

FLOW BEHAVIOUR IN MODEL OPEN-CHANNEL BENDS AND IMPLICATIONS FOR  
LATERAL MIGRATION IN RIVERS

by

George Okoye Krhoda

B.Ed.(Hons), University of Nairobi, Kenya, 1975

M.A. Wilfrid Laurier University, Ontario, Canada, 1980

THESIS SUBMITTED IN PARTIAL FULFILLMENT OF  
THE REQUIREMENTS FOR THE DEGREE OF  
DOCTOR OF PHILOSOPHY  
in the Department  
of  
Geography



George Okoye Krhoda 1985

SIMON FRASER UNIVERSITY

All rights reserved. This work may not be  
reproduced in whole or in part, by photocopy  
or other means, without permission of the author.

## ERRATUM

Table 3.2 and Figure 3.26 are missing due to an error in labeling.

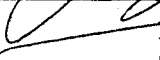
APPROVAL

Name: George O. Krhoda  
Degree: Doctor of Philosophy  
Title of Thesis: Flow Behaviour in Model Open-Channel  
Bends and Implications for Lateral  
Migration in Rivers

Examining Committee:

Chairman: Roger Hayter

---

  
Edward J. Hickin  
Senior Supervisor

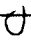
---

Ian Hutchinson

---

Michael C. Roberts

---

  
Gary Parker  
Professor  
External Examiner  
Department of Civil and Mineral Engineering  
University of Minnesota

Date Approved: Nov 10<sup>th</sup> 1984

PARTIAL COPYRIGHT LICENSE

I hereby grant to Simon Fraser University the right to lend my thesis, project or extended essay (the title of which is shown below) to users of the Simon Fraser University Library, and to make partial or single copies only for such users or in response to a request from the library of any other university, or other educational institution, on its own behalf or for one of its users. I further agree that permission for multiple copying of this work for scholarly purposes may be granted by me or the Dean of Graduate Studies. It is understood that copying or publication of this work for financial gain shall not be allowed without my written permission.

Title of Thesis/Project/Extended Essay

Flow Behaviour in Model Open-Channel Bends and Implications for

Lateral Migration in Rivers

Author:

(signature)

George O. Krhoda

(name)

December 10, 1984

(date)

## ABSTRACT

An investigation was conducted at the Burnaby Mountain Experimental Watershed at Simon Fraser University to study flow behaviour of single and consecutive model open-channel bends with curvature ratio combinations of  $1.0 < r_c/w < 4.7$ . Detailed measurements of velocity, current direction and bed topography were collected from more than ten cross sections in each bend. The total bend deflection angles varied between 75 and 180 degrees. The results of data analysis are presented in isovel patterns, vertical and longitudinal variation of velocity, shear stress and friction coefficients.

The transverse secondary flow advection upstream of the bend becomes appreciable at 30 degrees and is maximised at 60 degrees. Between 80 and 120 degrees, the transverse secondary flow decreases to its former magnitude at the straight entrance; shear stress and boundary friction both decrease also. These flow parameters are periodic every 30 to 60 degrees of the bend. Hickin's postulate on the shift of the core of maximum velocity is verified in single and upstream bends but the downstream bends are influenced by inherited structure which delays the cross over and the location of the fully developed flow zone. Bends of  $r_c/w > 2.7$  generate an oscillatory flow structure with relatively higher amplitudes than tighter bends.

The increase of shear stress and friction coefficients in bends of  $2.7 < r_c/w < 3.5$  is associated with plane bed, nonuniform mean velocity and decreased secondary flow advection. The

longitudinal distribution of shear stress and friction coefficients skew downstream in bends of  $r_c/w < 1.7$ ; it is symmetrical in  $r_c/w > 3.0$ , but becomes uniform in  $r_c/w = 2.0$ . The uniform velocity distribution may be responsible for reduced shear in  $r_c/w = 2.0$ . Bagnold's separation-collapse model could not be verified; instead the separation zones continually interact with the mainstream flow by secondary flow advection. The observed location of pools and of maxima in velocity and shear stress imply a curvature-dependent downstream shift in the erosional axis of developing bends consistent with Hickin's earlier observations. The predominant mode of lateral migration of upstream and single bends is by translation-expansion; the downstream bends migrate by expansion and rotation.

## ACKNOWLEDGEMENTS

During the last four years, many people assisted me generously with the preparation and completion of this thesis. I am particularly grateful to my senior supervisor, Edward J. Hickin, for providing inspiration, tactful guidance, and encouragement at all stages of my degree program. I will always value - and maintain - his friendship.

The study benefitted from Ian Hutchinson and Michael Roberts who provided valuable assistance during the discussion on the subject matter, and reviews of the manuscript. I would like to thank fellow graduate students who provided an environment for hard work on one hand and for laughter on the other. However I solely remain responsible for any commission or omission in this research.

This research was made possible by funding from the National Research Council of Canada, made available by Ted Hickin from his operating grant. Additional funding was provided by Simon Fraser University through a scholarship and a stipend during this period of need.

## TABLE OF CONTENTS

Approval .....	ii
ABSTRACT .....	iii
ACKNOWLEDGEMENTS .....	v
List of Tables .....	xii
List of Figures .....	xiv
CHAPTER 1 INTRODUCTION .....	1
I INTRODUCTION .....	1
1.1 Rationale and Basis .....	1
1.2 Objectives .....	7
1.3 Organisation of the study .....	7
II THEORETICAL BASIS AND REVIEW OF PREVIOUS WORK .....	9
1.4 Flow Characteristics in Open-channel Bends .....	9
1.5 Flow Separation .....	17
1.6 Channel Deformation and Lateral Migration in Rivers .....	18
CHAPTER 2 MEASUREMENT AND ANALYSIS .....	27
2 MEASUREMENTS AND ANALYSIS .....	27
2.1 Introduction .....	27
2.2 The Experimental Model .....	29
2.3 Calibration and Measurements .....	32
2.4 Data Analysis .....	37
2.5 Data Presentation .....	38
CHAPTER 3 EXPERIMENTAL RESULTS: SINGLE OPEN-CHANNEL BENDS .....	40
3.1 THE VELOCITY DISTRIBUTION AND CURRENT DIRECTION ..	40
3.1.1 Introduction .....	40



3.2.1 The Isovel Patterns and Current Direction in Single Bends with $r_c/w > 3.2$ .....	41
3.1.3 Summary of Flow Characteristics in Bends of $r_c/w > 3.2$ .....	51
3.1.4 The Isovel Patterns and Current Direction in Bends with $r_c/w < 2.6$ .....	56
3.1.5 Summary of Flow Characteristics in Bends with $r_c/w < 2.6$ .....	67
3.2 THE VELOCITY DISTRIBUTION IN SINGLE OPEN-CHANNEL BENDS .....	73
3.2.1. Introduction .....	73
3.2.2 The Distribution of Mean Velocity .....	74
3.2.3 Summary of Velocity Distribution in Single Bends .....	87
3.3 THE DISTRIBUTION OF SHEAR STRESS AND FRICTION COEFFICIENT .....	89
3.3.1 Introduction .....	89
3.3.2 The Distribution of Shear Stress near the Channel Banks .....	89
3.3.3 Summary .....	96
3.3.4 The Distribution of Mean Shear Stress in Single Bends .....	97
3.3.5 The Distribution of Friction Coefficient .....	107
3.4 DISCUSSION OF FLOW CONDITIONS IN SINGLE-OPEN CHANNEL BENDS .....	117
CHAPTER 4 EXPERIMENTAL RESULTS OF CONSECUTIVE BENDS WITH CONSTANT UPSTREAM BEND GEOMETRY .....	122
4 VELOCITY DISTRIBUTION, CURRENT DIRECTION AND VORTEX INTERACTION .....	122
4.1 Introduction .....	122
4.1.2 The Isovel Patterns and Current Direction in Consecutive Bends of $r_c/w_{us} = 4.0$ and variable $r_c/w_{ds}$ .....	123

4.1.3 Summary .....	130
4.1.4 The Isovel Patterns and Current Direction in Consecutive Bends of $r_c/wus=3.65$ and variable $r_c$ /wds .....	131
4.1.5 Summary .....	140
4.1.6 The Isovel Patterns and Current Direction in Consecutive Bends of $r_c/wus=2.7$ and variable $r_c$ /wds .....	141
4.1.8 The Isovel Patterns and Current Direction in Consecutive Bends of $r_c/wus=1.5$ and variable $r_c$ /wds .....	154
4.1.9 Summary and Observations .....	161
4.2 THE DISTRIBUTION OF VELOCITY IN CONSECUTIVE BENDS .....	166
4.2.1 Introduction .....	166
4.2.2 The Distribution of Velocity in Single Bends with $r_c/wus=4.0$ and variable $r_c/wds$ .....	167
4.2.3 The Distribution of Velocity in Consecutive Bends with $r_c/wus =3.6$ and variable $r_c/wds$ .....	170
4.2.4 The Distribution of Velocity in Consecutive Bends with $r_c/wus =2.7$ and variable $r_c/wds$ .....	174
4.2.5 The Distribution of Velocity in Bends with $r_c$ /wus=2.0 and variable $r_c/wds$ .....	176
4.2.6 The Distribution of Velocity in Bends with $r_c$ /wus=1.5 and variable $r_c/wds$ .....	178
4.2.7 Summary and Observations .....	179
4.3 THE DISTRIBUTION OF SHEAR STRESS AND FRICTION COEFFICIENTS IN CONSECUTIVE BENDS WITH CONSTANT UPSTREAM BEND GEOMETRY .....	184
4.3.1 Introduction .....	184
4.3.2 The Distribution of Shear Stress and Friction Coefficients in Consecutive Bends with $r_c$ /wus=4.0 and variable $r_c/wds$ .....	185
4.3.3 The Distribution of Shear Stress and Friction Coefficients in Consecutive Bends of $r_c/wus=3.65$ and variable $r_c/wds$ .....	192

4.3.4 The Distribution of Shear Stress and Friction Coefficients in Consecutive Bends of $r_c/wds=2.70$ and variable $r_c/wds$ .....	199
4.3.5 The Distribution of Shear Stress and Friction Coefficients in Consecutive Bends of $r_c/wds=2.0$ and variable $r_c/wds$ .....	203
4.3.6 The Distribution of Shear Stress and Friction Coefficients in Consecutive Bends of $r_c/wds=1.5$ and variable $r_c/wds$ .....	209
4.3.7 Summary and Observations .....	214
CHAPTER 5 EXPERIMENTAL RESULTS OF CONSECUTIVE BENDS WITH DOWNSTREAM BEND GEOMETRY CONSTANT .....	220
5 THE BEND FLOW DEVELOPMENT AND VORTEX INTERACTION IN CONSECUTIVE BENDS WITH CONSTANT DOWNSTREAM GEOMETRY .....	220
5.1 Introduction .....	220
5.1.2 The Isovel Patterns and Current Direction in Consecutive Bends of $r_c/wds=4.0$ and variable $r_c/wds$ .....	221
5.1.2 The Isovel Patterns and Current Direction in Consecutive Bends of $r_c/wds=3.3$ and variable $r_c/wds$ .....	232
5.1.4 The Isovel Patterns and Current Direction in Consecutive Bends of $r_c/wds=2.5$ and variable $r_c/wds$ .....	242
5.1.5 The Isovel Patterns and Current Direction in Consecutive Bends of $r_c/wds=1.94$ and variable $r_c/wds$ .....	247
5.1.6 Summary and Discussion .....	256
5.2 THE DISTRIBUTION OF MEAN AND TRANSVERSE VELOCITY	258
5.2.1 Introduction .....	258
5.2.2 The Velocity Distribution in Consecutive Bends of $r_c/wds=4.0$ and variable $r_c/wds$ .....	259
5.2.3 The Velocity Distribution in Consecutive Bends of $r_c/wds = 3.3$ and variable $r_c/wds$ .....	264
5.2.4 The Velocity Distribution in Consecutive Bends in $r_c/wds=2.5$ and variable $r_c/wds$ .....	268

5.2.5 The Velocity Distribution in Consecutive Bends in $r_c/w=2.0$ and variable $r_c/wus$ .....	271
5.2.6 Summary .....	274
5.3 THE DISTRIBUTION OF SHEAR STRESS AND FRICTION COEFFICIENTS IN CONSECUTIVE BENDS WITH CONSTANT DOWNSTREAM BEND GEOMETRY .....	279
5.3.1 Introduction .....	279
5.3.2 The Distribution of Shear Stress and Friction Coefficients in Consecutive Bends with $r_c$ $/wds=4.0$ and varying $r_c/wds$ .....	280
5.3.3 The Distribution of Shear Stress and Friction Coefficients in Consecutive Bends with $r_c$ $/wds=3.3$ and variable $r_c/wus$ .....	286
5.3.4 The Distribution of Shear Stress and Friction Coefficient in Consecutive Bends with $r_c/wds=2.5$ and variable $r_c/wus$ .....	293
5.3.5 The Distribution of Shear Stress and Friction Coefficient in Consecutive Bends with $r_c$ $/wds=1.94$ and variable $r_c/wus$ .....	298
4.4.5 Summary .....	302
CHAPTER 6 DISCUSSION OF RESULTS AND LATERAL MIGRATION IN RIVERS .....	306
6.1 Introduction .....	306
6.2 Bend Flow Development .....	308
6.3 Bend Flow Interaction .....	313
6.4 Bend Flow Development and Interaction and Lateral Migration in Rivers .....	318
CHAPTER 7 CONCLUSION .....	331
7 CONCLUSION .....	331
APPENDIX 1 .....	336
Calibration of Current meter used in the present study .....	336
APPENDIX 2 .....	338

1. GEOMETRIC CHARACTERISTICS OF CONSECUTIVE BENDS SERIES WITH CONSTANT UPSTREAM CURVATURE RATIOS ..	338
2. GEOMETRIC CHARACTERISTICS OF CONSECUTIVE BENDS SERIES WITH CONSTANT DOWNSTREAM CURVATURE RATIO .	340
GEOMETRIC CHARACTERISTICS OF SINGLE BENDS .....	342
APPENDIX 3 .....	342
The relations between Bed deformation and Shear Stress .....	342
BIBLIOGRAPHY .....	373

## LIST OF TABLES

TABLE	PAGE
1.1	List of symbols used in the present study ..... 5
1.2	Different modes of lateral migration in rivers ..... 24
2.1	Specifications of the Baby Ott current meter propellers used in the present study ..... 33
2.2	Error estimates of instruments and measurements ..... 36
3.1	Summary of approximate limits of each vortex flow in single open-channel bends ..... 66
3.3	The location of minimum and maximum shear stress and flow separation zones ..... I04
3.4	The relationship between mean friction coefficients expressed as ratios of that of a straight channel ..... I09
4.1	The bend flow development and vortex inter- action in consecutive bends with $r_c/wus=4.0$ and variable downstream bend geometry ..... I29
4.2	The bend flow development and vortex inter- action in consecutive bends with $r_c/wus=3.65$ and variable downstream bend geometry ..... I38
4.3	The bend flow development and vortex inter- action in consecutive bends with $r_c/wus=2.7$ and variable downstream bend geometry ..... I47
4.4	The bend flow development and vortex inter- action in consecutive bends with $r_c/wus=2.0$ and variable downstream bend geometry ..... I52
4.5	The bend flow development and vortex inter- action in consecutive bends with $r_c/wus=1.5$ and variable downstream bend geometry ..... I59
4.6	The location of maximum shear stress in consecutive bends with $r_c/wus=4.0$ and variable downstream bend geometry ..... I89

4.7	The location of maximum shear stress in consecutive bends with $r_c/wus=3.65$ and variable downstream bend geometry .....	198
4.8	The location of maximum shear stress in consecutive bends with $r_c/wus=2.0$ and variable downstream bend geometry .....	205
4.9	The location of maximum shear stress in consecutive bends with $r_c/wus=1.5$ and variable downstream bend geometry .....	213
4.10	The variation of dimensionless shear stress with curvature ratio .....	216
5.1	The bend flow development and vortex interaction in consecutive bends with $r_c/wds=4.0$ and variable upstream bend geometry .....	228
5.2	The bend flow development and vortex interaction in consecutive bends with $r_c/wds=3.65$ and variable upstream bend geometry .....	240
5.3	The bend flow development and vortex interaction in consecutive bends with $r_c/wds=2.5$ and variable upstream bend geometry .....	246
5.4	The bend flow development and vortex interaction in consecutive bends with $r_c/wds=1.9$ and variable upstream bend geometry .....	255
5.5	The location of maximum and minimum velocity in consecutive bends with constant downstream bend geometry .....	275
5.6	The location and extent of convex and concave flow separation zones .....	277
5.7	The location of maximum shear stress in consecutive bends with $r_c/wus=4.0$ and variable downstream bend geometry .....	287
5.8	The location of maximum shear stress in consecutive bends with $r_c/wds=3.3$ and variable upstream bend geometry .....	291
6.1	The location of the free and forced vortices and the fully developed flow zones .....	310

## LIST OF FIGURES

FIGURE	PAGE
1.1 A definitional sketch of open-channel bend geometry .....	3
1.2 A schematic representation of variations of fluid hydraulic patterns with bend geometry and the rate of lateral migration in rivers.....	16
1.3 Modes of lateral migration and the potential of point bar preservation in river bends.....	24
2.1 Outline of experimental runs.....	28
2.2 Cumulative grain size distribution of sediment used in the present study.....	31
3.1 Selected isovel patterns of a straight channel .....	42
3.2 Cross stream and vertical velocity distribution of selected sections of a straight channel .....	42
3.3 Selected isovel patterns of a single bend with $r_c/w=4.7$ .....	44
3.4 Cross stream and vertical velocity distribution of selected sections of a single bend with $r_c/w=4.7$ .....	44
3.5 Selected isovel patterns of a single bend with $r_c/w=4.0$ .....	46
3.6 Cross stream and vertical velocity distribution of selected cross sections of a bend with $r_c/w=4.0$ .....	47
3.7 Selected isovel patterns of a single bend with $r_c/w=3.7$ .....	50
3.8 Cross stream and vertical velocity distribution of selected cross sections of a bend with $r_c/w=3.7$ .....	50



3.9	Selected isovel patterns of a single bend with $r_c/w=3.3$ .....	52
3.10	Cross stream and vertical velocity distribution of selected cross sections of a bend with $r_c/w=3.3$ .....	52
3.11	Selected isovel patterns of a single bend with $r_c/w=3.2$ .....	53
3.12	Cross stream and vertical velocity distribution of selected cross sections of a bend with $r_c/w=3.2$ .....	53
3.13	Selected isovel patterns of a single bend with $r_c/w=2.6$ .....	54
3.14	Selected isovel patterns of a single bend with $r_c/w=2.2$ .....	57
3.15	Cross stream and vertical velocity distribution of selected cross sections of a bend with $r_c/w=2.2$ .....	58
3.16	Selected isovel patterns of a single bend with $r_c/w=1.8$ .....	60
3.17	Cross stream and vertical velocity distribution of selected cross sections of a bend with $r_c/w=1.8$ .....	60
3.18	Selected isovel patterns of a single bend with $r_c/w=1.5$ .....	61
3.19	Cross stream and vertical velocity distribution of selected cross sections of a bend with $r_c/w=1.5$ .....	62
3.20	Selected isovel patterns of a single bend with $r_c/w=1.0$ .....	64
3.21	Cross stream and vertical velocity distribution of selected cross sections of a bend with $r_c/w=1.0$ .....	64
3.22	The dimensionless bend angles at which the free and forced vortex flows are initiated .....	68

3.23	The ratio of mean velocity at each cross section and the velocity near the channel bend, $n = 0.75$ ..	71
3.24(a)	The longitudinal distribution of mean velocity in a single bend with $r_c/w=1.0$ .....	75
3.24(b)	The longitudinal distribution of mean velocity in a single bend with $r_c/w=1.5$ .....	75
3.24(c)	The longitudinal distribution of mean velocity in a single bend with $r_c/w=1.8$ .....	76
3.24(d)	The longitudinal distribution of mean velocity in a single bend with $r_c/w=2.6$ .....	76
3.24(e)	The longitudinal distribution of mean velocity in a single bend with $r_c/w=2.2$ .....	77
3.24(f)	The longitudinal distribution of mean velocity in a single bend with $r_c/w=3.2$ .....	78
3.24(g)	The longitudinal distribution of mean velocity in a single bend with $r_c/w=3.3$ .....	78
3.24(h)	The longitudinal distribution of mean velocity in a single bend with $r_c/w=3.7$ .....	79
3.24(i)	The longitudinal distribution of mean velocity in a single bend with $r_c/w=4.0$ .....	79
3.25	The relationship between $r_o/r_i$ with curvature ratio .....	83
3.27	The distribution of shear stress along the channel banks of a bend with $r_c/w=4.0$ .....	91
3.28	The distribution of shear stress along the channel banks of bends with $3.2 < r_c/w < 3.7$ .....	92
3.29	The distribution of shear stress along the channel banks of bends with $r_c/w=2.2$ and $2.6$ .....	93
3.30	The distribution of shear stress along the channel banks of bends with $1.0 < r_c/w < 1.8$ .....	94
3.31	Channel bend deformation characteristics of selected single bends .....	99
3.32	The distribution of mean shear stress in bends with $4.7 > r_c/w > 2.6$ .....	101

3.33	The distribution of mean shear stress in bends with $1.0 < r_c/w < 2.2$ .....	I02
3.34	The location of the bend sections at which the shear stress has maximum and minimum values .....	I05
3.35	The distribution of friction coefficients in single bends .....	II0
3.36	The distribution of friction coefficients in single bends with $r_c/w > 2.5$ .....	II2
3.37	The distribution of friction coefficients in single bends of $r_c/w < 2.5$ .....	II3
3.38	Comparison between computed $\tan \alpha$ and the maximum current direction .....	II6
4.1	Selected isovel patterns of consecutive bends with $r_c/w_{us}=4.0$ and $r_c/w_{ds}=3.1$ .....	I24
4.2	Selected isovel patterns of consecutive bends with $r_c/w_{us}=4.0$ and $r_c/w_{ds}=2.0$ .....	I25
4.3	Selected isovel patterns of consecutive bends with $r_c/w_{us}=4.0$ and $r_c/w_{ds}=1.8$ .....	I26
4.4	Selected isovel patterns of consecutive bends with $r_c/w_{us}=3.65$ and $r_c/w_{ds}=3.91$ .....	I32
4.5	Selected isovel patterns of consecutive bends with $r_c/w_{us}=3.65$ and $r_c/w_{ds}=2.2$ .....	I33
4.6	Selected isovel patterns of consecutive bends with $r_c/w_{us}=3.65$ and $r_c/w_{ds}=1.56$ .....	I34
4.7	Selected isovel patterns of consecutive bends with $r_c/w_{us}=3.65$ and $r_c/w_{ds}=1.75$ .....	I35
4.8	Selected isovel patterns of consecutive bends with $r_c/w_{us}=3.3$ and $r_c/w_{ds}=3.8$ .....	I37
4.9	Selected isovel patterns of consecutive bends with $r_c/w_{us}=2.7$ and $r_c/w_{ds}=4.0$ .....	I42

4.10	Selected isovel patterns of consecutive bends with $r_C/wus=2.7$ and $r_C/wds=2.7$ .....	I43
4.11	Selected isovel patterns of consecutive bends with $r_C/wus=2.7$ and $r_C/wds=2.3$ .....	I44
4.12	Selected isovel patterns of consecutive bends with $r_C/wus=2.7$ and $r_C/wds=1.0$ .....	I45
4.13	Selected isovel patterns of consecutive bends with $r_C/wus=2.0$ and $r_C/wds=4.0$ .....	I48
4.14	Selected isovel patterns of consecutive bends with $r_C/wus=2.0$ and $r_C/wds=3.0$ .....	I49
4.15	Selected isovel patterns of consecutive bends with $r_C/wus=2.0$ and $r_C/wds=2.0$ .....	I50
4.16	Selected isovel patterns of consecutive bends with $r_C/wus=1.92$ and $r_C/wds=2.65$ .....	I51
4.17	Selected isovel patterns of consecutive bends with $r/wus=1.5$ and $r_C/wds=2.9$ .....	I55
4.18	Selected isovel patterns of consecutive bends with $r_C/wus=1.5$ and $r_C/wds=2.7$ .....	I56
4.19	Selected isovel patterns of consecutive bends with $r_C/wus=1.5$ and $r_C/wds=2.1$ .....	I57
4.20	Selected isovel patterns of consecutive bends with $r_C/wus=1.2$ and $r_C/wds=1.5$ .....	I58
4.21	The distribution of mean velocity in consecutive bends with $r_C/wus=4.0$ and variable downstream bend geometry .....	I68
4.22	The distribution of mean velocity in consecutive bends with $r_C/wus=3.65$ and variable downstream bend geometry .....	I71
4.23	The distribution of mean velocity in consecutive bends with $r_C/wus=2.67$ and variable downstream bend geometry .....	I73
4.24	The distribution of mean velocity in consecutive bends with $r_C/wus=2.0$ and variable downstream bend geometry .....	I75

4.25	The distribution of mean velocity in consecutive bends with $r_C/wus=1.5$ and variable downstream bend geometry .....	I77
4.26	The distribution of mean shear stress in consecutive bends with $r_C/wus=4.0$ (constant) and variable downstream bend geometry .....	I86
4.27	The distribution of friction coefficient in consecutive bends with $r_C/wus=4.0$ (constant) and variable downstream bend geometry .....	I87
4.28	The distribution of shear stress near the concave bank in consecutive bends with $r_C/wus=4.0$ (constant) and variable downstream geometry .....	I91
4.29	The distribution of mean shear stress in consecutive bends with $r_C/wus=3.65$ (constant) and variable downstream bend geometry .....	I93
4.30	The distribution of friction coefficient in consecutive bends with $r_C/wus=3.65$ (constant) and variable downstream bend geometry .....	I94
4.31(a)	The distribution of shear stress near the concave bank in consecutive bends with $r_C/wus=3.65$ (constant) and variable downstream geometry .....	I95
4.31(b)	The distribution of mean shear stress in consecutive bends with $r_C/wus=3.65$ (constant) and variable downstream bend geometry .....	I96
4.32	The distribution of mean shear stress in consecutive bends with $r_C/wus=2.67$ (constant) and variable downstream bend geometry .....	200
4.33	The distribution of friction coefficient in consecutive bends with $r_C/wus=2.67$ (constant) and variable downstream bend geometry .....	201
4.34	The distribution of shear stress near the channel banks in consecutive bends with $r_C/wus=2.67$ (constant) and variable downstream bend geometry .....	202

4.35	The distribution of mean shear stress in consecutive bends with $r_C/wus=2.0$ (constant) and variable downstream bend geometry .....	205
4.36	The distribution of shear stress near the channel banks in consecutive bends with $r_C/wus=2.0$ (constant) and variable downstream bend geometry .....	206
4.37	The distribution of friction coefficient in consecutive bends with $r_C/wus=2.0$ (constant) and variable downstream bend geometry .....	207
4.38	The distribution of mean shear stress in consecutive bends with $r_C/wus=1.5$ (constant) and variable downstream bend geometry .....	210
4.39	The distribution of friction coefficient in consecutive bends with $r_C/wus=1.5$ (constant) and variable downstream bend geometry .....	211
4.40	The distribution of shear stress near the channel banks in consecutive bends with $r_C/wus=1.5$ (constant) and variable downstream bend geometry .....	212
4.41	The relationship between nondimensional shear stress and curvature index .....	218
5.1	Selected isovel patterns in consecutive bends with $r_C/wus=3.0$ and $r_C/wds=4.0$ (constant) .....	222
5.2	Selected isovel patterns in consecutive bends with $r_C/wus=2.7$ and $r_C/wds=4.0$ (constant) .....	223
5.3	Current direction motifs for bends with $r_C/wus=2.7$ and $r_C/wds=4.0$ (constant) .....	224
5.4	Selected isovel patterns in consecutive bends with $r_C/wus=1.4$ and $r_C/wds=4.0$ (constant) .....	225
5.5	Vortex development and interaction in consecutive bends with $r_C/wus=1.4$ and $r_C/wds=4.0$ (constant) .....	227
5.6	Selected isovel patterns in consecutive bends with $r_C/wus=1.73$ and $r_C/wds=3.6$ (constant) .....	233

5.7	Selected isovel patterns in consecutive bends with $r_C/wus=1.7$ and $r_C/wds=3.03$ (constant) .....	234
5.8	Selected isovel patterns in consecutive bends with $r_C/wus=3.2$ and $r_C/wds=3.3$ (constant) .....	236
5.9	Selected isovel patterns in consecutive bends with $r_C/wus=2.0$ and $r_C/wds=3.2$ (constant) .....	237
5.10	Selected isovel patterns in consecutive bends with $r_C/wus=2.6$ and $r_C/wds=3.0$ (constant) .....	238
5.11	Selected isovel patterns in consecutive bends with $r_C/wus=1.5$ and $r_C/wds=3.3$ (constant) .....	239
5.12	Selected isovel patterns in consecutive bends with $r_C/wus=3.0$ and $r_C/wds=2.56$ (constant) .....	243
5.13	Selected isovel patterns in consecutive bends with $r_C/wus=3.2$ and $r_C/wds=2.4$ (constant) .....	244
5.14	Selected isovel patterns in consecutive bends with $r_C/wus=2.0$ and $r_C/wds=2.6$ (constant) .....	245
5.15(a)	Selected isovel patterns in consecutive bends with $r/wus=4.0$ and $r_C/wds=1.65$ (constant) .....	248
5.15(b)	Vortex development and interaction in conse- cutive bends with $r_C/wus=4.0$ and $r_C/wds=1.9$ .....	249
5.16	Selected isovel patterns in consecutive bends with $r_C/wus=2.75$ and $r_C/wds=1.65$ (constant) .....	250
5.17	Selected isovel patterns in consecutive bends with $r_C/wus=3.0$ and $r_C/wds=1.94$ (constant) .....	251
5.18	Selected isovel patterns in consecutive bends with $r_C/wus=1.64$ and $r_C/wds=1.94$ (constant) .....	252
5.19	Selected isovel patterns in consecutive bends with $r_C/wus=3.3$ and $r_C/wds=2.0$ (constant) .....	254
5.20	The distribution of mean velocity in consecutive bends with $r_C/wds=4.0$ and variable upstream bend geometry .....	260

5.21	The distribution of velocity near the channel banks of paired bends with $r_C/wds=4.0$ and variable upstream bend geometry .....	261
5.22	The distribution of mean velocity in consecutive bends with $r_C/wds=3.3$ and variable upstream bend geometry .....	265
5.23	The distribution of velocity near the channel banks of paired bends with $r_C/wds=3.3$ and variable upstream bend geometry .....	266
5.24	The distribution of mean velocity in consecutive bends with $r_C/wds=2.5$ and variable upstream bend geometry .....	269
5.25	The distribution of velocity near the channel banks of paired bends with $r_C/wds=2.5$ and variable upstream bend geometry .....	270
5.26	The distribution of mean velocity in consecutive bends with $r_C/wds=1.9$ and variable upstream bend geometry .....	272
5.27	The distribution of velocity near the channel banks of paired bends with $r_C/wds=1.9$ and variable upstream bend geometry .....	273
5.28	The distribution of mean shear stress in consecutive bends with $r_C/wds=4.0$ and variable upstream bend geometry .....	281
5.29	The distribution of shear stress near the channel banks of consecutive bends with $r_C/wds=4.0$ and variable upstream bend geometry .....	282
5.30	Contours of relative shear stress in consecutive bends with $r_C/wus=3.0$ and $r_C/wds=4.0$ .....	284
5.31	The distribution of friction coefficient in consecutive bends with $r_C/wds=4.0$ and variable upstream bend geometry .....	285
5.32	The distribution of mean shear stress in consecutive bends with $r_C/wds=3.3$ and variable upstream bend geometry .....	289



5.33	The distribution of shear stress near the channel banks of consecutive bends with $r_c/wds=3.3$ and variable upstream bend geometry .....	290
5.34	The distribution of friction coefficient in consecutive bends with $r_c/wds=3.3$ and variable upstream bend geometry .....	294
5.35	The distribution of mean shear stress in consecutive bends with $r_c/wds=2.5$ and variable upstream bend geometry .....	295
5.36	The distribution of shear stress near the channel banks of consecutive bends in $r_c/wds=2.5$ and variable upstream bend geometry .....	296
5.37	The distribution of friction coefficient in consecutive bends with $r_c/wds=2.5$ and variable upstream bend geometry .....	297
5.38	The distribution of mean shear stress in consecutive bends with $r_c/wds=1.94$ and variable upstream bend geometry .....	299
5.39	The distribution of friction coefficient in consecutive bends with $r_c/wds=1.94$ and variable upstream bend geometry .....	300
5.40	Contour map of dimensionless shear stress distribution in consecutive bends with $r_c/wus=1.64$ and $r_c/wds=1.94$ .....	30I
6.1	The relationship between the initiation of free and forced vortices and the fully developed flow zones .....	3II
6.2	The location of free vortex along the upstream and downstream bends .....	3I7
6.3	The location of maximum erosional axis in river bends of the Beatton .....	320
6.4	The location of the points where velocity, shear stress and the strength of the vortex flow have maximum values .....	32I
6.5	The location of maximum velocity, shear stress and vortex strength in single and upstream bends .....	325
6.6	The location of the areas liable to erosion in downstream bends .....	327

## LIST OF PLATES

PLATE		PAGE
2.1	The Experimental model: An example of a single bend .....	30
3.1	The bedform characteristics of a straight channel .....	45
3.2	Vortex roll-up at the bend apex due to flow acceleration near the concave bank and deceleration near the convex bank .....	85
3.3	The periodic surface flow characteristic typical in the present model bends and river .....	86

## CHAPTER 1 INTRODUCTION

### I INTRODUCTION

#### 1. Rationale and Basis

River channels do not remain straight for any appreciable distance. The winding of river planforms and the tendency to create a succession of shoals and deeps have been of interest to navigators, hydraulicians, mathematicians and planners for more than a century (Thompson, 1876). The physical explanation of shoals and deeps has been identified as the attenuation of the velocity fields by secondary flow (Levliansky, 1955). Secondary flow or currents occur in a plane normal to the local axis of the primary flow and are brought about by the interaction between the primary velocity with gross channel properties (Ciracy, 1967), resulting in spirals or vortices. Both terms are used interchangeably in the literature. Thompson (1876) correctly ascribed such secondary flow to friction (see also Rozovskii, 1961).

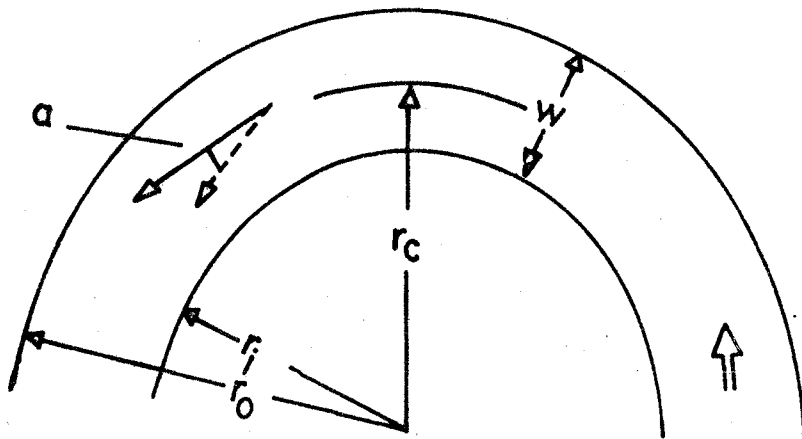
One hundred years later, investigators continue to put together the puzzle of cause(s) of meander initiation. Several workers have linked meandering tendency with sediment transport,

stream load and oscillation of the core of maximum velocity (Werner, 1954; Friedkin, 1945; Ackers and Charlton, 1971). The manner in which velocity distribution becomes nonuniform in order to cause localised scour and shoal (Quraishy, 1944) has been a staging ground for investigating meander initiation. After a bend has been initiated, meanders become self-perpetuating by increasing nonuniform transverse and longitudinal velocity, shear stress and friction to flow. The sharp alternate bends aggravate the meander development.

This study examines the relationships among bend flow, shear stress, friction to flow and the curvature of model stream bends. The principal aim of the investigation is to better understand the nature of velocity fields in tight bends with curvature ratios of  $1.0 < r_c/w < 4.0$  and in bend sequences of varying curvature combinations. Figure 1.1 gives a definitional sketch of the geometry of an open-channel bend. The symbols used in the present study are given in Table 1.1 for reference. The ultimate goal of this research is to relate the spatial variation of velocity and shear stress fields to different modes of lateral migration in rivers.

Numerous studies have examined velocity and shear stress distribution in single isolated open-channel bends. Few studies, however, have examined flow interaction in a series of bends (Jackson, 1975; Yen, 1965; Hickin, 1978; Siebert and Gotz, 1975; Bhowmik, 1979).

Figure I.I. A definitional sketch of open-channel bend geometry



- a current direction deviation
- $r_i$  inner bank radius
- $r_o$  outer bank radius
- $r_c$  channel centreline radius
- w channel width

Such studies have increased our knowledge of the mechanics and kinematics of flow in river bends but the conclusions which relate to lateral migration are limited by lack of a systematic criterion for evaluating the degree of upstream and downstream effects on either the proceeding or preceding bends. They also are limited by the mathematical assumptions built into the analytical models examined.

It is necessary to investigate the distribution of velocity, shear stress and friction to flow in open-channel bends in order to understand how the stream can modify its geometry through erosion in certain zones but not in others. A general picture of bend modification shows that erosion occurs on the outside (concave) bank and deposition on the inside (convex) bank. It is necessary also that the flow in open-channel bends be compared to fluid flow in other conduits in order to see the various results of research in the most general conceptual context. Evidence exists already on the spatial variation of flow characteristics and on how these characteristics relate to channel geometry, vortex and turbulence production including flow separation (Yen, 1970; Jackson, 1975; de Vriend, 1980).

List of Symbols used in the present Study

- a - current direction in degrees
- C - Chezy's friction coefficient
- D - hydraulic depth, the ratio of area of cross section to channel width
- f - unknown functional relationship
- ff - Darcy-Weisbach friction coefficient
- ff<sub>b</sub> - mean friction coefficient of a bend
- ff<sub>s</sub> - mean friction coefficient of a straight channel
- Fn - Froude number,  $V/\sqrt{gD}$
- g - acceleration due to gravity, 9.81m.s<sup>-1</sup>
- h - water elevation, m.
- k<sub>1</sub>, ... k<sub>n</sub> - unknown coefficient
- m - number of revolutions of propeller per sec.
- n - relative depth, y<sub>0</sub>/y<sub>1</sub>
- P - channel perimeter, m.
- q - sediment transport
- r - radius of a streamline
- r<sub>c</sub> - channel centreline radius, m.
- r<sub>i</sub> - inner (convex) bank radius, m.
- r<sub>o</sub> - outer (concave) bank radius, m.
- s - rate of change of secondary flow
- t - exponent of any vortex in equation 1.4.
- T<sub>o</sub> - shear stress, Newtons/m<sup>2</sup>.

$T_x$  - dimensionless shear stress ratio

$\bar{T}_o$  - mean shear stress at each cross section, in equation 2.3.

$u$  - radial velocity,  $m\ s^{-1}$

$U$  - kinematic viscosity,  $m.\ s^{-1}$

$v$  - vertical velocity,  $m\ s^{-1}$

$V$  - mean velocity at a cross section,  $m.\ s^{-1}$

$V$  - mean velocity near the channel bed,  $n > 0.75$

$w$  - surface channel width,  $m$ .

$*$  - fluid density

$y$  - depth of the flow,  $m$ .

$\bar{y}$  - mean depth;  $z$  - radial coordinate

#### subscripts

$r_i$  - subscript for the convex bank

$r_o$  - subscript for the concave bank

$us$  - subscript for upstream bends

$ds$  - subscript for downstream bends

$max$  - subscript for maximum

$min$  - subscript for minimum



## 1.2 Objectives

The aim of this study is to examine bend flow, shear stress and friction to flow in various model streams in order to better understand the flow dynamics in open-channel bends and also predict various patterns of lateral erosion. The detailed objectives are five-fold:

1. to measure, describe and map the distribution of primary and secondary velocity in single and successive bends;
2. to study bend-flow development and interaction, and compare the results with analytical-theoretical formulations in tight bends;
3. to compare and incorporate information on macro-eddies and bend-flow structure with previous results obtained from closed conduits at similar Reynolds numbers;
4. to relate flow structure in tight bends to modes of lateral migration in rivers;
5. to provide measurements for testing analytical solutions where they may be applicable.

## 1.3 Organisation of the study

The various aspects of bend flow development and interaction in the present study correspond with phases of experimental design. The following section outlines the

theoretical basis and reviews also the pertinent literature on bend flow structure. Chapter 2 outlines the methods and procedures adopted in the experiment. It provides the basis of evaluating measurement errors, and includes a discussion of data analysis and presentation of experimental results.

Experimental results are discussed in Chapters 3 to 5. Each chapter deals with single bends (chapter 3), consecutive bends of which the upstream curvature ratios are constant (chapter 4) and chapter 5 treats those in which downstream curvature ratios are constant. A synthesis of the discussion of bend flow development and interaction and the implications for lateral erosion in rivers is treated in chapter 6. The conclusions drawn from this exercise provide an assesment of the results and the shortcomings of this investigation; these are discussed in chapter 7.

II THEORETICAL BASIS AND REVIEW OF PREVIOUS WORK

1.4 Flow Characteristics in Open-channel Bends

The dominating characteristic of flow in open-channel bends is the centrifugal force which causes transverse acceleration on one hand, and flow deceleration and superelevation on the other. Assuming that the flow in a bend is irrotational and the distribution of pressure is hydrostatic, Mockmore (1944) describes the need for centrifugal force to move an element of water in a curved path by an equation in the form:

$$dh/dz = u^2/(gr) \dots \dots \dots 1.1$$

where h is elevation of water surface above a horizontal datum, z is a radial coordinate measured outward, u is radial velocity along a streamline, r is the radius of the streamline, and g is acceleration due to gravity.

Yen and Yen (1971) integrated equation 1.1 accounting for resistance to flow and found that dh/dz varies little with u. For a rough approximation, we set  $r=r_c$  and  $u=V$ , where V is the mean velocity. At a cross section of small width, the water surface slope, dh, is inclined towards the concave bank, and may be estimated by an equation in the form:

$$dh = V^2 w / (g r_c) \dots \dots \dots 1.2$$

where w is channel width, and r is the centre

line radius; the other symbols are as defined earlier.

In deriving equations 1.1 and 1.2, it is assumed that the flow is two-dimensional and the transverse velocity is constant and does not depend on the change of bend curvature. Such a bend flow pattern is preceded by a transitional zone where velocity is higher near the convex bank than on the concave and varies across the channel in close agreement with the law of the free vortex (Mockmore, 1944). The angular velocities and accelerations inherent in the free vortex move bed load from the inner (convex) bank towards the channel centreline.

Using the same assumptions as for equation 1.1 to write the energy equation and after differentiation, the energy equation can be combined with equation 1.1 to take the form (Einstein and Harder, 1954):

$$dv/dr - v/r = 0 \dots\dots\dots 1.3$$

Equation 1.3 may be simplified to:

$$v = k_1 r^t \dots\dots\dots 1.4$$

where  $k_1$  and  $t$  respectively are coefficient and exponent.

From equation 1.4,  $k$  varies from one section to another depending on the position of the core of maximum velocity. For forced vortex,  $t = + 1.0$  and for a free vortex,  $t = - 1.0$ . In the present study, a transitional vortex (parabolic flow) is defined for  $- 0.15 < t < + 0.15$ .

Vortex development and decay in open-channel bends (Bagnold, 1960; Soliman and Tinney, 1968) has been a controversial subject (Hickin, 1978) because its measurement has

eluded geomorphologists. Vortices are common whenever there are frictional forces (Einstein and Shen, 1964). As flow approaches the bend entrance, a potential vortex will be initiated as a result of the imbalance of pressure forces in equation 1.1; this theoretical notion is confirmed by experimental results in rigid rectangular channels (Mockmore, 1944; Rozovskii, 1961; Muramoto, 1967) , those of trapezoidal sections, (Rozovskii, 1961; Yen, 1965; Desaulniers and Frenette, 1972) and in field examples (Jackson, 1975; Hickin, 1978). As flow reaches the bend, radial forces shift the core of maximum velocity as well as the axis of maximum shear stress towards the concave bank. Further downstream the flow becomes steady and two-dimensional, i.e. the flow does not change its characteristics with increasing bend angle and the bend-flow is said to be fully developed. Because the developed flow regime is two-dimensional (Muramoto, 1967), its location may be detected by transverse surface and bottom currents directed respectively towards the concave bank and convex bank (Jackson, 1975). Although there is no agreement on whether a developed flow regime can be obtained for any appreciable length in tight bends (Shukry, 1949; Gotz, 1980), the debate has been confusing because of the lack of a standardised frame of reference. To this end it may be useful to express equation 1.4 as a function of the bend angle and curvature ratio.

Muramoto (1967) measured the distribution of vorticity using an improved pitot tube in model meander bends of  $r_c/w=1.5$

and 3.0 and concluded that secondary flow varies in relation to bend angle. Some of the major findings of Muramoto are summarised below.

1. the secondary flow directed towards the surface increases in magnitude from the channel bend entrance and reaches its maximum at bend angle of 60 degrees, then it gradually decreases in the curved section.
2. the secondary flow directed radially outwards (free vortex) maintains its magnitude at the bend entrance until a bend angle of 15 degrees, then it gradually decreases in the downstream curved section. At the bend exit, it recovers to approach its initial magnitude.
3. the secondary flow directed towards the bottom of the channel remains zero until a bend angle of 60 degrees and then it gradually increases in the latter half of the bend. Past the bend apex, it becomes zero again.

Fox and Ball (1968) observed secondary flow development between 15 and 60 degrees in a 180 degree bend. Hawthorne (1951), Yen (1970), Einstein (1972), Siebert and Gotz (1975) and Varshney and Garde (1975) also have arrived at values within that broad range. The location of the fully developed flow zone has been estimated by Rozovskii (1961) using an expression in the form:

$$X = [(2.3 C/\sqrt{g}) (h/r)] \dots \dots \dots 1.5$$

where X is the angular distance from the bend entrance, C is Chezy's friction coefficient, h is depth.

$$C = \sqrt{8g/ff} \dots\dots\dots 1.6$$

where  $g$  is acceleration due to gravity and  $ff$  is Darcy's friction coefficient.

Substituting for  $C$  in equation 1.5 gives:

$$x = k_2 [(\sqrt{8g/ff}) (h/r) \dots\dots\dots 1.7$$

Equation 1.7 shows that the location of the fully developed flow zone is an inverse function of friction coefficient and the ratio of depth of flow to radius of bend curvature. Smith (1976) and Mullin and Greated (1980) found that the location of the fully developed flow zone is 1.5 and 1.9 channel widths from the bend entrance respectively, although these data are difficult to compare with those reported by the authors cited earlier.

The controversy about vortex development and location centres on the way streamlines converge and diverge continuously through the bend. On the one hand is Wilson's (1973) model of a single vortex at the bend apex and double vortices with bed-divergent currents at bend inflection. On the other is the Hey and Thorne's (1975) model which resembles Wilson's concept at the bend apex, except with a subsidiary vortex that rotates in the opposite sense to the main one. It has bed-divergent currents at the bend inflection. The Wilson's model is supported by results of Leopold and Wolman (1960, Baldwin creek, U.S.A), Rozovskii (1961, Desna and Snov rivers, U.S.S.R.) and Jackson (1975, Wabash river, U.S.A.). Hey and Thorne's model is supported by their own examples including results of Bathurst et al (1979), and also flume studies (Einstein and Harder, 1954;

Einstein and Shen, 1964; Onishi et al; 1976). While both models appear to be applicable to some bends, they probably represent a system of threshold bifurcation or break down (Bagnold, 1960) in vortex development. The shift of the core of maximum velocity (Hickin, 1978) and the axis of maximum shear stress possibly are related to the number of vortices at the bend apex and inflections. In fact the presence of double vortices at the bend apex has been used to discriminate between stable and unstable flows (see for example Tietjens, 1934).

Given a cross section of a bend with isovels it is possible to estimate whether the secondary flow is directed towards the channel bed (downwelling) or towards the water surface (upwelling). Assuming that the pattern of the isovels act as a set of flexible membranes held in place by constant fluid of equal velocity, any surface bulge of the isovels towards the bottom will imply downwelling, and the converse is true. At the water surface, secondary flow convergence at the channel centreline depresses the core of maximum velocity.

Analytically, Rozovskii (1961) made the same assumptions as those used for deriving equations 1.1 and 1.2 and obtained an expression for the distribution of vertical velocity in the form:

$$v/V = -1.5/x^2 (h/r)^2 (y/n - (y/n)^2) \dots\dots\dots 1.8$$

where  $v$  is the vertical velocity component,  $V$  is longitudinal velocity component,  $y$  is the depth of measurement,  $n$  is the relative depth,  $y_1/y_0$ , and  $x$  is von



Karman's constant.

Equation 1.8 yields only secondary flow directed towards the channel bed and therefore can be restricted to bend angles downstream of 60 degrees (Muramoto, 1967). Einstein (1972) integrated a simplified Navier-Stokes equation and derived an expression for the rate of change of secondary flow,  $s$ , in the form:

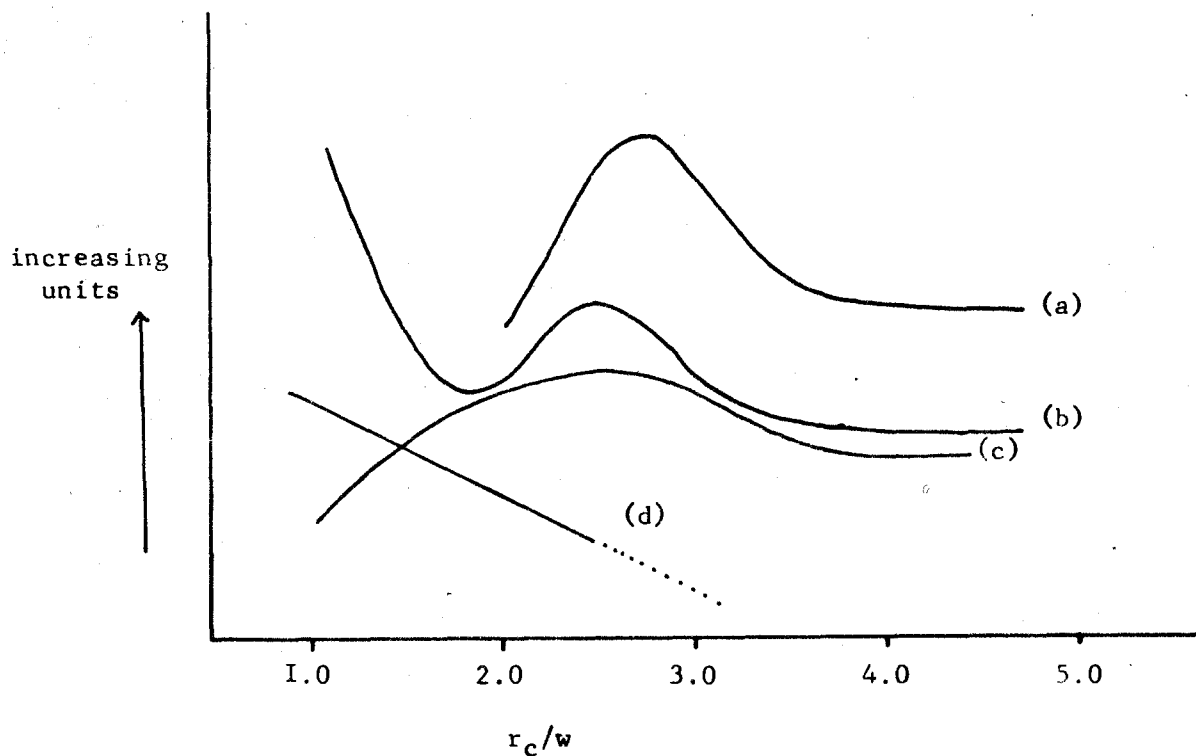
$$s = du/dy \cdot f(a) \dots \dots \dots 1.9$$

where  $f$  is an unknown function and  $a$  is the current direction.

Equation 1.9 is supported by Muramoto's (1967) results and appears to be readily applicable to meander bends of diverse geometry.

The relationships amongst fluid hydraulic variables, bend geometry and the rate of lateral migration in rivers are complex (cf. Nanson and Hickin, 1983). Figure 1.2 summarises the variations of shear stress, friction to flow, the location of the core of maximum velocity and the strength of the spiral flow reported in various literature. Hickin (1978) suggested that the core of maximum velocity, and therefore the axis of maximum shear stress, tend to locate at the centre of the channel in bends of  $r_c/w > 4.0$ . The velocity distribution and friction to flow are similar also to that of a straight channel (Bagnold, 1960). The rate of lateral erosion is small compared to that in rather tighter bends. However the core of maximum velocity shifts towards the concave bank in bends between  $3.0 < r_c/w < 4.0$

Figure I.2. A schematic representation of variations of fluid hydraulic patterns with bend geometry and the rate of lateral migration in rivers.



- Definitions of each curve:
- (a) rate of lateral migration, m./yr. (Hickin and Nanson, 1975).
  - (b) distribution of friction coefficient,  $F_n^2$  (Bagnold, 1960)
  - (c) the location of the core of maximum velocity, measured from the outer bank to the inner bank and expressed as  $W/W$ . The data is adopted from Hickin's (1979) hypothetical discussion.
  - (d) strength of the spiral flow (Shukry, 1949).

see also Yen, 1970; Onishi, et al. 1976). Within these bends secondary flow and lateral erosion increase, then both decrease (Shukry, 1949) as the bends approach  $r_c/w=3.0$ . Finally the core of maximum velocity shifts towards the centre of the channel, but more or less at the toe of the point bar in  $r_c/w<3.0$ . This simple model of transverse variation of high velocity core with decreasing  $r_c/w$  may be applicable to single isolated bends; the flow structure in the downstream bends are influenced by flow conditions that persist from the upstream bends.

### 1.5 Flow Separation

A study of flow and vortex interaction in bends of  $r_c/w<4.0$  cannot be complete without a discussion on separation of flow. Flow separation is due to adverse pressure gradient whenever the flow changes direction sufficiently more rapidly than the boundary geometry, as it does at the bend apex. The separated flow takes the form of rollers or vortices near the channel boundary. At Reynolds number greater than 100, separation bubbles are shed periodically into vortex trails (Roshko, 1961).

The presence of flow separation reduces the size of the 'live width' of the cross section and causes additional energy losses in channel bends (Leopold et al; 1960). The separation zones may locate on the concave (Woodyer, 1975; Hickin, 1979) or on the convex (Leopold et al; 1960; Bagnold, 1960; Hickin, 1977), or on both banks (Ippen and Drinker, 1962). The occurrence of flow separation depends on flow rate, bed and bend geometry

and roughness of the channel banks. Leeder and Bridges (1975) found that flow separation occurs at moderately low Froude numbers ( $Fn < 0.4$ ) on bends of  $r_c/w > 4.0$ . At higher Froude numbers,  $Fn > 0.6$ , flow becomes unstable and surface waves predominate (Soliman and Tinney, 1968).

Flow separation has other implications for understanding bend flow structure. Velocity and shear stress decrease rapidly along the separated zone and then increase steeply at the reattachment point (Bradshaw and Wong, 1972; Raudkivi, 1966). At separation zones, the boundary layer increases its thickness (Einstein and Harder, 1954) and it entrains more and more fluid as its size increases. Further downstream at reattachment, the boundary layer thickness decreases and a series of vortex rollups develops (Brown and Roshko, 1974). Whatever the results of separation to flow, the tendency is to increase velocity fluctuations and increase shear stress and friction to flow at reattachment points. Such fluctuations affect sediment entrainment and deposition (Jackson, 1976). Hickin (1977) has suggested that the flow separation on the concave side of the bend may arrest lateral migration in rivers.

### 1.6 Channel Deformation and Lateral Migration in Rivers

Lateral erosion is one degree of freedom by which rivers achieve dynamic equilibrium. Others include adjustment of width, depth, slope and velocity; and have been discussed in detail

elsewhere (cf. Maddock, 1970; Smith, 1974; Yang, 1976; Hey, 1978). The rate of lateral erosion depends on channel shape (Hickin and Nanson, 1975), bank stability (Fisk, 1952; Allen, 1965; Daniel, 1971; Nanson and Hickin, 1983) and variation of hydrometeorological factors (Knighton, 1972). The mode of migration is considerably varied within short channel lengths because of differing influences of each of the factors and depends on the interaction of flow development and decay between each bend. The latter is not so well known and it will be the focus of discussion in Chapter 6.

Like the contribution of upstream and downstream flow conditions to lateral migration, the initiation of meanders remains a contentious area of research. Several analytical, quasi-theoretical and experimental models have been suggested. What is known is that there is an initial instability of the flow which interacts with the mobile channel bed and which amplifies secondary flow in an organised manner as to cause alternate wandering of the thalweg (see for example Kennedy, 1963; Raudkivi, 1963; Engelund, 1970; Nakagawa and Tsujimoto, 1980; and Callander, 1978 for a review). The secondary flow associated with the wandering primary flow undermines the channel banks and the debris which falls into the stream is carried away.

Elementary fluid kinematics indicate that fluids translate, rotate or angularly deform (Rouse, 1965). The overall rotation at a section cannot contribute shear strain because there is no

relative motion. But rotational-flow equations have been applied successfully to model curvilinear flows provided  $r_c/w$  is small and width-depth ratio is large (Hawthorne, 1951; Squire and Winter, 1951). Humphrey et al (1977) show that the intensity of secondary flow decreases with rotational flow but increases when the core of maximum velocity shifts towards the outer bank.

Turbulent friction-dominated flow in rivers may develop rotational flow which takes the form of horse-shoe vortices in cross sectional plane. The horse-shoe vortices are eddies which develop between the channel and free water surface; they stretch asymmetrically in the direction of the flow and move water up along the banks and out of the banks towards the centre at the surface (Einstein and Shen, 1964). The circulation is counterclockwise at the right bank and the converse is true at the left bank. The circulation of the vortices alternates from one bank to the other and develops alternate scour holes more readily than steady flow (Shen and Komura, 1968).

The point of maximum erosion may be a function of the angle of attack of the undisturbed flow at the bend entrance (Parsons, 1960), and be proportional to the shear stress along the channel bank (Hooke and Rohre, 1979), or to the radial force per unit area of the bank (Begin, 1981). Hooke (1975) observed that the local shear stress along the bank where the erosional axis locates is about double the mean shear stress at that cross section. Appman (1972) found that shear stress increases as the bend curvature ratio decreases. Ippen and Drinker (1962),

however, noted that bends of  $r_c/w=3.0$  had a less deformed channel bed than either wider or tighter ones because secondary flow decreases to a minimum value (Shukry, 1949).

Langbein and Leopold (1966) found that as meanders approach "sine-generated curve" in form, the waves become more oblique to the mean pathlength and high momentum velocity approach different portions of the outer bank. According to Desaulniers and Frenette (1973), the surface streamlines tend to impinge on the concave bank at the exit of a 90-degree bend, at the bend apex of a 180-degree bend and further downstream of the exit in a 60-degree bend. The maximum current deviation of each streamline lies between 20 and 37 degrees (Bagnold, 1960), although Hooke (1980) argues that the role of secondary flow may have been overemphasised. The intensity of secondary flow increases with decreasing  $r_c/w$  (Shukry, 1949). Unlike Bridge and Jarvis (1983), Zimmerman (1977) concluded that the spiral that develops as a result of intense secondary flow is a function of bed roughness.

Riffle-pool sequence is ubiquitous in open-channel bends as in straight rivers. Riffles are topographic high points with coarser sediment size in an undulating bed profile; they are spaced every 5 - 7 channel widths apart (Leopold et al; 1964). Pools are low points which act as dams along the channel reach and are located between riffles. Double vortices with convergent currents are associated with braiding and riffles while bed-divergent currents are associated with pools (Leopold et al;

1964). The greater depth of the bend pools, including the backwater effect they cause at the bend axis, reduces mean velocity at the bend apex (cf. Yen, 1967). Stable mean longitudinal velocity is maintained, therefore, by the optimum interaction of riffles located at bend inflections and pools at the bend apex (cf. Leopold and Wolman, 1957). Beyond some critical pathlength, the sequence of riffles and pools tends to break down because the secondary flow convection cannot maintain itself (Hey and Thorne, 1975; Knighton, 1973). Field examples have shown that many bends which have more than one riffle tend to develop complex planforms (Carson and Lepointe, 1982).

River meanders in the process of lateral migration expand, rotate and translate (Daniel, 1971). In the context of a whole river system, these processes of lateral migration may change the meander path length. Assuming a uniformly erodable medium, the path length increases during the processes of expansion and rotation or both but remains constant during the process of translation. Jackson (1975) associated such modes of lateral migration with depositional facies and their potential for preservation (Figure 1.2 and Table 1.2). He categorised the depositional facies as transitional, intermediate or fully developed using the velocity magnitude and mean sediment size. The transitional facies incorporated a zone where both the velocity magnitude and mean sediment size do not increase outwards possibly because this is the zone at which the upstream flow influences begin to decay on one hand, while a forced

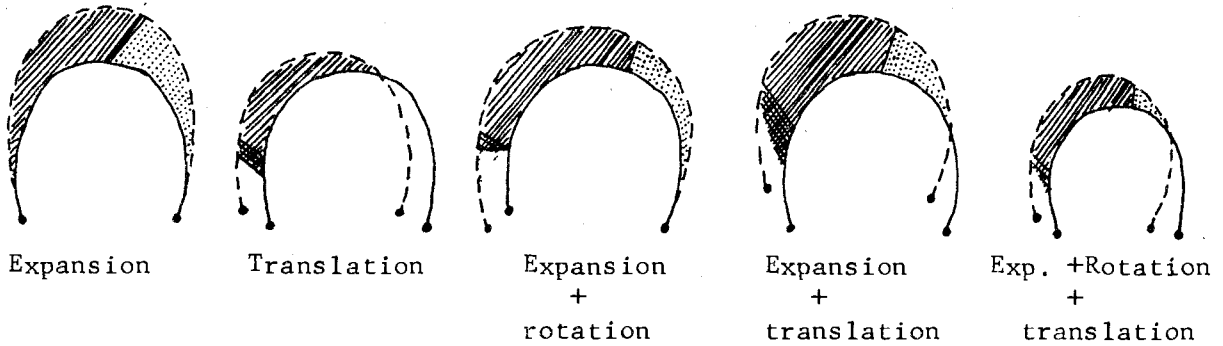


vortex flow begins to develop. Intermediate depositional facies are products of the fully developed flow regime although the mean sediment size is of translational flow as a result of a lag in sediment transport response. This is the zone where there is a mutual interference between the primary and secondary flow (Muramoto, 1967). Such a state of equilibrium likely is represented by parabolic flow. A fully developed depositional facies has both the velocity magnitude and the mean sediment size increasing from the convex (inner) bank toward the concave (outer) bank. The intermediate and fully developed zones depend on the development and decay rate of the forced vortex flow. These modes of lateral migration are by no means exclusive but may be associated with the bend flow structure. Hickin (1974), with the use of aerial photographs, explained that simple modes discussed above become rather more complex in bends with  $r_c/w < 2.0$  and also because of the influences of the upstream and downstream bends.

The relationship between simple modes of lateral migration may be shown qualitatively by using transverse and longitudinal distribution of discharge,  $q$ , (cf. Daniel, 1971; Begin, 1981) and sediment transport,  $q_s$ , (Hooke, 1975; Kikkawa et al; 1975)

Figure I.3. Modes of lateral migration and the potential of point bar preservation in river bends (Jackson, 1975 (b))

Gentle curvature ( $r_c/w > 3.0$ ).



Intermediate curvature ( $r_c/w = 1.5$  to  $3.0$ ).

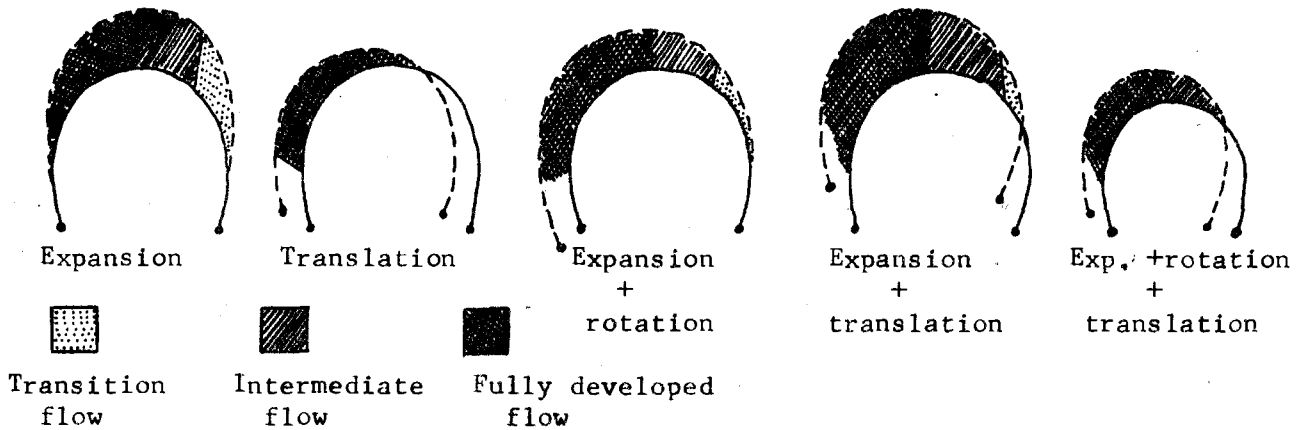


TABLE I.2

Different modes of lateral migration in river bends.

$r_c/w$	mode	source
0.5	n.i	Jackson (1975 (b))
1.8	expansion/rotation	"
3.3	translation	"
3.5	translation	Bridge and Jarvis (1982)
4.0	expansion	Begin (1981)
5.5	translation	Jackson (1975 (b))

nb. n.i. indicates not given by the author.

and from Figure 1.3. In the expansion mode of lateral migration, the erosional axis locates between bend angles of 40 and 170 degrees along the concave bank. Sediment continuity demands that  $q$  leaving the outer bank must be greater than  $q$  coming in to the region while the converse is true for the inner bank in order to maintain a stable width-depth ratio. The pattern of sediment transfer requires a forced vortex with secondary flow from the concave towards the convex side of the channel near the bed, and another from the convex towards the concave bank near the water surface (Chiu and Hsiung, 1981). Since depth and velocity will vary, shear stress becomes a dependent variable.

In expansion and rotation (type A), the erosional axis locates at a bend angle between 0 and 40 degrees along the convex bank and also between 40 and 180 degrees along the concave bank. Examples of expansion and rotation mode are generally referred to as freely meandering (Kondrat'yev, 1968). The erosional pattern requires a free vortex with secondary flow advection from the inner bank towards the outer bank near the bottom and the converse near the surface. The sediment load transported from the inner bank is greater than that transported in to the region. Along the concave bank, however, a forced vortex flow develops to a maximum value at 130 degrees before it decreases towards the bend exit. The sediment transported to the concave bank is less than that transported out; the converse is true for the convex bank.

In expansion and rotation (type B), the erosional axis locates near the concave bank downstream of the bend apex. The forced vortex flow attains its maximum strength at 150 degrees of the bend (Onishi et al; 1976; Hooke, 1975). On the other hand, the translation mode requires maximum erosion from the bend entrance until 90 degrees along the convex bank, and along the concave bank downstream of the bend axis. The bend apex maintains a combined vortex to reduce bank erosion; width and bend curvature both remaining sensibly constant. For translational mode, the free vortex flow locates between the bend entrance and 90 degrees while a forced vortex flow locates downstream of the bend apex. Figure 1.3 shows that the point of maximum erosion and point bar deposition locate downstream of the bend apex. The strength of the forced vortex, i.e. the fully developed flow zone, locates also downstream of the bend axis. This ensures downvalley migration of channel bends (Leopold et al; 1964). The flow patterns described above, however, may depart from that of natural rivers because of geologic and hydrologic variations. Different types of flow structure (vortices) therefore may combine to create compound bends (Hickin, 1974; Lewin et al; 1977; Parker et al; 1982) with double-valued planforms (Langbein and Leopold, 1966; cf. T-bends of Hickin, 1974). The present study investigates bend flow development in order to relate the different modes of lateral migration discussed above to the flow structure.

## CHAPTER 2 MEASUREMENT AND ANALYSIS

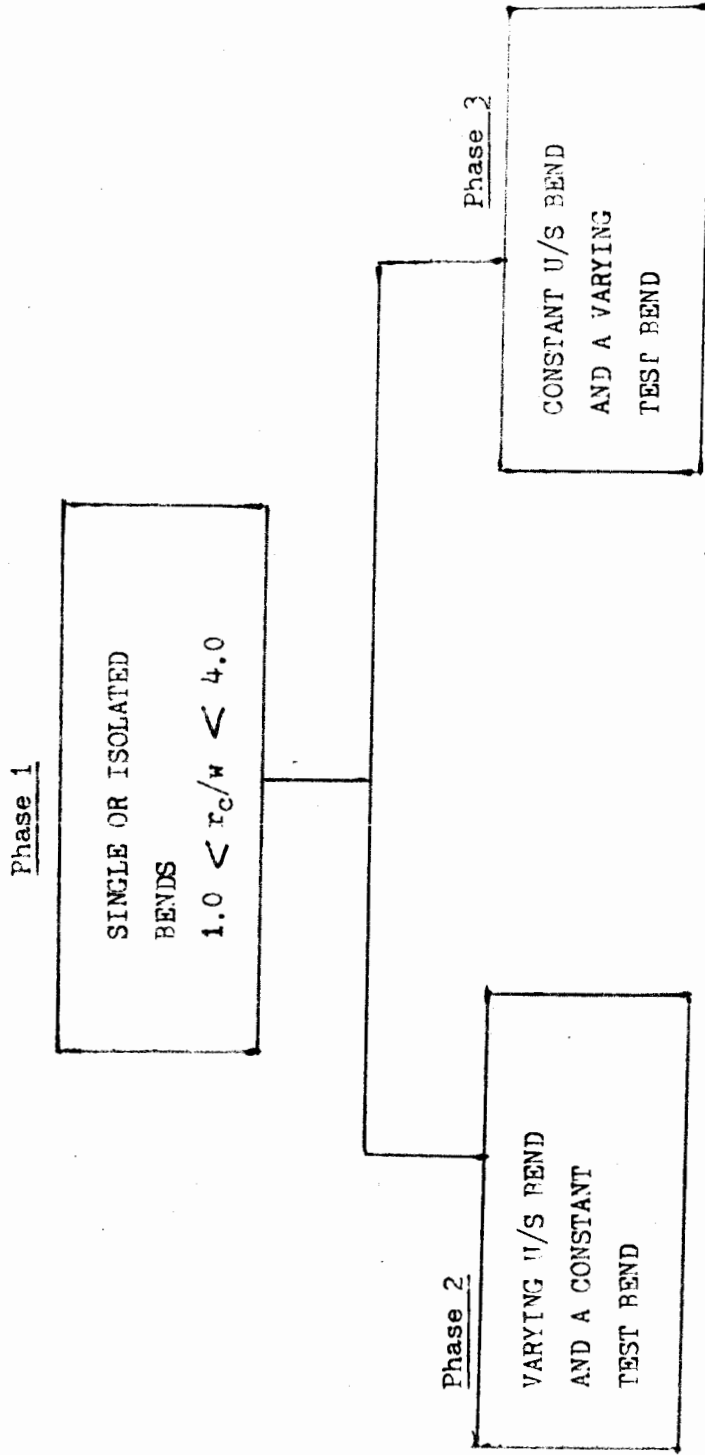
### 2 MEASUREMENTS AND ANALYSIS

#### 2.1 Introduction

Model open-channel bends were studied instead of natural rivers so that discharge, channel planform and sediment input could be regulated. The investigation was organised in three phases (Figure 2.1). The first phase of the investigation was to design and examine the flow characteristics of 10 isolated single bends of various curvature ratios as control experiments. The character of the fully developed flow zone was measured in the control bends to provide a basis of comparison in the analysis of consecutive bends. The second phase of experiments constituted sets of paired bends of which the curvature ratio of the upstream bends were held constant. The final phase constituted the same number of experiments as in phase two except the curvature ratios of the downstream bends were held constant. The geometric characteristics of the bends investigated are shown in Appendix 2. Some selected runs were repeated and the internal consistency was found to be acceptable in spite of variations caused by ruggedness of the channel banks and the locations of bedforms.

Fig. 2. I

Outline of Experimental Runs



## 2.2 The Experimental Model

The experimental site for this study was a 9.0m by 7.0m quadrat located at the Burnaby Mountain Experimental Watershed (BMEW) at Simon Fraser University. The model incorporated a manual sediment-feed system composed of three parts; a settling well, the channel test section, and a stilling well (Plate 2.1). The settling and stilling wells, each 0.24m in capacity, were made of 0.0019m thick plywood. The settling well was open at the top and at the bottom to allow it to be set on the ground while the stilling well was closed at the bottom and supported to give an average channel gradient of 0.00314. A rectangular weir capable of discharging a maximum flow volume of  $0.028\text{m}^3\text{s}^{-1}$  was fitted at the downstream end of the settling well. The channel bed was veneered with sand upto 4cm. thick at the beginning of each run.

Water was discharged by a 0.06m diameter hose into the settling well where it was mixed with fine washed sand,  $d_{50}=0.2\text{mm}$ . The selection of sediment size was based on trial and error through washing since the other parameters (gradient, width, depth and bend curvature ratio) were fixed. Figure 2.2 shows the grain size distribution of the sediment input for all the experiments. It can be noted that there is a 'break' of grain size - cumulative percent coarser at 10% ,  $d_{50}=0.125\text{mm}$ . and 0.2mm; probably separating sediment load

PLATE 2. I.

The Experimental model : An example of a single bend



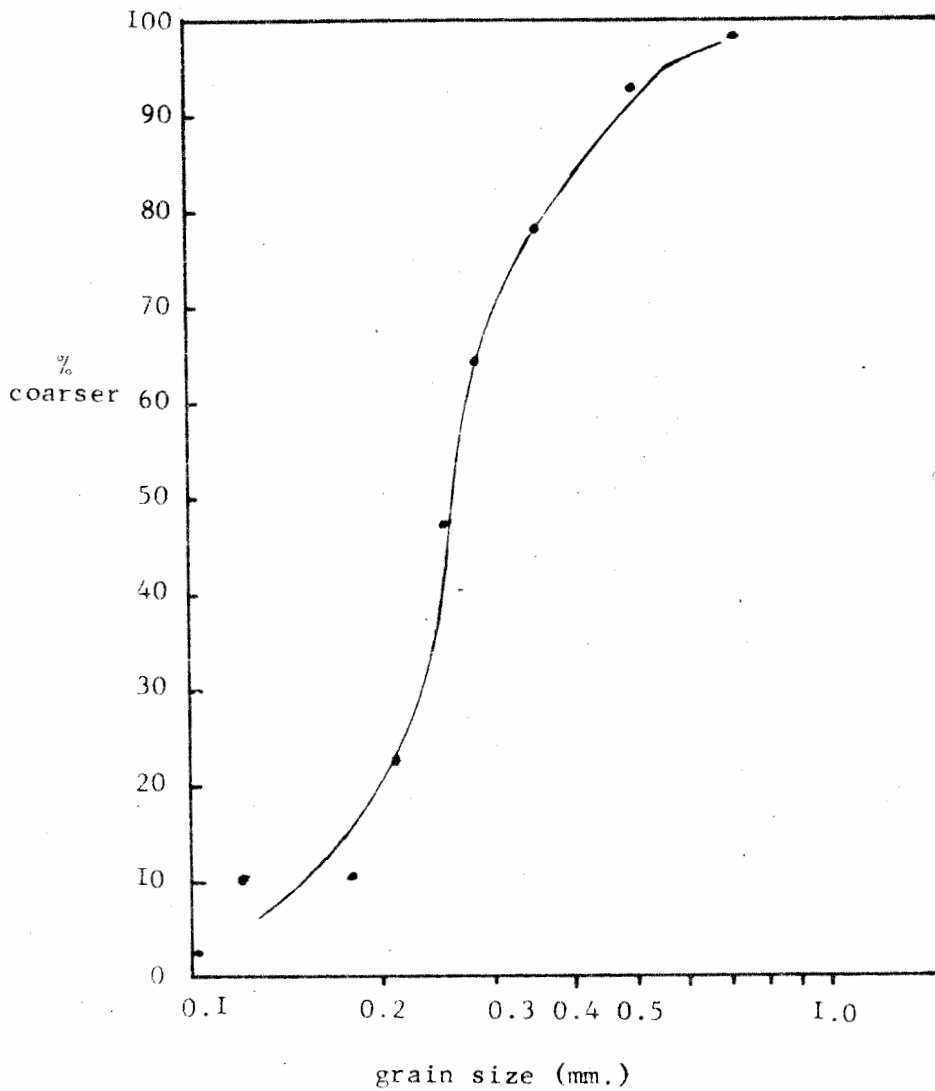
stilling  
well

settling well

The flow is from the bottom of the photograph towards the top.



Figure 2.2. Cumulative grain size distribution of sediment used  
in the present study.



carried intermitently in suspension and those in constant traction (cf. Middleton, 1976). The channel width varied between 0.4m and 0.7m in different runs, while mean depth varied between 0.09m and 0.12m. Such variations of width and depth were intended to accomodate an average velocity of 0.18m s<sup>-1</sup>. The channel planforms and bedform patterns were photographed for further analysis.

### 2.3 Calibration and Measurements

The variables used in the study are derived from measurements of velocity, current direction, and channel geometry. The flow was considered to be stable after the ripples developed throughout the channel and point bars became sensibly stable; usually after 4 to 10 hours. The velocity was measured by a baby Ott current meter. The current meter was chosen because it has a forward mounted propeller which makes it less sensitive to nonparallel flows. The specifications of the propellers are shown in Table 2.1. The 50mm propellor which is calibrated by the manufacturers was used to calibrate the 30mm propeller in a flume at the Geomorphology Laboratory at Simon Fraser University. Several variable speeds were run to give a least-square calibration equation in the form:

$$V=0.4929m+0.0416.....2.1$$

where m is the number of revolutions of the propeller per second.

TABLE 2.1

Specifications of the Baby Ott Current meter propellers used in the study.

Propeller #	Diameter (mm.)	Pitch (m.)	$V_{min}$ (m. s <sup>-1</sup> )	$V_{max}$ (m. s <sup>-1</sup> )	Obliquity %	$\frac{\text{Hub radius}^2}{\text{Blade area}}$
I5823/3	50	0.25	.0035	4.0	±10	.003
I9280/6	30	0.10	.055	2.0	±10	.051

The estimated variation from the regression line was 1.4%.

The accuracy of velocity measurements depends also on the obliquity of the flow, turbulence and on the spatial and temporal sampling procedures. The effect of turbulence and obliquity of the flow is a function of the ratio of the square of hub radius and blade area. As shown in the Appendix 1, turbulence causes the propeller to under-register the actual velocity (cf. Dickinson, 1967) while the effect of vertical and horizontal flow obliquity in curved channels was not measured. Instead the error suggested by manufacturers of plus or minus 10% in still water tank calibration was adopted for the present study. The 30mm propeller may under-register the velocity by as much as 6% compared to the 50mm one because the latter has a higher blade ratio (cf. Charlton, 1978); but the absolute errors involved in using the 30mm propeller were not assessed. The 6% relative error is, however, insignificant given the nature of the depth-averaged velocity data. The flow rate was kept above  $0.15\text{ m s}^{-1}$  as recommended by Hoyt (1910) and Barrows (1905) in order to avoid blade slippage and threshold friction effects of bearings. The current meter was cleaned and oiled before each run.

Velocity was measured over an interval of 35 to 60 seconds, depending on the position of cross section and flow rate. This time interval is sufficiently long to integrate most but not all of the major sources of velocity fluctuations and long enough to eliminate the influence of propeller inertia. Although the

effect of velocity fluctuations and of propeller inertia were not estimated, they have negligible impact on the mean flow.

Measurements were taken every 0.0762m across the channel width, and at 0.03m depth intervals. The surface velocity was measured at 0.015m below the water surface and the bottom velocity was measured at 0.01m above the channel bed. Rumpf (1914) found that the current meter over-registers consistently near the channel boundary while Godfrey (1958) disagrees; he found that the errors contributed by the channel boundary are small in flumes. It is generally known that velocity is higher on top of dunes and megaripples than on the downstream sheltered part where turbulence is predominant. In any case, the actual errors due to boundary effects are not known. In situations where the propeller was either located behind a bedform or the velocity was too small to give an accurate estimate of the flow, several readings were taken and averaged; this average was presumed to be representative.

Depth at each vertical was measured by a thin plastic ruler graduated in mm. The effects of surface tension and velocity of approach were considered to be negligible. The time interval between depth and velocity measurements was less than 10 seconds near the point bar area to avoid errors that may result from sediment avalanche (cf. Hooke, 1975). Because the channel width was constant, the section orientation for measuring the current direction was chosen by visual inspection to be perpendicular to the banks and the general path of the channel.

Table 2.2 Error estimates of instruments and measurements

Instrument	Causes of error	Type of error	Estimated magnitude
current meter I5823	calibration	consistent	$\pm 0.7\%$
	properties of flow	random	not known
	channel pattern/bed- forms	varies with bedforms	$\pm 10\%$
Depth measurement	surface tension	random	negligible
	velocity of approach	consistent	negligible
	sampling	consistent	not known
	sediment transport	random	negligible
Current direction	properties of flow and eddies	random	not known
	sampling	consistent	negligible
Precision of time piece	signal rate of timer and stop watch	random	negligible
Channel geometry	averaging and human error	consistent	negligible

Details of the calibration techniques and results are discussed in the Appendix 2.1.

The current direction was measured by a deflectometer consisting of a protractor glued on a thin wire, 0.001m diameter and 0.2m long, and a thread subtended at one end. The current direction was read after immersing the thread to an appropriate depth for 10 seconds. The water was clear at the time of measurements. The accuracy of all the measurements depended on the level of eddies and the flow rate (Table 2.2).

#### 2.4 Data Analysis

Shear stress, friction coefficient and vortex strength are derived from velocity measurements. Shear stress at each vertical was calculated using an equation in the form:

$$T_o = [ ((v_2 - v_1) / 5.75) (y_2 / y_1) ] \dots\dots\dots 2.2$$

where T is shear stress,  $v_1$  and  $v_2$  are velocity measured near the channel bottom and the next measurement on the same vertical,  $y_1$  and  $y_2$  are depth at which velocity  $v_1$  and  $v_2$  are measured respectively. The assumptions of the law of the wall were assumed to hold.

The mean shear stress for each cross section was determined using an equation in the form:

$$\bar{T}_o = (1/P \int_{r_o}^{r_i} T_o dP) \dots\dots\dots 2.3$$

where P is the wetted perimeter of the channel.

Maps of dimensionless shear stress distribution,  $T_o / \bar{T}_o$ , were prepared as the ratio between the point shear stress to the mean shear stress of the cross section.

The D'Arcy Weisbach friction coefficient was calculated using an equation in the form:

$$ff = \bar{T}_o / \rho V^2 \dots \dots \dots 2.4$$

where ff is friction coefficient, V is mean velocity and  $\rho$  is density of the fluid.

The strength of the vortex, t, was calculated from equation 1.4. Because there were six to eight verticals at each cross section, no further statistical tests were deemed necessary. The exponent t defined the following vortex conditions: forced vortex when  $t > +0.15$ , free vortex when  $t > -0.15$  and parabolic flow when  $t < |0.15|$ . Current direction has been computed as the deviation angle between the surface currents and the bottom currents. Attempts to measure the current direction at each point of velocity measurement in order to mathematically examine secondary flow in detail were dropped after a few initial runs because differences were too small to give reliable readings.

### 2.5 Data Presentation

Data analyses are presented in various forms in order to characterise the different flow properties reviewed in part II of chapter 1. The flow deformation rates are represented by isovels, or "contours" joining points of equal velocity. As mentioned earlier, the isovel patterns show the direction of secondary flow and the geometry of vortices imbedded in the flow structure. The isovel diagrams are prepared from the left



(concave) bank to the right (convex) bank to an observer facing downstream. In addition to isovel patterns, the distribution of average velocity at each vertical and the cross stream (radial) velocity for every section are shown on the same scale. The cross stream velocity profiles are intended to show the type of the vortex flow and its strength ( value of  $t$  in equation 1.4) and are scaled from  $w_1/w_0$  from the top (concave bank) toward the bottom (convex bank) in each diagram. The distribution of vertical velocity is given for each relative depth,  $n$  ( $n = y_1/y_0$ ).

The surface and bottom currents are shown respectively by bold and broken lines for each cross section. The shear stress ratio,  $T_0/\bar{T}_0$ , and bed deformation are shown by contour lines.

## CHAPTER 3 EXPERIMENTAL RESULTS: SINGLE OPEN-CHANNEL BENDS

### 3.1 THE VELOCITY DISTRIBUTION AND CURRENT DIRECTION

#### 3.1.1 Introduction

The phase of the investigation reported here involving a straight control channel and single open-channel bends with curvature ratios of  $1.0 < r_c/w < 4.7$  was carried out for three specific reasons. First, to establish the relations among the velocity field and the development and decay of the spiral flow. Secondly, to identify the location of the fully developed flow zone in order to relate it to bends of various curvature ratios. Thirdly, to test empirically the hypothesis that, at the bend apex, the core of maximum velocity tends to be displaced towards the concave bank in bends of  $r_c/w > 3.0$ , and towards the convex bank in bends of  $r_c/w < 3.0$  (Hickin, 1978).

The results are presented in various ways. Isovel patterns and current direction are examined in section 3.1 and the lengthwise velocity distribution is discussed in section 3.2. The aim is to show various aspects of flow deformation both at a station and also in the downstream direction.

### 3.2.1 The Isovel Patterns and Current Direction in Single Bends with $r_c/w > 3.2$

The three-dimensional velocity distribution at each cross section shown by the isovel patterns were plotted from point velocity measurements taken every 0.03m apart along each vertical profile and 0.076m intervals across the channel section. A total of approximately 36 points were located in each cross section. These isovel patterns display considerable irregularity caused by the effect of secondary flow generated by the nonuniform or skewed distribution of shear stress (Chiu and Hsiung, 1981; Rozovskii, 1961).

The isovel patterns of a straight channel (Figure 3.1) show a steep velocity gradient towards the channel bottom in the first two-thirds of flow depth, and a marked retardation towards the channel bed. The isovels near the water surface display a W-shaped pattern showing accelerated flow near the water surface and secondary flow advection towards the bottom near the banks and towards the surface at the central portion. Continuity demands that there be two counterrotating bed-convergent spirals in order to create upwelling at the central portion of the channel. These bed-convergent spirals generate horse-shoe vortices in straight turbulent flows (Einstein and Li, 1958; Perkins, 1970).

Figure 3.1. Selected isovel patterns of a straight channel. The digrams are presented from left bank to right bank facing downstream. The velocity measurements are in cm. sec.<sup>-1</sup>.

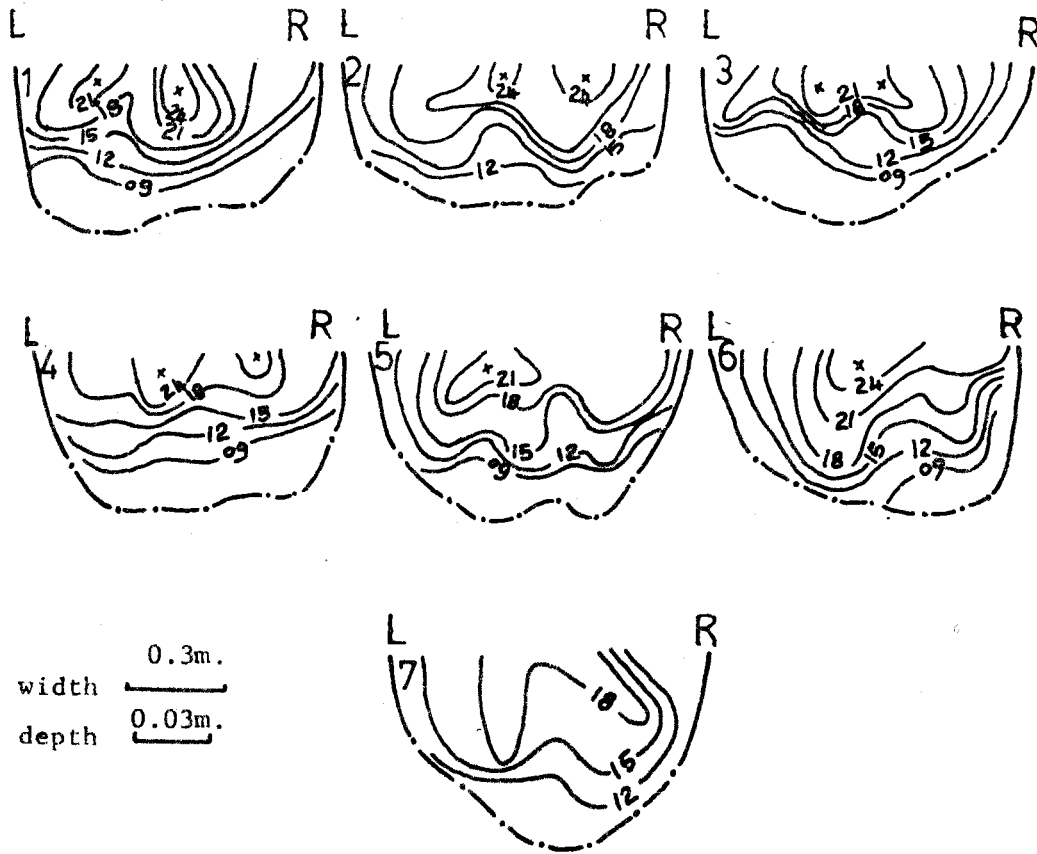


Figure 3.2. Cross stream and vertical velocity of selected cross sections of a straight channel. The relative depth ( $y_1 / y_0$ ) and width ( $w_1 / w_0$ ) are shown along the vertical axis. The flow direction is from left to right.

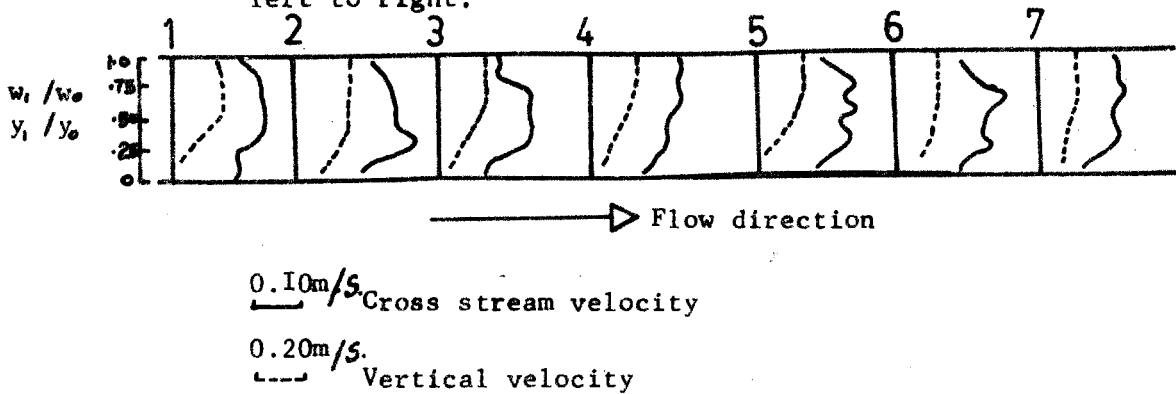
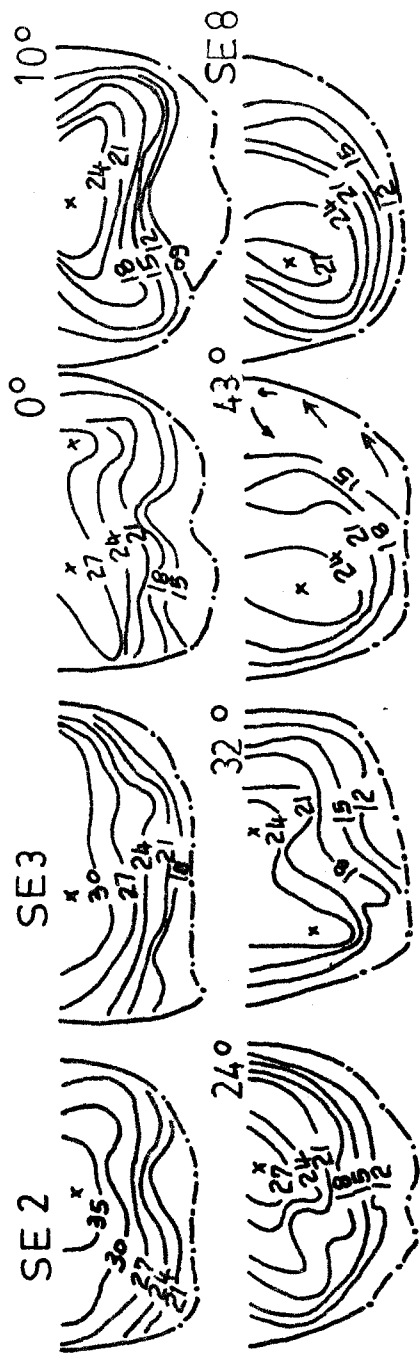


Figure 3.2 shows the cross stream and the vertical velocity for a straight channel. The cross stream profiles are parabolic in most sections except at section #4 where the rough channel banks retard the flow. The current direction deviates from the mainstream flow by less than 3 degrees, an observation consistent with those made by Hall (1972) who explained that two counterrotating spirals tend to reduce the magnitude of secondary flow. The differences between the cross stream profiles are caused by variations in bedform size and location factors that are responsible for boundary layer growth (see Plate 3.1; Van Dyke, 1970). The effect of the secondary flow advection is to retard the flow near the channel bed (cf. De Vriend, 1980).

For a bend of  $r_c/w=4.7$  (Figures 3.3 and 3.4), the isovel patterns and cross stream velocity profiles along the bend entrance to a bend angle of 10 degrees has a velocity field similar to that of a straight channel. The retarded flow locates near the outer (concave) bank at the bend apex and secondary flow advection at the centre of the channel reduces the mean velocity and radial acceleration. From a bend angle of 32 degrees, the maximum velocity core shifts towards the concave (outer) bank and remains there along the straight exit portion of the bend (see SE2 #8).

Figure 3.3. Selected isovel patterns of a single bend with  $r_c/w=4.7$ . The diagrams are presented from left bank to right bank facing downstream. The velocity measurements are in cm. sec.<sup>-1</sup>



width  $\frac{0.3m.}{\text{---}}$   
 depth  $\frac{0.03m.}{\text{---}}$

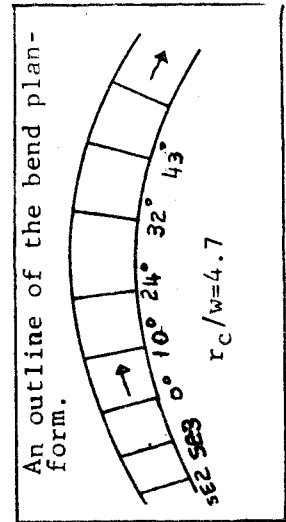
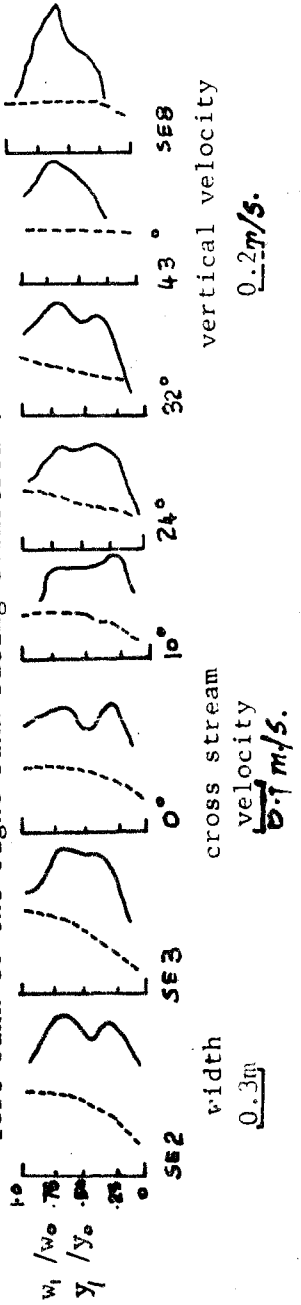


Figure 3.4. Cross stream and vertical velocity distribution of selected cross sections of a bend with  $r_c/w=4.7$ . The relative depth ( $y_i/y_0$ ) and width ( $w_i/w_0$ ) are shown along the vertical axis. The cross stream velocity distribution is shown from the left bank to the right bank facing downstream.



width  $\frac{0.3m}{\text{---}}$   
 velocity  $\frac{0.2m/s.}{\text{---}}$

PLATE 3. I.

The bedform characteristics of a straight channel. The flow is from left to the right of the photograph.



Figure 3.5. Selected isovel patterns of a single bend with  $r_c/w=4.0$ . The diagrams are presented from left bank to right bank facing downstream. The velocity measurements are given in cm. sec.<sup>-1</sup>

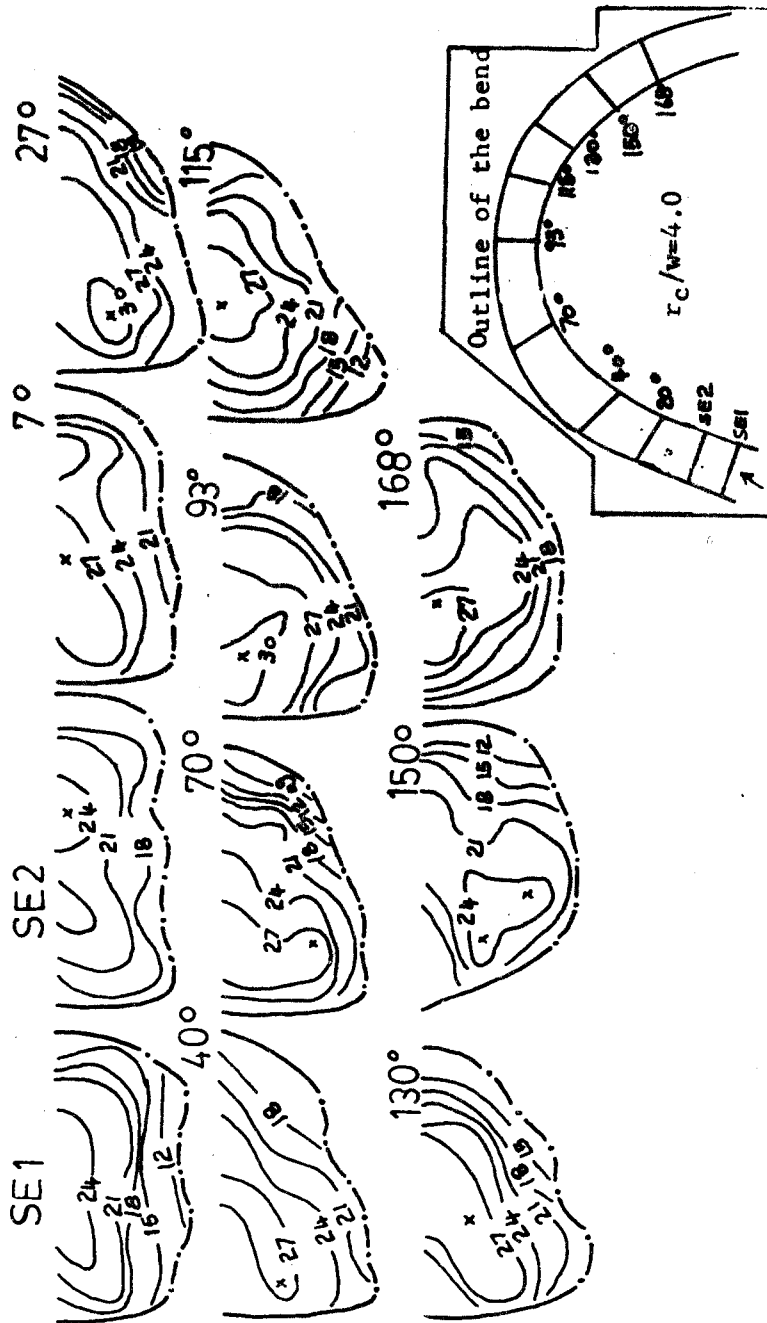
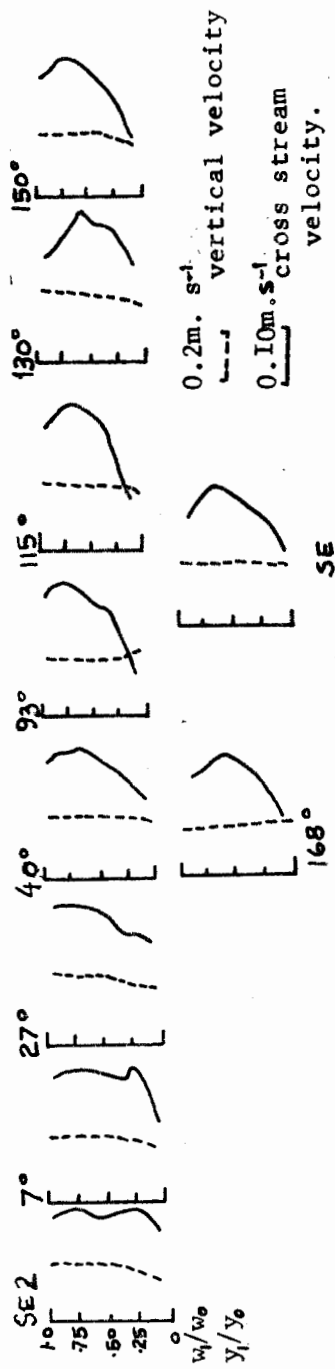




Figure 3.6. Cross stream and vertical velocity distribution of selected cross sections of a bend of  $r_c/w=4.0$ . The relative depth and width are shown along the vertical axis. The cross stream velocity is shown from the left bank to the right bank facing downstream. See Figure 3.5 for the bend outline and the location points of the cross sections.



The W-shaped isovel patterns in  $r_c/w=4.0$  (Figure 3.5) are limited to the entrance of the bend as are those in  $r_c/w=4.7$ . Within the bend, the high velocity core shifts from the water surface near the channel banks to lie asymmetrically towards the concave bank. As the intensity of the spiral increases, the isovels bulge towards the concave bank at mid depth and towards the convex bank near the surface and channel bed at a bend angle of 75 degrees (horse-shoe vortex: Einstein and Shen, 1964). The anticlockwise rotating secondary flow develops near the bed, reduces the influence of its clockwise rotating counterpart near the surface and establishes a parabolic flow at 116 degrees. The intensity of the forced vortex flow at first increases but then decreases again towards the bend exit. The location of flow cross overs at the bend entrance, and at 40 and 116 degrees makes it difficult for the fully developed flow characteristics to establish for any appreciable bend length (cf. Gotz, 1980).

The flow development in bends of  $r_c/w>4.0$  supplements previous results (cf. Fox and Ball, 1968) in several ways, but also differs in two main areas. The initiation stage of bend flow development marked by a free vortex flow does not exist in these wide bends (see Figure 3.6), perhaps because cross stream momentum overwhelms angular acceleration (cf. Mullin and Greated, 1980). The maximum strength of the forced vortex flow ( $t=0.33$ ) occurs at a bend angle of 60 degrees depicting the characteristics of a fully developed flow although it does not persist because of the generation of an anticlockwise secondary

flow at the bend apex near the channel bed. The characteristics of fully developed flow are initiated again at 130 degrees.

The same characteristics of the W-shaped isovels, parabolic flow profiles and logarithmic distribution of vertical velocity exist for a bend of  $r_c/w=3.7$  (Figure 3.7) as for the previous ones. The core of maximum velocity locates at the channel centreline between the bend entrance and 25 degrees, then towards the convex at mid depth along the bend zone between 25 and 44 degrees. Relatively retarded flow occupies the inner (convex) bank and causes flow separation at 60 degrees of the bend angle. In the separated zone, the high momentum fluid is injected towards the convex bank near the channel bed and towards the surface where it generates eddies because of vertical mixing. The separated zone therefore interacts continuously with the mainstream flow.

Along the bend zone between 80 and 115 degrees, the transverse surface secondary flow convergence depresses the core of maximum velocity towards the channel bed. The maximum current direction at 115 degrees where the bottom currents are directed towards the convex bank is the main locus of point bar deposition. Simultaneous bank erosion likely occurs along the concave bank.

Figure 3.7. Selected isovel patterns of a single bend with  $r_c/w=3.7$ . The diagrams are presented from the left bank to the right bank facing downstream. The velocity measurements are given in cm. sec.<sup>-1</sup>

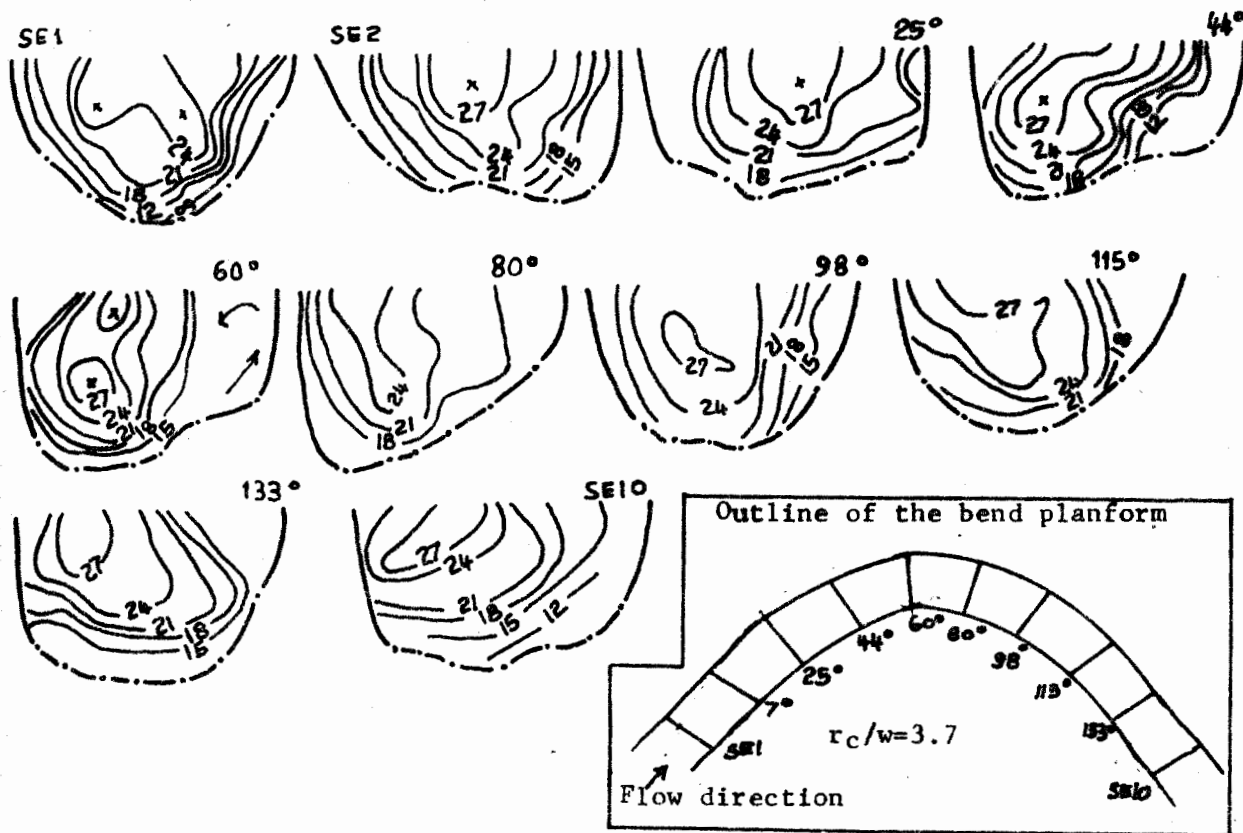
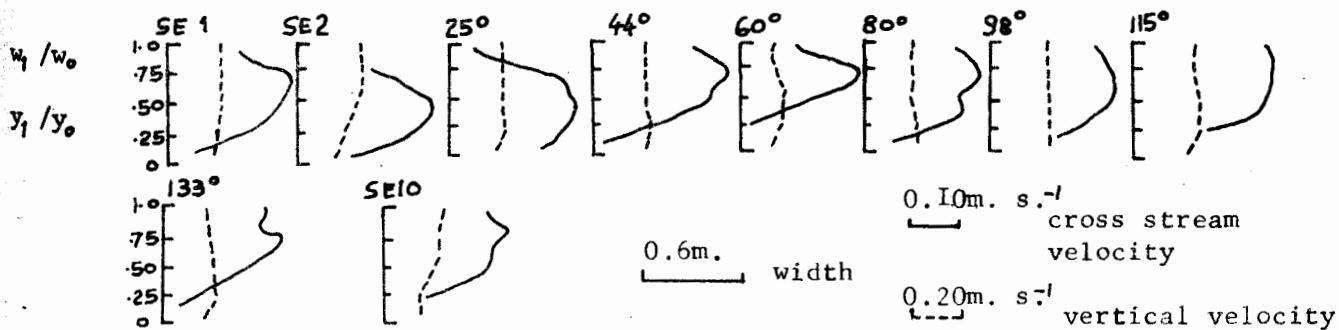


Figure 3.8. Cross stream and vertical velocity distribution of selected cross sections of a bend of  $r_c/w=3.7$ . The relative depth and width are shown along the vertical axis. The cross stream velocity distribution is shown from the left bank to the right bank facing downstream.



Unlike the flow structure in a bend with  $r_c/w=3.7$ , the forced vortex flow forms between 15 and 37 degrees in that of  $r_c/w=3.3$  (Figures 3.9 and 3.10). The accelerating fluid shifts towards the concave bank, then diverges towards the surface near the concave bank while flow decelerates at the bottom near the convex bank. The transitional flow at a bend angle of 37 degrees has the characteristics of a free vortex flow in a bend with  $r_c/w=3.3$  compared to 60 degrees in that of  $r_c/w=3.7$ . The core of maximum velocity locates at the centre of the channel near the surface at the bend apex while the maximum strength of the spiral locates along the bend zone between 37 and 77 degrees (Figure 3.13; cf. Muramoto, 1967). Both the flow cross over and convex flow separation zone locate at the bend apex. The initiation of a free vortex flow in bends with  $r_c/w=3.3$  and 3.2 at the bend entrance (Figures 3.9 to 3.12; cf. Mockmore, 1944; Shukry, 1949) shows that angular acceleration increases and shifts downstream as  $r_c/w$  decreases.

### 3.1.3 Summary of Flow Characteristics in Bends of $r_c/w > 3.2$

Some characteristics of isovel patterns in bends of  $4.7 < r_c/w < 3.2$  are that the point at which the direction of the secondary flow shifts towards the concave (outer) bank moves upstream from bend angle of 80 degrees to 17 degrees with  $r_c/w$ ; however the strength of the spiral is low.

Figure 3.9. The isovel patterns of selected cross sections of a single bend with  $r_c/w=3.3$ . The diagrams are presented from the left bank to the right bank facing downstream. The velocity measurements are given in cm. sec.<sup>-1</sup>

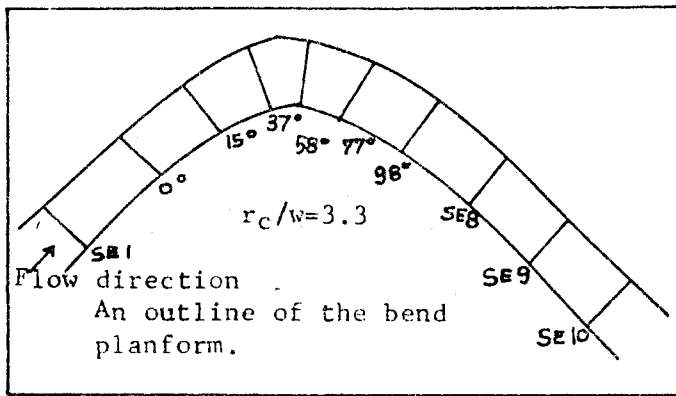
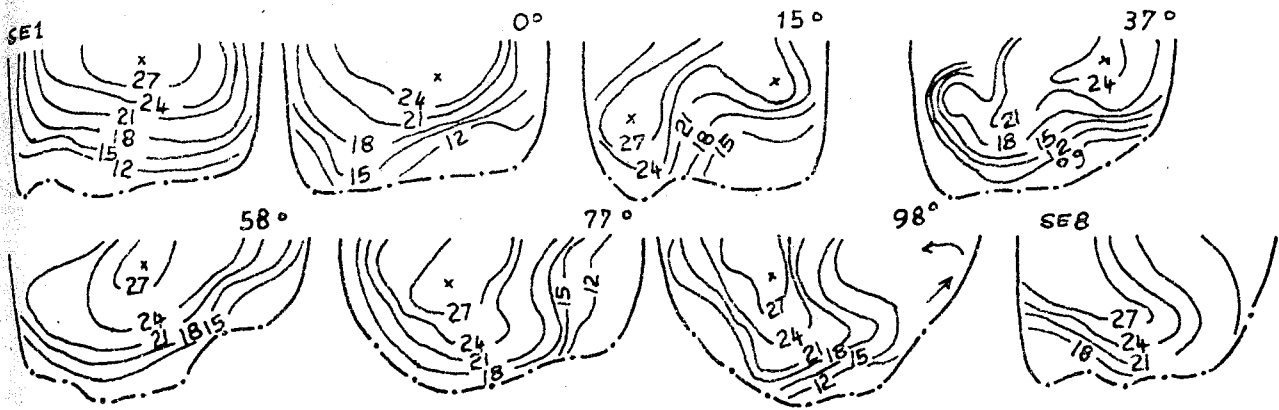
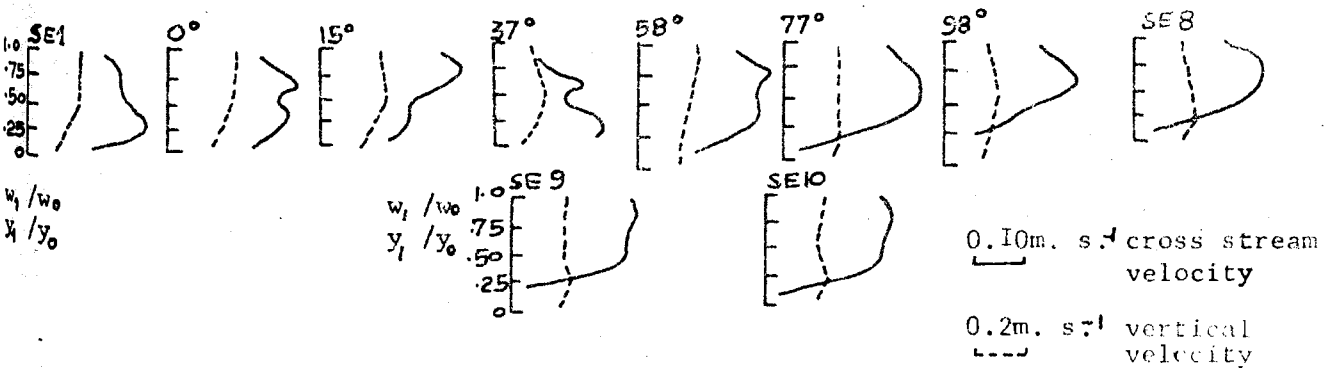


Figure 3.10. Cross stream and vertical velocity distributions of selected cross sections of a bend of  $r_c/w=3.3$ .



NB. The cross stream velocity distribution is shown from the left bank to right bank facing downstream.

Figure 3.II. The isovel patterns of selected cross sections of a single bend with  $r_c/w=3.2$ . The diagrams are presented from the left bank to right bank facing downstream. The velocity measurements are given in cm. sec. <sup>-1</sup>

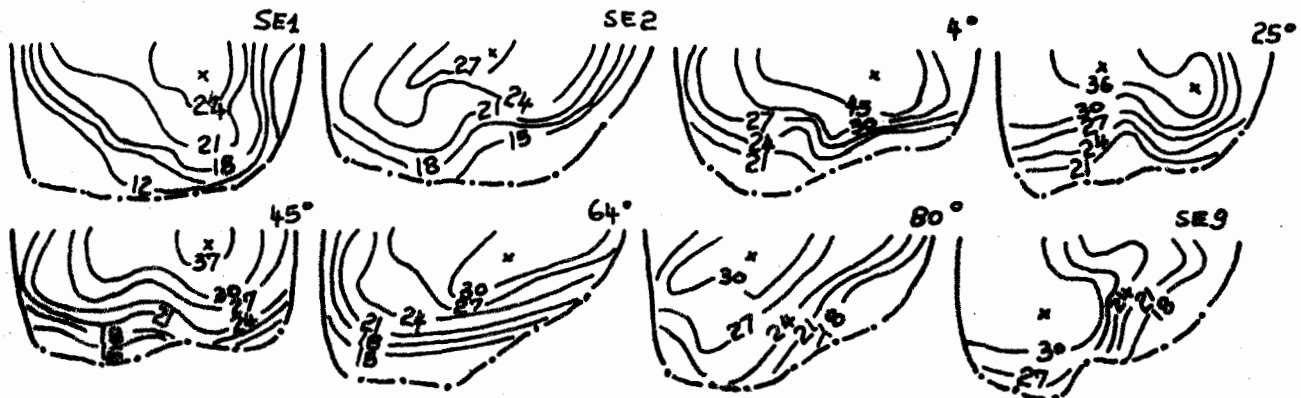


Figure 3.I2. Cross stream and vertical velocity distributions of selected cross sections of a bend with  $r_c/w=3.2$ . The cross stream velocity is presented by solid lines from the left bank to the right bank facing downstream. The vertical velocity is presented by broken lines. The relative depth and width are shown along the vertical scale of each diagram.

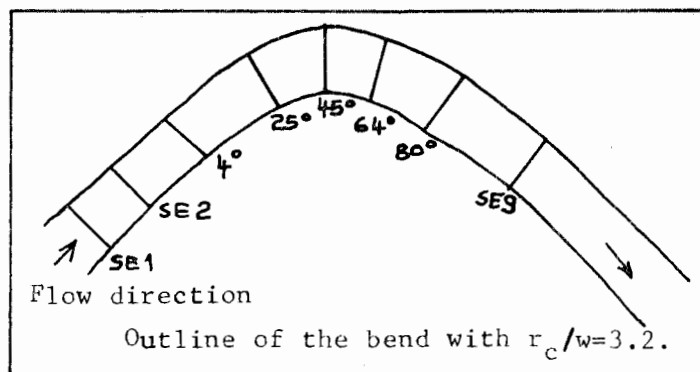
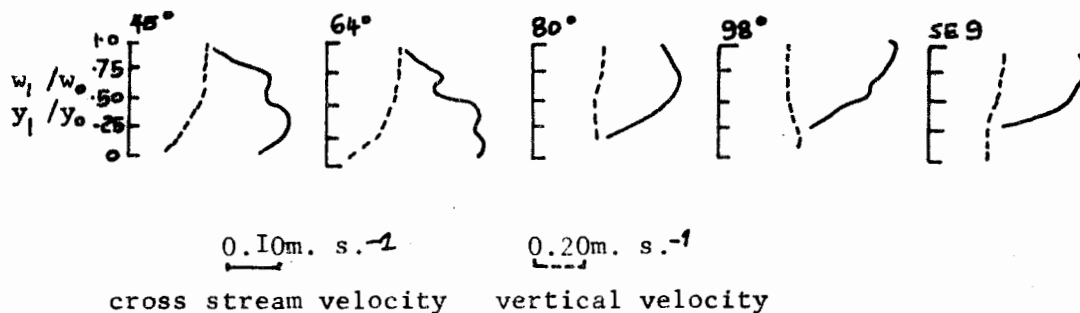
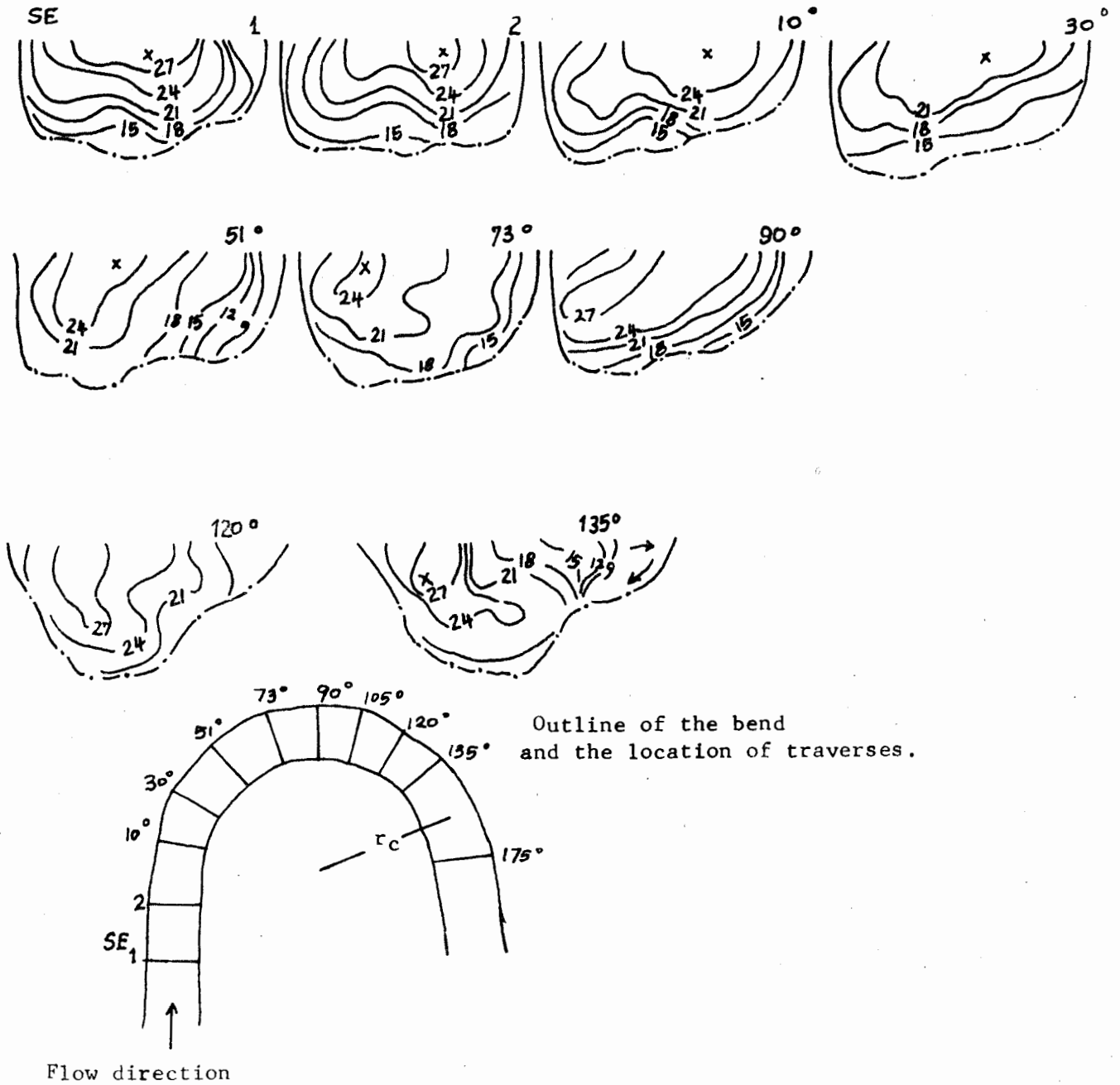


Figure 3.13. Selected isovel patterns of a single bend with  $r_c/w=2.6$ . The diagrams are presented from left bank to right bank facing downstream. The velocity measurements are given in cm. s<sup>-1</sup>





But the zone where the forced vortex flow develops moves downstream from a bend angle of 37 degrees to one of 80 degrees as the curvature ratio decreases. This is because the high velocity core remains at the channel centreline along the bend apex instead of crossing to the concave bank. On the converse, the convex flow separation zone locates between 30 and 44 degrees in  $4.7 > r_c/w > 3.7$ , but at 98 degrees and along the exit portion in  $r_c/w = 3.3$ . In  $r_c/w = 3.3$ , the convex flow separation shifts downstream because the high velocity core shifts to the convex bank (free vortex flow) and the the flow separates from the concave bank at 37 degrees. These particular results show that conservation of angular momentum overwhelms cross-stream transfer of momentum increasingly earlier as  $r_c/w$  decreases. The results also show that the parabolic flow and free vortex flow do not flatten the logarithmic distribution of vertical velocity because secondary flow advection reduces the velocity near the channel bed.

The streamlines impinge on the concave banks, sink towards the bottom and then redirects transversely across the channel between 25 and 60 degrees. This region has the characteristics of the fully developed bend flow zone. A secondary counterrotating spiral that develops near the bed at the bend apex reduces the strength of the clockwise directed secondary flow advection and that of the forced vortex. The high velocity core locates near the concave bank below the water surface at the bend apex because the secondary and primary spirals converge

there (cf. Hey and Thorne, 1975). The second zone of the fully developed flow does not occur until downstream of the bend apex (cf. Leopold et al; 1964). The isovel patterns, current direction and vortex development in bends of  $r_c/w > 4.0$  lend support to Hey and Thorne's (1975) model of double spirals at the bend apex while bends of  $2.6 < r_c/w < 3.2$  lend support to Wilson's (1973) model of a single spiral.

#### 3.1.4 The Isovel Patterns and Current Direction in Bends with $r_c/w < 2.6$

The discussion in section 3.1.3 shows that angular acceleration overwhelms cross stream momentum transfer as  $r_c/w$  decreases. Further tightening of the bends to  $r_c/w = 2.6$  recreates symmetrical isovel geometry and increases the extent of parabolic flow at the bend entrance. The spiral directed towards the inner bank near the bottom lies under the one that owes its existence to the bend entrance. At the bend apex (95 degrees) both spirals transfer high momentum fluid, near the surface and bottom, towards the inner bank and weakens the forced vortex flow from  $t = 0.26$  to  $t = 0.15$ . Although this forced vortex translates to parabolic flow at 130 degrees, the superposed spirals reverse their direction at 150 degrees and the fully developed flow characteristics develop. As the superposed spirals coalesce along the exit portion, the convex flow separation entrains more fluid and its areal extent increases.

Figure 3.14. The isovel patterns of selected cross sections of a single bend with  $r_c/w=2.2$ . The diagrams are presented from the left bank to the right bank facing downstream.

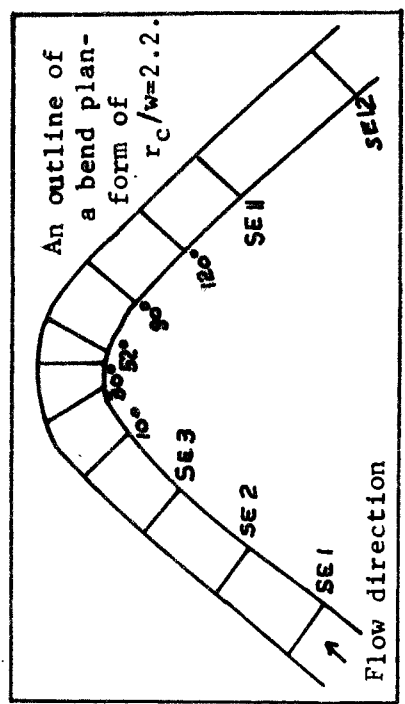
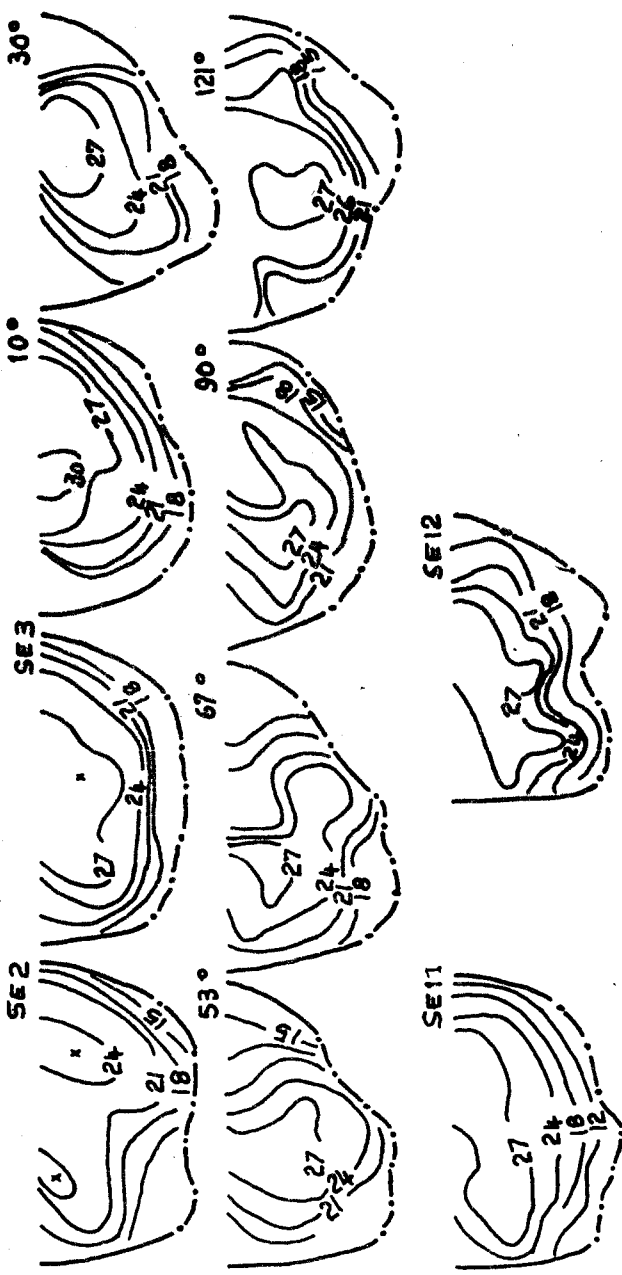
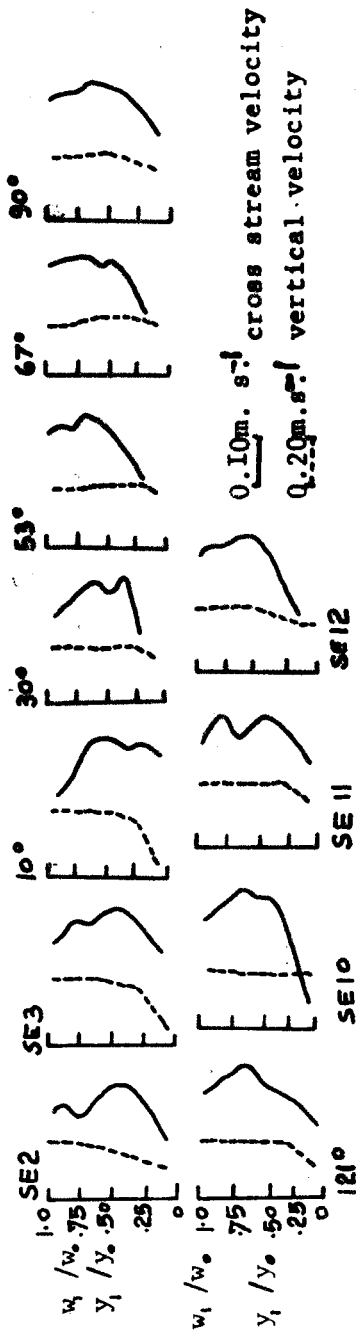


Figure 3.15. Cross stream and vertical velocity distributions of selected cross sections of a bend with  $r_c/w=2.2$ . The cross stream velocity are presented by solid lines from the left bank to the right bank facing downstream. The vertical velocity are shown by broken lines. The relative depth and width are shown along the vertical scale on each diagram. The outline of the bend geometry is shown in Figure 3.14.



The extent of parabolic flow and symmetrical isovels decreases with  $r_c/w$ . It appears that there is a threshold in a bend with  $r_c/w=2.6$  in which flow development becomes rather shorter (cf. Mullin and Greated, 1980). The transition from parabolic flow to free vortex flow occurs at 10 degrees in a bend with  $r_c/w=2.2$  (Figure 3.14) and logarithmic distribution of vertical velocity is sustained upto a bend angle of 53 degrees (Figure 3.15) but is restricted to the bend zone between 15 and 30 degrees of wider bends. The anticlockwise spiral near the bottom becomes strong at 67 degrees and shifts the core of maximum velocity towards the inner bank. These bed-divergent currents reduce the intensity of the superposed spirals at a bend angle of 121 degrees and limit the growth of the forced vortex flow through the rest of the bend.

Further tightening of the bend to  $r_c/w=1.8$  (Figure 3.16) reduces the intensity of the deformed isovels that bulge towards the outer bank as in Figure 3.14. The secondary flow towards corners are not limited to the straight entrance as for a bend with  $r_c/w=2.2$ , but are sustained until a bend angle of 25 degrees. The ridge of secondary flow advection towards the surface decreases and a free vortex forms ( $t=-0.45$ ) between 25 and 56 degrees of the bend angle. Because the high velocity core shifts rapidly to the concave bank, the forced vortex flow has a maximum strength,  $t=0.30$ , at 56 degrees; the same position an anticlockwise spiral directed towards the inner bank develops. The secondary flow advection near the inner bank directed

Figure 3.16. The isovel patterns of selected cross sections of a single bend with  $r_c/w=1.8$ . The diagrams are presented from the left bank to the right bank facing downstream. Velocity contours are shown in cm. s.<sup>-1</sup>

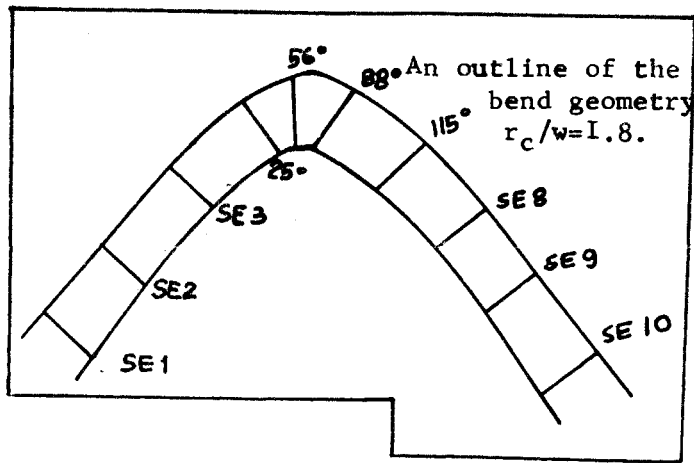
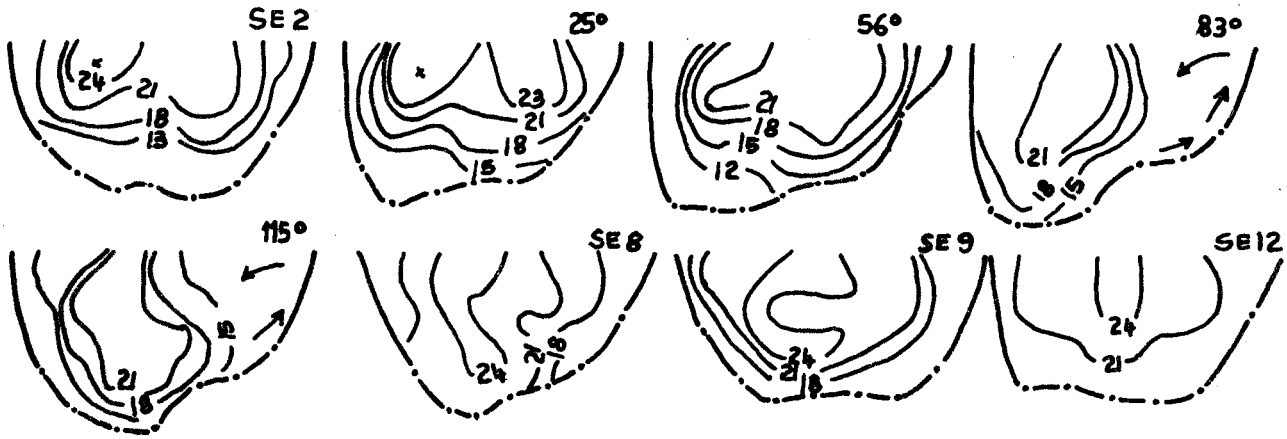
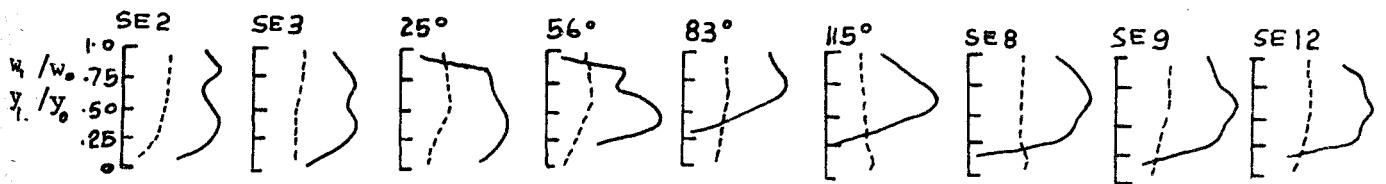


Figure 3.17. Cross stream and vertical velocity distributions of selected cross sections of a bend with  $r_c/w=1.8$ . The cross stream velocity distribution is shown by solid lines while the vertical velocity distribution is shown by broken lines: both in cm. s.<sup>-1</sup>



$w_1/w_0$  and  $y_1/y_0$  represent relative width and depth respectively.

Figure 3. 18. The isovel patterns of selected cross sections of a single bend with  $r_c/w=1.5$ . The diagrams are presented from the left bank to the right bank facing downstream. Velocity contours are shown in  $\text{cm. s}^{-1}$ .

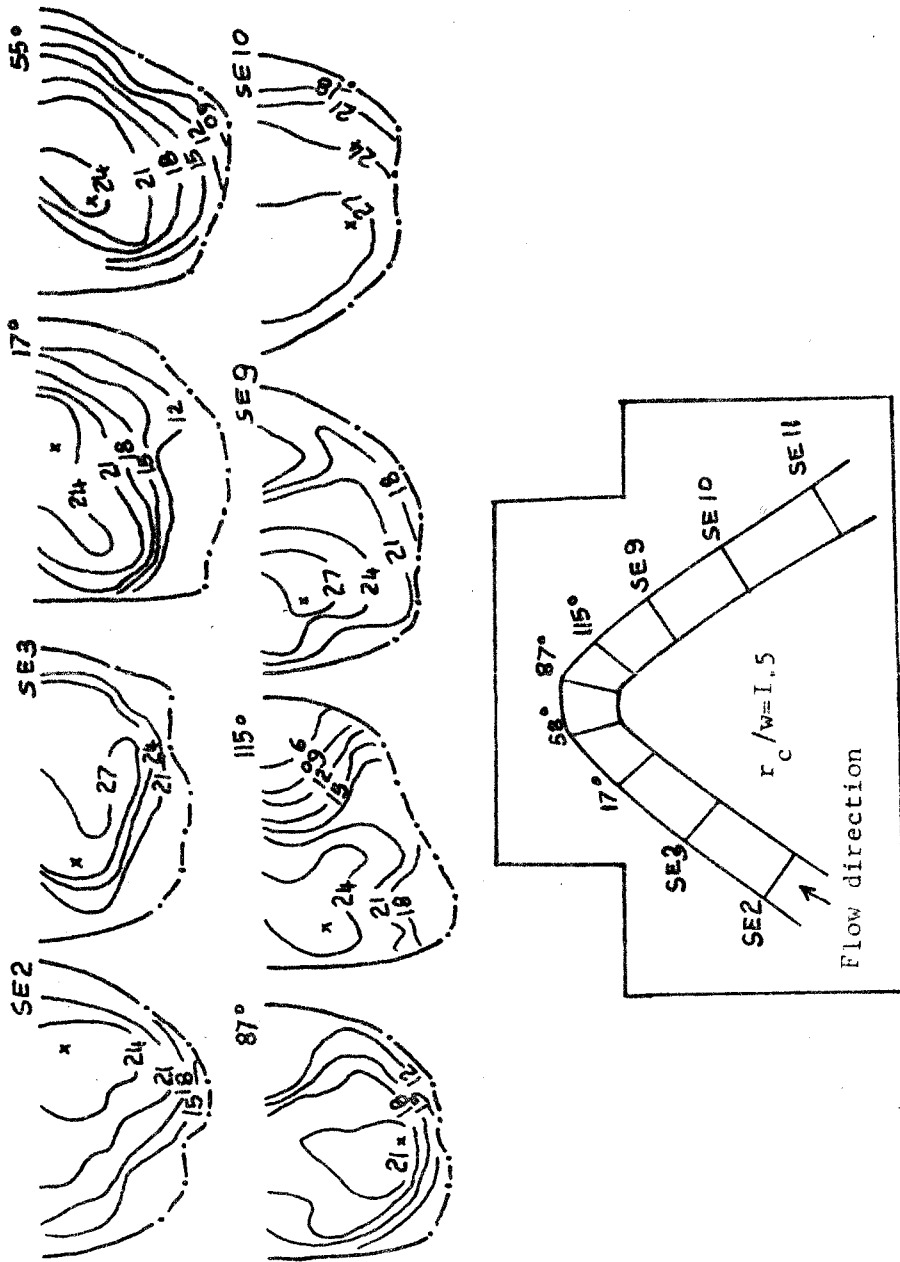
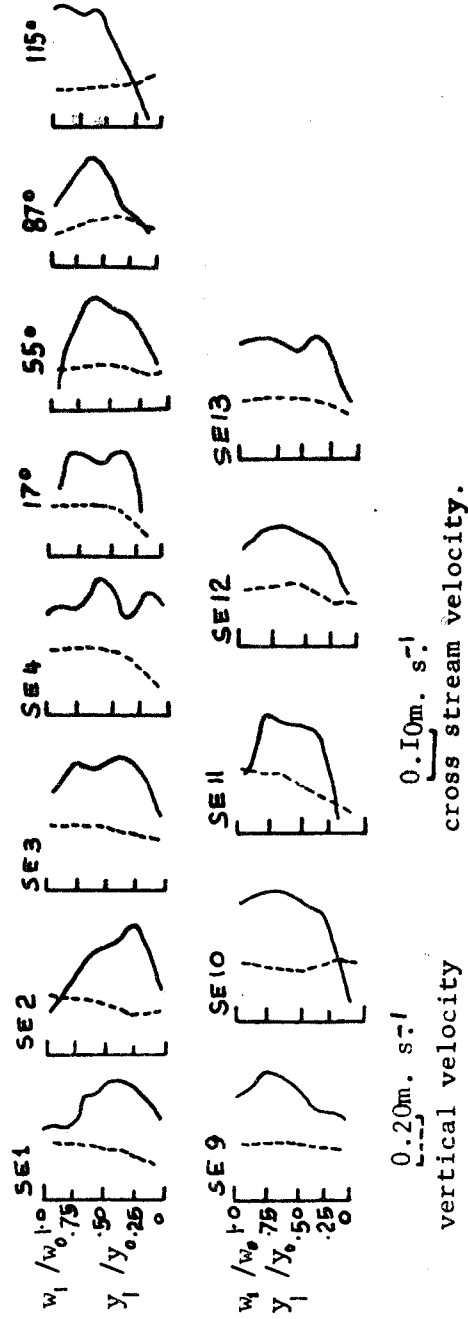


Figure 3. I9. Cross stream and vertical velocity distributions of selected cross sections of a bend with  $r_c/w=1.5$ . The cross stream velocity distribution is shown by solid lines while the vertical velocity distribution is shown by broken lines; both in  $\text{cm. s}^{-1}$ . The relative width ( $w_1/w_0$ ) and depth ( $y_1/y_0$ ) are shown on the vertical scale on each diagram.



Nb: The location diagram is shown in Figure 3. I8.



towards the surface increases its influence along the bend zone between 83 degrees and 115 degrees as the separated flow entrains more and more fluid. But the rotational flow that develops at section #9 along the exit weakens the forced vortex flow considerably, restores isovel symmetry and the logarithmic vertical velocity profile. Unlike a bend of  $r_c/w=2.2$ , a bend of  $r_c/w=1.8$  has simple isovel patterns at the bend apex. Convex flow separation zones ( at 83 and 115 degrees of the bend) reduce the size of the "live width" and absorb eddies which otherwise are transported downstream.

There is little secondary flow advection in a bend with  $r_c/w=1.5$  (Figure 3.18) compared to that for  $r_c/w=1.8$ . Instead there is a progressive development of a free vortex flow which reaches its maximum strength ( $t=-0.28$ ) at the bend entrance. The superposed spirals transfer high momentum fluid towards the concave bank at the surface and towards the convex bank near the channel bed at section #3 along the straight entrance. The flow profile is more or less parabolic due to transverse velocity redistribution. Within the bend (17 degrees), the velocity near the channel bed is retarded and there is secondary flow advection directed towards the surface. This flow pattern assures the existence of parabolic cross stream flow profiles, but distorts the distribution of vertical velocity.

Figure 3.20. The isovel patterns of selected cross sections of a single bend with  $r_c/w=1.0$ . The diagrams are presented from the left bank to the right bank facing downstream. Velocity contours are shown in  $\text{cm. s}^{-1}$ .

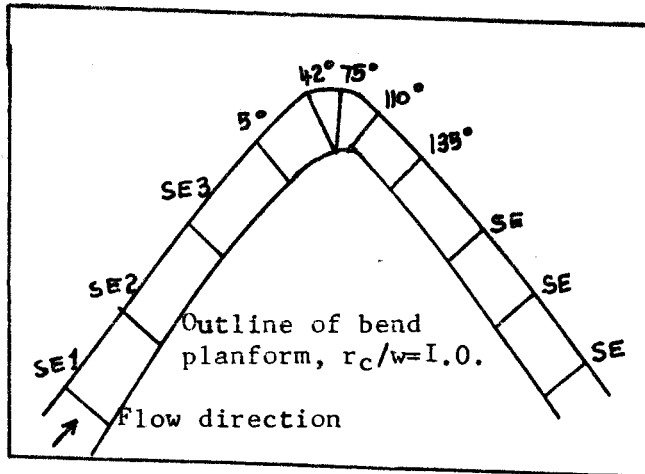
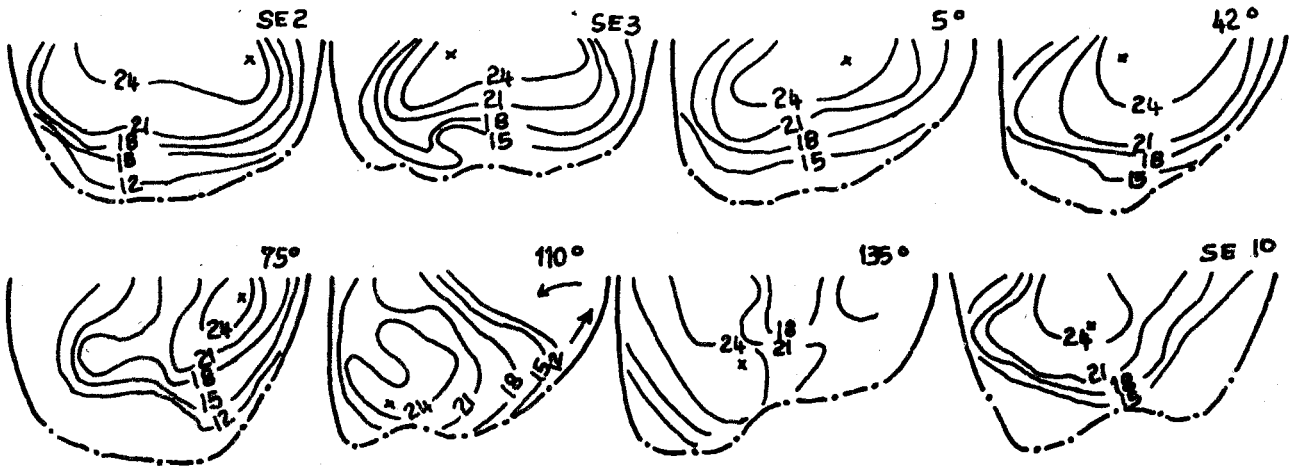
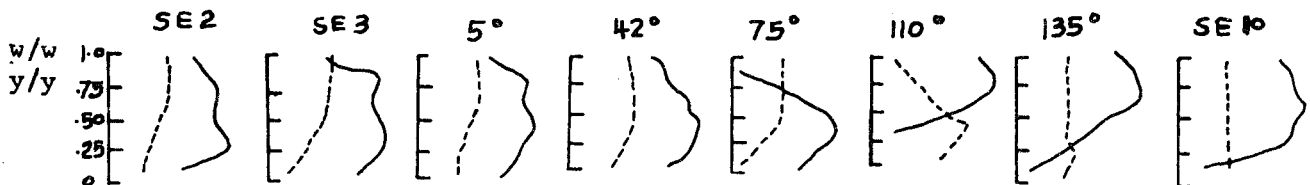


Figure 3.21. Cross stream and vertical velocity distributions of selected cross sections of a bend with  $r_c/w=1.0$ . The cross stream velocity distribution is shown by solid lines while the vertical velocity distribution is shown by broken lines; both in  $\text{cm. s}^{-1}$ . The relative depth and width are shown on the vertical scale on each diagram.



0.10  $\text{m. s}^{-1}$   
cross stream  
velocity

0.20  $\text{m. s}^{-1}$   
vertical velocity

Between bend angle of 17 and 55 degrees the strength of the spiral increases to 22 degrees near the convex bank (Figure 3.13). The bed-divergent double spirals with transverse secondary flow at 87 degrees depresses the core of maximum velocity towards the bottom. Towards the bend exit, the surface currents tend to lie parallel to the channel banks while the bottom currents incline towards the convex (inner) bank; they facilitate point bar deposition. Parabolic flow profiles and logarithmic distribution of vertical velocity are obtained indicating that the bend effects have been suppressed to a minimum.

Figure 3.20 shows the isovel patterns while Figure 3.21 shows the distribution of vertical and radial velocity in a bend with  $r_c/w=1.0$ . Secondary flow advection towards the corners is readily suppressed at the bend entrance. The complex interaction between fluid obeying the principle of conservation of angular momentum near the surface and those transferring high momentum from the concave bank towards the convex bank at section #3 is probably an example of upstream transmission of the bend effects towards the straight entrance. Leschziner and Rodi (1979) in a comparison of a turbulence-based computational model of secondary flow with experimental measurements noted that in strongly curved channels, a unidirectional, radially inward motion prevailed along the straight portion upstream from the bend entrance. But within the bend zone, there is a consistent transfer of fluid towards the concave bank at a bend

Table 3.I. Summary of approximate limits of each vortex flow in single open-channel bends.

$r_c/w$	SE	0°	30°	60°	90°	120°	150°	180°	SE
1.0	parabolic flow		free vortex	forced vortex	forced vortex	forced vortex	forced vortex	parabolic flow	parabolic flow
1.5	free vortex	parabolic flow		forced vortex		forced vortex		forced vortex	forced vortex
1.8	parabolic flow	free vortex	forced vortex		forced vortex		forced vortex	parabolic flow	parabolic flow
2.2	parabolic flow	free vortex	forced vortex		forced vortex		forced vortex		forced vortex
2.6	parabolic flow	forced vortex		forced vortex	T	forced vortex	forced vortex	parabolic flow	parabolic flow
3.2	parabolic	free vortex		forced vortex		forced vortex		forced vortex	
3.3	parabolic	forced	free	forced vortex		forced vortex		forced vortex	
3.7	parabolic	forced		forced vortex		forced vortex		forced vortex	
4.0	parabolic	forced vortex		forced vortex		forced vortex		forced vortex	
4.7	parabolic	free	parabolic flow	forced vortex	forced vortex	forced vortex	forced vortex	forced vortex	forced vortex

NB. SE represents the straight entrance and exit sections of the bend.

T transitional zone

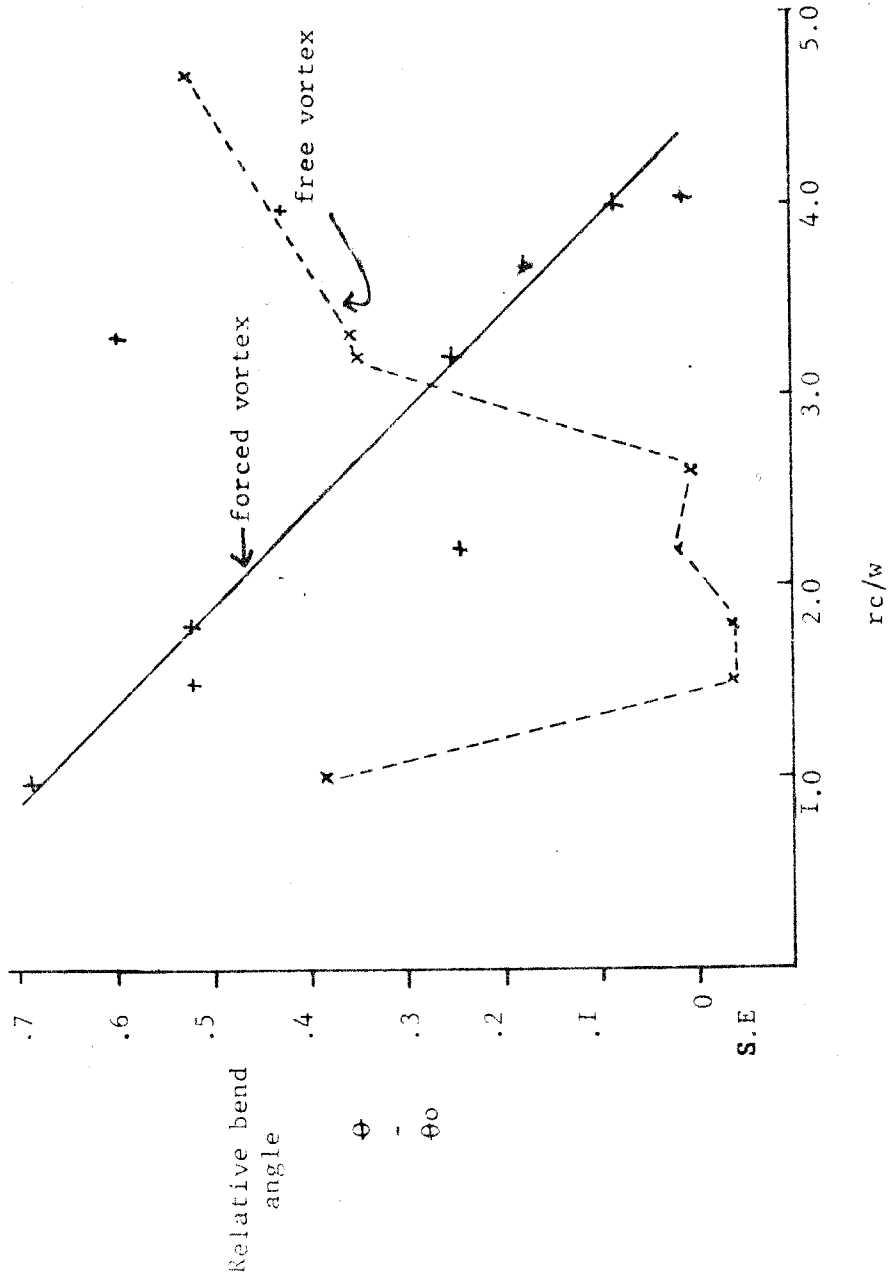
angle of 5 degrees. As the secondary flow advection directed towards the surface at the centre of the channel changes the current direction from 9 degrees at a bend angle of 42 degrees to 42 degrees at 75 degrees of the bend (Figure 3.13), upwelling increases and the flow separates from the concave bank.

The initiation of forced and free vortices in single bends also varies with  $r_c/w$ . Figure 3.22 was prepared by calculating the ratio of the bend angle at which each vortex flow is initiated to total bend angle. There may be, however, some differences between the plotted points because the interval between sections at which the measurements were taken are not standardised. In any case the point at which a free vortex flow is initiated shifts upstream while that of a forced vortex flow shifts downstream as the bends become rather tighter. The upstream shifts of the free vortex flow is due to the influence of the curvature upstream of the bend (cf. Pratap and Spalding, 1975).

### 3.1.5 Summary of Flow Characteristics in Bends with $r_c/w < 2.6$

The main characteristics of isovel patterns and current direction in bends of  $2.6 > r_c/w > 1.8$  is that the positions at which the forced vortex flow forms shifts downstream to 80 degrees while that of the free vortex flow migrates upstream as  $r_c/w$  decreases; the converse of those of  $r_c/w > 3.2$  (cf. Bagnold, 1960).

Figure 3.22. The dimensionless bend angles at which free and forced vortex flows are initiated. The bend apex location is at  $\theta = 0.50$ .



The free vortex flow is represented by 'x' while the forced vortex flow is represented by '+'. The distinction is based on the strength of the flow,  $t$ , in the expression  $V=kr \frac{t}{r}$ .

It has been known for sometime that a transitional flow occurs at the bend apex while the forced vortex (fully developed) flow locates downstream of the bend apex (Leopold and Wolman, 1960; Rozovskii, 1961; Jackson, 1975). But the evidence that the fully developed flow is preceded by parabolic flow at the bend apex has not received much attention. The existence of the parabolic flow at the bend axis is closely associated with the variation of the flow development patterns as described in the present work. The evidence of such downstream migration of the fully developed flow zones do exist in the literature as being consequences of either increasing or decreasing discharge (Jackson, 1975; Bathurst et al; 1979). As discharge decreases, channel width decreases while radius of curvature remains sensibly the same. The bend geometry therefore becomes less tight. Leschziner and Rodi (1979) have argued that strongly curved flows transmit bend effects upstream through radial asymmetry of tranverse velocity that delays the formation of fully developed flow (cf. Humphrey et al; 1977).

The presence of strong secondary flow towards corners in straight rectangular channels compares well with results of measurements at the bend entrance (Perkins, 1970; Humphrey et al; 1977; 1981). The radial forces direct the secondary flow from corners towards the water surface but close to the outer bank upstream of 60 degrees and then towards the inner bank near the bend apex. The currents near the channel bed are directed towards the outer bank zone between 30 and 60 degrees, and then

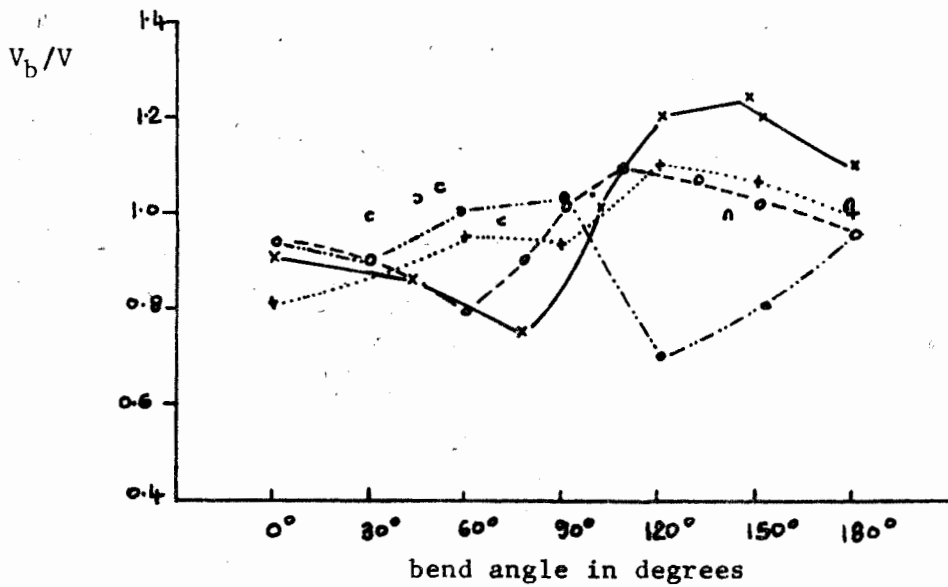
towards the centre upstream of the bend apex (between 60 and 90 degrees). The surface currents are , on the other hand, parallel to the channel banks up to 60 degrees where they approach the concave bank at an angle, after which they converge towards the centreline. The streamlines that impinge on the concave bank generates turbulence (cf. Yao and Berger, 1975) and provide eddies which are transported across the channel by secondary flow. These eddies become entrapped with the mainstream flow and cause flow deceleration.

Along the bend zone between 60 and 105 degrees, the transverse secondary flow convergence depresses the core of maximum velocity towards the channel bed. The present results complement those of Hawthorne (1951) and Rowe (1970) who suggest that a secondary spiral with opposite sense of rotation develops at the bend apex and reduces the intensity of the initial spiral. Further downstream, the bottom currents are directed towards the convex bank and are responsible for point bar deposition.

The depression of the core of maximum velocity is shown by comparing the ratio of velocity near the channel bed and the mean velocity at each cross section at  $y_1/y_0 > 0.75$  (Figure 3.23). The ratio of velocity near the channel bed,  $V_b$ , and the mean



Figure 3.23. The ratio of mean velocity at each cross section and the velocity near the channel bed,  $n=0.75$ .



symbols represent:

— x —	$r_c/w=1.0$	c	$r_c/w=3.2$
..... + .....	$r_c/w=1.5$	n	$r_c/w=3.3$
- - - ● - - -	$r_c/w=2.2$	o	$r_c/w=3.7$
- - - ○ - - -	$r_c/w=1.8$		

velocity for each cross section,  $V$ , depicts the growth of the boundary layer including interferences by the bedforms. The  $V_b/V$  reaches a maximum value along the bend zone between 60 and 180 degrees; the same section where the core of maximum velocity depresses towards the channel bed in agreement with Muramoto's (1967) findings. Maximum  $V_b/V$  locates towards the bend exit in  $r_c/w < 3.2$ . The secondary flow towards the concave bank between 30 and 60 degrees may cause bank failure there. Near the concave bank, the cross stream velocity is directed towards the outer bank near the surface, then towards the channel bed and inwards towards the channel centreline. Assuming that the velocity magnitude exceeds that of bank competence, sediments will be transported towards the centreline by traction.

Bagnold (1960) describes the separated zones as "...an intervening space occupied by a zone of unstable and confused motion..." (cf. Rozovskii, 1961). Observations from this study and others (Mockmore, 1944; de Vriend, 1980; O'Brien, 1981; Fox and Ball, 1968) suggest that the separated zone has organised strong secondary flow advection near the bottom from the concave bank towards the surface near the convex bank. The secondary flow displaces the core of maximum velocity towards the centreline and weakens the forced vortex at the bend apex. The inner vortex of the separated flow has an anticlockwise circulation to that of the primary vortex. The onset of flow separation is, therefore a flow response to decreasing  $r_c/w$ .

## 3.2 THE VELOCITY DISTRIBUTION IN SINGLE OPEN-CHANNEL BENDS

### 3.2.1. Introduction

Nearly all models of sediment transport (Bogardi, 1971) and meander initiation apply some kind of perturbation parameter to the mainstream velocity. Morphological processes - erosion, transport and sedimentation - cannot be explained without considering velocity fluctuations (Sundborg, 1956). Einstein and Shen (1968) properly suggested that unsteady velocity is a prerequisite for the development of 'organised' alternate pools and riffles in straight channels. Hayashi (1973) found that velocity fluctuations near the bed facilitate the development of bedforms because of differential shear stress (cf. Leeder, 1980). Although the temporal and spatial periodic variations of such unsteady flow vary considerably (cf. Kalinske, 1947), the variations have to be persistent in order to create morphological impact.

In section 2.2, it was observed that secondary flow from the outer bank directed towards the inner bank near the channel bed and towards the surface at the convex bank encourages flow deceleration and separation zones. The isovel patterns show in varying magnitudes the presence of macroeddies whose geometrical axes vary in relation to mainstream velocity and bedform

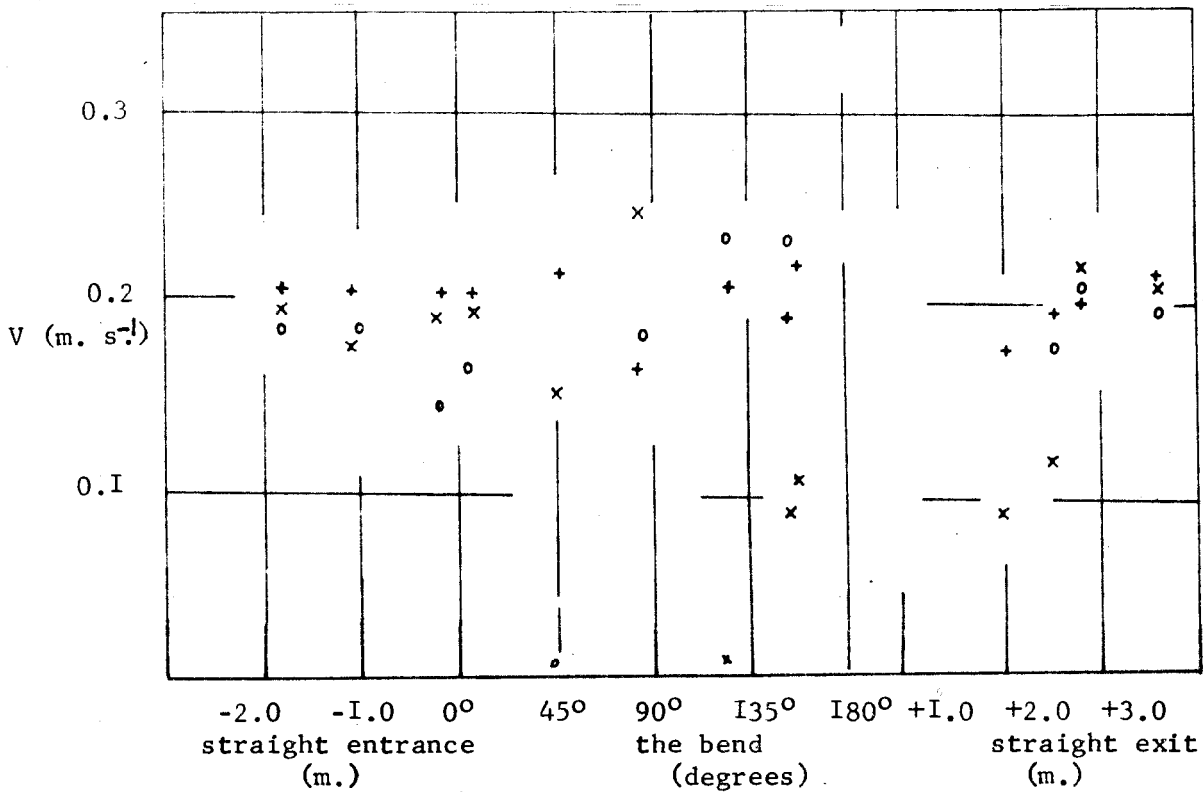
characteristics. Superposed on such macroeddies must be other types of eddies of all sorts which interact with the mainstream velocity. Section 3.3 describes the distribution of longitudinal and transverse velocity in single bends of  $1.0 < r_c/w < 4.7$ .

### 3.2.2 The Distribution of Mean Velocity

The velocity distribution in open-channel bends is inherently unsteady and nonuniform. The periodic vertical oscillation moves the core of maximum velocity towards the channel bed upstream of the bend apex and towards the surface downstream of the bend apex (Figure 3.22 and section 3.1); the pattern is generated by boundary layer development (Squire and Winter, 1951; Einstein and Li, 1958). The transverse oscillation moves the core of maximum velocity from one bank to the other causing alternate accelerations and decelerations every 3 to 4 channel widths; they represent organised secondary flow towards the banks (Einstein and Shen, 1964). The riffle-pool spacing is, therefore, a response to such organised secondary flow (Richards, 1978).

The sequential diagrams in Figure 3.24 show the velocity distribution near the channel banks and also the mean cross sectional velocity. The mean velocity is shown by "x" symbols, the velocity near the outer bank are represented by "o" symbols and "+" symbols represent the velocity near the convex (inner)

Figure 3.24 (a). The longitudinal distribution of mean velocity in a single bend with  $r_c/w=1.0$ .



The symbols x represents velocity near the inner bank, + represents velocity near the outer bank and o represents velocity mean at each cross section.

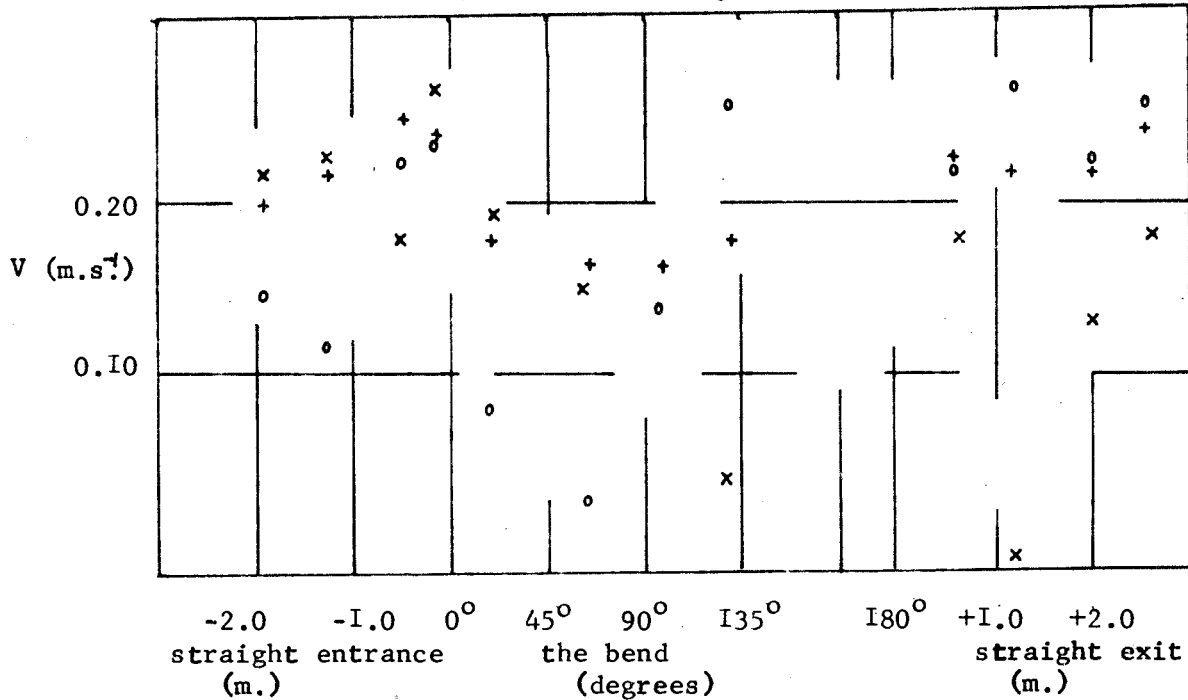
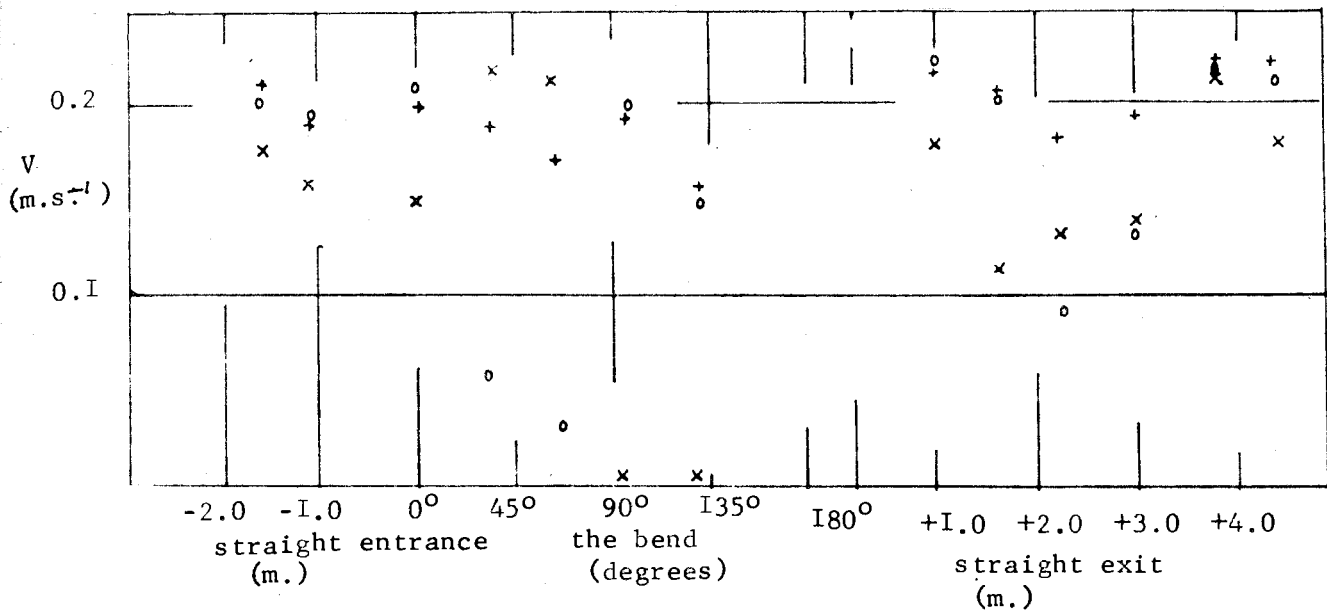


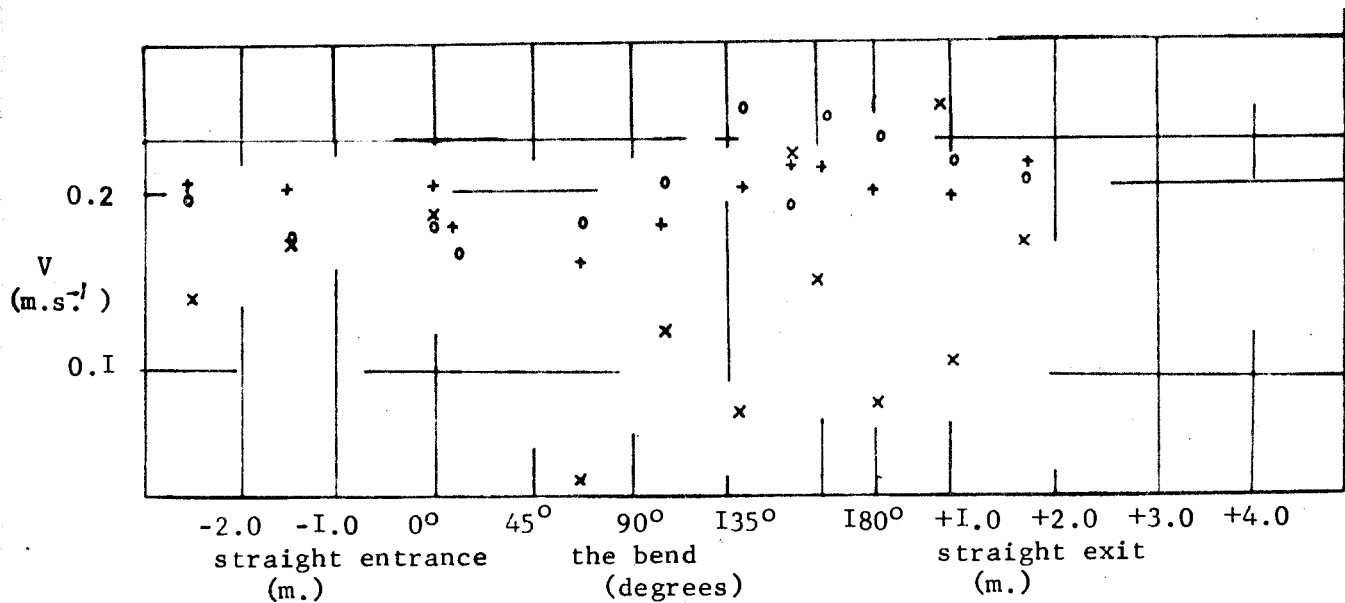
Figure 3.24 (b). The longitudinal distribution of mean velocity in a single bend with  $r_c/w=1.5$ . The symbols are as explained earlier.

Figure 3.24 (c). The longitudinal distribution of mean velocity in a single bend with  $r_c/w=1.8$ .



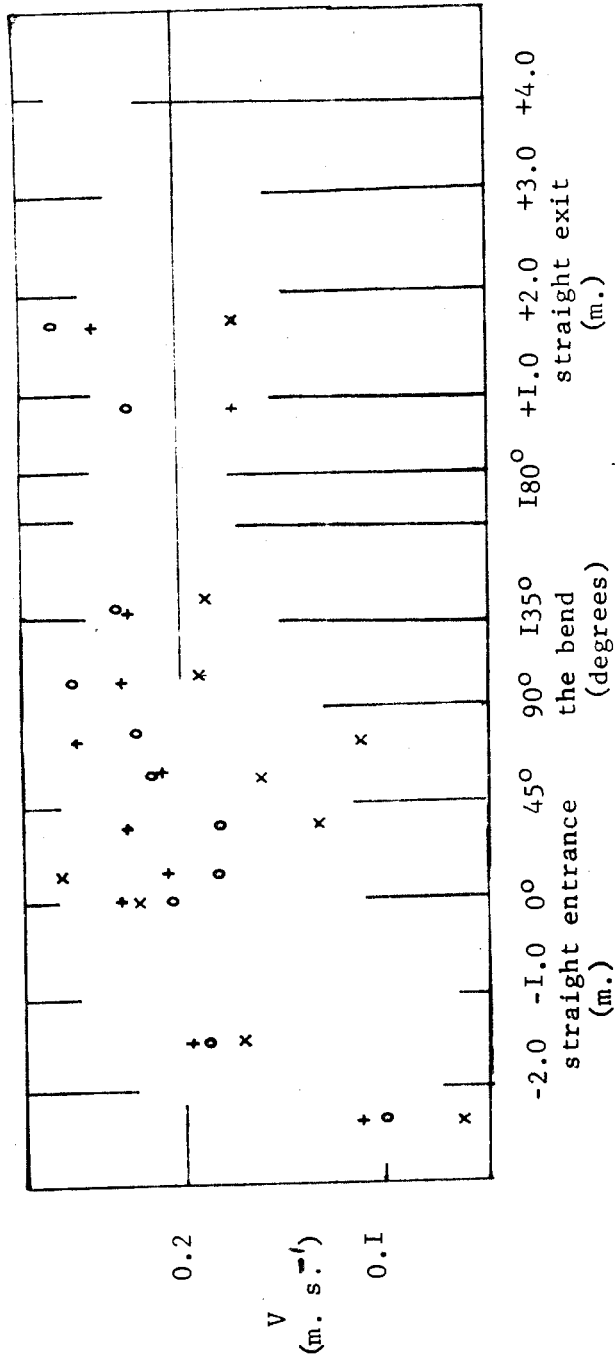
The symbols x represents velocity near the inner bank, + represents velocity near the outer bank and o represents the mean velocity.

Figure 3.24 (d). The longitudinal distribution of velocity in a single bend with  $r_c/w=2.6$ .



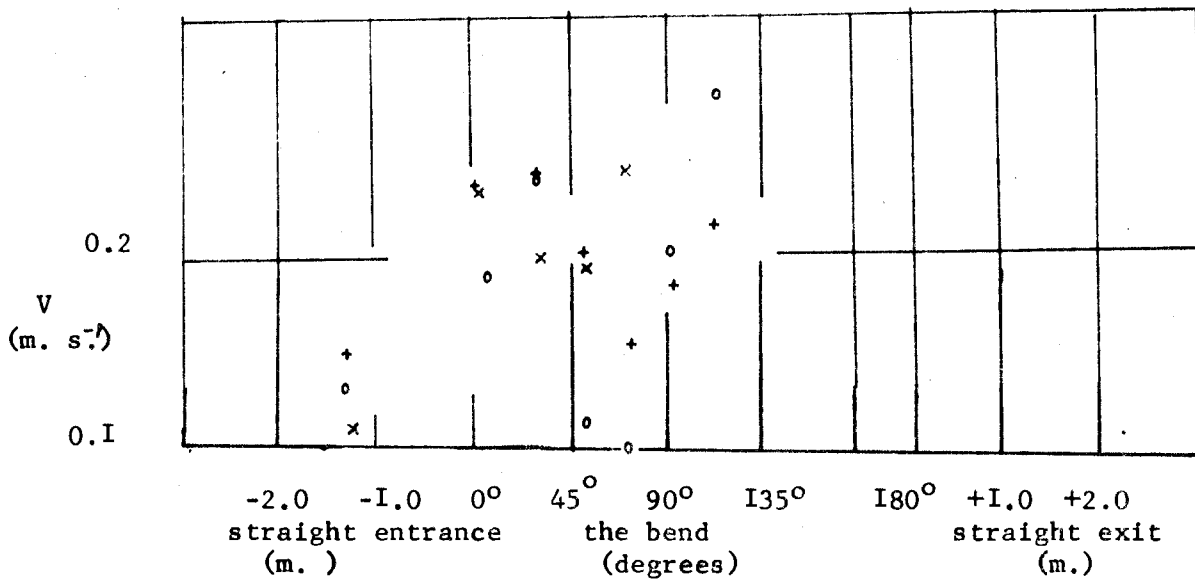
The symbols are as explained earlier.

Figure 3.24 (e). The longitudinal distribution of velocity in a single bend with  $r_c/w=2.2$ .



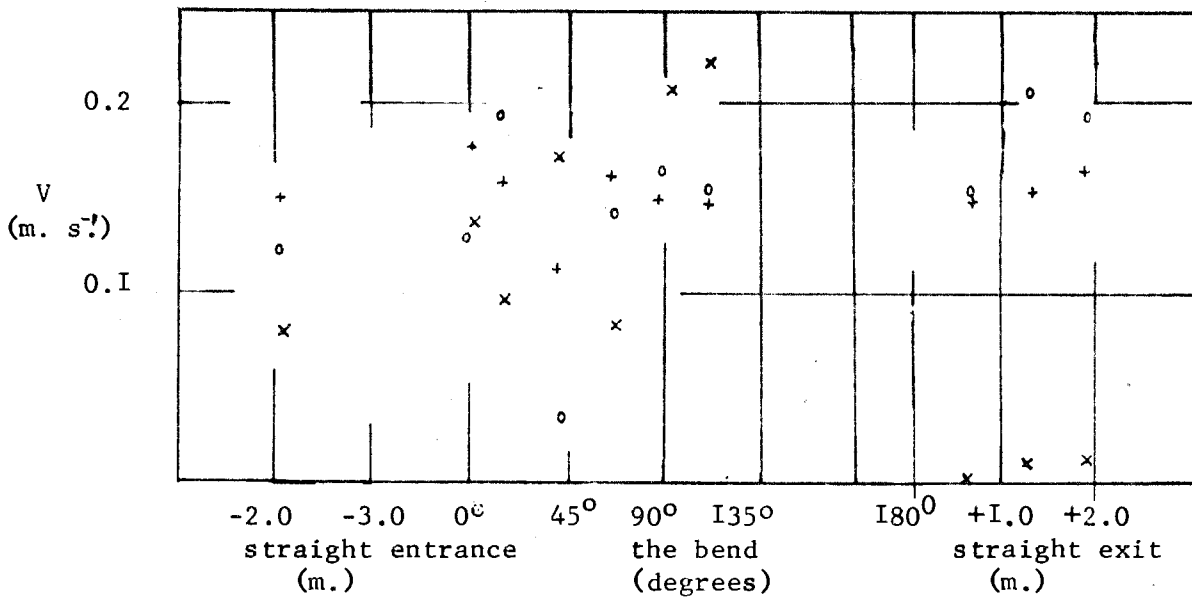
The velocity near the inner (convex) bank is represented by x symbols, the one near the outer (concave) is represented by + symbols and the mean velocity is shown by o symbols.

Figure 3.24 (f). The longitudinal distribution of velocity in a single bend with  $r_c/w=3.2$ .



The symbols are as explained earlier.

Figure 3.24 (g). The longitudinal distribution of velocity in a single bend with  $r_c/w=3.3$ .



x symbols represent the velocity near the inner bank, + symbols represent velocity near the outer bank while o symbols represent the mean velocity.



Figure 3.24 (h). The longitudinal distribution of velocity in a single bend with  $r_c/w=3.7$ .

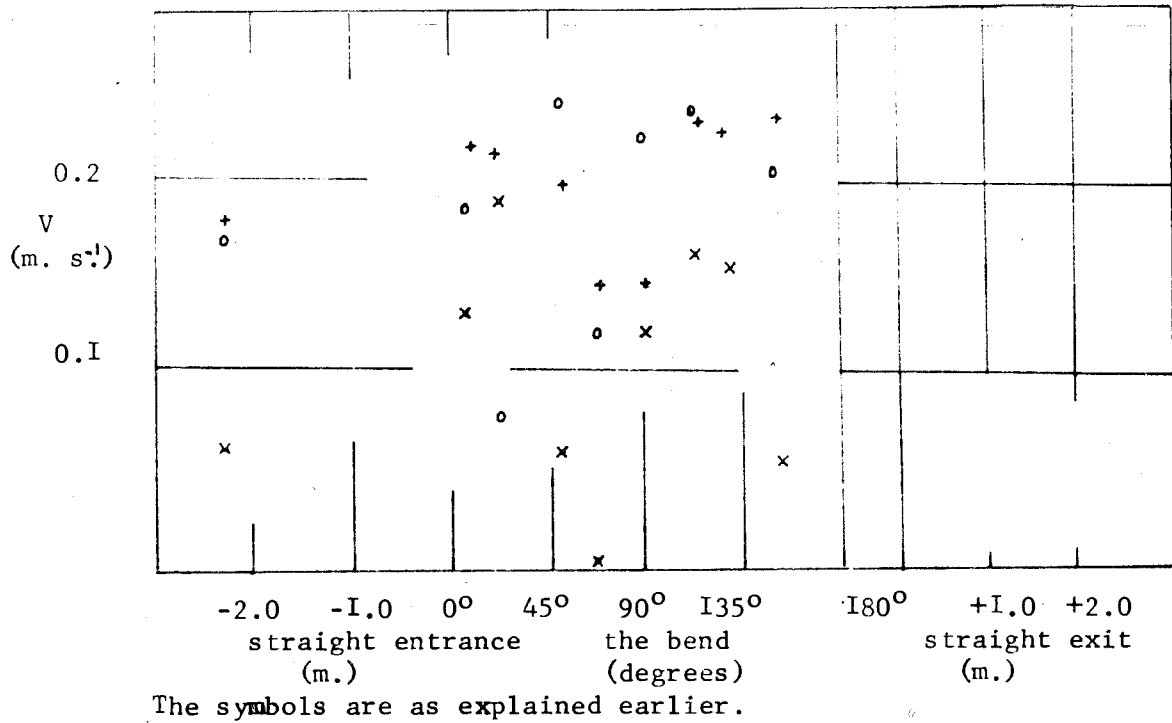
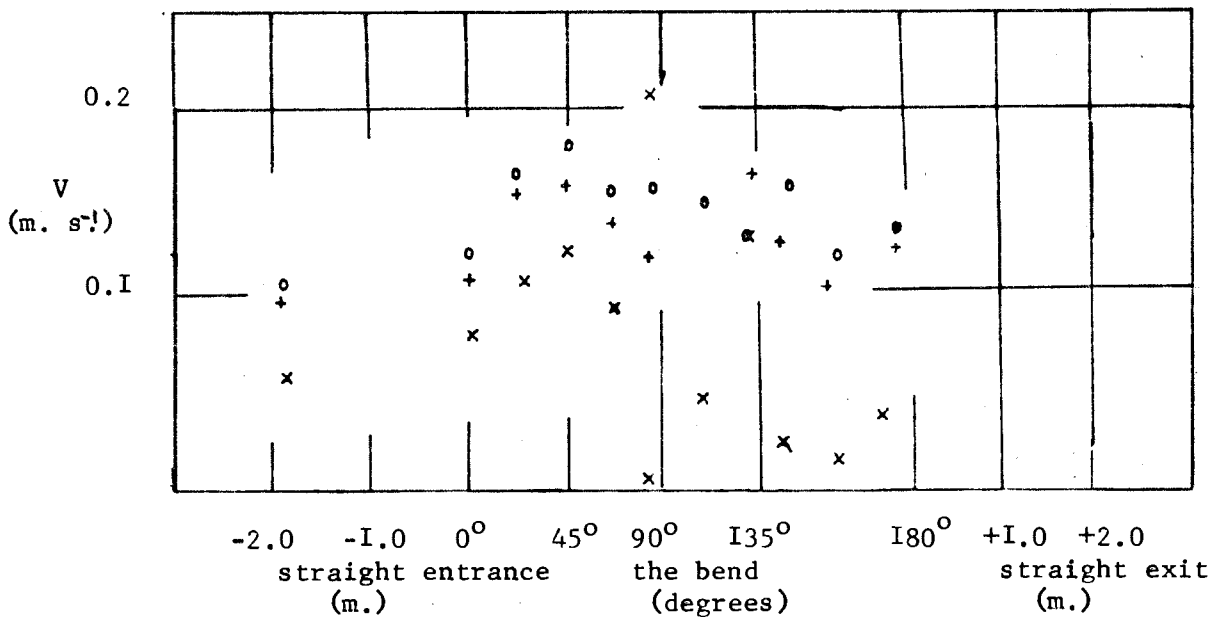


Figure 3.24 (i). The longitudinal distribution of velocity in a single bend with  $r_c/w=4.0$ .



x symbols represent the velocity near the inner bank, + symbols represent velocity near the outer bank and o symbols represent the mean velocity.

bank. The velocity near the banks was measured at 0.076m from the water's edge. The channel length, shown along the horizontal scale in the figures was measured in meters from the straight entrance, and in degrees along the bend curvature. The straight exit portion was measured in meters away from the bend exit.

The profiles of velocity near both banks that are of the same pitch are probably due to flow accelerations punctuated with flow decelerations and may be caused by the variations in bedform size and location factors that are responsible for boundary layer growth near the channel banks in bends of  $r_c/w > 3.7$  and  $r_c/w = 1.0$ . The velocity profiles that are of opposite pitch for bends of  $3.3 > r_c/w > 1.8$  represent alternate vortices that travel in a manner similar to that produced by velocity reflectivity concept (Leliavsky, 1955). The sections where flow decelerations occur have bank eddies with quasi-vertical axes.

The mean velocity decreases to a minimum value in the bend zone between 60 and 120 degrees except in  $r_c/w = 3.3$  in which it decreases to a minimum at 37 degrees. The maximum superelevation (Shukry, 1949), the location where the core of maximum velocity depresses towards the channel bed, the location of the secondary spiral, and the maximum shear stress and friction to flow (Nakomura and Tomonari, 1982; Choi et al; 1979) all lie along the bend zone between 60 and 120 degrees.

Flow in curved conduits is usually unstable. The threshold at which bend flow becomes unstable has received little

attention compared to flow in closed conduits or between rotating cylinders (for example, see Taylor, 1923; Stuart, 1971; Simpson et al 1983). The only attempts presently known are by Soliman and Tinney (1968) in which transverse oblique waves become predominant in bend flow when Froude number exceeds 0.6 and Bagnold's (1960) concept of separation-collapse theory. In support of the theory, Bagnold concluded that "... a confused zone of flow ..." that develops near the inner bank collapses and friction coefficient decreases in  $r_c/w=2.0$ . Hickin (1975) appealed to the same concept to explain a decrease of lateral migration in bends of  $r_c/w < 2.0$ . separation.

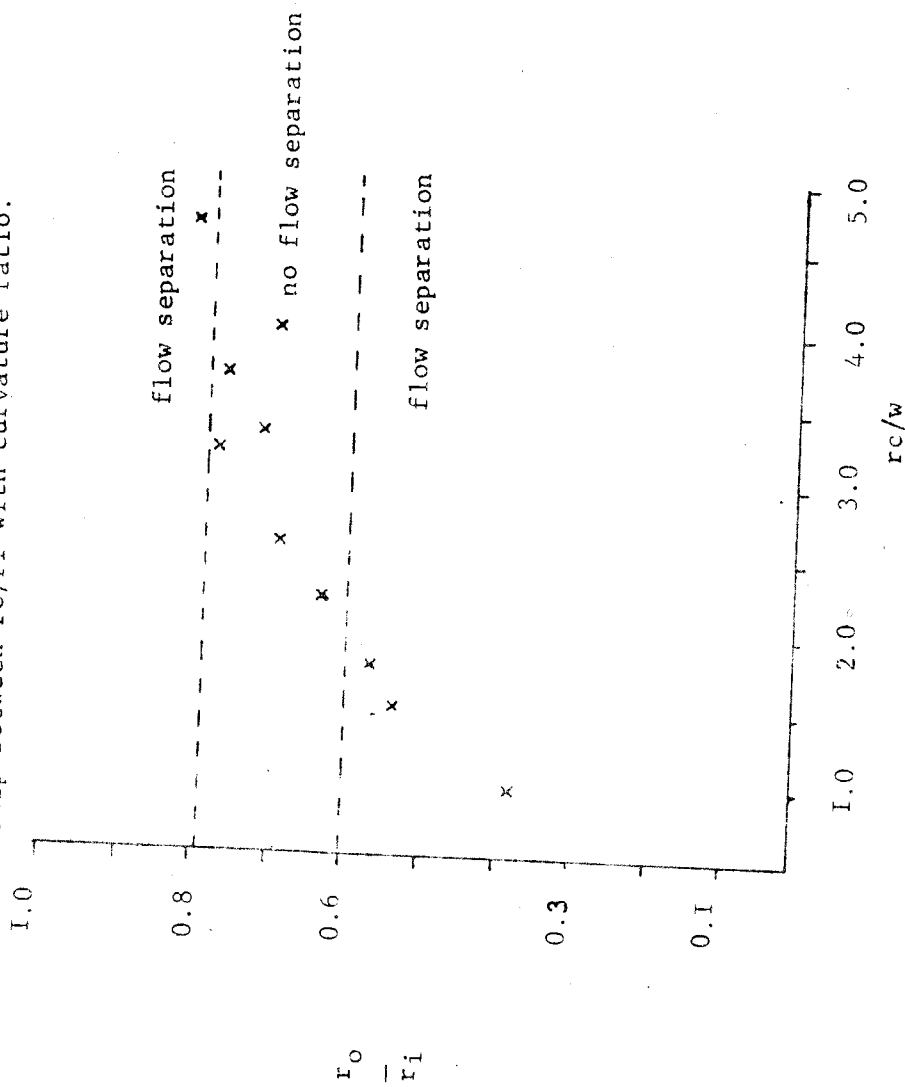
It has been known for some time that elbows of pipes are designed with flared or bulged vertex to reduce bend loss (Mockmore, 1937). Flow separation causes the flow cross section to maintain a constant width in some rivers by reducing the 'live width' at the bend apex while in others mid-channel bar deposition (cf. Lewin, 1978) eliminates the incidence of flow separation although friction to flow may increase considerably. Experimental models of flow behavior in bends, on the other hand assume that the channel width remains constant while the bend geometry changes (Leopold et al; 1964). Hickin (1975) compared the relationship between the theoretical and observed ratio of centreline radius,  $r_c$ , and inner radius,  $r_i$ , as bends become rather tighter to confirm the assumption of constant channel-width with decreasing  $r_c/w$ .  $r_o$  is chosen in this study because it is easier to measure in rivers than  $r_c$ . Figure 3.25

shows the ratios of radii of the outer and inner banks. With constant channel width of 0.6m, the relationship between the ratio of outer (concave) radius and the inner (convex) radius increases steeply with decreasing  $r_c/w$  in bends with  $1.0 < r_c/w < 2.5$  then remains sensibly constant for bend with  $2.5 < r_c/w < 4.7$  conforming to that arrived at theoretically by Hickin (1975).

The mean velocity distribution shows that bends with  $r_c/w < 2.0$  and  $r_c/w > 3.7$  have separation zones while  $2.2 < r_c/w < 4.0$  do not have separation zones. Any decrease in  $r_c/w$  is often compensated by an increase of depth (Levliansky, 1955). The difference between Hickin's (1975, Figure 4) results for the Beatton river is due to lacustrine deposits (Nanson, 1977) which have inhibited channel incision and resulted in "flared" widths at the bend apex. Hickin (1977) confirms such geological control by his observation that discharge-width relationship is more consistent than that of width-bend wavelength.

The separatrix between bend apices with flow separation zones and those without may be explained by the interaction between vertical and longitudinal oscillations of the main flow. The causes of longitudinal oscillation are not well known (Stuart, 1971), but represent the response of flow to the boundary layer conditions and the rate of sediment transport (Engelund, 1970; Despard and Miller, 1971; Jackson, 1976; Leeder, 1980). The vertical and transversal oscillations are superposed on the longitudinal oscillations. Matthes (1947) argued that the upward directed vortices are intermittent

Figure 3.25. The relationship between  $r_o/r_i$  with curvature ratio.



(cf. Jackson, 1976) while the downward directed vortices caused by changes of current direction are persistent. Although it is difficult to separate the influences of each vortex type on periodic velocity distribution in the present study, it is obvious that all types of vortices occur in varying intensity in response to changes in  $r_c/w$ . The composite effect is that when velocity decelerates near the channel bed at a bend angle of 30 degrees, the mainstream velocity accelerates and quasi-vertical eddies form (Prandtl, 1949). Bagnold (1960) suggested that flow separation may be reduced by the increasing number of eddies towards the inner bank where in this study, the same purpose is fulfilled by secondary flow advection towards the corners and towards the surface.

The general patterns were photographed for laboratory analysis. Bubbles were created in the flow by dumping dry fine sand into the settling well. This mixture of sand with the flow made the pattern of vortices and vortex trails visible (see in Plates 3.2 and 3.3 below). Flow visualisation techniques were employed to investigate further the progressive development and decay of macroeddies. The flow in a straight channel and along the straight portions of bends depicts random movements of bubbles, perhaps because of intense secondary flow advection there. Towards the bend entrance, however, the bubbles concentrate linearly along the centre of the channel where the velocity gradient is steep. Because the point bar is less developed and the high velocity core is near the convex (inner)

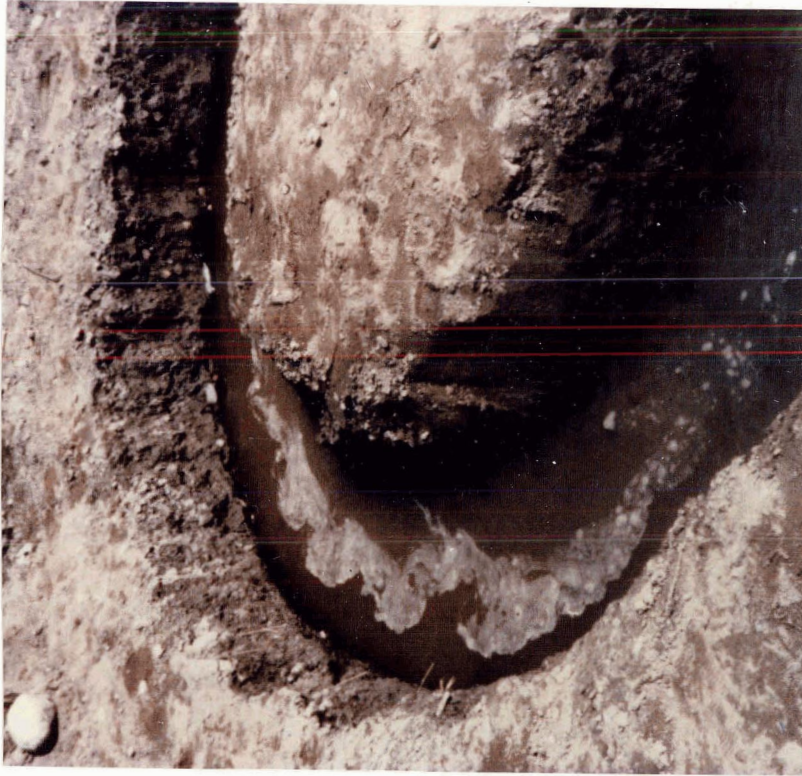
PLATE 3.2

Vortex roll-up at the bend apex due to flow acceleration near the concave (outer) bank and deceleration near the convex (inner) bank. The flow direction is from the bottom part towards the top left corner of the photograph.



PLATE 3, 3

The white trace in the channel shows the periodic surface flow characteristic typical in the present model bends and in rivers. The vortices are elongated towards the concave (outer) bank; they possibly are responsible for undermining the channel banks.



The flow direction is from the top right corner towards the bottom of the photograph.



bank and velocity along the concave (outer) bank decelerates upstream of the bend apex, the double counterrotating spirals shear on each other and the bubbles tend to roll up. These roll-ups had the same geometry as those observed in flows behind bluff bodies (Rouse, 1965).

Downstream of the bend apex (Plate 3.3), the vortex trails become elongated, because of flow acceleration near the concave bank, and disintegrate finally towards the bend inflexion. These vortices did not reverse their direction when viewed by an observer from a fixed point. As Matthes (1947) observed in freely meandering rivers, the quasi-vertical bank eddies, the spiral vortices and quasi-horizontal velocity oscillations transfer flow momentum to the walls which likely will cause lateral erosion through increased shear stress. Because the increase of these vortices has a nonlinear relationship with curvature, it probably is expected that the rate of lateral bend movement will be nonlinear as erosion proceeds to tighten the curvature.

### 3.2.3 Summary of Velocity Distribution in Single Bends

The minimum values of mean velocity locate along the bend zone between 60 and 120 degrees (cf. Yarnell and Nagler, 1933) except in  $r_c/w=3.3$  in which the flow rapidly transforms from a forced vortex to free vortex and then to forced vortex again. The secondary flow transports turbulence at the bend entrance

towards the inner bank upstream of 30 degrees of the bend, but reverses its direction towards the mainstream flow between 30 and 60 degrees. The effect of turbulence on the mainstream flow causes flow deceleration there. Hawthorne (1951) has shown in pipe flow experiments that the local pressure reaches a maximum value at 45 degrees then decreases rapidly to a minimum value between 120 and 180 degrees (cf. Achenbach, 1971; Nakomura and Tamonari, 1982; Patel et al, 1980). Marris (1963) argued that the flow regime along the inner bank tends to be sensibly steady at 90 degrees because the free vortex flow at the bend entrance strains turbulence from reaching this section. This is the bend zone where the intensity of the secondary flow and the strength of the forced vortex flow decrease.

The velocity distribution of bends considered in the present study shows the importance of macroeddies and vortex flow in stream geometry adjustment. The sediment transport near the channel bed likely follows the same orientation of the secondary flow and zones with high velocity. On the other hand, the deposition of fine sediments that depend on the quasi-vertical bank eddies and flow separation may be predicted by examining the isovel patterns.

### 3.3 THE DISTRIBUTION OF SHEAR STRESS AND FRICTION COEFFICIENT

#### 3.3.1 Introduction

Open-channel bends dissipate energy through shear stress (internal distortion) and secondary flow (bend resistance) (Leopold et al; 1960). Secondary flow in bends with  $1.0 < r_c/w < 4.0$  and that of a straight channel has been described in section 3.1. The mean flow structure and velocity near the channel bottom and banks (section 3.2) are unsteady and nonuniform. Ippen and Drinker (1962) found that unsteady flow structure causes rapid periodic variations between minimum and maximum shear stress and friction coefficient. The distribution of shear stress near the banks and also mean shear stress are described in sections 3.3.2 and 3.3.4 respectively. The distribution of friction to flow is discussed in section 3.3.5.

#### 3.3.2 The Distribution of Shear Stress near the Channel Banks

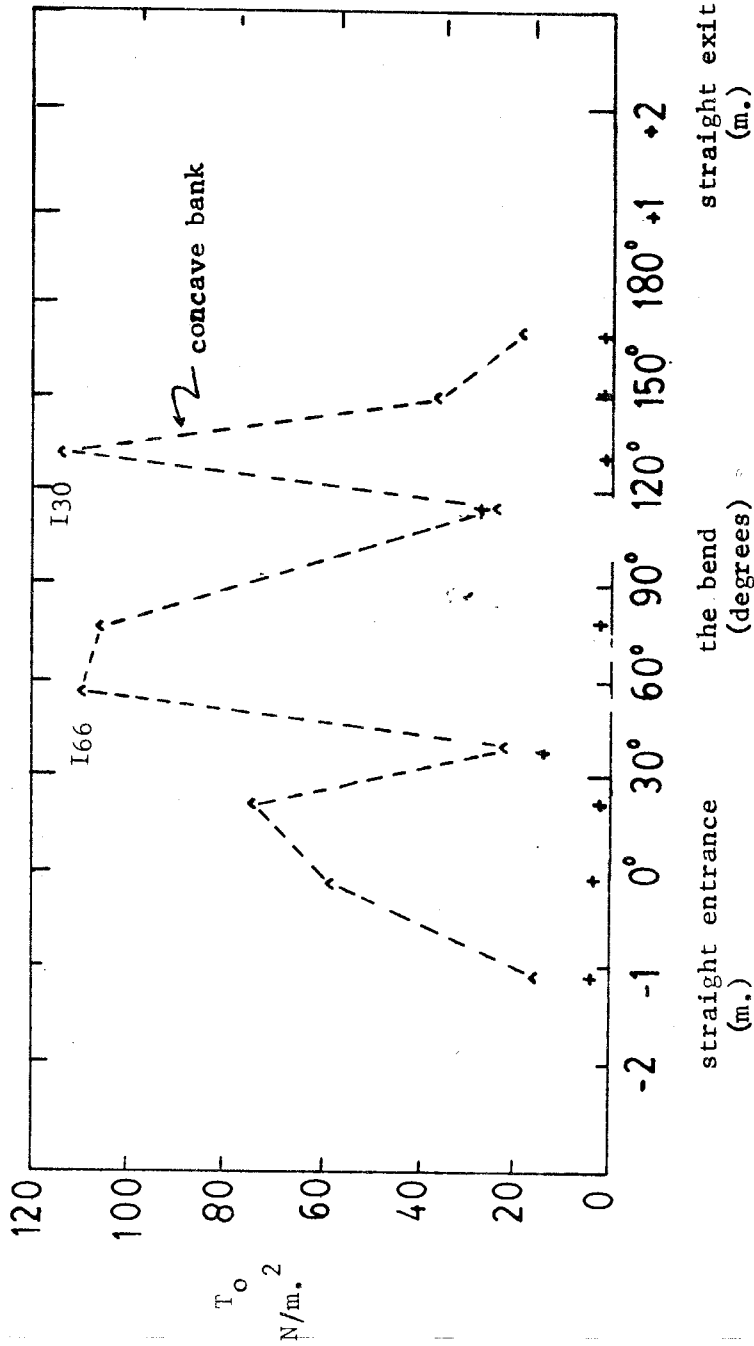
The shear stress distribution was calculated using equation 2.2 ( for the depth range,  $y_1/y_0 > 0.75$ ) for velocities measured along the channel banks 0.076m from the water's edge. The aim is to determine the nature of maximum/minimum shear stress along each bank of various bends in order to determine the bank areas

where most of the stream energy is dissipated. The second aim is to determine the magnitude and variation of stress each bend supports along the concave bank. Bagnold (1960) suggested in support of his separation-collapse model that the concave banks support considerable shear stress, and that shear magnitude decreases after break-away in  $r_c/w=2.0$  (cf. Hickin, 1975).

The resultant of shear stress along the banks is shown by the relative direction of secondary currents. The maximum mean shear stress points locate every 1.0m which represents 3 to 4 channel widths in a straight channel (cf. Leopold et al; 1960). The filament of the maximum shear along the banks alternate from one bank to the other because the secondary flow alternates its direction towards the banks near the channel bed. The spiral near the channel bed moves fluid towards the surface close to the channel bank and centreline thus opposing sediment deposition. These spirals likely will enhance bank erosion if the critical shear stress for a specific bank material is exceeded. In a straight channel, the minimum shear stress distribution along the banks alternate; this alternation likely develops deeps and shoals (cf. Friedkin, 1945).

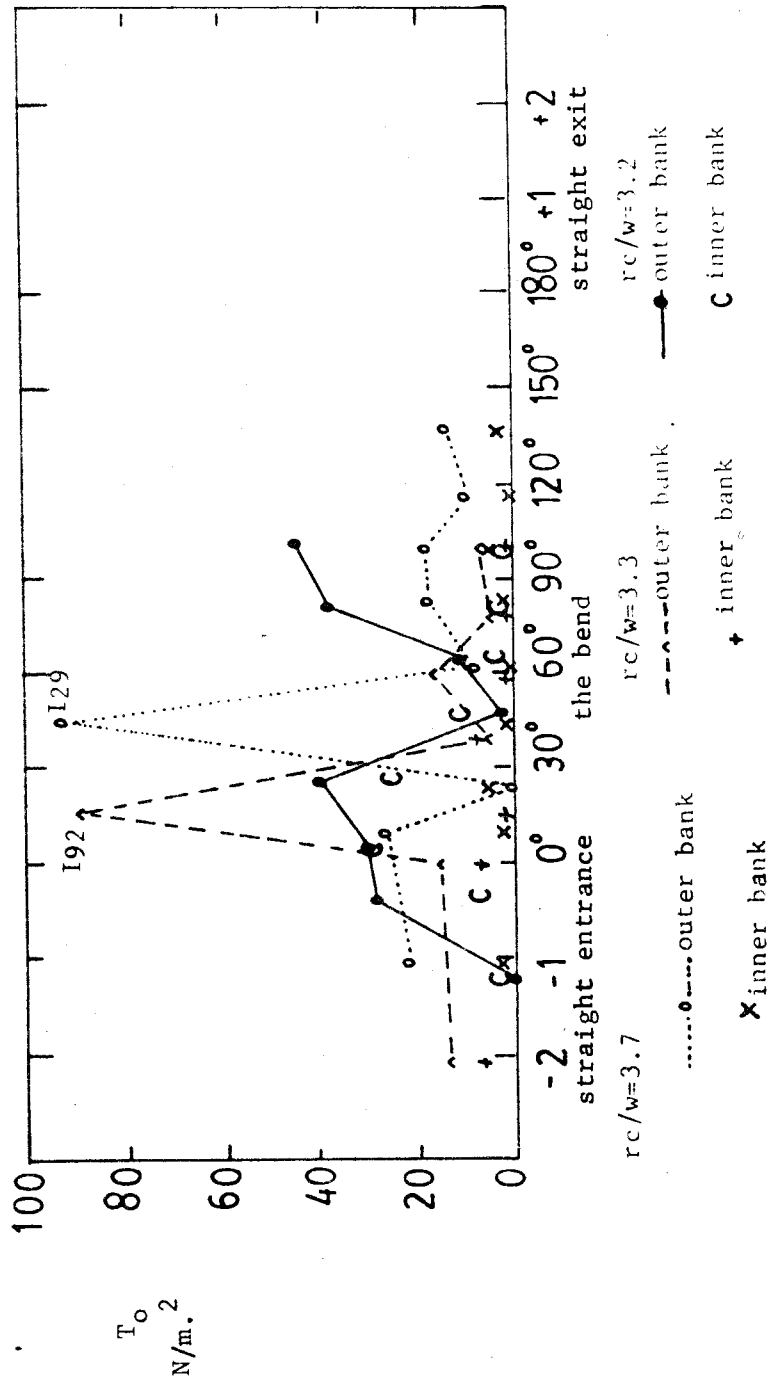
Figures 3.27 to 3.30 show that the distribution of shear stress near the channel banks is periodic every 60 degrees. Assuming that the periodic shear stress distribution is competent to erode the channel banks, erosion will occur every

Figure 3.27. The distribution of shear stress along the channel banks of a bend with  $r_c/w = 4.0$ .



nb. The shear stress along the inner (convex) bank are shown by '+' symbols and are not connected by any lines.

Figure 3.28. The distribution of shear stress along the channel banks.



nb. The shear stress along the convex bank are shown by symbols not joined by lines.

Figure 3.29. The distribution of shear stress along the channel banks. The shear stress along the convex (inner) bank are shown by symbols which are not joined by lines.

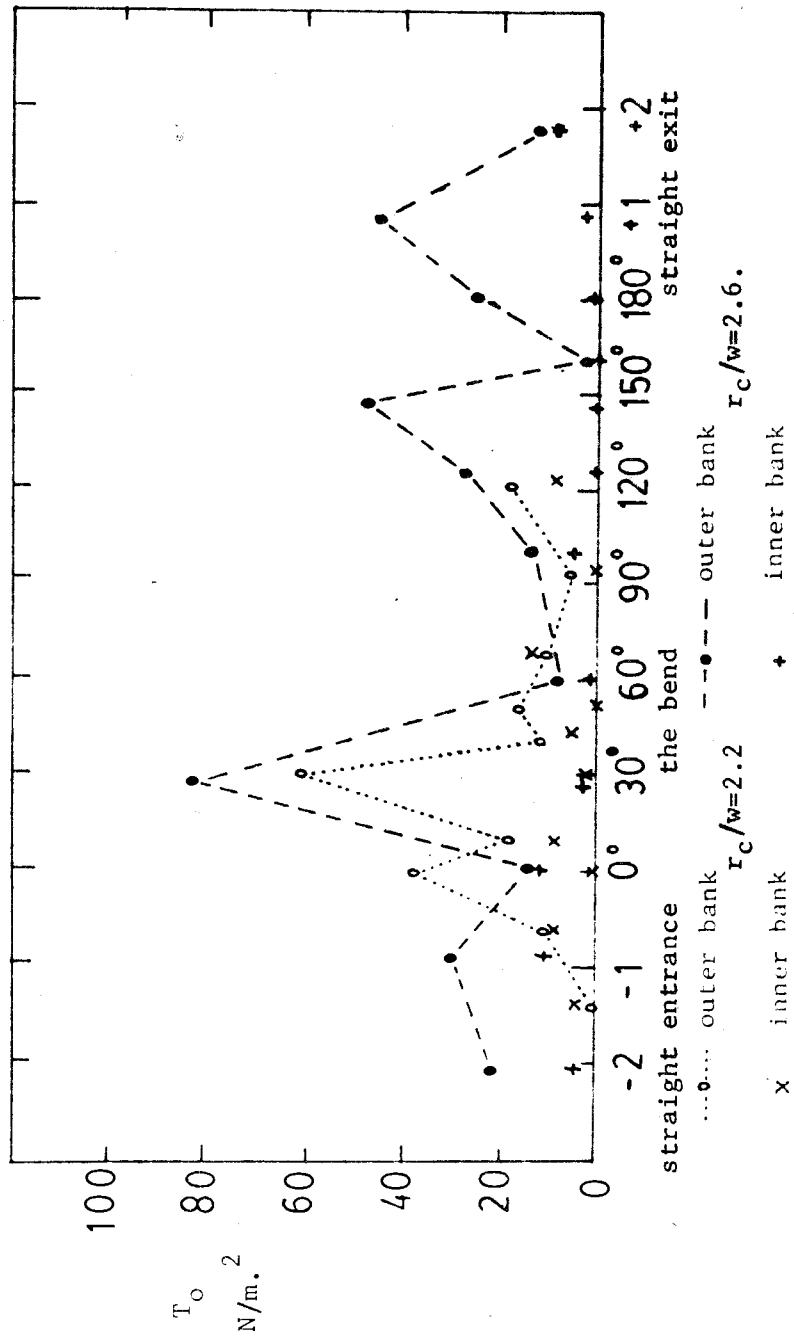
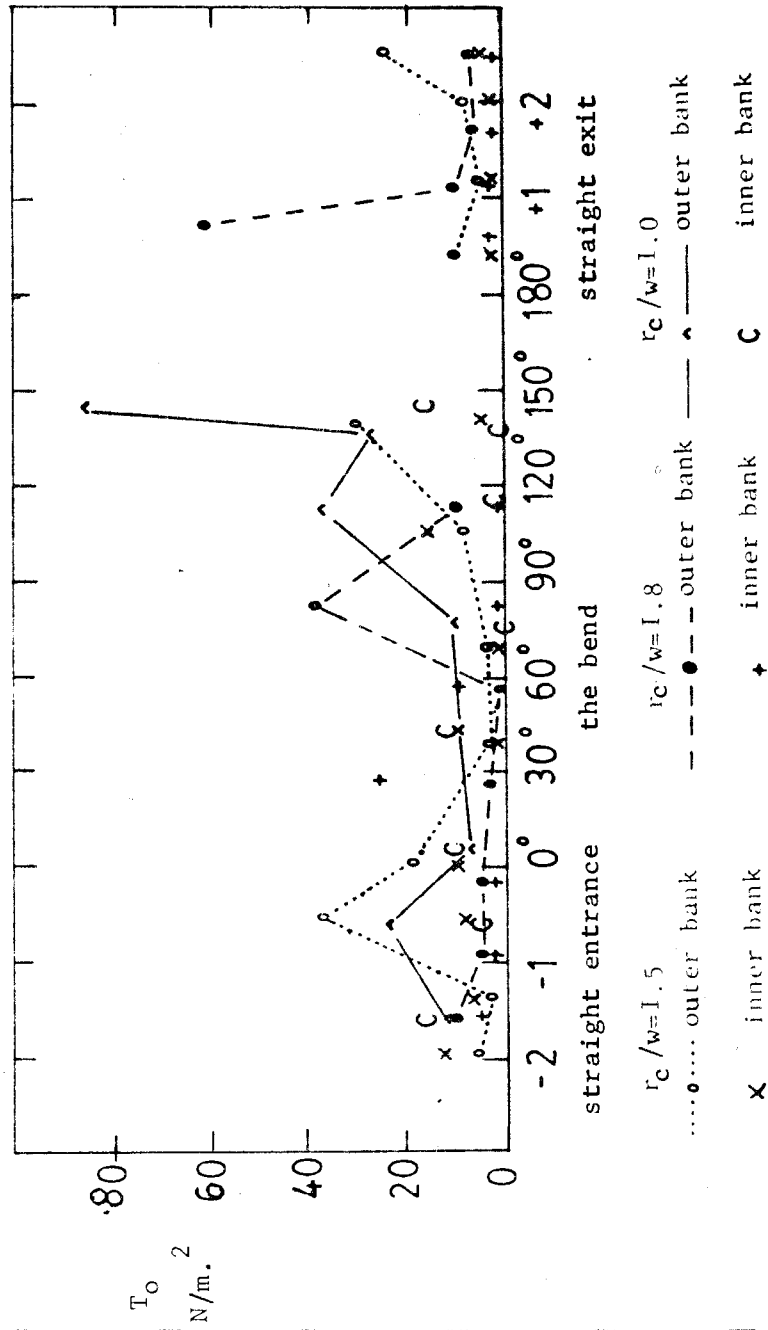


Figure 3.30. The distribution of shear stress along the channel banks. The shear stress along the convex (inner) bank are shown by symbols which are not joined by lines.





60 degrees on alternate banks. The result of such erosion may create a meandering stream with a shorter wavelength than the meandering valley. Such meandering channels have been suggested to be underfit streams. Dury's (1965) manifest underfit and a section of the Red river in Alberta (Government of Mines, Energy and Resources photograph) have shorter channel wavelength than that of the valley; a characteristic that probably develops in wide bends (cf. Tinkler, 1971; Keller, 1972).

In a bend of  $r_c/w=4.0$ , the shear stress distribution is nonperiodic. The maximum shear along the concave bank locate at bend angles of 20, 60 and 130 degrees and at 40 and 116 degrees along the convex bank. There is more than one pool along the bend (cf. Leopold and Wolman, 1960). The shear stress along the convex bank in bends with  $3.3 < r_c/w < 3.7$  is very low compared to those in  $r_c/w=3.2$  and  $r_c/w > 4.0$ ; but near the concave bank it is periodic every 40 degrees instead of every 60 degrees in bends with  $r_c/w=4.7$ . The pools locate every 40 degrees also. The magnitude of shear stress of a bend with  $r_c/w=3.2$  is equal along both banks through the rest of the bend and the bedforms are barely perceptible (see also Ippen and Drinker, 1962). The maximum shear stress along the concave bank in  $r_c/w=2.6$  locates at 27, 145 and 180 degrees of the bend while the one near the convex bank is low except at the bend entrance. The maximum shear stress in  $r_c/w=2.2$  is periodic between 30 to 40 degrees as in  $r_c/w=3.3$ .

The shear stress along the convex bank in  $r_c/w=1.8$  is high and periodic every 1.0m along the entrance and exit portions. The distribution in  $r_c/w=1.0$  and 1.5 is irregular because of flow separation zones along both banks.

In general, bends of  $2.6 < r_c/w < 4.0$  support considerable shear stress at the bend apices. In bends with  $r_c/w < 2.0$ , the magnitude of shear stress along the concave bank decreases but increases for those of  $r_c/w < 1.8$ . In addition, there is a general decrease of shear stress in all bend zones between 30 and 90 degrees along the concave bank (cf. Ippen and Drinker, 1962). Bagnold (1960) argued that shear stress decreases rapidly along the concave bank in a bend of  $r_c/w = 2.0$  which coincides with the critical curvature ratio at which resistance to flow becomes minimum. Figures 3.29 and 3.30 are in support of Bagnold's findings.

### 3.3.3 Summary

The shear stress distribution near the channel banks of bends with  $4.7 > r_c/w > 2.2$ , and also in a straight channel is periodic every 3 to 4 channel widths ( equivalent of 45 to 60 degrees in bends). The distribution of boundary shear along the straight channel and in bends with  $2.6 < r_c/w < 3.3$  are of opposite pitch, while those with  $r_c/w = 3.2$  and 3.3 are periodic every 60 degrees and their bedforms are barely perceptible (see figure 3.31). The present results concur with those of Bathurst et al;

(1979) who observed that, without strong double vortices, the shear stress pattern becomes too diffuse (cf. Figure 3.27). Generally, high relative shear stress locates along the convex bank at the bend entrance and along the concave bank in  $2.6 < r_c/w < 4.0$  and  $r_c/w < 1.8$ , but decreases in a bend with  $r_c/w = 2.2$  along the concave bank.

Variation in the location of the maximum shear stress along the concave (outer) bank was not totally unexpected. Several natural river bends have planforms that are asymmetrical and more complex than that suggested by the proponents of the "sine-generated" planforms (Langbein and Leopold, 1966). Keller (1972) notes that the processes that are operative in creating meander bends paradoxically are the same as those that produce straight reaches. The present study correlates the factors that increase the bend path length with the decrease of the intensity of the secondary flow along the bend zone between 60 and 120 degrees. It is this bend zone that forms the straight segment of the T-bend geometry (cf. Hickin, 1974).

#### 3.3.4 The Distribution of Mean Shear Stress in Single Bends

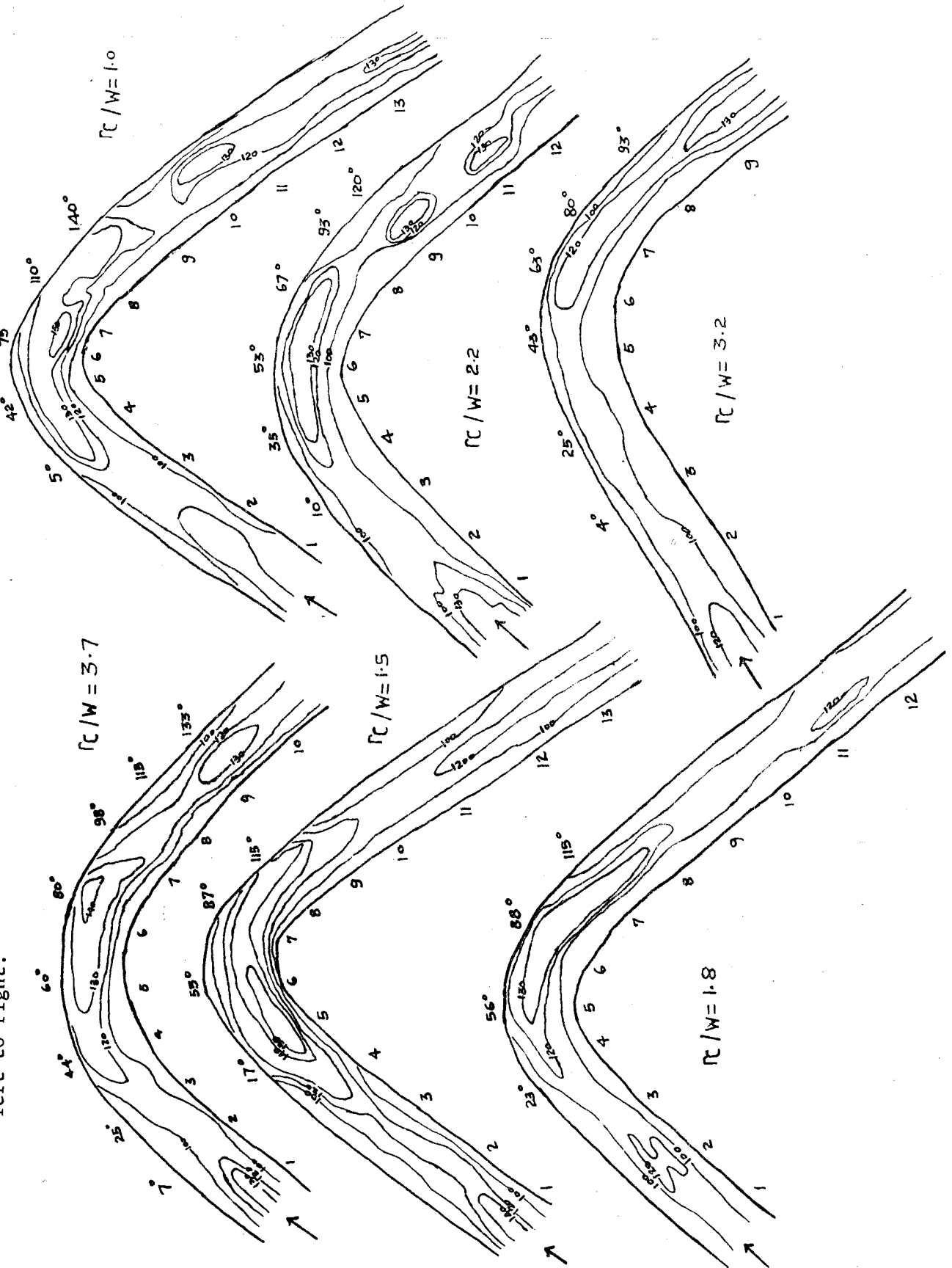
The distribution of mean shear stress in open-channel bends of  $1.0 < r_c/w < 4.7$  depicts various bend effects on entry and exit portions (Van Dyke, 1970). Ippen and Drinker's (1962) figures show that the location of maximum shear stress ratio shifted slightly upstream when the bend curvature was decreased from

$r_c/w=1.6$  to  $r_c/w=1.3$ , but the shear stress ratio was relatively higher and the cross stream asymmetry was barely perceptible for a bend with  $r_c/w=3.6$ . The location of bend sections that have maximum and minimum shear stress values identifies the nature of asymmetry of the longitudinal distribution by tracing the growth and decay of such peaks with variations of bend curvature. A steep decreasing shear stress gradient indicates the imminence or occurrence of flow separation (Choi et al; 1979) while a steep increasing gradient shows the thinning (transitional) of boundary layer flow (Achenbach, 1971). Research in closed conduits with blockage (Ramamurthy and Ng, 1973) and in accelerating cylinders (Lug and Haussling, 1974) shows that increased blockage causes an early flow transition because of vortex shading which causes low shear stress.

Figure 3.31 shows the character of channel bed deformation of selected single bends. Each map was prepared by plotting depth measurements on the outline map of each bend; the contours were smoothed to remove minor irregularities.

The variation of shear stress in a straight channel has a maximum standard deviation of 10% from the average. Figures 3.32 and 3.33 show that the shear stress rises steadily in bends of  $r_c/w=2.6$ , 1.8 and 1.0 because of long uninterrupted development of the boundary layer while those of  $r_c/w = 1.5$ , 2.2 and  $r_c/w > 3.2$  rise steeply to a maximum value 3.0m downstream of the settling well (cf. Ippen and Drinker, 1962). The steep rise along the bend entrance is caused by an early transition to parabolic flow

Figure 3.31 Channel bed deformation characteristics of selected single bends. Flow direction is from left to right.



to forced vortex flow as shown in Table 3.1. The minimum shear stress locates along the bend zone between 40 and 80 degrees (compare to 60 and 120 degrees in Dietrich et al; 1979). The zone of minimum shear stress along the bend zone between 30 and 60 degrees locates where the secondary flow has a maximum value (Hawthorne, 1951; Muramoto, 1967; Einstein, 1972; Rowe, 1970). It will be recalled that downstream of a bend angle of 60 degrees is where a secondary spiral rotating in an opposite sense to the primary one develops. The superelevation and the location of a pool at 60 degrees may also act in concert to decrease shear at the bend apex (cf. Shukry, 1949).

The differences that exist between the shear stress distribution for each bend curvature show the nature of energy dissipation in some regions and not in others. The mean shear stress distribution in  $r_c/w=4.7$  decreases at the bend entrance until 10 degrees, then increases steadily until 32 degrees. By tightening the bend to  $r_c/w=4.0$ , the mean shear stress increases along the bend entrance, levels to a plateau at the bend axis before it decreases towards the exit.

In a bend with  $3.2 > r_c/w > 3.7$ , the first peak of maximum shear stress migrates upstream and the subpeak increases its magnitude as the curvature decreases. For a bend of  $r_c/w=3.2$ , the subpeak has a greater amplitude than the primary peak. The first peak locates along the bend zone between 20 and 40 degrees and a sub peak locates between 80 and 100 degrees. The shear

Figure 3.32. The distribution of mean shear stress in bends with  $4.7r_c/w > 2.6$ .

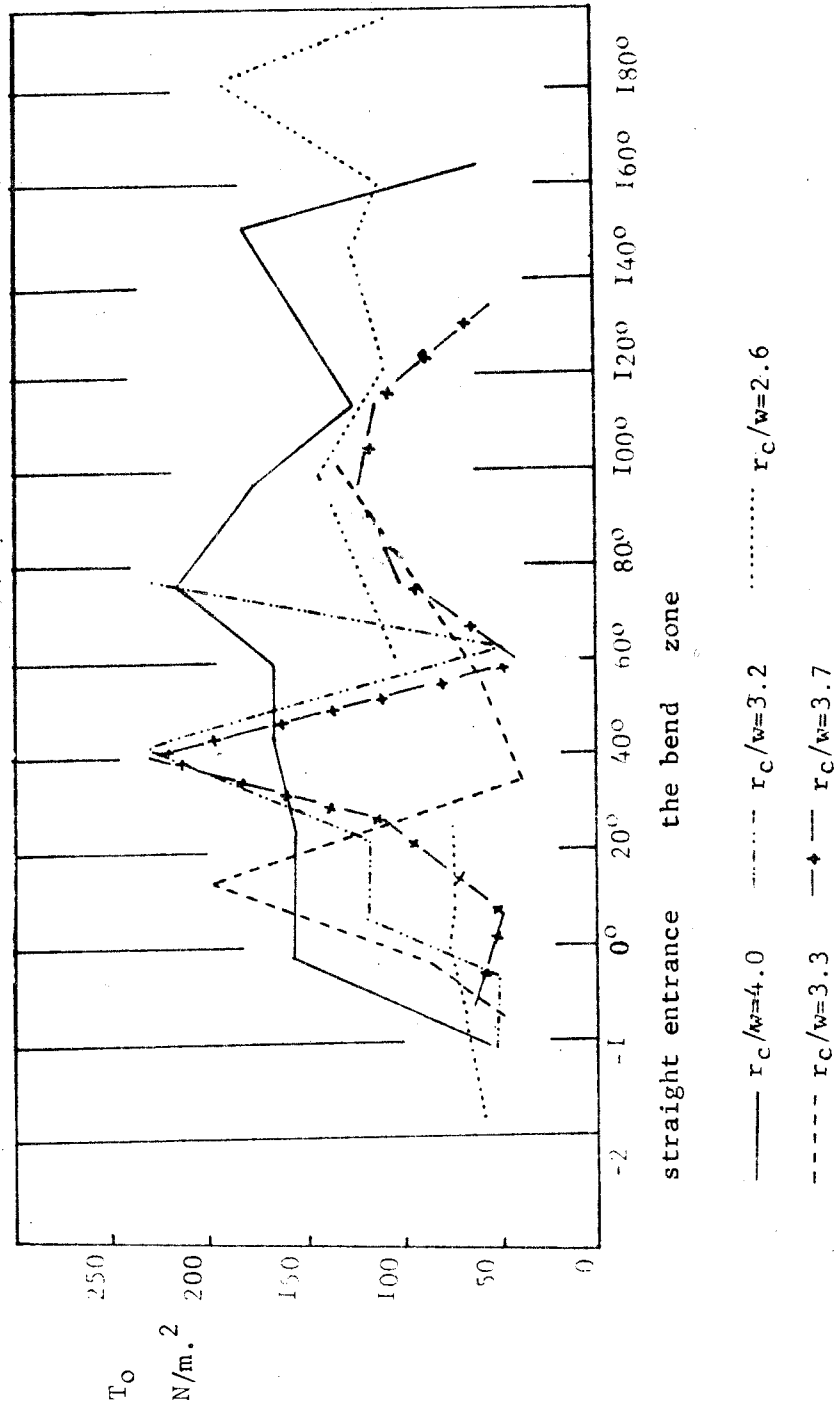
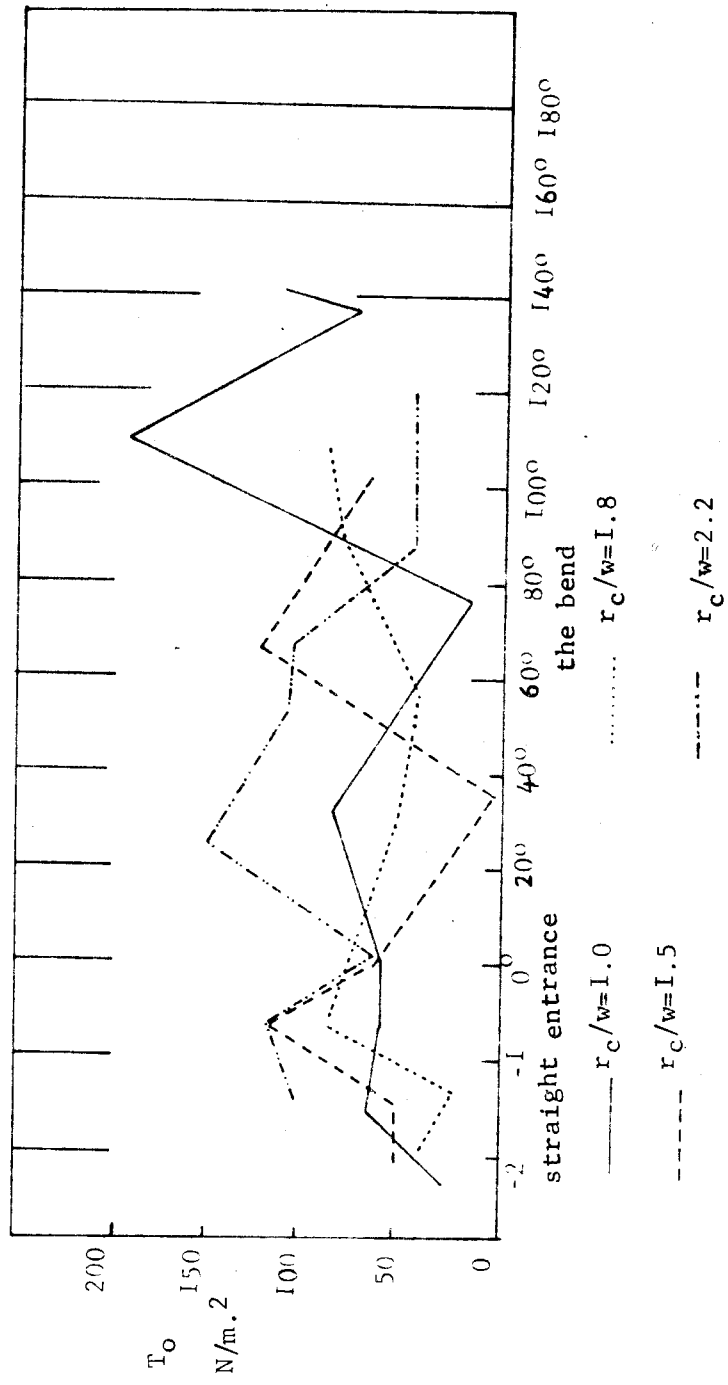


Figure 3.33. The distribution of mean shear stress in bends with  $1.0 < r_c/w < 2.2$ .





distribution in a bend of  $r_c/w=2.6$  is similar to that in  $r_c/w=4.0$  except at the bend entrance along which the shear stress is relatively lower. The mean shear stress distribution in a bend with  $r_c/w=2.2$  skews upstream of the bend apex; the maximum locates at the bend entrance and at 30 degrees but the shear distribution becomes rather uniform in  $r_c/w=1.8$ . The primary peak in  $r_c/w=1.0$  migrates downstream to lie between 80 and 130 degrees.

The shift of the location of maximum shear stress discussed above is in agreement with the pattern observed in many model bends (cf. Ippen and Drinker, 1962) and to those behind bluff bodies (cf. Ramamurthy and Ng, 1973). However, the present study also shows that the transition zone shifts upstream of the bend axis upto a limit in a bend with  $r_c/w=2.2$ , stabilises in that of  $r_c/w=1.8$  and finally shifts downstream in bends with  $r_c/w<1.8$ . In other words, the relationship is nonlinear and has a threshold behavior in bends with  $2.2 < r_c/w < 1.8$ .

The location of maximum and minimum shear stress points and flow separation zones are shown in Table 3.3. Some bends which have two or more peaks are included for the sake of completeness. The flow separation zones were identified from the diagrams of isovel patterns because the shear drop, in some bends, resulted from secondary flow advection. These flow separation zones locate at approximately 35 degrees of bends with  $r_c/w=3.3$  and 4.7; this suppresses the formation of free

Table 3.3. The location of minimum and maximum shear stress and flow separation zones

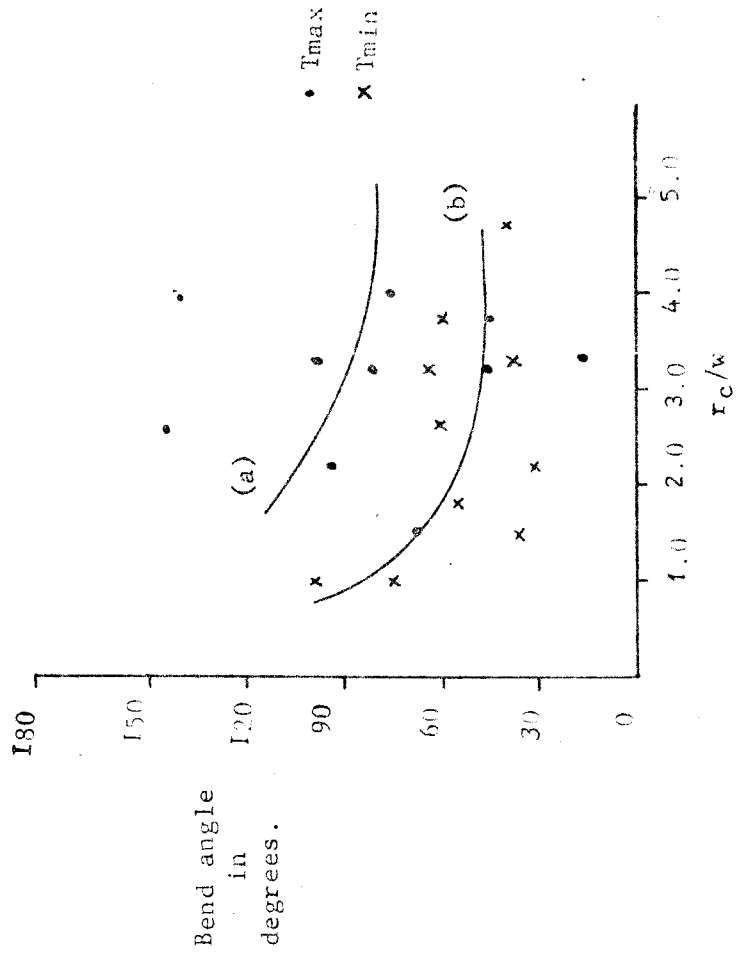
$r_c/w$	$F_n$	$T_{min} (0^\circ)$	$T_{max}(0^\circ)$	flow separation ( $0^\circ$ )	$rc < (0.5 + 13 F_n)^{**}$
1.0	0.2	75	110	75; 135; SE 10	3.1
1.5	0.2	35	67	35; 105	3.1
1.8	0.2	57	n/a	57; 83; 115	3.1
2.2	0.23	30	94	n/a	3.5
2.6	0.23	60	30; 135	n/a	3.5
3.2	0.28	63	45; 80	SE 9	4.1
3.3	0.2	37	15; 98	37	3.1
3.7	0.2	60	44	60; SE 10	3.1
4.0	0.24	n/a	75; 150	n/a	3.6
4.7	0.2	43	SE 8	SE 8	3.1

Nb. SE1 means straight entrance portion of the bend.  
SE2 means the straight exit portion of the bend.

n/a could not be identified from the diagrams.

\*\* source (Leeder and Bridges, 1975).

Figure 3.34. The location of bend sections at which the shear stress has maximum and minimum values; the curves marked (a) and (b) depict the best-fit lines for the upstream trend of shear stress points with decreasing bend geometry.



vortex flow. The extent of flow separation also increases from 30 degrees of the bend zone of  $r_c/w=1.8$  to occupy between 60 and 70 degrees of bends with  $r_c/w=1.5$  and 1.0 because as the bends become rather tighter, the separated zone entrains more fluid and increases in extent. From Table 3.3, it is noted that the location of the minimum shear stress migrates downstream in bends with  $r_c/w > 3.3$  and 1.5 while it remains stationary in those with  $r_c/w=2.0$  and 2.6. In general, the lengthwise mean shear stress distribution is periodic every 45 to 60 degrees.

Leeder and Bridges (1975), after examining the bend flow structure of intertidal meandering channels in the Solway Firth, England, observed that flow separation occurs in meanders with modest Froude numbers (cf. Leopold et al; 1960; Soliman and Tinney, 1968). Their discriminant curve relating  $r_c/w$  to Froude number may be expressed in the form of  $r_c < (0.5 + 13 F)$  shown in the last column in Table 3.3. Figure 3.34 shows the location of zones with maximum and minimum values of boundary shear stress. It can be noted that the maximum shear value occurs in a wide range of bend zones. However there appears to be a trend showing the upstream migration of maximum shear points as  $r_c/w$  decreases. These results are in agreement with those of Hooke (1975).

The evidence that the locations of maximum velocity and shear stress near the outer bank (between 30 to 60 degrees and downstream of 120 degrees) likely causes erosion there is consistent with a complex erosional motif (Hickin, 1974).

However, instead of a single orthogonal describing simple phases, several orthogonals may be suggested within one single erosional period in order to create compound bends (cf. Brice, 1973). The formation of additional pools (Lewin, 1972) and decrease of secondary flow, mean velocity and shear stress between 60 and 120 degrees support the need for a complex erosional axis.

Maximum point bar deposition occurs at two zones also; one a little upstream of the bend apex and the other downstream of 120 degrees. The upvalley point bar is probably a result of an oblique sand wave (cf. Dietrich et al; 1979) while that downvalley may be due to reduced velocity and occurrence of flow separation near the convex bank. Models which show that the point bar usually hugs the convex bank downstream of the bend apex (Leopold et al; 1964) and also those that show lateral erosion being unidirectional (Begin, 1982) may need revision (cf. Hickin, 1974).

### 3.3.5 The Distribution of Friction Coefficient

The mean friction coefficient in the present study for bends of  $1.0 < r_c/w < 4.7$  range between 0.19 and 0.34 while that of a straight channel is 0.06. Resistance in a straight channel is 60% less than that in  $2.0 < r_c/w < 3.0$  (cf. Leopold et al; 1960). Resistance to flow (Bagnold, 1960) and shear stress (Varshey and Garde, 1975) increase rapidly in  $r_c/w < 1.5$  and  $2.0 < r_c/w < 3.0$ . The

ratio of friction coefficients of a straight channel and bends shown in Table 3.4 depicts relatively higher ratios for bends of  $r_c/w=1.5$  and  $4.0$  than for  $1.8 < r_c/w < 2.2$  in agreement with the results of the authors cited earlier. The relationship between maximum friction coefficients and  $r_c/w$  is shown in Figure 3.35. The maximum resistance to flow increases as the bends become rather tighter within the limit  $4.7 < r_c/w < 3.3$ ; drops in  $2.2 < r_c/w < 3.0$  and increases in  $r_c/w < 1.8$ .

Within bend variations are shown by the ratio of maximum and minimum friction coefficients in Table 3.4. The bends with low  $ff_b/ff_s$  ratios have relatively uniform distribution of resistance through out the bend and those with high ratios have localised regions of high resistance. The high ratios also depict the impact of flow reattachment after separation. Bends of  $r_c/w=2.2$ ,  $2.6$  and  $4.0$  have lower ratios; but the ones for  $r_c/w=1.8$  and  $4.7$  are even lower than those for  $r_c/w=3.2$  and  $3.7$ . It has been argued that rivers tend to have uniform distribution of energy and minimise local variation to maintain dynamic equilibrium (Langbein and Leopold, 1966). The bends with  $2.2 < r_c/w < 2.6$  and  $r_c/w=4.0$  therefore satisfies the above criterion.

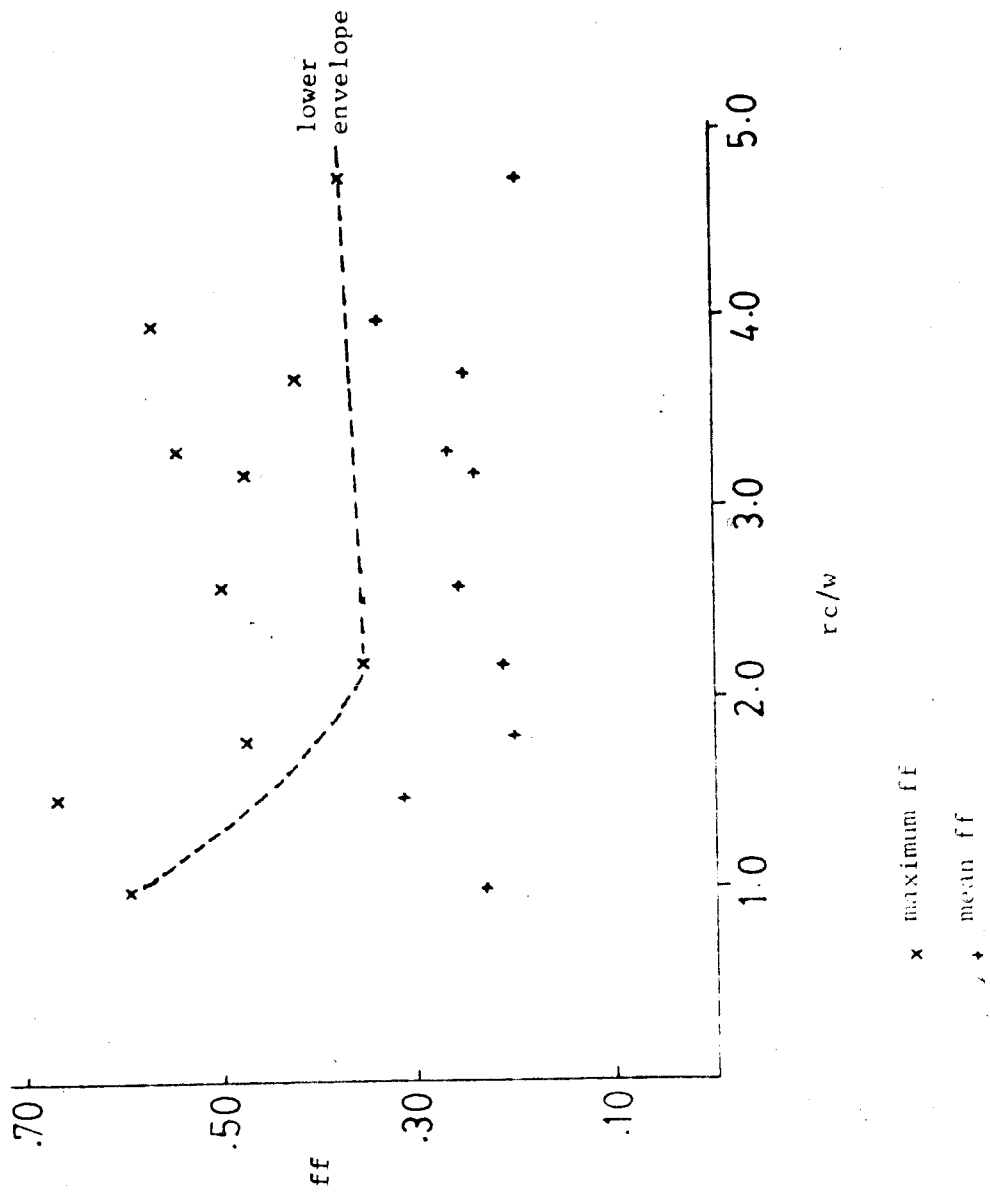
Figures 3.36 and 3.37 show the lengthwise distribution of friction coefficient. The maximum resistance is concentrated upstream of the bend apex in  $3.3 < r_c/w < 4.7$ ; it increases slowly along the bend zone between  $60$  and  $160$  degrees and decreases towards the bend exit.

Table 3.4. The relationship between mean friction coefficients expressed as ratios of the straight channel;  $ff_s=0.06$ .

$rc/w$	$ff_b/ff_s$	$ff_{max} (^\circ)$	$ff_{min} (^\circ)$	$ff_{max}/ff_{min}$
1.0	3.91	110	75; 135	8.29
1.5	5.08	55	17	16.36
1.8	3.24	115	SE8	6.62
2.2	3.25	SE1; 30-67	10; SE11	2.87
2.6	4.30	180; 60	97-145	2.06
3.2	3.92	64; 30	48	4.10
3.3	4.70	15; 98	37-58	3.69
3.7	4.09	44	7; 60	3.49
4.0	5.60	150; 75; 0	116; 168	2.64
4.7	3.16	SE8	43	6.89

Note: SE1 and SE2 means the straight entrance and exit portions of the bends respectively.

Figure 3.35. The distribution of friction coefficients in single bends.





Bends with  $2.2 < r_c/w < 2.6$  and  $3.7 < r_c/w < 4.0$  have resistance to flow distributions that are skewed towards the downstream part of the bend. There are two peaks of maximum resistance at the bend entrance and exit; and the minimum value is between 37 and 80 degrees

The decrease of friction coefficient at the apex of tighter bends may be caused by a decrease of the size of the point bar (cf. Onishi et al; 1976). Because the core of maximum velocity lies more or less near the convex (inner) bank, sediment deposition decrease there. Most of the sediment load in traction is transported downstream while the fines carried in suspension accumulate at the separated zones (cf. Woodyer, 1975). This is in agreement with the notion that tight bends have shorter point bars than wide bends (cf. Hickin, 1969). The present study suggests that reduced rate of lateral migration in  $r_c/w < 2.0$  and  $r_c/w > 3.5$  may be due to a reduction of 'live width' by flow separation. The flared bend widths shown in Figure 3.26 (cf. Prandtl, 1949; Hickin, 1977) and cylindrical vortices sandwiching retarded flow (i.e. C-shaped isovels patterns) inhibit boundary flow separation at the expense of increasing friction in  $r_c/w < 2.0$ . The convex and concave flow separation zones in  $r_c/w = 3.3$  and  $3.7$  respectively probably are thresholds at which the influence of the flared bend widths shift flow deceleration from the inner bank to the outer bank as in those of  $r_c/w < 1.5$  (Table 3.3).

Figure 3.36. The distribution of friction coefficient in bends of  $r_c/w$  2.5. Two examples of skin friction trends in cross flow are included for comparison.

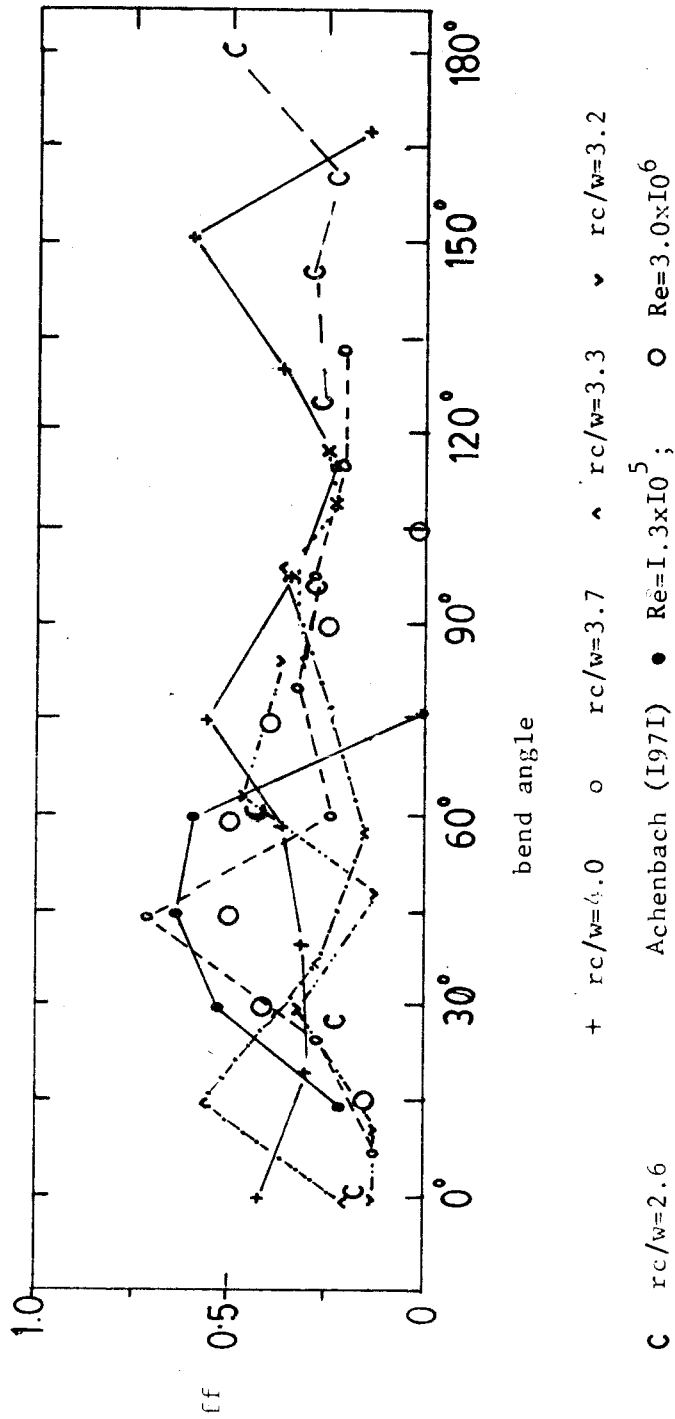
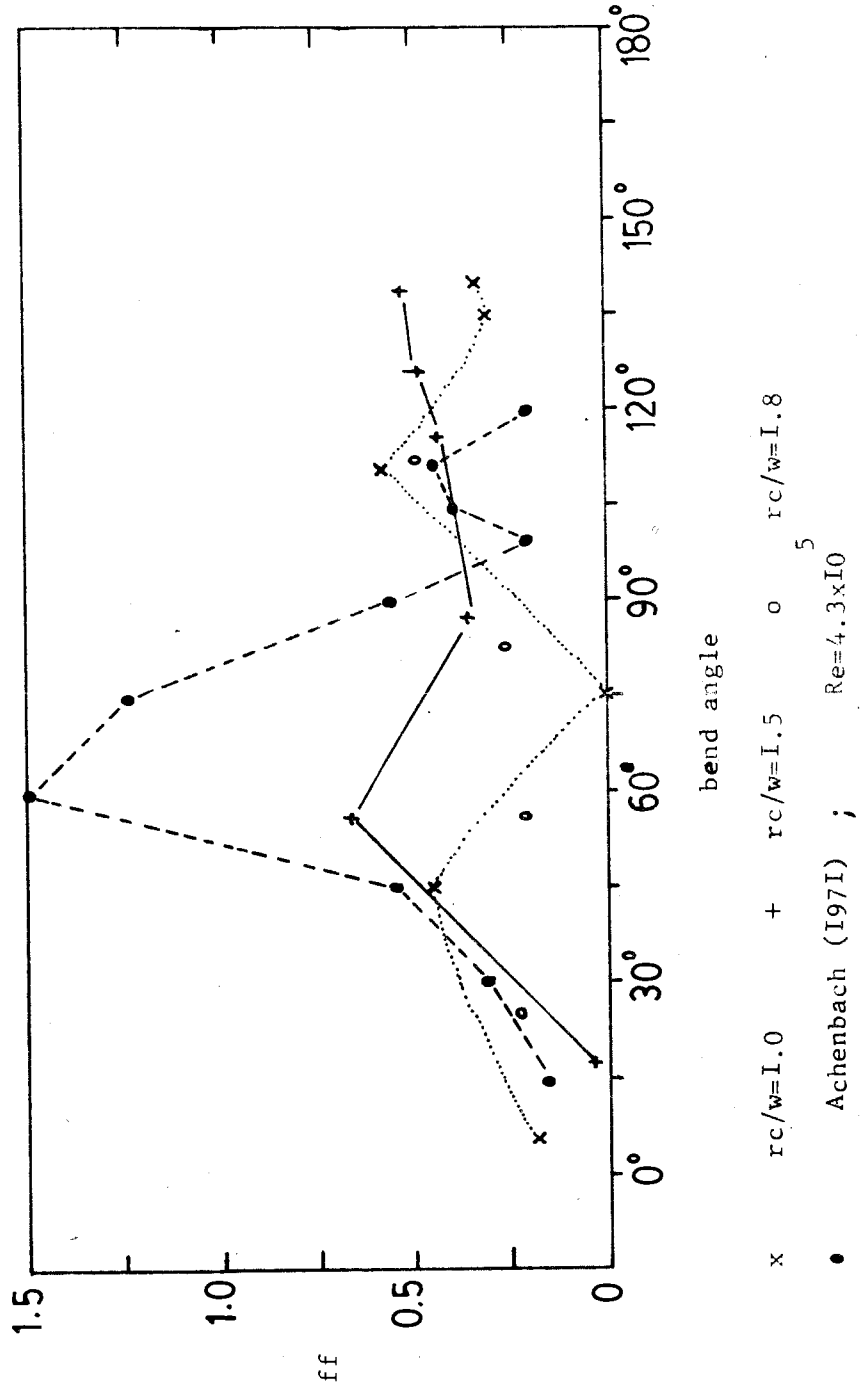


Figure 3.37. The distribution of friction coefficient in bends of  $r_c/w = 2.5$ .  
 Two examples of skin resistance trends in cross flow are  
 included for comparison.



The bends in which resistance to flow increases rapidly are the same as those which have been shown in Figures 3.25 and 3.26 to have no flow separation zones. Leopold et al; (1960), Bagnold (1960), Ippen and Drinker (1962) and Appman (1972) explain the decrease in resistance in  $1.5 < r_c/w < 2.0$  as a response to collapse of convex flow separation zones and the consequent development of large eddies. Unlike Bagnold (1960), Hickin and Nanson (1975) argue that the core of maximum velocity near the concave bank which is responsible for erosion there becomes disrupted by such eddies at  $r_c/w$  approaching 2.0. Flow separation was not observed in bends with  $2.2 < r_c/w < 2.6$  and  $r_c/w = 4.0$ . These differences may be because the Froude number and width-depth ratio of the present model bends are small compared to those cited earlier. Because flow separation can occur in a wide range of  $r_c/w$ , the variation of the Froude number may be an important factor (Soliman and Tinney, 1968; Leeder and Bridges, 1975). As Froude number increases, the boundary between the mainstream flow and the separated flow periodically deforms into large eddies (vortex trails) discussed earlier. But as the high velocity core shifts towards the inner bank, the separated flow is entrained with the mainstream flow to create complex isovel geometry .

The increase of resistance may be associated also with plane bed profiles in a bend with  $r_c/w = 3.3$ . In alluvial rivers, the monotonous increase of velocity as observed in these bends likely will wash out the bedforms to give way to plane bed; resistance to flow ( Simmons et al; 1965) and sediment transport

(Onishi et al; 1976) also will increase. Figure 3.30 shows that the bed profile of  $r_c/w=3.2$  is nearly plane and the distribution of shear stress at a cross section is nearly symmetrical. For these reasons, bends of  $r_c/w=3.0$  have been considered to behave dynamically as straight channels (Soliman and Tinney, 1968; Davies and Sutherland, 1980).

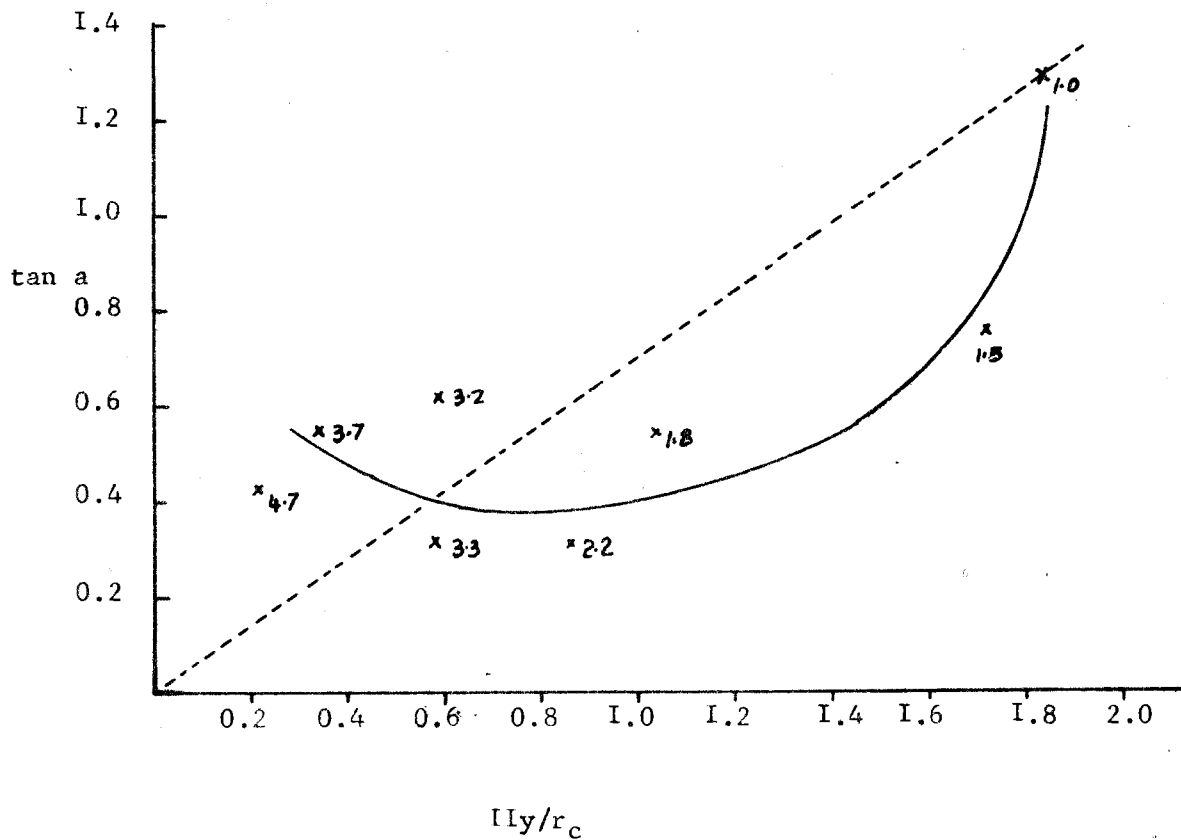
The interaction between secondary flow advection and bedforms determines the magnitude of boundary friction in channels. Rozovskii (1961) expressed the relation between bend geometry and secondary flow using an expression in the form:

$$\tan a = 11(y/r) \dots \dots \dots 3.4$$

Zimmerman (1977), argued that  $\tan a$  is an inverse function of resistance to flow because the bedforms influence the distribution of vertical velocity. The mobilised plane channel bed of  $r_c/w=3.3$  tends to have relatively higher velocity than the other bedforms.

Figure 3.38 shows a comparison between calculated  $\tan a$  using equation 3.4 (shown along the x-axis) and  $\tan a$  based on the maximum difference between the surface and bottom current direction at cross sections between a bend angle of 70 and 105 degrees. The choice of this bend zone is a compromise between those bends with delayed fully developed flow zone and those that have the fully developed flow zone upstream of the bend axis. The curvature ratio of single bends are shown for each plotted point. The figure shows that  $\tan a$  increases with friction coefficient.

Figure 3.38. Comparison between computed  $\tan a$  and the maximum current direction ( $\tan a$  measured).



The dotted line is the perfect identity curve while the solid line is a possible trend line. The numbers beside the marked points are curvature ratios of the bends.

### 3.4 DISCUSSION OF FLOW CONDITIONS IN SINGLE-OPEN CHANNEL BENDS

Detailed measurements of flow conditions have been made in a straight control channel and in single bends of  $1.0 < r_c/w < 4.7$ . The isovel patterns of a straight channel and bend entrances have a characteristic secondary flow towards the corners and towards the water surface at the channel centreline. These flow patterns are typical of the developed turbulent flow in straight rectangular channels. The velocity profiles are parabolic except for a few departures which are contributed by the size and location factors of the bedforms. The secondary flow that moves retarded flow from the bank corners upwards to the surface causes the mean flow to decelerate near the channel banks. As a result of the flow retardation near the channel walls there is a small azimuthal component of cross stream velocity at the centreline as the boundary layer thickness of the channel bed decreases towards the bend entrance.

Towards the bend entrance, the secondary flow from corners moves towards the water surface, but close to the banks. The strength of the spiral increases between the bend entrance to a bend angle of 30 degrees (cf. Prus-Chacinki, 1956; Rowe, 1970) where free vortex locates in  $r_c/w = 3.2$  only. The secondary flow directed towards the surface moves towards the concave bank finally vanishing as cross flow sets in along the bend zone between 30 and 60 degrees. Near the water surface, the secondary

flow converges, depresses the core of maximum velocity below the water surface and diverges near the channel bed. A secondary spiral that rotates anticlockwise to the main spiral develops at approximately 60 degrees near the concave bank near the bed and moves the core of maximum velocity towards the convex bank. This secondary spiral is the one that establishes within the bend as opposed to that which develops along the bend entrance (Shukry, 1949). In  $r_c/w < 2.0$ , the secondary spiral is strong enough to establish parabolic flow. The small variations of the flow development observed are due to changes of  $r_c/w$ .

The relative locations of the free and forced vortices migrate upstream of the bend axis as  $r_c/w$  decreases (cf. Figure 3.37); a pattern which likely is responsible for generating different phases of lateral migration in rivers. Free vortex and parabolic flow maintains a logarithmic distribution of vertical velocity while forced vortex flow tends to increase the velocity near the bed. This difference may be explained by the complementary effect of decreasing radial acceleration in a free vortex flow and increasing advective acceleration for parabolic flows (cf. de Vriend, 1980). The interaction of radial and advective accelerations decreases the magnitude of the mean velocity also. The mean velocity decreases to a minimum value between 60 and 120 degrees. Muramoto (1967) argues that this is the bend region where there is a mutual interference between the mainstream velocity and the secondary flow (transitional zone). It is this region also that generates the longitudinal



oscillations that manifest as bubbles which roll up but remain entrained by the mainstream flow. The causes of such roll-ups have been studied in flows behind bluff bodies but not in rivers.

The transverse oscillation is the cause of velocity and shear stress reflectivity (Levliansky, 1955; Desaulniers and Frenette, 1973; Engelund and Skovgaard, 1973), and probably is responsible for selective and alternate bank erosion in rivers. The distribution of velocity and shear stress near the banks that are of opposite pitch represents bends in which the core of maximum velocity shifts with shorter wavelengths than that of the bend geometry (cf. Dury, 1965) and therefore intensify thalweg wandering. The ones that have the same pitch likely are responsible for widening the channel because the high velocity is attenuated towards the bed near both banks. If erosion of the channel banks continue uncontrolled, the channel may begin to braid.

The velocity and shear stress distribution for bends with  $r_c/w > 3.7$  are periodic every 45 degrees while those of  $r_c/w = 3.0$  are periodic every 60 degrees. Because of this sensible constance of the periodic flow, the core of maximum velocity locates near the inner bank in bend apices of  $r_c/w < 2.0$  and the fully developed flow zone locates downstream of the bend itself. Alternatively, if the core of maximum velocity locates near the concave bank, the fully developed flow locates there also. There appears to be no reason why the fully developed flow zone should

locate downstream of the bend apex in a wide range of curvature ratios (cf. Gotz, 1980).

The longitudinal distribution of shear stress is one approach by which the behavior of the boundary layer can be examined. In bends with  $3.7 < r_c/w < 3.0$ , there are two shear peaks at 40 and 90 degrees of the bend and each peak represents the point where the high velocity core is located near the bed. These points represent also the location of the bend pools. The amplitude of the first peak decreases while that of the second peak increases as the curvature ratio decreases. In a general manner, the mean shear stress decreases to a minimum value along the bend zone between 60 and 120 degrees, probably because of the presence of a transitional flow. These transitional flows are associated with several pairs of vortices in contrast to a single vortex at the fully developed flow zone. Similar trends have been observed in closed conduits with cross flow and vary with Reynolds number (see for example Achenbach, 1970; Browand, 1966; Wang, 1970).

The decrease of shear stress and friction to flow in bends of  $1.8 < r_c/w < 2.6$  likely are due to parabolic flow that occurs along most of the bends while those which have higher shear stress values have either strong vortices at the bend entrance ( $r_c/w > 3.0$ ) or towards the bend exit ( $r_c/w < 1.8$ ). Leopold et al (1964) thought that because the apices are deeper than the inflections, more energy is conserved there. The present results supports this contention but restricts it to those bends with

$1.8 < r_c/w < 2.6$  only (Bagnold, 1960).

The flow conditions that have been described above have some implications for lateral erosion in rivers. The bed-divergent spirals cause the mainstream velocity to increase and causes channel incision (cf. Leliavsky, 1955). The high momentum fluid near the surface is transmitted below the water surface and depresses the high velocity core towards the channel bed. On the other hand, the bed-convergent spirals decelerate the mainstream flow and causes deposition at the channel centreline. These spirals interact and are maintained by pool and riffle sequences (cf. Hey and Thorne, 1975).

## CHAPTER 4 EXPERIMENTAL RESULTS OF CONSECUTIVE BENDS WITH CONSTANT UPSTREAM BEND GEOMETRY

### 4 VELOCITY DISTRIBUTION, CURRENT DIRECTION AND VORTEX INTERACTION

#### 4.1 Introduction

The preceding discussion of single bends demonstrates that secondary flow advection at the centreline shifts towards the surface close to the banks at the bend entrance and causes shear stress and friction to increase there. The intensity and rate of secondary flow and magnitude of shear stress near the banks increase in bends with  $r_c/w > 2.6$  and  $r_c/w < 1.5$ , but decrease for those with  $r_c/w = 2.6$  and  $1.0$ . The rate at which high momentum is redistributed between the inner bank at the bend entrance and the outer bank downstream of the bend apex varies with the onset of a secondary spiral that develops along the bend zone between 40 and 80 degrees. These variations likely cause erosion on different segments of the bend.

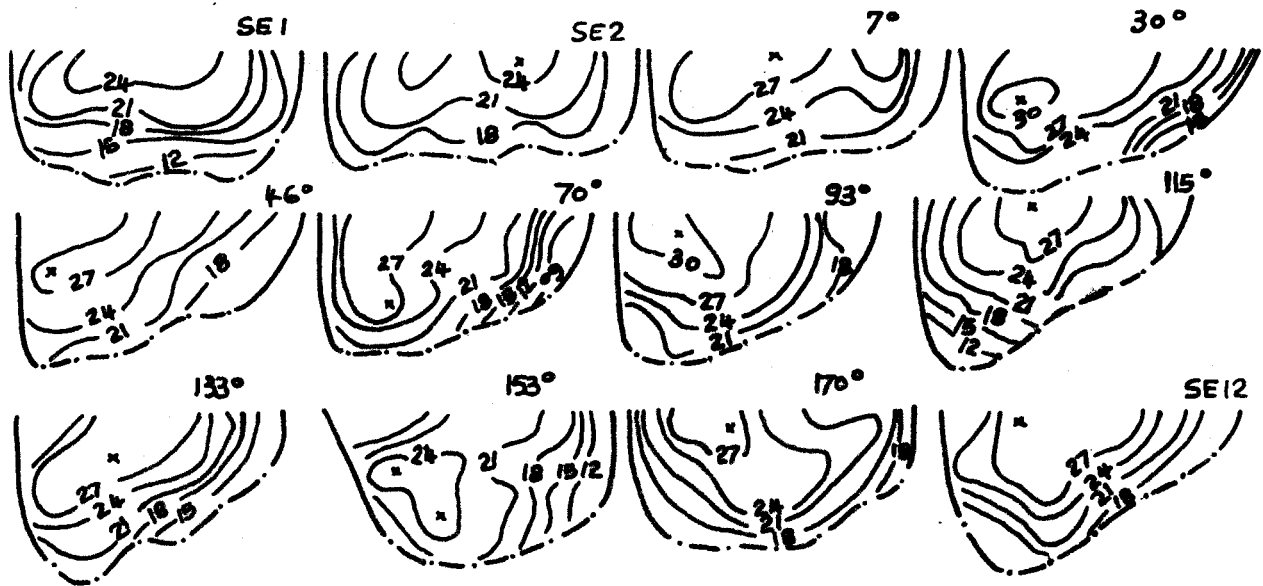
This chapter discusses the flow development in a series of paired bends in which the upstream bend geometry is constant while that in the downstream bends varies. The aim is to

identify the manner in which upstream bend flow conditions are transmitted downstream thus influencing flow development there. Section 4.2 discusses the distribution of mean velocity while section 4.3 discusses the variation of shear stress and friction to flow. The upstream bends are expressed as  $r_c/w_{us}$  while  $r_c/w_{ds}$  represents the downstream cases.

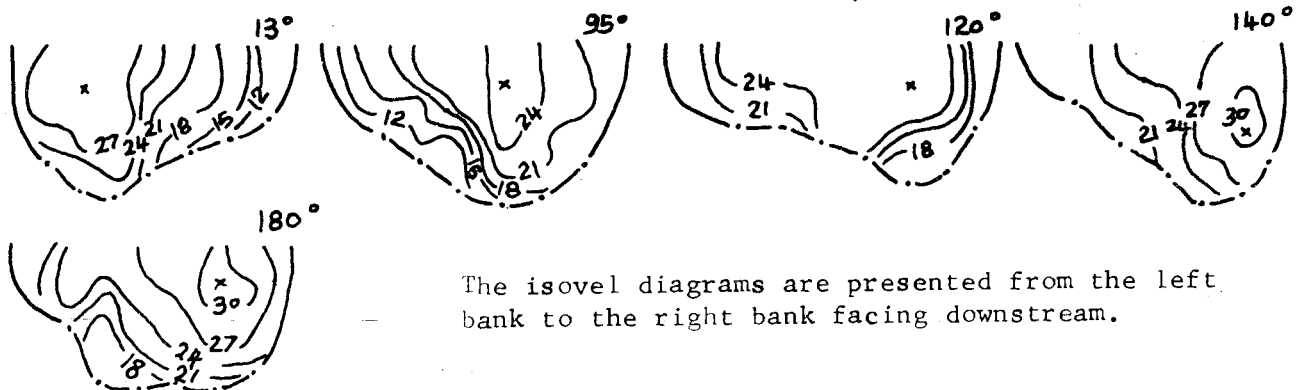
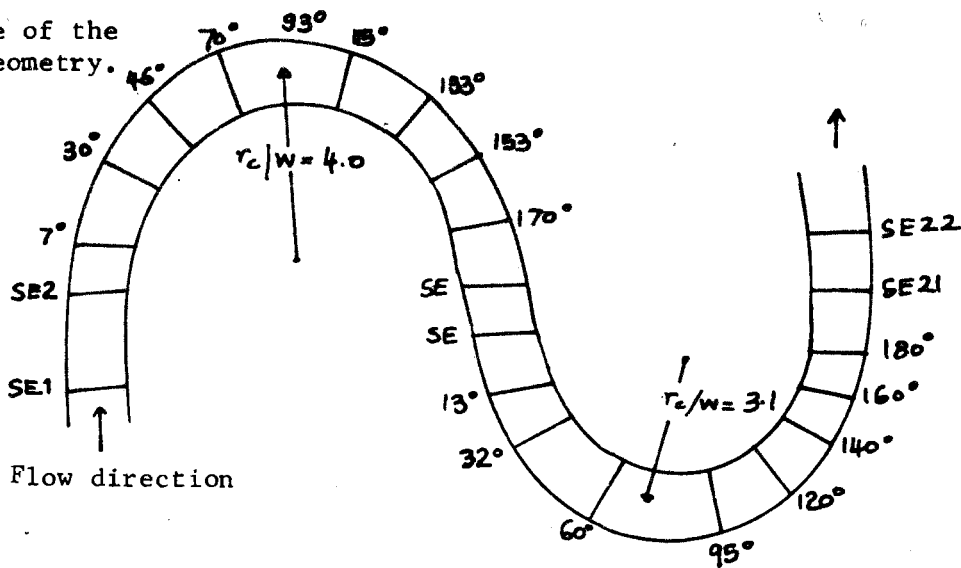
#### 4.1.2 The Isovel Patterns and Current Direction in Consecutive Bends of $r_c/w_{us}=4.0$ and variable $r_c/w_{ds}$

Figures 4.1 to 4.3 show selected isovel patterns in this run of experiments. The isovel patterns display typical characteristics of turbulent flow along the bend entrance. The secondary flow is directed towards the section corners as well as towards the water surface at the centre of the channel. The intensity of the secondary flow that is directed towards the inner bank, however, decreases at the bend entrance and this trend continues into the bend. At a bend angle of 30 degrees, the secondary flow advection directed towards the outer bank increases while that towards the inner bank is suppressed showing the influence of cross stream momentum transfer. Further in to the bend, the secondary spiral that initiates within the bend zone develops at 70 degrees, and the initially parabolic flow translates to a forced vortex flow at 90 degrees (Table 4.1).

Figure 4.1. Selected isovel patterns in consecutive bends with  $r_c/w_{us}=4.0$  and  $r_c/w_{ds}=3.1$ . The isovels are shown in  $cm. s^{-1}$  and the symbol x represents the location of the maximum velocity measurement.



Outline of the bend geometry.



The isovel diagrams are presented from the left bank to the right bank facing downstream.

Figure 4.2. Selected isovel patterns in consecutive bends with  $r_c/w_{US}=4.0$  and  $r_c/w_{DS}=2.0$ . The isovels are shown in cm, s<sup>-1</sup>. The isovel diagrams are presented from the left bank to the right bank facing downstream.

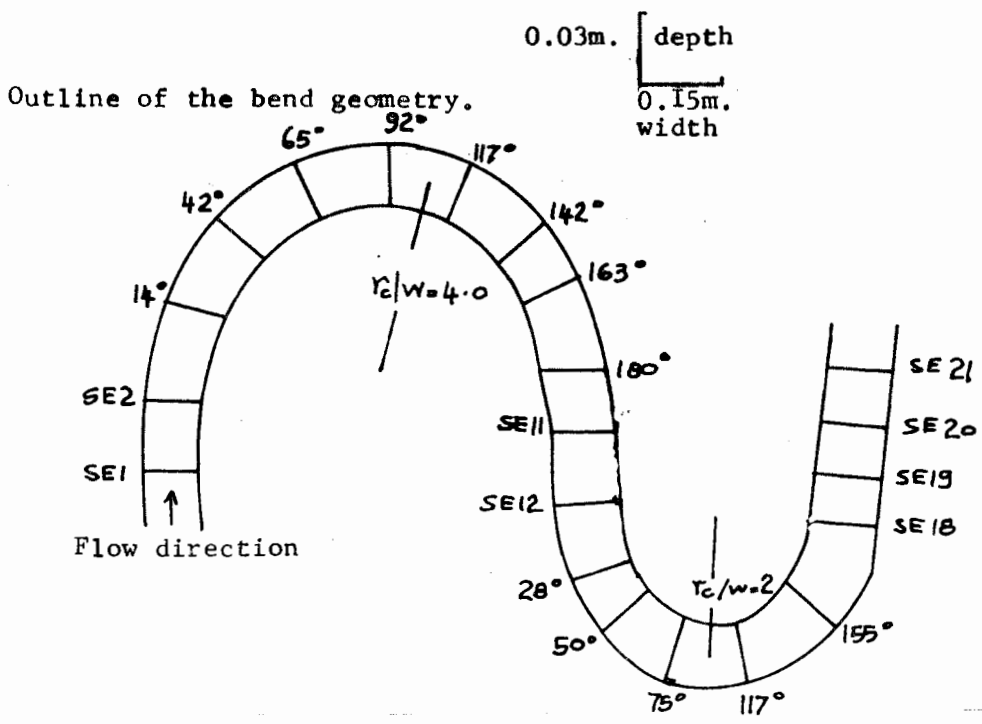
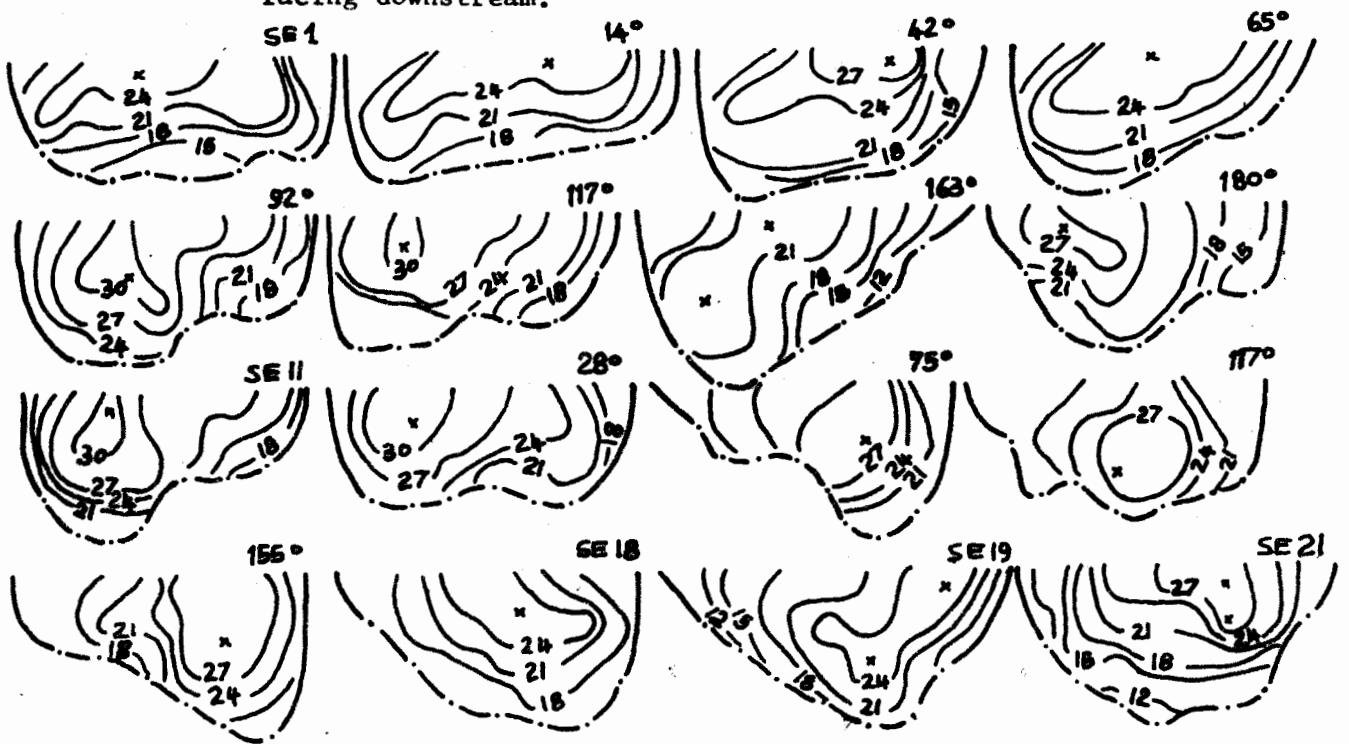
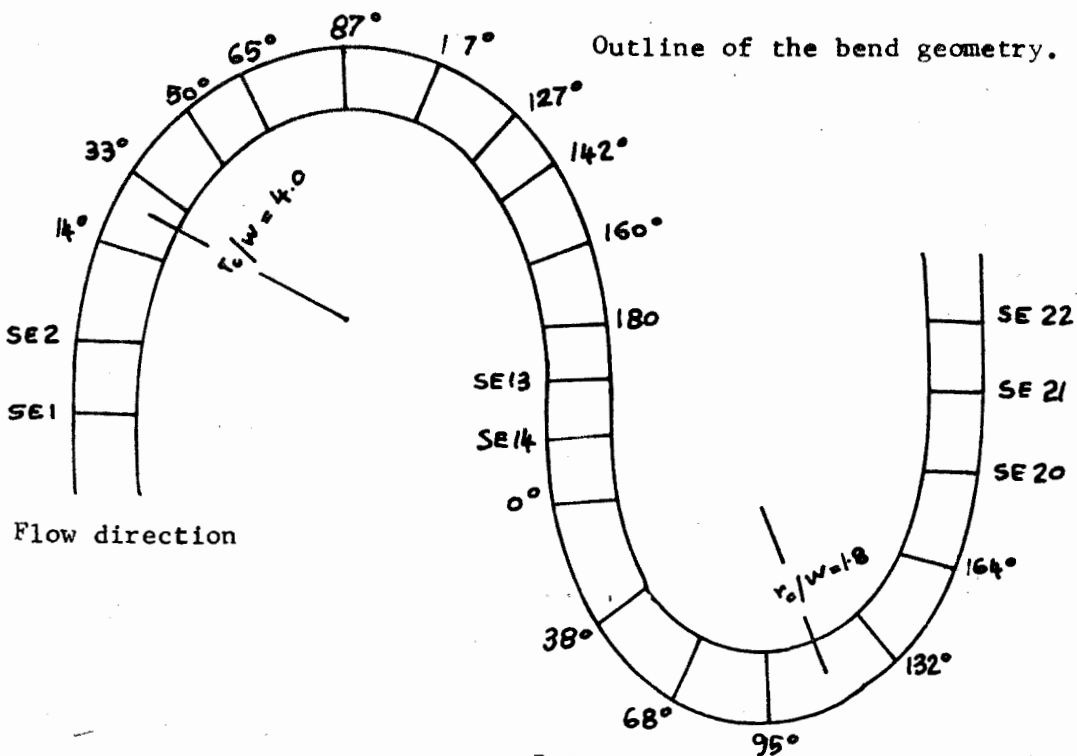
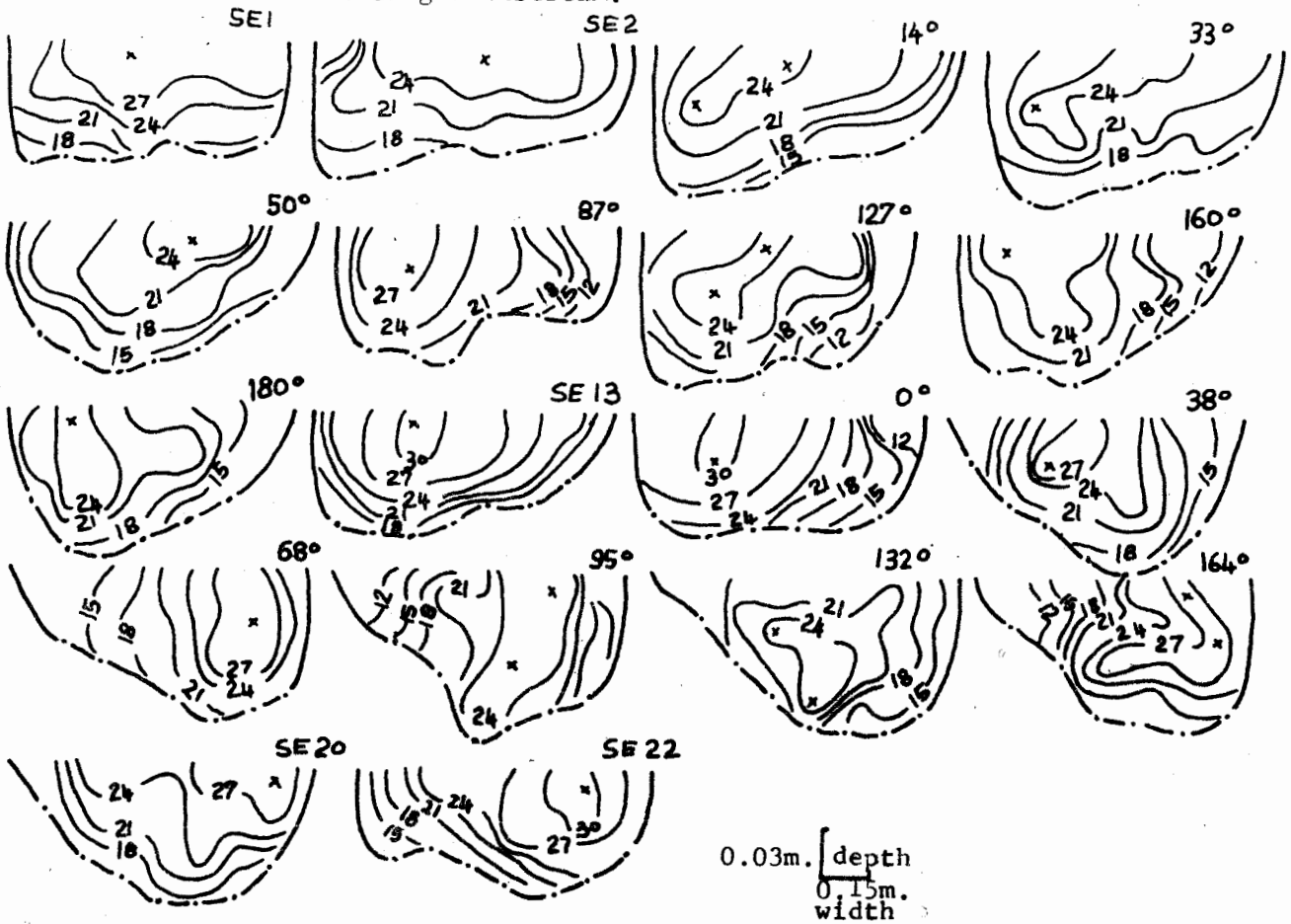


Figure 4.3. Selected isovel patterns in consecutive bends with  $r_c/w_{us}=4.0$  and  $r_c/w_{ds}=1.8$ . The isovels are shown in cm. s<sup>-1</sup>

The isovel diagrams are presented from the left bank to the right bank facing downstream.





Within the bend zone between 115 and 130 degrees, the forced vortex reverts to parabolic flow, reflecting the growth of that second spiral (cf. Shukry, 1949). The maximum magnitudes of the forced vortex locate at 70 and 133 degrees, but decreases downstream as the core of maximum velocity shifts towards the channel bottom. A parabolic flow profile exists along the 1.33m straight reach at the inflection between the two bends.

The cross over in the flow structure locates at the bend entrance. Along the downstream bend, the core of maximum velocity remains along the inner bank (free vortex flow) while transverse secondary flow directs slow moving flow along the concave (outer) bank to about 13 degrees of the bend angle. The free vortex reaches its maximum value at 13 degrees, after which it decreases downstream. The current direction is less than 17 degrees until a bend angle of 60 degrees where the free vortex flow translates to a forced vortex flow (cf. Bluck, 1971; Bridge and Jarvis, 1976). However, the forced vortex flow does not persist for long because a second spiral forms near the channel bed and shifts the core of maximum velocity towards the inner bank at 140 degrees (Callander, 1978). There appears to be no carry over of the upstream bend effects to the downstream bend since a parabolic flow profile is obtained along the inflection of the bend. The development of the secondary spiral near the channel bed likely delays the core of high velocity from shifting towards the concave bank. The core of maximum velocity remains at the centre of the channel downstream of the bend axis

along the second bend in a manner likely to develop the transitional facies observed in Jackson's (1975) study.

Flow development in a bend of  $r_c/wus = 4.0$  and  $r_c/wds = 2.0$  and 1.8 shows remarkable similarities with those along the upstream bend in Figure 4.1 except for the increased extent of the parabolic flow at the bend entrance and the downstream migration of transitional flow. Table 4.1 shows the vortex flow interaction, each vortex being separated by a cross over. The transverse secondary flow depresses the core of maximum velocity towards the bottom and the outer bank at 32 degrees in a bend with  $r_c/wds = 2.0$  much earlier than in that with  $r_c/wds = 3.1$ , and displays a parabolic rather than a forced vortex flow. This parabolic flow extends the bend zone between 55 and 115 degrees, then transforms to a forced vortex flow. The forced vortex has a maximum strength ( $t = 0.26$ ) at 155 degrees and then it decays to a parabolic flow along the exit portion. In other words, tightening the downstream bend from  $r_c/wds = 3.1$  to 2.0 weakens the forced vortex along the bend zone between 55 and 115 degrees.

The free vortex contracts to 30 degrees and weakens in  $r_c/wds = 1.8$  because the high velocity core that locates near the convex bank rapidly shifts towards the concave (outer) bank. As a result, the forced vortex replaces parabolic flow at the bend apex in  $r_c/wds = 2.0$ .

TABLE 4.1

The bend flow development and vortex interaction in consecutive bends with  $r_c/w_{us} = 4.0$  and variable downstream bend geometry (3.1, 2.0 and 1.8).

$r_c/w$	SE1 0°	30°	60°	90°	120°	150°	180°	SE2 0°	30°	60°	90°	120°	150°	180°	SE2
4.0/ 3.1	parabolic		Forced vortex .33		parab. Forced vortex .32			parabol.	Free vortex -.44		Forced vortex .21		Free vort. -.15		Forced vortex
4.0/ 2.0	Parabolic flow			Forced vortex .23					Free vort. -.42		Parabolic flow		Forced vortex .26		Forced vortex
4.0/ 1.8	Parabolic Flow			Forced vortex .38					Free vort. -.37				Forced vortex .45		T

\* The numbers below are the maximum value of  $t$  in the equation  $\bar{V} = k r^t$ . SE1 and SE2 represent the straight entrance and exit portions of the bend respectively. T represent a transitional flow.

Because the bend is tight, the isovel patterns between 95 and 164 degrees have two spirals rotating anticlockwise in a manner not unlike the flow in a horse-shoe vortex.

#### 4.1.3 Summary

The isovel patterns along a constant bend of  $r_c/wds=4.0$  are reasonably consistent for different runs with variable  $r_c/wds$ . The secondary flow advection towards corners at the straight entrance lies near the outer bank at 30 degrees in Figure 4.1, but the intensity decreases with curvature ratio. With a decrease of  $r_c/wds$ , the secondary spiral near the bottom migrates upstream to 14 degrees in Figures 4.2 and 4.3. The elimination of parabolic flow along the inflection preceding  $r_c/wds=2.0$  possibly is the effect of the downstream bend transmitted to the inflection region. But as observed in single bends, the strength of forced vortex flow declines between 80 and 130 degrees due to the development of a secondary counterrotating spiral.

There is transitional flow every 30 degrees in a bend with  $r_c/wds=3.1$ , but its extent decreases as  $r_c/wds$  declines. The fact that free vortex flow decays earlier in  $r_c/wds < 3.0$  is consistent with the observation that the transition zone becomes correspondingly much longer in tight bends (cf. Ippen and Drinker, 1962). The core of maximum velocity depresses towards the bottom at 90 degrees and rotational flow associated with

horse-shoe vortices dominates from 90 to 140 degrees of the bend. The forced and free vortices between 60 and 120 degrees in Figure 4.1 are eliminated completely in Figure 4.3 probably because  $r_c/wds$  is rather tighter.

The velocity distribution in open-channels determine the nature and mode of lateral erosion, assuming geological controls are uniform (Schumm, 1977). A bend with  $r_c/wds=3.1$  may migrate in a complex T-bend system (Hickin, 1974) because the transitions between vortices are 30 degrees, far closer than the inflection in the bend geometry. Since the inherited free vortex is strong and parabolic flow dominates the bend axis,  $r_c/wds=2.0$  will experience erosion along the convex bank at the bend entrance and along the concave bank at the bend exit (cf. Kondrat'yev, 1968), giving rise to a translational mode of lateral migration. A bend with  $r_c/wds=1.8$  will experience expansion and translation because the extent of the free vortex is short and the forced vortex is strong around the bend axis. The secondary spiral that develops at the bend entrance is responsible for weakening the free vortex.

#### 4.1.4 The Isovel Patterns and Current Direction in Consecutive Bends of $r_c/wds=3.65$ and variable $r_c/wds$

Figures 4.4 to 4.7 show the isovel patterns and Table 4.2 summarises vortex development and interaction in paired bends with  $r_c/wds=3.65$  and  $1.5 < r_c/wds < 3.91$ .

Figure 4.4. Selected isovel patterns in consecutive bends with  $r_c/w_{ds}=3.65$  and  $r_c/w_{ds}=3.91$ . The isovels are shown in  $\text{cm. s}^{-1}$  and the symbol  $x$  represents the location of the maximum velocity measurement. The isovel diagrams are presented from the left bank to the right bank facing downstream.

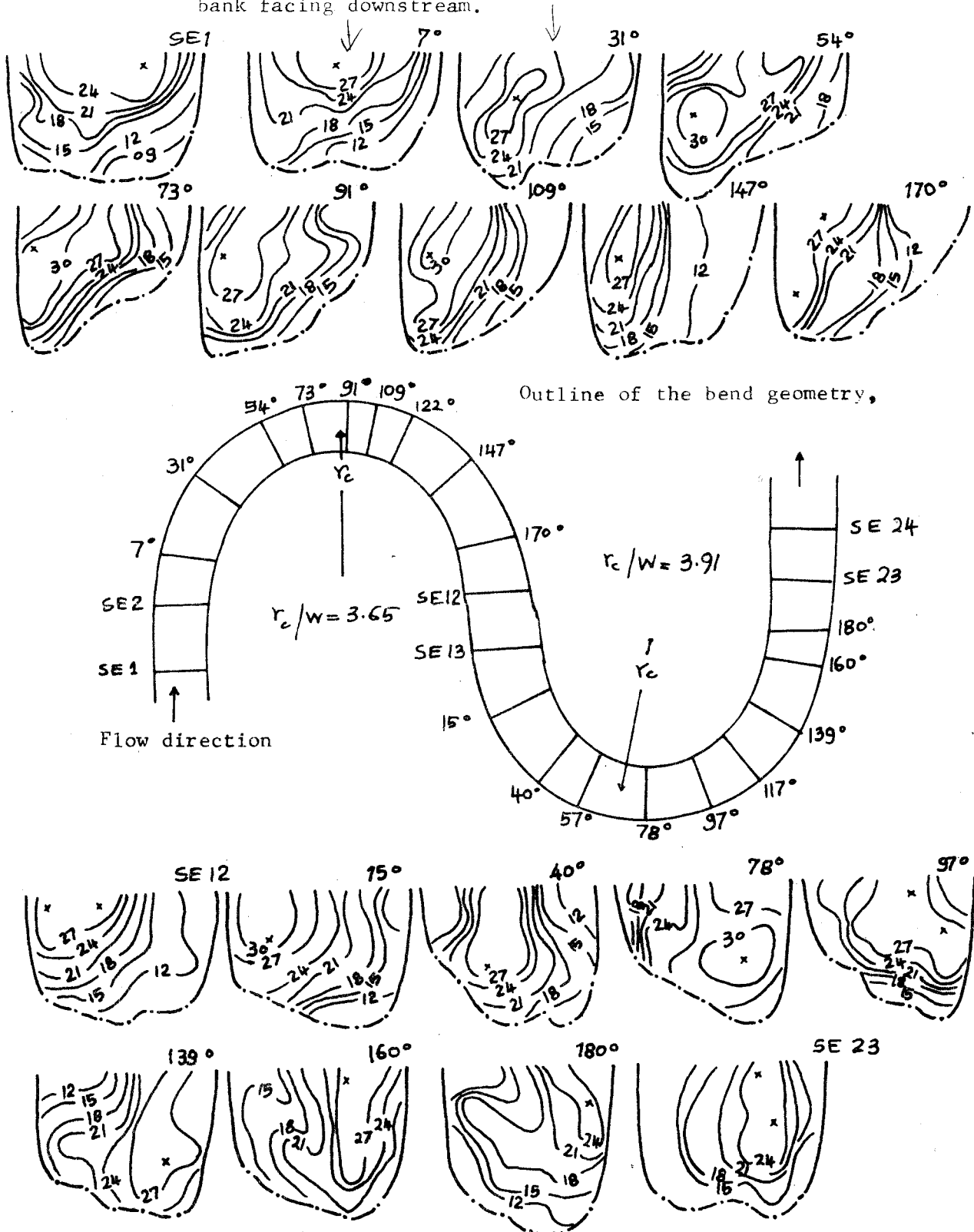


Figure 4.5. Selected isovel patterns in consecutive bends with  $r_c/w_{US}=3.65$   $r_c/w_{DS}=2.2$ . The isovels are shown in cm. s<sup>-1</sup> and the symbol x represents the location of the maximum velocity measurement.

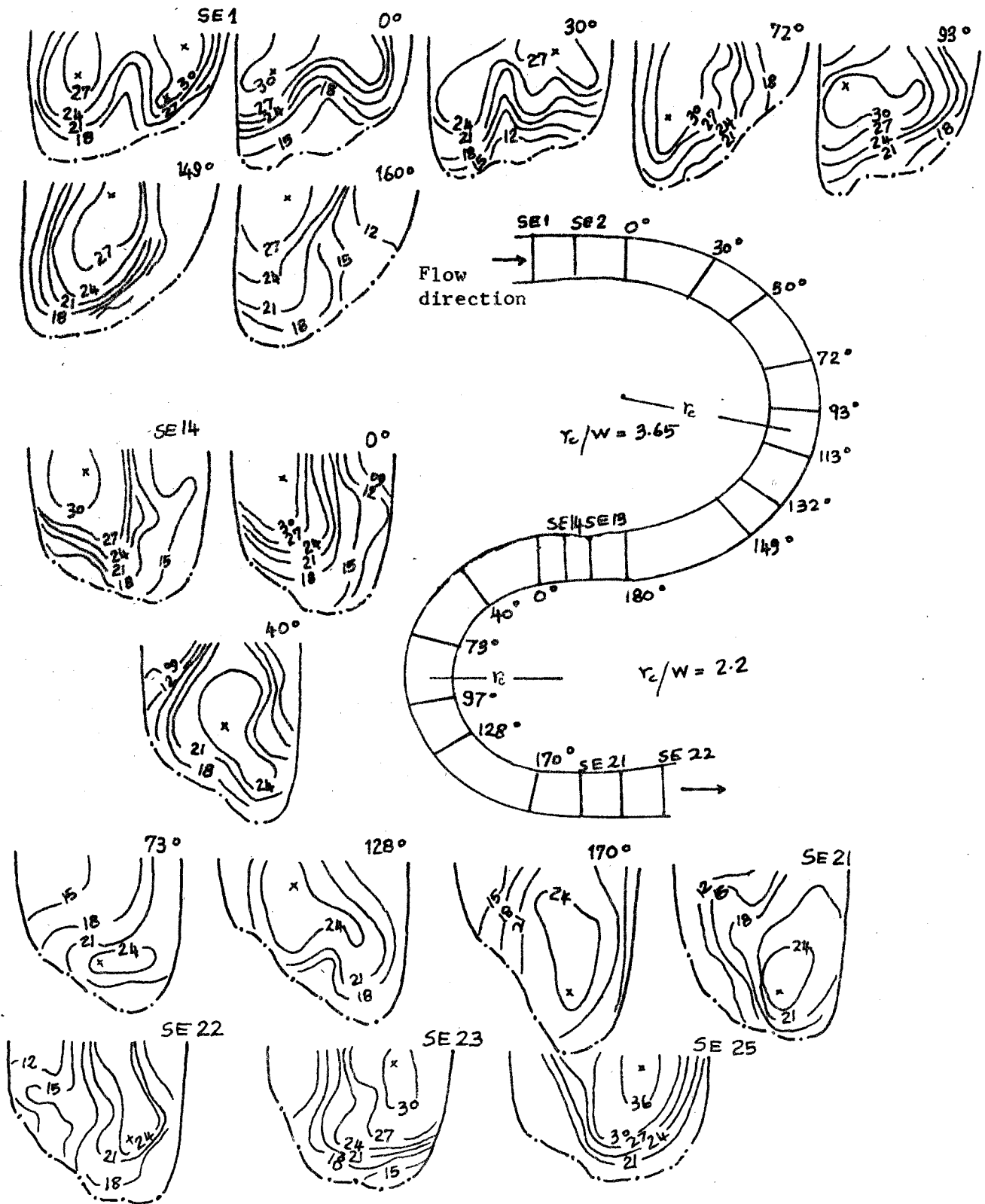


Figure 4.6. Selected isovel patterns in consecutive bends with  $r_c/w_{ds}=3.65$  and  $r_c/w_{ds}=1.56$ . The isovels are shown in  $\text{cm. s}^{-1}$ . The diagrams are presented from the left bank to the right bank facing downstream.

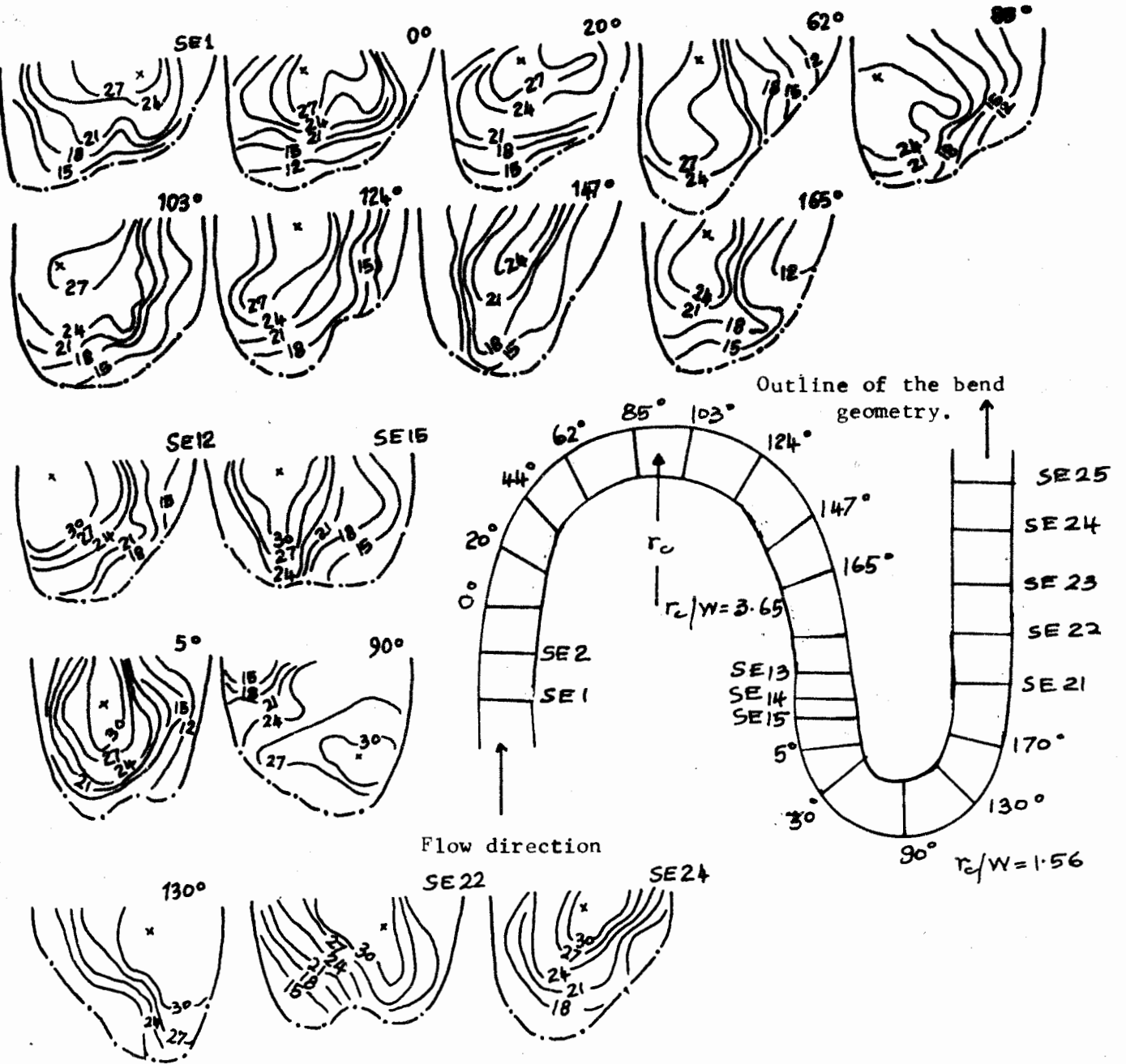
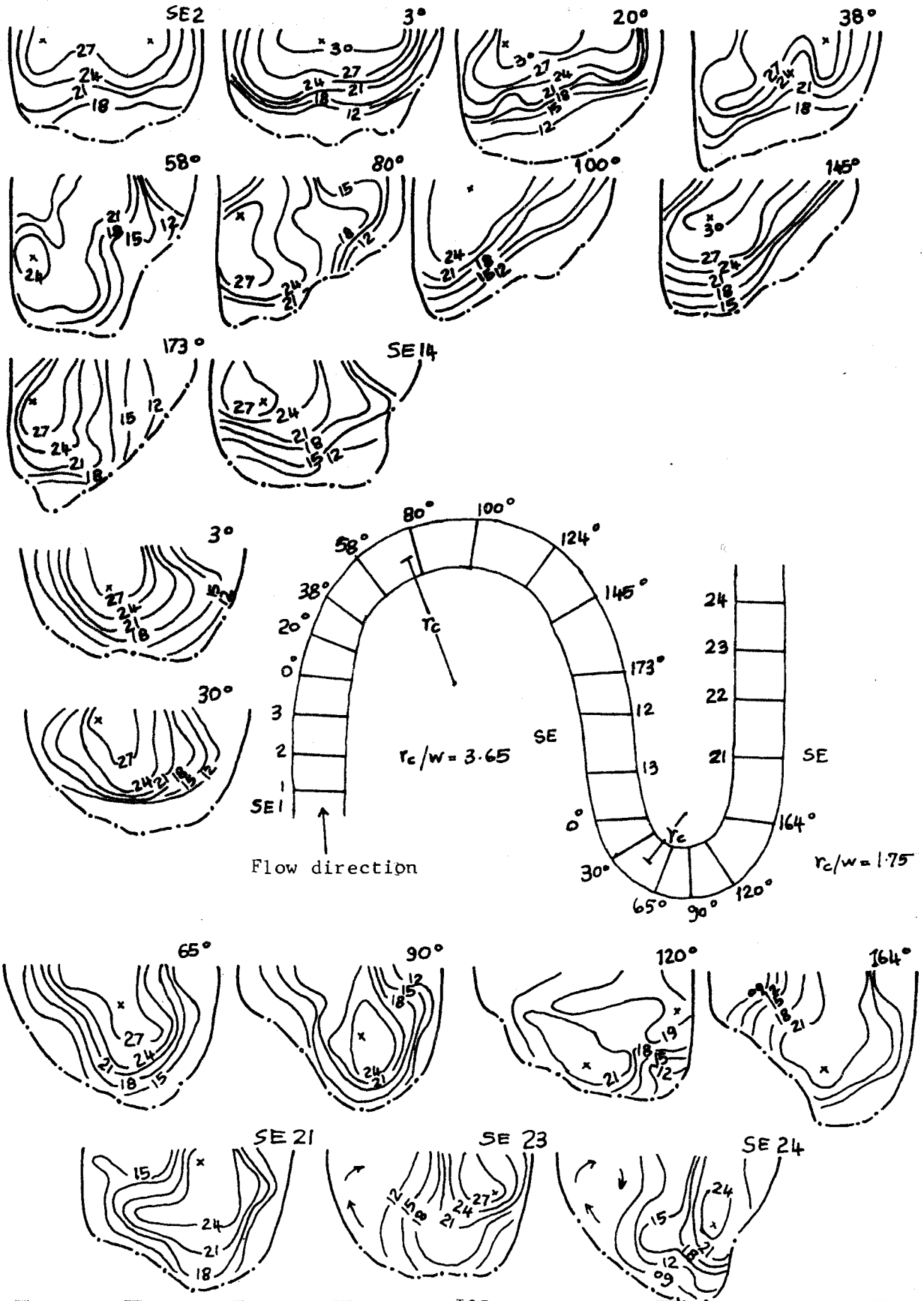




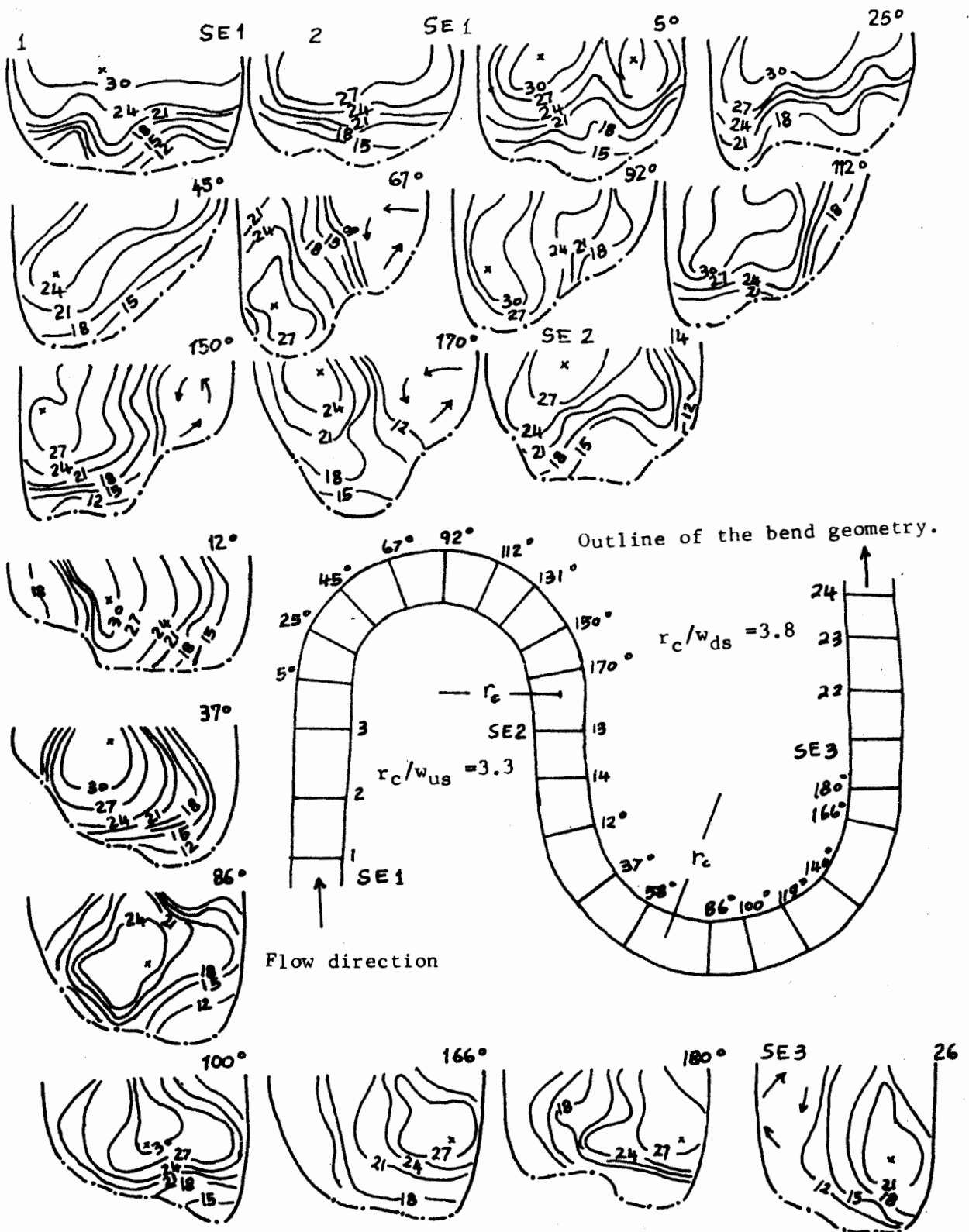
Figure 4.7. Selected isovel patterns in consecutive bends with  $r_c/w_{us}=3.65$  and  $r_c/w_{ds}=1.75$ . The isovels are shown in  $cm. s^{-1}$



The secondary flow advection towards the corners and surface at the centreline is limited to less than 60 degrees of the initial bend. The isovels progressively bulge towards the concave bank while those that bulge towards the convex bank become suppressed between the bend entrance and 30 degrees. The core of maximum velocity depresses towards the bottom between 54 and 95 degrees of the bend marking the transition from parabolic to forced vortex flow. The spirals become rather more developed as the current direction increases from 7 to 18 degrees at a bend angle of 73 degrees. Upstream of 73 degrees of the bend, the secondary spiral directed towards the convex bank near the bed sends secondary flow upwards and with it fine sediment along the bank towards the water surface. The convex flow separation zone locates at 67 degrees in Figure 4.8 but not in the other tighter bends. This is because the bends preceded by one with  $r_c/wds < 2.0$  develop strong rotational C-shaped isovels between 80 and 95 degrees and at the bend exits unlike those preceded by  $r_c/wds > 2.0$ .

Along the downstream bends, the inherited free vortex flow decays between 50 and 80 degrees and increases the extent of the transitional zone for a bend with  $r_c/wds = 1.56$  than in those of  $2.2 > r_c/wds > 1.75$ .

Figure 4.8. Selected isovel patterns in consecutive bends with  $r_c/w_{ds}=3.3$  and  $r_c/w_{ds}=3.8$ . The isovels are shown in  $\text{cm. s}^{-1}$



Nb. The symbol 'x' shows the location of maximum velocity. The diagrams are presented from the left bank to the right bank facing downstream.

TABLE 4.2.

The bend flow development and vortex interaction in consecutive bends with  $r_c/w_{us} = 3.65$  and variable downstream geometry (1.56, 1.75, 2.2, 3.8 and 3.91).

$r_c/w$	SEI	0°	30°	60°	90°	120°	150°	180°	0°	30°	60°	90°	120°	150°	180°	SE2
3.65/ 1.56	Parabolic flow		Forced vortex .69		T vortex				Free vort. -.47		Forced vortex			T vortex		.87
3.65/ 1.75	Parabolic flow		Forced vortex 0.42						Free vort. -0.28							Parabolic flow
3.65/ 2.2	Parabolic flow		Parabolic flow	Forced vortex 0.62		Forced vortex 0.79			Free vort. -.66		Forced vortex .26					Forced vortex .46
3.3/ 3.8	Parabolic flow			Forced vortex .47					Free vort. -.34			Forced vortex .38				
3.65/ 3.91	Parab. flow		Forced vortex .58						Free vort. -.59		Forced vort. .21			Forced T vort. .59		Parabolic flow

The numbers below each type of vortex is the maximum value of  $t$  in the expression  $V=kr.t$ .  
T means transition and SEI and SE2 represent the straight entrance and exit respectively.

As the secondary flow converges near the surface and the isovels deform downwards increasing the vertical velocity gradient (between 40 and 160 degrees), the free vortex flow transforms to a forced vortex. But in a bend of  $r_c/wds=1.75$ , the transition to a forced vortex flow is replaced by a parabolic flow that occupies the rest of the bend. This parabolic flow occurs because the high velocity core locates at the channel centreline (cf. Hickin, 1978) near the bed. The other bends considered here have a strong secondary spiral directed towards the inner bank between 120 and 150 degrees, the same region the width of the point bar is a maximum. The growth of the point bar is enhanced by the presence of the convex flow separation that creates a low energy environment for deposition, shifts the core of maximum velocity towards the outer (concave) bank and increases the strength of the forced vortex flow. This pattern of flow development ensures downvalley migration (translation) of meander bends.

The patterns of secondary flow discussed above are in accord with the general model of spiral flow in meander bends (cf. Rozovskii, 1961; Yen, 1967; Wilson, 1973). Secondary flow convergence near the surface (double spirals) at the bend apex is rather more common than single spirals. With the double spirals, the core of maximum velocity depresses towards the channel bottom and transmits high velocity fluid towards the bed to cause erosion and increase sediment transport. The single spirals at the bend apex are maintained, on the other hand, by

the presence of retarded (sometimes separated) flow near the bed close to the convex (inner) bank (Figure 4.5 at a bend angle of 73 degrees and in Figure 4.7 at 100 degrees). Einstein and Harder (1954) show that the upper layers of the flow close to the concave bank may not be affected by bed shear stress if the secondary vortex is completely dominated by the primary one. Hey and Thorne's (1975) results confirm the reduction of bed shear stress and channel roughness decrease along the concave (outer) bank. The occurrence of these single spirals at the bend apex and low shear stress along the outer bank in particular may be insightful in studies of bend erosion (cf. Woodyer, 1975; Hickin, 1979); this idea will be pursued further in chapter 6.

#### 4.1.5 Summary

The free vortex flow is inherited from the forced vortex of the upstream bends. It extends until 30 degrees in bends with  $r_c/wds=1.75$  and 2.2; and to 60 degrees in those of  $r_c/wds=3.8$ , 1.56 and 3.91. The parabolic flow at the bend apex results from the dual effect of the free vortex at the bend entrance and a developing second spiral that rotates anticlockwise within the downstream bend. Humphrey et al (1981) show that in turbulent flows in bends of strong curvature the core of maximum velocity does not shift towards the concave bank until 70 degrees of which the present data is in agreement. In  $r_c/wds>3.0$ , however, the core of maximum velocity shifts towards the outer bank at

the bend entrance and stays there through the rest of the bend (cf. Wilson, 1973). A bend with  $r_c/wds=1.56$  has the strongest forced vortex flow ( $t=0.89$ ) and it is associated with convex flow separation zone.

#### 4.1.6 The Isovel Patterns and Current Direction in Consecutive Bends of $r_c/wds=2.7$ and variable $r_c/wds$

The isovel patterns along the straight entrance shown in Figures 4.9 to 4.11 have secondary flow advection towards the corners and also to the water surface. The latter secondary flow advection directed towards the surface creates a ridge of decelerated flow and causes the isovels at 44 degrees of the bend to become complex. Near the water surface, the secondary flow converges (current direction is 25 degrees) and depresses the core of maximum velocity towards the bottom. But because the velocity near the concave bank is greater than that near the convex bank, the eddies that develop near the convex bank retard the flow. These quasi-vertical eddies are responsible for flow separation along the bend zone between 132 and 180 degrees where there is a maximum rate of point bar deposition. The convex flow separation strengthens the forced vortex ( $t=0.55$ ) at 154 degrees (see Table 4.3) because the flow has to accelerate to fulfill

Figure 4.9. Selected isovel patterns in consecutive bends with  $r_c/w_{us} = 2.7$  and  $r_c/w_{ds} = 4.0$ . The isovels are shown in cm. s<sup>-1</sup>. The diagrams are drawn from the left bank to the right bank facing downstream.

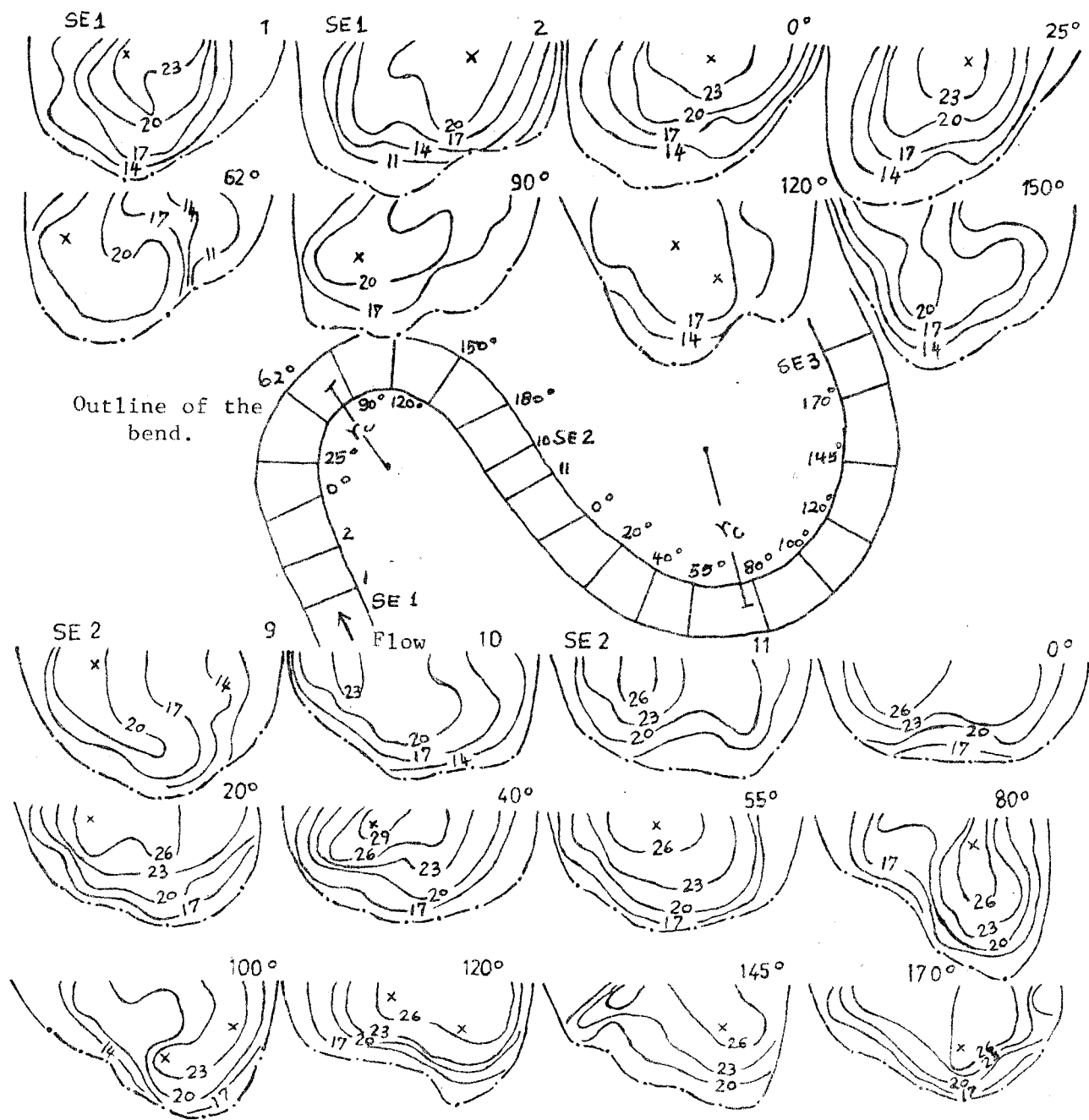




Figure 4.10. Selected isovel patterns in consecutive bends with  $r_c/w_{us}=2.7$  and  $r_c/w_{ds}=2.7$ . The isovels are shown in  $\text{cm. s}^{-1}$ . The diagrams are presented from the left bank to the right bank facing downstream.

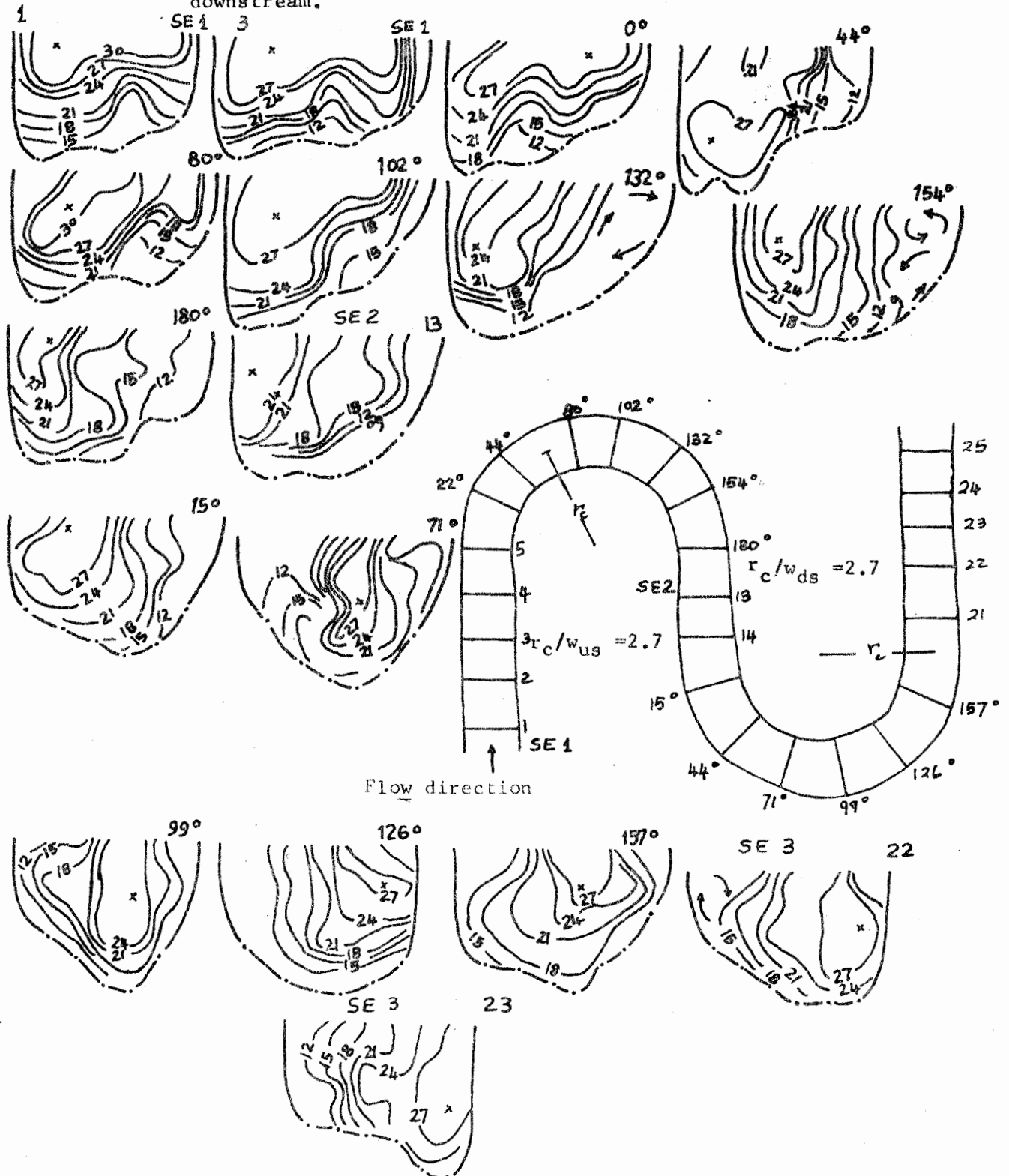


Figure 4.II. Selected isovel patterns in consecutive bends with  $r_c/w_{us}=2.7$  and  $r_c/w_{ds}=2.3$ . The isovels are shown in cm. s<sup>-1</sup>. The diagrams are presented from the left bank to the right bank facing d/s.

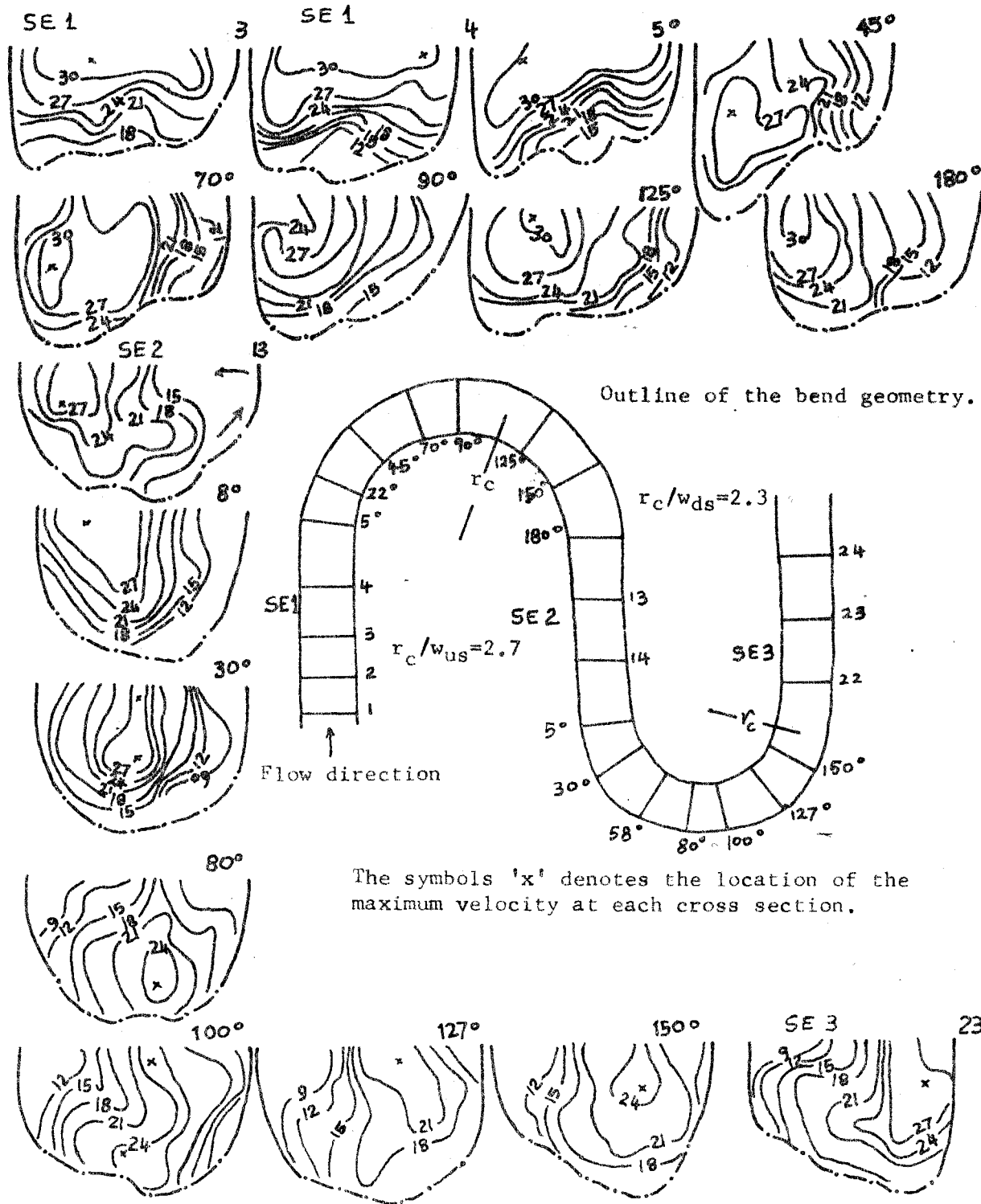
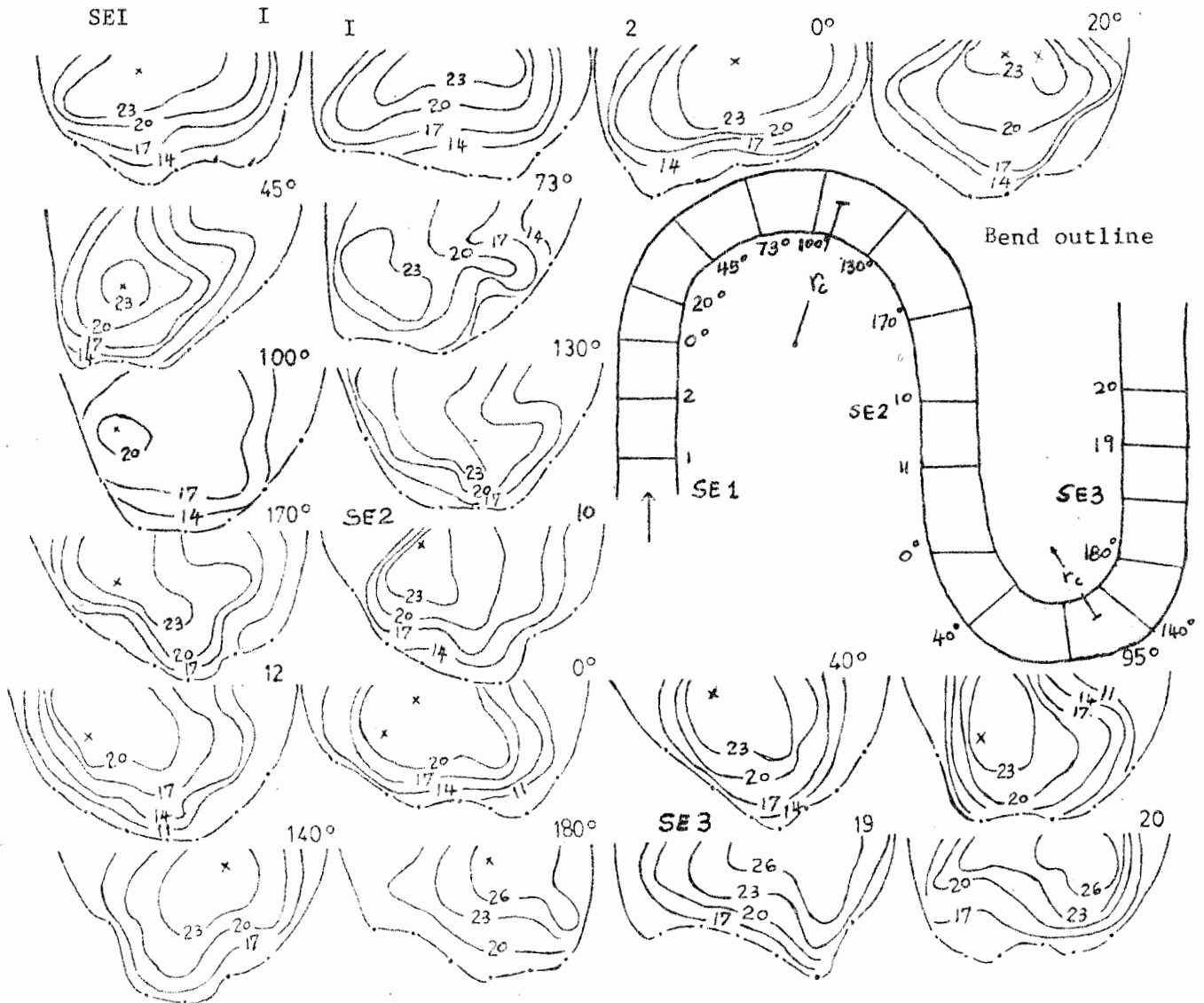


Figure 4.12. Selected isovel patterns in consecutive bends with  $r_c/w_{US}=2.7$  and  $r_c/w_{DS}=1.0$ . The diagrams are shown from the left bank to the right bank facing downstream. The isovels are given in  $\text{cm. s}^{-1}$



nb. SE1 and SE2 represent respectively straight entrance and exit of the bend.

continuity demands as the area of the section decreases.

The parabolic flow in the upstream bends translates to a forced vortex flow at the bend entrance in Figure 4.10 to 4.13 and 4.15 and at 60 degrees in Figure 4.14. A saddle-like flow separation near the channel bottom along the entrance in Figure 4.14 due to the influence of the bedforms likely is responsible for sustaining the parabolic flow long into the bend. The core of maximum velocity depresses towards the bottom along the bend zone between 54 and 90 degrees. As the upstream bends are tightened from  $r_c/w=2.7$  to 2.0 (Figures 4.13 to 4.16), the location of complex isovel patterns shifts from a bend angle of 44 degrees to lie between 80 and 90 degrees. In other words, the cross stream momentum transfer is overwhelmed by vertical secondary flow and flow convergence near the surface. But in Figure 4.13, the high velocity core splits into two filaments; one close to the concave bank at mid depth and the other near the water surface close to the convex (inner) bank.

Along the downstream bends, the forced vortex flow inherited from a bend of  $r_c/w_{us}=2.0$  continues through the rest of that of  $r_c/w_{ds}=4.0$ , after the vortex flow crosses the channel centreline to the concave (outer) bank along the inflection zone (sections 12 - 13, Figure 4.13). The core of maximum velocity depresses towards the bottom between 50 degrees (Figure 4.16) and 90 degrees where U-shaped isovels move towards the inner bank in accord with the other tight bend flow structures (cf. Fox and Ball, 1975).

TABLE 4.3

The bend flow development and vortex interaction in consecutive bends with  $r_c/w_{us}=2.7$  and variable downstream bend geometry (2.67, 2.26 and 2.1).

$r_c/w$	SEI 0°	30°	60°	90°	120°	150°	180° SE2	0°	30°	60°	90°	120°	150°	180° SE3	
2.7/ 2.7	Parabol. flow	Forced vortex							Free vort.	Forced vortex					
						.55		-.44						.49	
2.7/ 2.3	Parab.	Forced vortex							Free vort.	Forced vortex					
						.51		-.43						.48	
2.7/ 2.1	not measured														
2.0/ 1.0	Forced vort.	Forced vortex	Forced vortex	Forced vortex	Forced vortex	Forced vort.	Forced vort.	Free vort.	Free vortex	Free vortex	Free vortex	Free vortex	Parabolic Flow	Forced vort.	
	T 0.28	T 0.23	T	T	T	0.15	0.27	-0.15	-0.19	-0.19	-0.19	-0.19	0.23	0.23	

\* The numbers below are the maximum value of  $t$  in the expression  $V=kr^t$ . T means transition between vortex types while SE1 and SE2 represent the straight entrance and exit portions of the bend respectively.

Figure 4.13. Selected isovel patterns in consecutive bends with  $r_c/w_{us}=2.0$  and  $r_c/w_{ds}=4.0$ . The isovels are shown in cm. s<sup>-1</sup>. The diagrams are presented from the left bank to the right bank facing downstream. The symbol 'x' denotes the position of the maximum velocity.

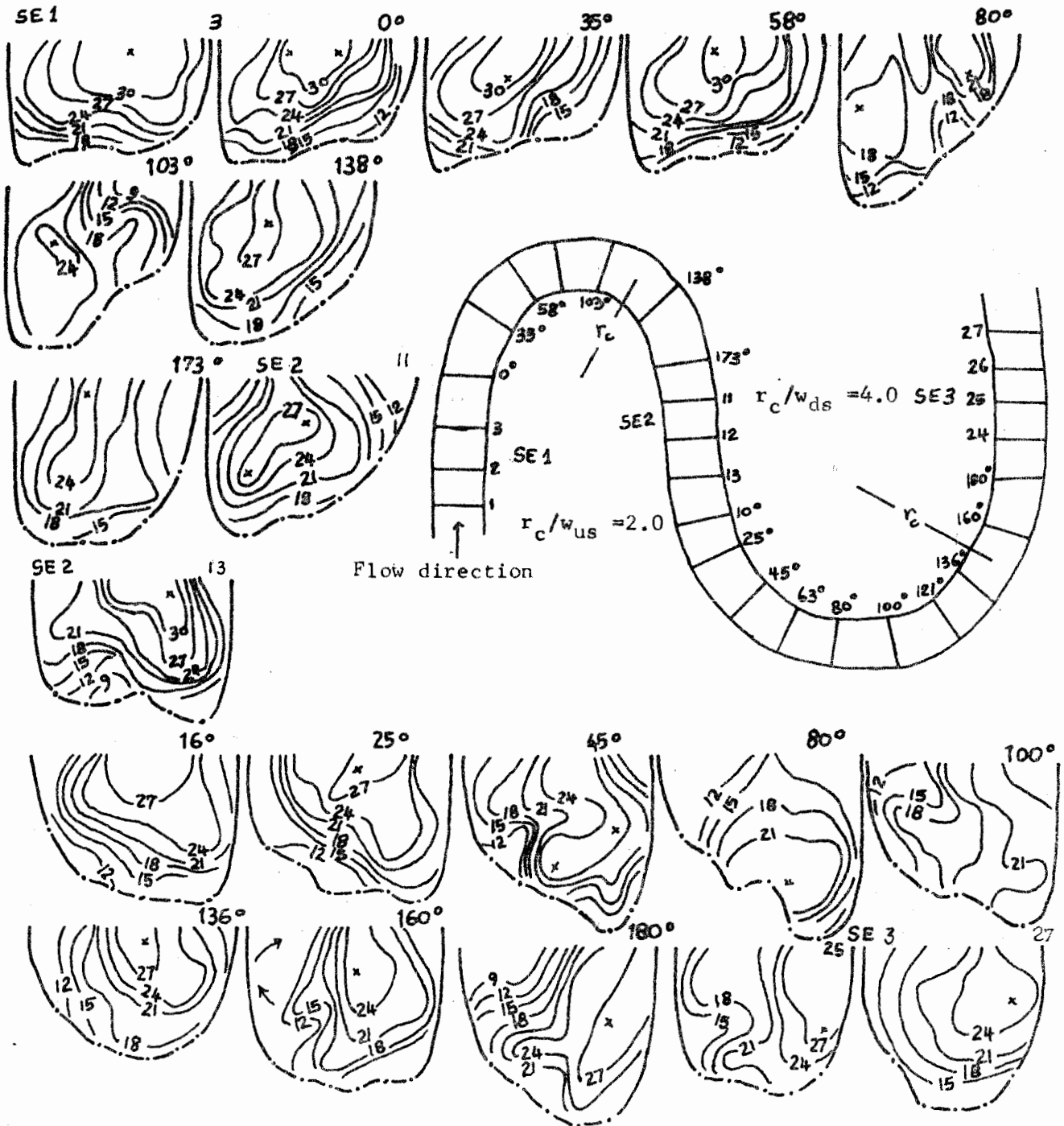


Figure 4.14. Selected isovel patterns in consecutive bends with  $r_c/w_{us}=2.0$  and  $r_c/w_{ds}=3.0$ . The isovels are shown in cm. s<sup>-1</sup>

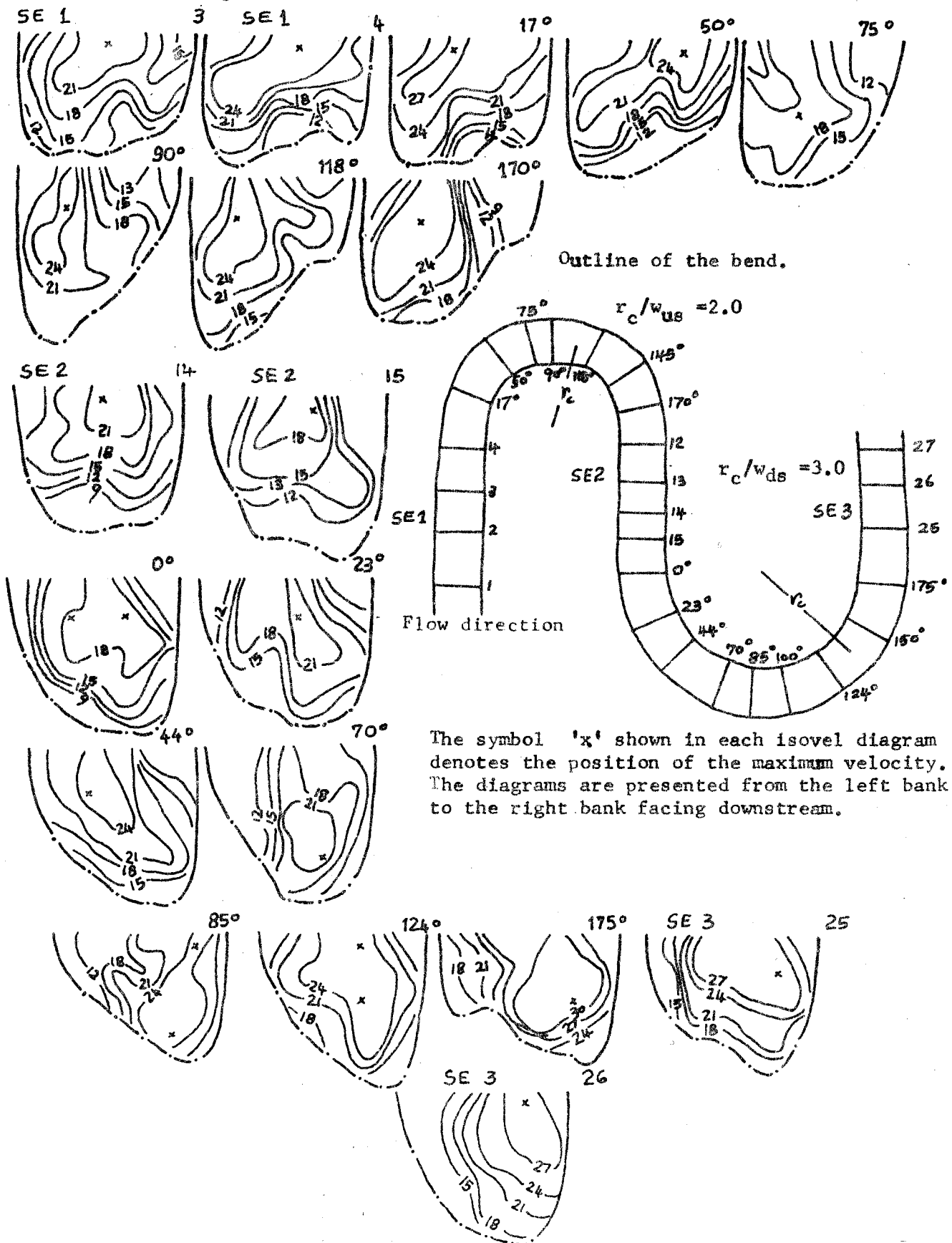


Figure 4.15. Selected isovel patterns in consecutive bends with  $r_c/w_{ds}=2.0$  and  $r_c/w_{ds}=2.0$ . The isovels are shown in  $\text{cm. s}^{-1}$

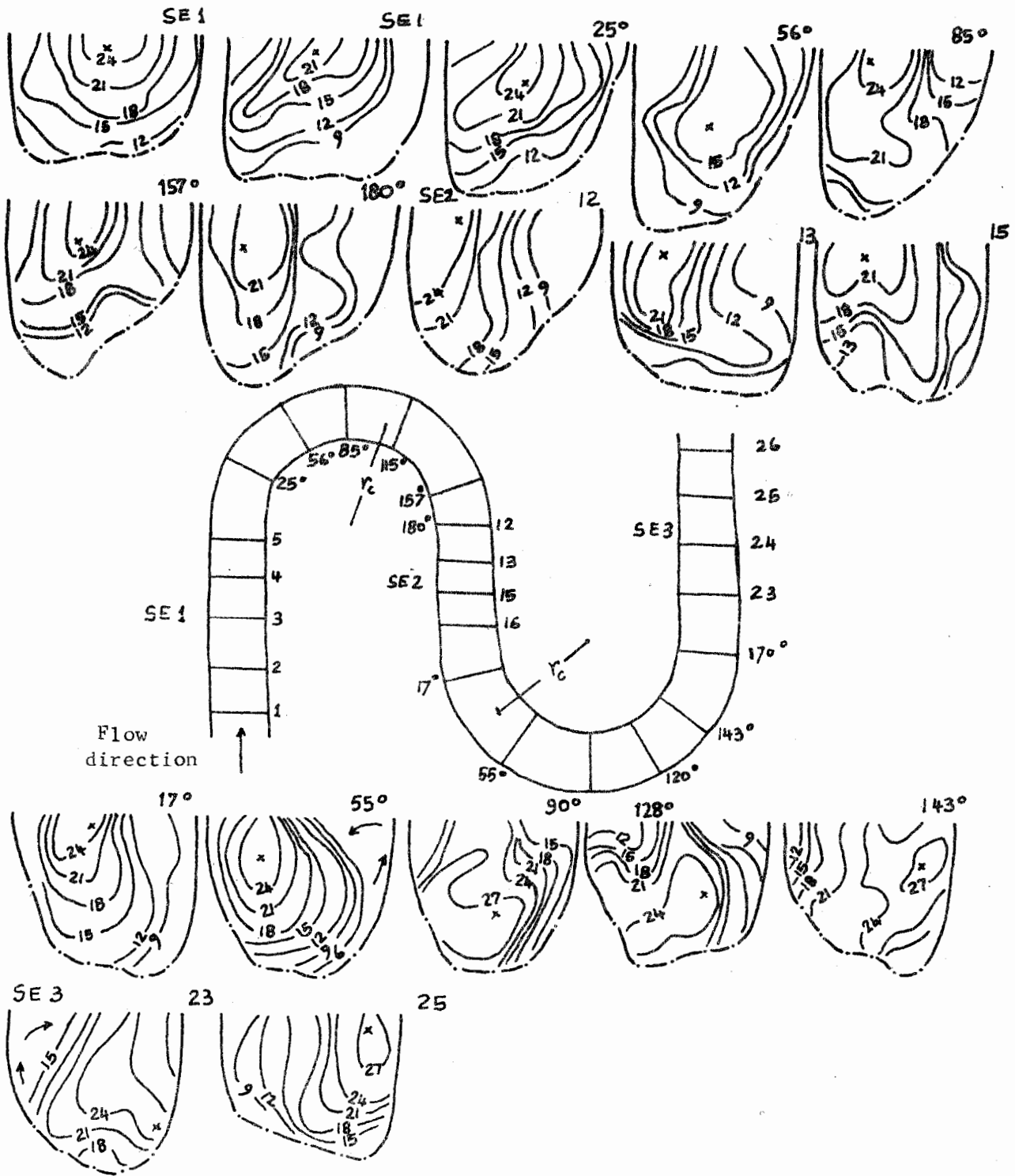




Figure 4.16. Selected isovel patterns in consecutive bends with  $r_c/w_{us}=1.92$  and  $r_c/w_{ds}=2.65$ . The isovels are shown in  $cm. s^{-1}$

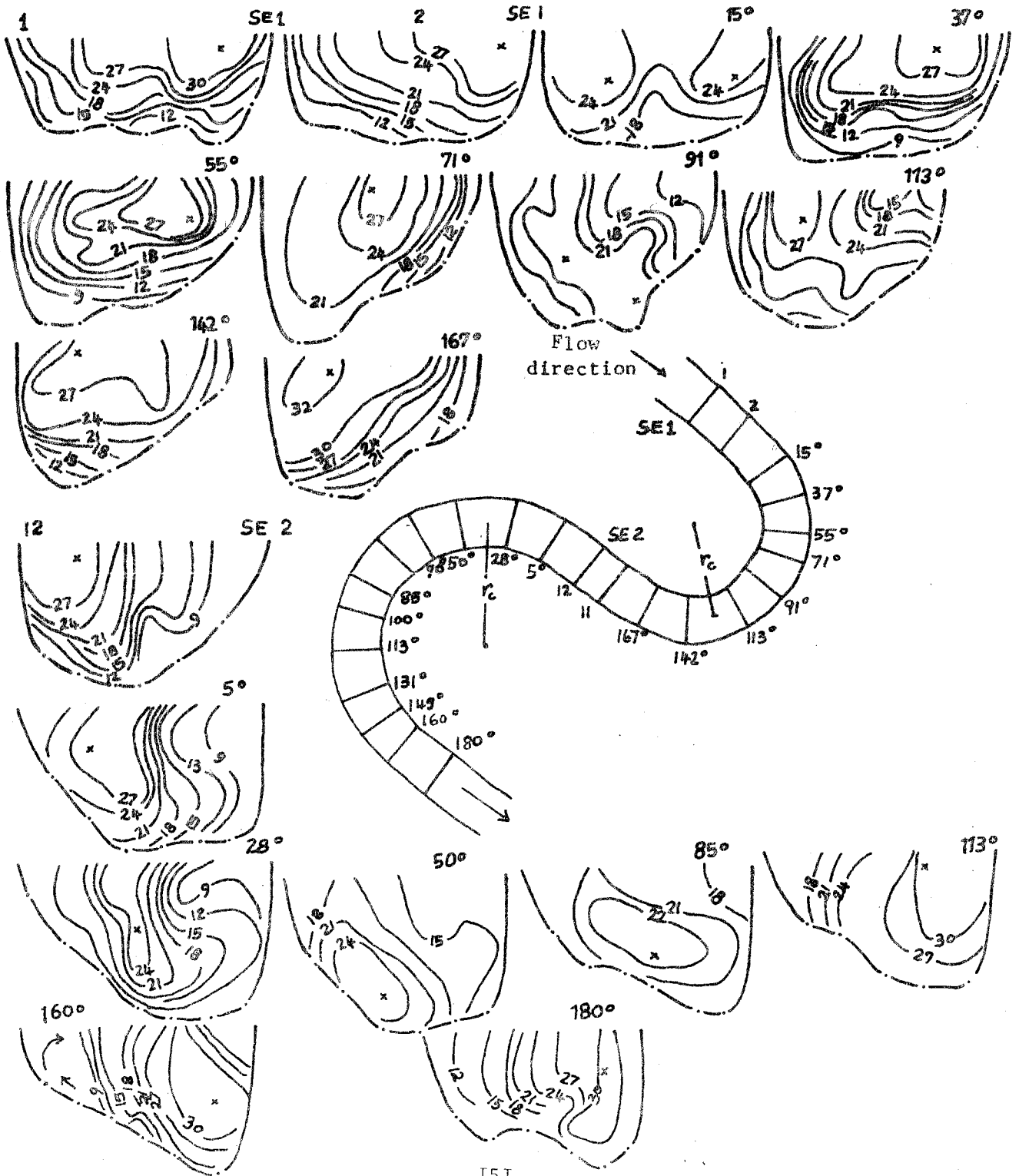


TABLE 4.4

The bend flow development and vortex interaction in consecutive bends with  $r_c/w_{us}=2.0$  and variable downstream bend geometry (4.0, 3.0 and 2.0).

$r_c/w$	SEI	0°	30°	60°	90°	120°	150°	SE2	0°	30°	60°	90°	120°	150°	180°	SE3
2.0/ 4.0			Forced T .61		vortex .13			.15	Forced T .35				vortex .30			.45
2.0/ 3.0					Forced vortex .55			Parab. Free vort. -.44					Forced vortex T .69			
2.0/ 2.0	Parab.	Forced T vort. .30			Forced Vortex .71				Free vortex .41							Forced vortex .47
2.0/ 1.0	Forced vort. 0.23	Parabolic flow	Forced 0.24		Parabolic flow vort .15			Free T					vortex -0.2			Forced vortex .31

\* The numbers below are the maximum values of  $t$  in the equation  $V = kr^t$ .

T means transition between vortex types while SE1 and SE2 represent the straight entrance and exit portions of the bend respectively.

The convex flow separation develops at 55 and 160 degrees and also along the downstream bend exit portions. Since convex flow separation zones are areas of deposition, the downstream bends likely may have three loci of point bars as well as points of erosion on the concave bank. Because these point bars may not be preserved during the process of lateral erosion (cf. Jackson, 1975), they complicate any simple flood plain reconstruction (cf. Hickin, 1974).

The extent of the forced vortex flow decreases as the downstream bends become tighter. It occupies the zone between the bend entrance until 180 degrees in a bend with  $r_c/wds=4.0$ , between 50 and 180 degrees in that of  $r_c/wds=3.05$ , and between 120 and 180 degrees in  $r_c/wds=2.0$ . The extent of the free vortex is limited to the bend portion upstream of 50 degrees in bends with  $4.0 > r_c/wds > 2.0$  the bend zone where erosion occurs (Suga, 1967). The parabolic (transitional) flow locates at 45 degrees in a bend with  $r_c/wds=4.0$ , at 135 degrees in that of  $r_c/wds=3.0$  and at 120 degrees in  $r_c/wds=2.0$ . These parabolic flow zones also are cross overs in the flow structure, and therefore the thalweg of a bend with  $r_c/wds=2.0$  crosses the channel centreline more abruptly than in wider bends. Jackson (1975) has shown that the preservation of point bar deposits depends on the location and extent of the transitional (parabolic) flow. These bends ( $2.0 < r_c/wds < 3.0$ ) likely have longer bend zones with intermediate point bar depositional facies because the flow structure is partly transitional and partly fully developed (Jackson, 1975).

#### 4.1.8 The Isovel Patterns and Current Direction in Consecutive Bends of $r_c/wds=1.5$ and variable $r_c/wds$

Figures 4.17 to 4.20 show that isovel patterns along the straight entrance are consistent with the previous observations. The secondary spiral develops near the bottom and shifts low momentum fluid towards the water surface near the convex bank at 50 degrees of the bend. The C-shaped isovels in a bend of  $r_c/wds=2.1$  at 105 degrees in Figure 4.19 and reverse C-shaped ones at 80 degrees in Figure 4.17 are two spirals that rotate anticlockwise near the surface and clockwise near the bottom (cf. Einstein and Shen, 1964). It should be noted that these isovel shapes display further twists of the secondary flow pattern described earlier as W- and U-shapes. The effect of these spirals is to transfer accelerated fluid towards the channel bottom, where it is retarded and redirected to the inner bank towards the surface. As expected, the core of maximum velocity locates also along the convex bank at the bend apex (Hickin, 1978).

Along the downstream bends, the free vortex flow extends from the bend entrance until 60 degrees; except for a bend of  $r_c/wds=1.5$  because the latter is preceded by a tighter upstream bend. Further downstream, the free vortex flow weakens and the core of maximum velocity shifts towards the outer bank.

Figure 4.17. Selected isovel patterns in consecutive bends with  $r_c/w_{US}=1.5$  and  $r_c/w_{DS}=2.9$ . The isovels are shown  $\text{cm. s}^{-1}$

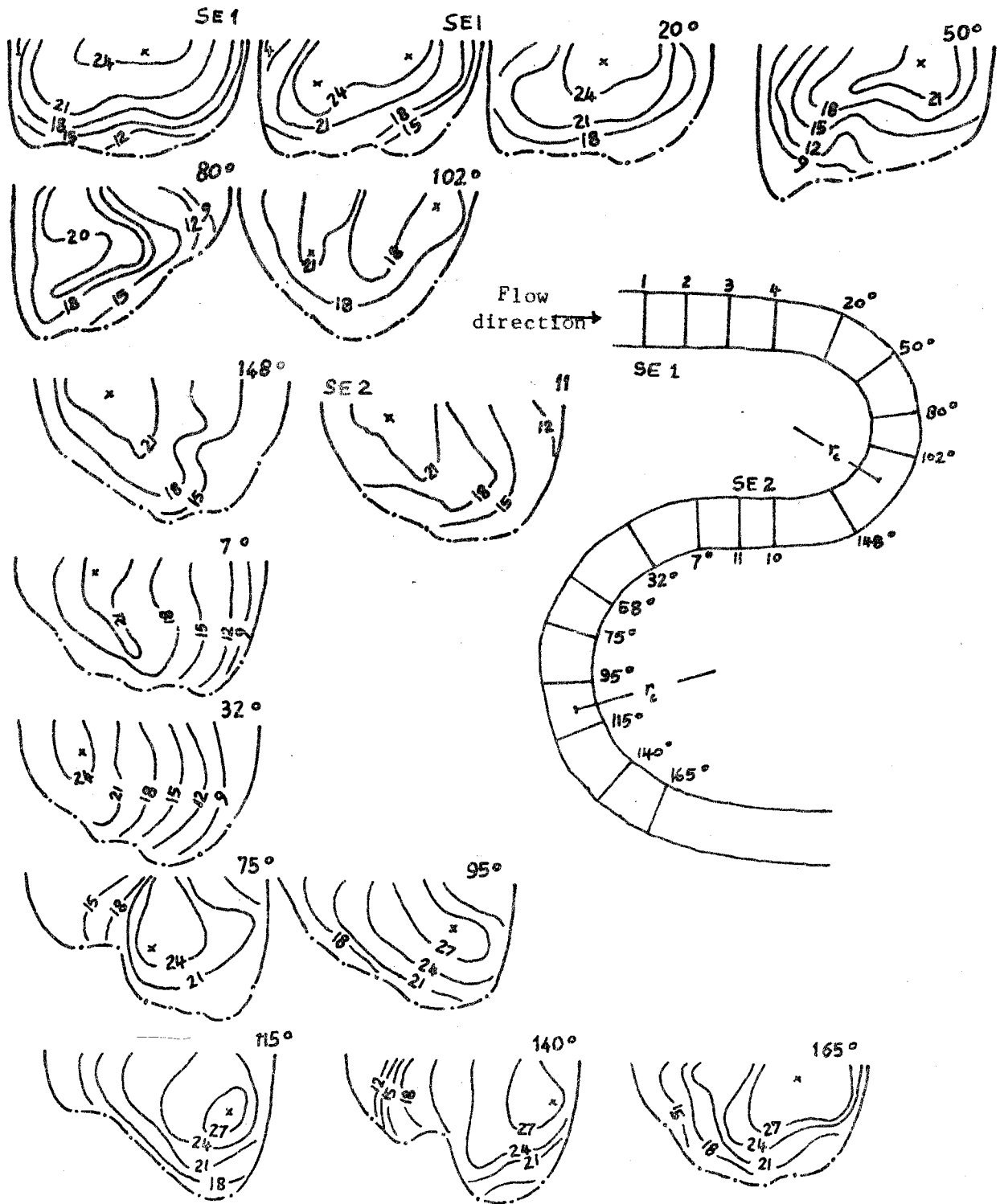
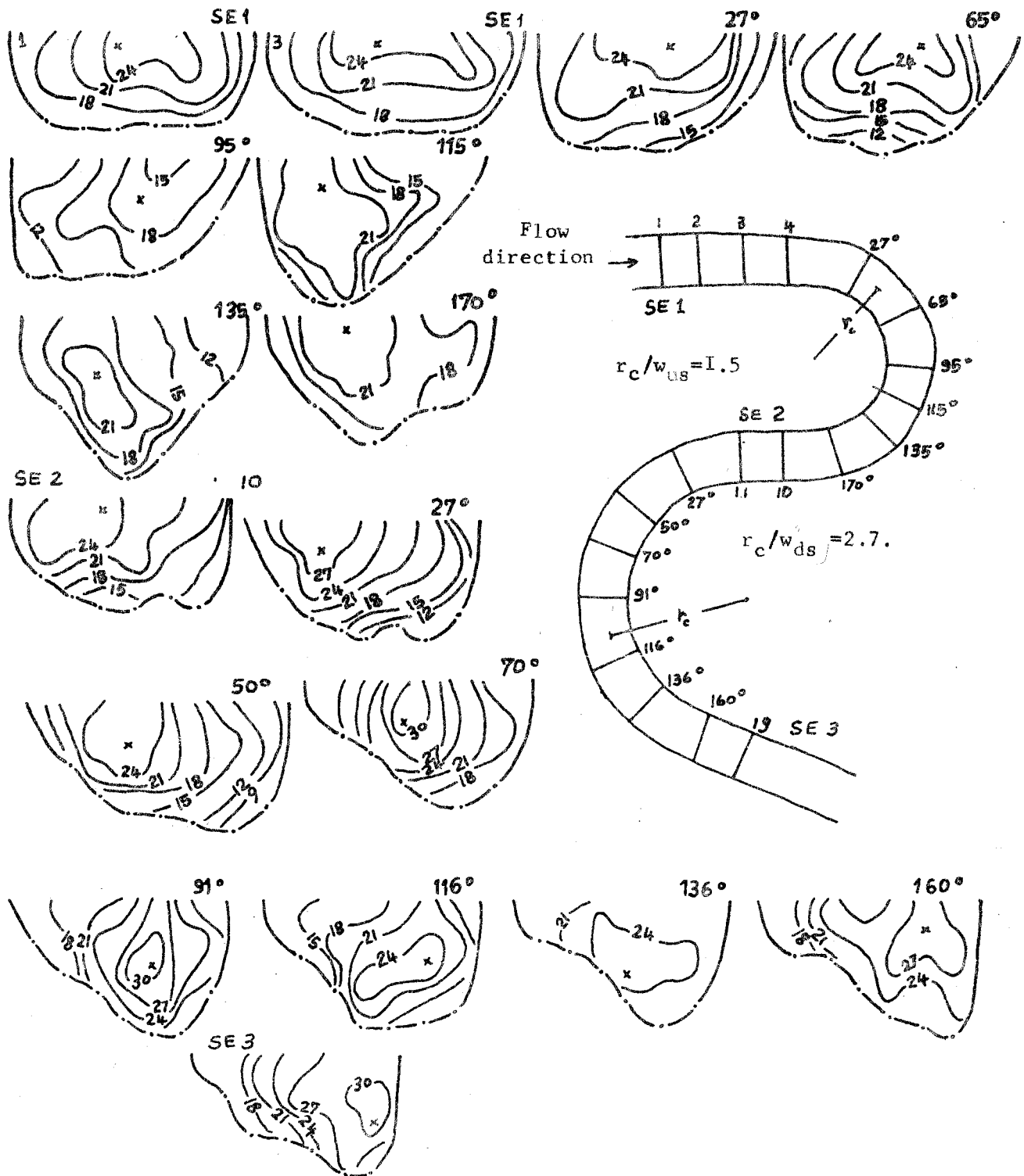


Figure 4.18. Selected isovel patterns in consecutive bends with  $r_c/w_{us}=1.5$  and  $r_c/w_{ds}=2.7$ . The isovel interval is 3 cm.  $s^{-1}$



nb. The isovel diagrams are presented from the left bank to the right bank facing downstream. The symbol 'x' denotes the position of maximum velocity.

Figure 4.19. Selected isovel patterns in consecutive bends with  $r_c/w_{us} = 1.5$  and  $r_c/w_{ds} = 2.1$ . The diagrams are presented from the left bank to the right bank facing downstream. The isovels are given in  $cm. s^{-1}$

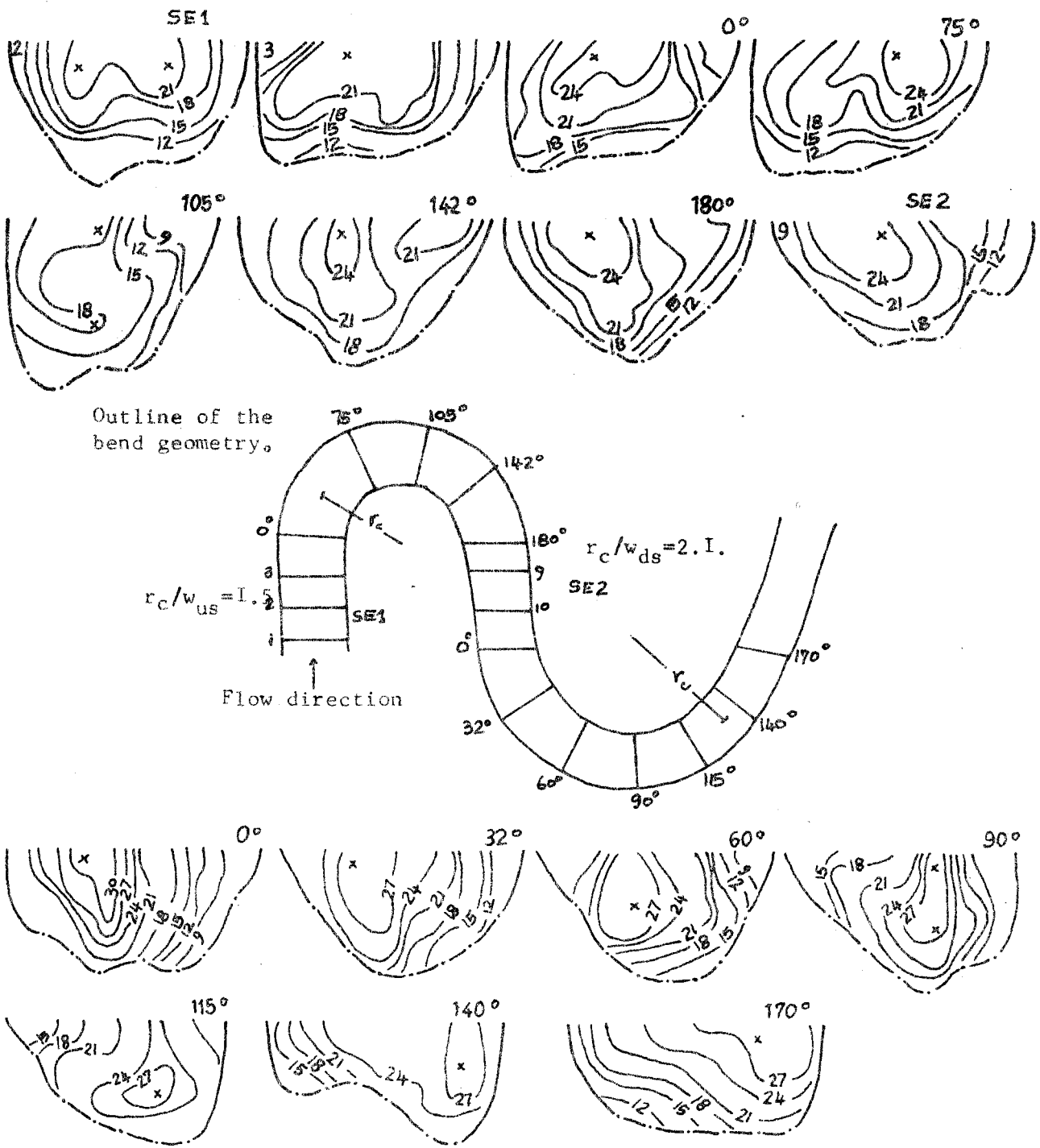


Figure 4.20. Selected isovel patterns in consecutive bends with  $r_c/w_{us} = 1.2$  and  $r_c/w_{ds} = 1.5$ . The diagrams are presented from the left bank to the right bank facing downstream. The isovels are shown in  $\text{cm. s}^{-1}$ . The symbol 'x' denotes the location of maximum velocity at each cross section.

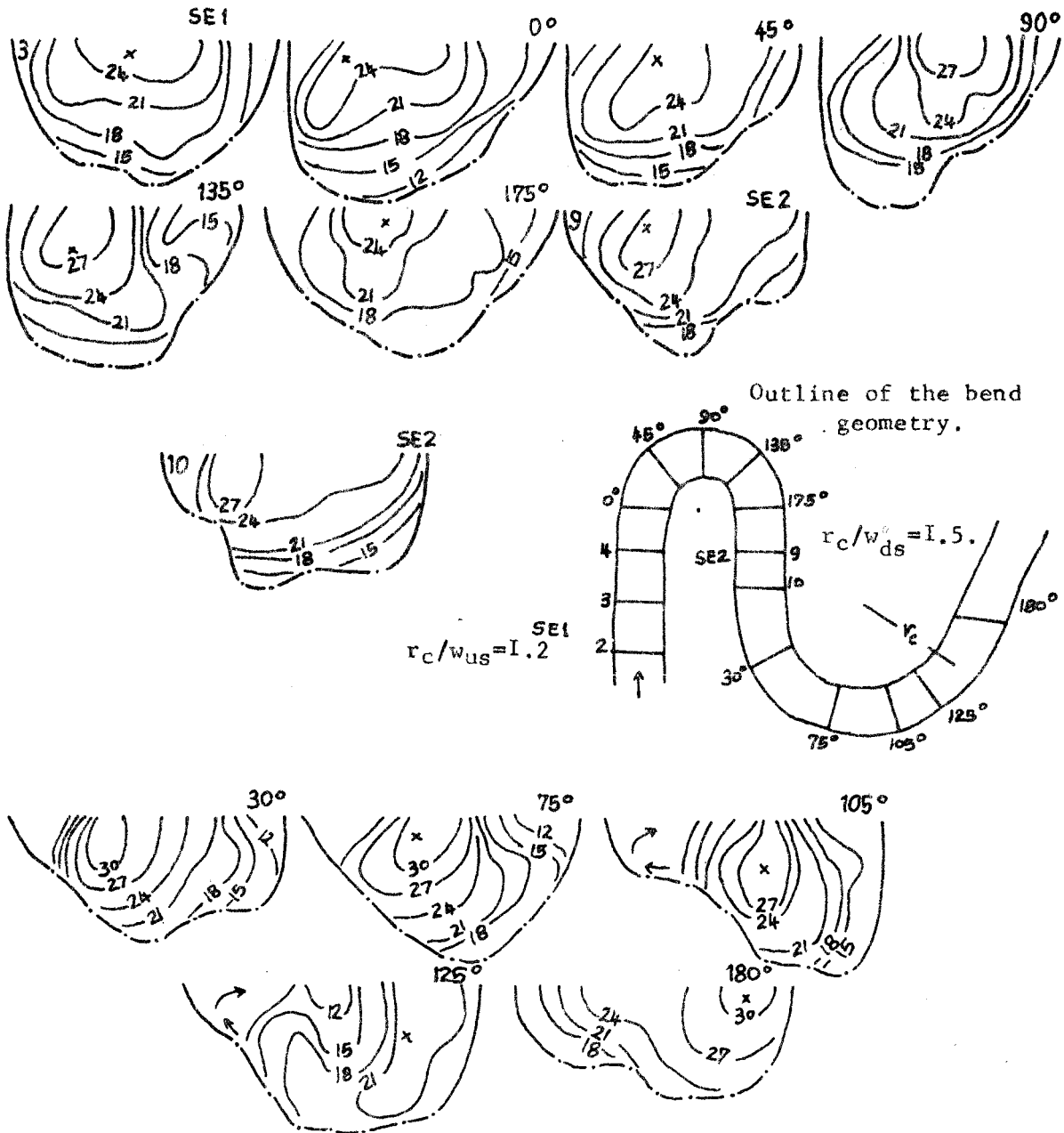




TABLE 4.5

The bend flow development and vortex interaction in consecutive bends with  $r_c/w_{us} = 1.5$  and variable downstream bend geometry ( $2.6 r_c/w_{ds} = 1.5$ ).

$r_c/w$	SE1	0°	30°	60°	90°	120°	150°	180°	0°	30°	60°	90°	120°	150°	180°	SE2
1.92/ 2.65	Free vort.	T Free vort.	Forced	T	vortex .43				Free vortex -.57	Parab.	Forced vortex .54					
1.5/ 2.9	Parabolic flow	T	Forced .27	T	vortex				Free vortex -.42	Parab.	Forced vortex .37					
1.5/ 2.7	Free vort.	Parabolic	Free vort. .18	Forced vortex .22					Free vort. .29	Parab.	Forced T vortex .49					
1.5/ 2.1	Parabolic flow	Parabolic flow	Forced .29	T	vortex .51				Free vortex -.36	Parab.	Forced vortex .26					
1.2/ 1.5	Parabolic flow	Forced vortex .21							Free vortex -.44	Parab.	Forced vortex .23					

\* The numbers below each type of vortex flow are the maximum value of  $t$  in the expression  $V=kr.t$ .  
T means transition between vortex types

The difference between the bends discussed above and those of  $r_c/wds=1.2$  and  $r_c/wds=1.5$  is the persistence of parabolic flow until 90 degrees along the upstream bends. Leischziner and Rodi (1979) pointed out that in tight bends a symmetrical spiral motion prevails along the bend zone between 40 and 130 degrees because there is neither flow acceleration nor deceleration so that a state of axial symmetry is obtained. This flow pattern likely inhibits bank erosion. At the bend apex, secondary flow bulges the isovels towards the inner bank and weakens forced vortex flow; it decays along the exit.

The other difference is that the free vortex along the downstream bend ( $r_c/wds=1.5$ ) does not have any history from the upstream bend because parabolic flow forms along the inflection. Bridge and Jarvis (1982) note that within the parabolic flow at the bend inflection, each cell is intimately associated with the end or the beginning of a major cell that dominates the point bar (cf. Thorne and Hey, 1975). Along the downstream bends, the free vortex extends until 130 degrees; its maximum strength locates at 75 degrees of the bend angle. This shows that in the downstream bend of opposite curvature, the imbalance of inertial and radial forces takes longer to develop; the extreme result of such an imbalance likely is a flow separation which is prevalent in tight bends. Humphrey et al (1981) suggested that the imbalance of radial over inertial forces is responsible for shifting the core of maximum velocity from the convex to the concave bank as flow approaches the bend axis (see also Squire

and Winter, 1965; Hawthorne, 1951; Rozovskii, 1965; Ananyan 1965). However over the point bar zone, the core of maximum velocity is forced to shift towards the concave bank by the occurrence of convex flow separation at 105 degrees.

#### 4.1.9 Summary and Observations

The differences between vortex interactions and patterns of secondary flow reflect the influences that are conveyed from the downstream bends to the bend inflection through radial acceleration. In a bend of  $r_c/w = 1.2$ , the parabolic flow extends from the bend entrance until 90 degrees and also along the inflection. The parabolic profiles that locate at the bend apex are either associated with C-shaped isovels in which retarded flow is sandwiched by accelerating fluid or because the core of maximum velocity locates at the channel centreline (Hickin, 1978). The secondary flow convergence near the surface depresses the core of maximum velocity towards the bottom (cf. Hey and Thorne, 1975). Along the downstream bends, the free vortex extends to 130 degrees in bend series of  $r_c/w = 1.5$  and  $r_c/w = 2.0$ , but only up to 60 degrees in the other paired bends.

The straight entrance of bends have secondary flow advection directed towards the corners and also towards the water surface at the centre of the channel. It extends from the bend entrance until 60 degrees of bend zones of  $r_c/w > 3.0$  and  $r_c/w < 2.0$ , and to 90 degrees in  $r_c/w = 2.0$ . The development of

an anticlockwise rotating secondary spiral near the bed at the axis of tight bends shifts the high velocity core towards the channel centreline. The growth of a secondary spiral as opposed to the main one explains why the secondary flow intensity decreases along the bend zone between 60 and 120 degrees erasing the transverse flow components layer by layer, beginning with the channel bottom where they are of least intensity (cf. Mockmore, 1944).

The parabolic flow translates to a forced vortex; its maximum strength locates at the bend apex of  $r_c/wus > 3.0$  or at the bend exit for tighter bends. Only in bend series with  $r_c/wus = 4.0$  and  $r_c/wds = 3.1$ , and  $r_c/wus = 1.2$  and  $r_c/wds = 1.5$  did the forced vortex strength become reduced completely and parabolic flow occupied the inflections.

The inherited forced vortex flow structure translates to a free vortex at the bend entrance along the downstream bends. The extent of the free vortex flow varies with a decrease in  $r_c/wds$  and then translates to a parabolic flow along the bend zone between 30 and 50 degrees. In fact parabolic flow occupies the rest of the bend with  $r_c/wds = 1.75$ ; but only between 30 and 90 degrees in that of  $r_c/wds = 1.5$  and between 55 and 115 degrees in  $r_c/wds = 2.0$ . The forced vortex flow extends between 120 and 180 degrees, along the downstream bend series with  $r_c/wus = 2.07$  and  $r_c/wds = 2.0$ ;  $r_c/wus = 1.5$  and  $r_c/wds = 2.07$ ; and  $r_c/wds = 1.5$ . These are the bends with a higher potential of erosion along the exit portions.

The secondary flow structure in subsequent bends accords well with the general model of flow development in bends (see Rozovskii, 1961, Muramoto, 1967; Mosonyi and Gotz, 1973; Hickin, 1978). The region of the maximum bend influence on flow structure between 30 and 60 degrees, the decrease of vortex strength between 80 and 130 degrees, and the location of fully developed flow downstream of 135 degrees are in agreement with the notion that the development of spirals are discontinuous (contrast with Leopold et al; 1964). Mosonyi and Gotz (1973) in a model of three consecutive bends found that the spiral developed between 50 and 70 degrees of the bend; the variation of width depth increased the spiral intensity but did not alter the pattern of development (cf. Muramoto, 1967; Einstein, 1972).

The spiral inherited from the upstream bends decays between 50 and 65 degrees in the downstream bend, in agreement with Mosonyi and Gotz (1973). Further in to the bend, the development of a secondary spiral between 65 and 105 degrees twists the isovels into a C-shaped geometry. The upper spiral sometimes reaches the water surface. The congruence of these results confirm that flow development in subsequent bends are radically influenced by the upstream bend conditions (cf. Hickin, 1978), a notion that is further developed in Chapter 5.

The isovel patterns of the bend zone between 30 and 180 degrees are of particular interest to sedimentologists concerned with floodplain formation (cf. Fenneman, 1906; Melton, 1936; Mackin, 1937; Fisk, 1946). The heterogeneity of point bar

deposits (Wolman and Leopold, 1957) and ridge and swale topography represent the effect of the location of the high velocity core, secondary flow convection and sediment supply. Two hypotheses on point bar deposition, namely, the influence of the flow separation zone and Langmuir circulation (Bagnold, 1954) can be examined using the present data to identify the type(s) of flow structure which may be associated with point bar deposition. The flow structure in the upstream bends represents undisturbed flow pattern, while that in the downstream bends represents situations typical in natural rivers.

The secondary flow towards corners and from the channel bed at the centreline towards the surface may erode the banks and deposit sediment along the centreline (cf. Einstein and Li, 1958). The recruited sediments likely are swept towards the concave bank at the onset of the cross flow along the bend zone between 30 and 60 degrees. Further downstream, the secondary spiral that develops along the bend zone between 80 and 130 degrees will move bed load sediments towards the channel centreline again. The intensity of this spiral increases as the bends become tighter. Assuming sediment movement follows the same pattern of secondary flow, sediments in traction will be deposited at the upstream portion of the point bar (cf Bluck, 1972; Jackson, 1976; contrast with Bridge, 1975). The occurrence of parabolic flow along the bend apex would imply that most small calibre sediments can be deposited in a slack water environment where Langmuir circulation occurs.

Further downstream (135 to 180 degrees), the secondary spiral near the bottom increases its magnitude and shifts the core of maximum velocity towards the outer bank. The secondary flow advection towards the inner bank near the bed and surface where the convex flow separation occurs is limited in its capacity to lift larger sediment calibre; this flow structure is responsible for the rapid deposition of fine granules there (Bluck, 1972). It is worth noting that bends of  $r_c/w < 2.0$  have parabolic flow and the core of maximum velocity locates near the convex bank; they will probably witness little erosion along the convex bank zone (Hickin and Nanson, 1975; Jackson, 1976).

The mode of point bar deposition along the downstream bends differs from those along the upstream because of the inherited free vortex with its attendant sediment load from the concave bank of the upstream bend. Dietrich and Smith (1979) observed that high sediment load travelled downstream as a convex sand-wave as the core of maximum velocity shifts towards the outer bank. The outward directed spiral near the convex bank pertinent to free vortex flow structure winnows out fine granules from the upstream end of the bar. The secondary flow from the centreline directed towards the convex bank, on the other hand recruits fine sediment for deposition along the downstream end of the bar (cf. Bluck, 1972; Jackson, 1975; Nanson, 1980). The composite effect of long transitional flow along the downstream bends probably is the reason why the point bars there are topographically lower and locates further

downstream towards the bend exit when compared to the one that forms along the upstream bends (cf. Bluck, 1972). The downvalley migration of river bends is therefore assured.

## 4.2 THE DISTRIBUTION OF VELOCITY IN CONSECUTIVE BENDS

### 4.2.1 Introduction

The velocity distribution in channels shows the segments in which stream energy is lost through eddies and boundary roughness (Leopold et al; 1964). But many river bends tend to maintain a uniform distribution of velocity (steady state) by conserving energy at the bend apex where the water is deep and dissipating more along the inflection reaches. The energy gradient ( $S + V/2g$ ), where  $S$  is water surface elevation, has a steeper profile in meandering sections because of the necessity to overcome bend resistance (Leopold et al; 1964). Because the water surface and mean depth of flow do not change very much compared to the mean velocity in the present study, the distribution of mean velocity is indicative of the influence of eddies in total energy dissipation.

An aim of this research was to investigate velocity unsteadiness (macro-eddies) in open-channel bends, to identify the regions where stream energy is concentrated, and also to compare the distribution with nonuniform flow past bluff bodies.



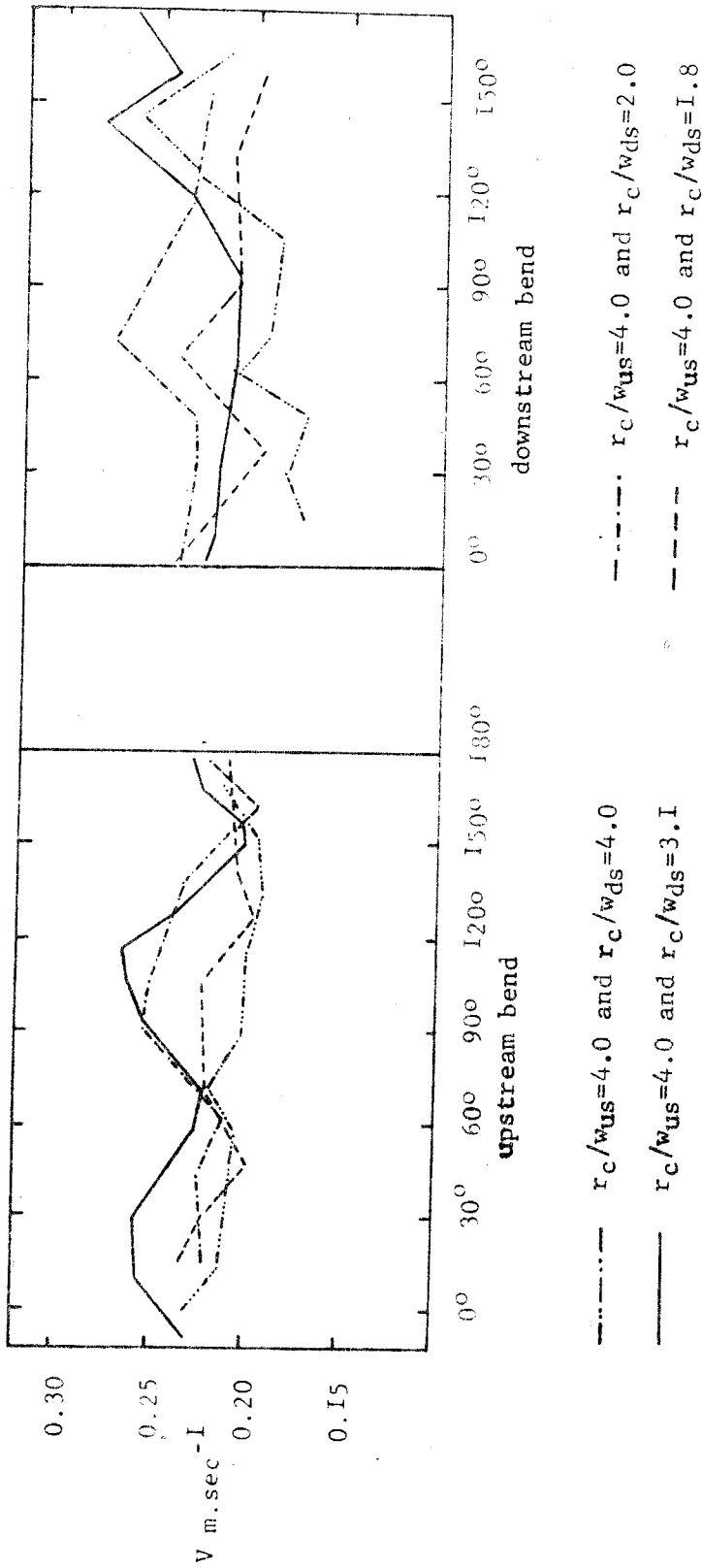
Chapter two shows that the flow structure in single bends exhibits longitudinal, transverse and vertical unsteadiness due to the effect of the bend. Flow visualisation method showed that the surface bubbles congregate at the centre of the channel as the flow approaches the bend entrance. Within the bend, the bubbles tend to form vortex trails similar to the ones which have been observed behind bluff bodies (cf. Roshko, 1971; Hall, 1972). Such vortices were observed also in natural rivers like the Squamish in British Columbia. Figures 4.20 and 4.24 summarise the trends of the longitudinal mean velocities for all bends considered in this Chapter.

#### 4.2.2 The Distribution of Velocity in Single Bends with $r_c/w_s=4.0$ and variable $r_c/w_s$

The velocity near the channel banks was measured 0.076m from the water's edge while the means are calculated from depth-averaged measurements. There were six or more verticals at every cross section.

Along the upstream bends the mean velocity increases and reaches a maximum value at 30 degrees, and then it falls to a minimum value along the bend zone between 45 and 60 degrees (Figure 4.21). It increases again from 60 degrees to reach a second maximum value at a bend angle of 105 degrees.

Figure 4.2I. The distribution of mean velocity in consecutive bends with  $r_c/w_{us}=4.0$  (constant) and variable downstream bend geometry.



These observations accord well with the previous results in tight bends (cf. Shukry, 1949; Yen and Yen, 1970). On the other hand, the velocity near the convex bank fluctuates every 60 degrees in wider bends but it decreases to every 30 degrees as the downstream bends become tighter. The velocity along the concave bank is uniformly distributed and rather higher compared to the lengthwise distribution of the mean velocity except downstream of 90 degrees in bends preceded by  $r_c/w_s$  of 3.0 and 1.8 in which there possibly are upstream transmission of downstream bend influences.

It has been observed that the maximum velocity locates downstream of the bend apex near the concave bank (Leliavsky, 1955), but little is known of the changes that may occur in the flow structure as the bend geometry changes through the processes of erosion and deposition. The present studies shows that the point of maximum mean velocity migrates from a bend angle of 150 degrees in  $r_c/w_s=3.1$  to 60 degrees in a bend of  $r_c/w_s=2.0$  but decreases along the concave bank while increasing along the convex bank between the bend entrance and 30 degrees (cf. Shukry, 1963). These trends become reversed at 90 degrees where the thalweg shifts towards the outer bank. In  $r_c/w_s < 2.0$ , the velocity trends near the banks are of opposite pitch upstream of 45 degrees and downstream of 120 degrees, but becomes uniform and have the same pitch along the bend axis because of the strong double vortices in the flow structure. Further downstream of the bend apex, the flow near both banks is

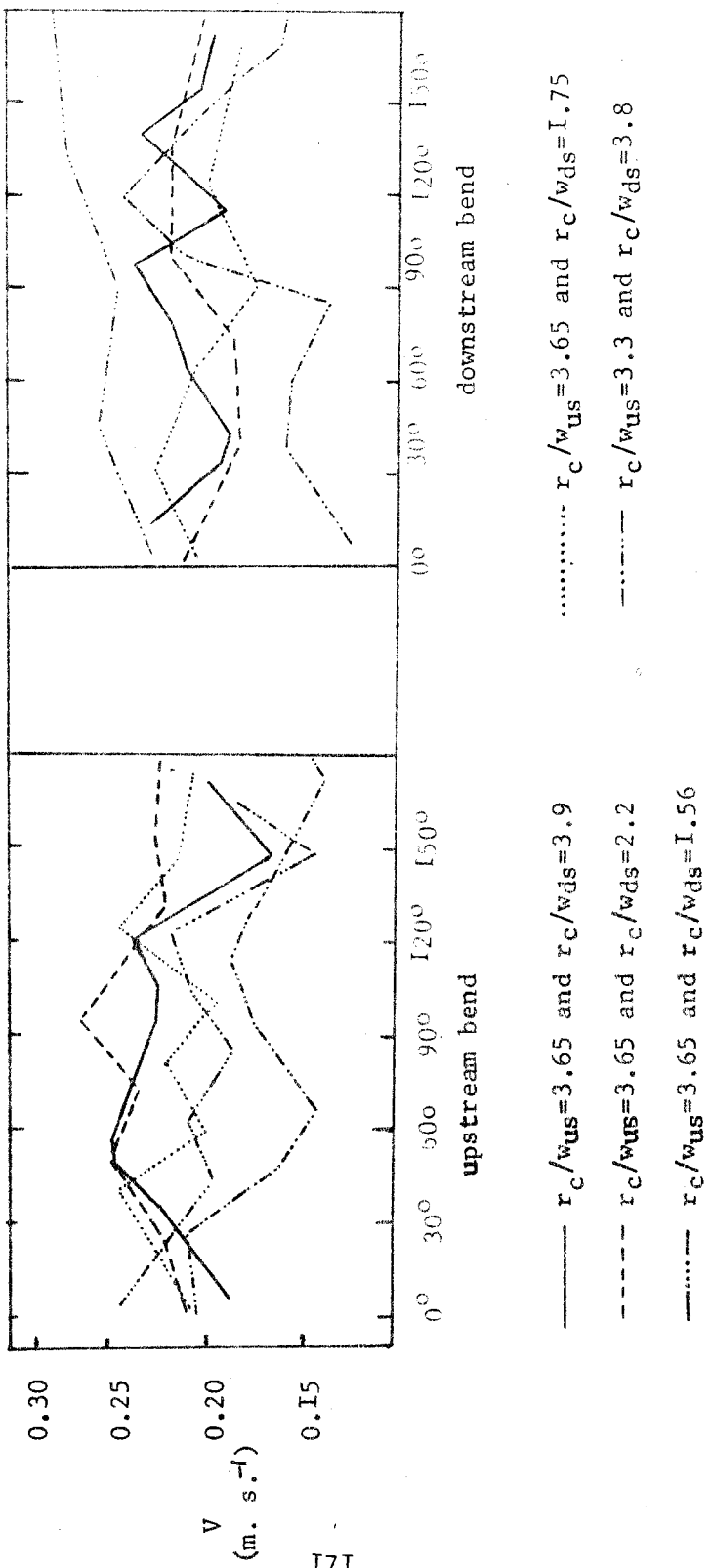
retarded to a minimum value at 135 degrees of bend angle; the same position the bend pool locates.

The changes of velocity distribution in various bend geometry can be associated with those of migrating rivers. Jackson (1975) shows that mean cross sectional velocity increases at the bend apex with discharge (his traverses 1 and 3) in  $r_c/w=3.3$ . This increase in discharge is accommodated by width rather than depth. Since width increased and radius of curvature remained sensibly constant, the bed asymmetry shifted from inner bank to the outer bank over a longer transition than at lower discharges. Such long transitional flow delays the establishment of a fully developed flow zone while a shorter transition directs currents towards the outer bank and promotes erosion (Ferguson, 1973) at the bend apex.

#### 4.2.3 The Distribution of Velocity in Consecutive Bends with $r_c/w_{us} = 3.6$ and variable $r_c/w_{ds}$

The mean longitudinal velocity increases at the bend entrance to a maximum value at 30 degrees (Figure 4.22). The minimum value of mean velocity locates along the bend zone between 60 and 90 degrees, and this region becomes deeper and the flow separates as  $r_c/w_{ds}$  decreases.

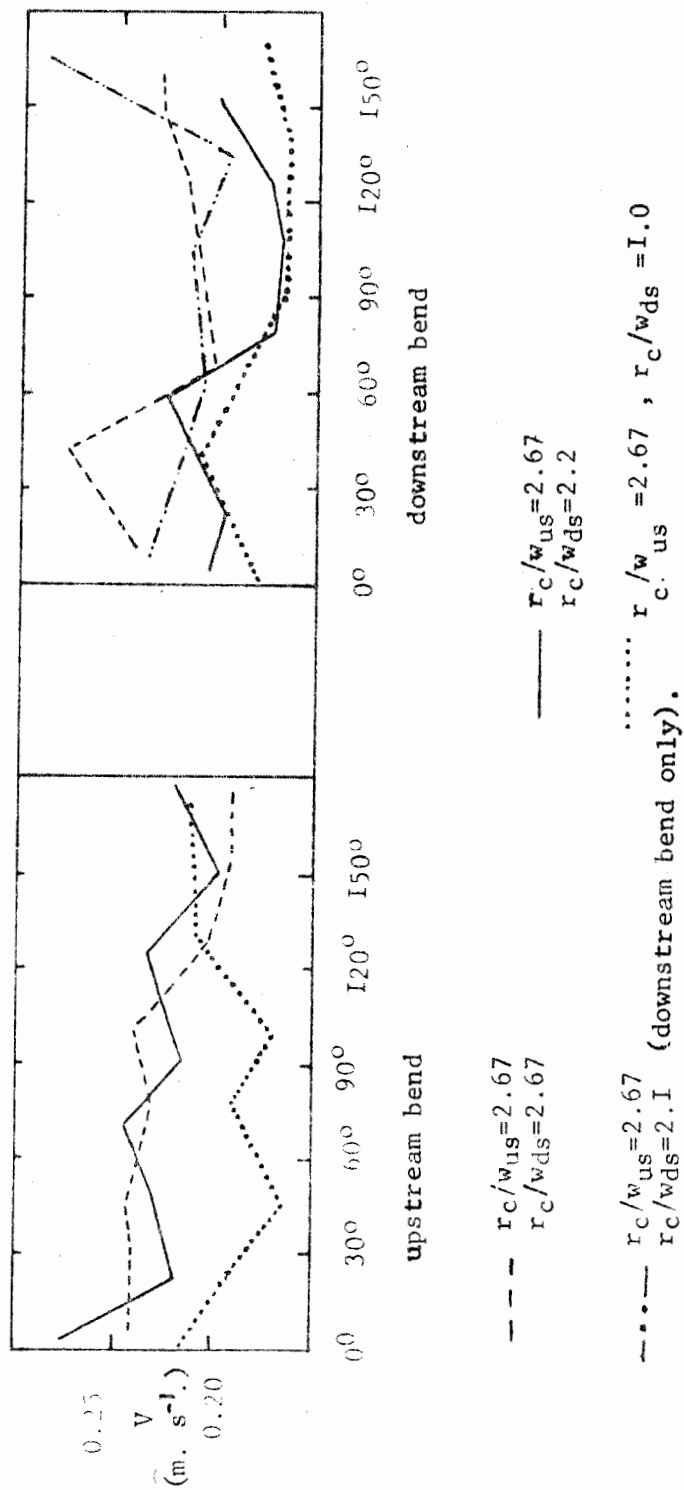
Figure 4.22. The distribution of mean velocity in consecutive bends with  $r_c/w_{us}=3.65$  (constant) and variable downstream bend geometry.



Leopold et al (1960) appealed to an analogy of a broad-crested weir and suggested that the pool at the bend apex dams the channel and velocity decelerates while it accelerates both upstream and downstream of the bend apex. It is possible that such a distribution of velocity will reduce energy loss at the bend apex and increase it along the entrance and inflection. Figures 4.21 and 4.22 also show that the velocity distribution skews towards the first half of the upstream bends that are preceded by  $r_c/wds > 2.0$ , and that a uniform distribution applies to those preceded by tighter bends. Along the downstream bends of  $r_c/wds > 3.8$ , the mean velocity distribution skews towards the bend exit while those of  $r_c/wds < 3.6$  remain sensibly uniform. These differences reflect the variety of the wavelength of the incoming spiral from the upstream bends.

The present results show that the mean velocity distribution is nonuniform. It is periodic every 60 degrees which agrees well with the results reported by Muramoto (1967) and Einstein (1972) that the secondary flow attains its maximum effect on the mainstream velocity every 60 degrees. This 60 degrees interval is associated with upwelling and downwelling flow conditions. The channel bend therefore interferes with the flow conditions rather than the converse. The flow separation is a response of the flow pattern to overcome such interferences. The separation zones migrate upstream as  $r_c/wds$  decreases.

Figure 4.23. The distribution of mean velocity in consecutive bends with  $r_c/w_{us}=2.67$  (constant) and variable downstream bend geometry.

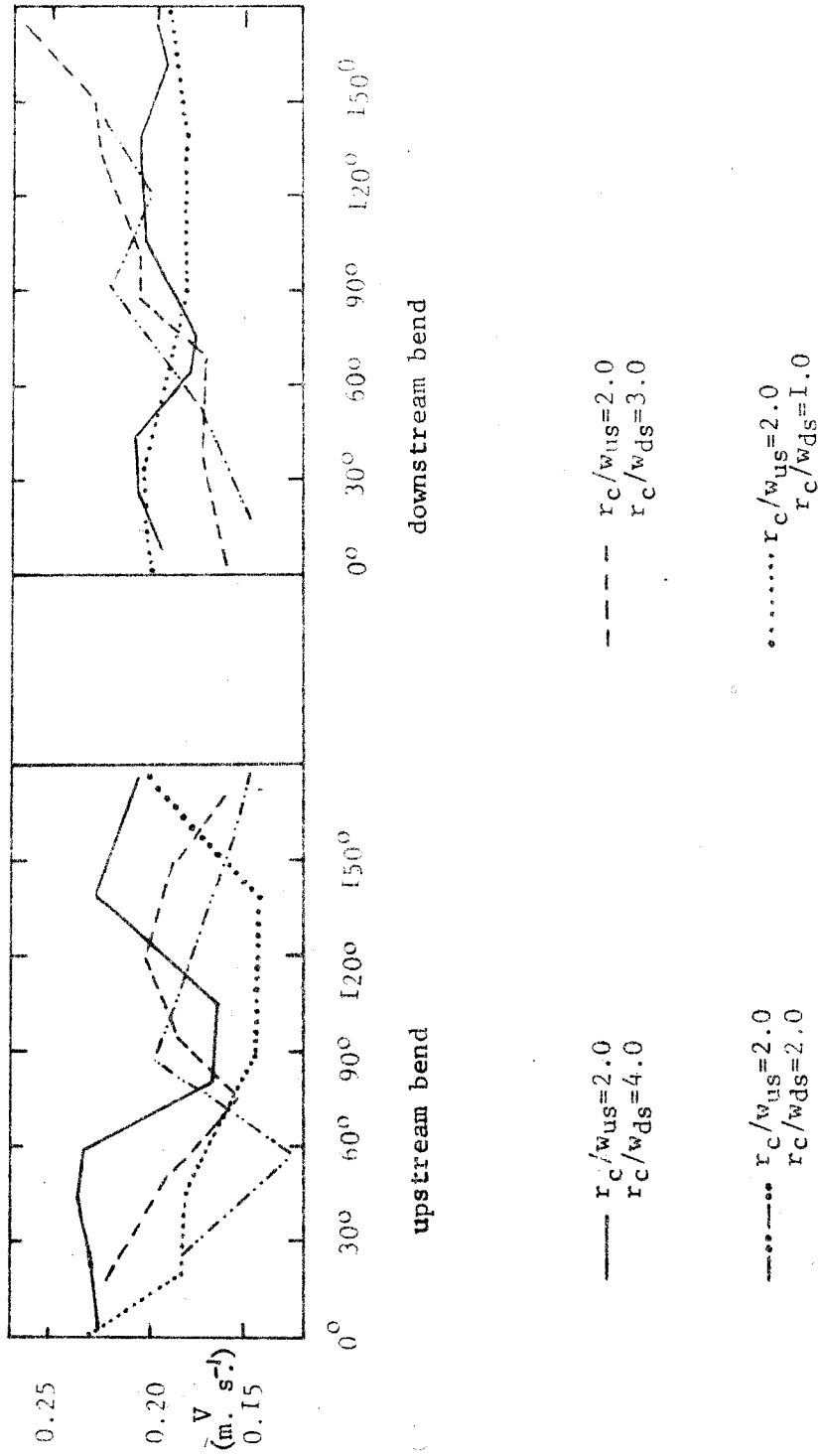


#### 4.2.4 The Distribution of Velocity in Consecutive Bends with $r_c/wus = 2.7$ and variable $r_c/wds$

The mean velocity distribution in bends of  $r_c/wus=2.7$  (Figure 4.23) is periodic every 60 degrees, like those of  $r_c/wus>3.65$ . The convex flow separation zones locate at 30 and 90 degrees of the bend. The mean velocity along the downstream bends reaches a maximum value upstream of 60 degrees and a minimum value along the bend zone between 60 and 120 degrees. The valley associated with minimum mean velocity between 60 and 90 degrees increases its depth and extends, probably because of the backwater effect discussed earlier. But the extent of the valley increases because secondary flow convection directs fluid towards the bank and piles it near the surface. This depresses the core of maximum velocity further towards the bottom at the centreline. Although Richards (1978) confirms that piling of water near the surface generates uniform distribution of velocity, most of the examples are obtained from straight channels with riffle-pool sequences and are not applicable to channel bends. Associating backwater phenomenon with examples observed in this study therefore demands that there be a pool at the bend apex and riffles at the inflections; the bend profiles in fact show the contrary.



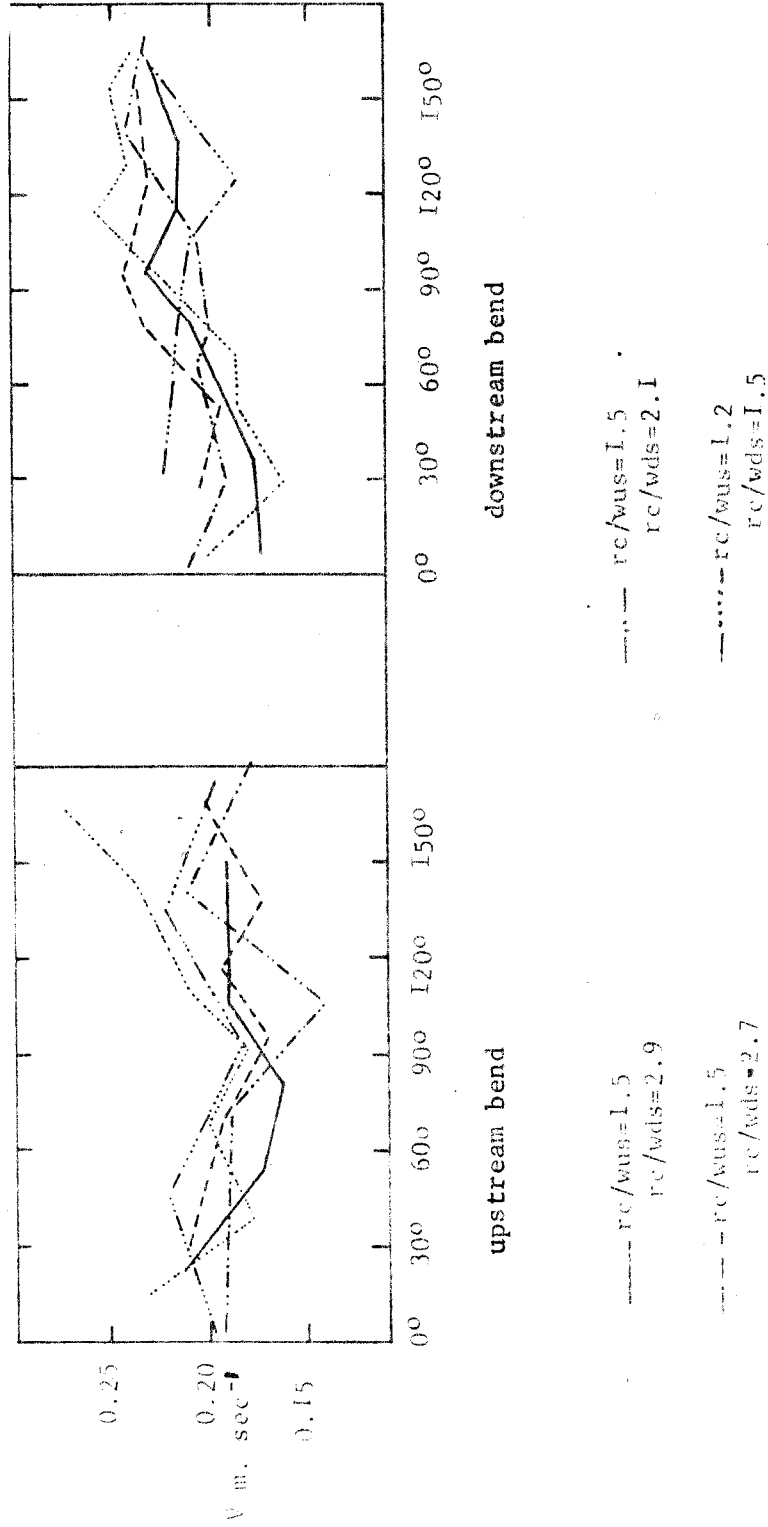
Figure 4.24. The distribution of mean velocity in consecutive bends with  $r_c/w_{us} = 2.0$  (constant) and variable downstream bend geometry.



#### 4.2.5 The Distribution of Velocity in Bends with $r_c/wds=2.0$ and variable $r_c/wds$

The lengthwise variation between minimum and maximum velocity points increases for bends of  $r_c/wds=2.2$  (Figure 4.23). The locations of minimum velocity migrate upstream from 90 degrees in co-association with the migration of the convex flow separation zones as the downstream bend curvature decreases. Along the downstream bends the mean velocity is uniform but increases downstream with minor valleys along the bend zone between 30 and 120 degrees. Convex flow separation zones locate in  $r_c/wds>3.0$  and concave flow separation in  $r_c/w<2.0$  at 60 degrees; this indicates a shift of the high velocity core from the inner (convex) bank towards the outer (concave) bank and the upstream migration of the cross over in the flow structure upstream as  $r_c/w$  decreases. This high velocity near the convex bank is due to transverse secondary flow near the channel bed from the inner bank which pushes decelerating fluid towards the outer bank (cf. Dietrich et al; 1983). Hickin's (1978) hypothesis on the location of the core of maximum velocity near the inner bank therefore is supported by the present results. Such bends generally incise the toe of the point bar and shifts its locus towards the downstream.

Figure 4.25. The distribution of mean velocity in consecutive bends with  $r_c/w_{us} = 1.5$  (constant) and variable downstream bend geometry.



The bends also have concave flow separation (cf. Hickin, 1979). In general, lateral migration may be discontinued but most bends likely will respond to this flow pattern by migrating downvalley (translational) although at a lower rate than that of wider bends.

#### 4.2.6 The Distribution of Velocity in Bends with $r_c/w_{us}=1.5$ and variable $r_c/w_{ds}$

The mean longitudinal velocity along the upstream bends increases to a maximum value at 30 degrees, decreases at the bend apex, then increases again towards the bend exit (Figure 4.25). The concave flow separation zone locates at 30 degrees in a bend with  $r_c/w=1.92$  and along the bend zone between 60 and 90 degrees in bend series of  $r_c/w_{us}=1.5$  and  $r_c/w_{ds}=1.2$ . The velocity decelerates along the convex bank between 90 and 120 degrees, the bend section where point bar deposition is greatest. There is an upstream migration of the locations of maximum mean velocity (high energy zone) and a downstream migration of flow separation zones (depositional zone) as the main flow structure follows a sinuous path. Assuming that the bend sections with maximal velocity will erode faster than those with less than the average velocity, it follows that such erosional axes likely will migrate downstream according to the present results. Hickin (1974) suggests that the regions of maximum erosion and deposition tends to change as the bend

amplitude increases.

The flow decelerates along the bend zone between 30 and 60 degrees in the downstream bends, the same region free vortex flow transforms into forced vortex. Measurements by Jackson (1975) on the Wabash River show that there is a rapid adjustment of the vortex flow to local curvature; the adjustment takes only 20 to 30% of each bend zone as observed in the present study.

#### 4.2.7 Summary and Observations

The nature of flow in rivers is gradually varied due to boundary resistance and internal distortion by secondary flow. There are periodic longitudinal and vertical oscillations of the mean velocity and velocity near the banks. Yalin (1971) suggested that the oscillations in a straight channel are periodic every  $2\pi$  times channel width while that of a meander wavelength is  $4\pi$  times channel width (both in c.g.s units) when measured along the meander axis (cf. Richards, 1976). Clearly the meander wavelength is invariant with the mean flow oscillation. The model bends discussed here have a constant width of 0.6m and the oscillations occur every 60 degrees. Minor departures from the 60 degrees wavelength probably are due to vortex coalescence and also interferences caused by the bend geometry and bedforms. The position where the mean velocity distribution has a minimum value is the same as those points where the forced vortex strength has a maximum value. This

coincidence may be because of eddies generated when the streamlines approach the outer (concave) bank at wide angles. The bend in which  $r_c/w=2.0$  has a sinuous velocity oscillation which is more regular than those of other bends considered in this section.

Talbot and Gong (1983) found that secondary circulation in closed conduits reaches a maximum value at 30 degrees (cf. Muramoto, 1967; Einstein, 1972). The maximum mean velocity at 30 degrees occurs where parabolic flow translates to a forced vortex or a free vortex flow; these vortices generate a surplus of momentum acceleration (cf. de Vriend, 1980).

The flow separation zones are regions of pressure surplus caused by an abrupt change of streamlines from the boundary. They locate at either 60 degrees, 90 or 120 degrees; each at an interval of 30 degrees which compares well with the occurrence of major velocity amplitudes. The secondary flow in separated zones near the bed are directed towards the side walls and then up towards the water surface. Because low momentum fluid shifts from the mainstream flow near the channel bed towards the separated zone, a complete breakaway of the inner vortex (Bagnold, 1960) was not observed in the present runs.

Decreasing  $r_c/w$  increases the variation of longitudinal mean velocity by way of increasing the intensity of the secondary flow advection near the banks and the channel centreline (de Vriend, 1980). Secondary flow advection reduces the depth-averaged velocity because it transports fluid of

longitudinal momentum deficit to the mainstream flow wherever the isovel bulge inwards ( away from the boundary). The fluid near the concave bank, on the other hand has surplus longitudinal momentum because the isovels bulge outwards (towards the boundary). This pattern of secondary flow facilitates deposition along the inner bank and erosion on the outer (concave) bank.

Cassidy and Falvey (1970) found that the locations of minimum longitudinal velocities are associated with flow oscillations that are of "opposite pitch", i.e. the velocities near the banks are out-of-phase. It is known that this asymmetric velocity distribution is conducive to alternate erosion and deposition (Quraishy, 1944). Assuming that the velocity near the banks is competent to cause erosion, the banks will be eroded at 60 and 120 degrees of the bend because these are points where the velocity has a maximum value. The expansion mode of lateral erosion requires that maximum velocity and the erosional axis locate at the bend apex as observed for a bend with  $r_c/w=3.3$  (Figure 4.22). Other modes will require different combinations of periodic flow patterns.

The mean longitudinal velocity along the downstream bends is irregular. The irregularity tends to increase with an increase in bend curvature at a constant upstream condition. The velocity distribution along the banks tends to criss-cross at 60 degrees, the same location where the free vortex inherited from the upstream bends translates to a forced vortex. The effect of

the upstream bends are eliminated completely by 60 degrees of the bend (see also Bluck, 1971).

The mean energy gradient in meander bends is steeper than in straight channels (Leopold et al; 1964) and meander bends therefore depend on such surplus energy to overcome bend resistance, erode the concave bank, and form point bars on the convex bank. The increased bend resistance is probably accommodated by the greater depth of the pool at the bend apex that encourages backwater effects and reduces resistance. The backwater effect envelopes the bend zone between 60 and 120 degrees where the minimum mean velocity was measured.

The valley of the mean longitudinal velocity at 90 degrees is due to flow deceleration along the banks because of pressure surplus and boundary roughness. Because the core of maximum velocity locates near the bed, the effect of the boundary roughness likely is accompanied by high sediment charge. But the longitudinal velocity in a bend of  $r_c/w=2.6$  is sensibly steady without flow separation zones conforming to the suggestion made by Choi et al (1979) that no flow separation forms in experiments with steady flow. Further tightening of such bends increases the depth of the "valley" in bends of  $r_c/w=2.0$ . But by  $r_c/w=1.5$  the velocity depression has decreased considerably and by  $r_c/w=1.2$ , the distribution of the flow is quasi-steady again.

According to Shen and Komura (1968), well developed scour holes and skewed shoals may be obtained with nonuniform flow.



The velocity distributions that are steady for bends of  $r_c/w < 1.5$  and  $r_c/w = 2.6$  likely are related to the processes of bank erosion and deposition along the straight entrance and exit portions of the bend (cf. Carey, 1963). Bends with approximately  $r_c/w = 2.0$  have low rates of erosion (Hickin and Nanson, 1975) perhaps because stream competence is reduced at the bend apex as a result of decreased mean velocity. Sato and Okada (1966) have suggested that mean velocity first decreases and secondly becomes irregular behind bluff bodies with an increase of the angle of attack. Any decrease in bend curvature increases the angle at which the flow has to turn in order to fulfil continuity demands. The streamlines therefore will impinge on the concave (outer) bank at a large angle as the bend become tighter and this establishes large eddies which decrease the mainstream velocity.

The velocity near the banks tends to show more extreme excursions than the mean longitudinal velocities. The maximum velocity near the concave bank locates at 30 degrees where the maximum shear stress was observed also by Ippen and Drinker (1962). The second position at which the velocity near the concave (outer) bank is high locates downstream of 120 degrees where erosion likely may be appreciable (cf. Parsons, 1960). Yen (1970) demonstrates also the persistence of low shear stress and velocity at 80 degrees near the concave bank in diverse bend geometries; a characteristic that the present study supports. The effect of a sinusoidal core of maximum velocity on shear

stress distribution is examined below.

### 4.3 THE DISTRIBUTION OF SHEAR STRESS AND FRICTION COEFFICIENTS IN CONSECUTIVE BENDS WITH CONSTANT UPSTREAM BEND GEOMETRY

#### 4.3.1 Introduction

A general model of shear stress distribution in open-channel bends (cf. Ippen and Drinker, 1962) shows that high shear stress occurs along the convex bank along the bend entrance, shifts towards the concave bank midway past the bend apex, and remains there through the rest of the bend. The mean shear stress was calculated by graphical integration of point shear through the cross section. The measurements are applicable near the channel bed at  $y_1/y_0 > 0.75$ . The magnitude of shear stress was found to be dependent on the strength of the secondary flow (cf. Brooks, 1963).

The discussion in sections 4.1 and 4.2 has identified regions of the bend which have relatively high velocity and explains how the mainstream velocity interacts with secondary flow advection. This section examines the distribution of shear stress and friction to flow in the same bends in order to relate points of maximum and minimum shear stress and friction to isovel patterns and types of vortices. The bend effects transmitted to subsequent bends will also be examined by

comparing the distribution of shear stress and friction coefficients of different bend series.

4.3.2 The Distribution of Shear Stress and Friction Coefficients in Consecutive Bends with  $r_c/wus=4.0$  and variable  $r_c/wds$

The longitudinal distribution of mean shear stress shown in Figure 4.26 reflects the distribution of friction coefficient shown in Figure 4.27. The maximum shear along the bends locates at 40 degrees, 90 degrees and 150 degrees, while the minimum values locate at 60 degrees, 120 degrees and also along the exit portions of the upstream bends of  $r_c/wus=4.0$  and  $r_c/wds>2.0$ . The maximum shear moves towards the outer bank at 30 degrees, then more or less towards the channel centreline at the bend apex and finally it returns to the outer bank along the downstream portion of the bend apex.

Erosion or deposition may occur anywhere along a bend as they depend on the ability of the local shear stress to transport more or less of the sediment load supplied (Hooke, 1975). Onishi et al (1976) have shown that the sediment supplied towards the inner (convex) bank is greater than the competence of the local flow conditions to transport all of it. This facilitates point bar deposition.

Figure 4.26. The distribution of mean shear stress in consecutive bends in consecutive bends with  $r_c/w_{us}=4.0$  (constant) and variable downstream bend geometry.

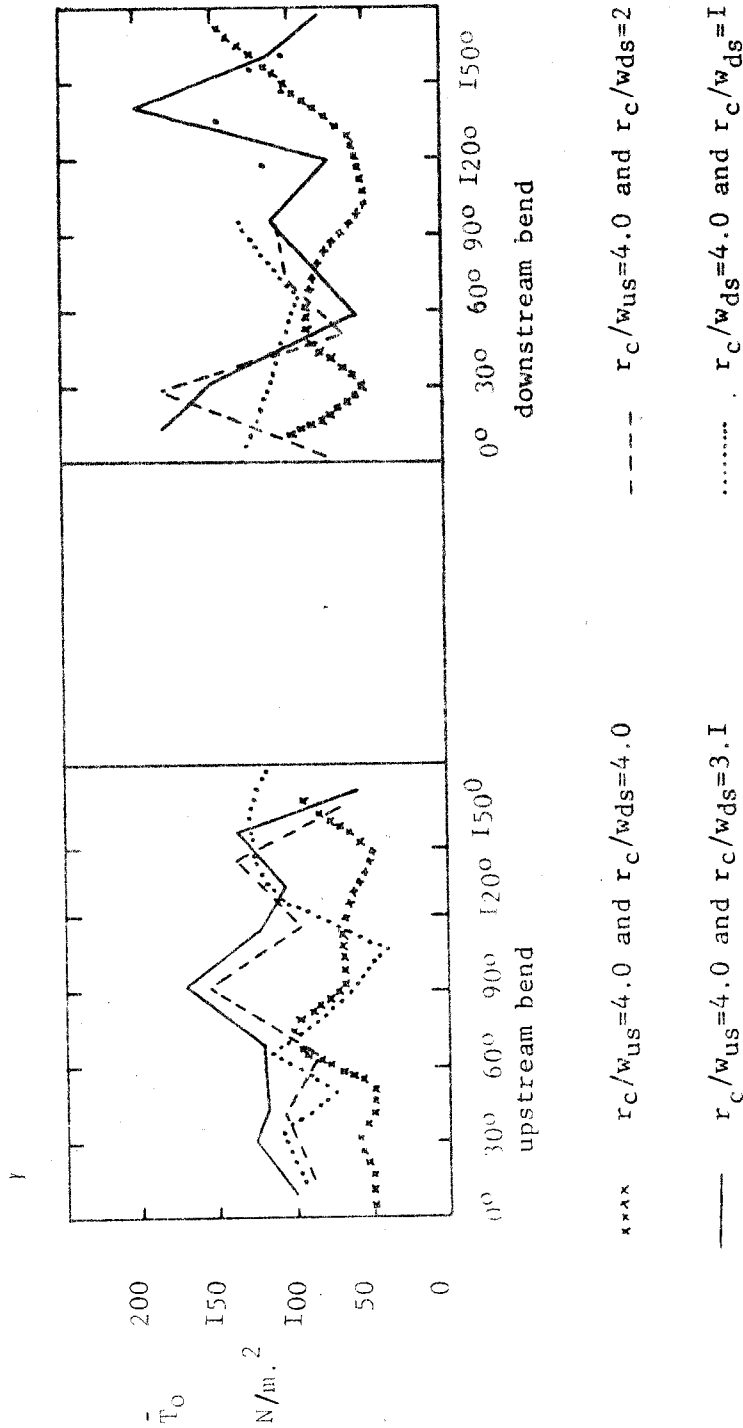
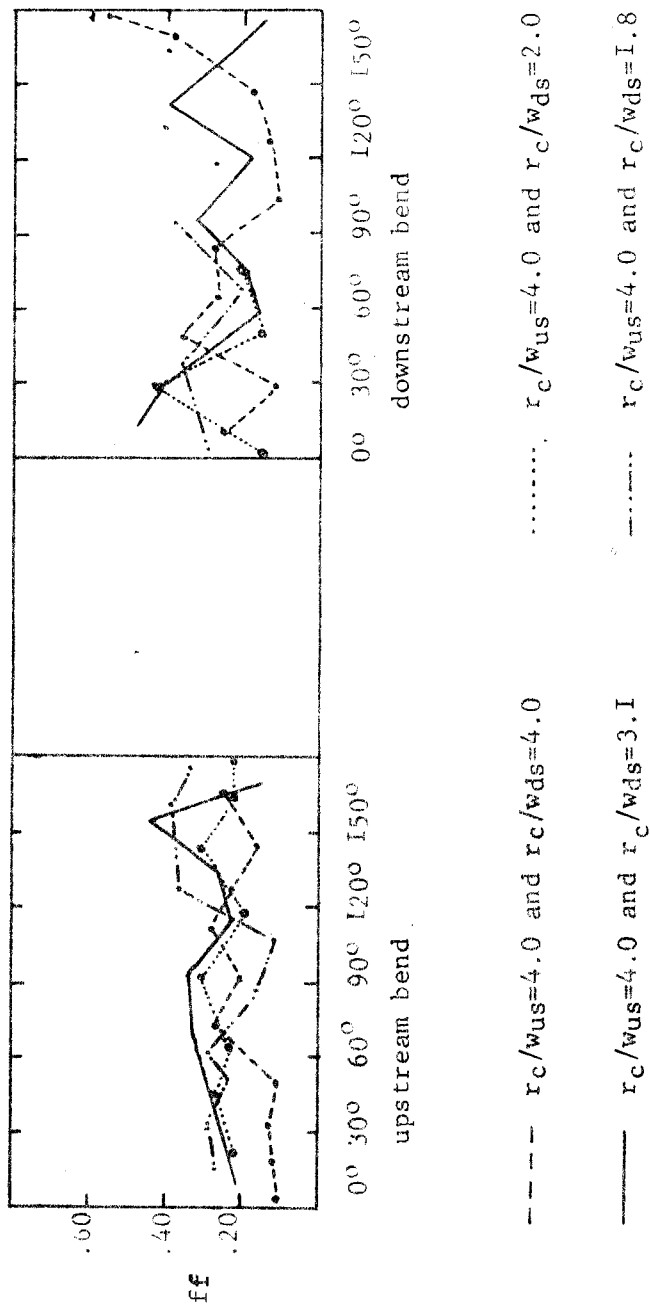


Figure 4.27. The distribution of friction coefficient in consecutive bends with  $r_c/w_{us}=4.0$  (constant) and variable downstream geometry.



For bends with  $r_c/wds=4.0$ , erosion may be appreciable at a bend angle of 30 degrees and also downstream of 100 degrees along the concave bank. Assuming that this pattern of erosion is not interrupted, a T-shaped bend geometry will develop (cf. Hickin, 1974; Figure 7, type C or F).

The distribution of shear stress is periodic every 50 to 60 degrees. The upstream bend preceded by  $r_c/wds=1.8$  has a maximum value of the mean shear stress at 30 and 60 degrees and also in the region of the bend exit. If erosion occurs at these points of maximum shear, the erosional motif conforms to that described by Hickin (1974, figure 6) where three points of erosional axes occur; two points at the bend entrance and also towards the bend exit. The minimum shear stress value occurs along the bend zone between 75 and 105 degrees in bends preceded by  $r_c/wds=4.0$  and 1.8. In other words, the centre of the maximum value of shear stress has moved to occupy a bend angle upstream of 60 degrees and downstream of 105 degrees. These are the points where the velocity near the channel bed is high and pools locate also. A summary of the locations of minimum and maximum shear stress is shown in Table 4.6.

TABLE 4.6

The location (in degrees) of the maximum and minimum values of shear stress in consecutive bends with  $r_c/w_{us}=4.0$  and variable downstream bend geometry.

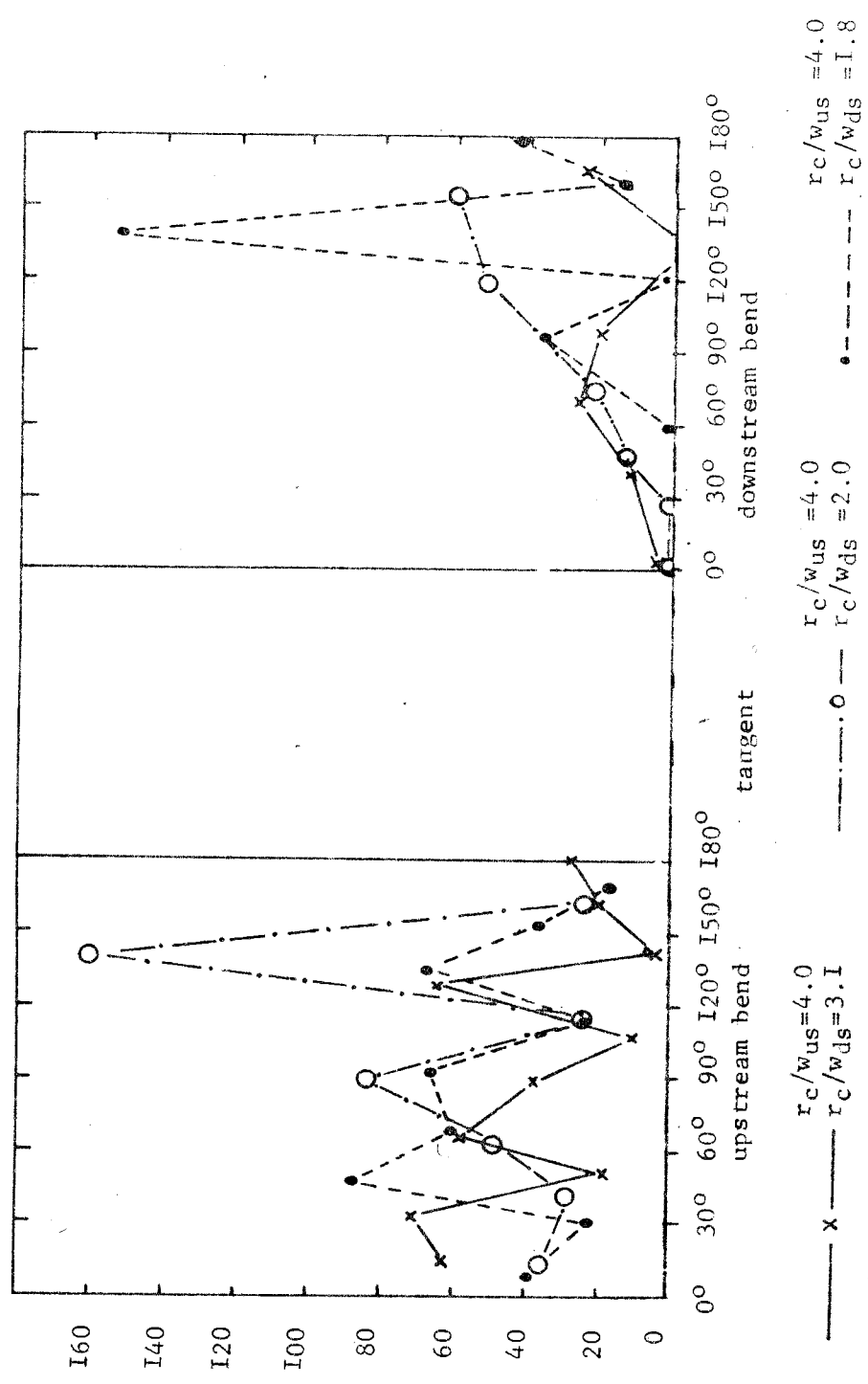
$r_c/w_{us}$	$T_{\text{max}}$	$T_{\text{min}}$	$r_c/w_{ds}$	$T_{\text{max}}$	$T_{\text{min}}$
4.0	75	50;150	4.0	30;105	150
4.0	90	170	3.1	135	60;120
4.0	90	170	2.0	30	50
4.0	120;150	50;105	1.8	30;105	150-180

Figure 4.28 shows the distribution of shear stress along the banks, 0.076m away from the water's edge. The shear stress distribution along the concave (outer) bank are connected by lines while the one near the inner bank are shown by various symbols that are not connected by lines. The shear stress distribution along the concave bank in  $r_c/wds=3.1$  and  $1.8$  is periodic every 60 degrees; but increases monotonically in  $r_c/wds=2.0$ . The inherited high shear along the convex bank dissipates along the downstream bend zone between 50 and 60 degrees, then it shifts and increases along the concave bank. Erosion tends to occur along the convex bank upstream of 60 degrees in a wide range of  $r_c/w$  (cf. Kondrat'yev, 1968).

Figure 4.27 shows a narrow band of mean friction coefficient around  $ff=0.20$ . The location of the pool and the decrease of the strength of secondary flow along the bend zone between 60 and 120 degrees may cause friction at the bend apex to decrease. But the decrease of friction coefficient in the bend corresponds also with the bend axis where the pool is supposedly located. The present study has identified two pool locations: one is upstream of 60 degrees and the other is downstream of 120 degrees. Instead of a pool there is a tendency for a riffle to locate at the bend axis of some but not all bends (cf. Bluck, 1972). Evidence presented by Keller (1972) demonstrates the variability of the location of pools and riffles as meandering streams increase their amplitudes ( $r_c/w$  decreasing).



Figure 4.28. The distribution of shear stress near the concave bank in consecutive bends with  $r_c/w_{us}=4.0$  (constant) and variable downstream bend geometry.



nb. The shear stress along the convex (inner) bank are not shown because it is low.

### 4.3.3 The Distribution of Shear Stress and Friction Coefficients in Consecutive Bends of $r_c/wus=3.65$ and variable $r_c/wds$

Unlike a bend with  $r_c/wus=4.0$ , the mean shear stress distribution in one of  $r_c/wus=3.65$  is nonperiodic; except in a bend preceded by  $r_c/wds=2.2$  (Figure 4.29). The maximum mean shear stress concentrates along the bend zone between 30 and 70 degrees but becomes steady downstream of the bend apex (120 - 150 degrees). The upstream bend preceded by  $r_c/wds=2.2$  is periodic every 60 degrees as for  $r_c/wus=4.0$ . Table 4.7 shows the specific points since there are minor variations due to flow variability.

Along the downstream bends, the inherited high shear zone along the convex bank is considerably reduced in bends of  $r_c/wds=3.8$ , 2.2 and 1.56, but the reasons for this trend are not obvious. The minimum value locates upstream of 45 degrees (Figure 4.31). The shear along the concave bank has a maximum value between 90 and 120 degrees of the bend, except in that with  $r_c/wds=1.75$ , the same bend zone liable for erosion in the expansion mode of channel migration (cf. Daniel, 1971). The point at which shear stress trends near the banks cross each other moves upstream by 20 degrees in these runs compared to 60 degrees in bends preceded by  $r_c/wus=4.0$  (Figure 4.28). The upstream shift of the cross over of the high shear stress distribution possibly is related to the relatively lower shear

Figure 4.29. The distribution of mean shear stress in consecutive bends with  $r_c/w_{us}=3.65$  (constant) and variable downstream bend geometry.

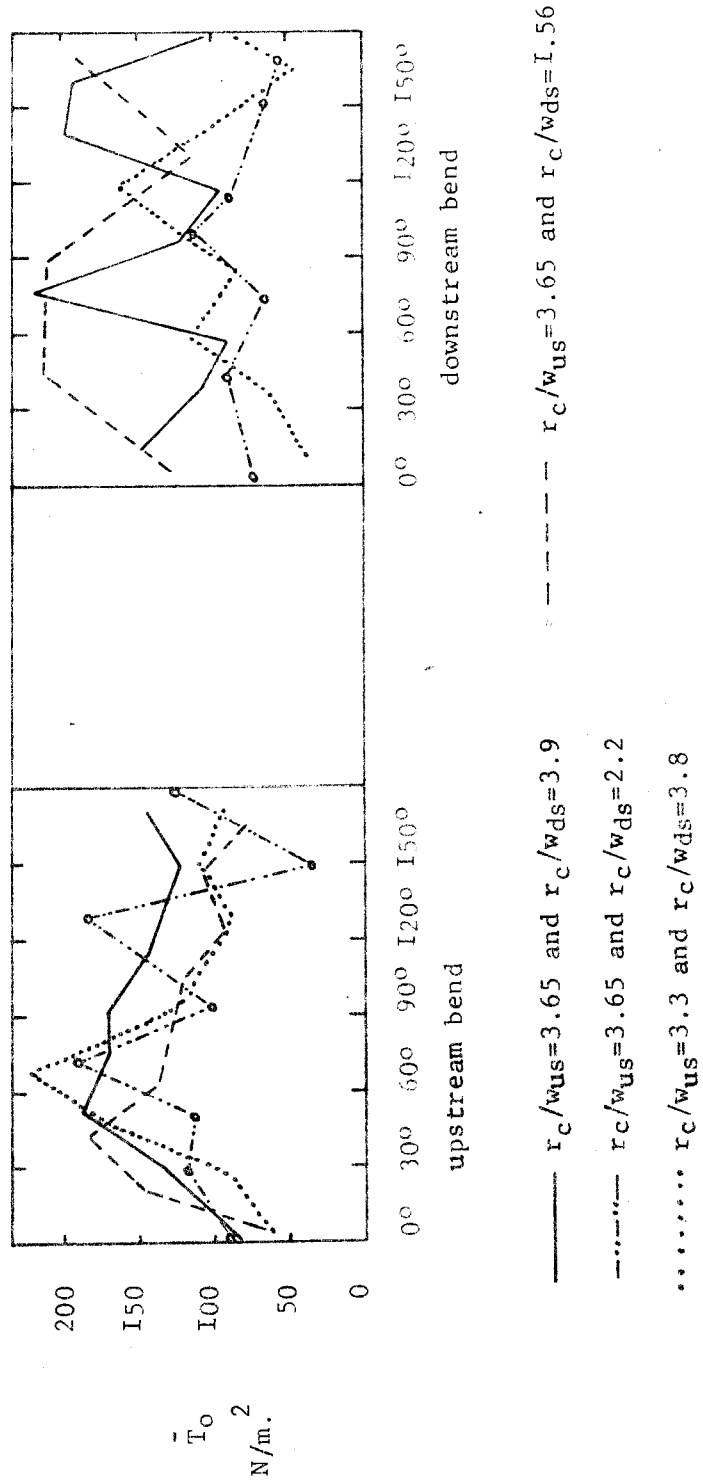
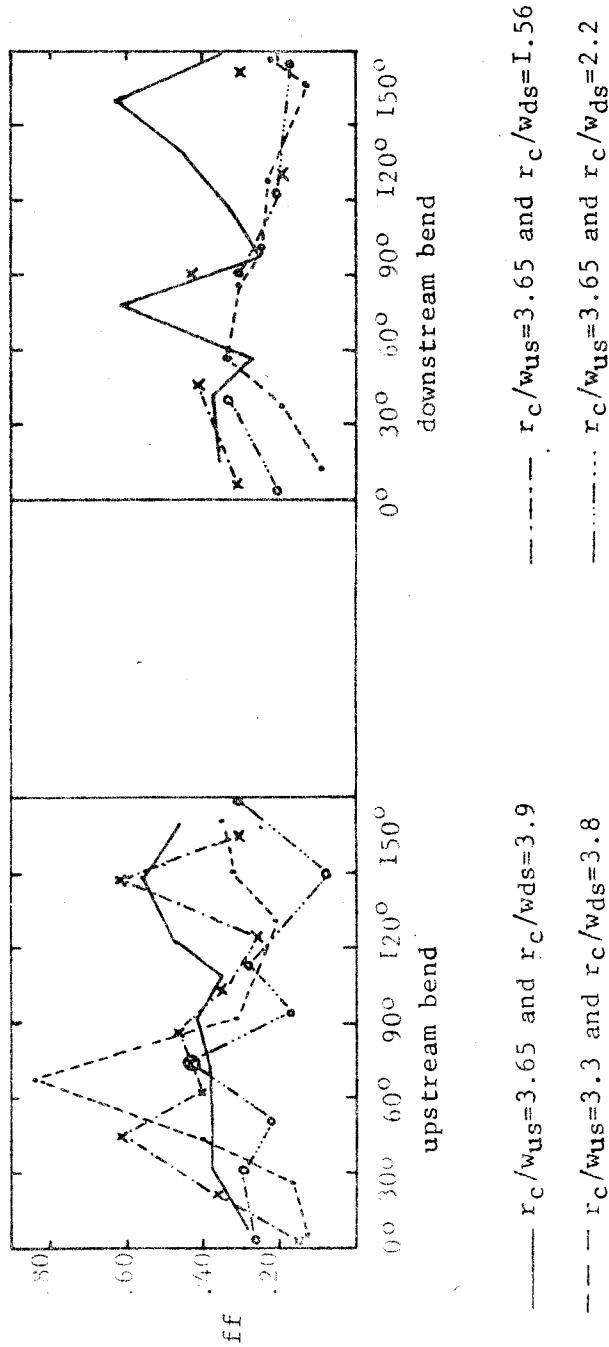
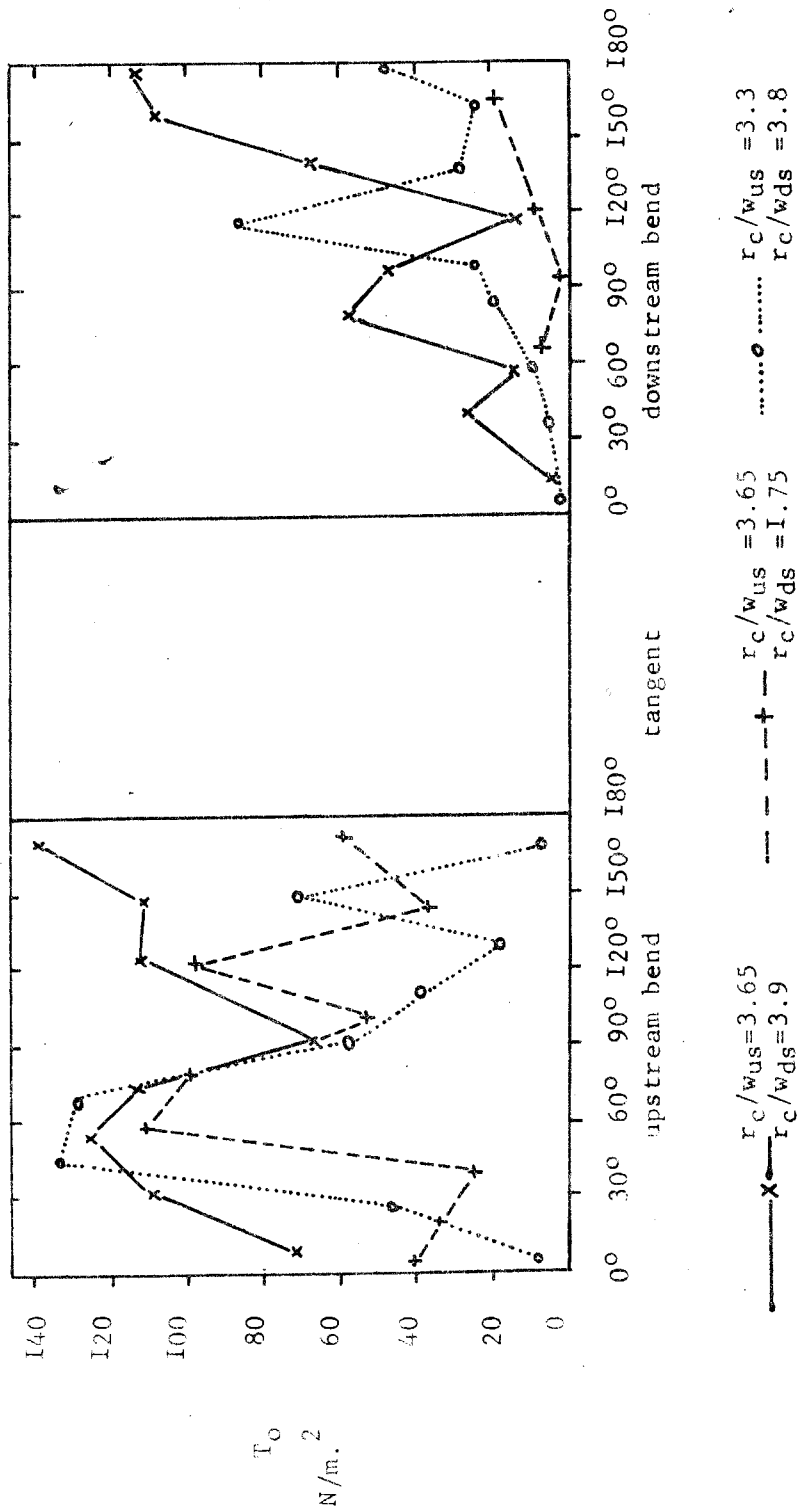


Figure 4.30. The distribution of friction coefficient in consecutive bends with  $r_c/w_{us}=3.65$  (constant) and variable downstream bend geometry.



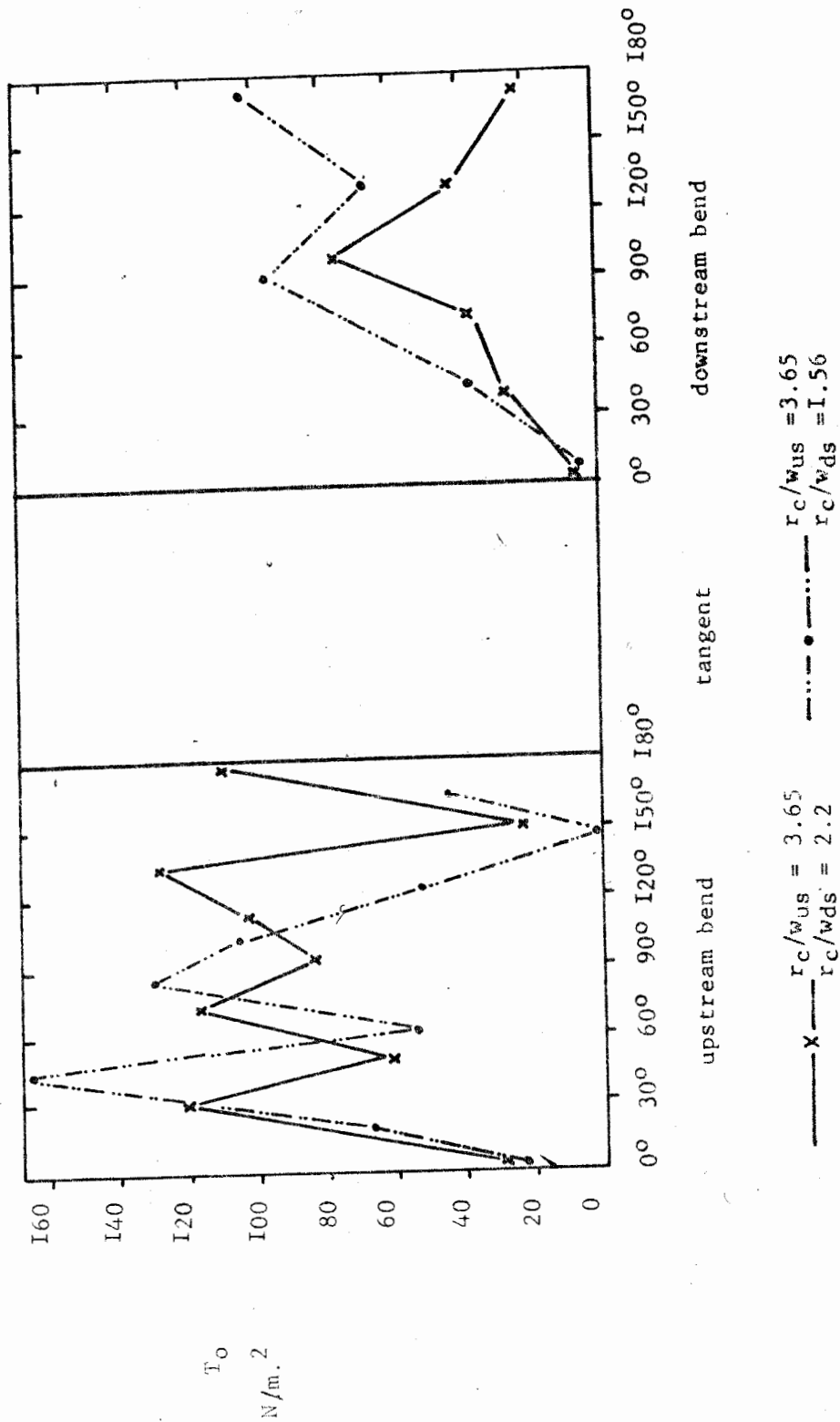
Nb. Note that the friction coefficient values for  $r_c/w_{ds}=1.56$  are not connected by any lines.

Figure 4.31(a). The distribution of shear stress near the concave bank of consecutive bends with  $r_c/w_{us} = 3.65$  (constant) and variable downstream bend geometry.



nb. The shear stress values along the convex bank are low; they are not included in this diagram.

Figure 4.3I(b). The distribution of shear stress near the concave bank of consecutive bends with  $r_c/w_{us} = 3.65$  (constant) and variable downstream bend geometry.



nb. The shear stress values along the convex (inner) bank are generally low; they are not included in this diagram.

rates along these downstream bends.

The identification of regions of maximum energy dissipation and bank erosion can be made by examining the location of maximum shear points. The shear stress distribution near the banks along the downstream bends can be categorised as double peaks and single peaks as shown in Table 4.8. A bend of  $r_c/wds=3.91$  has two peaks at 75 and 150 degrees while the minimum value locates at 60 and 105 degrees. The wavelength of the shear stress distribution is about 60 to 70 degrees. The upstream position of maximum shear stress decreases in a bend with  $r_c/wds=3.8$  and 2.2 while the second peak moves simultaneously upstream from 150 to 120 degrees. A bend of  $r_c/wds=1.7$  has a single maximum shear value at 90 degrees while that  $r_c/wds=1.56$  has a maximum value between 45 and 90 degrees. In general, the maximum shear stress locates at either 45 degrees, 90 or at 150 degrees in most channel bends. These locations also are the points where the intensity of secondary flow attains a maximum value.

The mean shear stress distribution and that along the concave bank in bend series of  $r_c/wus=3.65$  are relatively higher than those measured in  $r_c/wus=4.0$ , in spite of their equal mean velocity and width-depth ratio. The minimum friction coefficient locates along the bend zone between 90 and 150 degrees in agreement with the pattern of secondary flow discussed earlier. In general, the maximum friction coefficient along the upstream bends occupies the bend zone upstream of 90 degrees and

TABLE 4.7

The location of maximum shear stress in consecutive bends of  $r_c/w_{us}=3.65$  (constant) and variable downstream bend geometry.

(measurements in degrees of bend angle)

$r_c/w_{us}$	$T_{omax}$	$T_{omin}$	$r_c/w_{ds}$	$T_{omax}$	$T_{omin}$
3.65	55	SE I	3.91	75; I50	60; I20
3.65	75; I30	90; I50*	2.2	100	-
3.65	45	SE I- I80	1.56	45-90 I75	I30
3.3	70	SE I*	3.8	60; I20	80; I65

\* SE straight Entrance



decreases towards the exit portions. There are two peaks of maximum friction at 45 degrees and 150 degrees along the upstream bends. The downstream trends, however, are reduced to one peak that locates between 60 and 90 degrees, except in bend series with  $r_c/wus=3.65$  and  $r_c/wds=3.91$  in which double peaks occur at 75 and 150 degrees as for the upstream bends. The high shear stress and friction coefficient may be attributed to internal flow distortion in the pools and to boundary roughness over the riffles or cross overs (Leopold et al; 1960).

#### 4.3.4 The Distribution of Shear Stress and Friction Coefficients in Consecutive Bends of $r_c/wus=2.70$ and variable $r_c/wds$

The mean shear stress and boundary shear along the concave bank in bends with  $r_c/wus=2.70$  concentrates at 35 degrees; other points of concentration locate at 100 and 150 degrees of the bend (Figure 4.32). Along the bend zone between 60 and 90 degrees and at 120 degrees, the dimensionless shear stress ( $T_o/\bar{T}_o$ ) is totally borne by the concave (outer) bank; the same points where the maximum erosion likely occurs. Bends preceded by  $r_c/wds=4.0$  and 1.0, however do not have any major boundary shear peaks, probably because of steady flow at the bend apex. The distribution along the concave bank is periodic every 40 to 50 degrees, but is generally high at the bend entrance (cf. Ippen and Drinker, 1962).

Figure 4.32. The distribution of mean shear stress in consecutive bends with  $r_c/w_{us}=2.67$  (constant) and variable downstream bend geometry.

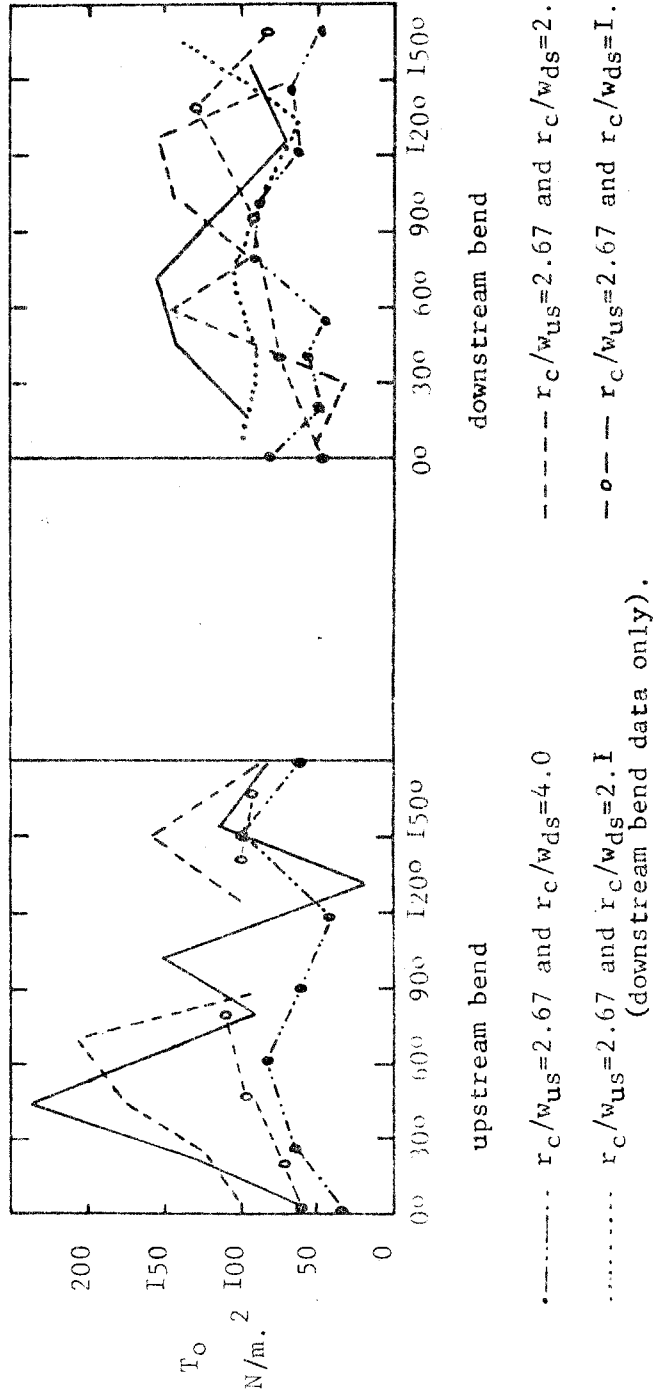


Figure 4.33. The distribution of friction coefficient in consecutive bend with  $r_c/w_{us}=2.67$  (constant) and variable downstream bend geometry.

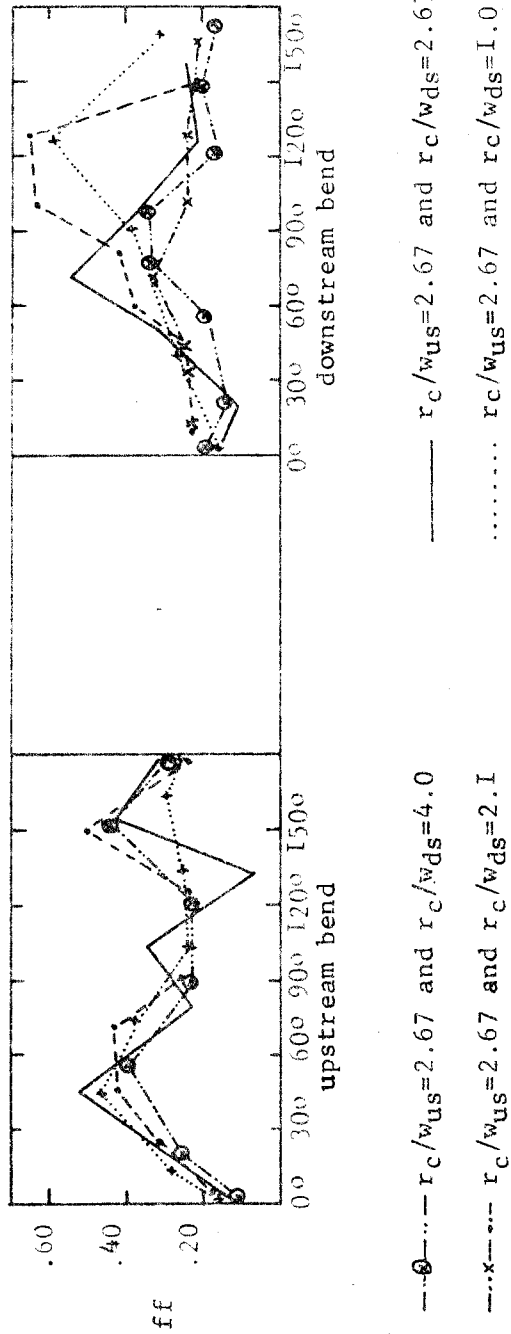
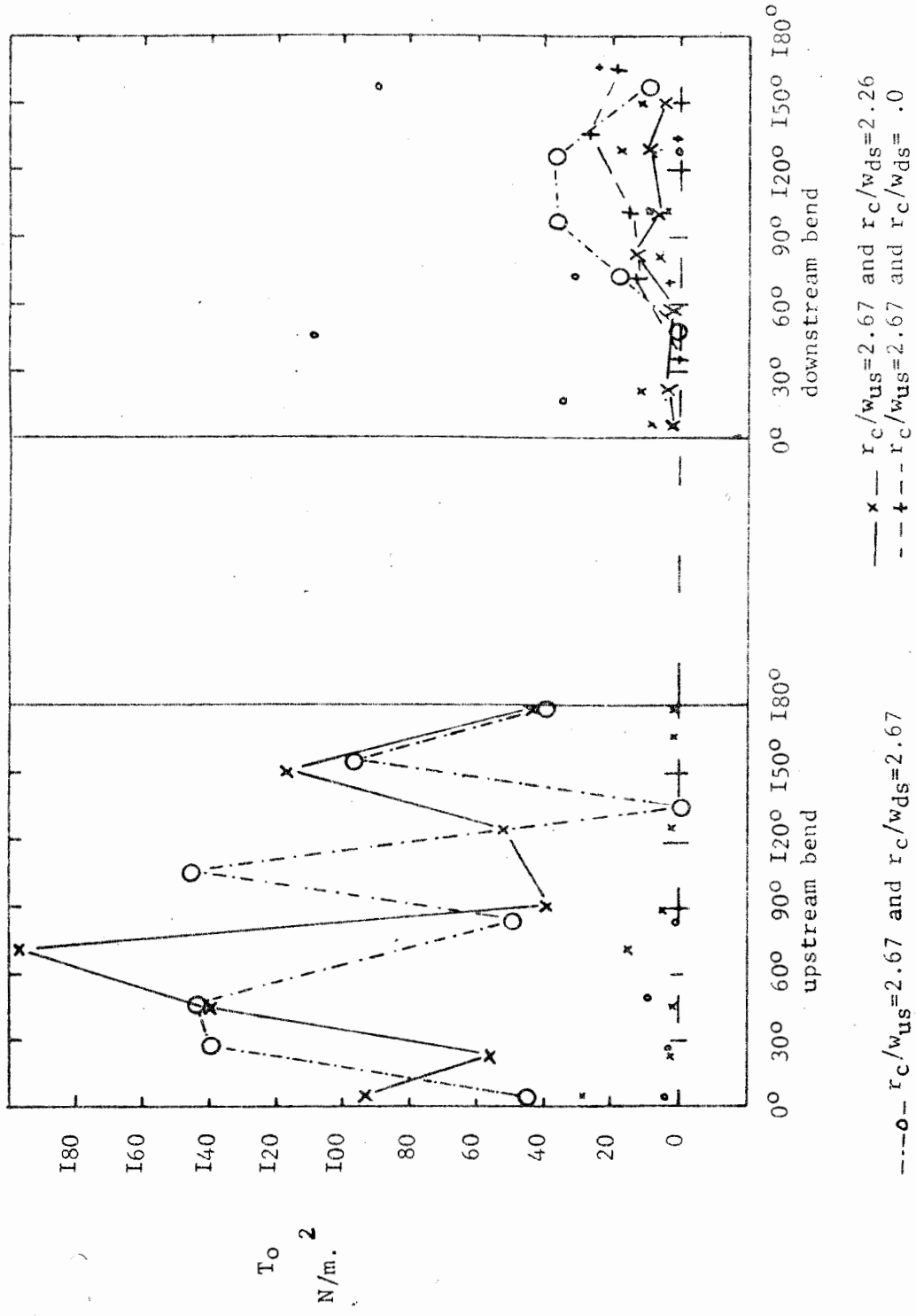


Figure 4.34. The distribution of shear stress near the channel banks in consecutive bends with  $r_c/w_{us}=2.67$  (constant) and variable downstream bend geometry. The shear stress near the concave bank are connected by lines while that near the convex bank are shown by symbols only.



Nb. The shear stress along the convex bank are shown by smaller symbols than that near the concave bank.

Along the downstream bends, the maximum shear stress locates upstream of 60 degrees in a bend with  $r_c/wds=2.70$ ; between 90 and 120 degrees in those of  $r_c/wds=2.26$  and 1.0. These differences in the location of the maximum shear stress occur because the time the flow takes to become fully developed varies from one bend series to the other (see for example  $r_c/wds=2.26$  and 4.0). The shear distribution along the convex bank is relatively high upstream of 60 degrees and downstream of 150 degrees, as observed in the previous bends (cf. Nough and Townsend, 1978). This is the bend zone where most of the bank calving occurs (Parsons, 1960). Figure 4.33 ( $r_c/wds=2.70$ ) has three peaks of maximum friction coefficient at 45, 120 and 150 degrees along the upstream bends and at 75 degrees along the downstream bends (variable  $r_c/wds$ ). But the zone with maximum friction coefficient shifts to the bend exit in  $r_c/wds=2.26$  (from 75 degrees in other bends) where the channel is deep and secondary flow divergence near the bed is predominant. Erosion possibly occurs along this exit portion of the bend.

#### 4.3.5 The Distribution of Shear Stress and Friction Coefficients in Consecutive Bends of $r_c/wds=2.0$ and variable $r_c/wds$

The lengthwise distribution of mean shear stress is symmetrical at 90 degrees in bends preceded by  $r_c/wds=2.0$ ; but concentrates downstream of the bend apex in those preceded by  $r_c/wds>1.9$ , except the one preceded by  $r_c/wds=1.0$  whose

distribution skews upstream of the bend apex. The reasons for these differences are not presently known. The minimum mean shear locates between 30 and 90 degrees (Table 4.9). Leopold et al (1960) argued that although flow depth increases and relative roughness declines in the bend pool zones, energy dissipation through increased secondary flow results in a net increase in resistance to flow there. The present data shows that the increase of secondary flow along the bend zone is discontinuous and also varies with  $r_c/w$ . In some cases, the pool does not locate at the bend apex. The low shear stress along the bend apex likely is a result of the decrease of secondary flow associated with the backwater effect. The shear stress along the concave bank decreases from the entrance to 30 degrees, then increases to a maximum value between 60 and 90 degrees. In general the distribution is periodic every 60 degrees.

The mean shear stress distribution along the downstream bends centres upstream of the bend axis in bend series with  $r_c/wds=2.70$  and  $2.26$ , downstream of 90 degrees in  $r_c/wds=1.0$ ,  $2.1$  and  $2.26$ ; but it remains uniform in  $r_c/wds=4.0$ . These locations reflect the characteristics of secondary flow development. Along the convex bank, the shear stress is generally low, but the maximum values locate at 60 and 120 degrees while the minimum values locate at 45 degrees and between 100 and 160 degrees except in  $r_c/wds=2.0$ . The boundary shear along the concave bank increases gradually

TABLE 4.8

The location (in degrees) of maximum and minimum shear stress of consecutive bends of  $r_c/w_{us}=2.0$  and varying  $r_c/w_{ds}$ .

$r_c/w_{us}$	$T_{omax}$	$T_{omin}$	$r_c/w_{ds}$	$T_{omax}$	$T_{omin}$
2.0	35; 105	60	4.0	90	180
2.0	15; 90	40	3.0	100; 150	30; 105
2.0	15; 95	60	2.0	90	-
1.92	15; 110	40	2.65	105	-

Figure 4.35. The distribution of mean shear stress in consecutive bends with  $r_c/w_{us}=2.0$  (constant) and varying  $r_c/w_{ds}$ .

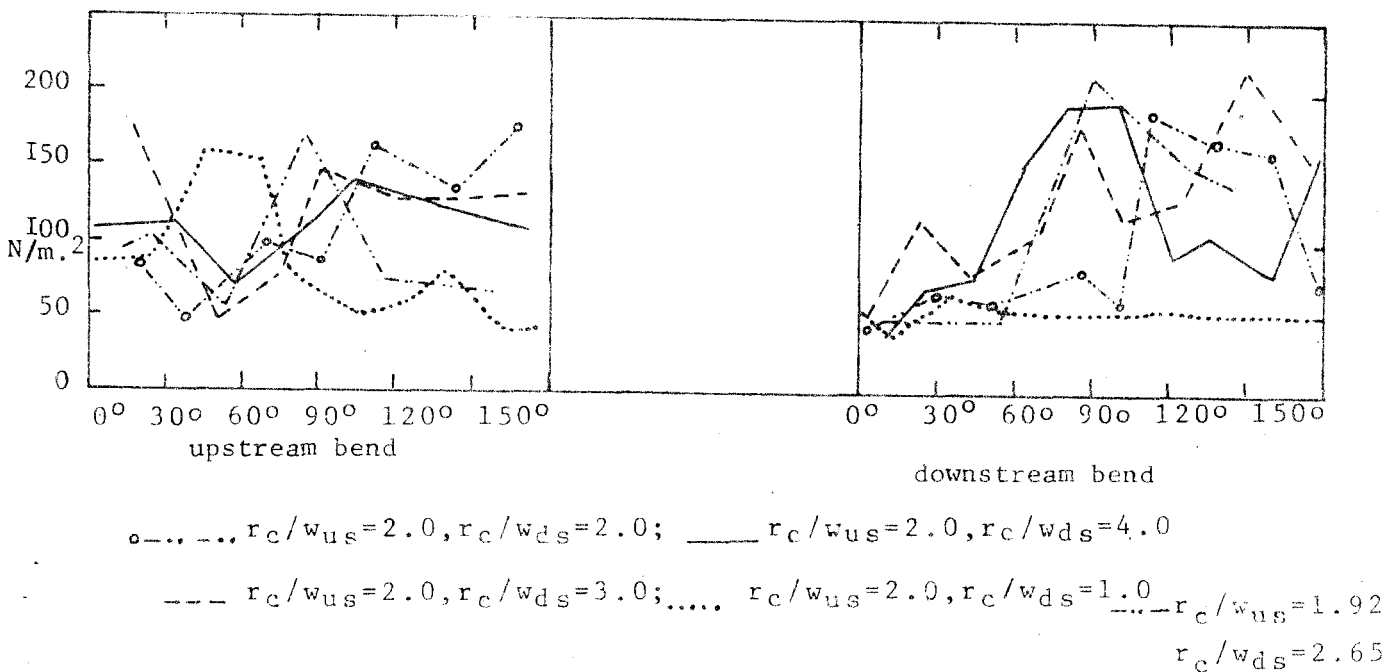


Figure 4.36. The distribution of shear stress near the channel banks of consecutive bends with  $r_c/w_{us} = 2.0$  (constant) and variable downstream bend geometry. The shear stress near the concave (outer) bank is shown by symbols connected by lines while the symbols for the convex bank are not connected by any lines.

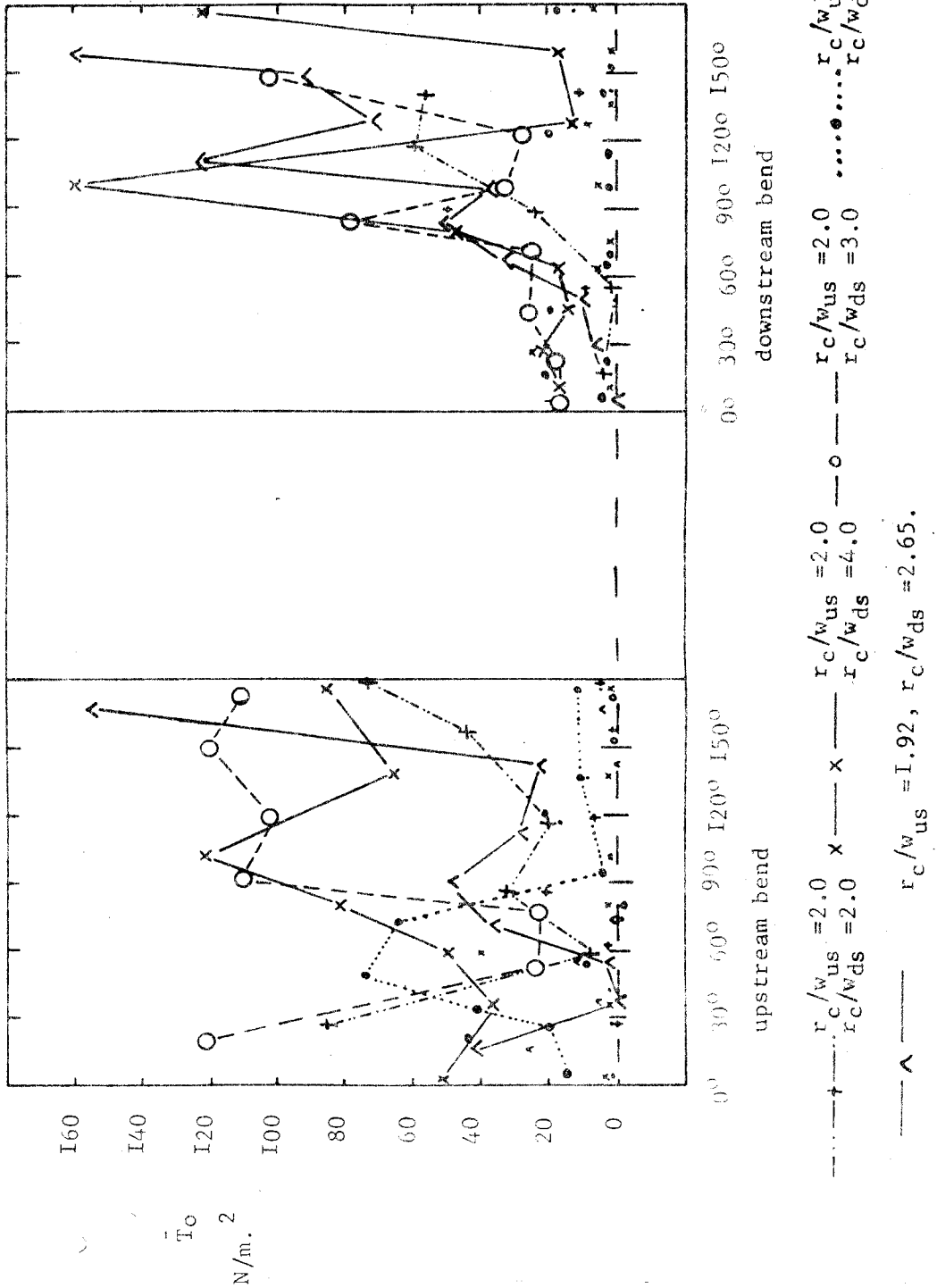
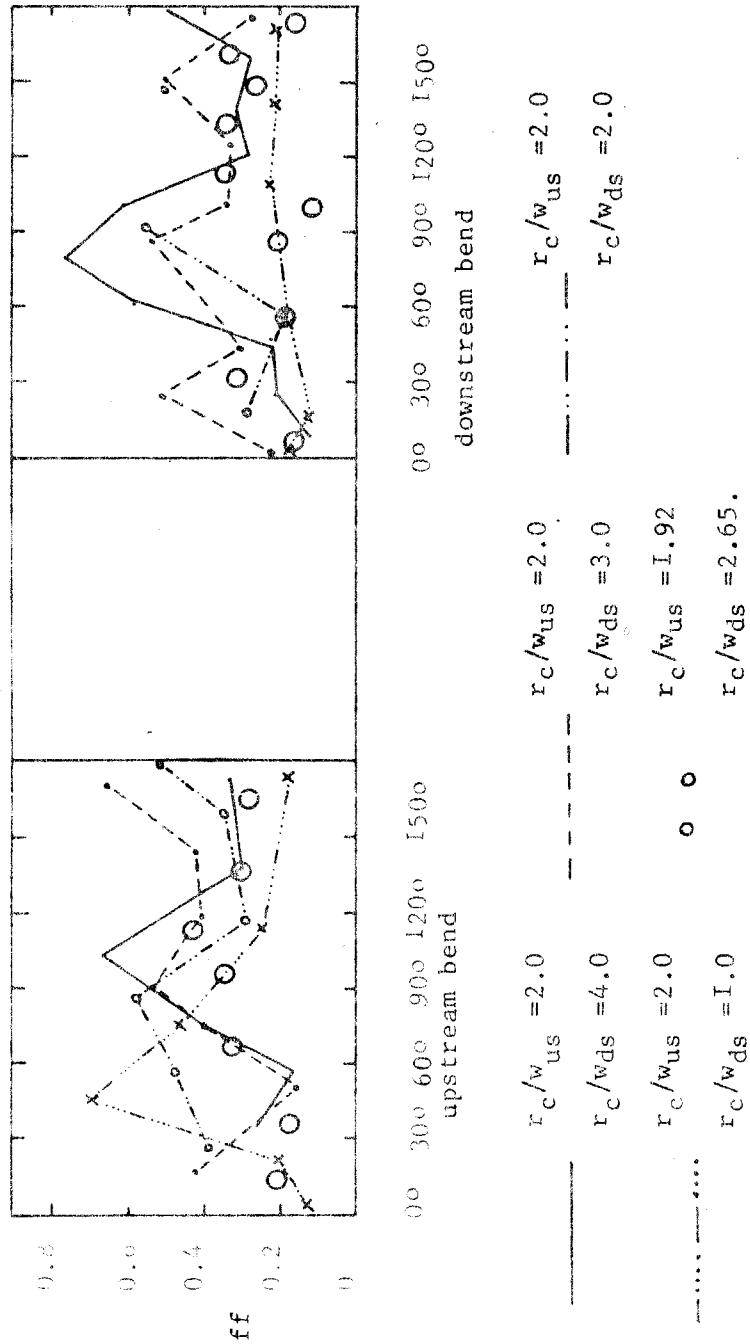




Figure 4.37. The distribution of friction coefficient in consecutive bends with  $r_c/w_{us}=2.0$  and variable downstream bend geometry.



and reaches a maximum value along the bend zone between 90 and 120 degrees where erosion is appreciable (Parsons, 1960). There are two points with maximum values along the bend zone between 30 and 120 degrees along the convex bank in  $r_c/wds > 2.0$ , but because sediment supply is greater than that which can be removed by the local shear (cf. Onishi et al; 1976), there is little erosion along the convex bank of such wide bends. Those proceeded by  $r_c/wds < 2.0$  have only one maximum value that locates at 90 degrees.

Dietrich and Smith (1983) have shown that the high boundary shear along the convex bank decreases in magnitude from the upstream part of the bend to the downstream end. Such a distribution reflects the limiting depth caused by the point bar and the abrupt shift of the high shear from the convex (inner) bank to the concave bank. The results of Ippen and Drinker (1962) and those of the present study identify two points near the convex bank where there is high shear stress in bends of  $r_c/wds > 2.0$  and one point in those of  $r_c/wds < 2.0$ . The basis for these differences is that the maximum velocity core locates near the concave bank in  $r_c/w < 2.0$  and erodes the point bar (see for example Carey, 1963; Yarnkh, 1978).

#### 4.3.6 The Distribution of Shear Stress and Friction Coefficients in Consecutive Bends of $r_c/wus=1.5$ and variable $r_c/wds$

The mean shear stress distribution is skewed towards the downstream portion of the bend (Figure 4.38). It decreases between the bend entrance and 60 degrees, increases along the bend zone between 60 and 105 degrees and decreases finally towards the bend exit (Table 4.9). This distribution displays the same pattern as that of secondary flow. The trend in a bend of  $r_c/wus=1.2$  is opposite to that in  $r_c/wus=1.5$ : the filament of maximum shear shifts from the concave bank towards the convex bank at the bend entrance and between 75 and 115 degrees along the concave bank in  $r_c/wus=1.2$ .

Along the downstream bends, the profiles are sinuous every 60 degrees and trends upwards with increasing bend angle; this reflects the progressive development of the secondary flow and the location of the fully developed flow zone. The distribution of friction coefficient shown in Figure 4.39 displays the same characteristics as those of shear stress. The double shear peaks, typical of more open bends, emerge as the downstream bends become tighter. Figure 4.40 shows the lengthwise distribution of shear stress near the channel banks. It can be seen that high shear locates downstream of the bend apex and likely facilitates concave bank erosion there.

Figure 4.38. The distribution of mean shear stress in consecutive bends with  $r_c/w_{us} = 1.5$  and variable downstream bend geometry (2.9, 2.7, 2.1 and 1.5).

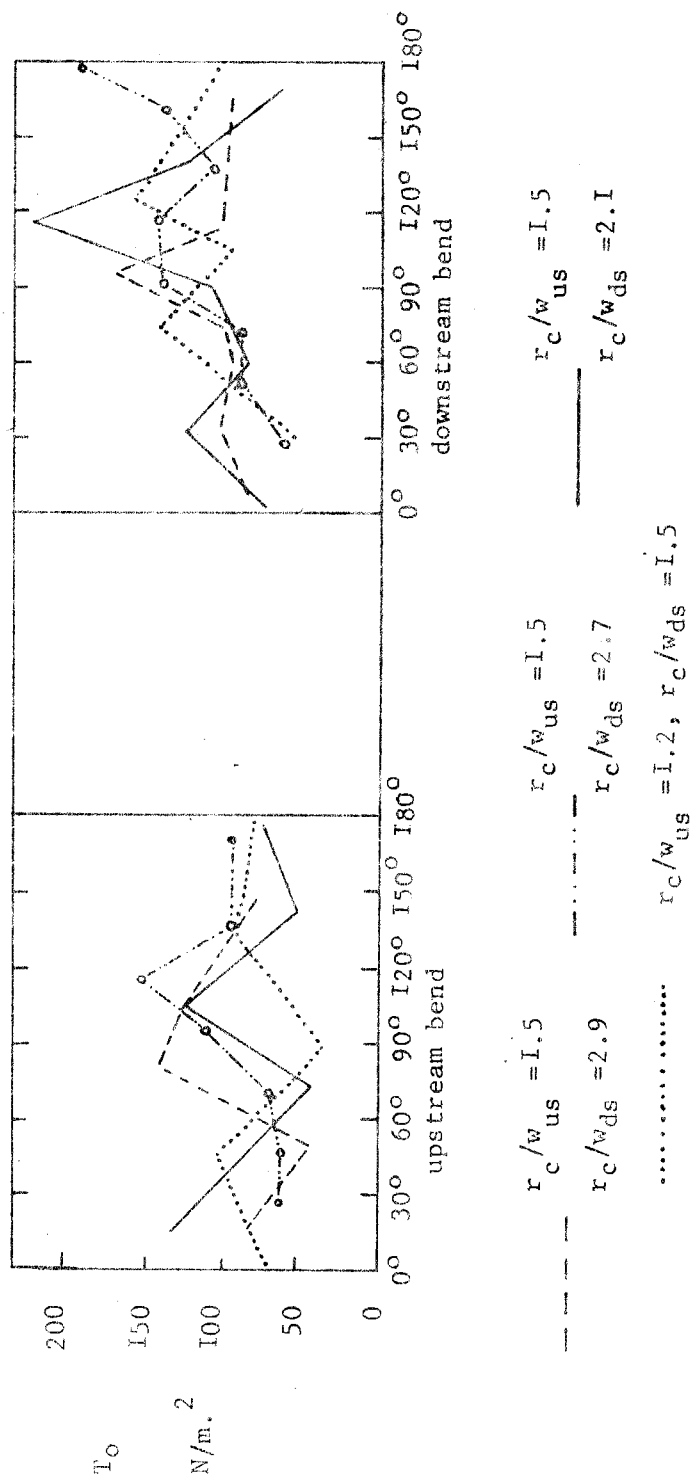


Figure 4.39. The distribution of friction coefficient in consecutive bends with  $r_c/w_{us} = 1.5$  and variable downstream bend geometry.

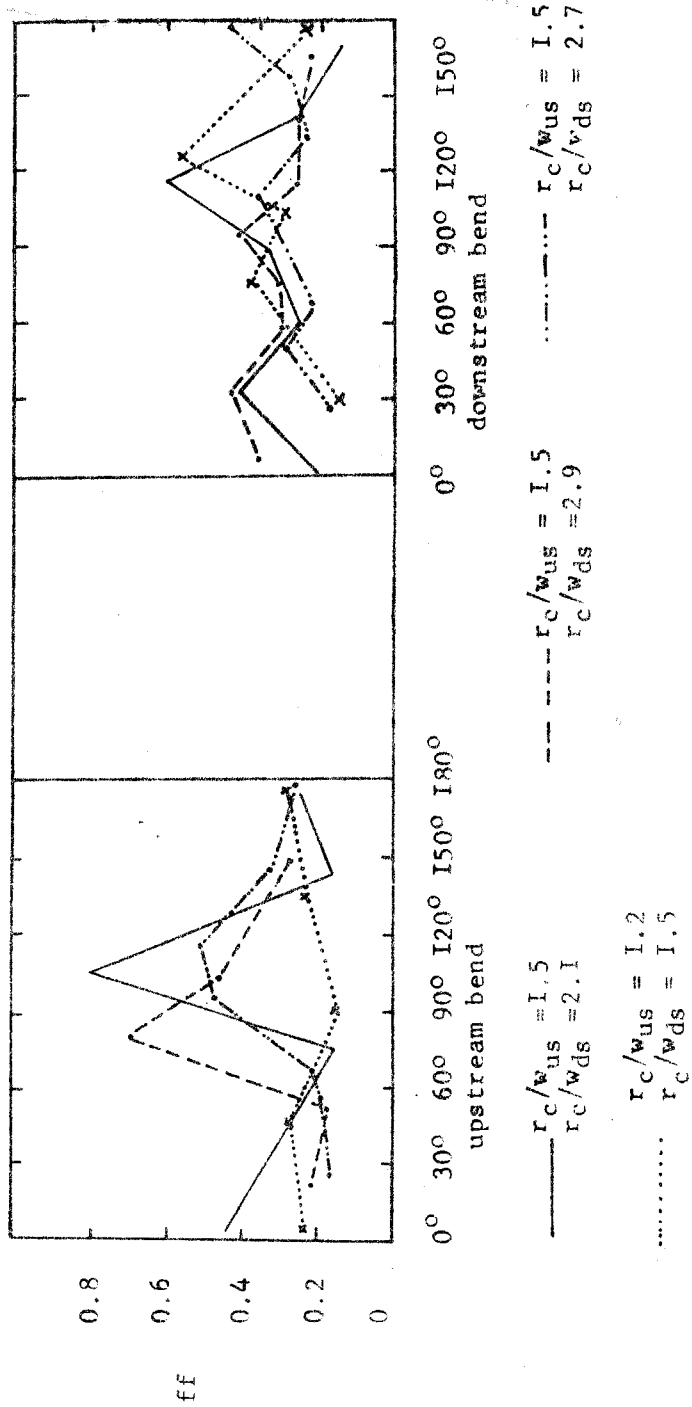


Figure 4.40. The distribution of shear stress near the concave banks of bends with  $r_c/w_{us} = 1.5$  and variable downstream bend geometry. The shear stress near the convex bank had low magnitudes and are not shown in this diagram.

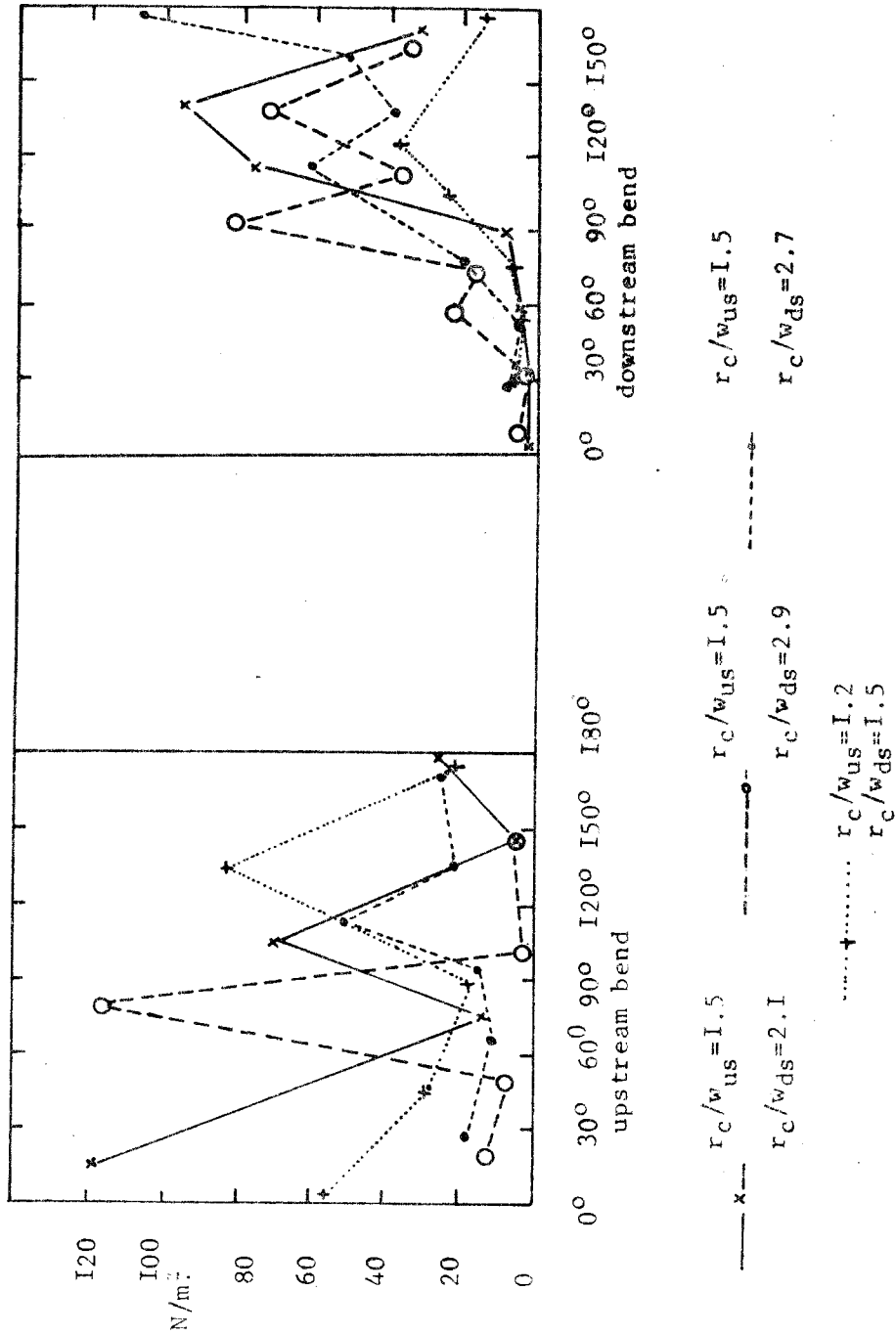


TABLE 4.9

The location (in degrees) of the maximum and minimum shear stress in consecutive bends of  $r_c/w_{us}=1.5$  and varying  $r_c/w_{ds}$ .

$r_c/w_{us}$	Tmax	Tmin	$r_c/w_{ds}$	Tmax	Tmin
1.5	100	50	2.9	100	60-90
1.5	115	60	2.7	105; 180	30; 135
1.5	105	75	2.1	30; 120	60; 180
1.2	40; 135	90	1.5	75; 120	30; 105; 180

#### 4.3.7 Summary and Observations

Downstream variation of mean shear stress and friction coefficient are in agreement with general patterns observed in meandering streams (cf. Ippen and Drinker, 1962). The description has centred on the location of maximum points, cross overs and flow separation zones. Because of the nonuniform distribution of velocity, the oscillation of the high velocity core corresponds with the periodic variation of the boundary layer characteristics and the zones at which stream energy is dissipated.

The general trend of shear stress distribution is the periodic variation of peaks every 60 degrees. Einstein (1972) corroborated Muramoto's (1967) results and confirmed that maximum secondary flow is reached every 60 degrees. Evidence from single bends confirms the same (cf. Ippen and Drinker, 1962; Yalin, 1971; Varshney and Garde, 1974; Nouh and Townsend, 1978). Minor variations observed in the present study likely are caused by upstream migration of such points due to changes in curvature ratio.

Bends of  $r_c/w_{us}=1.5$  and  $4.0$  have peak shear stress at the bend apex except those preceded by bends with  $r_c/w_{ds}=1.8$  and  $4.0$ . Bends of  $r_c/w_{us}=3.65$  and  $2.0$  have upstream skewed peaks. Ito (1954) showed that 90% of the total bend shear stress occurs downstream of tight bend apices. Bridge and Jarvis (1982) noted



also that the zones of maximum shear migrate downstream as discharge increases (i.e  $r_c/w$  decreases; cf. Soliman and Tinney, 1968). The downstream migration of points with maximum shear stress are associated with the location where the high velocity core crosses from one channel bank to the other. As  $r_c/w$  decreases, the flow takes longer to display the characteristics of the fully developed flow zone.

In wide bends, friction to flow increases gradually to a maximum value at a bend angle of 60 degrees and in the second half of the bend, but decreases along the bend apex. The decrease of friction coefficient along the bend zone between 75 and 150 degrees is associated with the point at which the high velocity core and shear stress cross the channel centreline towards the concave bank. The location of the bend pool and the decrease of secondary flow along this bend section both cause the relative roughness to decline. The shifts of the centres at which friction coefficient has a maximum value reflect the variability of the location of the fully developed flow zone, the bend pool and flow separation zones. Subsequent bends following  $1.5 < r_c/w < 2.67$  have lower and less variability of shear stress distribution than those preceded by  $r_c/w > 3.65$  and are comparable to Hickin's (1978) data. It is possible that secondary flow advection and free vortex development along the downstream bends are able to dampen the disturbances transmitted from tight upstream bends.

TABLE 4.10

The variation of dimensionless shear stress,  $T_o/\bar{T}_o$ , with curvature ratio,  $r_c/w$ , for paired bends of the present study.

$r_c/w_{us}$	$T_o/\bar{T}_o$	$r_c/w_{ds}$	$T_o/\bar{T}_o$
1.5	2.4	2.9	2.4
1.5	2.8	2.7	2.1
1.5	2.7	2.1	3.5
1.2	2.5	1.5	2.4
2.0	2.4	4.0	3.1
2.0	2.3	3.0	2.9
1.92	4.0	2.65	3.7
2.0	2.9	2.0	3.6
2.67	2.2	2.67	2.3
2.67	2.6	2.3	2.9
2.67	-	2.1	3.6
4.0	2.9	3.1	2.7
4.0	3.2	2.0	2.4
4.0	2.8	1.8	2.6

Ito (1954) showed that subsequent bends proceeding tight ones tended to have only 40% of the shear stress observed in the upstream bends. Hickin (1976) surmised that the rate of erosion in a given bend depends on the curvature ratio of the adjacent ones, a pattern which likely is associated with a decrease of shear along the concave bank also.

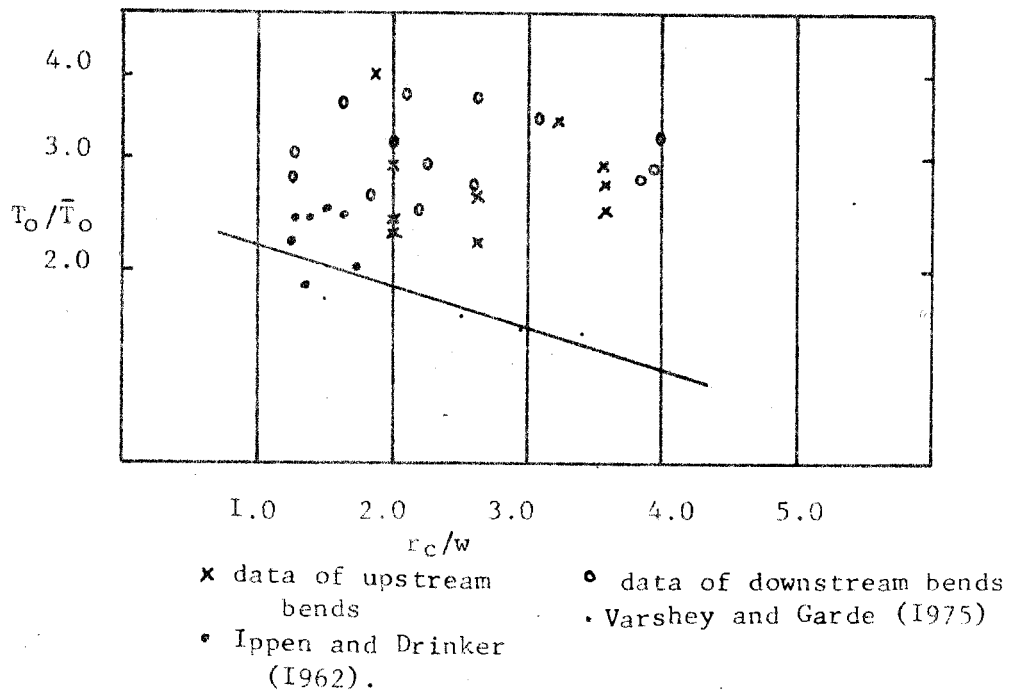
The local shear stress ratio ( $T_o/\bar{T}_o$ ) is one and a half to three times greater in zones where the core of maximum velocity depresses towards the channel bed and the secondary flow is high (Ippen and Drinker, 1962; Hooke, 1975; Bathurst et al; 1979; Bridge and Jarvis, 1982). The shear stress ratio increases also as bends become tighter (cf. Appman, 1972; Varshney and Garde, 1975). Figure 4.41 compares published data with those of the present study. Although there is wide scatter, the least square regression equation based on data from Table 4.11 is:

$$T_o/\bar{T}_o = k_u + r/w \dots\dots\dots 4.5$$

where e is an exponent.

$k_u$  has a value of 2.8 and 2.54 respectively for upstream and downstream bends, while e is -0.16 and -0.198 for the upstream and the downstream bends (R (correlation coefficient) is insignificant at 98% ). The value of  $k_u$  possibly varies with the hydraulic conditions of the channel including rates of sediment transport, width-depth ratio, etc. The slope of the curve is the same as that reported by Appman (1972) although the ratios of the present study are higher, probably because of differences of

Figure 4.4I. The relationship between nondimensional shear stress,  $T_o/\bar{T}_o$ , and curvature index,  $r_c/w$ .



Note that there is considerable scatter, however, each data set shows a decreasing trend with curvature, see for example those by Varshey and Garde (1975).

flow regime (Onishi et al; 1976) and bedforms (Bridge and Jarvis, 1982).

High shear stress increases the stream's competence to erode and transport its load (cf. Kirkby, 1977). The zones of high shear stress and resistance to flow discussed above can be related to patterns of bank erosion and bend migration. The low shear stress zone between 30 and 60 degrees near the concave bank is due to flow deceleration caused by a very gentle water surface slope which inclines upstream (Hooke, 1975; Dietrich et al 1979) with the onset of cross stream momentum transfer. The periodic variations of the maximum shear stress are more pronounced for bends of  $r_c/w=3.65$  and  $2.7$ , and likely will cause erosion while the same variations concentrate downstream for those of  $r_c/w=1.5$  and uniform for  $r_c/w=4.0$ . Along the downstream bends, the maximum shear occurs along the inner bank upstream of the point bar and downstream of the bend apex along the concave bank; this pattern assures the process of downvalley migration of bends.

## CHAPTER 5 EXPERIMENTAL RESULTS OF CONSECUTIVE BENDS WITH DOWNSTREAM BEND GEOMETRY CONSTANT

### 5 THE BEND FLOW DEVELOPMENT AND VORTEX INTERACTION IN CONSECUTIVE BENDS WITH CONSTANT DOWNSTREAM GEOMETRY

#### 5.1 Introduction

This part of the study was designed to investigate the distribution of velocity, shear stress and friction to flow in consecutive bends in order to identify the influences of upstream bends on flow development and interaction along the downstream ones. Chapter 3 showed how isovel patterns, vortex interaction, friction to flow and shear stress vary with increasing bend angle and curvature ratio. The consecutive bends discussed in Chapter 4 have identified the differences that exist between bends of  $r_c/w > 3.0$ ,  $r_c/w = 2.0$  and  $r_c/w < 2.0$  and their various but related influences on the downstream bends.

This chapter describes and discusses results of experiments on consecutive bends with constant downstream geometry while that for  $r_c/w$  is allowed to vary. Jackson (1975) and Bridge and Jarvis (1976) have suggested that the cross over located within the bend depicts the strength of the inherited flow. The

extent and magnitude of free vortex flow and superposed spirals (Callander, 1978) are some of the criteria used in this study to identify such an upstream influence. Other criteria include shear stress and friction distribution, boundary layer development, flow separation, and the location of fully developed flow (Mullin and Greated, 1980). The final analysis in Chapter 6 relates the variations of velocity and shear stress to lateral migration in rivers. The isovel patterns, current direction and vortex interaction are discussed in section 5.2, while section 5.3 examines the longitudinal and transverse distribution of velocity. The distribution of shear stress and friction to flow are discussed in section 5.5.

#### 5.1.2 The Isovel Patterns and Current Direction in Consecutive Bends of $r_c/wds=4.0$ and variable $r_c/wus$

Figures 5.1, 5.2 and 5.4 show the isovel patterns while Table 5.1 summarises vortex development and interaction along consecutive bends with  $r_c/wds=4.0$  and  $r_c/wus$  varying between 3.0 and 1.4. Figure 5.3 shows the current direction near the surface (solid lines) and near the bottom (broken lines) in one of the paired bends to be discussed in this section.

Figure 5.I. Selected isovel patterns in consecutive bends with  $r_c/w_{US}=3.0$  and  $r_c/w_{DS}=4.0$ . The isovel are shown in  $cm. s^{-1}$ . The diagrams are presented from the left bank to the right bank facing downstream.

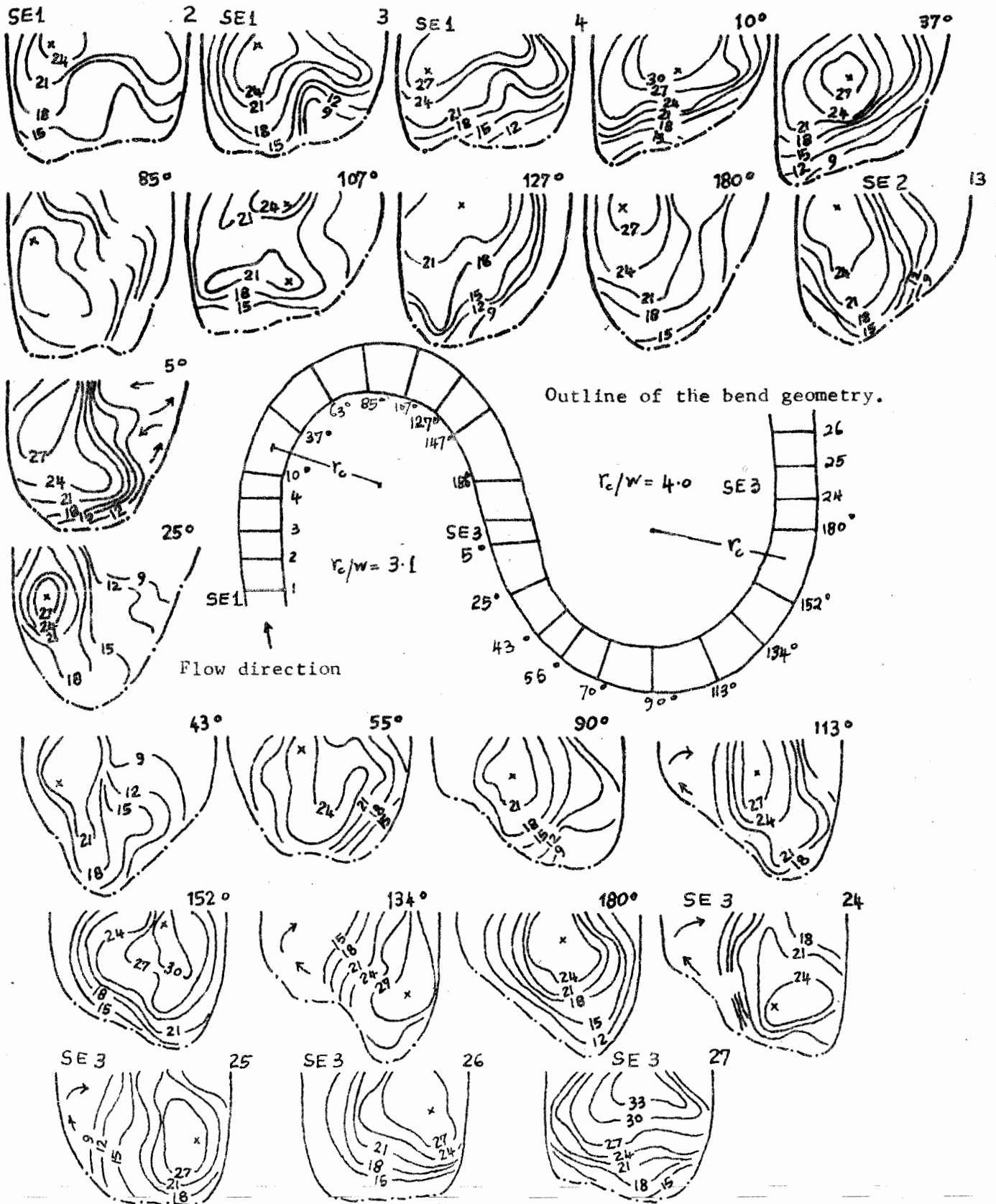




Figure 5.2. Selected isovel patterns in consecutive bends with  $r_c/w_b = 2.7$  and  $r_c/w_d = 4.0$ . The isovels are shown in cm. s<sup>-1</sup>. The outline of the bend and traverse locations are given in Figure 5.3. The isovel diagrams are presented from the left bank to the right bank facing downstream.

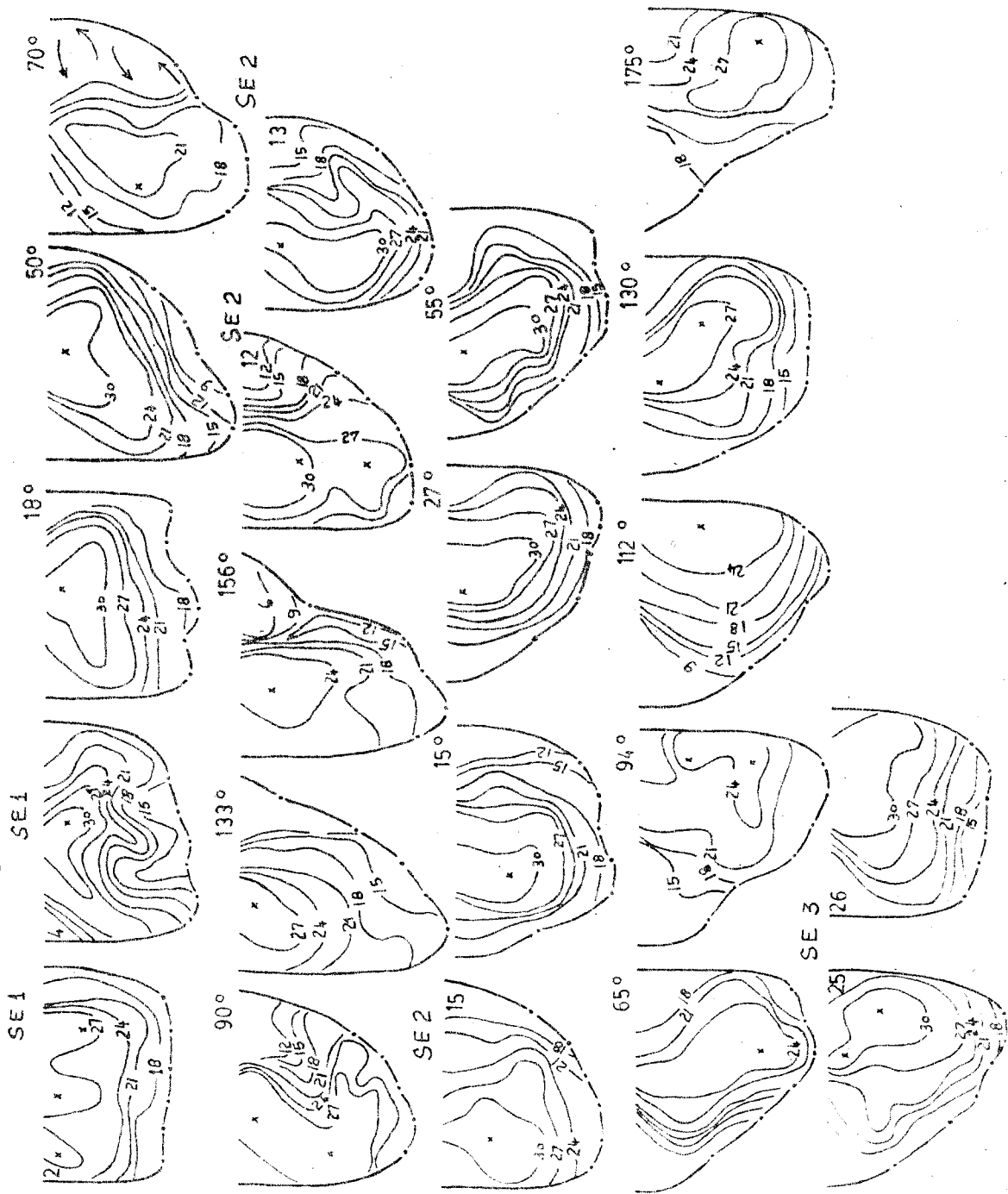


Figure 5.3. Current direction motifs for  $r_c/w_{us}=2.7$  and  $r_c/w_{ds}=4.0$ .

The bottom currents are shown by broken lines while the surface currents are shown by complete lines.

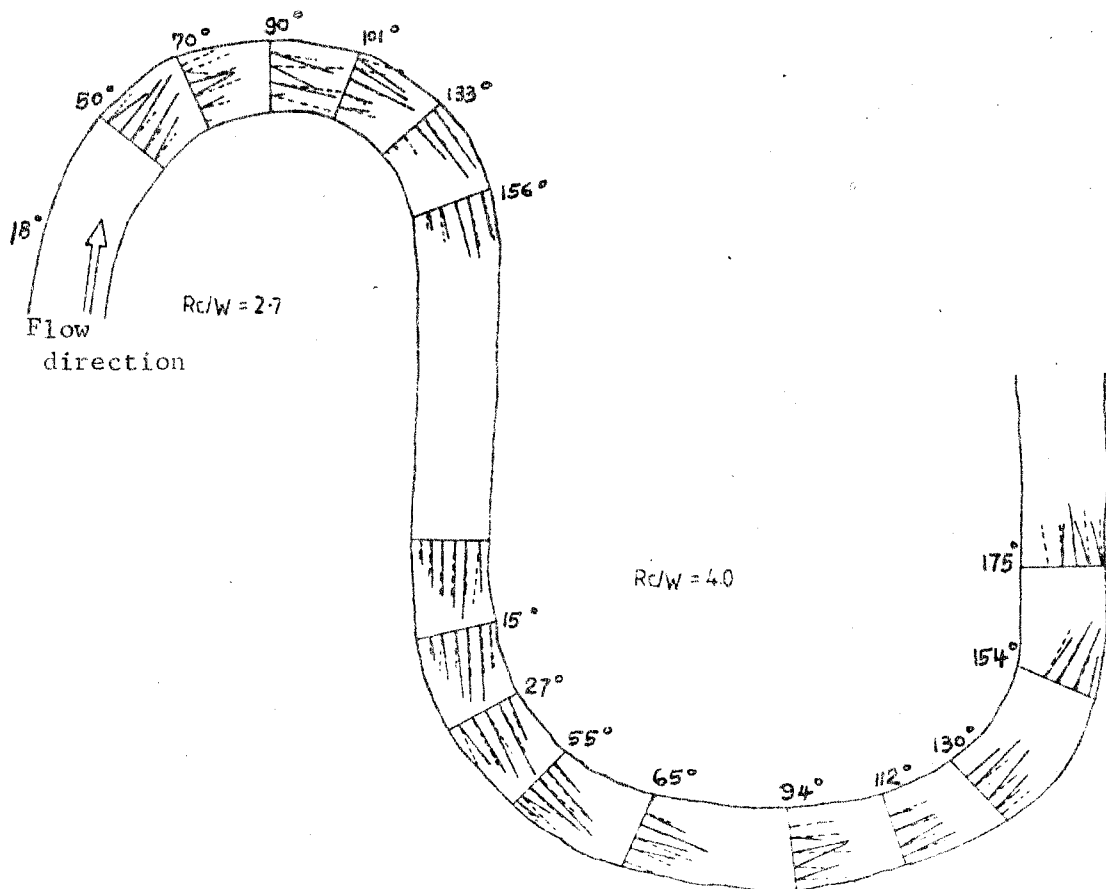
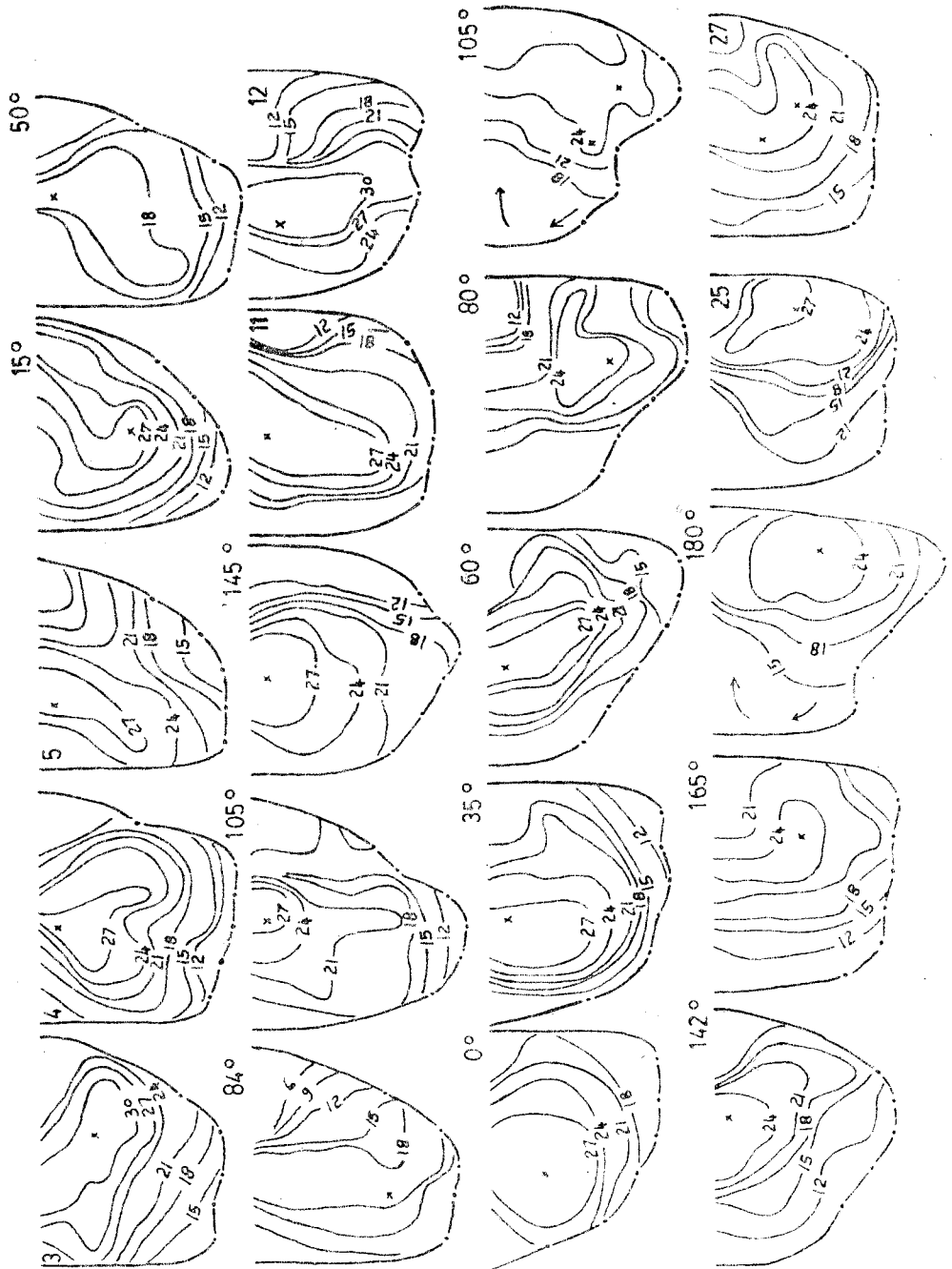


Figure 5.4. Selected isovel patterns in consecutive bends with  $r_c/w_{ds} = 1.4$  and  $r_c/w_{ds} = 4.0$ . The outline of the bends and traverse locations are given in Figure 5.5. The isovels interval is 3 cm. s<sup>-1</sup>. The isovel diagrams are presented from the left bank to the right bank facing downstream.



The patterns of secondary flow and current direction are similar to those of bends with constant upstream geometry shown in Figure 4.1; but with minor modifications. For example, the double spirals lie obliquely towards the water surface at 85 degrees of the bend in Figures 5.1 and 5.2 compared to a bend angle of 54 degrees in Figure 4.4. The surface currents are intensely deformed while the bottom ones lie more or less parallel to the channel banks at the bend apex (Figure 5.3). The isovel pattern near the water surface shows that the effect of the centrifugal force begins at the water surface and deforms the water column layer by layer (cf. Mockmore, 1944) and reaches a maximum value approximately at 60 degrees of the bend angle (cf. Muramoto, 1967). At 101 degrees of the bend angle, the bottom currents are directed towards the channel banks and likely are responsible for undermining the concave bank.

The effect of the bend is transmitted upstream through velocity acceleration and intense secondary flow in the form of C-shaped isovel geometry at 15 degrees in a bend of  $r_c/wus=1.4$  compared to 90 degrees in that of  $r_c/wus=2.7$ . This upstream migration of the bend effects reduces also the extent of the parabolic flow along the channel entrance. The C-shaped isovels represent a developed secondary spiral moving accelerating fluid towards the bottom. Near the channel bed, the developed spiral retards mainstream flow through drag and directs currents towards the banks as it shifts the core of maximum velocity towards the centreline (cf. Dietrich et al; 1979).

Figure 5.5. Vortex development and interaction in consecutive bends of  $r_c/w_{us} = 1.4$  and  $r_c/w_{ds} = 4.0$ . The location of each cross section is shown in degrees; the value of vortex strength,  $\tau$ , in the expression  $I.4$  is given also for each cross section.

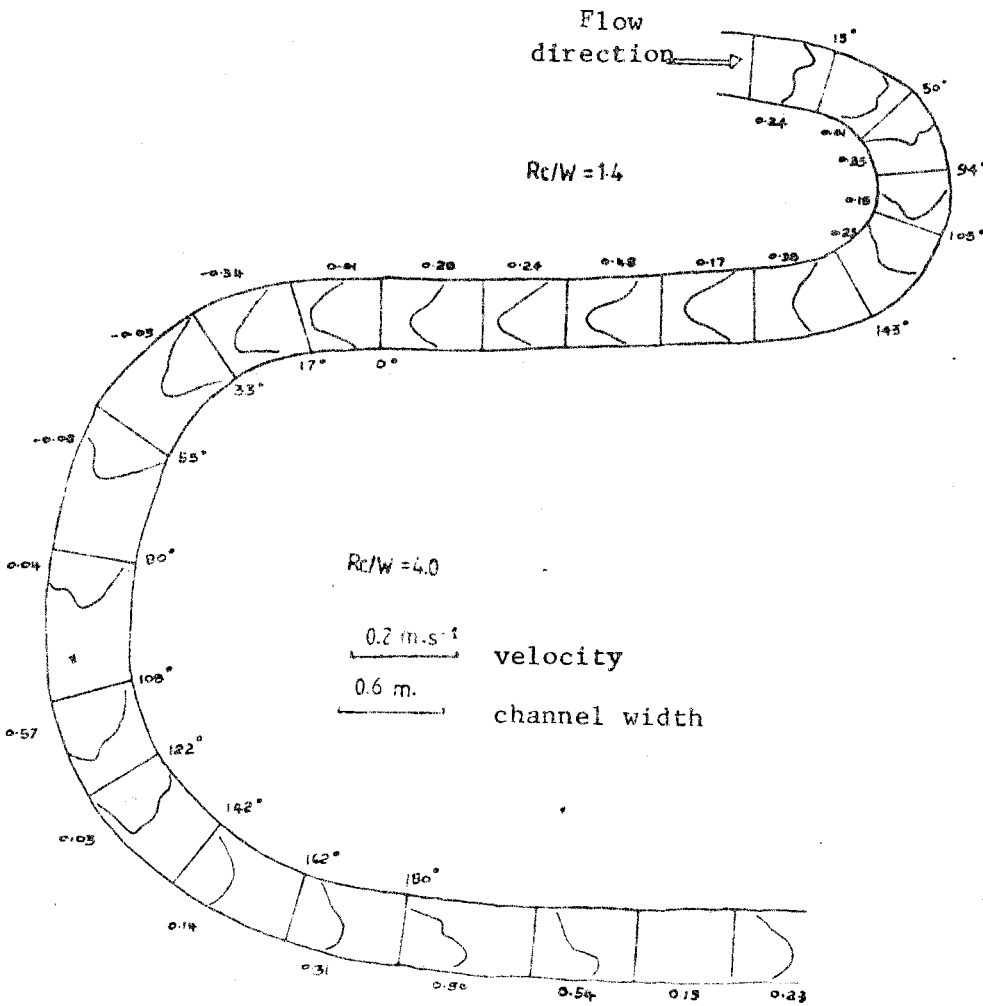


Table 5.I.

The bend flow development and vortex interaction in consecutive bends with  $r_c/wds = 4.0$  and variable upstream bend geometry (3.0, 2.7, 2.2 and 1.4). The numbers below each vortex type is the maximum value of  $t$  in the expression  $V=kr^t$ . T means transitional flow.

$r_c/w$	SEI	0°	30°	60°	90°	120°	150°	180°	SE2	0°	30°	60°	90°	120°	150°	180°	SE3			
3.0/ 4.0	Para.	Forced vortex														0.57	Forced vortex	0.60	Parab.	
2.7/ 4.0	Parab. flow	Forced vortex														0.59	Free Parab.	Forced vortex	0.68	
2.2/ 4.0	Parabolic flow	Forced vortex														0.58	Free vortex -0.41	Forced vortex 0.85		
1.4/ 3.91	Parabol. flow	Forced vortex														0.43	Free vort. -0.34	Parab.	Forced vortex 0.54	

Nb. SE1 and SE2 represents straight entrance and exit portions of the bend respectively.

In general, the oscillation of the high velocity core is similar to that of the other bends discussed earlier.

The core of maximum velocity moves towards the channel bottom between 50 and 94 degrees and towards the water surface along the rest of the bend. Further in to the bend (between 94 and 127 degrees), the vortex strength decreases (cf. Figure 5.5). The velocity increases near the channel bed with downwelling upstream of the bend axis but decreases with upwelling downstream of the bend apex, in agreement with the results of Muramoto (1967).

Along the downstream bend ( $r_c/wds=4.0$ ) the secondary flow near the bottom directed towards the concave bank, then towards the centre of the channel at the bend entrance causes flow separation at 5 degrees of the bend (see Figure 5.1). This flow separation is a result of delayed adaptation of the incoming helical flow to the following channel bend geometry (i.e. the high velocity filament and the channel bend are not synchronous). The inherited free vortex may occupy the zone from the bend entrance to 105 degrees of the bend in Figure 5.1, but is limited to a bend angle of 15 degrees in Figure 5.2 and to 45 degrees in Figure 5.3. In other words, the transition zone (cross over) migrates upstream and the high velocity core takes longer to shift towards the concave (outer) bank. According to Jackson (1975), the transitional zone associated with the intermediate depositional facies (see Figure 1.3) does not locate upstream of the bend apex except where expansion and

rotation processes of lateral migration occur. The preservation or absence of the intermediate facies is a function of the extent of the free vortex flow at the downstream bend entrance.

The free vortex flow at the downstream bend entrance translates to forced vortex flow at 35 degrees after which parabolic flow establishes between 35 and 100 degrees for bend series  $r_c/wus=1.4$  and  $r_c/wds=4.0$ . The absence of a strong vortex flow along the bend zone between 35 and 100 degrees is particularly noteworthy because this is the bend zone where bank erosion has to occur for an expansion mode of bend migration. It appears that the influence of the upstream bend in controlling the extent to which a free vortex may occur decreases to a minimum value for bends with  $r_c/wus=2.7$  and  $1.4$  [the inflections were of the same length]. In bend series of  $r_c/wus=3.0$  and  $r_c/wds=4.0$ , the core of maximum velocity is depressed towards the bottom between 5 and 43 degrees of the downstream bend; it changes to a U-shaped configuration at 55 degrees, where the velocity profile at  $y_1/y_o=0.5$  has a valley at the centre. This complex isovel geometry mainly is due to strong converging secondary flow from the banks which splits the core of maximum velocity in to two filaments (cf. Hey and Thorne, 1975, their Figure 4).

The occurrence of the free vortex flow at the downstream bend entrance is responsible for erosion along the convex (inner) bank. The erosion that occurs here is due to inertial forces (Suga, 1967) manifested in the form of a strong free



vortex inherited from the upstream bend. The present study also shows that the extent of this free vortex flow varies with  $r_c/w$ ; generally it decays at about 60 degrees of most bends. Exceptional cases are, for example, bend series of  $r_c/w_{us}=3.0$  and  $r_c/w_{ds}=4.0$  in which the free vortex flow extends from the bend entrance until 105 degrees while for those of  $r_c/w_{us}=2.7$  and  $r_c/w_{ds}=4.0$ , the free vortex extends until 15 degrees. The bend series with  $r_c/w_{us}=3.0$  and  $r_c/w_{ds}=4.0$  represents flow characteristics which are consistent with the translation mode while the latter cases ( $r_c/w_{us}=2.7$  and  $r_c/w_{ds}=4.0$ ) have a parabolic flow profile between 15 degrees and 90 degrees of the bend which is necessary for the expansion and rotation mode of bend movement.

De Vriend and Geldolf (1983) also observed that the secondary flow towards the inner bank becomes enhanced and causes the core of maximum velocity to take longer to get to the concave bank in a following opposite bend (cf. Callander, 1978). The transitional zone in the downstream bend shown in Figure 5.1 is shorter than those shown in Figures 5.2 and 5.4 because of decreasing  $r_c/w_{us}$ . The consequence of long transition zones is that the flow does not become fully developed until the bend exit, and the point bar also is topographically lower than that of the upstream bank. The erosion along the inner bank at the bend entrance and on the concave (outer) bank downstream of the bend apex ensures downvalley migration of river bends.

### 5.1.2 The Isovel Patterns and Current Direction in Consecutive Bends of $r_c/wds=3.3$ and variable $r_c/wus$

Figures 5.6 and 5.7 show the isovel patterns in  $r_c/wus=1.73$  and  $r_c/wds=3.62$  and  $r_c/wds=3.0$  respectively. The free vortex and parabolic flow profiles locate along the bend entrance because the upstream bend is tight. From the bend entrance until 25 degrees, the secondary flow directed towards the convex bank is progressively suppressed while the one towards the concave bank is amplified, except in  $r_c/wus=1.5$  (Figure 5.11) where a free vortex flow forms at 50 degrees of bend angle. The parabolic flow translates to a forced vortex flow and it extends until 70 degrees of the bend where inertial forces cause transverse surface-convergent secondary flow advection that depresses the core of maximum velocity towards the channel bed at the centreline. Fully developed flow occurs towards the bend exit.

Secondary flow towards corners occurs along the 2.26m inflection reach, indicating that the upstream and downstream bends have negligible effect for the bend series shown in Figure 5.6. Along the downstream bend, the free vortex forms between the bend entrance until 15 degrees in Figures 5.6 to 5.11, but between 45 and 75 degrees in Figures 5.8 and 5.9. The strongest free vortex flow was measured in bend series with  $r_c/wus=1.7$  and  $r_c/wds=3.0$  ( $t=-0.55$ ). The parabolic (transitional) flow locates at 60 degrees of bend angle in agreement with the results of Hooke (1975) for what he refers to

Figure 5.6. Selected isovel patterns in consecutive bends with  $r_c/w_{us} = 1.73$  and  $r_c/w_{ds} = 3.6$ . The diagrams are presented from the left bank to the right bank facing downstream. The isovels are shown in cm. s<sup>-1</sup>. The symbol 'x' denotes the position of the maximum velocity.

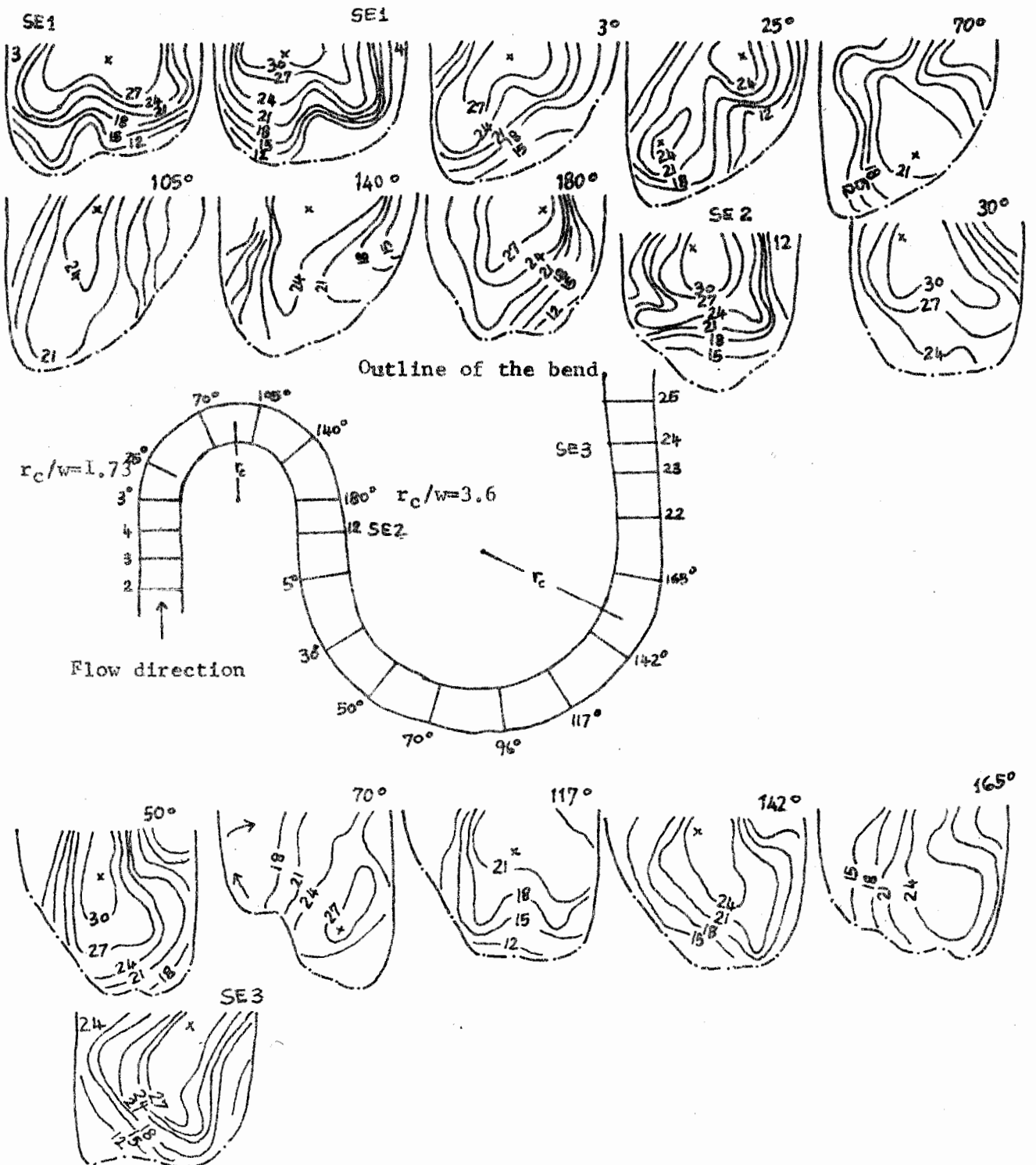
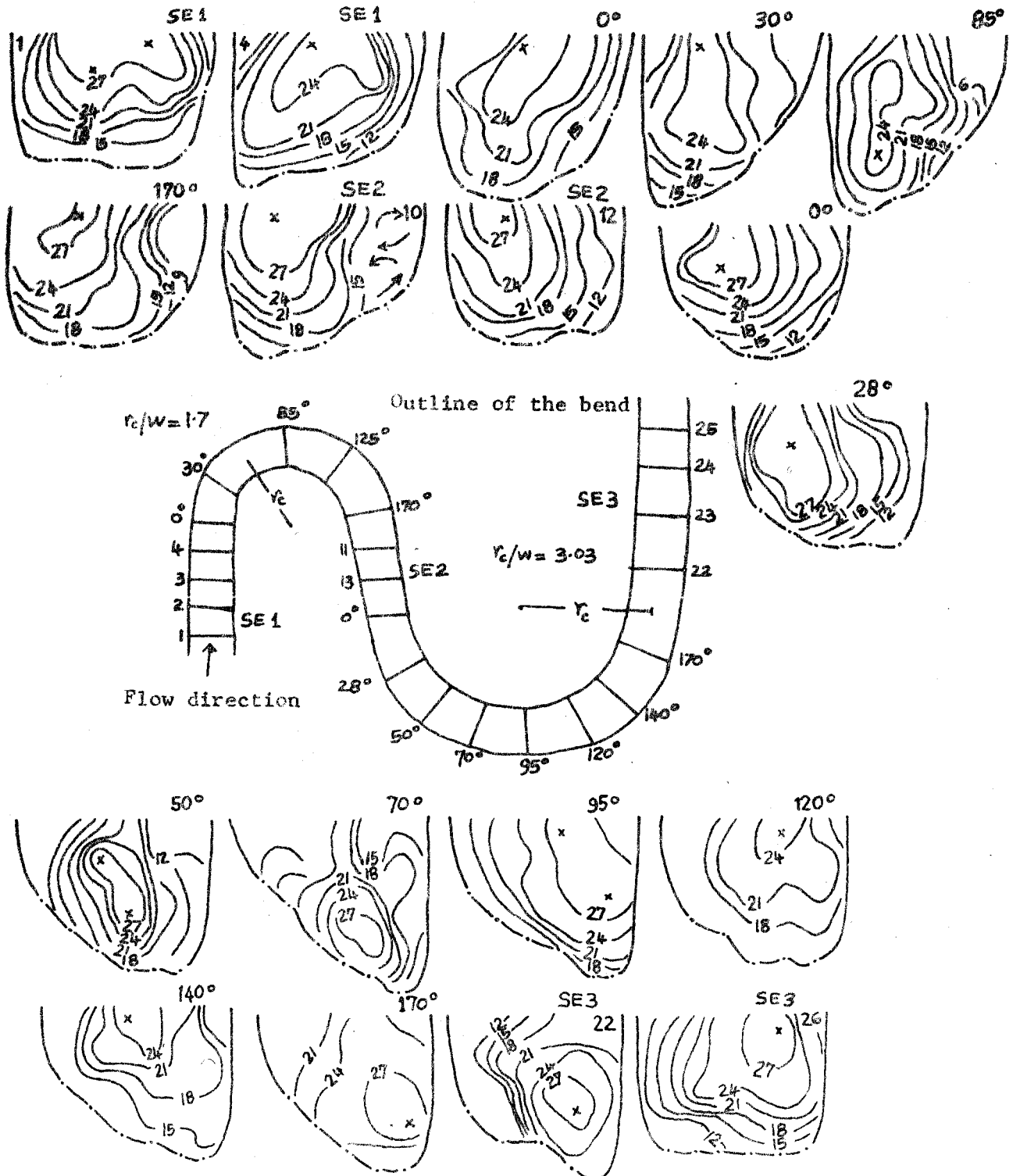


Figure 5.7. Selected isovel patterns in consecutive bends with  $r_c/w_{us} = 1.7$  and  $r_c/w_{ds} = 3.03$ . The diagrams are presented from the left bank to the right bank facing downstream. The isovels are shown in cm. s. The symbol 'x' denotes the position of the maximum velocity.



as an equilibrium channel bend. Along the bend zone between 70 and 117 degrees (see Figure 5.6) and 50 to 70 degrees (see Figure 5.7) the core of maximum velocity remains close to the bottom but it inclines obliquely across the channel. This indicates the existence of a superposed spiral; the lower one rotates anticlockwise to the upper one and consequently decreases the strength of the forced vortex flow. Dietrich et al (1979) observed a similar counterrotating spiral along their cross sections 12 to 18 located at the same bend area as observed in these experiments. They attributed the origin of the spiral to the interaction of the bar and pool topography which causes a net outward flow over the point bar. In the present study, the point bars are less developed between 80 and 120 degrees because the secondary flow intensity decreases. Several field examples (cf. Hickin, 1974) show that the point bar orientation is relatively downstream of the bend axis as observed in the present model bends.

Because of rapid translation from one type of vortex flow to the other, the core of maximum velocity depresses towards the channel bed at 28, 70 and also at 170 degrees (the same locations as the bend pools) along the downstream bends shown in Figure 5.7. Further bend development may be associated with the formation of these additional pools and riffles (Hey and Thorne, 1975) which often involves differential limb migration (cf. Brice, 1973). Such bends may become complex as erosion progresses.



Figure 5.9. Selected isovel patterns in consecutive bends with  $r_c/w_{118} = 2.0$  and  $r_c/w_{ds} = 3.2$ . The diagrams are presented from the left bank to the right bank facing downstream. The isovels are shown in cm. s<sup>-1</sup>. The symbol 'x' denotes the position of the maximum velocity.

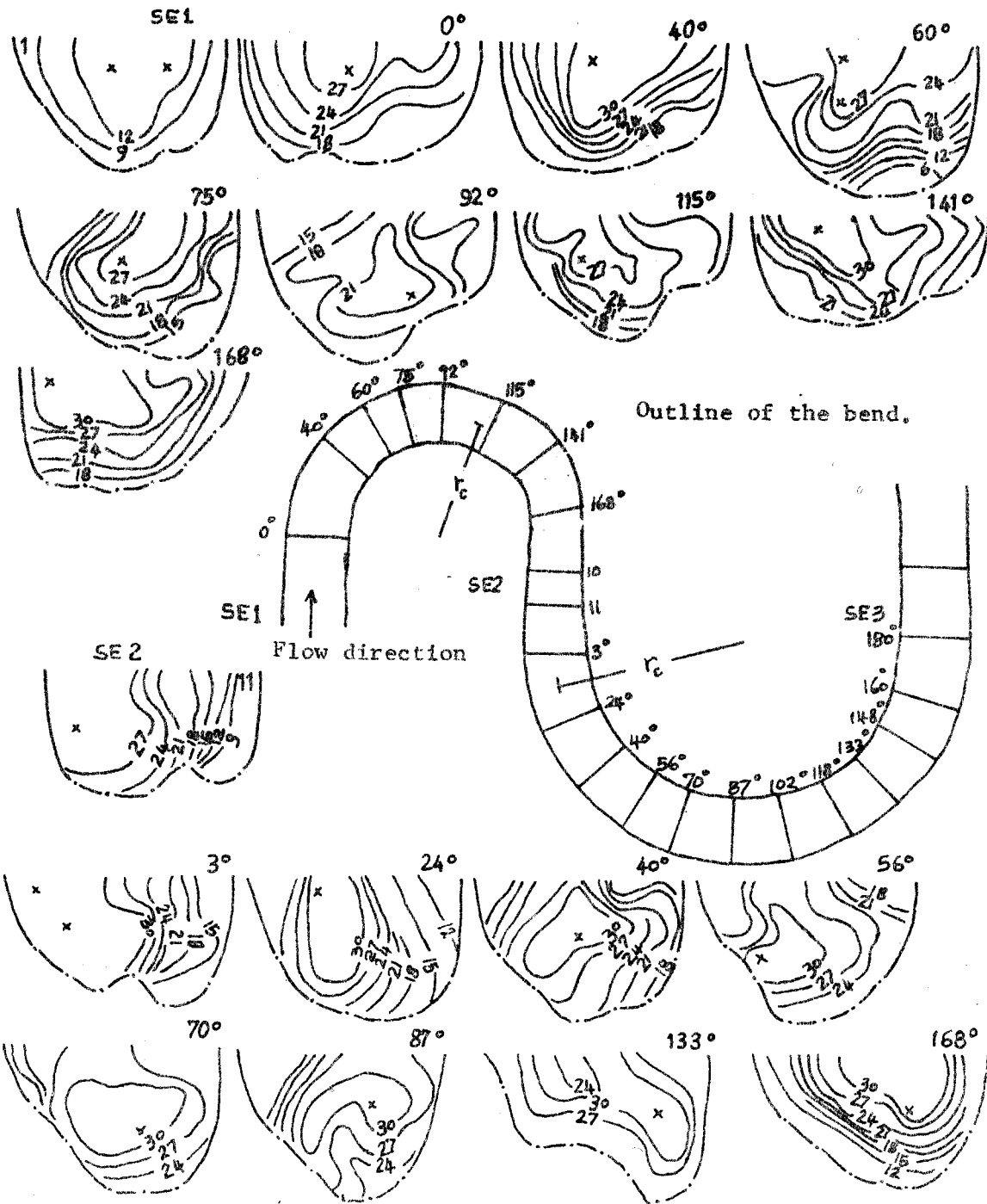


Figure 5.10. Selected isovel patterns in consecutive bends with  $r_c/w_{us} = 2.6$  and  $r_c/w_{ds} = 3.0$ . The diagrams are presented from the left bank to to the right bank facing downstream. The isovels are shown in cm. s<sup>-1</sup>. The symbol 'x' denotes the position of the maximum velocity.

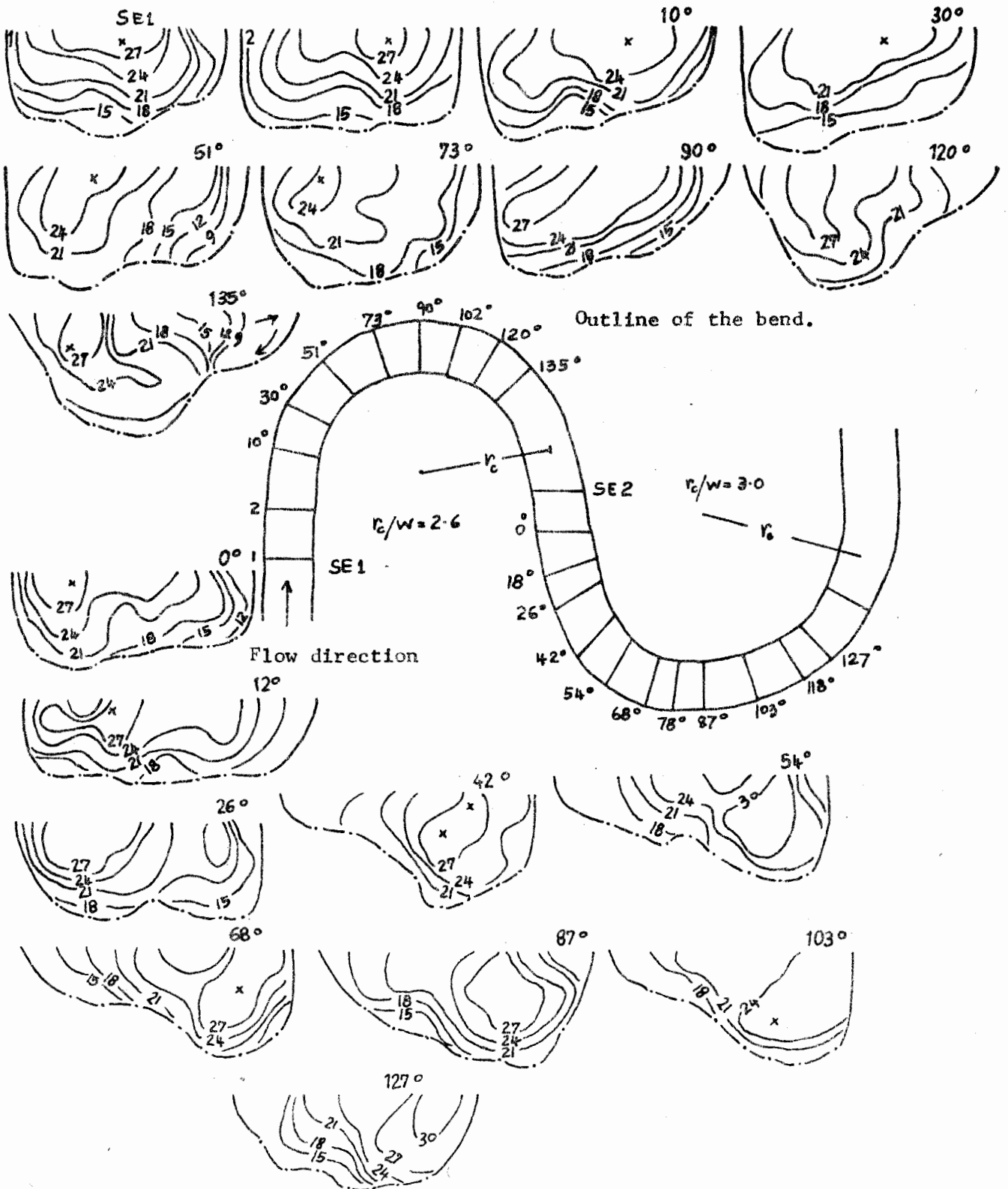




Figure 5.II. Selected isovel patterns in consecutive bends with  $r_c/w_{us} = 1.5$  and  $r_c/w_{ds} = 3.3$ . The diagrams are presented from the left bank to the right bank facing downstream. The isovels are shown in cm. s.<sup>-1</sup> The symbol 'x' denotes the position of the maximum velocity.

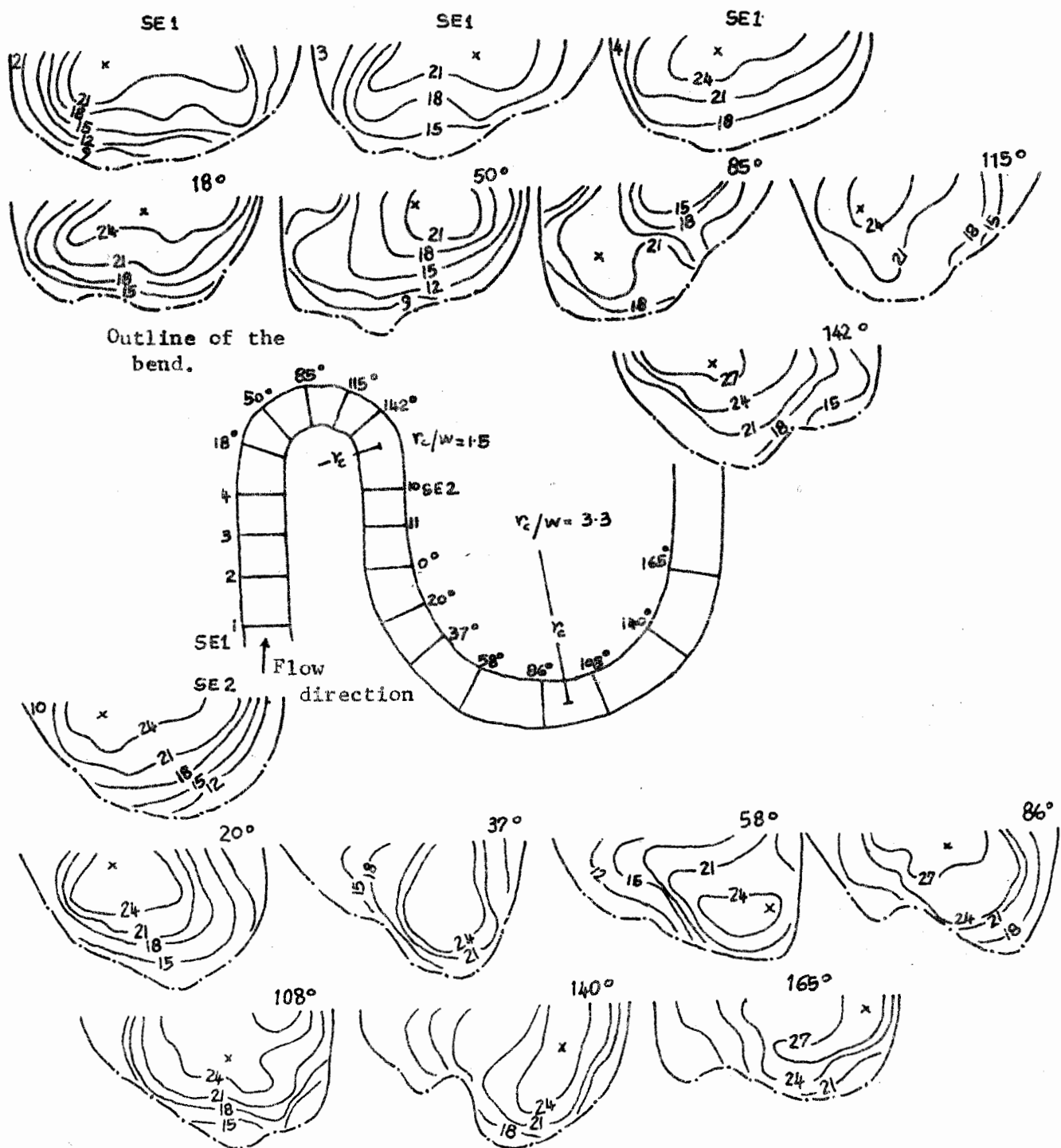


TABLE 5.2.

The bend flow development and vortex interaction in consecutive bends with  $r_c/w_{ds} = 3.3$  and variable upstream bend geometry (3.2, 2.0, 1.7, 1.73 and 1.5). The numbers below each vortex type is the maximum value of  $t$  in the expression  $V = kr^t$ . T means transition while SE1 and SE2 each represents the straight entrance and exit portions of the bend.

$r_c/w$	SE1	0°	30°	60°	90°	120°	150°	180°	SE2	0°	30°	60°	90°	120°	150°	180°	SE3
3.2/ 3.3	Parabolic flow		Forced vortex 0.36		Free vort. -0.31		Forced vortex 0.42										
2.0/ 3.2	Parabolic flow		Forced vortex 0.89		Free vort. -0.24		Forced vortex 0.46										
1.5/ 3.3	Parabolic flow		Free vort. -0.21		Forced vortex 0.30		Forced vortex 0.24										
1.73/ 3.62	Parab. flow	Forced vort. 0.16	Parabolic		Forced T	vortex	Free -0.30		T	Forced	vortex						
1.7/ 3.0	Parabolic flow		Forced vortex 0.63		Free vort. -0.55		Forced vort. 0.21		Parab.		Forced vortex 0.40						

In tight bends, it is the transmission of the effects arising from the downstream water surface elevation changes that causes the asymmetrical flow profile along the straight entrance portion. This is evident from the fact that the flow reverts to parabolic profiles at the inflections. The secondary flow towards corners extends from the bend entrance until 40 to 60 degrees (see Figures 5.9 and 5.10), but only up to 15 degrees in a bend with  $r_c/w=3.2$  shown in Figure 5.8 (cf. Fox and Ball, 1968; for 180 degree bend). The longest extent of the parabolic flow (from 0 to 120 degrees) occurs in  $r_c/w=2.0$  in which bend migration rate also decreases (Nanson and Hickin, 1975). It is likely that the decrease of the secondary flow may be a major contributing factor in limiting the rate of bank erosion.

The isovel patterns discussed above accord well with the general model of flow development in open-channel bends. The upstream influence on the following bends are depicted by the extent of the free vortex flow. For example, paired bends with  $r_c/w=1.73$  and  $3.62$  have short flow transitions between one vortex type to the other, and therefore the vortices do not have enough length to increase their strengths. Siebert and Gotz (1976) have suggested that the short flow transition zones may be due to what they term the hysteresis of the core of maximum velocity (alternating lateral shifts in the main velocity filament). In these bends, the core of maximum velocity depresses towards the bottom due to the presence of strong vortex pairs that counterrotate along the bend zone between 60

and 120 degrees. The transition zones between forced vortices in the downstream bend apices remain sensibly stationary between 60 and 150 degrees in all the bends.

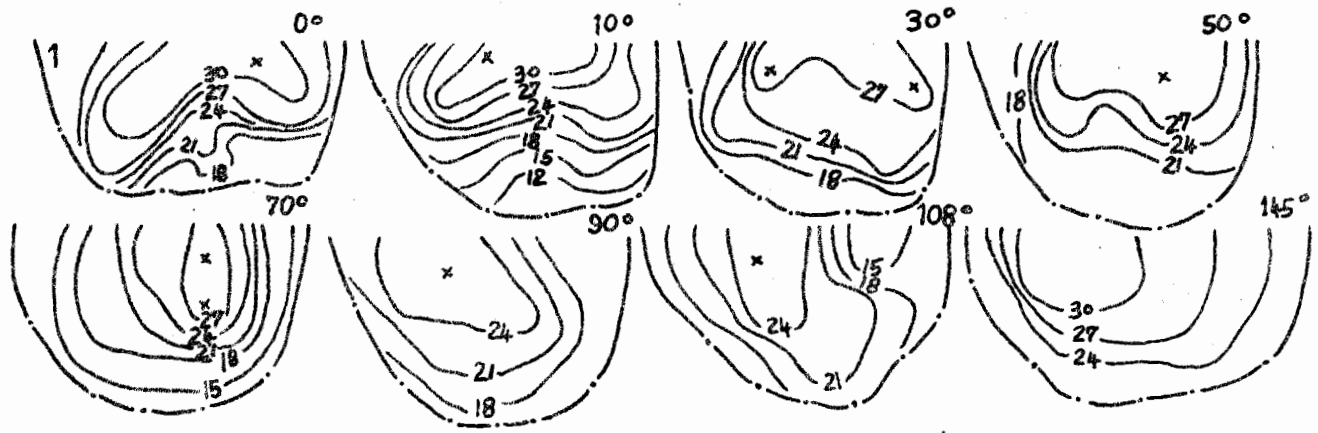
#### 5.1.4 The Isovel Patterns and Current Direction in Consecutive Bends of $r_c/wds=2.5$ and variable $r_c/wus$

Figures 5.12 to 5.14 show isovel patterns in bends with  $r_c/wds=2.5$  and varying  $r_c/wus$ . The core of maximum velocity depresses progressively towards the channel bottom between 52 and 90 degrees and a parabolic parabolic flow sometimes develops there. The secondary flow directed towards the channel bed near the concave (outer) bank develops at approximately 20 degrees (cf. Shukry, 1949; Fox and Ball, 1968). As  $r_c/wus$  decreases, the parabolic flow that transforms into a forced vortex flow in bends of  $r_c/wus=3.0$  and 3.2 establishes a free vortex flow within the the first half of the bend with  $r_c/wus=2.0$ . The transverse oscillation of high velocity core is periodic every 30 to 60 degrees. Along the downstream bend zone between 60 and 80 degrees, the core of maximum velocity depresses towards the bottom and the free vortex flow transforms into a forced vortex flow. Because the free vortex flow occupies nearly two-thirds of the bend and the forced vortex flow develops towards the bend exit, the point bar and the erosional axis locate further





Figure 5.14. Selected isovel patterns in consecutive bends with  $r_c/w_{us} = 2.0$  and  $r_c/w_{ds} = 2.6$ . The isovels are shown in  $\text{cm. s}^{-1}$  and the diagrams are presented from the left bank to the right bank facing downstream. The symbol 'x' denotes the position of the maximum velocity at each cross section.



Outline of the bend.

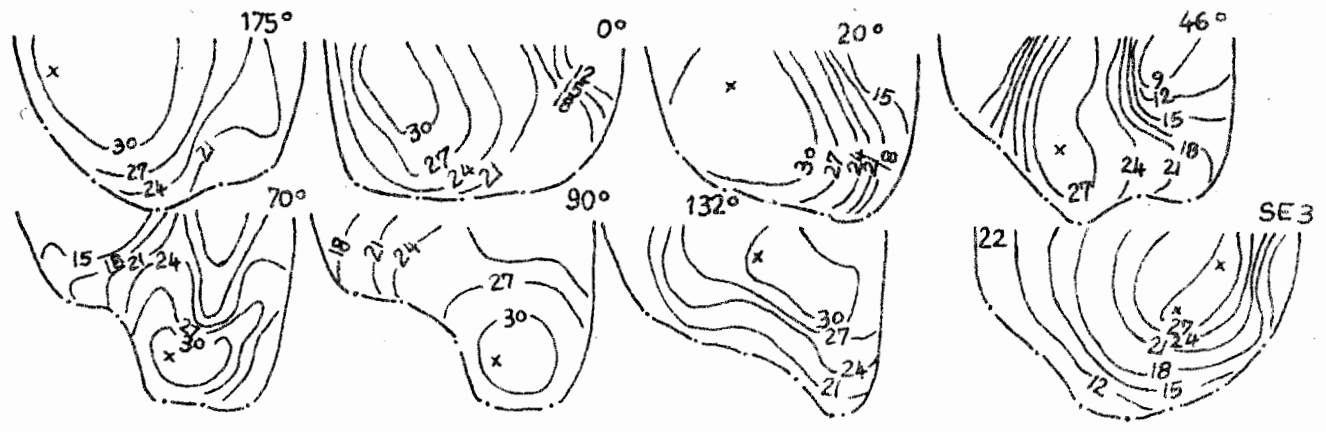
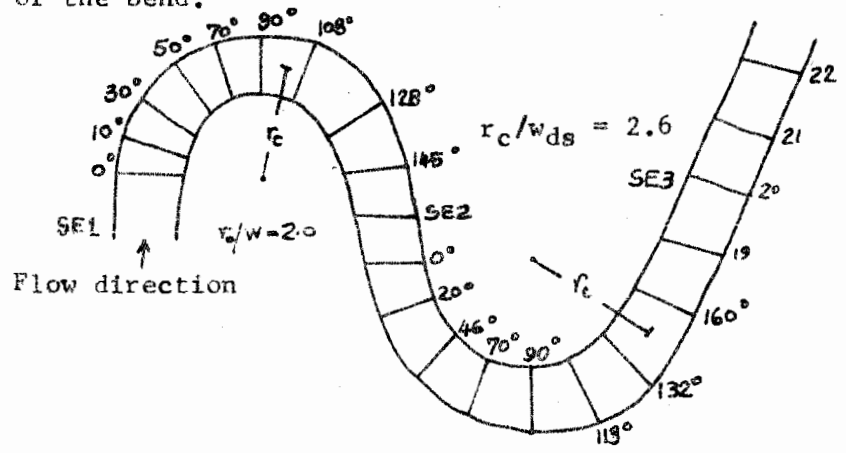


TABLE 5.3

The bend flow development and interaction in consecutive bends with  $r_c/w_{ds} = 2.5$  and variable upstream bend geometry (3.2, 2.56 and 2.6). The numbers below each vortex type is the maximum value of  $t$  in the expression  $V=kr^t$ .

$r_c/w$	SEI	0°	30°	60°	90°	120°	150°	180°	SE2	0°	30°	60°	90°	120°	150°	180°	SE3	
3.2/ 2.4	Parab. flow	Forced vortex													Free vortex		Forced vortex	
		0.64													-0.38		0.63	
3.0/ 2.56	Parab.	Forced vortex													Free vortex		Parabol. Forced	
		0.49													-0.14		0.16	
2.0/ 2.6	not measured	Free vortex													Free vort.		Forced vortex	
		-0.29													-0.58		0.47	

T\* represents transition, SEI and SE2 each represent straight entrance and exit portions of the bend.



downstream. But the variations of the extent of the free vortex flow show that the role of the point bar deposition on the rate of lateral erosion can be extremely varied (cf. Lewin, 1978) since a free vortex flow may straighten the point bar and possibly arrests lateral migration.

#### 5.1.5 The Isovel Patterns and Current Direction in Consecutive Bends of $r_c/wds=1.94$ and variable $r_c/wus$

Figure 5.15(a) shows the isovel patterns while Figure 5.15(b) shows vortex development and interaction in bend series with  $r_c/wus=4.0$  and  $r_c/wds=1.9$ . For each traverse shown in degrees (Figure 5.15(b)), the magnitude of the vortex strength (the value of the exponent  $t$ ) is given. The decrease of vortex strength along the bend zone between 70 and 103 degrees, which is the bend zone associated with downwelling, and the location of the fully developed flow zone towards the bend exit are typical characteristics of bend flow development discussed in this section. Along the downstream bends, the core of maximum velocity locates at the channel centreline until 125 degrees of bend angle, after which a forced vortex flow establishes downstream of 115 degrees of the bend. Figures 5.16 to 5.18 show that advective flow acceleration increases at the bend entrance as  $r_c/wus$  decreases. A comparison of flow structure at the bend apices indicates also that the high velocity core tends to

Figure 5.15(a). Selected isovel patterns in consecutive bends with  $r_c/w_{ds}=4.0$  and  $r_c/w_{ds}=1.65$ . The isovels are shown in  $\text{cm. s}^{-1}$  and the diagrams are presented from the left bank to the right bank facing downstream.

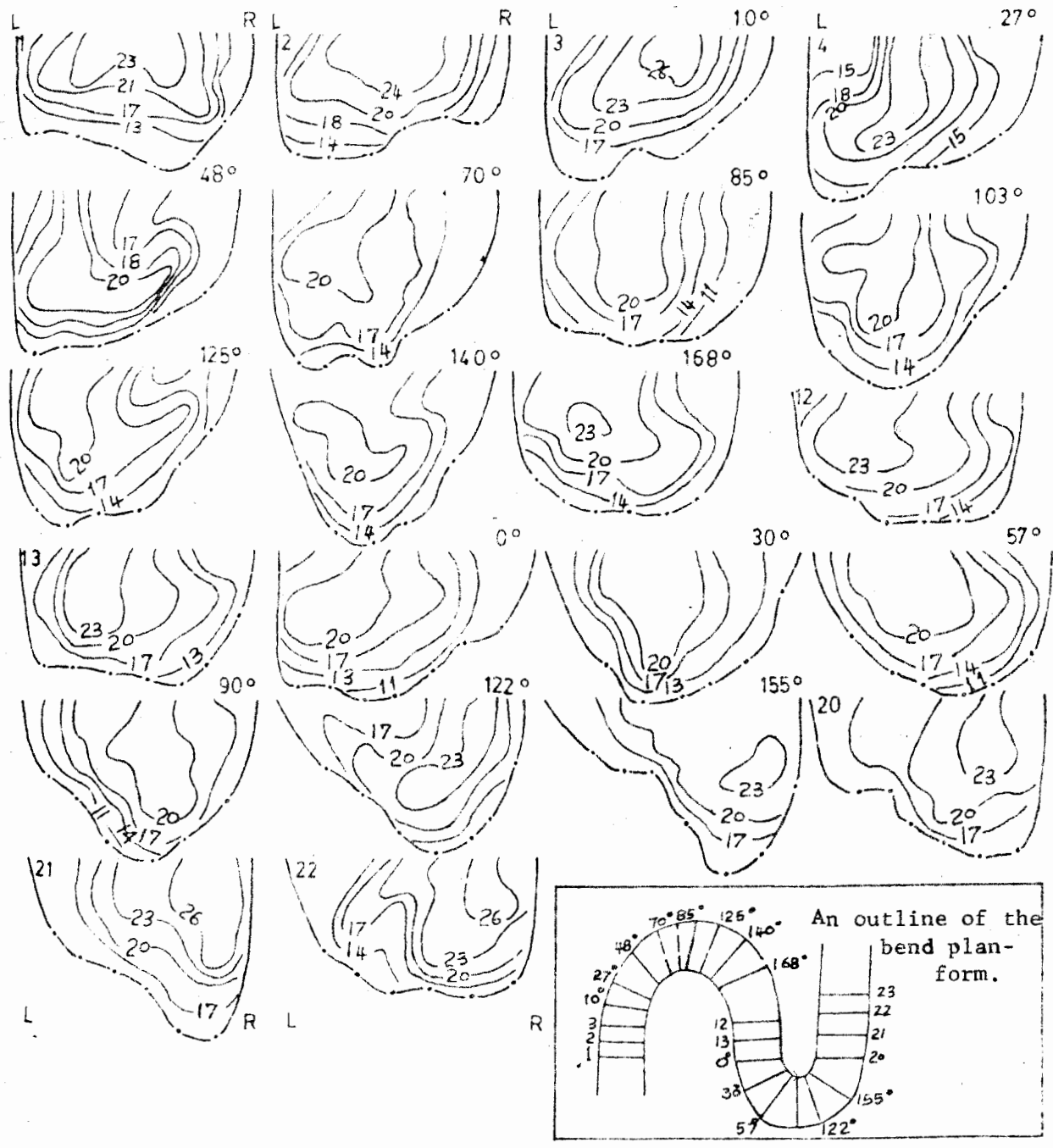




Figure 5.16. Selected isovel patterns in consecutive bends with  $r_c/w_{US} = 2.75$  and  $r_c/w_{DS} = 1.65$ . The isovels are shown in cm. s<sup>-1</sup>, and the diagrams are presented from the left bank to the right bank facing downstream. The symbol 'x' denotes the position of the maximum velocity.

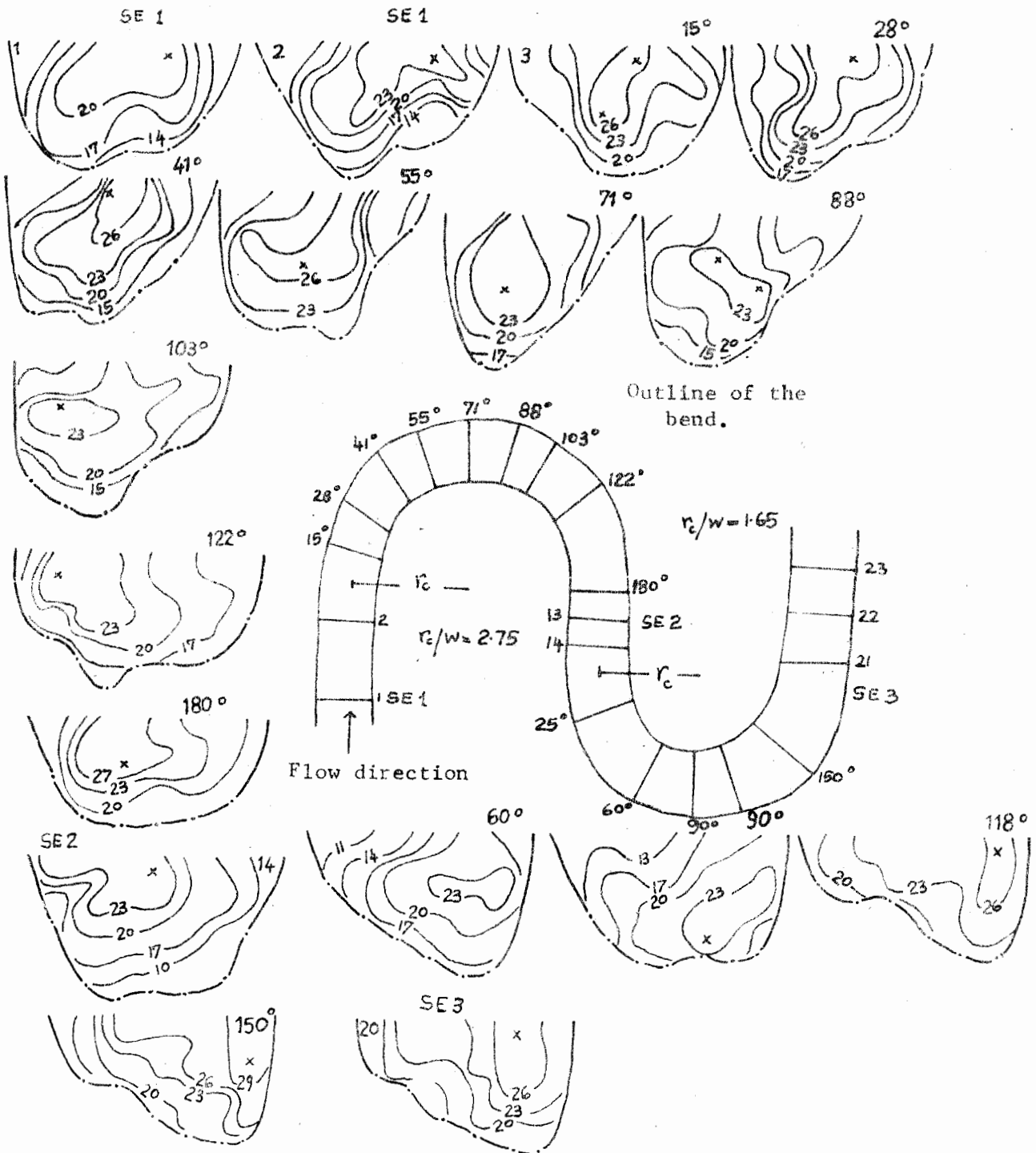
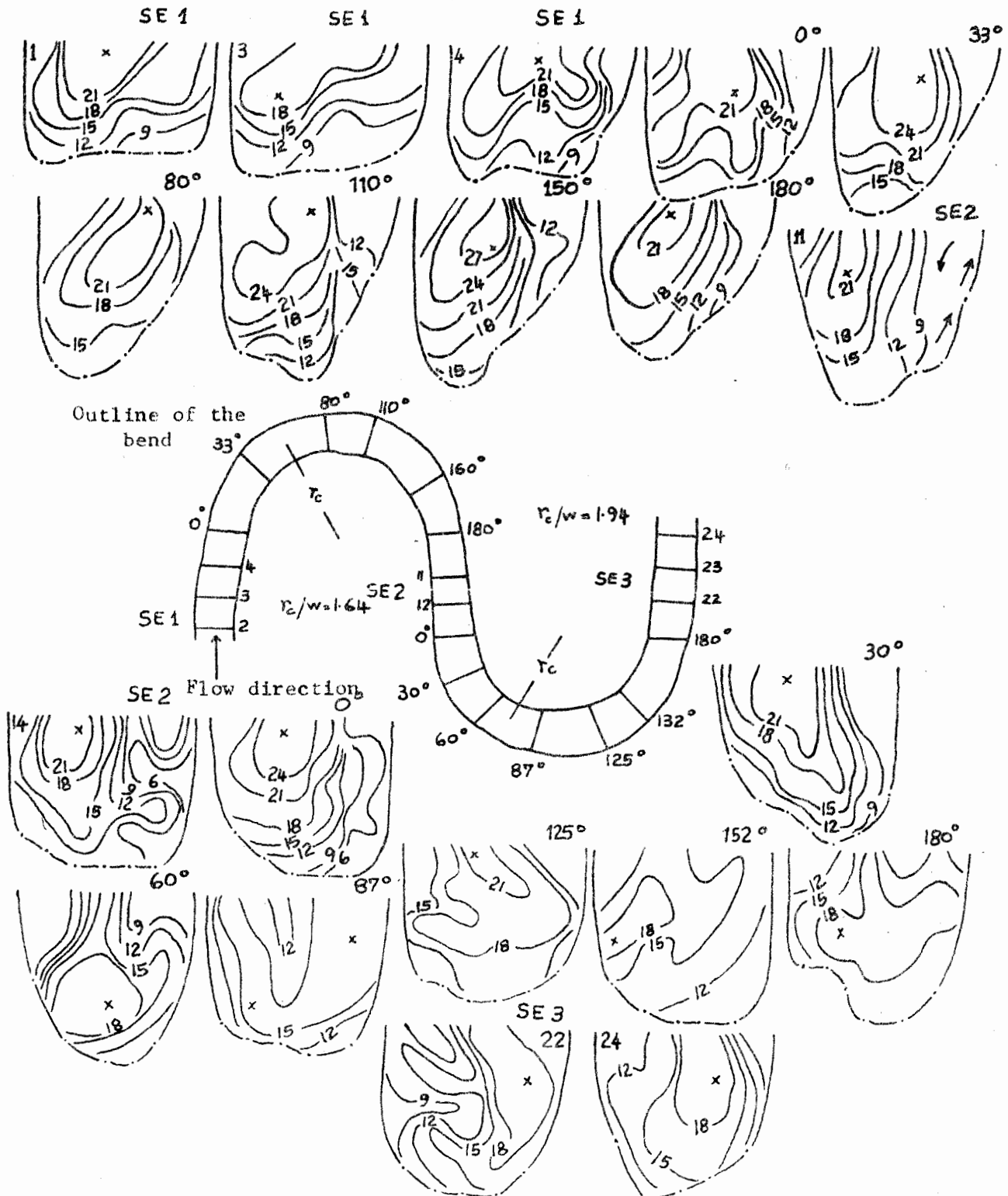




Figure 5.18. Selected isovel-patterns in consecutive bends with  $r_c/w_{us} = 1.64$  and  $r_c/w_{ds} = 1.94$ . The diagrams are presented from left bank to right bank facing downstream. The isovels are shown in  $cm. s^{-1}$



—nb. The location of the maximum velocity is shown by the symbol 'x'.

shift towards the water surface as the upstream bends become rather tighter. This probably is a result of the dominance of advective acceleration over cross stream momentum transfer.

Further tightening of the bends ( $r_c/wus=1.64$  and  $r_c/wds=1.94$ ) causes radical changes in the combination of vortices that occur. In Figure 5.18, the parabolic flow locates along the straight entrance but it translates to a forced vortex between the entrance and a bend angle of 45 degrees instead of the free vortex flow (see Figure 1.2,  $r_c/us=4.0$ ). Although the occurrence of this forced vortex flow may be due to local conditions, it translates to a free vortex flow further downstream between 45 and 105 degrees of bend angle.

Tightening of the upstream bends shifts the position of the C-shaped isovels upstream and delays the adjustment of the flow in the downstream bend. It causes the core of maximum velocity to shift towards the convex bank at the bend apex (compare Figures 5.16 and 5.17; cf. Hickin, 1978). But when these C-shaped superposed spirals coalesce, the resulting single spiral is unable to occupy the total channel width and the secondary flow near the bottom drives momentum deficit flow towards the banks and the surface (cf. Callander, 1978) and the flow separates from the boundary. In some cases, the retarded flow at mid depth surrounded by higher velocity flow near the channel boundary (C-shaped or U-shaped isovels) may be due to vortex trails that are captured by swift mainstream currents.

Figure 5.19. Selected isovel patterns in consecutive bends with  $r_c/w_{us} = 3.3$  and  $r_c/w_{ds} = 2.0$ . The diagrams are presented from left to right facing downstream. The isovels are shown in  $\text{cm. s}^{-1}$ . The symbol 'x' denotes the position of the maximum velocity.

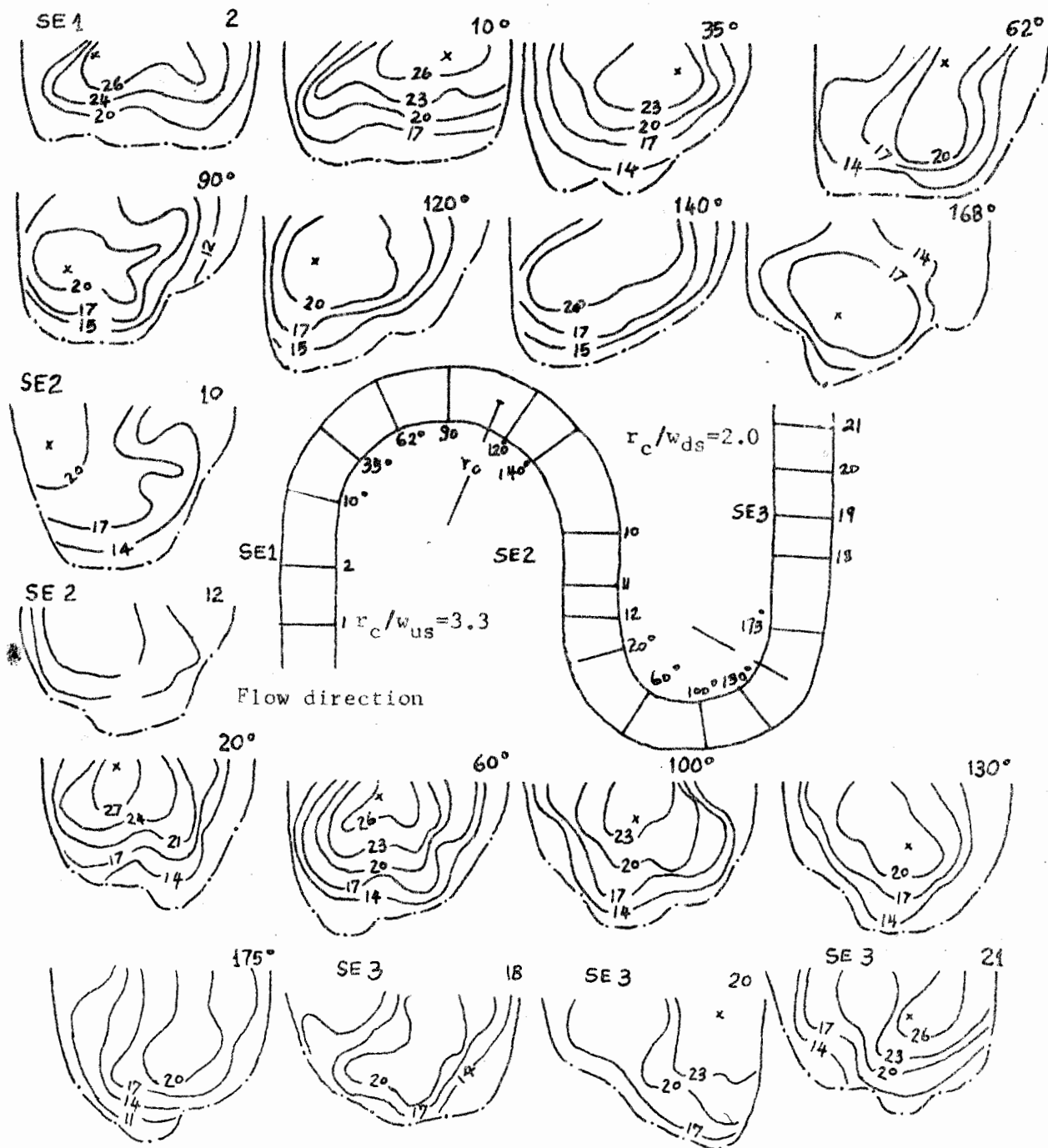




TABLE 5.4

The bend flow development and vortex interaction in consecutive bends with  $r_c/w_{ds} = 1.9$  and variable upstream bend geometry.

$r_c/w$	SEI	0°	30°	60°	90°	120°	150°	180°	SE2	0°	30°	60°	90°	120°	150°	180°	SE3
4.0/ 1.91	Parab. flow	Free vort. -0.51	Forced 0.41	T vortex	Free vort. -0.23	Forced vortex 0.33	vortex 0.40										
3.0/ 2.0	Parabolic flow	Forced 0.29	T vortex 0.22	Free vortex -0.33	Forced vortex 0.17	T vortex 0.35											
3.0/ 1.94	Parabolic flow	Forced 0.37	T vortex 0.20	Free vortex -0.21	Forced vortex 0.23	T vortex 0.35											
2.75/ 1.65	Parabol.	Free vort. -0.21	T Forced 0.42	T vortex 0.22	Free vort. -0.30	Forced vortex 0.33											
1.64/ 1.94	Parab. flow	Forced vort. 0.32	Free vortex -0.16	Forced vortex 0.48	Free vort. -0.41	Parabolic flow	Forced vortex 0.23										

nb. T represents transitional flow.

They also establish a parabolic flow at the bend apex where the core of maximum velocity depresses towards the channel bed. These U-shaped isovel patterns tilt 90 degrees anticlockwise (i.e reverse C-shaped) along the bend zone between 125 degrees and 165 degrees and a forced vortex flow establishes. This pattern of flow development inhibits point bar deposition between the entrance to a bend angle of 165 degrees. Instead, the channel width at the bend apex likely will flare, i.e. channel width at the bend apex becomes wider than that at the bend entrance or exit (cf. Hickin, 1975; Lewin, 1976).

#### 5.1.6 Summary and Discussion

The isovel patterns along the upstream bends are consistent with those for the upstream bends described in Chapter 4 and also to bend flow development in open-channel bends in general (cf. Mockmore, 1944). Although the strength of the free vortex at the upstream bend entrance is small ( $t$  is close to but less than  $-0.15$ ), it appears in the present analysis as parabolic flow. In to the bend, a forced vortex flow develops at 30 degrees and persists until 60 degrees. But still further downstream, a secondary spiral develops near the bed which tends to move accelerating fluid from the inner bank towards the outer bank (cf. Dietrich et al; 1979). This secondary spiral is the one that develops within the bend as opposed to that which owes its existence to the straight channel entrance zone (cf. Shukry,

1949); it reduces the strength of the forced vortex between 80 and 120 degrees through boundary friction.

The fully developed flow zone locates at about 60 degrees and downstream of 135 degrees. These are the two bend sections at which the loci of maximum erosion likely occurs in order for the bend to develop what Hickin (1974) refers to as a T-shaped bend geometry. In between these two fully developed flow zones, the core of maximum velocity depresses towards the bottom and secondary flow advects towards the water surface along the banks.

Along the downstream bends, the extent of the free vortex flow appears to be a reasonable indicator of upstream influence. The free vortex flow begins to disintegrate between 15 and 30 degrees, and in many cases it is overwhelmed by cross stream momentum at 60 degrees where the core of maximum velocity shifts towards the concave bank. The superposed spiral, the upper one inherited from the upstream and the lower one that develops at the bend entrance, are typical characteristics of the flow in subsequent bends (cf. Shukry, 1949; Mosonyi and Gotz, 1973; Ippen and Drinker, 1962). However, in both upstream and downstream bends, the secondary flow is periodic every 30 to 60 degrees and accords with results of Muramoto (1967), Einstein (1972) and Varshney and Garde (1975). The transitional zones occupied by parabolic flow cover less than 20 degrees in wider bends (less than 9% of the total bend) but increase with decreasing  $r_c/w$ . The short extent of such transitional zones

reflects an abrupt shift of the thalweg from one bank to the other which increases the potential for bend erosion and deposition that may be similar to those of underfit streams (cf. Tinkler, 1971).

## 5.2 THE DISTRIBUTION OF MEAN AND TRANSVERSE VELOCITY

### 5.2.1 Introduction

The systematic variation of the mean and transverse velocity oscillations along bends of diverse curvature ratios discussed in section 4.2 shows the zones at which most of the stream energy is lost to eddies and boundary roughness. The lengthwise velocity variations increase as the curvature ratio decreases; it signals that as large losses due to friction increase, energy is diverted to other segments of the bend. These longitudinal variations possibly are responsible for riffle and pool development. The discussion has shown that the velocity distributions along the downstream bends are more irregular than those of upstream bends because of the disturbances carried over from the upstream bends. A uniform distribution of mean velocity was observed only in a bend of  $r_c/w=2.0$ .

This section discusses experimental results of velocity measurements in paired bends with constant downstream bend

geometry. An attempt will be made to relate velocity near the channel banks to zones most liable to erode in river bends. Figures 5.20 to 5.27 show the mean longitudinal distribution of velocity and also velocity near the channel banks. The velocity near the channel banks was measured at 0.0762m from the water's edge. Velocities near the outer (concave) bank of various bend series are shown by different symbols that are joined by lines. Because the velocity near the inner (convex) bank is generally low, their distributions are shown by the same symbols as those of the concave bank, but for the sake of reducing clutter are not joined by any lines.

#### 5.2.2 The Velocity Distribution in Consecutive Bends of $r_c$ $/wds=4.0$ and variable $r_c/wds$

Velocity decreases along the upstream bends from the bend entrance to a minimum value along the bend zone between 60 and 90 degrees. It is this reach where the core of maximum velocity depresses towards the channel bed and the transition between free and forced vortices occurs (cf. Nagler, 1943; Shukry, 1963). The velocity distribution along the banks has irregular excursions where secondary flow moves accelerating fluid towards the banks, points that likely are candidates for erosion (Brooks, 1963).

Figure 5.20. The distribution of mean velocity in consecutive bends with  $r_c/w_{ds} = 4.0$  and variable upstream bend geometry.

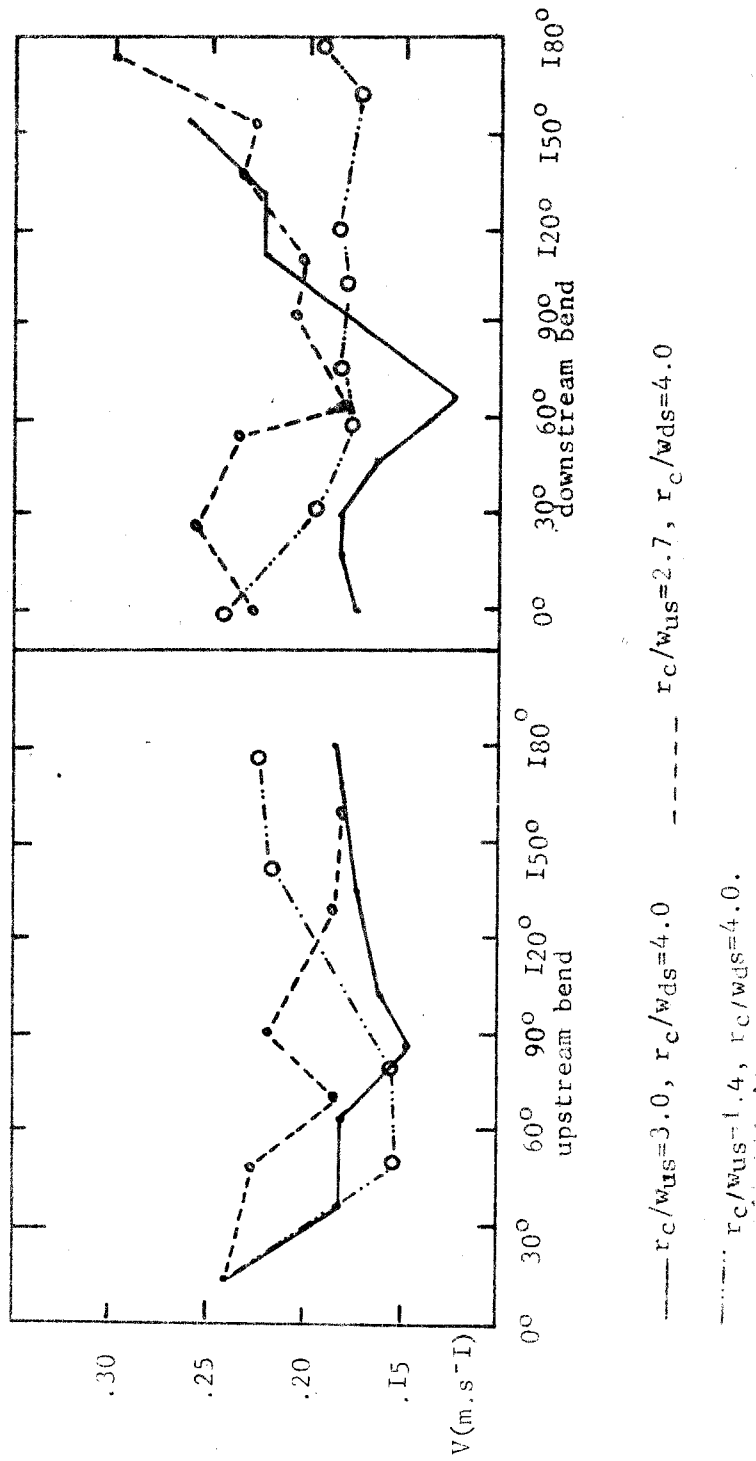
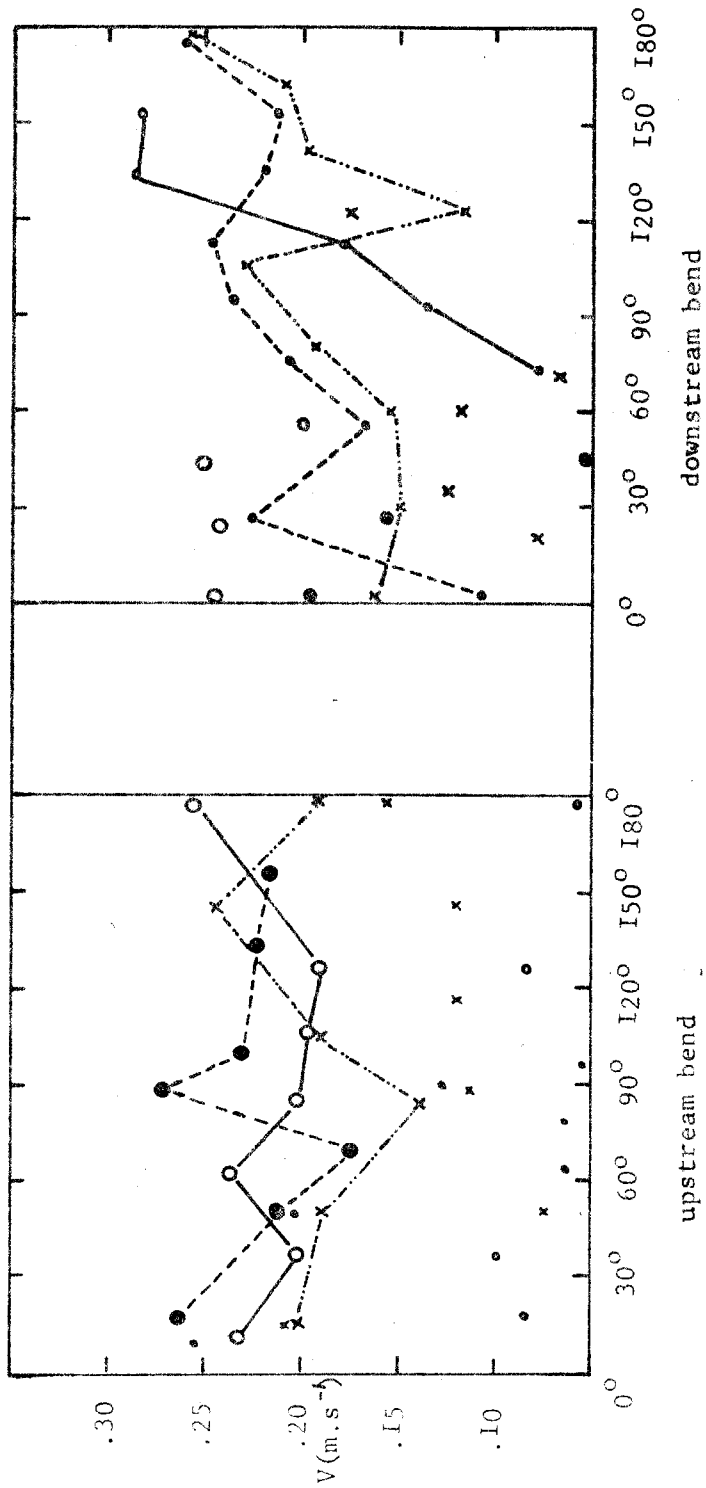


Figure 5.2I. The distribution of velocity near the channel banks of paired bends with  $r_c/w_{ds} = 4.0$  and variable upstream bend geometry. The velocity near the concave bank is joined by lines while the one near the convex bank is shown by symbols.



—  $r_c/w_{us}=3.0$ ,  $r_c/w_{ds}=4.0$ ; - - -  $r_c/w_{us}=2.7$ ,  $r_c/w_{ds}=4.0$  - · -  $r_c/w_{us}=1.4$ ,  $r_c/w_{ds}=4.0$

Note: The velocity along the outer banks is shown by symbols connected by lines while that near the convex bank is shown by the same symbol for each paired bend.

The upstream bends have minimum velocity between 60 and 120 degrees along the convex bank except in a bend with  $r/wus=1.4$  (shown by "x" symbols) in which the high velocity core is more or less near the inner bank. The minimum velocity occupies the bend zone between 30 and 60 degrees and also between 120 and 135 degrees near the concave bank. The location of the maximum velocity near the concave bank migrates downstream as the upstream bends become tighter. The zones with a minimum value near the inner bank have secondary flow towards the surface. Onishi et al (1976) observed that secondary flow directed vertically upwards tends to encourage suspension and reduce transport of bedload which makes these sections prime areas of point bar deposition.

The convex flow separation zones locate downstream of 60 degrees and do not reattach to the bank in bends with  $r/wus > 2.7$ . The velocity near the concave bank reaches a maximum value along the bend zone between 60 and 120 degrees and also downstream of 150 degrees except in a bend preceded by  $r/wus=1.4$ . This difference probably is because the arc length of the bend is shorter than that of the incoming spiral. In other words, the streamlines are subtended by radial forces away from the convex bank (separation zone) and the arc length of these streamlines is longer than that of the bend geometry. These streamlines do not therefore reattach to the convex bank within the bend zone. In this bend, the maximum velocity core shifts towards the channel centreline downstream of 120 degrees



of the bend angle. It also is interesting to note that convex flow separation zones contract along the upstream bend zones from 60 degrees in  $r_c/wus=3.0$ , 45 degrees in  $r_c/wus=2.7$  and 15 degrees in that of  $r_c/wus=1.4$ . Allen (1968) shows that the relative length of separation zone in a stepped channel decreases with relative step height. The step height is analogous to the curvature ratio in channel bends because the streamlines are curvilinear. The extent of the separated zone likely is related to the rate of point bar deposition and its topography. Onishi et al (1976) found that a single bend with  $r_c/w=3.0$  has a wider point bar which is topographically higher than those with greater or less curvature ratio. This increased rate of deposition concomitantly leads to a higher rate of erosion for the channel to maintain width-depth sensibly constant.

Along the downstream bends, the inherited high velocity near the convex bank decreases rapidly to a minimum value at approximately 60 degrees (cf. Bluck, 1972; Bridge and Jarvis, 1976). The transitional flow at 60 degrees of bend is accompanied by the presence of a riffle. In other words, the pool near the concave bank locates further downstream of the bend axis, thus assuring a downstream migration (translation) of the bend.

### 5.2.3 The Velocity Distribution in Consecutive Bends of $r_c/wds = 3.3$ and variable $r_c/wus$

The variations of mean longitudinal velocity along the downstream bends are periodic every 30 to 60 degrees (Figures 5.22 to 5.23) as observed in the previous bends. The maximum mean longitudinal velocity locates at 75 degrees in a bend with  $r_c/wus > 3.0$  and between 75 and 90 degrees in one of  $r_c/wus = 2.0$ . But the mean velocity increases with increasing bend angle in bends of  $r_c/wus < 2.0$ . The monotonous lengthwise increase of mean velocity likely is a product of the high velocity core that locates near the convex bank and which only shifts to the concave bank along the bend exit (cf. Blue et al; 1934). This flow pattern in tight bends straightens the point bar by erosion and deposits fine sediments in the abandoned scour pools on the concave bank (cf. Woodyer, 1975). Bagnold's (1960) model of a continuous presence of convex flow separation zone in tight bends may not reflect flow characteristics in natural rivers (see for example Lewin, 1976; Hickin, 1978). In a bend of  $r_c/w = 2.0$ , the core of maximum velocity follows a less sinuous path by as observed in the earlier cases.

Along the convex bank, the velocity distribution in upstream bends is more irregular (Figure 5.20).

Figure 5.22. The distribution of mean velocity in consecutive bends with  $r_c/w_{ds} = 3.3$  and variable upstream bend geometry.

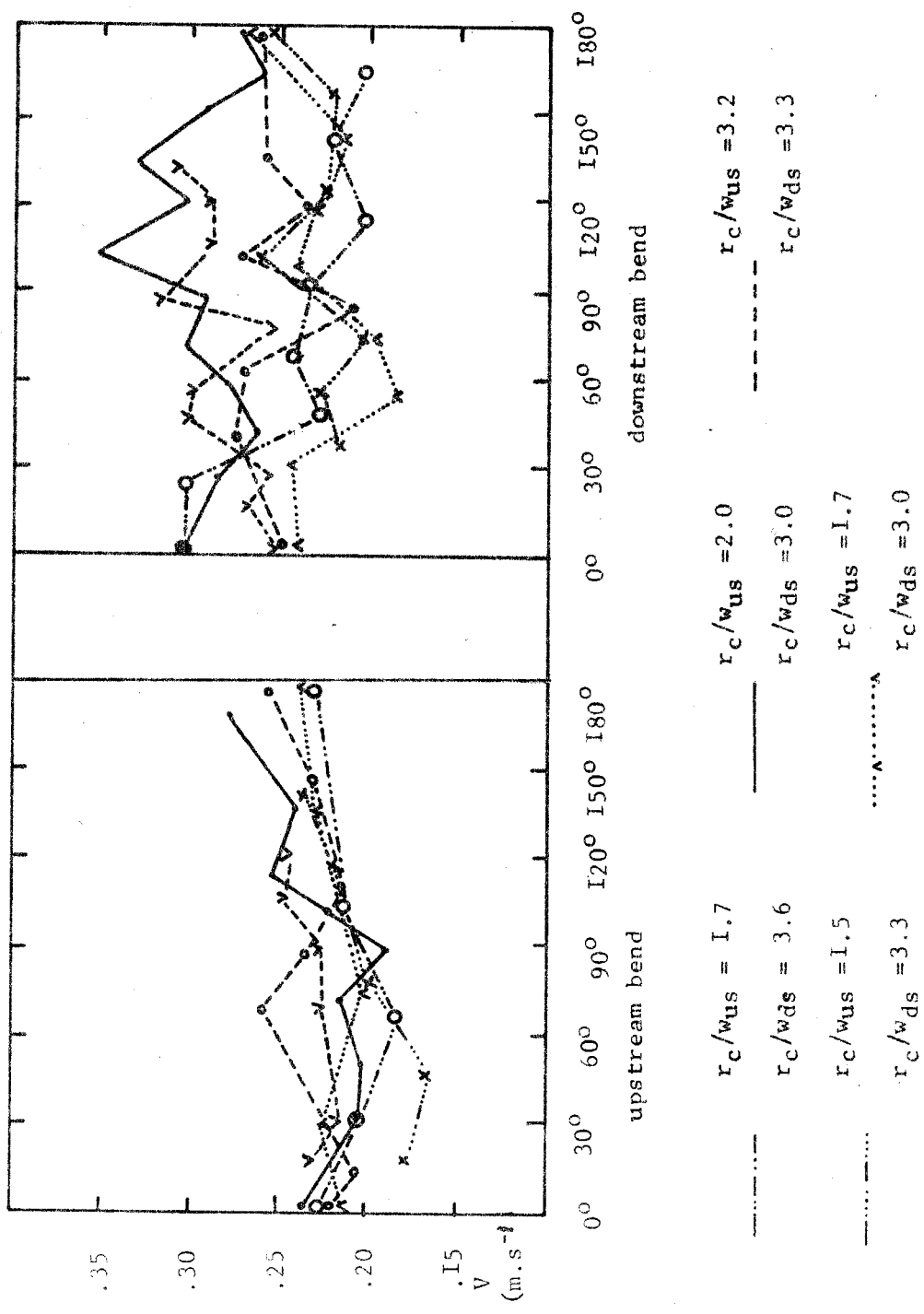
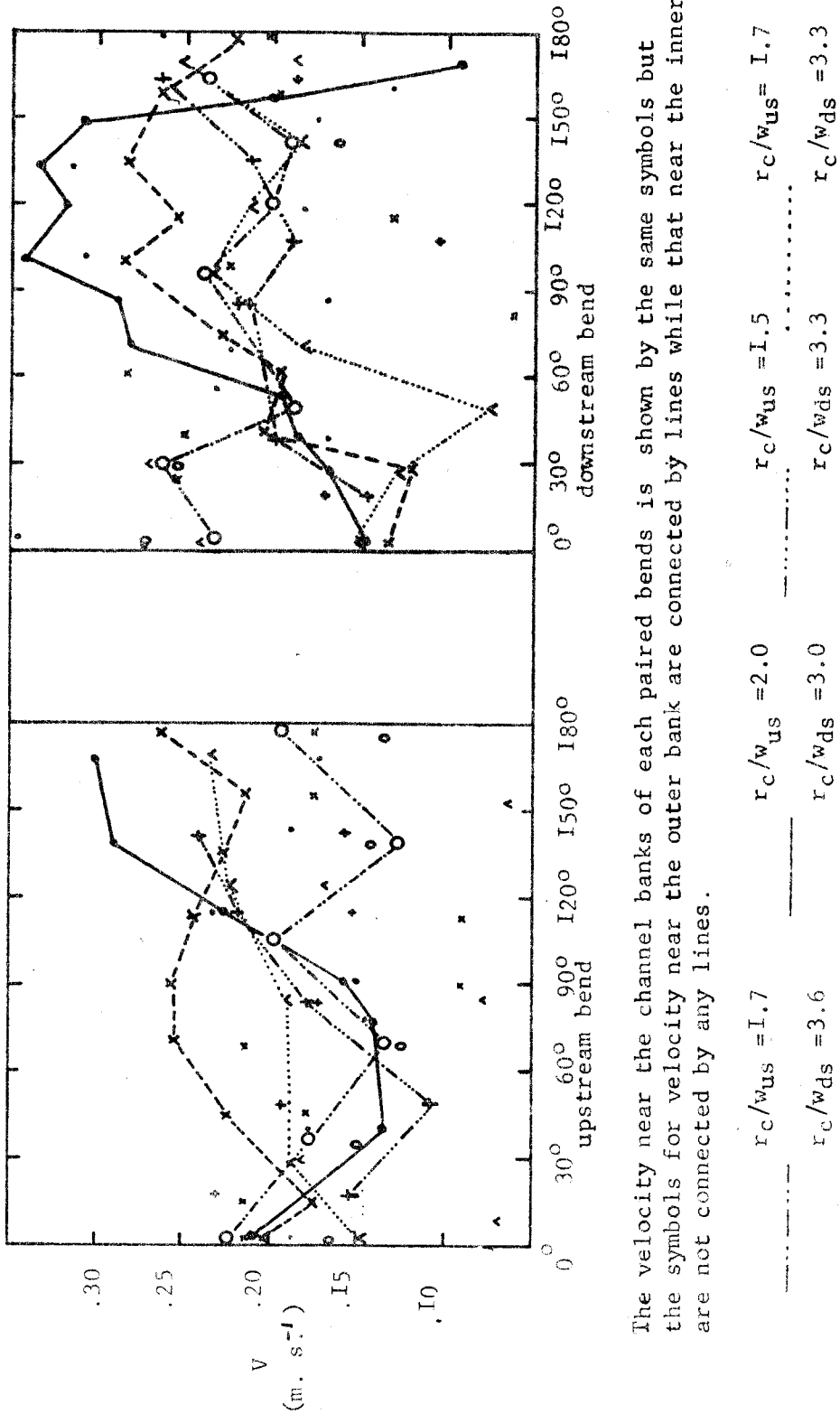


Figure 5.23. The distribution of velocity near the channel banks of consecutive bends with  $r_c/w_{ds} = 3.3$  and variable upstream bend geometry.



The velocity near the channel banks of each paired bends is shown by the same symbols but the symbols for velocity near the outer bank are connected by lines while that near the inner bank are not connected by any lines.

$r_c/w_{us} = 1.7$        $r_c/w_{us} = 2.0$        $r_c/w_{us} = 1.5$        $r_c/w_{us} = 1.7$   
 $r_c/w_{ds} = 3.6$        $r_c/w_{ds} = 3.0$        $r_c/w_{ds} = 3.3$        $r_c/w_{ds} = 3.3$   
 -----  $r_c/w_{us} = 3.3$ ,  $r_c/w_{ds} = 3.3$ .

The velocity near the concave bank decreases from the bend entrance until 45 degrees, then increases to a maximum value along the bend zone between 60 and 120 degrees where bank erosion occurs for the expansion type of bend movement. The maximum velocity near the convex bank locates at 70 degrees in  $r_c/wus=3.2$  only (free vortex), and between 120 and 150 degrees in the tighter bends. This high velocity core near the convex bank trims the topography of the point bar. However, along the downstream bends, the velocity distribution along the convex bank is periodic every 30 degrees in bends preceded by  $r_c/wus>2.0$ , and every 60 degrees in bends preceded by  $r_c/wus<2.0$ . As mentioned earlier, these differences are due to the influence of the incoming spiral flow from the upstream bend. A wider upstream bend contributes a spiral flow with a longer wavelength than that from a tighter bend. The velocity distribution near the concave bank, on the other hand, decreases along the downstream bend zone between 30 and 60 degrees, but increases to a maximum value at 90 degrees.

It has been known for some time that many meandering rivers migrate downvalley (Friedkin, 1945). This mode of migration likely is controlled by the velocity distribution near the concave bank. Figure 5.23 shows that relatively higher velocity occurs between 120 degrees and downstream of the subsequent bend apices of  $r_c/wus=2.0$  and between 60 and 150 degrees in the ones following  $r_c/wus=3.0$ . If the velocity is competent to erode the banks, these bends will migrate down valley. The high velocity

zone at the bend entrance along the convex bank in downstream bends may be responsible for "gutter" erosion observed by Suga (1967).

#### 5.2.4 The Velocity Distribution in Consecutive Bends in $r_c/wds=2.5$ and variable $r_c/wus$

The maximum mean longitudinal velocity along the downstream bends locates at 30 degrees and between 120 and 155 degrees, while the minimum value locates along the bend zone between 60 and 90 degrees (Figure 5.24). The mean velocity in a bend of  $r_c/wus=2.0$  is periodic every 60 degrees as observed in other bends of the same curvature ratio (see Chapter 4), but every 90 degrees in  $r_c/wus=3.0$  and 3.2. Along the concave banks, the velocity decreases from the bend entrance to a minimum value at 80 degrees but increases monotonically further downstream, except in a bend with  $r_c/w=2.0$  in which a flow separation zone locates at 150 degrees. As velocity near the concave bank decreases along the bend zone between 120 and 150 degrees in  $r_c/w=2.0$ . the one along the inner bank increases because the high velocity has shifted towards the convex bank. Bends with  $r_c/wus=3.0$  and 3.2 have relatively higher velocity along both banks which reduces the asymmetry of the channel cross section, shear stress (cf. Ippen and Drinker, 1962), and secondary flow (Shukry, 1949). This change is accompanied by an

Figure 5.24. The distribution of mean velocity in consecutive bends with  $r_c/w_{Ds} = 2.5$  and variable upstream bend geometry.

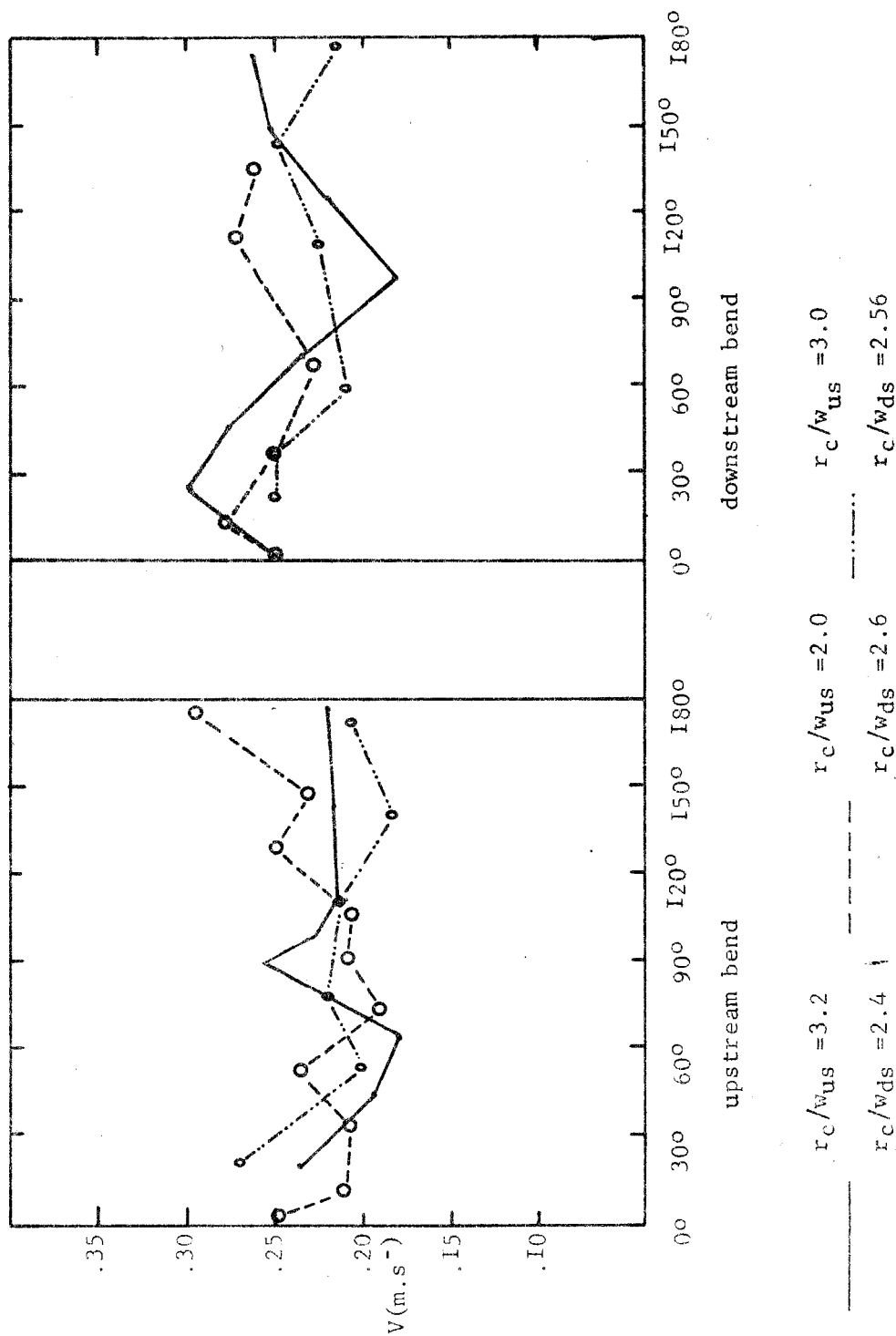
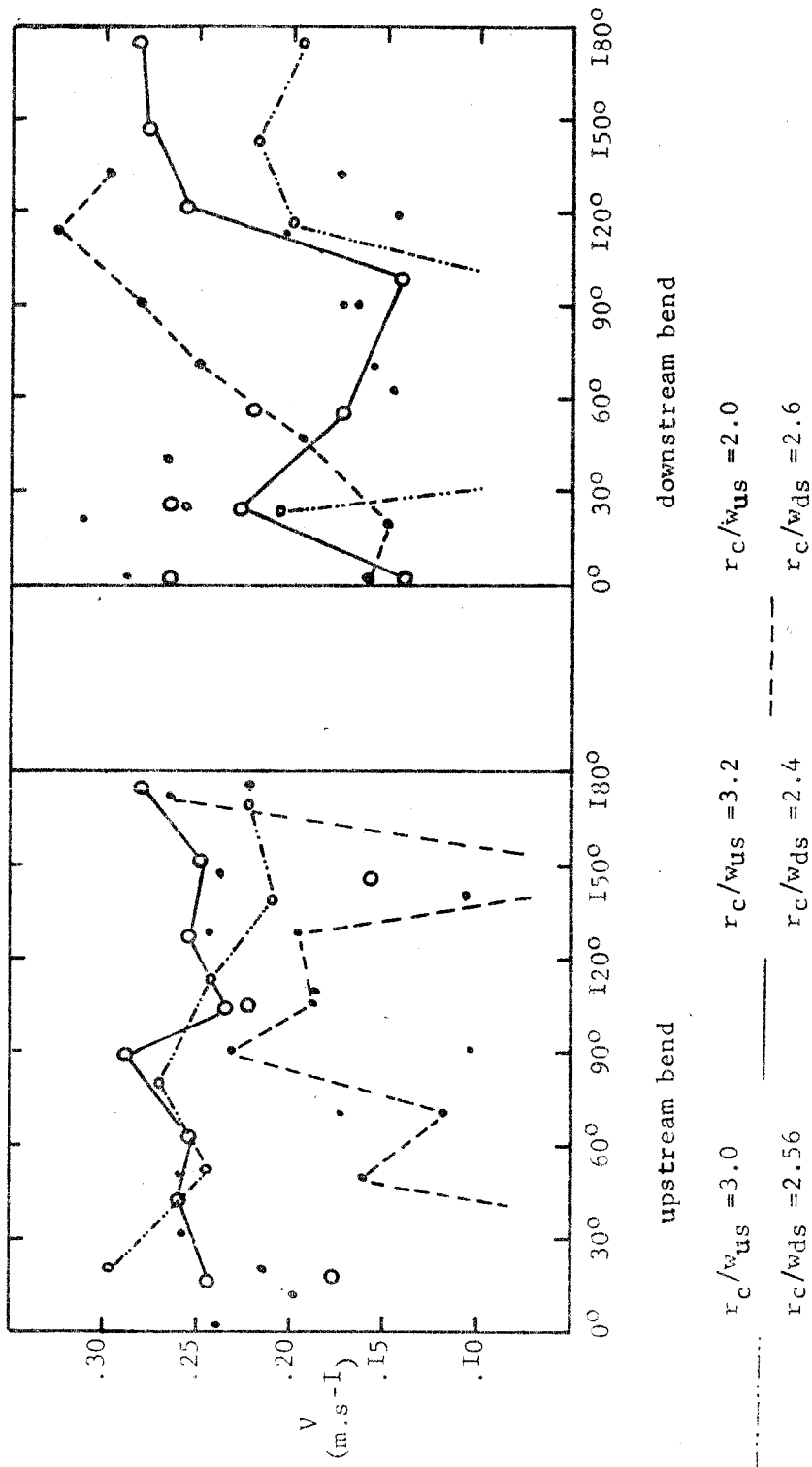


Figure 5.25. The distribution of velocity near the channel banks of consecutive bends with  $r_c/w_{ds} = 2.5$  and variable upstream bend geometry. The velocity for each paired bends is shown by the same symbols but the symbols for the outer bank are connected by lines while that of the inner bank are not connected by any lines.





increase of sediment transport rate (Onishi et al; 1976). The plane bed in these bends probably is responsible for the increase of periodicity of velocity distribution from 60 to 90 degrees.

Along the downstream bends, the valley of minimum velocity persists between 60 and 90 degrees. The velocity near the convex bank is initially high at the bend entrance, but decreases rapidly to a minimum value at the bend apex where point bar deposition occurs. The velocity along the concave bank increases from the bend entrance except in  $r_c/wds=2.56$  where concave flow separation locates between 30 and 90 degrees. The valley of minimum velocity that locates along the concave bank of the subsequent bend apices of  $r_c/wus=3.0$  and  $3.2$  likely will not experience an expansion mode of lateral migration. On the other hand, the concave bank of a bend with  $r_c/wds=2.6$  supports higher velocity between 60 and 120 degrees and likely causes erosion there (Bagnold, 1960; Begin, 1980). The general decrease of velocity at the bend apex is caused by the increased form drag associated with the shift of high velocity core towards the channel bed where the bend pool locates.

#### 5.2.5 The Velocity Distribution in Consecutive Bends in $r_c/w=2.0$ and variable $r_c/wus$

The difference between minimum and maximum mean velocity for the upstream bends is smaller than that shown in Figure 5.26

Figure 5.26. The distribution of mean velocity in consecutive bends with  $r_c/w_{ds} = 1.9$  and variable upstream bend geometry.

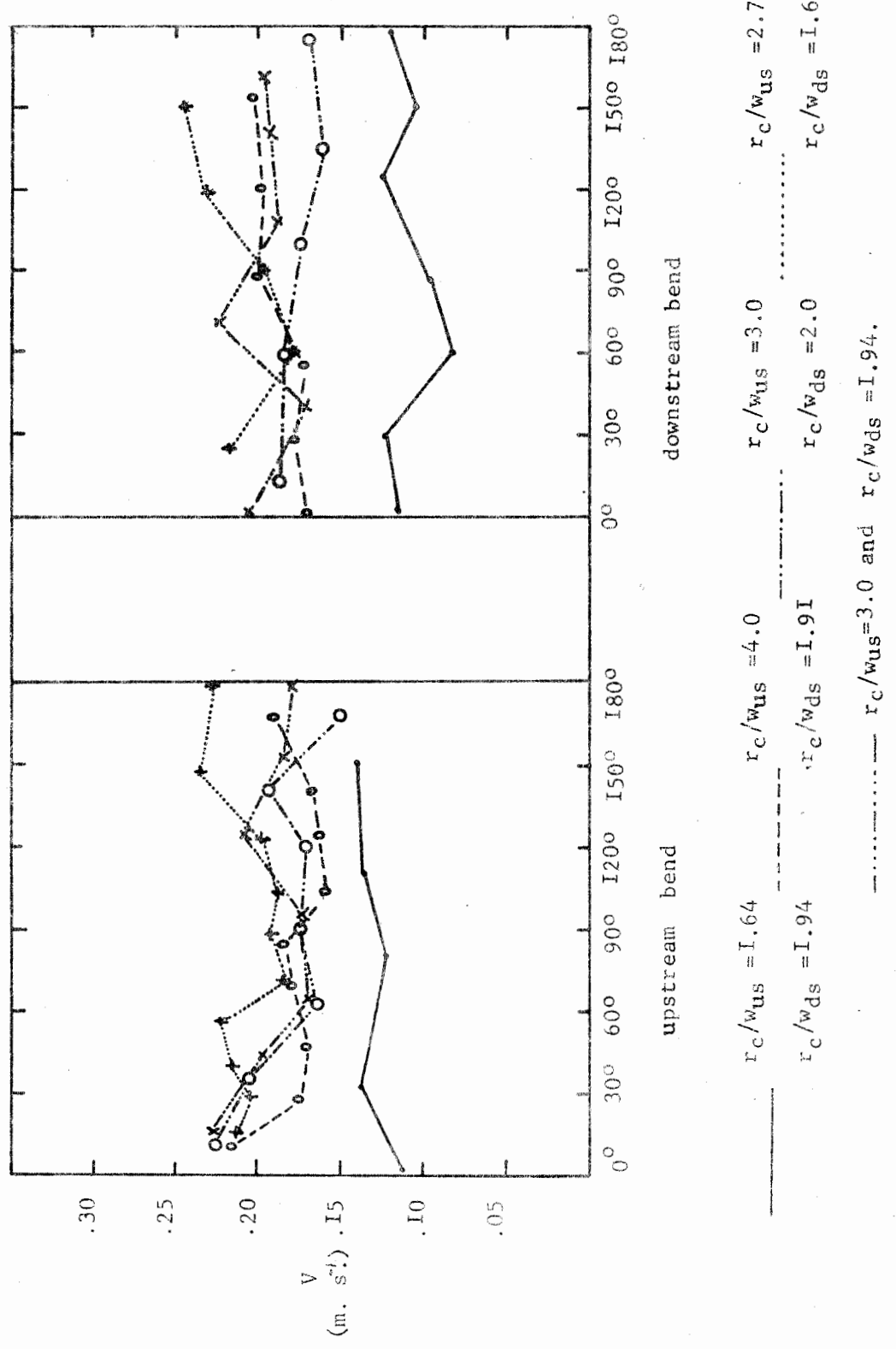
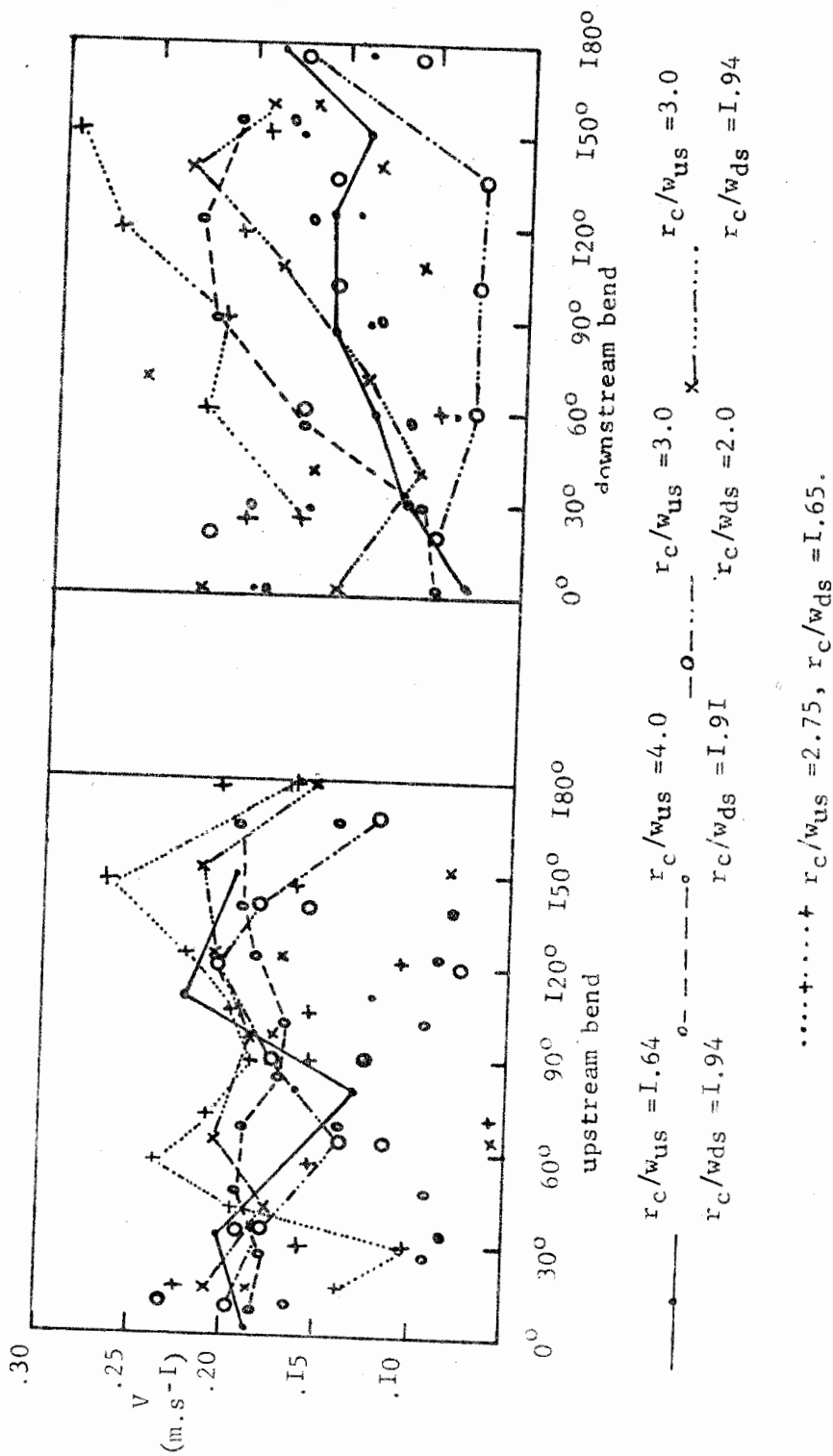


Figure 5.27. The distribution of velocity near the channel banks of consecutive bends with  $r_c/w_{ds} = 1.9$  and variable upstream bend geometry. The velocity for each paired bends is shown by the same symbols but the symbols for the outer bank are joined by lines while that of the inner bank are not connected by any lines.



( $r_c/wds=2.5$ ), but the valley of the minimum velocity locates in a more restricted zone between 60 and 90 degrees. Along the downstream bends the mean velocity profiles are sensibly uniform except for the bend preceded by  $r_c/wus=1.64$ ; a pattern similar to that observed in bends of  $r_c/wus=1.4$  (see section 3.3.2).

The velocity near the concave bank has a maximum value along the bend zone between 30 and 60 degrees and also between 120 and 150 degrees along the upstream bends. Because these sections support high velocity flow, bank calving likely will occur at these two points. Along the convex bank, the velocity is relatively higher at the bend apex in  $r_c/wus=2.7$  and 3.0 than in the other bends possibly because of the presence of a potential vortex flow. Unlike the upstream bends, the velocity along the concave bank in downstream bends increases monotonically through the rest of the bends, except in bends proceeding  $r_c/wus=1.64$  and 3.0.

#### 5.2.6 Summary

The variation of mean velocity can be shown as a ratio of maximum and minimum velocity shown in Table 5.5. The minimum velocity along the bend zone between 60 and 90 degrees and also between 110 and 150 degrees are consistent for both upstream and downstream bends. It appears, therefore, that the location of minimum mean velocity is neither controlled by differences of curvature ratio nor by the influence of upstream bends.

TABLE 5.5

The location of maximum and minimum velocity in consecutive bends with constant downstream curvature ratios.

$r_c/w_{us}$	$V_{max}$	$V_{min}$	$V_{max}/V_{min}$	$r_c/w_{ds}$	$V_{max}$	$V_{min}$	$V_{max}/V_{min}$
3.0	0	90	1.76	4.0	30;120	70	2.1
2.7	0;90	70;150	1.29	4.0	30;180	60	1.4
1.4	15;150	60	1.50	4.0	0	60	1.3
1.7	0	70	1.25	3.6	30	60;120	1.5
2.2	40;120	90	1.21	3.9	60;120; 150	15	1.4
2.0	120	90	1.52	3.2	105	40;150	1.4
3.2	70	15;110	1.22	3.3	40	74	1.4
1.5	150	80	1.41	3.3	55	90	1.3
1.7	30;120	90	1.17	3.0	30	50;135	1.3
3.0	15	50;135	1.49	2.56	30;140	60	1.2
3.2	15;90	60	1.43	2.4	30	100	1.7
2.0	0;180	70	1.5	2.6	15	70	1.2
1.6	30;150	0;75	1.08	1.94	30	60	1.3

The location of maximum mean velocity between the bend entrance and 30 degrees and between 120 and 180 degrees along the upstream bends that tend to vary with  $r_c/w$  possibly are bend effects that have been observed in the present study.

The valley of minimum velocity along the bend zone between 60 and 90 degrees is associated with the depression of the core of maximum velocity towards the channel bed. Along this bend zone, resistance may increase due to boundary roughness and with the intensity of secondary flow. Hickin (1978) observed a reduction of velocity near the water surface along the bend apex which he attributed to vertical vortices attached to fixed boundary elements (cf. Einstein and Shen, 1968). Muramoto (1967) measured vortex development in model bends of various curvature ratios and concluded that the secondary flow directed towards the channel bottom is zero until 60 degrees where it gradually increases in the second half of the bend. The data presented here lend support to such a development.

The maximum mean velocity that locates upstream of 30 degrees and downstream of 120 degrees is probably due to accelerated flow associated with the development of the forced vortex. It may be recalled also that the strength of the forced vortex flow decreases and parabolic (transitional) flow may develop in the region between 80 and 120 degrees. This bend zone witnesses a decrease of mean velocity and the high velocity core depresses towards the bed also.

TABLE 5.6

The location and extent of convex and concave flow separation zones of consecutive bends with downstream bend geometry constant and variable upstream bend curvature ratios.

UPSTREAM			DOWNSTREAM		
$r_c/w_{us}$	convex	concave	$r_c/w_{ds}$	convex	concave
3.0	60-120	-	4.0	60-180	0-60
2.7	70;120	-	4.0	30-180	-
1.7	90	-	3.6	30-120	-
1.7	-	-	3.0	30-150	-
1.4	-	-	4.0	60-105	-
2.2	90	-	3.9	60-150	-
2.0	-	30;150	2.6	45	-
1.5	-	-	3.3	30-60	-
3.0	60-120 170	-	2.5	30-90	-
3.2	60;120	-	2.4	90-180	-
1.6	120-180	-	1.9	-	-
1.0 <sup>*</sup>	40-160	-			
0.5 <sup>**</sup>	180	-			

\* Variations dependent on Reynolds number (Humphrey et al, 1981).

\*\* Shukry, 1949.

Such long flow transitions with bed-divergent spirals may scour the channel bed. This finding accords with that of Leopold et al (1964) that the mean velocity tends to increase at the lower ends of the riffle and the pool, but decreases at the pool.

The locations of concave and convex flow separation zones are shown in Table 5.6; it includes data from single bends of the same curvature ratio but varying Reynolds number in closed conduits (Humphrey et al; 1981) and data from model open-channel bends (Shukry, 1949). Bagnold (1960) argued for a relation between curvature ratio and the incidence of flow separation zones. He maintained that break-away (where the flow within the separated zone becomes confused and chaotic) developed in a bend with  $r_c/w=2.0$ . Evidence from the present study shows that the core of maximum velocity locates at the centre of the channel in  $r_c/w=2.0$ ; and it moves towards the inner bank in tighter bends causing flow deceleration near the concave bank rather than along the convex bank. The confused separated flow is probably swept downstream with the main flow and perhaps is responsible for the C-shaped vortices described in section 5.1. The monotonous increase of mean longitudinal velocity in bends of  $r_c/w=2.0$  indicates that they are rather more efficient conduits than either wider or tighter bends. In these bends, the core of maximum velocity takes a sinuous path but avoids impinging on the channel banks. The implications of such a trend on friction to flow and lateral migration in rivers will be discussed latter in this chapter.



## 5.3 THE DISTRIBUTION OF SHEAR STRESS AND FRICTION COEFFICIENTS IN CONSECUTIVE BENDS WITH CONSTANT DOWNSTREAM BEND GEOMETRY

### 5.3.1 Introduction

In section 4.3 it was stated that the distribution of shear stress and friction to flow is concentrated downstream of the bend apex in tight bends, but is uniform and periodic every 60 degrees in wider bends. This pattern of shear distribution results from a relatively higher shear filament that initially locates along the convex (inner) bank at the bend entrance. The high shear filament shifts towards the concave bank as the flow passes through the bend zone. The distribution shows also the general development of the boundary layer in conformity with other results from open-channel bends (Ippen and Drinker, 1962; Yen, 1965; Bridge and Jarvis, 1982) and in closed conduits (Ito, 1954; Choi et al; 1979).

The discussion which follows highlights the previous results and examines the influence of the upstream bends on the distribution of shear stress and friction to flow on the subsequent ones of constant curvature ratio.

### 5.3.2 The Distribution of Shear Stress and Friction Coefficients in Consecutive Bends with $r_c/wds=4.0$ and varying $r_c/wds$

Figure 5.28 shows the downstream variation of mean shear stress and Table 5.8 lists bend segments where shear stress reaches minimum and maximum values. The maximum and minimum shear points may be associated with areas of strong and weak decaying vortices respectively (Lugh and Hausling, 1974). The shear stress and friction coefficient decrease at the bend apex in  $r_c/wus=2.2$  (cf. Bagnold, 1960; Davies and Sutherland, 1980), but are much higher in  $r_c/wus=3.0$ . The filament of maximum shear stress shifts towards the convex bank along the straight entrance and towards the concave bank at the bend. As the bends become tighter ( $r_c/wus < 2.2$ ), the shear stress distribution becomes less peaked and the zone with maximum values shifts towards the downstream part of the bend apex. The high shear stress at the bend apex becomes a valley in  $r_c/wus=2.2$  (cf. Choi et al; 1979) due to long transitional flow in which the high velocity core lies near the channel bed. A bend with  $r_c/wus=4.0$  has relatively lower shear stress and is periodic every 60 degrees.

Figure 5.29 shows the distribution of shear stress at 0.0672m from the water's edge. The shear stress distribution along the concave bank for each  $r_c/w$  is shown by symbols joined by lines while that along the convex bank is shown by the same

Figure 5.28. The distribution of mean shear stress in consecutive bends with  $r_c/w_{ds} = 4.0$  and variable upstream bend geometry.

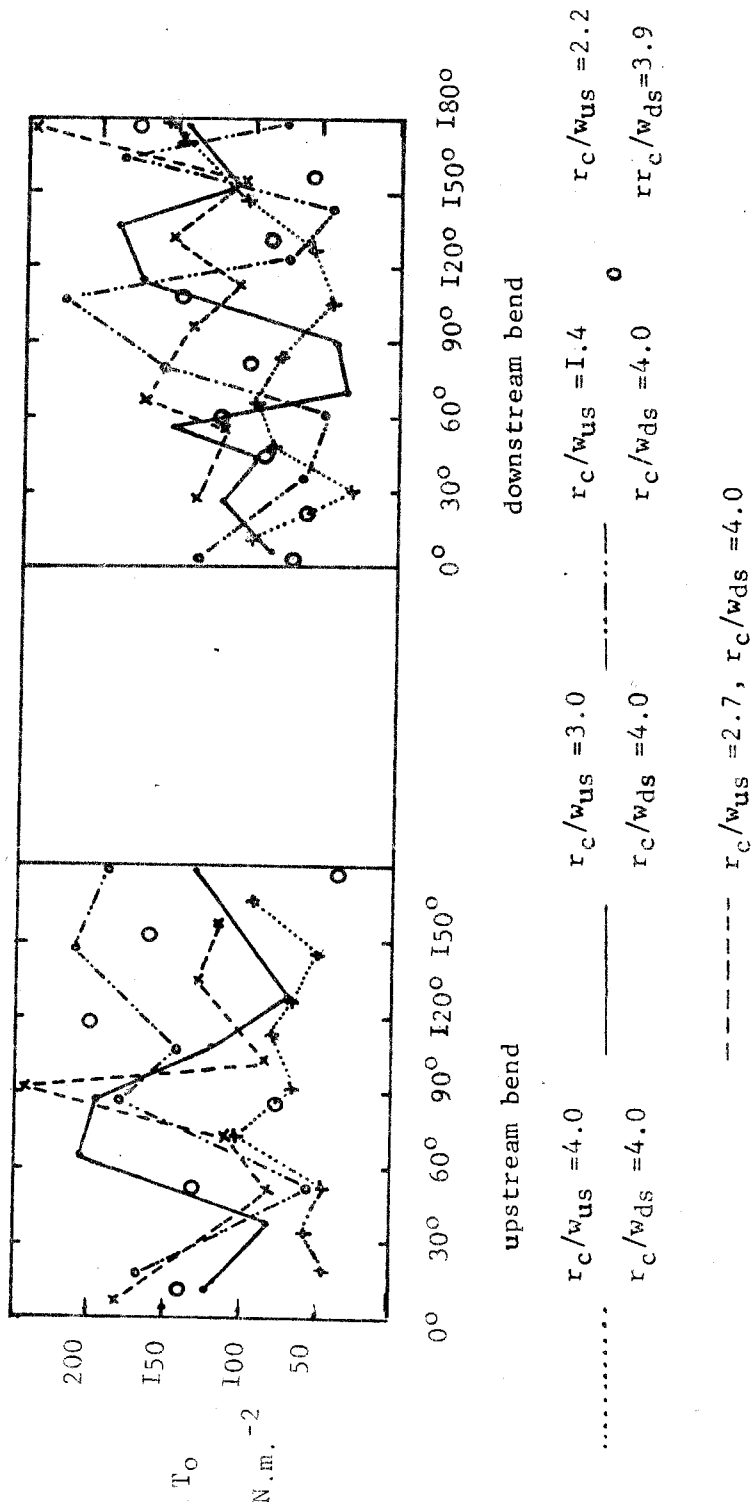
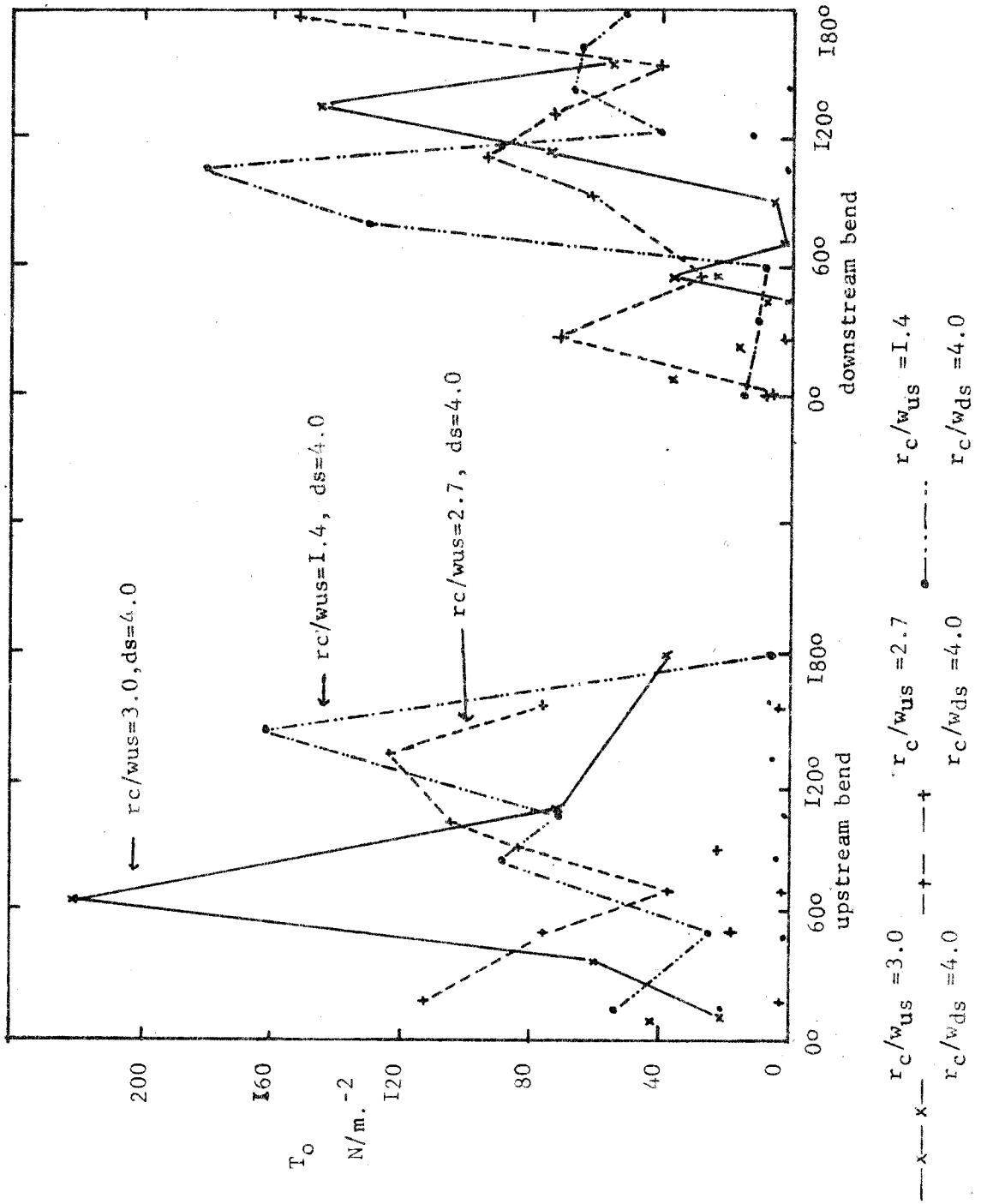


Figure 5.29. The distribution of shear stress near the channel banks of consecutive bends with  $r_c/w_{ds} = 4.0$  and variable upstream bend geometry. The shear stress for each paired bends is shown by the same symbols but the symbols for the outer bank are connected by lines while those near the inner bank are not connected by any lines.



symbols as on the concave bank but are not joined by lines. Figure 5.30 shows the isolines of the relative shear stress; the latter is expressed as the ratio of point shear stress and the mean at each section. This measure provides only a local value of shear stress pattern because it is not related to any standard station (in contrast to Ippen and Drinker's (1962) method). In spite of this shortcoming, the results are found to be internally consistent and the pattern is clear.

The shear stress near the banks along the upstream bends tends to be rather variable; maximum values locate between 60 and 90 degrees. As the bend is tightened ( $1.4 < r_c/wus < 2.7$ ), the shear stress along the concave (outer) bank decreases rapidly to a minimum value between 50 and 70 degrees of the bend then increases to a maximum value along the bend zone between 115 and 130 degrees. Since sediment transport increases with shear stress, the points of maximum shear along the concave bank will erode when the shear exceeds the resistance of the bank.

Along the downstream bends, the distribution of mean shear stress and friction coefficient is periodic every 60 degrees. The maximum mean boundary shear locates along the bend zone between 30 and 60 degrees and downstream of 120 degrees in bends subsequent to  $r_c/wus=3.0$  and  $4.0$ ; between 60 and 120 degrees in bends subsequent to  $r_c/wus=1.4$ , but is uniformly periodic in bends subsequent to  $r_c/wus=2.7$ . The filament of maximum shear shifts towards the convex bank at the bend entrance and towards the outer bank at 134 degrees in  $r_c/wds=4.0$ . But along the

Figure 5.30 Contours of relative shear stress in consecutive bends of  $r_c/w_{ds}=3.0$  and  $r_c/w_{ds}=4.0$ . The contour interval is 0.5.

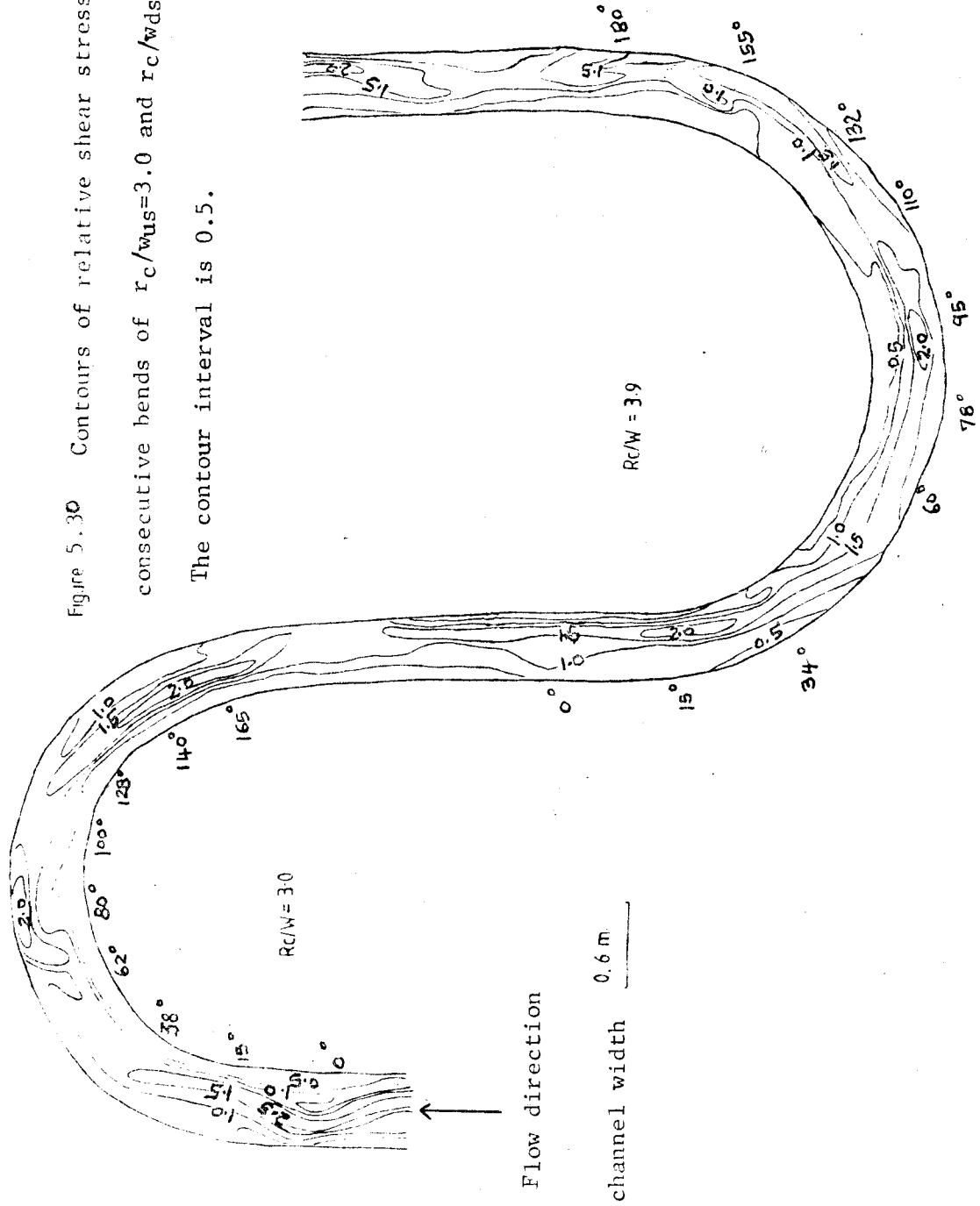
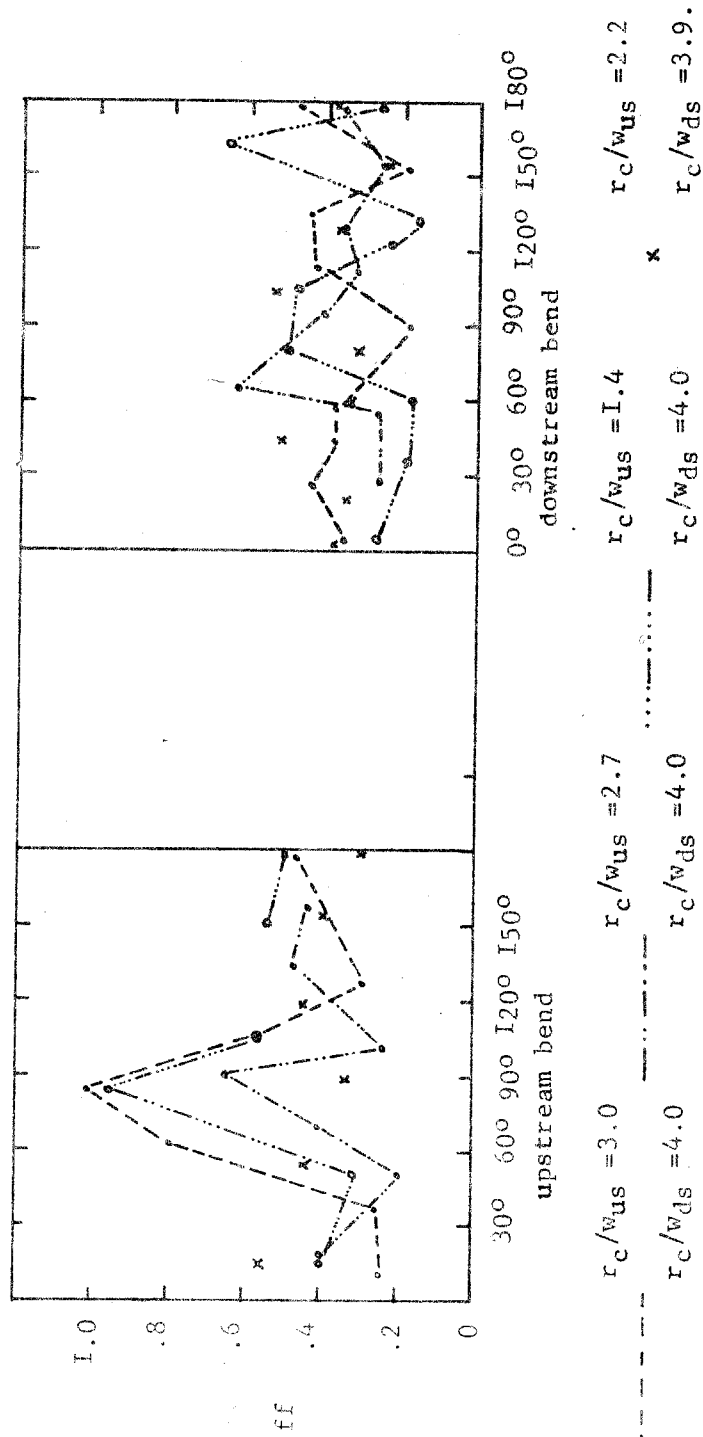


Figure 5.31. The distribution of friction coefficient in consecutive bends with  $r_c/w_{ds} = 4.0$  and variable upstream bend geometry.



downstream bends (Figure 5.30), the maximum shear filament hugs the convex bank up to 34 degrees then the point bar deflects it towards the channel centreline. The high shear filament remains near the concave bank from a bend angle of 60 degrees to the exit portion. In bend series with  $r_c/wus=1.4$  and  $r_c/wds=4.0$ , the filament of maximum shear remains along the centre of the channel until 145 degrees (cf. Ippen and Drinker, 1962). The distribution of friction to flow gives a maximum value at 90 degrees and thereafter it is periodic every 60 degrees (Figure 5.31).

Yen (1975) showed that the steep concave bank erodes when the effects of the spiral flow and weight acting to impel the grains are superposed on the bed shear stress. The present study shows that secondary flow is maximum between 30 and 60 degrees and also between 120 degrees and the bend exit. It is likely that erosion may occur at 60 degrees of the bend with  $r_c/wus=3.0$  and between 120 and 180 degrees in those with  $1.4 < r_c/wus < 2.7$  (cf. Kondrat'yev, 1968; Daniel, 1971).

### 5.3.3 The Distribution of Shear Stress and Friction Coefficients in Consecutive Bends with $r_c/wds=3.3$ and variable $r_c/wus$

There is a general decrease of mean shear stress from the bend entrance until 60 degrees in upstream bends. Figure 5.32 shows that mean shear increases towards the bend apex to a maximum value between 90 and 120 degrees, except in a bend with



TABLE 5.7

The location of maximum and minimum shear stress in consecutive bends with  $r_c/w_{ds} = 4.0$  and variable upstream bend geometry.

$r_c/w_{us}$	$\bar{T}_o$		$r_c/w_{ds}$	$\bar{T}_o$	
	Maximum	Minimum		Maximum	Minimum
3.0	60 - 90	40; I30	4.0	I20	60- 90
2.7	90	50; I00	4.0	60; I30	II5; I55
I.4	90; I50	50; I05	4.0	I05	60; I35
2.2	I5; I20	90	3.9	45; I05	75; I50

$r_c/wus=2.0$ . Tightening the upstream bend from  $r_c/wus=3.2$  to  $2.0$  increases the lengthwise shear stress variation and shifts the high shear filament from the concave bank towards the centreline at the bend apex. The distribution of shear stress along the concave bank (Figure 5.33) becomes symmetrical at the bend apex in  $r_c/wus=3.2$  and  $1.5$ , but shifts upstream and downstream of the bend apex in  $r_c/wus=1.7$  (cf. Ito, 1954). These are the points most liable to experience bank erosion in rivers (cf. Appman, Although the bends of  $1.7 < r_c/wus < 2.0$  show a relative decrease in shear stress at 90 degrees, it increases rapidly downstream of the bend apex. The downstream variations increase and the high shear zone shifts downstream of the bend apex in  $2.0 > r_c/wus > 1.7$ .

The individual bends tend to vary because the location of the maximum and minimum shear zones change with  $r_c/w$ . Table 5.8 shows regions of maximum and minimum values of shear stress along the channel banks and can be used to discern the areas of greater energy dissipation along the channel. The maximum shear stress along the concave bank in upstream bends shifts from 90 degrees of the bend with  $r_c/wus > 2.6$  to lie between 105 and 165 degrees in that of  $r_c/wus < 2.0$ ; the location of minimum shear points behave in a converse manner. Along the downstream bends, the maximum shear along the concave bank tends to locate downstream of 60 degrees, the same region with minimum values along the convex bank. This skewed distribution of boundary shear is an important characteristic in open-channel bends.

Figure 5.32. The distribution of mean shear stress in consecutive bends with  $r_c/w_{ds} = 3.3$  and variable upstream bend geometry.

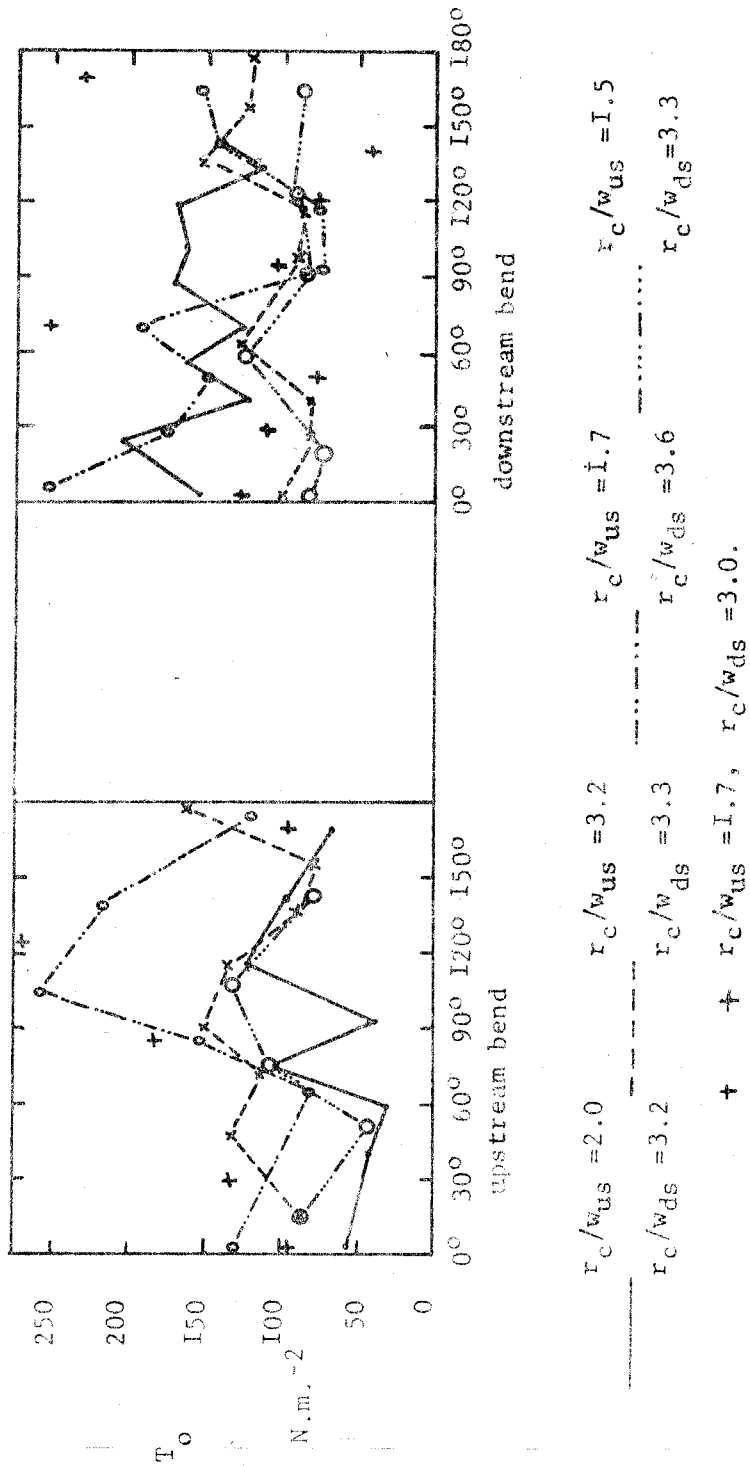




TABLE 5.8

The location of maximum and minimum shear stress near the channel banks of of consecutive bends with  $r_c/wds = 3.3$  (constant) and variable upstream bend geometry.

$r_c/wds$	$T_o$ Maximum		$T_o$ Minimum		$r_c/wds$	$T_o$ Maximum		$T_o$ Minimum	
	concave	convex	Concave	convex		concave	convex	concave	convex
3.2	45;90	15	15;135	15-180	3.0	60; 120	45	90	90
2.6	30;90	-	0;45;120	-	3.0	125	0	0;90	60;105
2.0	40;165	75;120	60	90	3.2	30;90-120	0;60;105	0;45	45;90
1.7	0;105	-	75;180	75	3.6	30;75	0-30	45;100	45-180
1.7	30;120	90-120	0;90	0;165	3.0	90;170	0	0-75;135	45-180
1.5	90-120	90	45	15	3.3	60	85	0;85	30-60;105-180

The average location of the point at which the high shear stress filament crosses from the inner (convex) bank to the outer (concave) bank (cross over) is also at 60 degrees of the bend angle, a flow characteristic typical in most natural rivers (cf. Bluck, 1971; Bridge and Jarvis, 1976). Further tightening of the bend,  $1.7 > r_c/w > 1.5$ , reduces the peakedness of the distribution and shifts the zone of maximum shear stress towards the bend apex. But in a bend with  $r_c/w = 1.5$ , the filament of maximum shear splits in to two: one near the concave bank and the other near the convex bank at 55 degrees (see also Ippen and Drinker, 1962, figure 8). If erosion may occur on both bends, the channel width likely will flare along this bend segment as postulated by Hickin (1975). There is only one peak at 60 degrees in a bend with  $r_c/w = 1.5$  compared to two peaks at 60 degrees (where the value of  $t$  has a maximum value) and 135 degrees (where the value of  $t$  begins to increase) in a bend preceded by  $r_c/w = 3.2$ . The two peaks sandwich a bend zone of low shear stress which likely is responsible for developing a complex bend geometry.

Along the downstream bends, the filament of maximum shear stress shifts from the centre line along the inflection reach towards the convex bank from the bend entrance to 27 degrees, after which it locates along the concave bank through out the rest of the bend. The maximum shear stress locates at 60 and 135 degrees as observed along the upstream bends also; but until 90 degrees in that proceeding  $r_c/w = 2.0$ . The periodic variations

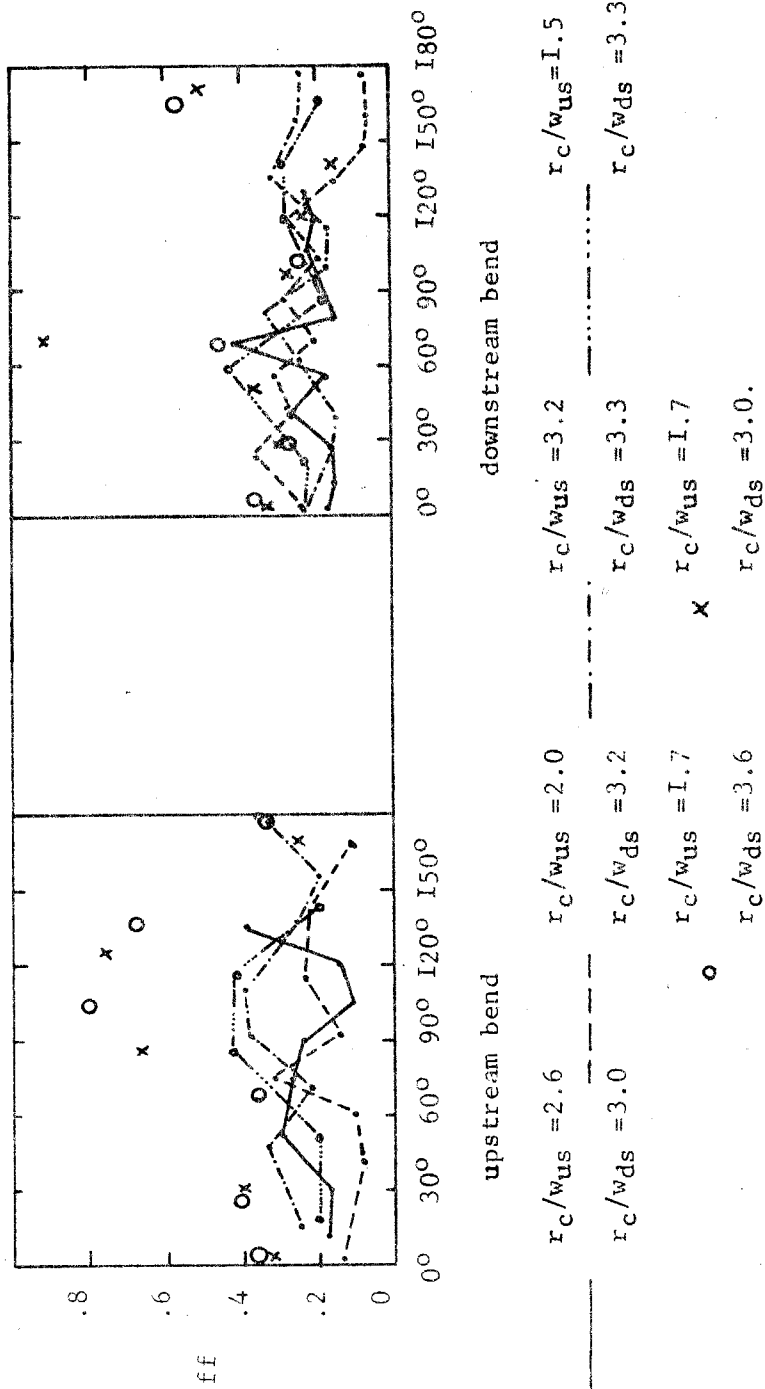
of shear stress distribution observed in the present study supplements Hooke's (1975) finding that the zone of maximum shear shifts downstream with increasing discharge in a model bend of constant width (i.e. decreasing curvature ratio).

Figure 5.34 shows the distribution of friction coefficient in bends with constant  $r_c/wds=3.3$ . Bends of  $2.0 < r_c/wus < 2.6$  show an appreciable decrease of friction between 90 and 120 degrees; bends of  $r_c/wus=3.2$  and  $3.3$  have less dramatic increases compared to those with  $r_c/w=1.5$  and  $1.7$ . These patterns are in accord with published results (cf. Bagnold, 1960).

#### 5.3.4 The Distribution of Shear Stress and Friction Coefficient in Consecutive Bends with $r_c/wds=2.5$ and variable $r_c/wus$

Figures 5.35 to 5.37 show the distribution of shear stress and friction coefficients in bends with  $r_c/wds=2.5$  (constant). The mean shear stress and friction coefficient decrease to a minimum value along the bend zone between 90 and 120 degrees; the maximum value locates between 30 and 90 degrees and along the exit. The shear stress is lower in a bend with  $r_c/wus=2.0$  and in bends proceeding it than in the other bends conforming to the previous results discussed earlier (cf. Bagnold, 1960). Along the concave bank, shear increases from the bend entrance to 60 degrees, the same point the intensity of secondary flow has a maximum value. But in downstream bends, the boundary shear

Figure 5.34. The distribution of friction coefficient of consecutive bends with  $r_c/w_{ds} = 3.3$  and variable upstream bend geometry.



Nb. The symbols showing friction coefficient in some bends are not connected by lines for the sake of clarity.



Figure 5.35. The distribution of shear stress in consecutive bends with  $r_c/w_{ds} = 2.5$  and variable downstream bend geometry.

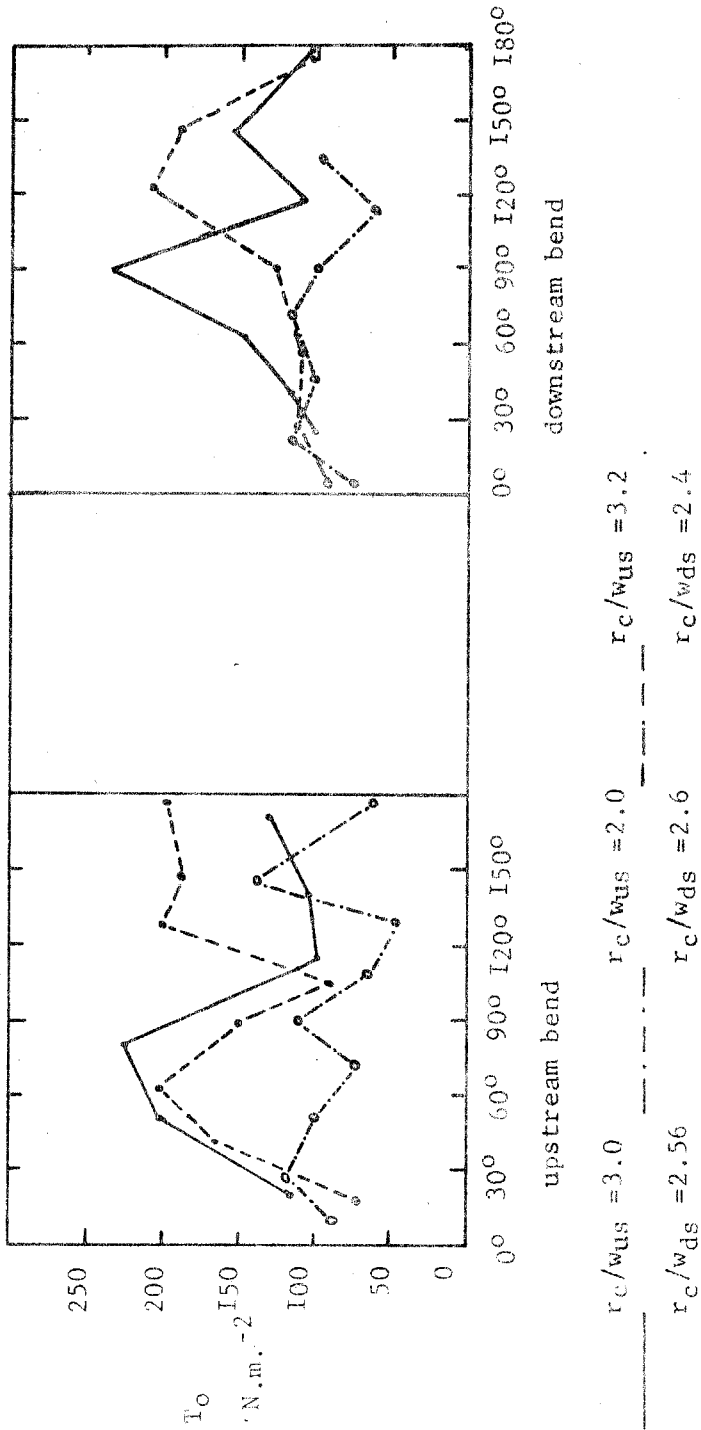


Figure 5.36. The distribution of shear stress near the channel banks of consecutive bends with  $r_c/w_{ds} = 2.5$  and variable upstream bend geometry. The shear stress for each paired bends is shown by the same symbols but the symbols for the outer bank are connected by lines while those of the inner bank are not connected by any lines.

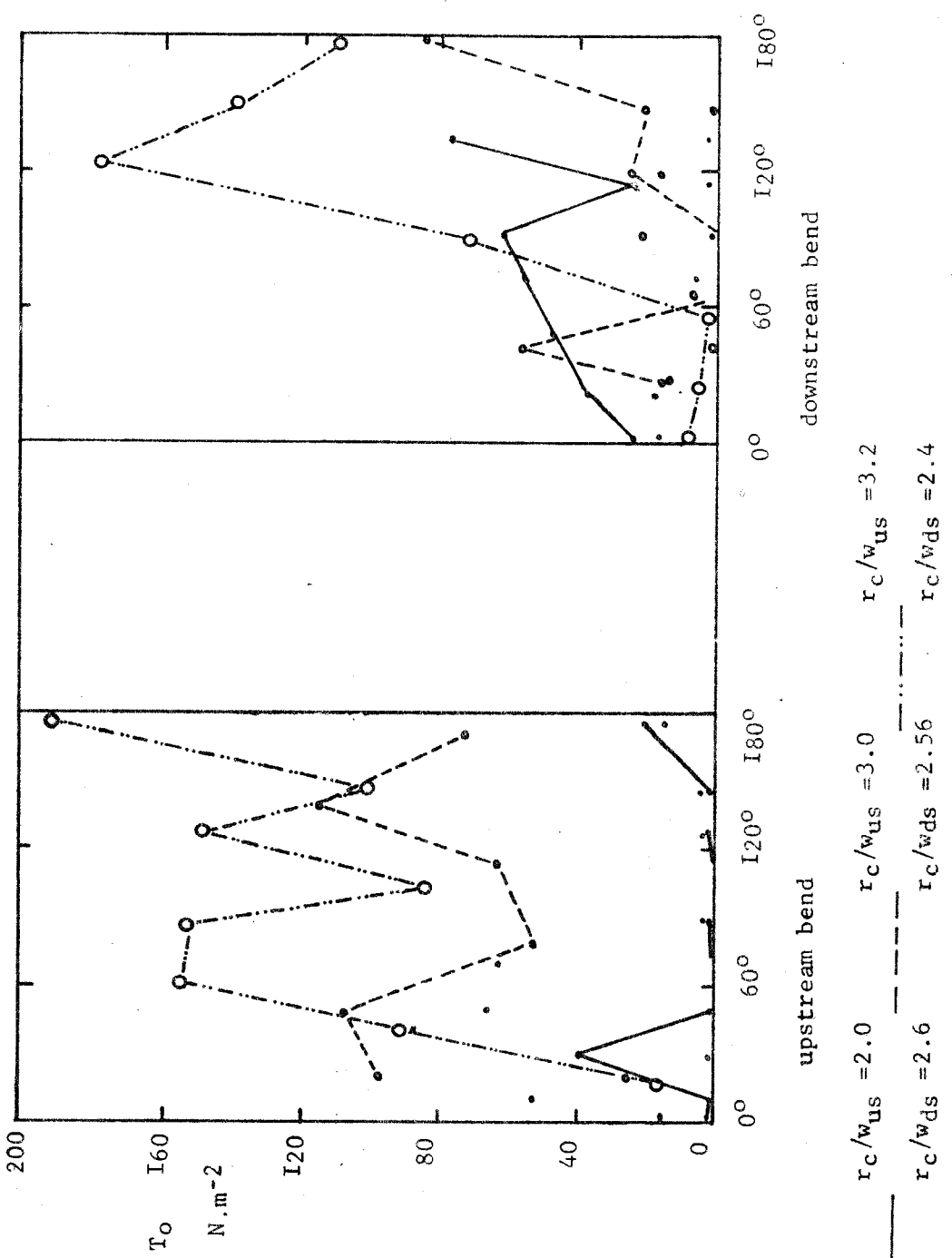
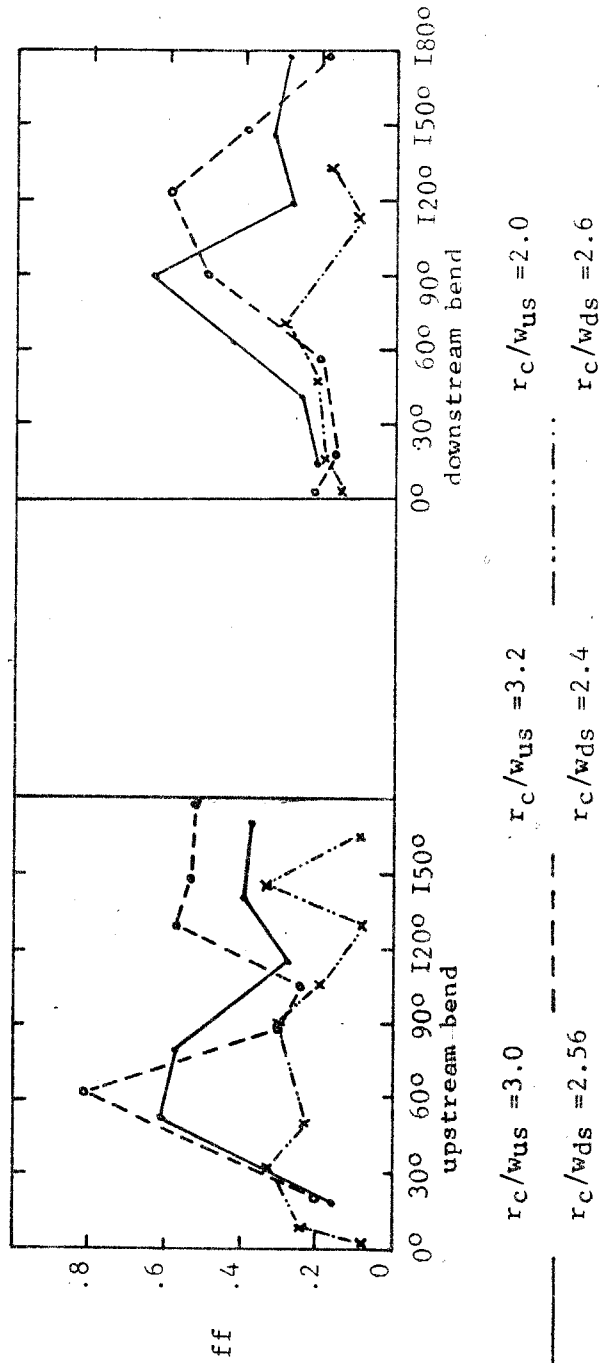


Figure 5.37. The distribution of friction coefficient of consecutive bends with  $r_c/w_{ds} = 2.5$  (constant) and variable upstream bend geometry.



near the concave bank is generally higher and concentrates downstream of the subsequent bend apices of  $r_c/wus=3.0$ .

### 5.3.5 The Distribution of Shear Stress and Friction Coefficient in Consecutive Bends with $r_c/wds=1.94$ and variable $r_c/wus$

The distribution of mean shear stress and friction coefficient (Figures 5.38 and 5.39) are skewed towards the upstream portion of the bend axis in bends with  $r_c/wus > 3.0$  and towards the downstream in those of  $r_c/wus < 1.64$ . The relative decrease of mean shear stress along the downstream bends was especially unexpected (Figure 5.38) because the preceding bends are tight. However the shear increase towards the bend exit portion was observed earlier in tight upstream bends ( $r_c/wus=1.7$ ).

Dietrich et al (1979) found that the skewed shear stress distribution at a cross section reflects the orientation of the bedforms. A uniform distribution of  $T_o/\bar{T}_o$  at any section therefore implies that the channel bed is mobilised and little depth variation may be detected. Figure 5.40 ( $r_c/wus=1.64$  and  $r_c/wds=1.94$ ) shows that the transverse variation of  $T_o/\bar{T}_o$  is reduced at the bend apices as it will be recalled that the high velocity core shifts more or less towards the water surface as  $r_c/w$  decreases.

Figure 5.38. The distribution of mean shear stress in consecutive bends with  $r_c/w_{ds} = 1.94$  and variable downstream bend geometry.

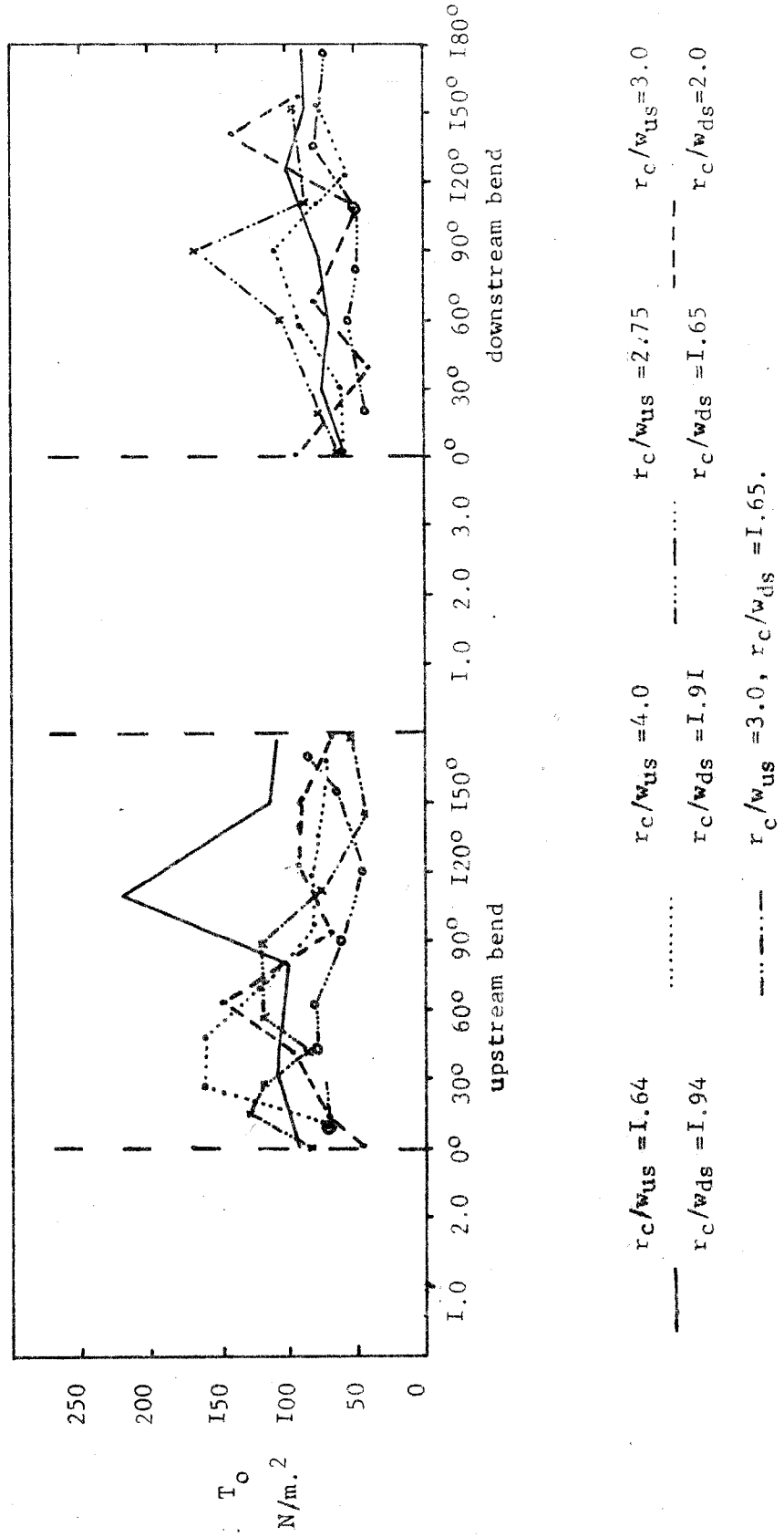
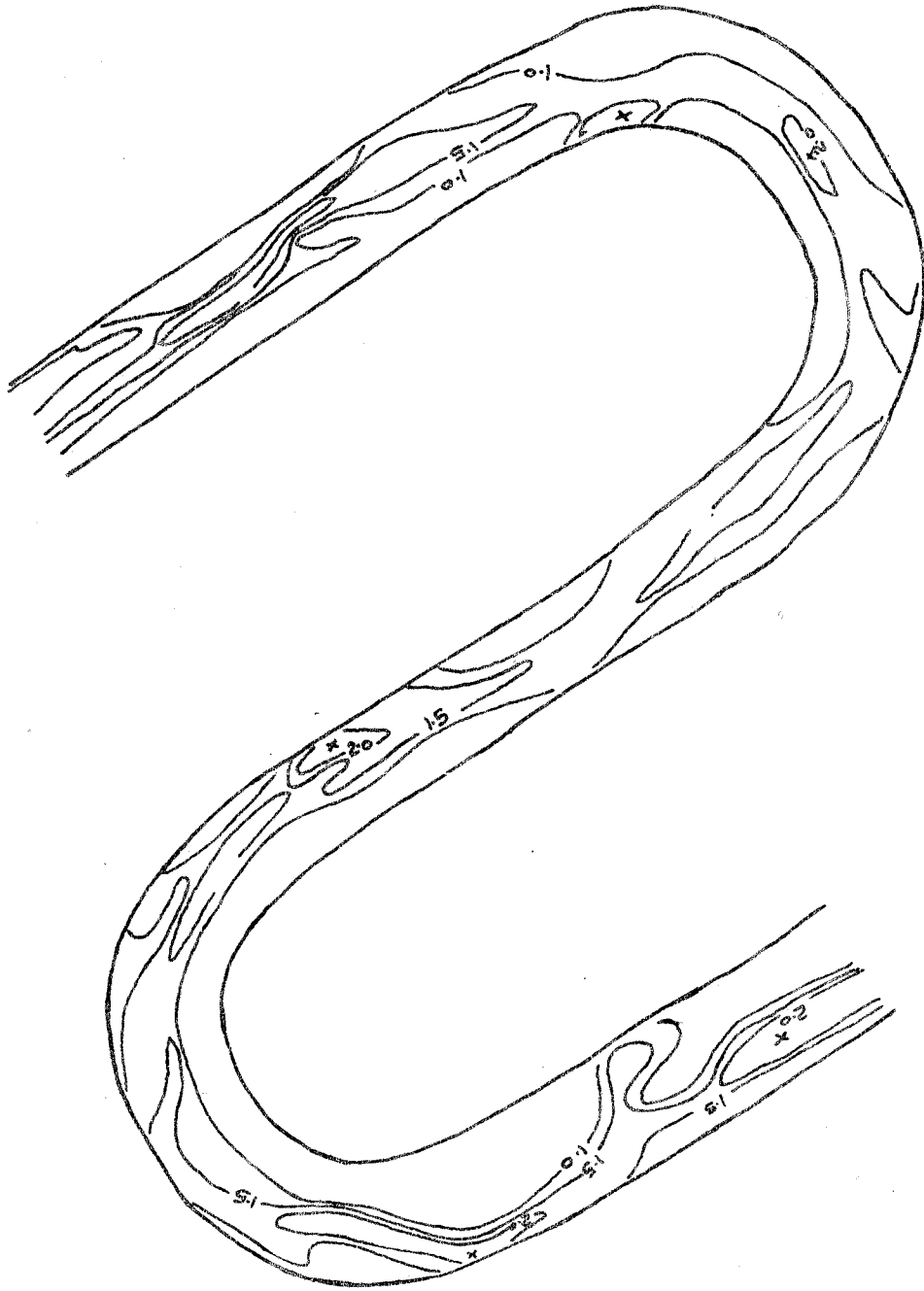




Figure 5.40. Contour map of dimensionless shear stress distribution in consecutive

bends of  $rc/wus=1.64$  and  $rc/wds=1.94$ .



#### 4.4.5 Summary

The results of shear stress distribution and friction to flow follow the general trend reported in other open-channel bends (cf. Ippen and Drinker, 1962; Hooke, 1975; Dietrich et al; 1979; Bridge and Jarvis, 1982). The zone of maximum boundary shear stress locates near the convex bank upstream of the bend axis then crosses to the concave bank downstream of the bend apex. The crossing is delayed more in a bend with  $r_c/w < 2.2$  than in that of  $r_c/w > 2.2$ . In other words, the cross over at which the filament of maximum shear stress moves from the convex bank towards the concave bank shifts downstream of the bend apex as  $r_c/w$  decreases. This downstream migration of the cross over is responsible for skewing the lengthwise distribution of mean shear stress downstream of the bend apex.

The longitudinal variation of the location of the maximum and minimum shear stress with  $r_c/w$  results from the upstream transmission of the bend effects. Ito (1954), Pratap and Spalding (1975), Humphrey and Whitelaw (1975) and Yao (1978) have suggested that bends tend to transmit their influences upstream through increased pressure near the convex bank. As pressure increases along the convex bank, velocity, shear stress and friction to flow decrease. The pressure surplus along the inner bank therefore is greater for bends of  $r_c/w > 2.0$  than for tighter ones because the high velocity core shifts towards the



inner bank. The cross over also is more abrupt (cf. Ippen and Drinker, 1962; Jackson, 1975). The minimum shear stress has a tendency to locate along the bend zone between 30 and 90 degrees; the same position intense secondary flow advection increases the momentum deficit near the channel bottom (cf. Dietrich et al; 1979). To maintain flow continuity, the accelerating fluid near the surface moves towards the concave (outer) bank while the retarded flow near the channel bed moves towards the convex (inner) bank.

The locations of the minimum values of shear stress and cross over vary more along the downstream bends than those of the upstream bends because of the influence of the incoming flow structure. Generally, the variations of shear stress distribution decrease with  $r_c/w$ . The mean shear stress and friction coefficient in bends with  $r_c/w > 4.0$  and 2.2 is less than those of  $r_c/w = 3.0$  and 1.5 (see also Bagnold, 1960; Davies and Sutherland, 1980). The ratio of the local shear stress ( $T_o/\bar{T}_o$ ) decreases in bends with  $2.5 < r_c/w < 3.0$  in coassociation with the development of a plane bed as a result of the symmetrical flow structure at each cross section. The combined effect of the plane bed, high sediment transport and a topographically high point bar likely are responsible for high shear stress and friction to flow in bends with  $r_c/w = 3.0$ .

The meandering process has been suggested to be the most probable river behavior because it minimises variations of shear stress and friction to flow (Leopold et al; 1964). Langbein and

Leopold (1966) found that the ratio of the meander arc length (S) to total distance along a bend (M) has a maximum value at approximately 45 and 135 degrees for 180 degree bend.

Kondrat'yev (1968) analysed data of meanders in many Russian rivers and found that 50% of all the cases had a total bend angle of 138 degrees. Although the proof of minimisation of variation may best be approached by use of spectral analysis, the present data set are too few and short (Tukey, 1967) to allow this approach. Despite this shortcoming, the periodicity of the mean shear stress distribution every 60 degrees is close to the maximum angle the path of meanders make with the mean downvalley direction (cf. Langbein and Leopold, 1966). The difference between the theoretical value of 45 degrees and that of the present data (60 degrees) may be attributed partly to changes of  $r_c/w$  and measurement and design errors. But the skewed longitudinal distribution of shear stress and friction to flow shows that some bend geometry may depart from the simple geometric convenience to possess double-valued (i.e. T-bend geometry of Hickin, 1974) planforms. The locations of these double-values have been identified in this study as those points at which shear stress and friction coefficient have a maximum value (i.e. at 60 and 130 degrees).

The discussion which follows examines the relationship between flow properties and bank and bed deformation. The primary assumption is that regions of maximum shear stress and velocity have high sediment transport rate. Assuming further

that sediment supply is limited, such sections will erode more quickly than regions of low shear stress.

## CHAPTER 6 DISCUSSION OF RESULTS AND LATERAL MIGRATION IN RIVERS

### 6.1 Introduction

The distribution of velocity, shear stress and friction to flow has been studied in model open-channel bends with the aim of developing a basis for interpreting modes of lateral migration in rivers. The present findings on flow development and interaction complement previous studies in several ways. First, the study confirms that the transverse secondary flow begins upstream of the bend axis and becomes appreciable at 30 degrees and reaches a maximum value at 60 degrees. Between 80 and 120 degrees, the transverse secondary flow decreases to its former magnitude at the straight entrance. Second, the hydraulic parameters are periodic every 30 to 60 degrees in most bends, conforming to results of Muramoto (1967) and Einstein (1972). Thirdly, shear stress and friction to flow have maximum values in bends with  $r_c/w > 3.0$  and  $r_c/w = 1.5$  but decrease for bends in which  $r_c/w$  approximates 2.0 (Bagnold, 1960; Davies and Sutherland, 1980). Fourth, the core of maximum velocity locates near the concave bank at the bend apex in  $r_c/w > 3.0$ , shifts towards the centre in  $2.0 < r_c/w < 3.0$ ; and towards the convex bank in  $r_c/w < 2.0$  (cf. Hickin, 1978). The transverse shift of the core of maximum velocity towards either bank represents a localised

force that may cause bank erosion.

There is ample evidence from this study and from other reports (cf. Ippen and Drinker, 1962; Suga, 1967; Hooke, 1975; Dietrich et al; 1979; Leeder, 1980) that associates the rate of sediment transport with velocity and shear stress distribution which in turn is a function of curvature ratio (Onishi et al; 1976). Although lateral erosion was not measured directly in the present study, Leighly (1938) showed that the shift of the core of maximum velocity and increase of discharge account for meander evolution. The evidence from the present study showing shifts of velocity pattern, the location of separation zones and the distribution of shear stress provide a basis for predicting zones of bend erosion and changes in channel configuration.

Three distinct areas demand further discussion and review in order to better understand the different modes of lateral erosion. First is the matter of spatial development of flow in various bends and their interactive consequences on the downstream bends. Second is the interaction of secondary flow advection and its effect on the mainstream velocity including vortex development, spiral bifurcation and flow separation. Third is that corpus of work which seeks to show the spatial relationship of vertical and horizontal modifications of the stream geometry and bend flow development.

## 6.2 Bend Flow Development

Assuming uniform entry conditions and steady flow, there is an initial increase of velocity near the convex bank due to the effects of the bend (cf. Smith and Greated, 1980). Further into the bend, centrifugally driven secondary flow shifts the core of maximum velocity towards the concave bank and the flow becomes fully developed. Jackson (1975) defines the fully developed flow zone as the bend segment where 'relatively normal asymmetry in the transversal distribution of velocity' is obtained. But the present study shows that neither uniform entry conditions, steady flow nor fully developed flow may exist for any appreciable bend length (cf. Gotz, 1980). In fact flow is developed at 60 and also downstream of 120 degrees; its specific location varies slightly with curvature ratio.

The flow in open-channel bends is unsteady and nonuniform; it is periodic every 30 to 60 degrees. Macroeddies are initiated near the channel bottom (Einstein and Shen, 1964) due to the roughness of the channel banks and bed and are directed towards the corners along the straight entrance. The double spirals with bed-convergent currents along the straight entrance, usually less than 10 degrees, cause cross stream variation of shear stress and friction to flow; these currents create three-dimensional megaripples shown in Plate 3.1.

The streamwise (longitudinal) vortices are overwhelmed by cross stream secondary flow at the bend approximately upstream of 30 degrees. The secondary flow directed towards the concave bank becomes amplified and a forced vortex forms. The secondary flow towards the convex bank is amplified in bends of  $r_c/w=3.0$  only. The characteristics of  $r_c/w=3.0$ , perhaps the most studied curvature ratio (Yen, 1975; Onishi et al; 1976; Varshey and Garde, 1975) appears to be nonrepresentative of other curvature ratios, a feature which has been known but ignored for some time (Shukry, 1949). The cross stream secondary flow is wall-bound at 60 degrees near the surface; but it is redirected towards the centreline near the bottom and to the surface near the convex bank. As defined earlier in this study, the velocity reflectivity (Levliansky, 1955; Desaulnier and Frenette, 1973) may be redefined now as a phenomenon involving alternate centrifugal acceleration near the surface and deceleration near the bottom. Prus-Chacinki (1956), Muramoto (1967), Suga (1967), Einstein (1972) and Varshey and Garde (1975) concur that velocity and shear stress both have a maximum value at 60 degrees; the same region which is prone to erosion (Parsons, 1960).

The location of fully developed flow is expressed as a ratio of the bend angle  $[\theta_p]$  to the total curvature  $[\theta]$  and is shown in Figure 6.1 and Table 6.1.

TABLE 6.1.

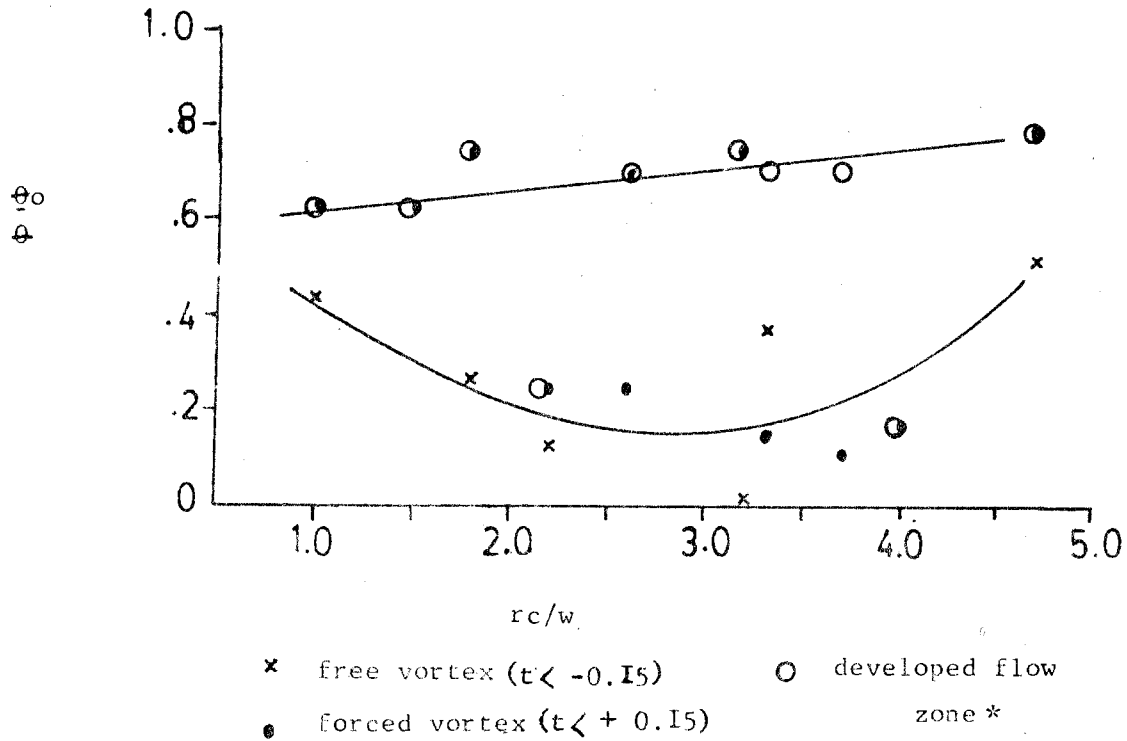
\* The location of free and forced vortices and the fully developed flow zones (data from single bends only).

$r_c/w$	Free vortex	Forced vortex	Developed flow
4.7	0.52	0.78	0.78
4.0	-	0.17	0.17
3.7	-	0.11	0.61
3.3	0.36	0.15	0.61
3.2	0.03	0.71	0.71
2.6	-	0.25	0.66
2.2	0.12	0.25	0.25
1.8	0.26	0.65	0.65
1.5	SEI	0.52	0.52
1.0	0.43	0.53	0.53

\* nb. The location of the vortices are given as the ratio of the point at which the vortex exists and the total bend angle.



Figure 6.I . The relationship between the initiation of free and forced vortices and developed flow zones (data from single bends only).



nb. \* The location of the fully developed flow zone is based on the transverse increase of velocity from the inner bank toward the outer bank (cf. Jackson, 1975). The current direction near the bed are directed towards the inner bank while the surface currents are directed towards the outer bank.

Bends of  $r_c/w=4.0$  and  $2.0$  have developed flow upstream of  $45$  degrees and downstream of the bend apex while the others examined in the study have developed flow characteristics downstream of the bend apex (Figure 6.1). The reason why the fully developed flow zone does not locate at the bend axis is due to a secondary spiral that develops along the bend zone between  $60$  and  $80$  degrees; it initiates parabolic flow in  $r_c/w < 2.0$  (cf. Choi et al; 1980). These results are in accord with observations that the fully developed flow usually locates towards the bend exit (Leopold et al; 1964).

The double spirals with bed-divergent currents (Hey and Thorne, 1975) take a different form in tighter bends. The spirals become superposed on each other and C-shaped secondary flow is directed towards the same bank near the surface and at the bottom. The retarded flow is sandwiched within the profile at mid depth. The shapes of such superposed spirals vary from reverse C-shaped, U-shaped and inverted U-shaped geometries. It may be recognised that these are different twists of the W-shaped pattern typical of turbulent flow in straight channels but distorted by bend effects. Einstein and Shen (1964) referred to such spirals as horse-shoe vortices in an attempt to describe flow geometry of straight channels with meandering tendencies.

The core of maximum velocity depresses towards the bottom upstream of the bend apex and increases sediment transport; but it moves towards the surface downstream of the bend apex and sediment transport is reduced. Yang (1972) shows that there is a

threshold at which the product of shear stress and velocity erodes the channel bank selectively to create meander bends. The maximum cross stream secondary flow occurs between 30 and 60 degrees, in agreement with theoretical formulations. The alternate scour holes created as a result have meanderlike characteristics but their spacings vary with the wavelength of the core of maximum velocity to form pseudomeanders (Shen and Komura, 1968; Wolman and Brush, 1961; Hickin, 1969) The experiments on meander development have not incorporated this fact(see also Schumm and Khan, 1972).

The transitional zone where the core of maximum velocity shifts from the channel bottom towards the surface is marked by a decrease of vortex strength and current direction. The core of maximum velocity and the filament of maximum shear shift towards the outer bank and are associated with wall-bound transverse secondary flow towards the concave bank at 120 degrees. The trends vary slightly with the skewness and peakedness of the lengthwise distribution of shear stress friction to flow at the bend apex. The effects of such variations along the downstream bends are discussed below.

### 6.3 Bend Flow Interaction

Measurements taken along the downstream bends offer an opportunity to compare flow development and interaction with real rivers because there is neither uniform entry nor steady

flow along the downstream bends. The magnitude of the inherited flow is approximated by the extent and strength of the free vortex flow along the downstream bend. This method was chosen because it was simple and expedient. The transitional region between free and forced vortices marks the cross over where the thalweg shifts from the inner bank towards the outer bank (Bridge and Jarvis, 1976). Callander (1978) describes the influence of the upstream bend by superposed spirals in which decelerated flow near the bed directed towards the convex bank is caught and returned across the channel by the spiral inherited from upstream.

As flow approaches the downstream bends, it decelerates near the concave bank and accelerates along the convex bank. The acceleration along the convex bank is inherited from the concave zone along the upstream bends. Evidence from a large body of literature on flow development (Yao and Berger, 1975) concur that the location of the free vortex at the bend entrance is a result of the influence of the bend. Pratap and Spalding (1975) attribute the free vortex at the bend entrance with uniform entry conditions to be due to pressure travelling upstream. Although Hickin (1978) argues strongly that the development of a free vortex at the bend entrance is a matter of continuity and mainflow inertia (cf. Dietrich et al; 1979) in agreement with other flume studies (cf. Yen, 1967), it appears that the variety of free vortex flow observed in this study cannot be explained fully in this way. What is known is that the high velocity

filament along the convex bank in subsequent bends cause erosion there in many rivers (see for example Kondrat'yev, 1968; Daniel, 1971; Hickin, 1974; Jackson, 1975; Lewin et al, 1977; Ratlaft, 1981).

The location of the free vortex along the single bends are shown in Figure 6.2. The first occurrence of the free vortex flow with an exponent of  $t > -0.15$  was identified and the bend zone occupied by that flow was plotted. In other words, the figure represents the extent of the influence of free vortex flow. The choice of the criterion  $t > -0.15$  may bias the results because some bends have weaker vortex flow than the others, but the method was expedient. The plotting pattern for single bends (best-fit line marked (a)) is straight forward. But in bend series, the plotting positions along the horizontal axis ( $r_c/w$ ) was determined in the following manner. The curvature ratio of the downstream bends is plotted for bend series in which the upstream bend geometry are constant to characterise the influence of the upstream bend on the flow structure of the following bend. For series of experiments in which the downstream bend geometry is constant, the upstream bend curvature ratio is plotted to assess the influence on flow structure along the downstream bend. In both cases, the zone occupied by the free vortex flow is for downstream bends only.

The free vortex flow extends from the bend entrance until a bend angle of 60 degrees in single bends. The entry flow conditions are assumed to be sensibly uniform. It can be noted

that best-fit line for single bends (marked a) shows that the location of the free vortex migrates downstream as curvature ratio increases from  $r_c/w=1.5$  to 5.0. The free vortex flow is associated with secondary flow that is directed radially outwards near the channel bed and inwards near the water surface. The best-fit line marked (b) is for the bend series with a constant downstream bend geometry but the plotted points along the horizontal axis are for the upstream bends. The free vortex locates upstream of 60 degrees but the extent decreases as the bend becomes tighter. The best-fit line marked (b) is steeper than that of (a) because of the strong free vortex flow inherited from the upstream. The curve marked (c) is for bend series with constant upstream curvature ratio. The points plotted along the horizontal axis are for the downstream bends ( $r_c/wds$ ). The curve shows that the free vortex flow limits its influence as the downstream bend becomes wider but remains constant in a bend of  $r_c/w < 2.0$ .

The trends of best-fit lines (a) and (b) can be explained by the fact that the fluid hydraulic parameters are periodic every 30 to 60 degrees in the present model bends of constant width (0.6m) conforming to the results of Langbein and Leopold (1966). Noting that the arc length increases by  $r_c \cdot d a$  (where  $a$  is expressed in radians), it follows that the location of free vortex flow must shift upstream as  $r_c/w$  decreases. The bend zone occupied by the free vortex determines the extent of the bend



that may be liable to erosion.

#### 6.4 Bend Flow Development and Interaction and Lateral Migration in Rivers

Bend flow development and interaction is complex. The flow is composed of organised periodic vortices due to strong secondary flow advection, and shear stress and friction coefficients vary with  $r_c/w$ . The distribution of these parameters is asymmetrical at each cross section and skewed longitudinally. There is a tendency towards self-preservation—the mainstream velocity is in a moving equilibrium that changes only slowly as roughness decreases. This section explores the relationship between bend flow development and interaction and its possible effects on the mode of lateral migration in rivers. The single and upstream bends represent "undisturbed" flow entry conditions while the downstream bends represent entry conditions that are more realistic counterparts to natural channels.

Meander bends have a tendency to migrate downvalley by reworking their former deposits (Leopold et al; 1964) although some workers suggest that downvalley migration is not ubiquitous (Desaulniers and Frennette, 1974; Hickin, 1974; Hooke, 1975). Hickin in this paper identified the direction of maximum erosion by extrapolating erosional pathlines of the scroll bar sequence. The erosional pathline of each bend was defined as the pathline along which the rate of lateral migration achieves a maximum

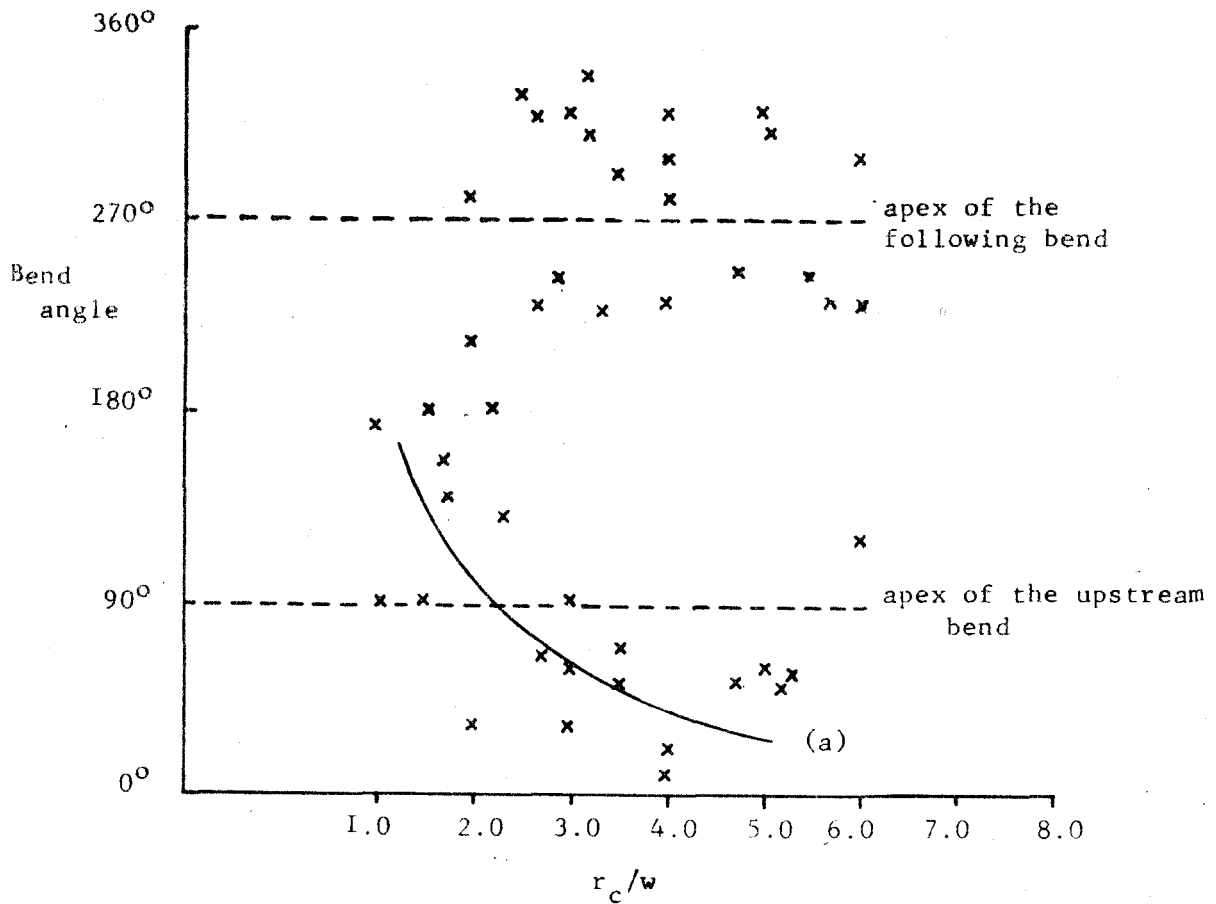


value. The maximum erosional axis shifted downstream as the amplitude of the meander increased (i.e. bend curvature ratio decreased). The migration rate reached a maximum value in bends with  $2.2 < r_c/w < 3.5$  (Nanson and Hickin, 1983); the same bends shown in Figures 2.25 and 2.26 that do not have flow separation zones. Nanson (1977) showed that the meander bends of the Beatton River have preferred orientation of the erosional axis. Expressing the preferred orientation using wind rose diagrams, Nanson was able to deduce a hypothetical model of channel migration and cutoff. Nanson's data are reproduced in Figure 6.3; the downvalley trend can be differentiated despite an overlap of data between  $1.5 < r_c/w < 2.5$ .

The points of maximum erosion and point bar deposition may be proposed on the basis of the location of the core of maximum velocity, location of pools, velocity and shear near the banks and maximum friction coefficient. There is close association between the locations of pools and maximum dimensionless shear stress (Appendix 3) which facilitates a comparison between maximum erosional axis although some bends have two or more pools. Multiple pool-bends have been described in flumes (Shukry, 1949) and in rivers (Milne, 1971). The pools and maximum shear stress were identified and their locations in various  $r_c/w$  were plotted in Figure 6.4. The two best-fit lines marked (a) and (b) respectively represent the pools that locate upstream of the bend apex and those that locate downstream of the bend axis.

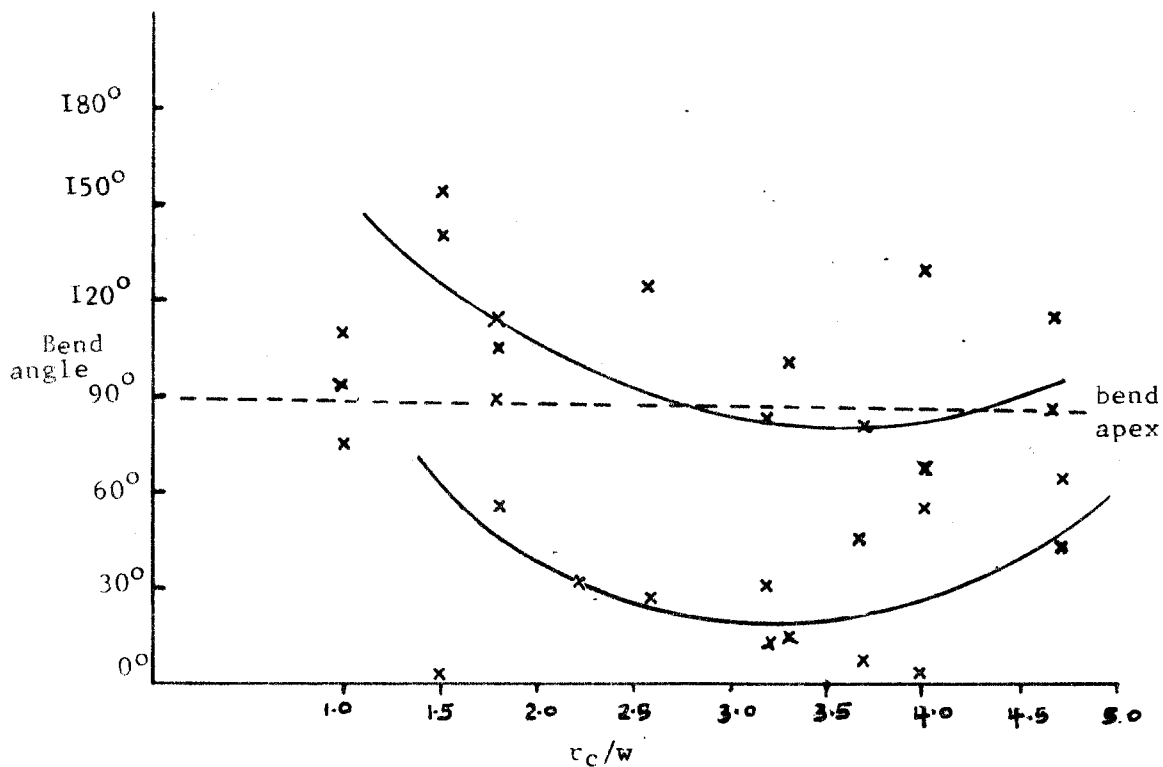
Figure 6.3. The location of maximum erosional axis in river bends of the Beatton.

(source: Nanson, 1977; Appendix I, p 336(b))



The curve marked (a) shows the downstream trend of maximum erosional axis for the upstream bends. The trend for the downstream bends are rather more scattered.

Figure 6.4. The location (in degrees) of the points where velocity, shear stress and strength of the vortex flow have maximum value.



The line marked (a) represents maximum values upstream of the bend apex while the line marked (b) represents points where the maximum values lie within the margin of  $\pm 15$  degrees downstream of the bend apex. Data includes single bends only.

Figure 6.4 shows that downvalley and upvalley oriented pools occur in a wide range of  $r_c/w$  in agreement with field examples of Hickin (1974) and Brice (1974). The convergence of data between  $1.5 < r_c/w < 2.5$  compares well with Nanson's (1977) data.

The application of the concept of velocity reflectivity in predicting points of maximum erosion has gained a large following (Lelviatsky, 1955; Parsons, 1960; Kondrat'yev, 1968; Appman, 1972). The concept involves transverse generation of waves towards alternate banks, each wave making an angle with the channel banks. A complete description of this method is given in detail in Lelviatsky (1955). Theoretically such waves can develop only in a flow with Froude number greater than 1.0 (Ippen and Knapp, 1936). Soliman and Tinney (1968), however, reported an oblique jump at a lower Froude number (0.6) and Shukry (1949) pointed out the influence of water surface elevation in bendflow development. The zones where the maximum water surface depression and elevation locate represent positive and negative wave fronts (cf. Chow, 1959).

Consider the flow consisting of stream tubes parallel to the channel banks along the straight entrance. As the flow enters the bend, the stream tubes change their direction, the force needed for this change must be a function of the rate of change in curvature. The average current direction near the water surface at the bend entrance is between 7 and 13 degrees while the bend forms an arc of 25 degrees per m. The surface stream tube near the inner bank will reach the outer bank

between 64 and 120 degrees of the bend angle. This is the bend zone at which the secondary flow decreases after impinging on the concave (outer) bank.

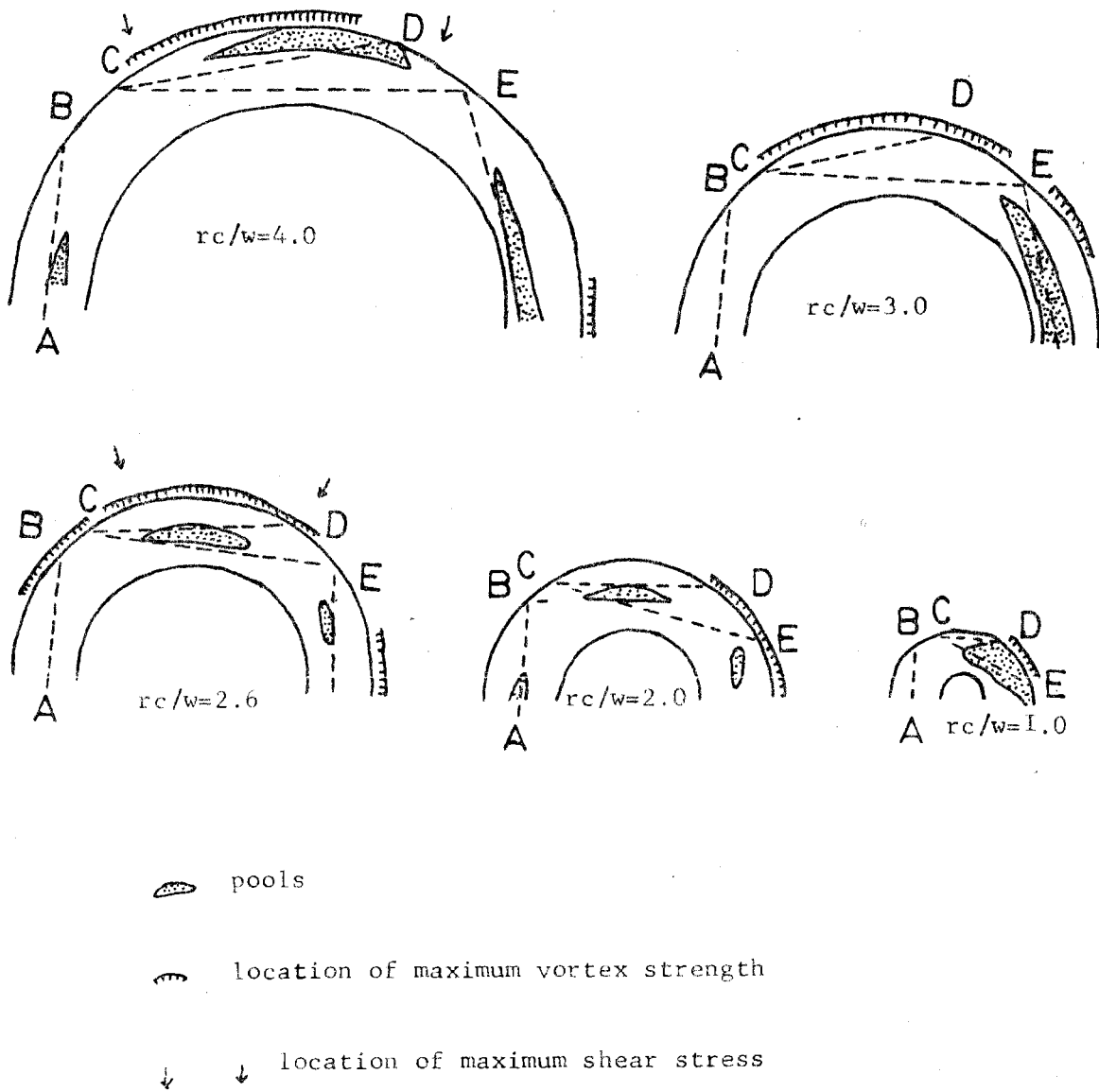
An attempt to apply the concept of velocity reflectivity in its redefined form to construct the points at which maximum erosion may occur is done in the following manner. The axis of the straight reach A is extended to the intersection with the concave bank at point B, from which a chord BC is extended one-half channel width (Kondrat'yev, 1968). Assuming that velocity is reflected from the concave bank at an angle ABC towards the concave bank further downstream to a point D, the reflection will interfere with the streamlines; this reduces the strength of the forced vortex and current direction as observed earlier. Further downstream, the chord from point D is extended one channel width to a point E. The coefficients of one-half channel width at BC and one channel width at DE may be rationalised by the presence of double and single vortices at these two locations respectively. Figures 6.5 and 6.6 were prepared using the technique described above.

Figure 6.5 shows the zones where velocity, shear stress and vortices along single and upstream bends reach the maximum value. The splitting of the pool-riffle sequence associated with multiple shift of flow from the concave bank within a single bend ( $2.0 < r_c/w < 2.6$ ) is among the main features of lateral migration. Secondary flow is directed towards the channel bottom at the pools and towards the surface at riffles. The points of

maximum shear stress are located at the pools also. The location of the points BC and DE vary considerably with  $r_c/w$ . These are the points that erosion likely occurs. But this variation is expected because there are various combinations of simple modes of lateral erosion. For example, a permutation of the three simple modes of migration (expansion, translation and rotation) into double and tripple combinations, including downvalley and upvalley trends of each combination forms a composite of 78 different models. It is not surprising, therefore, that various types of bend asymmetry have been documented (cf. Brice, 1974; Hickin, 1974). Brice in this excellent paper remarked that the bend asymmetry are "...not consistent relative to flow direction". The present data shows, however, that each asymmetry is a product of various characteristics of the bend flow development.

The flow characteristics are consistent because it has been shown that the fully developed flow locates upstream of 60 degrees of the bend angle and downstream of 120 degrees in most bends. Although the character of the delayed cross over has received more attention (cf. Parker et al; 1982; Ikeda et al; 1982) than the idea that of the fully developed flow locates at or upstream of 60 degrees (Muramoto, 1967, Varsney and Garde, 1975), evidence from the present study shows that this complex flow behaviour is responsible for developing compound loops. The role of the inherited vortex flow from the upstream bend persists well past the axis of the following bend and it is

Figure 6.5. The location of maximum velocity, shear stress and vortex strength in single and upstream bends.

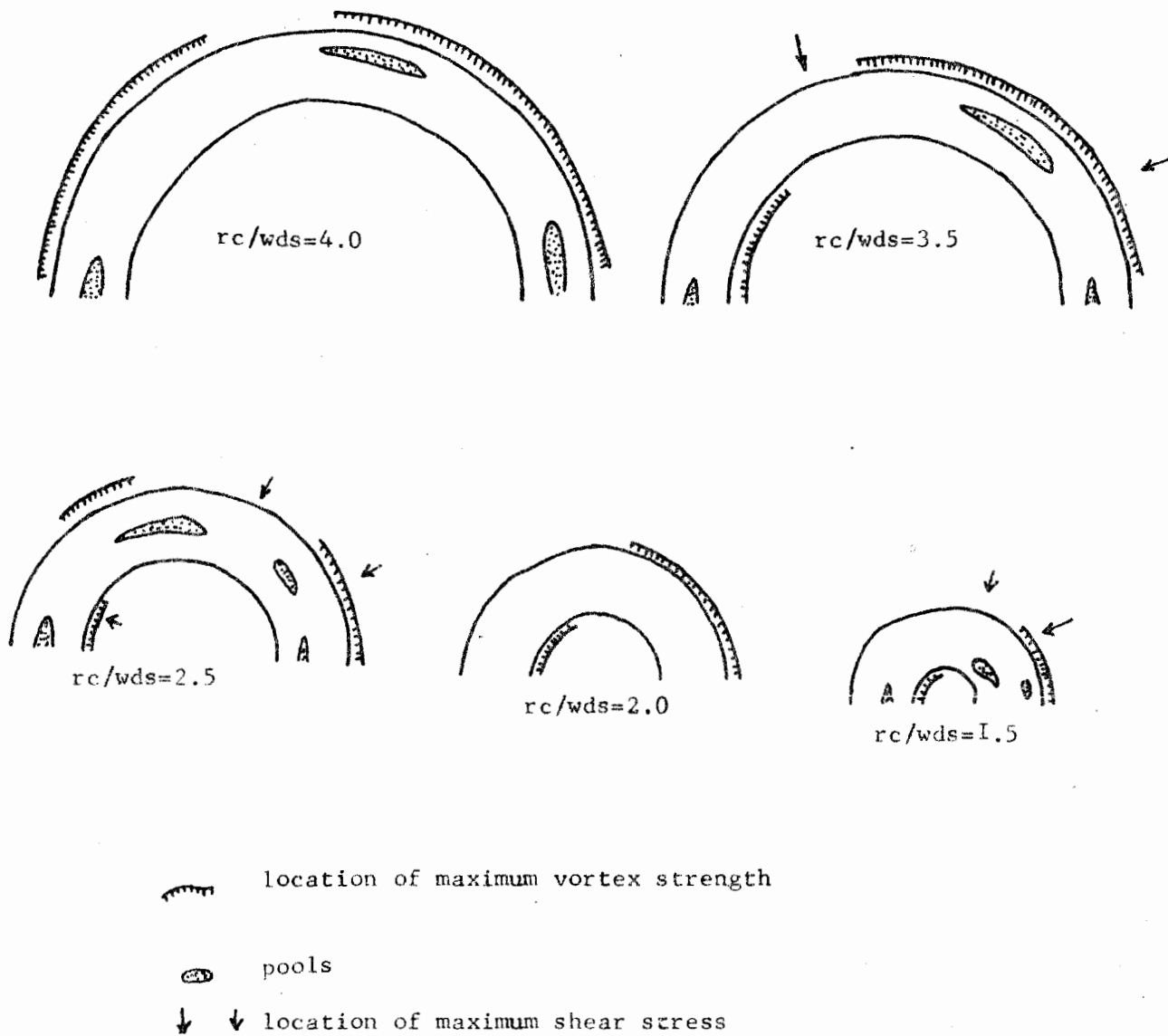


this residual effect that complicates further the flow characteristics. In single and upstream bends,  $r_c/w=4.7$  have maximum velocity along the convex bank upstream of the bend axis while there are only sporadic spots along the concave bank; erosion will occur on the convex bank along the bend entrance (see also Ippen and Drinker, 1962). Bends of  $r_c/w=3.0$  may experience translation and expansion (cf. Jackson, 1975 (b)) because of the location of the free vortex along the entrance and forced vortex along the concave bank towards the bend exit. The bends of  $r_c/w=2.0$  may experience expansion and rotation (type A) because parabolic flow locates upstream of the bend apex and the forced vortex reaches its maximum strength at 150 degrees. Bends of  $r_c/w=2.6$  and 4.0 may experience the expansion mode because the maximum velocity and shear stress locate between 40 and 160 degrees.

The points of maximum shear stress and velocity, and the location of vortices and pools along the downstream bends are shown in Figure 6.6. The vortex strength between 80 and 120 degrees is high in  $2.7 < r_c/w < 4.0$  and they are likely to experience expansion and rotation while those with  $r_c/w > 4.0$  may experience simple expansion. The expansion and rotation modes appear to be predominant along the downstream bends and also widespread in real rivers (Carson and Lapointe, 1983; Parker et al, 1982).



Figure 6.6. The location of areas liable to erosion in downstream bends.



Three associated flow phenomena act in concert along these bends. First, there is a carryover effect of a strong free vortex due to flow inertia from the upstream bends which persists until 60 degrees and sometimes to 120 degrees into the downstream bends. Second, there are riffles at the points where free vortex translates to forced vortex; the thalweg shifts from the inner bank towards the outer bank causing a delay of the fully developed flow zone (see also Bridges and Jarvis, 1976; Parker et al, 1982). Third, the delayed fully developed flow zone shifts the erosional axis downstream; this is a necessary prerequisite for the expansion and rotation mode of lateral erosion.

The downstream bends that do not have the tendency to experience expansion and rotation have maximum velocity along the outer bank located upstream of 60 degrees of bend angle as for single and upstream bends. The distribution of mean velocity and shear stress is skewed upvalley. If a second erosional axis occurs downstream of 130 degrees, the bends will develop a T-shaped geometry (cf. Hickin, 1974).

The experimental results show the uniqueness of bends of  $r_c/w=2.0$ . These bends are characterised by low shear stress and friction to flow and are dominated by parabolic flow along the bend axis. The core of maximum velocity and shear stress locate more or less at the centre of the channel. The decrease of shear stress, friction to flow and the forced vortex flow in the bend zone, and possibly the rate of lateral migration (Hickin and

Nanson, 1975) are due to the long transitional (parabolic) flow rather than vortex break down (Bagnold, 1960). The mainstream velocity decelerates alternately and rapidly with the result of increasing velocity away from the channel boundary along the sinuous path of reduced roughness.

The results of measurements of velocity, shear stress and friction coefficients suggest that tighter bends may not be products of a single bend as postulated in phase one experiments. The pools locate upstream of 60 degrees and downstream of 120 degrees in a bend with  $r_c/w > 3.0$ . Two bends likely will develop from these two erosional apices (see examples in Hickin, 1974; Brice, 1975). The results of Schumm and Khan (1972) confirm that unless some changes are made to the initial parameters, a straight channel may only progress to a meandering thalweg (see also Friedkin, 1945; Hayashi, 1973). Such changes includes discharge (cf. Shen and Komura, 1968) or sediment calibre. Desaulniers and Frenette (1973) found that erosional apices changed from the upstream of the bend apex through to the downstream end of the bend in different experiments involving bends of 180, 90 and 60 degrees.

The channel will create additional pools (Keller, 1972) by its periodic velocity and shear distribution and also erode to increase arc length. The wide variations of the wavelengths of the core of maximum velocity and the bend geometry demonstrate that riffles and pools are related to the periodic flow pulsations (Yalin, 1971) rather than the channel geometry. The

riffle-pool sequences may vary between three to twenty channel widths in diverse river regimes (Milne, 1982). The implications for lateral migration in rivers, although indirect, suggest that multiple erosional axes are more common than single ones.

Free vortices are typical and ubiquitous along the entrance of the downstream bends. The free vortex flow may erode the inner bank. Further downstream of a bend angle of 120 degrees, the same position maximum erosion occurs on the concave bank, a forced vortex has a maximum strength. The general pattern of maximum erosion is that bends with double pools may migrate through expansion and rotation while those with pools located upstream of the bend axis migrate upvalley and the ones with single pools migrate downvalley. In all cases, the limiting curvature ratio appears to be approximately  $r_c/w$  of about 2.0. These bends are more efficient conduits because their mean velocity increases. In other bends, the streamlines that impinge on the channel banks increase shear stress and reduce the mean longitudinal velocity in other bends but not in that with  $r_c/w=2.0$ .

## CHAPTER 7 CONCLUSION

### 7 CONCLUSION

The experimental work carried out for this dissertation has concentrated on investigating bend flow development and interactions in single and consecutive bends. The magnitude and extent of the influence of upstream and downstream bend flow conditions has been characterised by examining current direction, isovel patterns, vortex interaction, shear stress and friction to flow. The comparisons made between bend flow development and flow behind bluff bodies must remain speculative and discursive; its value can be judged by the limitations of experimental design, ruggedness of the instruments and errors discussed in chapter 2. The poor reproducibility of velocity measurements are of particular concern because of its transitional nature and the randomness of bedforms. The relationships between the states of flow deformation and modes of lateral erosion in rivers is to some extent speculative and therefore demand further refinement.

The present study confirms the dictum stated at the beginning of this investigation that river channels do not remain straight for any appreciable channel length. The flow is unsteady and nonuniform; the vortices interact in a complex

manner creating transverse and longitudinal oscillations. These oscillations are independent of the bend geometry. This possibly is the reason why various and dissimilar bend flow models tend to give realistic results. The flow dynamics in each curvature ratio is unique, a notion which is in agreement with Friedkin's (1945) results that each discharge forms a unique arc of curvature.

Although bend flow development varies with local conditions, it can be categorised into three regions. The first region is the straight entrance portion where there is no upstream influence of the bend. The flow is parabolic and secondary flow advection is directed towards the corners near the channel banks and towards the surface at the centre of the channel. This indicates that the influence of viscosity rather than inertial forces is predominant. However, as the bends become tighter,  $r_c/w < 3.0$ , there is an upstream transmission of bend effects that tend to destroy parabolic flow and develop a free vortex flow at the bend entrance.

The second region is between bend angles of 10 and 60 degrees. In this bend zone, the secondary flow directed towards the convex bank is suppressed, and a potential vortex is embedded in the flow. This position tends to vary because it is controlled by pressure travelling upstream through velocity acceleration near the convex bank as well as deceleration along the concave bank (free vortex flow). The cross stream transfer of momentum overwhelms the forces tending to conserve angular

acceleration in  $r_c/w < 3.0$ . The resulting imbalance of both forces determine the flow profile within this bend region in which instability is predominant.

The nonlinear instabilities generate fundamental oscillations, harmonics and subharmonics demonstrated by the doubling of the wavelengths of longitudinal and transverse velocity, shear stress and friction to flow. The mean longitudinal velocity and shear stress have valleys between 60 and 120 degrees; the region is dominated by parabolic (transitional) flow which impedes the formation of the fully developed flow zone and limits the role of expansion mode in lateral channel movement. The second region is poorly developed in bends of  $r_c/w < 2.0$  because the core of maximum velocity and the axis of maximum shear stress bounce from one bank to the other. In bends with  $r_c/w > 2.0$ , the bend effects migrate upstream as  $r_c/w$  decreases.

The shifts of maximum velocity towards the inner bank in  $r_c/w < 2.0$  may be a result of many factors. First, it may be due to the generation of a secondary spiral within the bend to supplement the one that develops along the straight portion or inherited from an upstream bend. Two, it may be due to an internal instability threshold (bifurcation) of the mainstream flow due to the dissimilarity between the wavelengths of the core of maximum velocity and the bend geometry (Figures 2.26 and 2.27). In both cases, the shift of high velocity core is important in assessing the rate and pattern of channel movement.

The third region and probably the best studied lies between approximately 120 and 180 degrees of the bend where the outer spiral dominates the inner one and the flow is said to be fully developed. The present study shows that there are two regions of fully developed flow ; one at approximately 60 degrees of the bend and the other as defined above. The fully developed flow zone that forms at 60 degrees breaks down at 80 degrees of the bend because of turbulence generated by streamlines that impinge on to the concave bank and also because high momentum fluid leaks towards the convex bank near the channel bed. The third region experiences the largest current deviation of all regions (cf. Bluck, 1971).

It is difficult to explain channel bank erosion by any single criterion developed in this study. The attempts to relate the location of velocity and boundary shear stress to bank erosion were based on the assumption that relatively higher magnitudes would locate near the channel banks. On the contrary, high boundary shear stress locates along the inner bank and at the channel centreline along the bend axis more often than near the concave (outer) bank in agreement with Hickin's (1978) postulate. The maximum velocity and boundary shear stress approaches the concave bank between 30 and 60 degrees of the bend and downstream of 120 degrees; the same bend zones that are liable to erosion (cf. Parsons, 1960; Suga, 1967; Kondrat'yev, 1968). The best comparison between the flow characteristics and modes of lateral migration was obtained by the use of the



principle of velocity reflectivity. The development of the pool is not a result of curved streamlines, but rather a matter of streamlines that approach the bank at approximately 90 degrees, sink towards the channel bed and then transversely move towards the channel centreline. The role of the channel geometry is to interfere with the flow pattern. The asymmetry of boundary shear stress and periodic flow unsteadiness cause the entire result of boundary instability and lateral erosion.

APPENDIX 1

Calibration of Current meter used in the present study

The Baby Ott current meter model #15823/3 (50mm propeller) has two variable calibration expressions as a function of the flow rate. These expressions were calibrated by the manufacturers and are in the form:

$$V = 0.7068m + 0.125 \dots\dots\dots A1$$

for  $V < 0.62 \text{ ft. s}^{-1}$

$$\text{and } V = 0.8026m + 0.066 \dots\dots\dots A2$$

for  $V > 0.62 \text{ ft. s}^{-1}$

Propeller model 19280/3 (30mm.) was calibrated in the Geomorphology Laboratory at Simon Fraser University. Sixty one velocity measurements at various flume speeds were taken using both propellers.

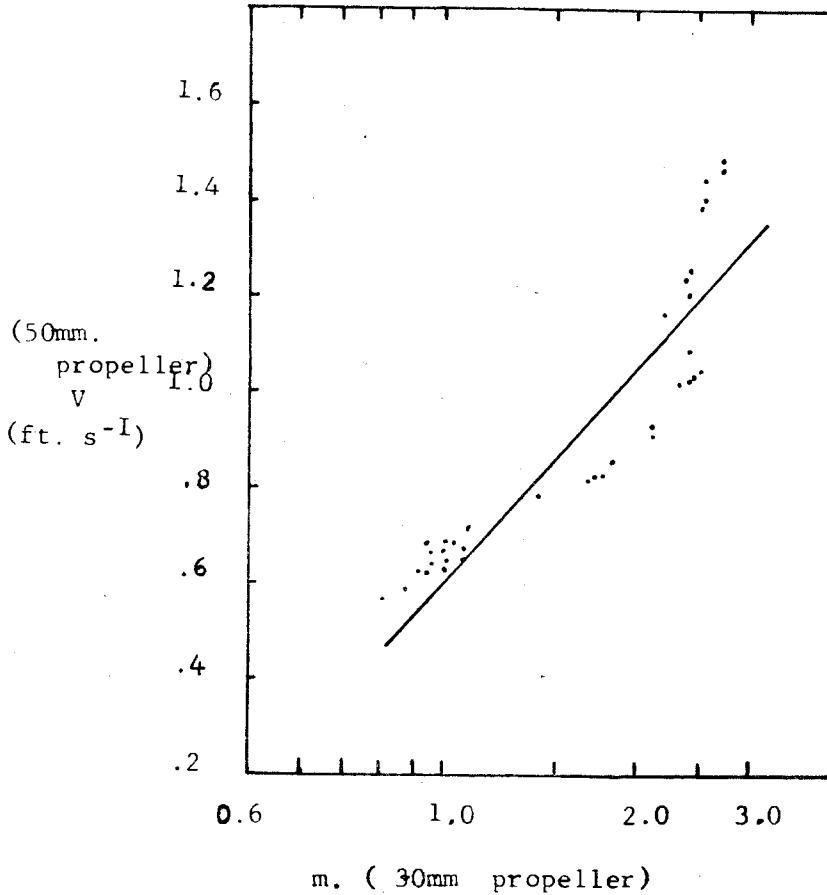
Figure A1-1 shows a nonlinear relationship between the number of revolutions per second for the 30mm propeller along the x-axis and the velocity (in  $\text{ft. s}^{-1}$ ) measured by the 50mm propeller. The velocity measurements were converted later in to SI Units. The resulting regression expression for the 30mm propeller was :

$$V = 0.4929m + 0.0146 \dots\dots\dots A3$$

$$r = 0.94$$

The nonlinearity of the distribution was not corrected because the flow rate of interest was between  $0.15 \text{ m. s}^{-1}$  and  $0.35 \text{ m. s}^{-1}$

Figure A1-1. Calibration data showing the relationship between the flow rate measured by the 30mm. propeller and the 50mm. propeller. The measurements taken by the 30mm. propeller are shown along the x-axis (number of propeller revolutions per second, m) and the measurements taken by the 50mm. propeller are shown in m. s<sup>-1</sup>



$$V = 0.4929m + 0.0416$$

$$r = 0.94.$$

APPENDIX 2

1. GEOMETRIC CHARACTERISTICS OF CONSECUTIVE BENDS SERIES WITH CONSTANT UPSTREAM CURVATURE RATIOS

entrance exit (m.)	$r_c/w_{us}$	$\theta_c$	tangent	$r_c/w_{ds}$	$\theta_c$
1.64 2.42	4.0	170	1.44	3.1	180
1.82 3.80	4.0	180	1.33	2.0	155
1.67 2.49	4.0	180	1.49	1.8	164
1.42 1.91	3.65	170	2.24	3.9	160
1.26 3.29	3.65	180	2.63	2.2	170
1.99 2.98	3.64	173	2.38	1.75	164
2.25 3.15	3.30	170	2.53	3.80	180
1.19 3.19	3.65	165	2.96	1.56	170
2.79 3.28	2.70	180	2.41	2.70	157
2.69 2.31	2.70	180	2.42	2.30	150

		2.69	2.70	180	2.42
2.10	165	2.27			
2.87	2.70	180	2.41	1.00	180
1.62					
1.71	2.07	173	2.73	4.00	180
2.55					
2.66	2.07	170	2.88	3.05	175
2.07					
2.67	2.07	180	3.37	2.00	143
2.80					
4.80	2.07	180	2.61	1.00	180
3.27					
0.93	1.92	167	1.42	2.65	180
0000					
2.28	1.50	180	1.92	2.15	170
0000					
2.71	1.50	148	1.87	2.90	165
0000					
2.13	1.50	170	1.77	2.75	177
0.79					
2.22	1.20	175	2.83	1.50	180
0.64					
1.77	3.65	170	1.83	2.10	170
3.02					
3.52	4.00	180	1.12	4.00	180
0.91					

		4.30	2.65	180	2.08
4.00	180	4.40			
4.30	2.65	180	2.08	4.00	180
4.40					

note: Measurements were not taken in bend segments denoted by 0000.

2. GEOMETRIC CHARACTERISTICS OF CONSECUTIVE BENDS SERIES WITH CONSTANT DOWNSTREAM CURVATURE RATIO

entrance	$r_c/wus$	$\theta_c$	tangent	$r_c/wds$	$\theta_c$
3.52	4.00	180	1.12	4.00	180
0000					
2.62	3.00	180	1.50	4.00	180
2.89					
2.49	2.70	156	2.64	4.00	175
3.29					
2.54	1.40	145	3.46	4.00	180
2.20					
3.78	3.65	180	1.78	4.00	180
1.83					
1.46	3.20	177	0.76	3.30	180
1.93					
0.50	2.00	168	1.36	3.20	180
0000					
2.85	1.50	142	2.25	3.30	165

0000					
2.34	1.73	180	2.62	3.60	165
3.30					
2.60	1.70	170	2.97	3.03	170
3.41					
2.98	3.00	170	2.69	2.56	180
3.15					
3.09	3.20	180	2.38	2.40	180
3.37					
0000	2.00	145	0.46	2.60	160
2.10					
3.91	3.30	140	0000	2.00	180
1.83					
1.90	1.64	180	2.57	1.94	180
1.94					
4.60	4.00	180	2.00	1.91	180
4.50					
4.14	2.75	180	0.78	1.65	180
2.89					
1.44	2.75	170	1.68	3.50	180
1.98					
4.37	2.79	180	2.59	3.00	180
3.58					
0000	2.60	135	0000	3.00	127
0000					

### GEOMETRIC CHARACTERISTICS OF SINGLE BENDS

entrance	$r_c/w$	$\theta$ (degrees)	exit(m.)>
5.16	4.7	42	000000
2.67	3.7	133	0.70
6.71	3.3	98	1.16
4.32	3.2	84	0.74
4.32	3.2	84	0.74
4.21	2.2	121	1.17
0000	2.6	180	0000
4.59	1.8	115	3.19
5.65	1.0	139	2.27
0000	4.0	180	0000

### APPENDIX 3

#### The relations between Bed deformation and Shear Stress

Maps of bed deformation were prepared from depth measurements for different models. There are six or more verticals for each traverse (cross section). The pattern of bed deformation of single bends has been shown in Figure 3.31 while Figures A3-1 through to A3-3 show those of selected consecutive bends. The flow direction is from the left to the top of the page; the numbers shown along the right bank facing downstream



are traverse numbers while those on the left are local bend angles (in degrees). The tangents between the upstream and the downstream bends were of equal length.

Figures A3-4 and A3-5 show the local shear stress ( $T_o/\bar{T}_o$ ) for the same bends shown in Figures A3-1 and A3-2. The correlation of decreasing shear stress and increasing channel depth at the bend pools are apparent. The shear stress distribution of the other bends are included for reference (Figures 3.5 through to A3-31).

The general aspect of high relative shear stress distribution in most but not all of these bends show three major zones. One is seen at the entrance vicinity near the convex bank of the bend; this is the region where a "gutter" develops during the process of erosion. The second position where the relative shear stress becomes maximiscal locates between 30 degrees and 60 degrees near the concave (outer) bank of the bend. This position locates where the centreline of the straight entrance zone intersects the concave bank. The flow is influenced to a large part by inertial forces. The third position locates downstream of the bend angle of 122 degrees or two-channel widths around the bend axis. Minor variations from these three trends, however, are possibly due to changes of  $r_c/w$ , total bend angle and inherited flow structures from the upstream bends which in turn reflects the rate of secondary flow development.

Figure A3-I. Variation of channel bed deformation of consecutive bends with  $r_c/w_{us} = 3.0$  and  $r_c/w_{ds} = 1.94$ . The measurements are shown in cm.

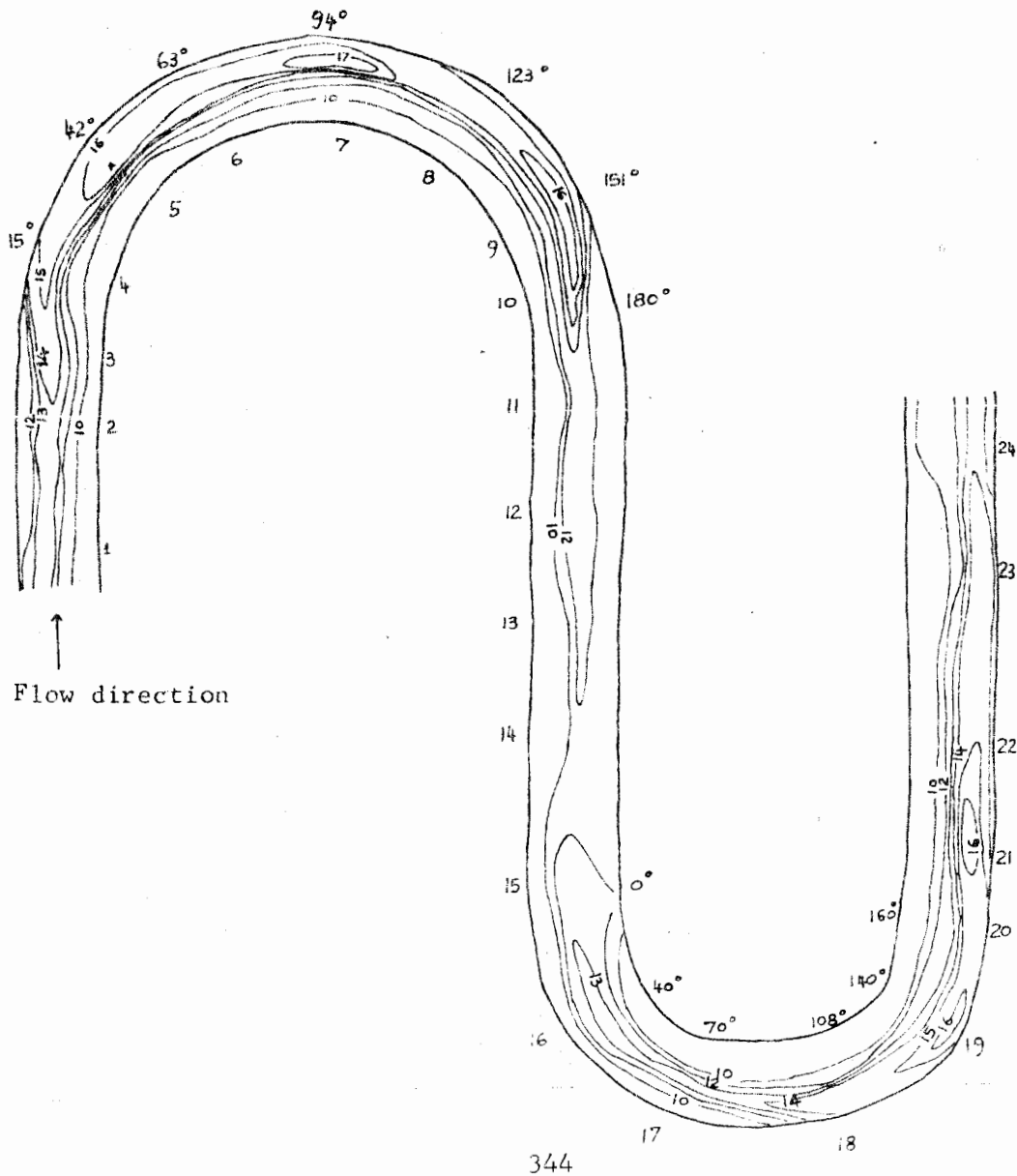


Figure A3-2. Variation of channel bed deformation of consecutive bends with  $r_c/w_{us} = 2.75$  and  $r_c/w_{ds} = 1.65$ . The contours are shown in cm.

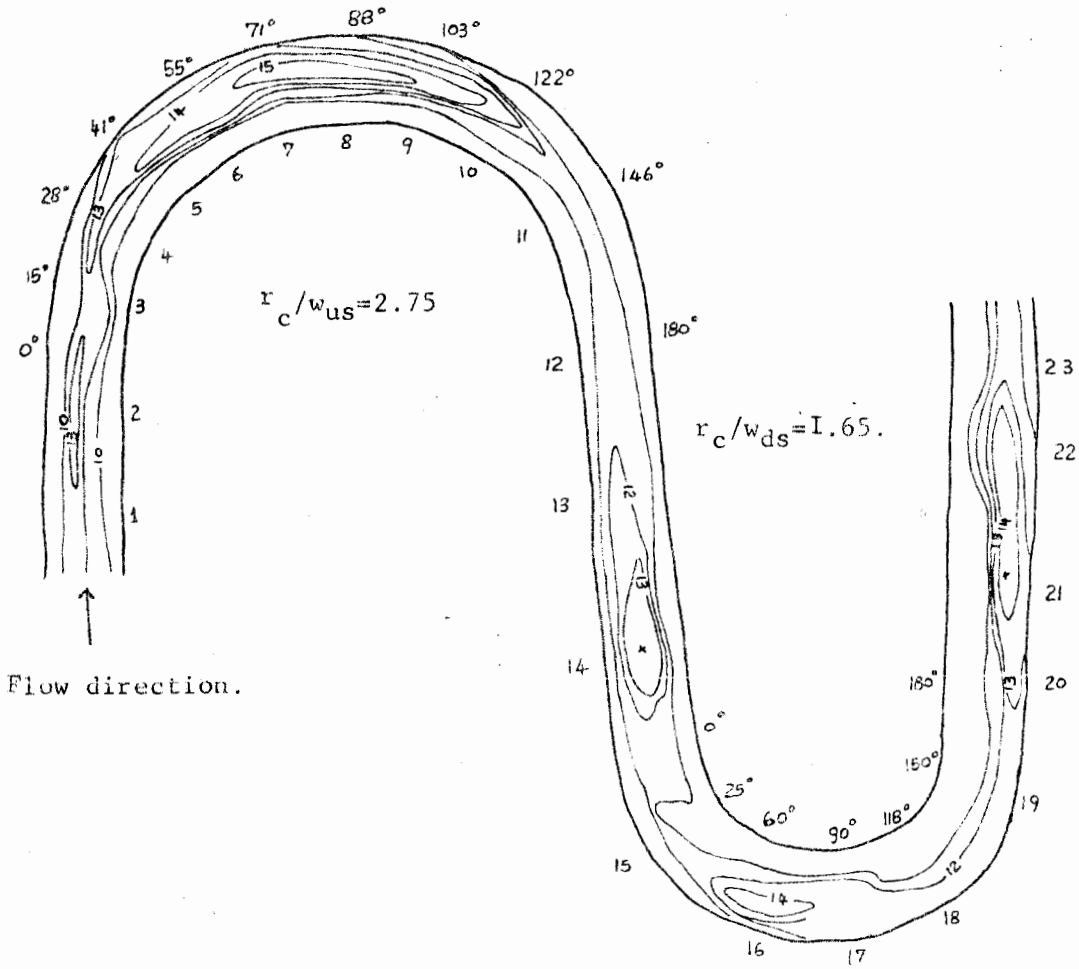
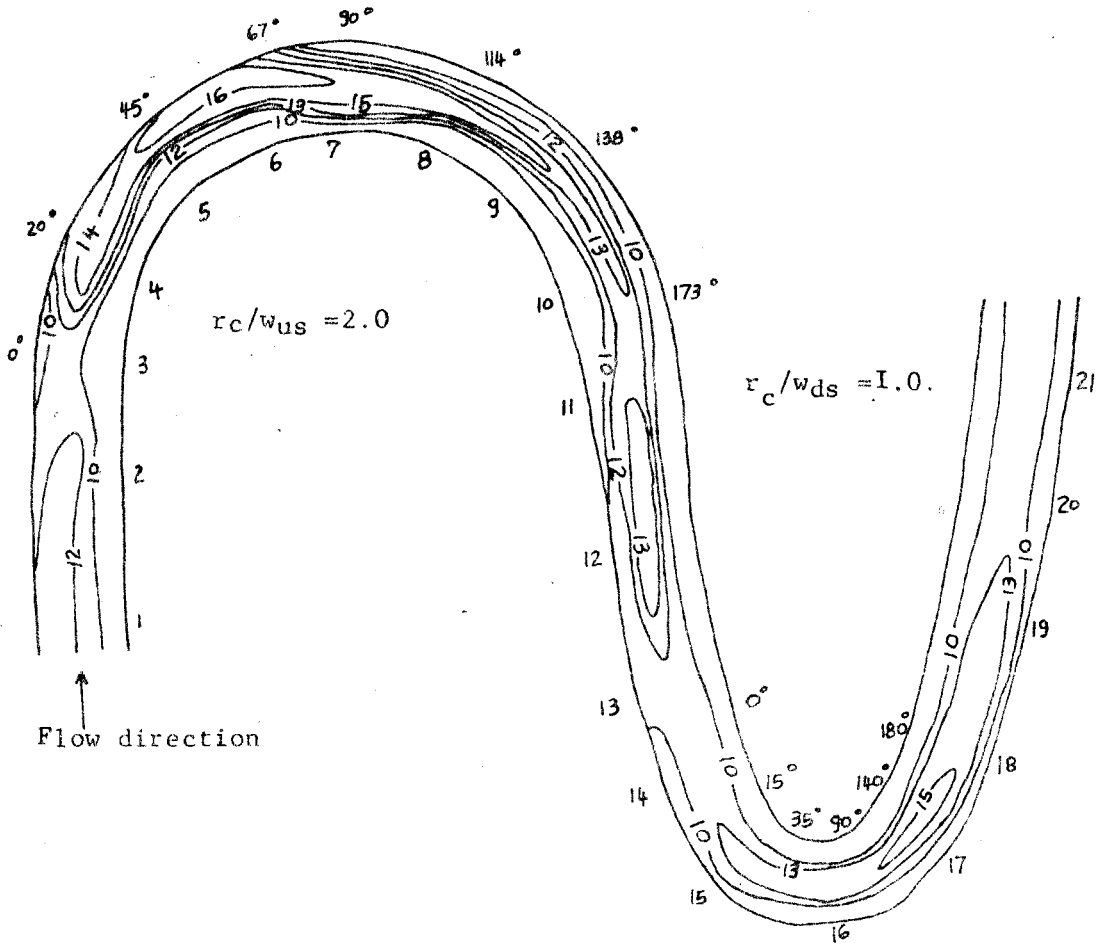


Figure A3-3. Variation of channel bed deformation of consecutive bends with  $r_c/w_{us} = 2.0$  and  $r_c/w_{ds} = 1.0$ . The contours are shown in cm.



nb. Note the pool that locates at the bend tangent contrary to single bend pool and tangent riffle.

Figures A3-4 and A3-5. The distribution of shear stress in consecutive bends. The contour interval is 0.5. The traverses (cross sections) and local bend curvature are shown on the diagrams.

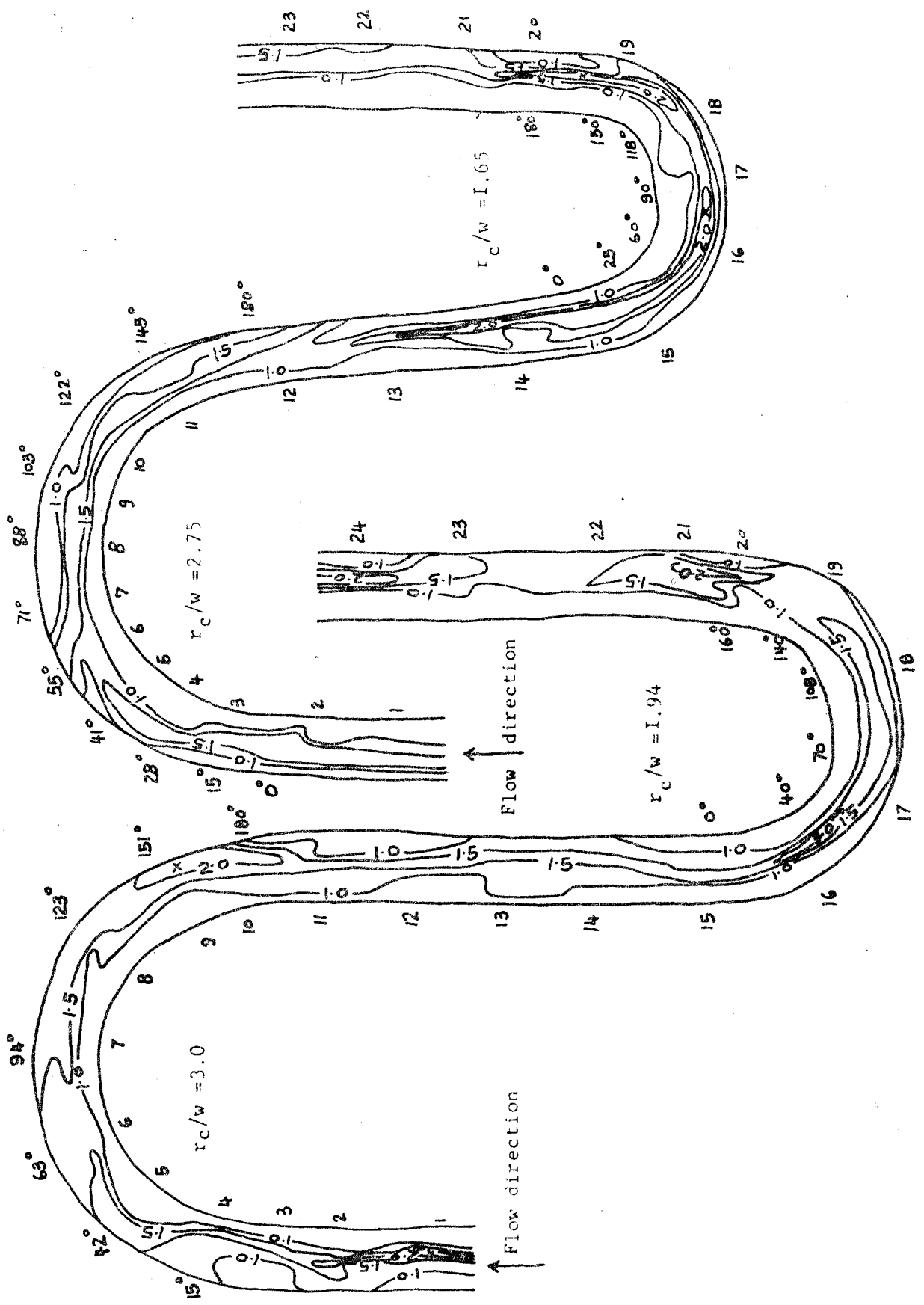


Figure A3-6. The distribution of shear stress in consecutive bends bends with  $r_c/w_{us} = 2.7$  and  $r_c/w_{ds} = 2.3$ . The contour interval is 0.5. The points at which  $T_0/\bar{T}_0$  has a maximum value are shown by the symbol 'x'

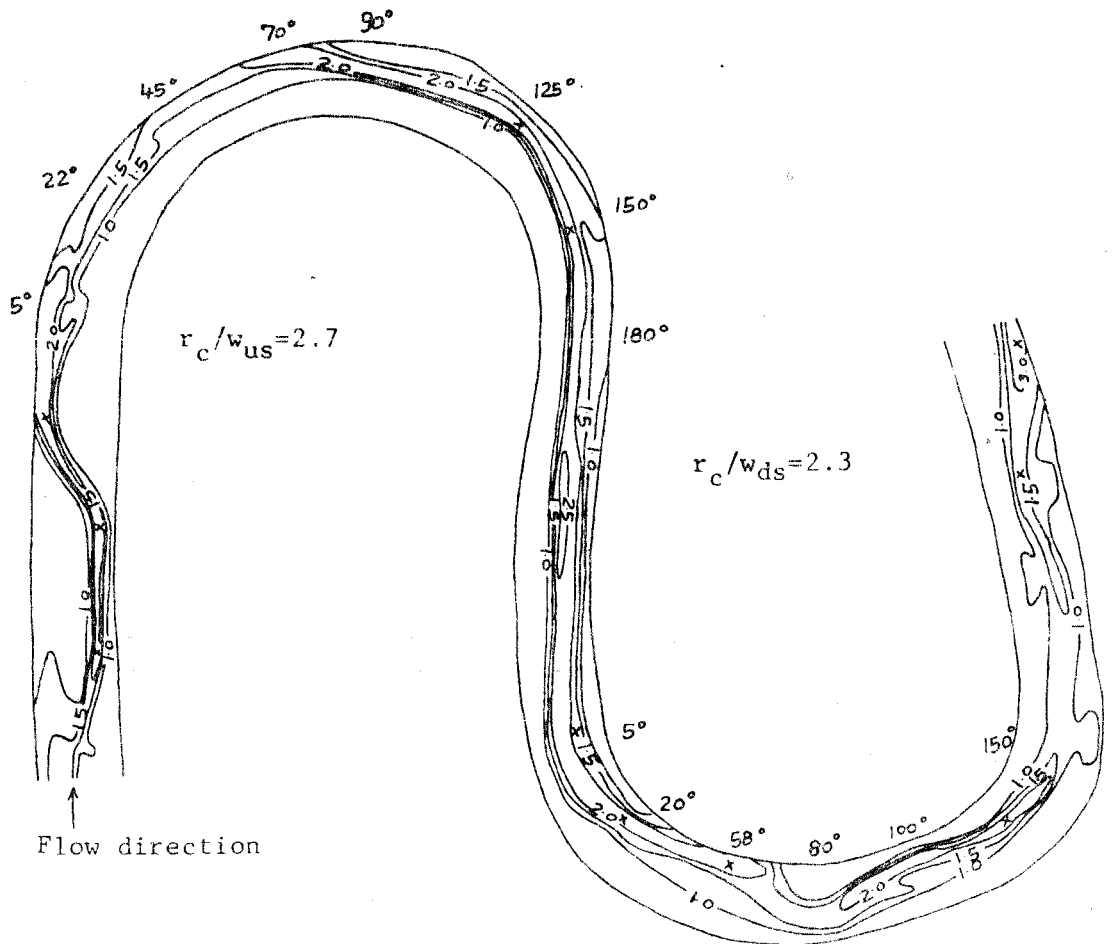


Figure A3-7. Variation of shear stress ( $T_o/\bar{T}_o$ ) for consecutive bends with  $r_c/w_{us} = 2.7$  and  $r_c/w_{ds} = 2.7$ . The contour interval is 0.5 and the points at which the shear stress has a maximum value are shown by the symbol 'x'

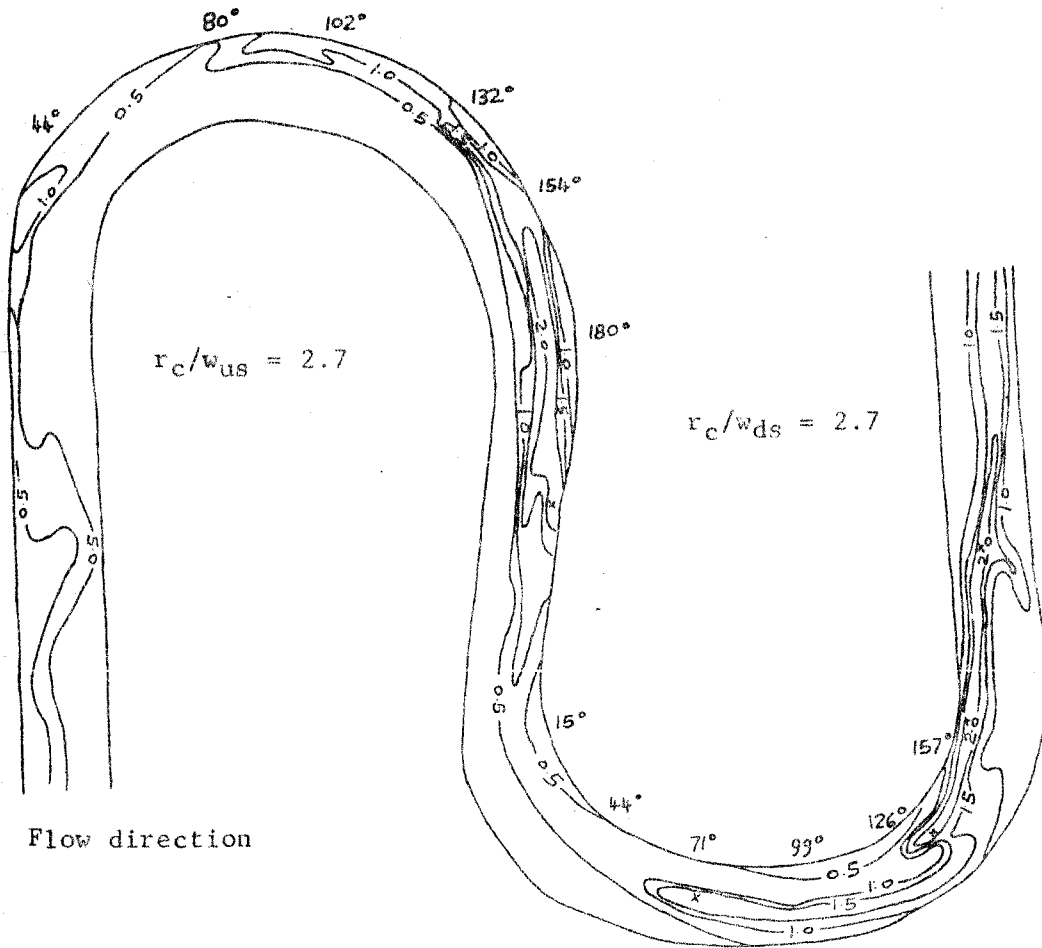


Figure A3-8. Variation of shear stress ( $T_o/\bar{T}_o$ ) for consecutive bends with  $r_c/w_{us} = 4.0$  and  $r_c/w_{ds} = 1.8$ . The contour interval is 0.5; the points at which the shear stress has a maximum value are shown by the symbol 'x'.

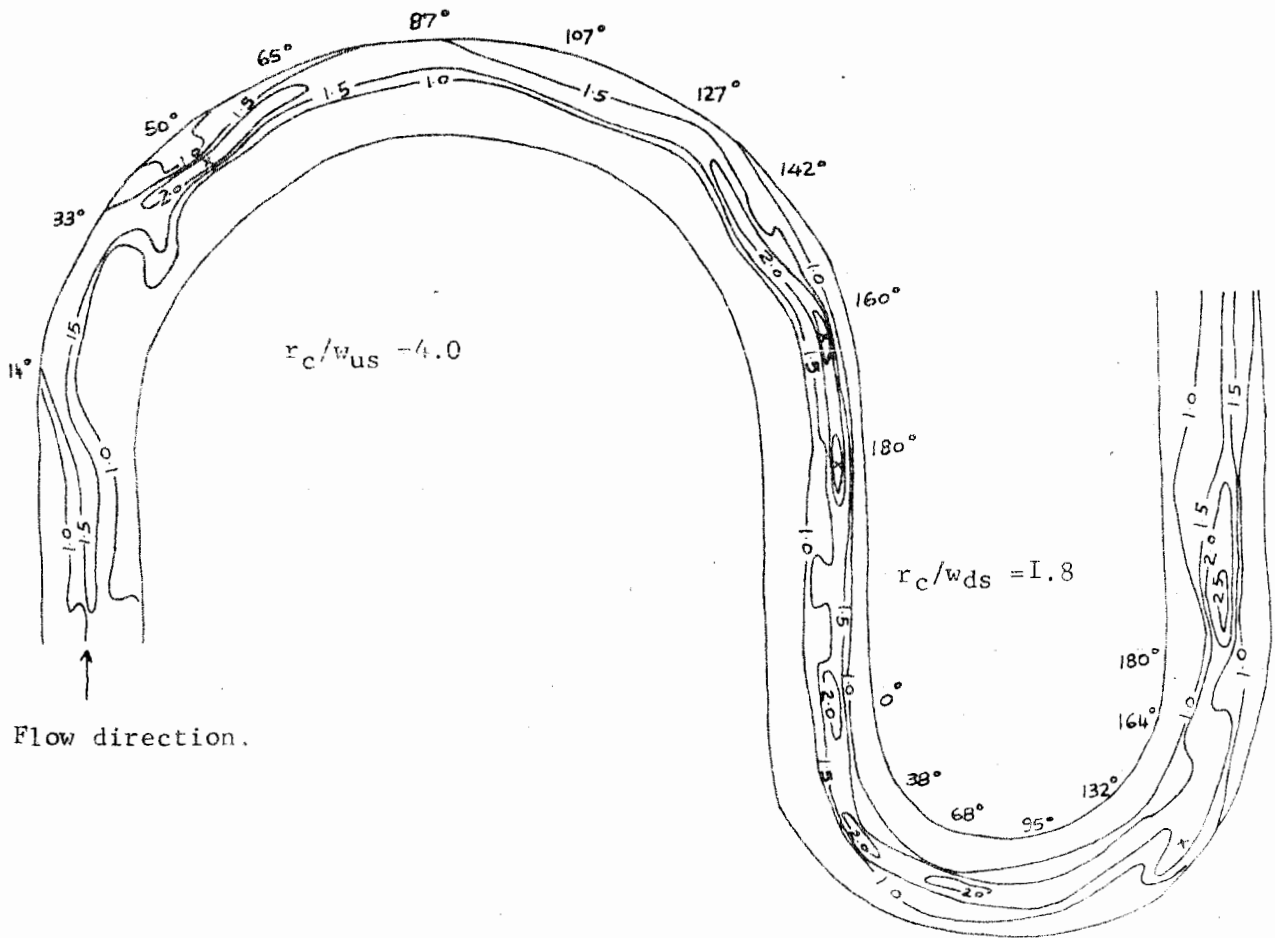




Figure A3-9. Variation of shear stress ( $T_o/\bar{T}_o$ ) for consecutive bends with  $r_c/w_{us} = 4.0$  (constant) and  $r_c/w_{ds} = 2.0$ . The contour interval is 0.5; the points at which the shear stress has a maximum value are shown by the symbol 'x'.

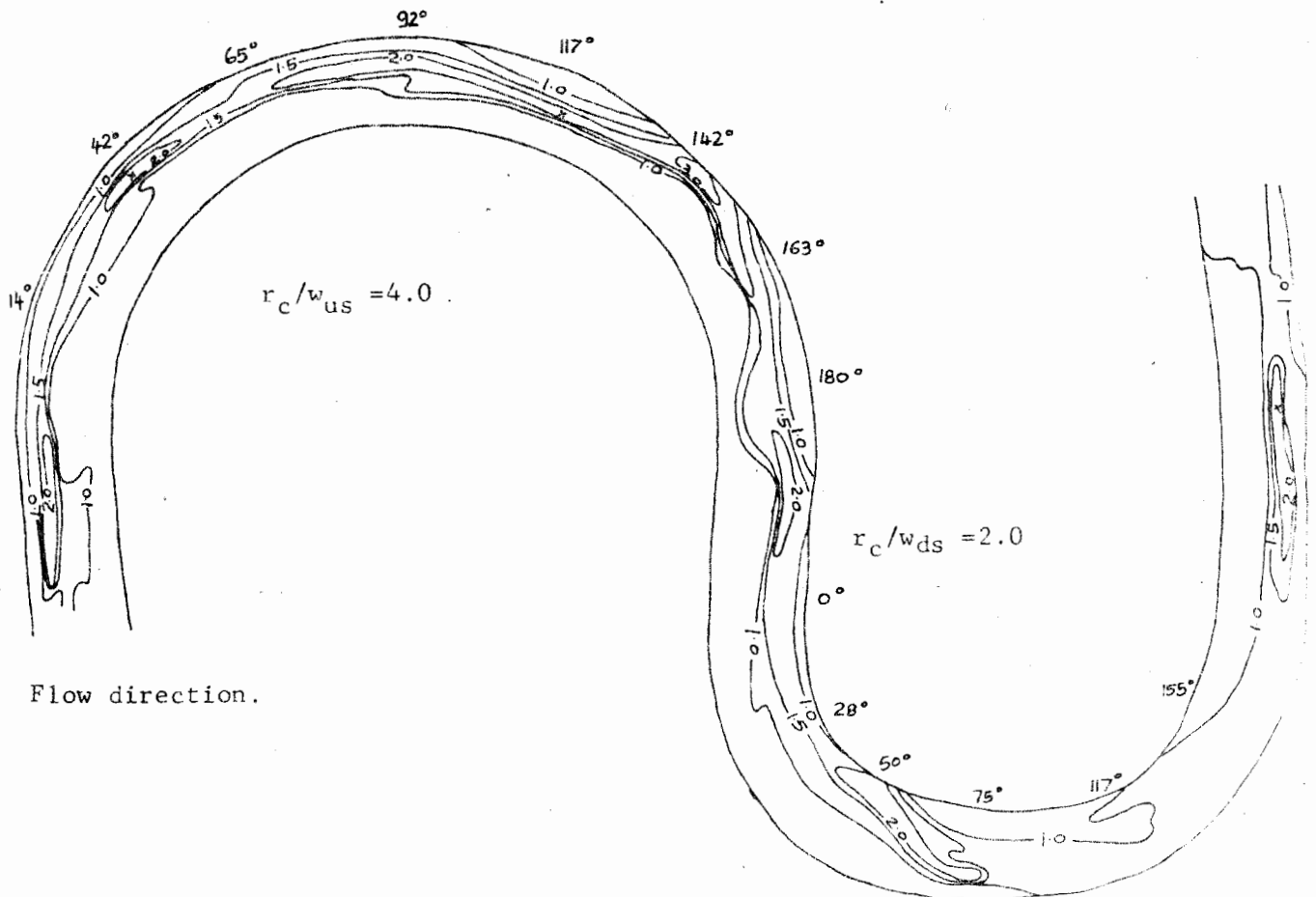


Figure A3-10. Variation of shear stress ( $\bar{T}_0/\bar{T}_0$ ) for consecutive bends with  $r_c/w_{us} = 4.0$  and  $r_c/w_{ds} = 3.1$ . The contour interval is 0.5; the points at which the shear stress has a maximum value are shown by the symbol 'x'.

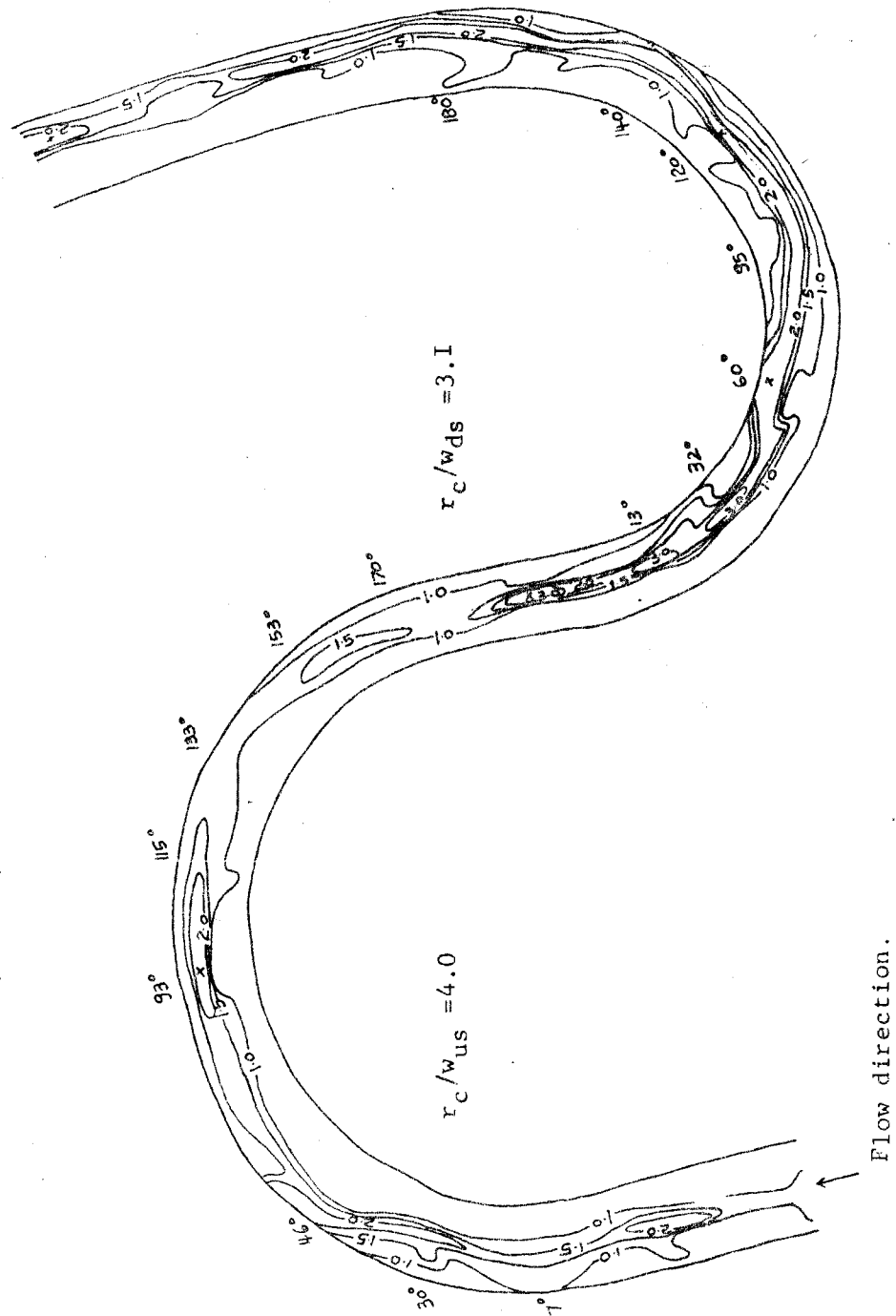


Figure A3-II. Variation of shear stress ( $T_o/\bar{T}_o$ ) for consecutive bends with  $r_c/w_{us} = 3.65$  (constant) and  $r_c/w_{ds} = 3.91$ . The contour interval is 0.5; the points at which the shear stress has a maximum value are shown by the symbol 'x'.

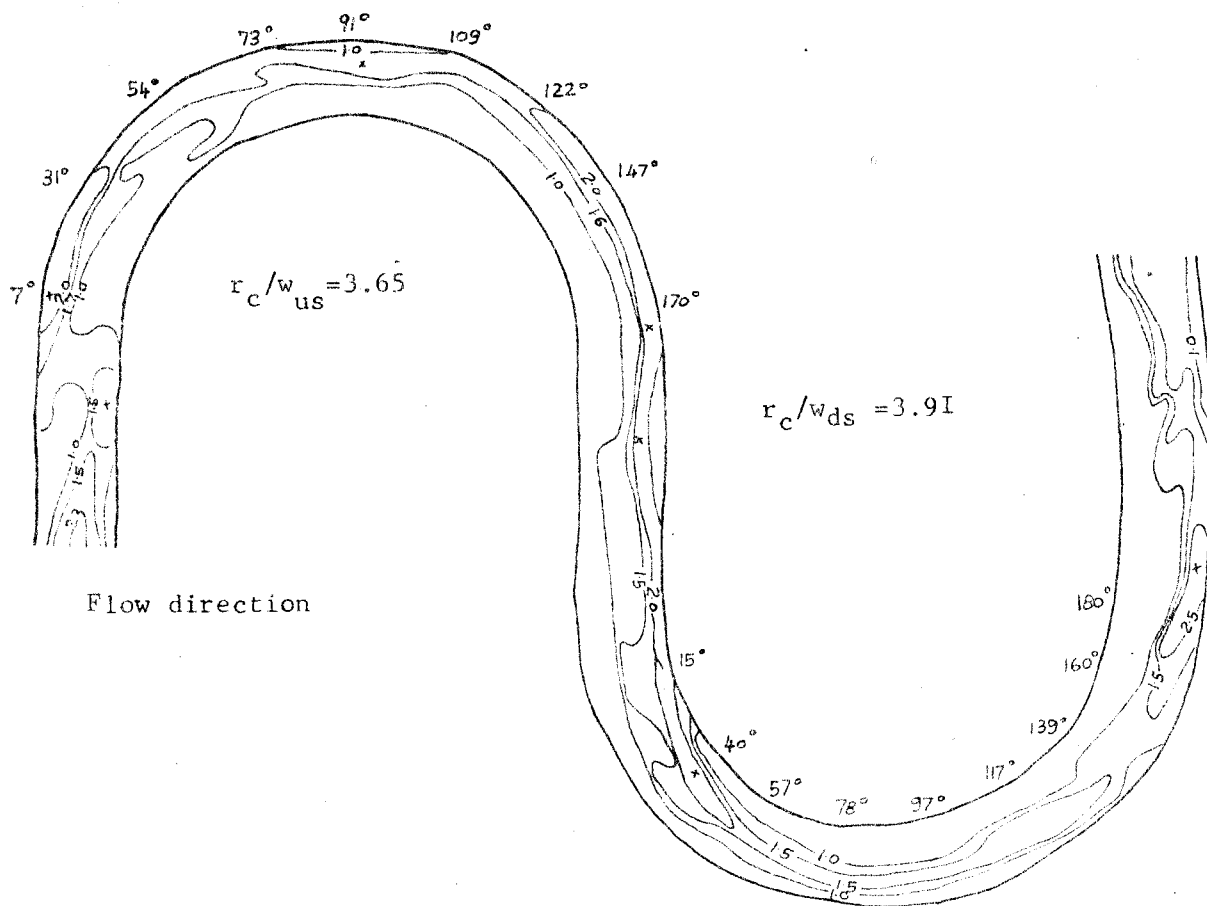


Figure A3-12. Variation of shear stress ( $T_0/\bar{T}_0$ ) for consecutive bends with  $r_c/w_{us} = 3.3$  (constant) and  $r_c/w_{ds} = 3.8$ .

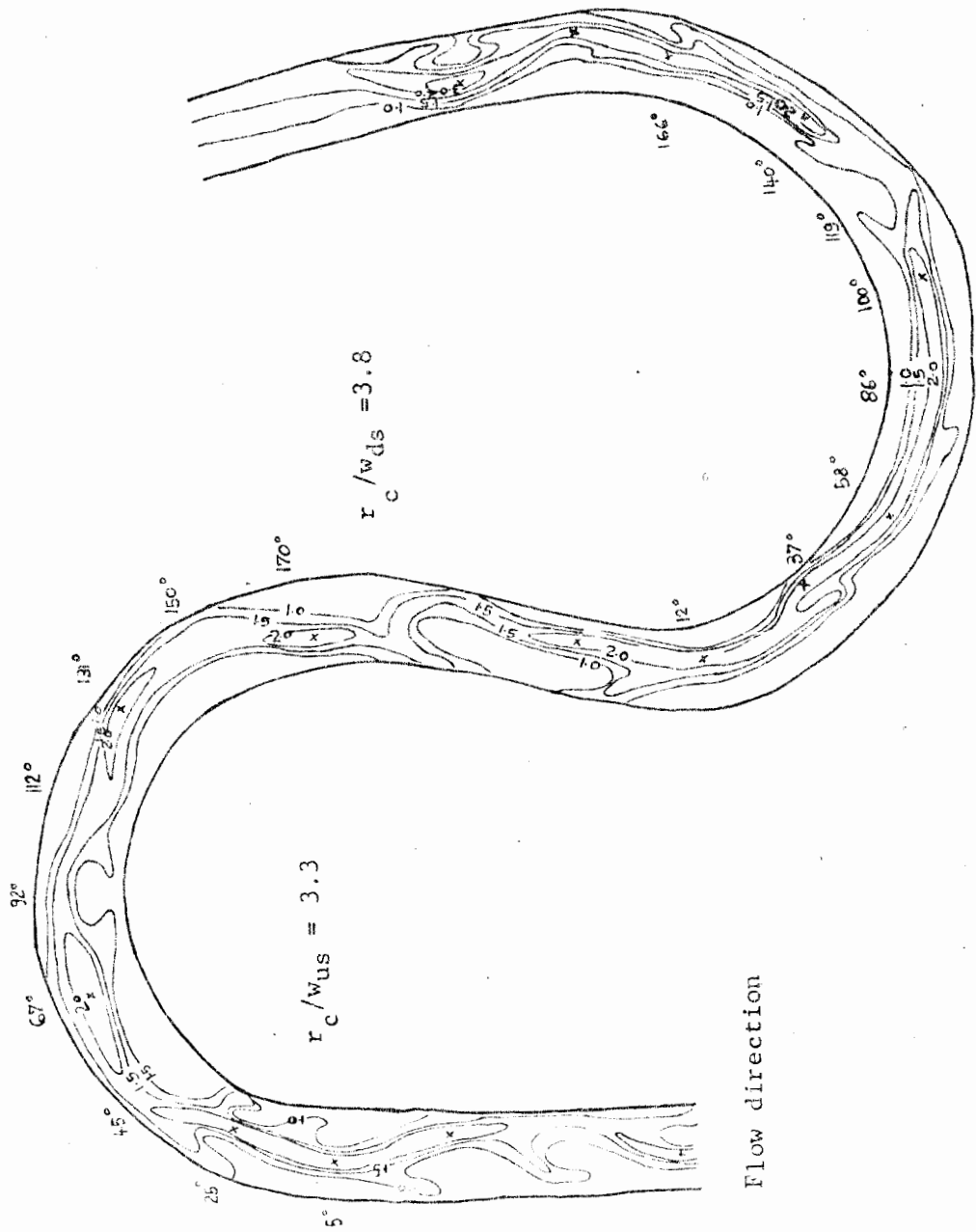


Figure A3-I3. Variation of shear stress ( $T_o/\bar{T}_o$ ) for consecutive bends with  $r_c/w_{us} = 3.65$  (constant) and  $r_c/w_{ds} = 2.2$ . The contour interval is 0.5; the points at which the shear stress has a maximum value are shown by the symbols 'x'.

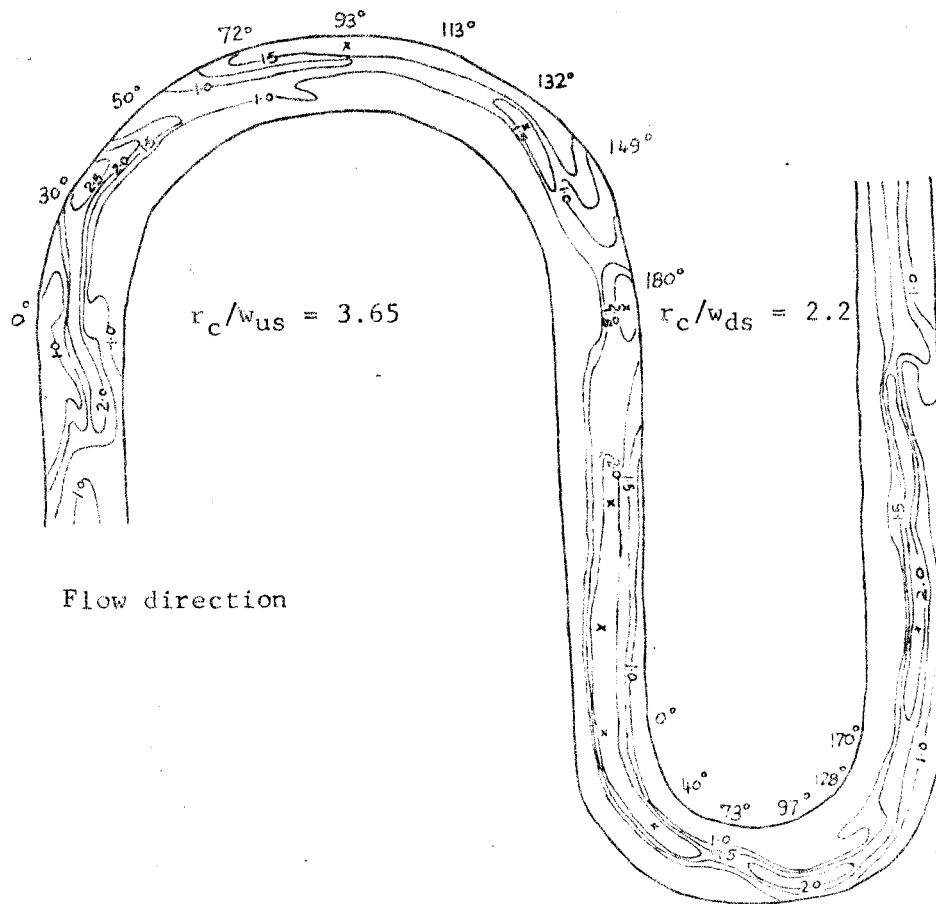
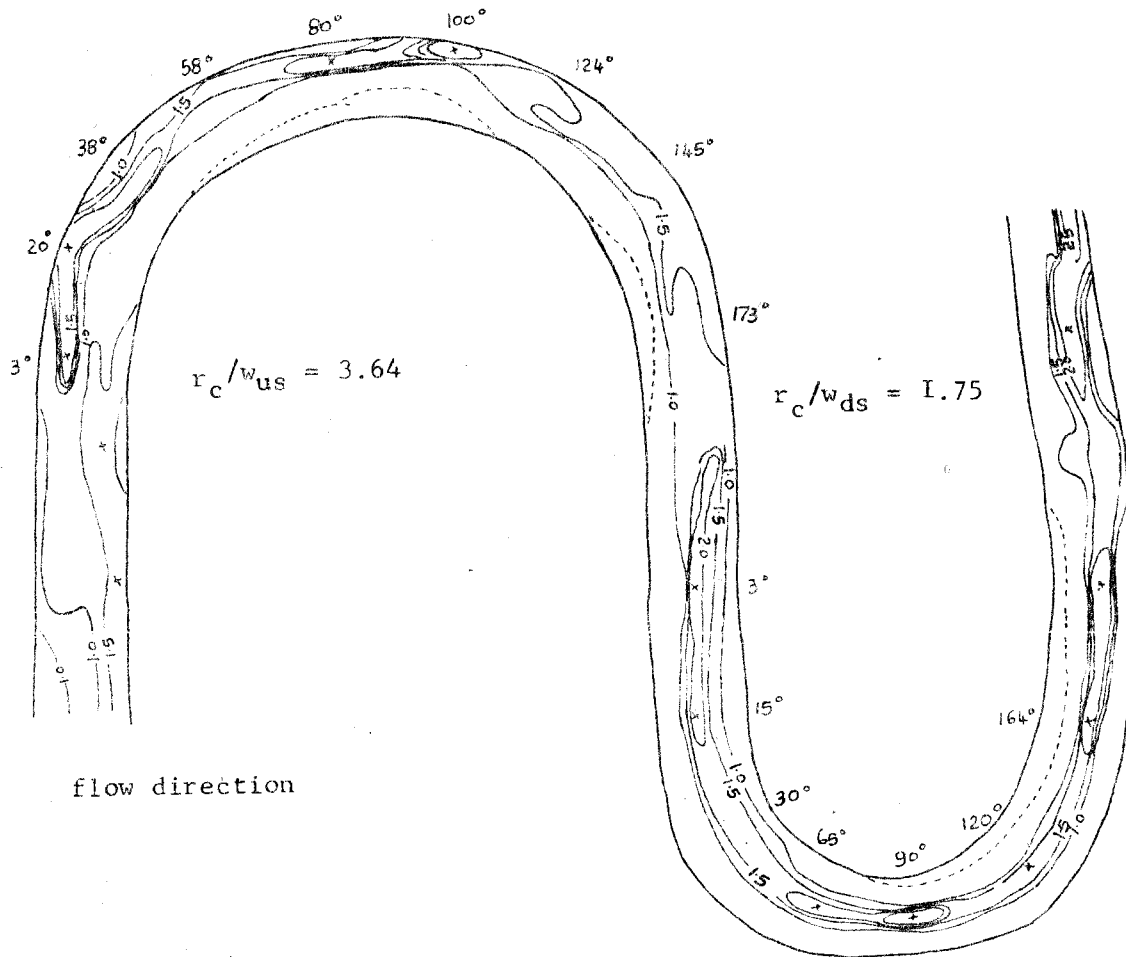


Figure A3-I4. Variation of shear stress ( $T_0/\bar{T}_0$ ) for consecutive bends with  $r_c/w_{us} = 3.64$  (constant) and  $r_c/w_{ds} = 1.75$ . The contour interval is 0.5.



nb. The points at which the shear stress has a maximum value are shown by the symbol 'x'.



Figure A3-I6. Variation of shear stress ( $T_o/\bar{T}_o$ ) for consecutive bends with  $r_c/w_{us} = 2.0$  (constant) and  $r_c/w_{ds} = 3.0$ . The contour interval is 0.3; the points at which the shear stress has a maximum value are shown by the symbol 'x'.

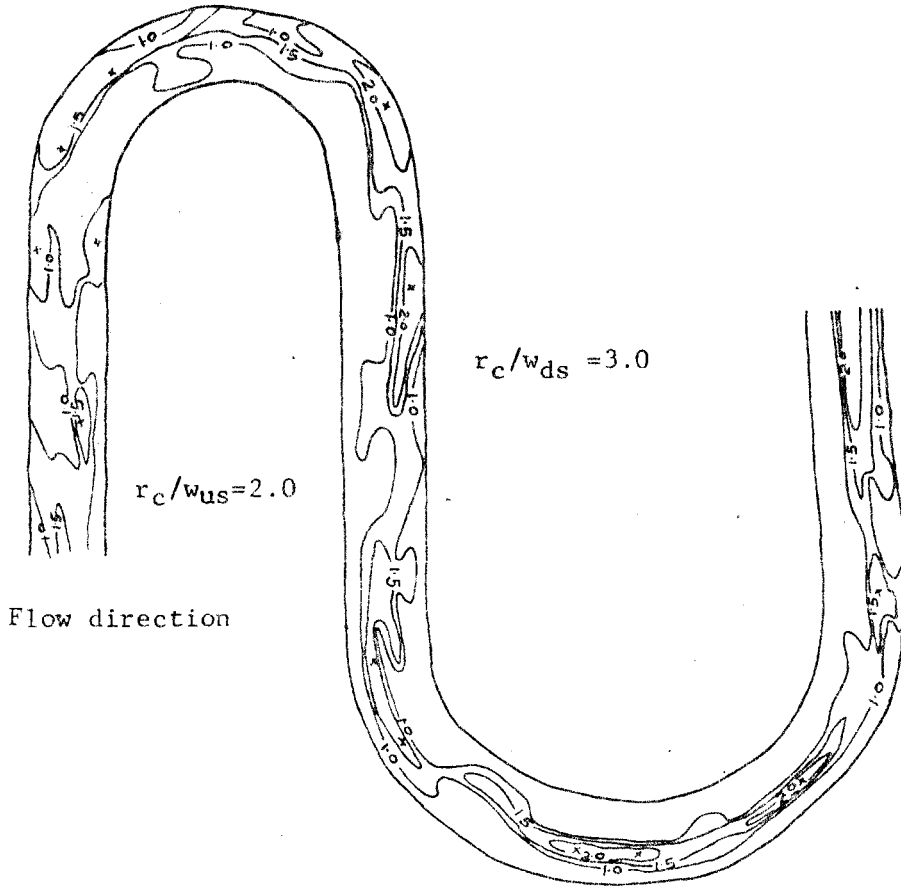




Figure A3-17. Variation of shear stress ( $T_0/\bar{T}_0$ ) for consecutive bends with  $r_c/w_{us} = 1.92$  (constant) and  $r_c/w_{ds} = 2.65$ .

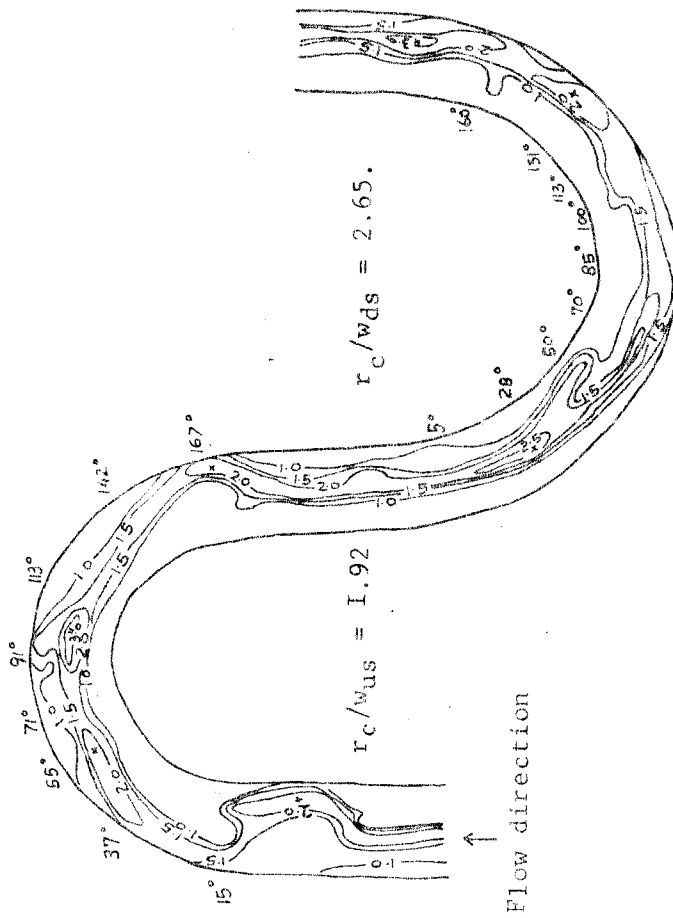


Figure A3-18. Variation of shear stress ( $T_o/\bar{T}_o$ ) for consecutive bends with  $r_c/w_{us} = 2.0$  and  $r_c/w_{ds} = 2.0$ . The contour interval is 0.5.

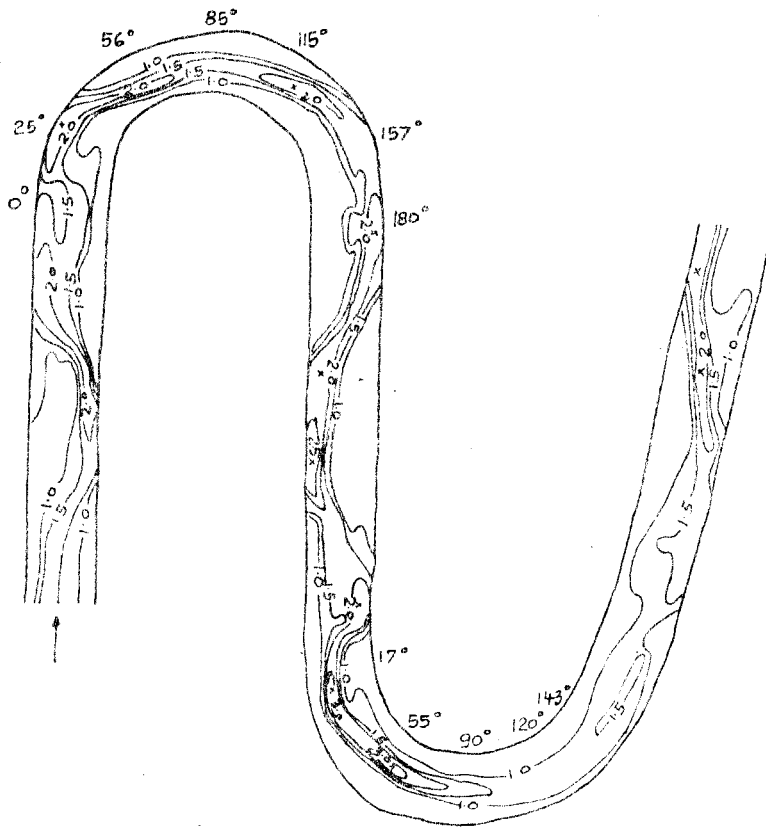


Figure A3-19. Variation of shear stress ( $T_0/\bar{T}_0$ ) for consecutive bends. The contour interval is 0.5; the points at which the shear stress has a maximum value are shown by the symbol 'x'.

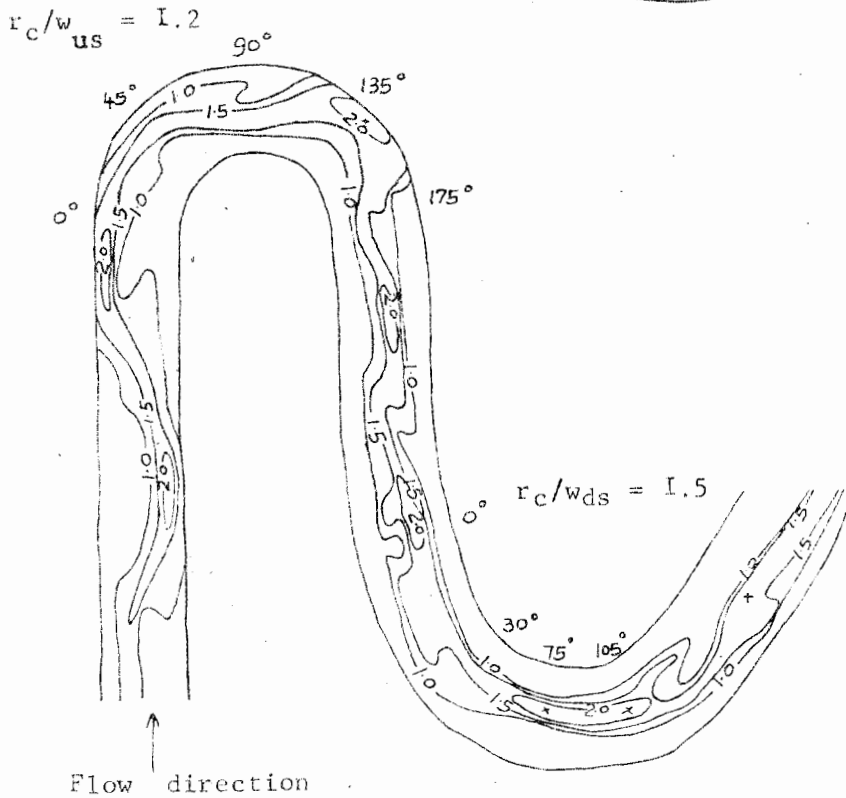
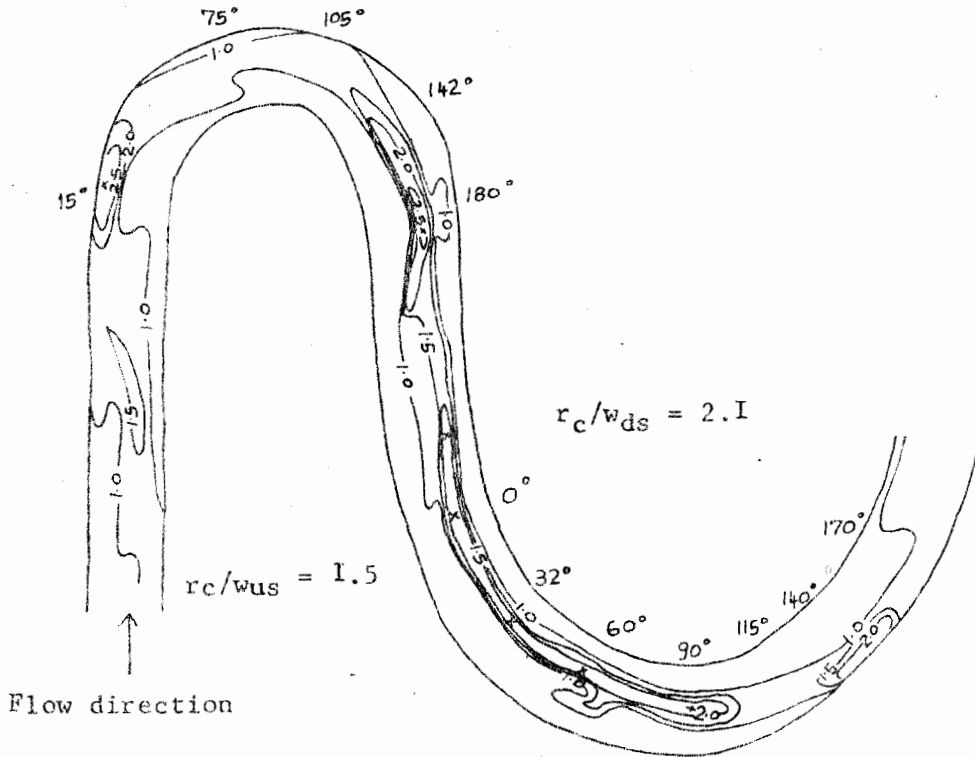


Figure A3-20. Variation of shear stress ( $T_o/\bar{T}_o$ ) for consecutive bends. The contour interval is 0.5; the points at which the shear stress has a maximum value are shown by the symbol 'x'.

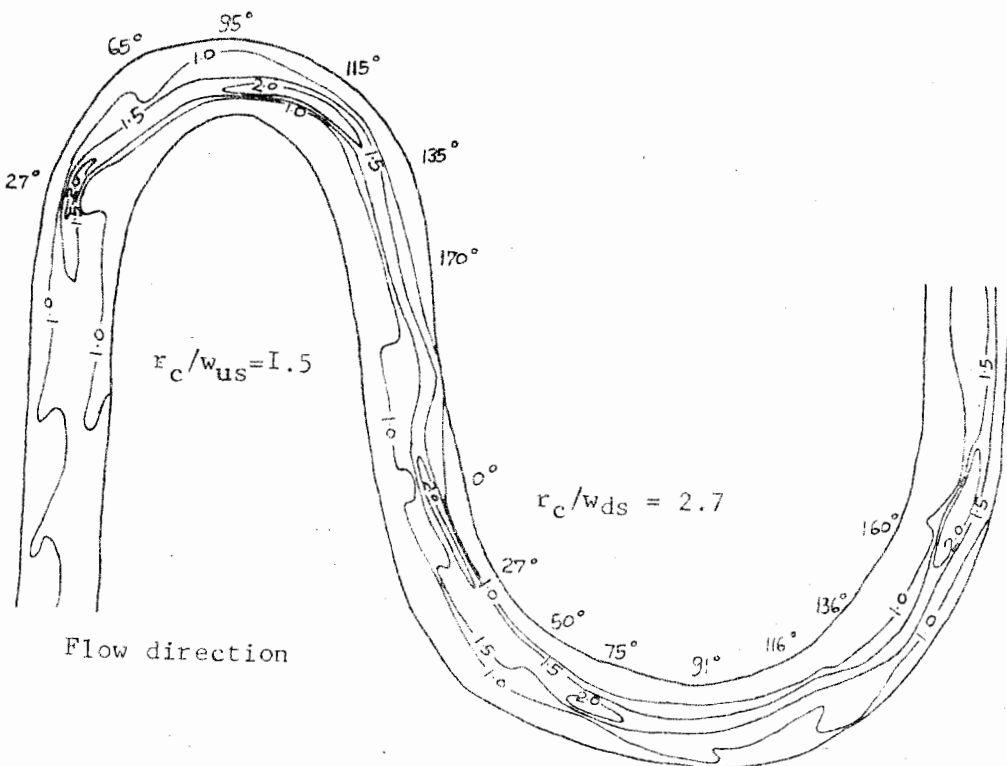
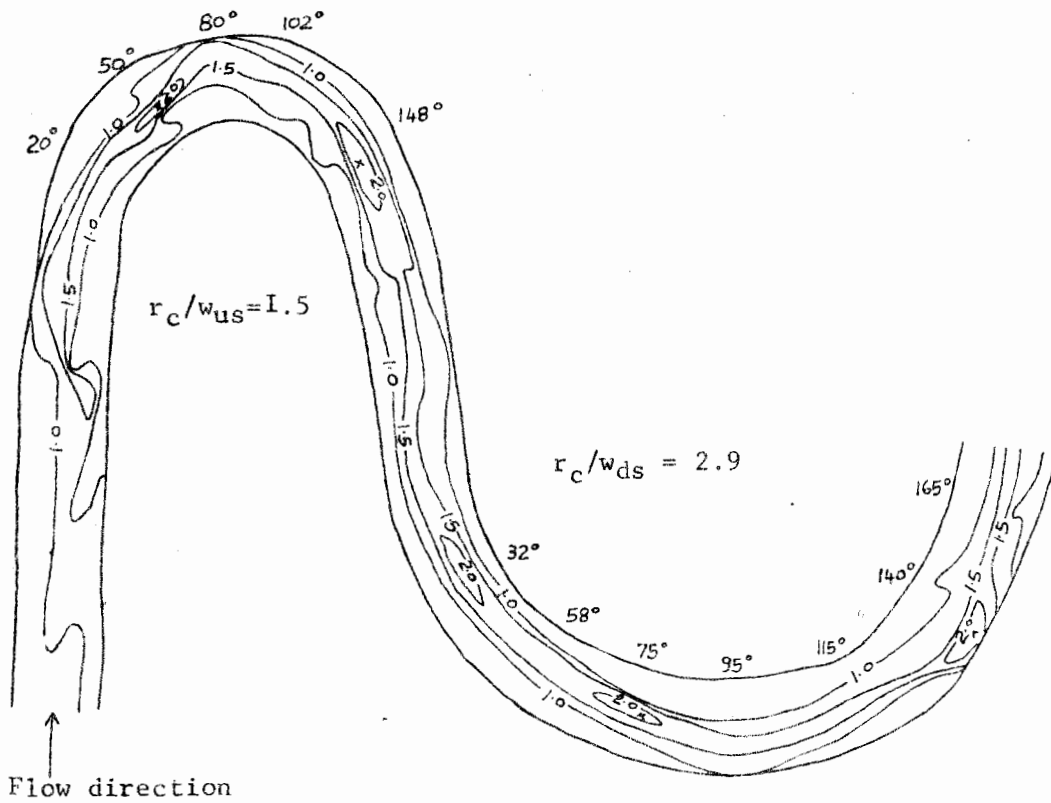


Figure A3-2I Variation of shear stress ( $T_o/\bar{T}_o$ ) for consecutive bends with  $r_c/w_{us} = 3.0$  and  $r_c/w_{ds} = 4.0$  (constant). The contour interval is 0.5. The points at which the shear stress has a maximum value are shown by the symbols 'x'.

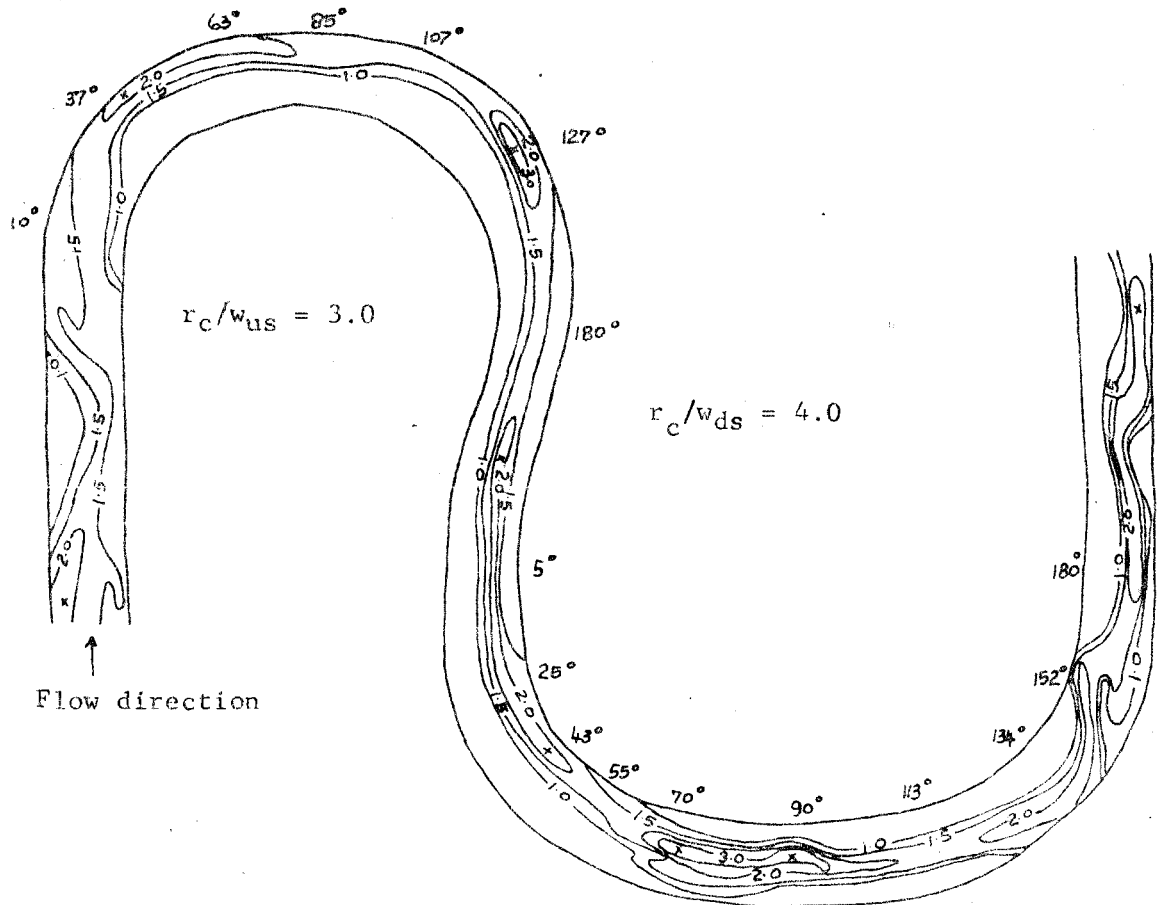


Figure A3-22. Variation of shear stress ( $T_o/\bar{T}_o$ ) for consecutive bends with  $r_c/w_{us} = 2.7$  and  $r_c/w_{ds} = 4.0$  (constant). The contour interval is 0.5; the points at which the shear stress has a maximum value are shown by the symbol 'x'.

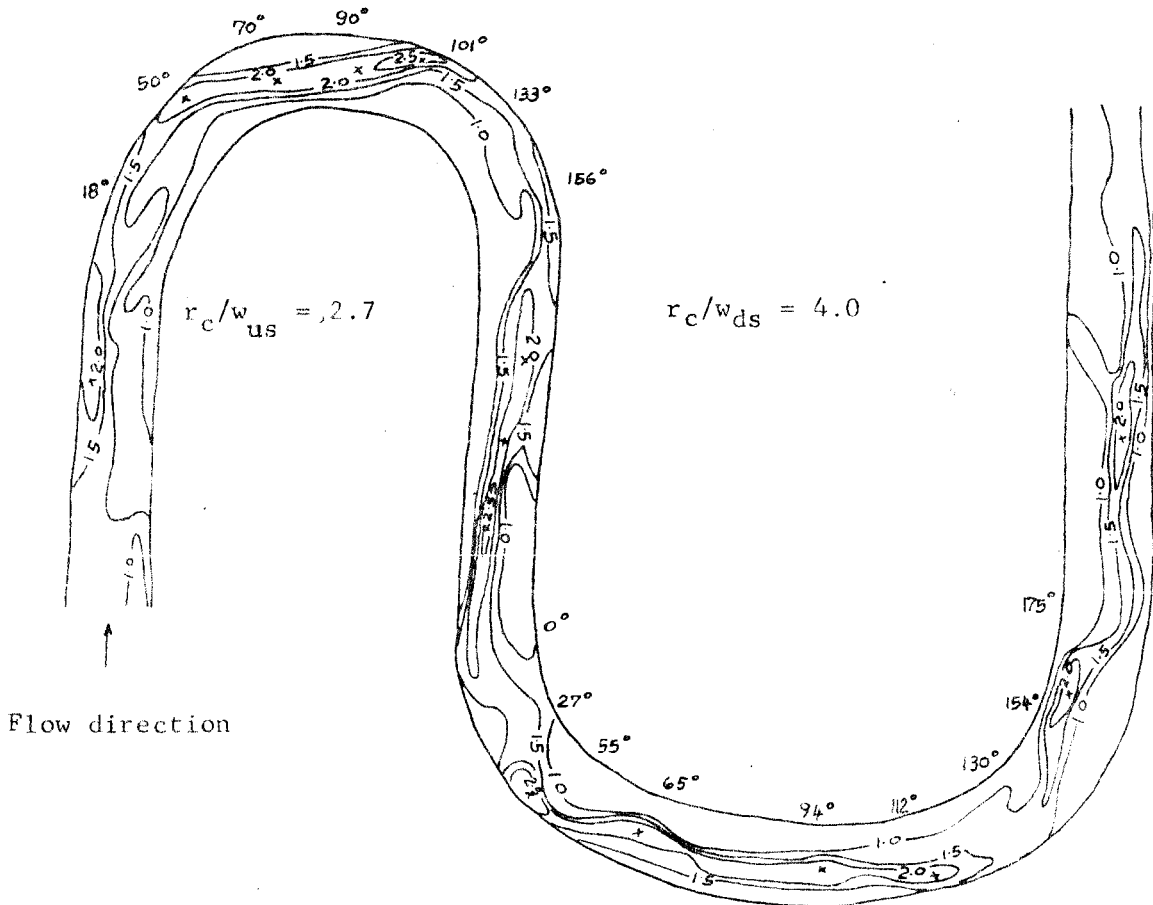


Figure A3-23. Variation of shear stress ( $T_0/\bar{T}_0$ ) for consecutive bends with  $r_c/w_{us} = 2.2$  and  $r_c/w_{ds} = 3.9$ . The contour interval is 0.5; the points at which the shear stress has a maximum value are shown by the symbol 'x'.

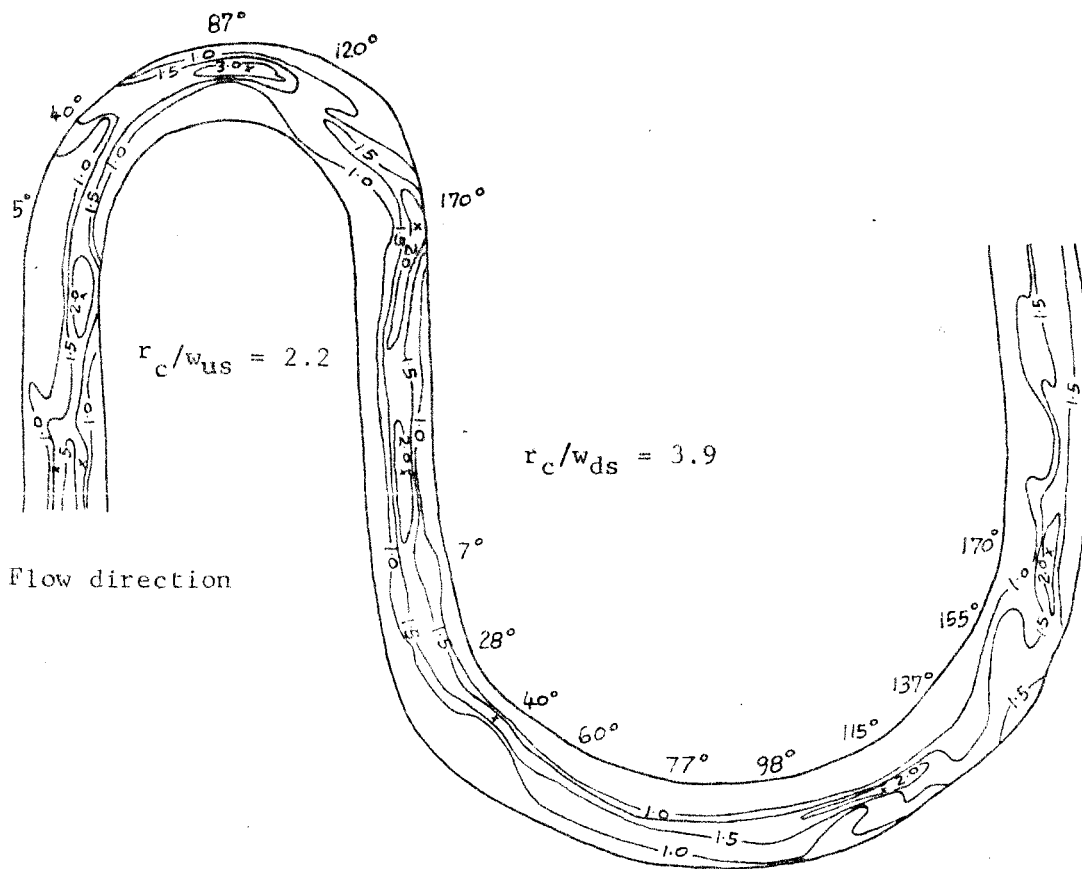


Figure A3-24. Variation of shear stress ( $T_o/\bar{T}_o$ ) for consecutive bends with  $r_c/w_{us} = 1.4$  and  $r_c/w_{ds} = 4.0$  (constant). The contour interval is 0.5; the points at which the shear stress has a maximum value are shown by the symbol 'x'.

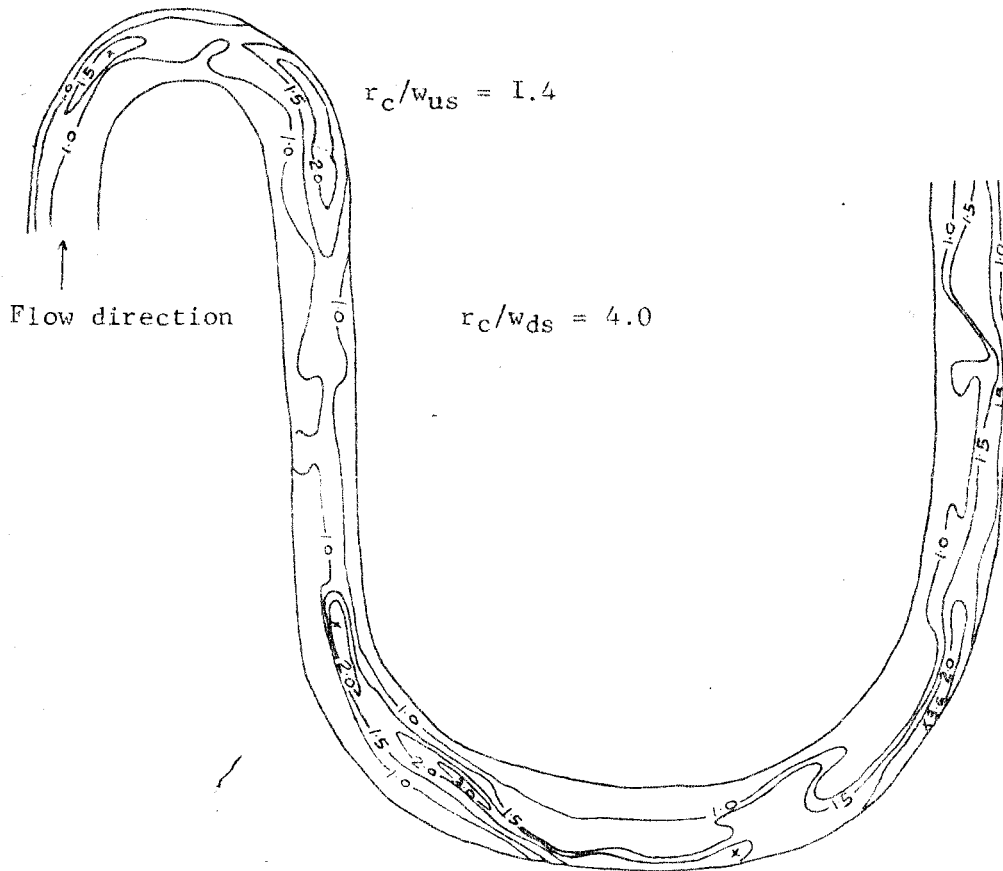




Figure A3-25. Variation of shear stress ( $T_0/\bar{T}_0$ ) for consecutive bends with  $r_c/w_{us} = 3.2$  and  $r_c/w_{ds} = 3.3$  (constant). The contour interval is 0.5; the points at which the shear stress has a maximum value are shown by the symbol 'x'.

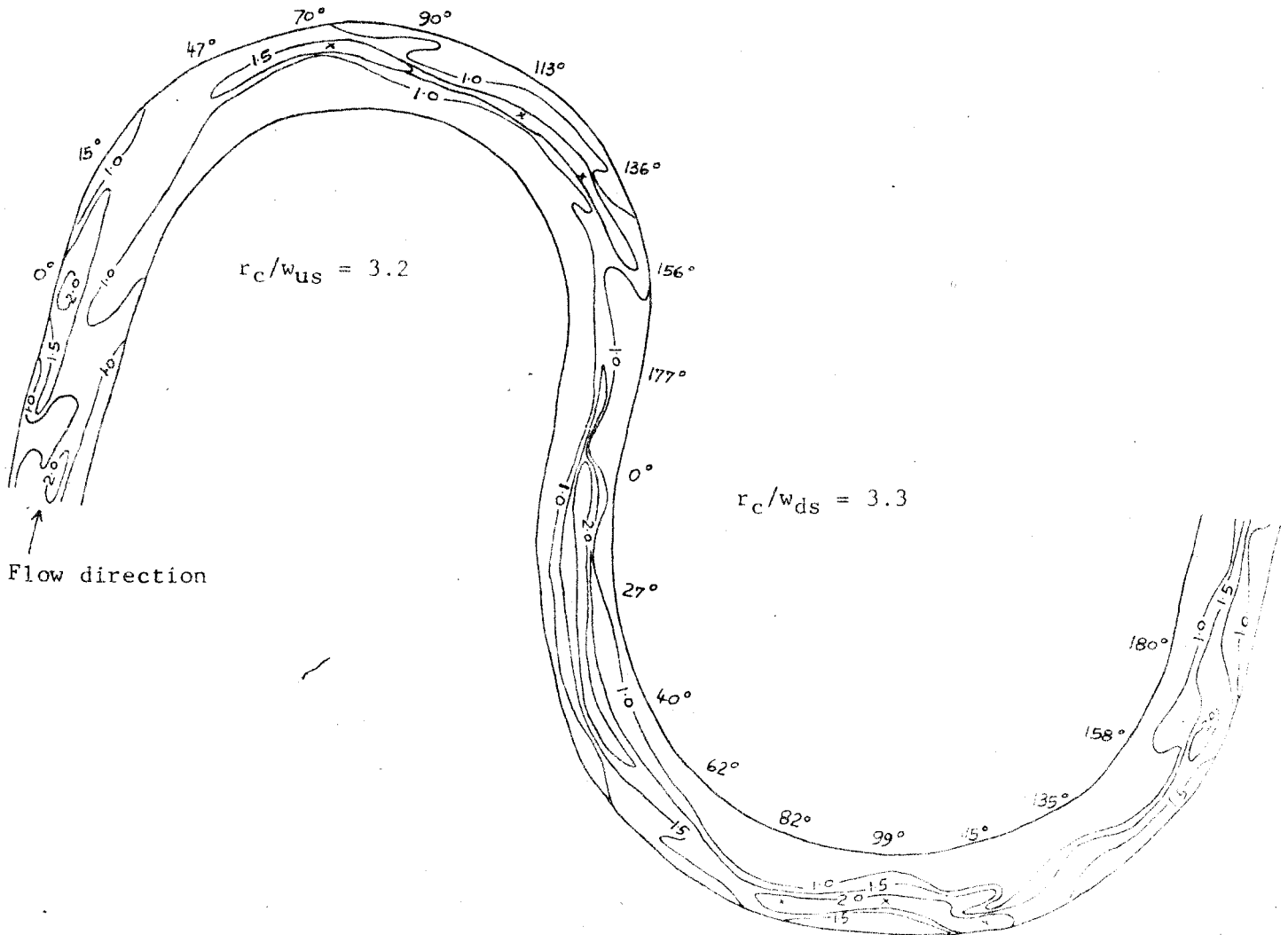


Figure A3-26. Variation of shear stress ( $T_o/\bar{T}_o$ ) for consecutive bends with  $r_c/w_{us} = 1.7$  and  $r_c/w_{ds} = 3.0$  (constant). The contour interval is 0.5; the points at which the shear stress has a maximum value are shown by the symbol 'x'.

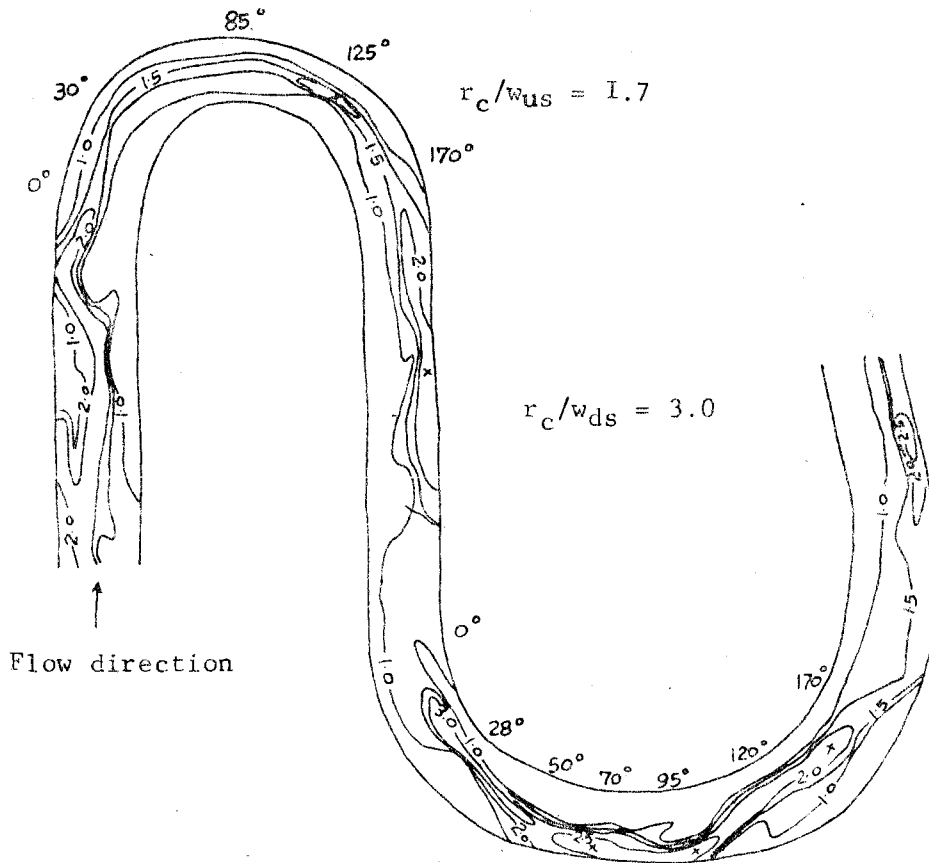


Figure A3-27. Variation of shear stress ( $T_o/\bar{T}_o$ ) for consecutive bends with  $r_c/w_{us} = 1.7$  and  $r_c/w_{ds} = 3.62$  (constant). The contour interval is 0.5; the points at which the shear stress has a maximum value are shown by the symbol 'x'.

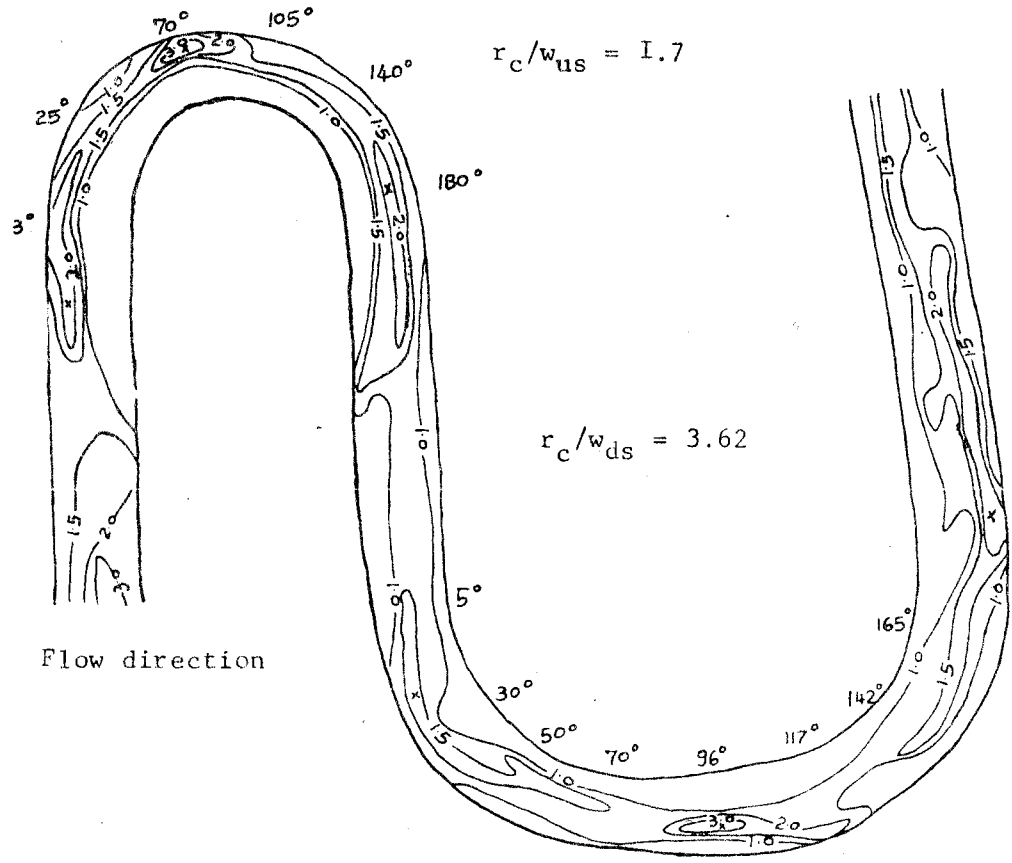


Figure A3-28. Variation of shear stress ( $T_o/\bar{T}_o$ ) for consecutive bends with  $r_c/w_{us} = 3.2$  and  $r_c/w_{ds} = 2.4$  (constant). The contour interval is 0.5; the points at which the shear stress has a maximum value are shown by the symbol 'x'.

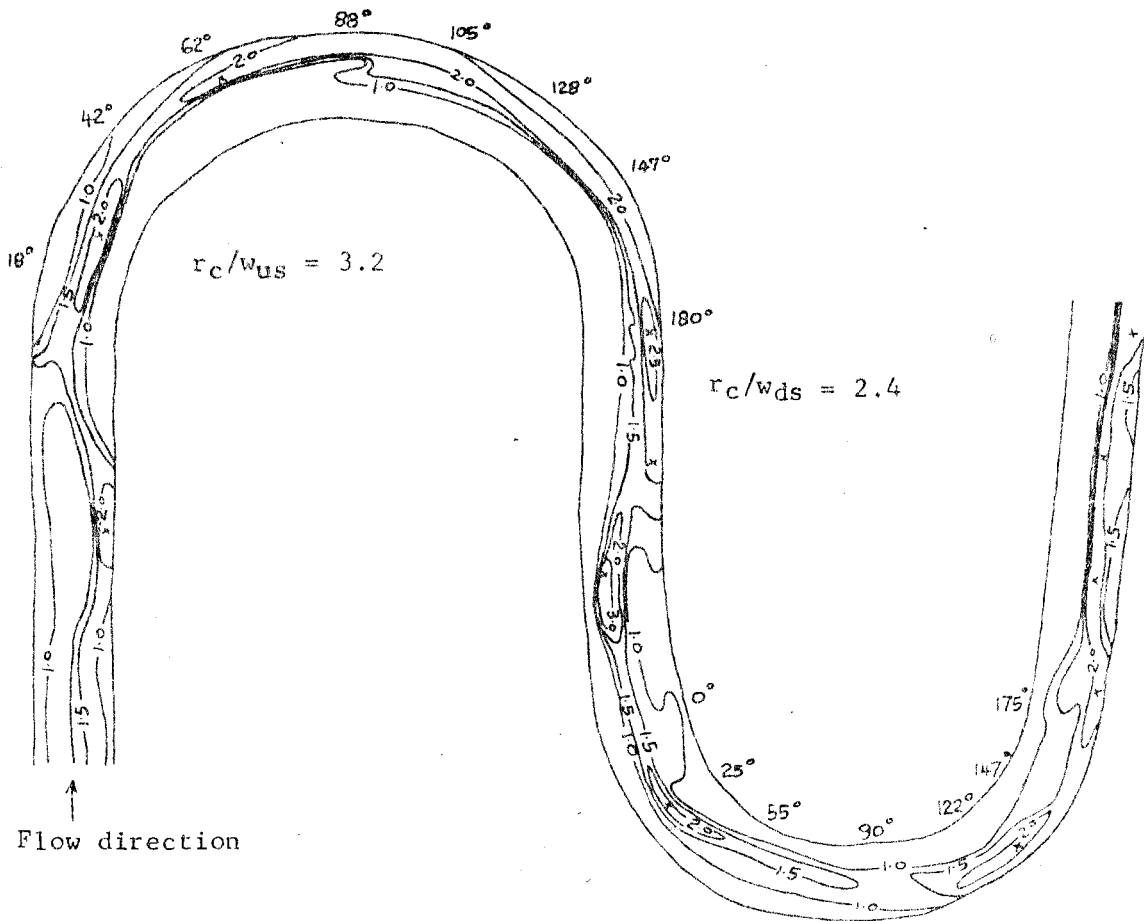


Figure A3-29. Variation of shear stress ( $T_0/\bar{T}_0$ ) for consecutive bends with  $r_c/w_{us} = 3.0$  and  $r_c/w_{ds} = 2.56$  (constant). The contour interval is 0.5; the points at which the shear stress has a maximum value are shown by the symbols 'x'.

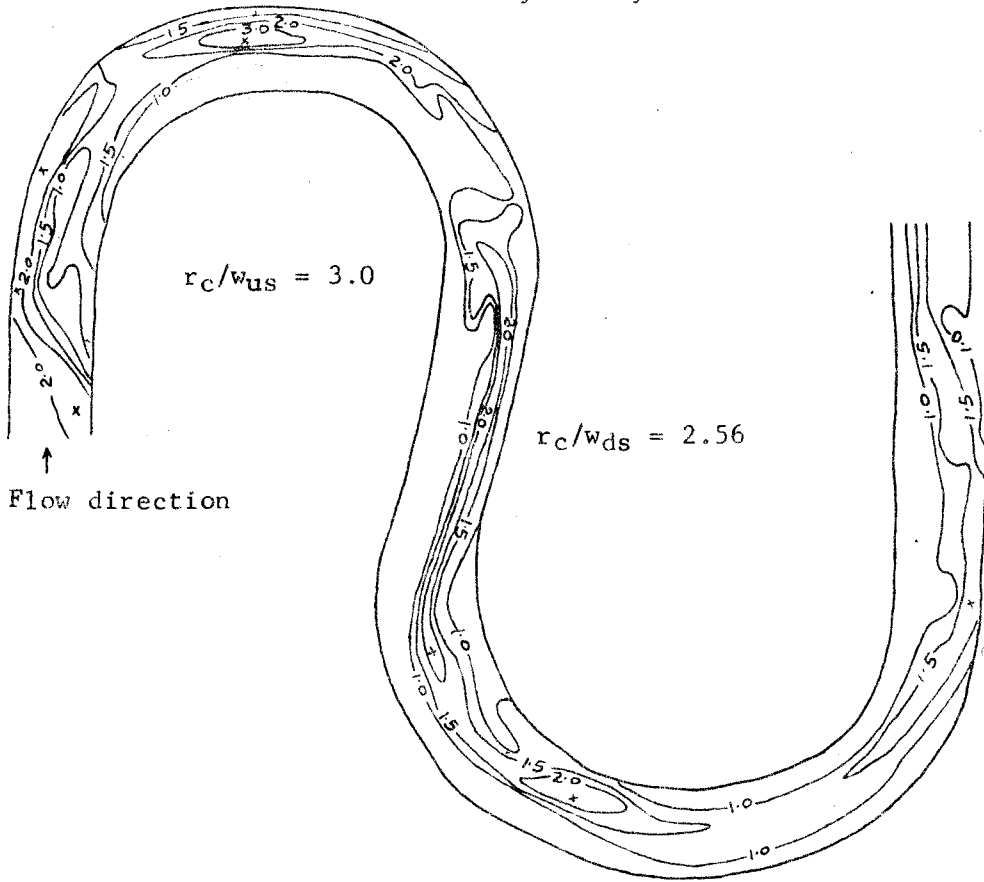


Figure A30. Variation of shear stress for consecutive bends with  $r_c/w_{us} = 2.0$  and  $r_c/w_{ds} = 3.2$  (constant).

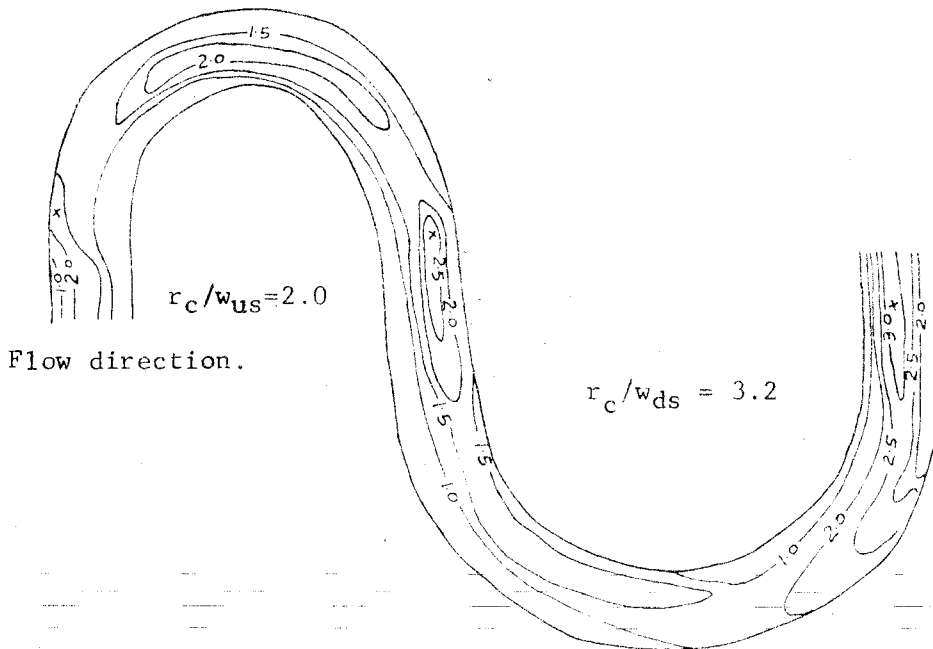
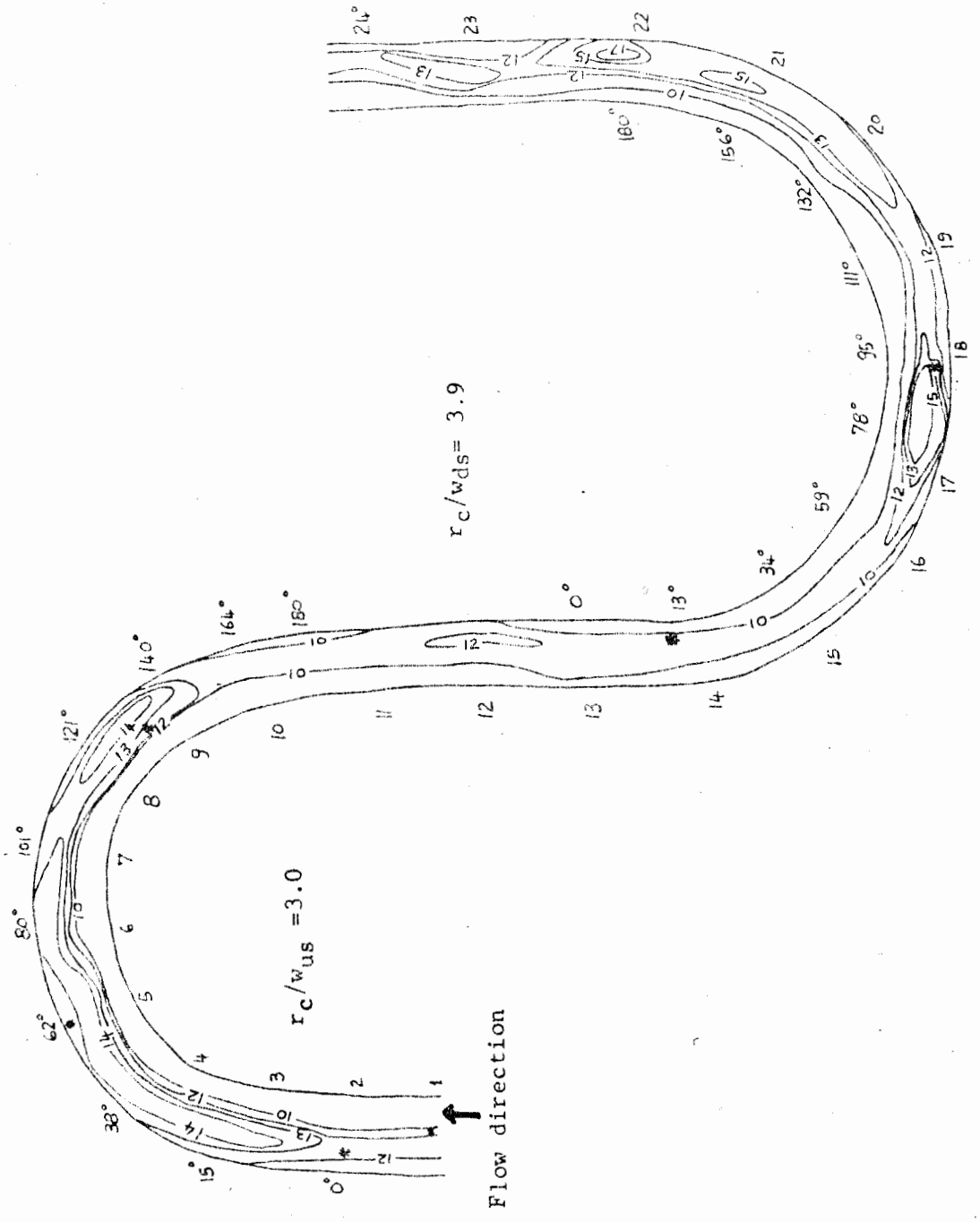




Figure A3-32. Variation of channel bed deformation in consecutive bends with  $r_c/w_{us} = 3.0$  and  $r_c/w_{ds} = 3.9$ . The symbol '\*' represents the points at which shear stress has a maximum value.



## BIBLIOGRAPHY

- Achenbach, E. 1970. Influence of surface roughness on cross-flow around a circular cylinder. *J. Fluid Mechanics* 46: 321-335.
- Achenbach, E. 1968. Distribution of local pressure and skin friction around circular cylinder in cross-flow upto Reynolds number 5 10 . *J. Fluid Mechanics* 34: 625-639.
- Ackers, P. and F.G. Charlton. 1971. The slope and resistance of small meandering channels. *Proceedings, Inst. Civil Engineers, Eng. Supplement* 15: 349-370.
- Allen, J.R. 1965. A review of the origin and characteristics of recent alluvial sediments. *Sedimentology* 5: 89 - 191.
- Annanian, A.K. 1967. An approximate theory of secondary flow at the bend of the river course. *Internl. Assoc. Hydraulic Res. Fort Collins, Colorado.*
- Appman, R.P. 1972. Flow processes in open-channel bends. *J. Hydraulic Div., Amer. Soc. Civil Engineers*, 98:795-810
- Bagnold, R.A. 1960. Some aspects of the shape of river meanders. *U.S.Geological Survey, Prof. Paper 282-E*, 10 p.
- Bagnold, R.A. *The Physics of Blown Sand and Desert Dunes.* Methuen, 1954.
- Barrows, H.K. 1905. Work of the hydrographic branch of U.S. Geological Survey in New England. *J.Assoc. Engineering Soc.* 35: 1- 33
- Bathurst, J.C., C.R. Thorne and R.D. Hey. 1979. Secondary flow and shear stress at river bends. *Proceedings, Amer. Soc. Civil Engineers, J. Hydraulic Div.* 105: 1277 - 1295.
- Begin, Z.B. 1981. The relationship between flow-shear stress and stream pattern. *J. Hydrology* 52: 307-319.
- Begin, Z.B. 1981. Stream curvature and bank erosion - a model based on momentum equation. *J. Geology* 89: 497-504.
- Bhowmik, N.G. 1979. *Hydraulics of flow in the Kaskaskia river, Illinois.* Illinois State Water Survey, Report 91, Urbana.
- Bluck, B.J. 1971. Sedimentation in the meandering River Endrick. *Scott. J. Geol.* 7: 93-138.
- Blue, F.L, J.K. Herbert and R.L. Lancefield. 1934. Flow around a river bend investigated. *Civil Engineering* 4: 258 - 260.



- Borgardi, J. Sediment Transport in Alluvial Streams. Budapest, 1974.
- Brice, J.S. 1973. Meandering pattern of the White river in Indiana - an analysis. In M.Morisawa (ed.), Fluvial Geomorphology. Publications in Geomorphology. Binhampton, N.Y.: 179-200.
- Brice, J.S. 1974. Evolution of meander loops. Geol. Soc. Amer. Bull. 85: 581-586.
- Bridge J.S.and J. Jarvis. 1976. Flow and sedimentary processes in the meandering river South Esk, Glen Clova, Scotland. Earth Surface Processes 1: 303-336.
- Bridge, J.S. and J. Jarvis. 1982. The dynamics of a river bend - a study in flow and sedimentary processes. Sedimentology 29: 499-541.
- Brooks, N.H. 1963. Boundary shear stress in curved trapezoidal channels. Discussion. J. Hydraulics Div., Amer. Soc. Civil Engineers 89: 327-333.
- Callander, R.A. 1978. River meandering. Annual Review of Fluid Mechanics 10: 129-158.
- Carson, M.A. and M.F. Lapointe. 1983. The inherent asymmetry of river meander planform. J. Geology 91: 41-55.
- Carey, W.C. 1963. Turn mechanisms of alluvial streams. Military Engineering, Jan - Feb.: 14 - 16.
- Carey, W.C. 1969. Formation of floodplain lands. Proceedings, Amer. Soc. Civil Engineers, J. Hydraulic Div. 95: 981 - 994.
- Cheng, K.C., R.C. Lin and J.W. Ou. 1976. Fully developed laminar flow in curved rectangular channels. Transactions, Amer. Soc. Mech. Enginners, J. of Fluid Engng. 98: 41 48
- Chiu, C and D.H.Hsiung. 1981. Secondary flow, shear stress and sediment transport. J. Hydraulic Div., Amer. Soc. Civil Engineers, 107: 879-898.
- Choi, U.S., L. Talbot and I. Cornet. 1979. Experimental study of wall shear rates in the entry region of a curved pipe. J. Fluid Mechanics 93: 465.
- Chow, V.T. 1959. Open Channel Hydraulics. McGraw Hill, N.Y.
- Choudhary, V.K. and S. Narasimhan. 1977. Flow in a 180 degrees open-channel rigid boundary bends. J. Hydraulics Div., Amer. Soc. Civil Engineers 103: 651-657.

- Ciracy, C. 1967. On secondary currents. Proceedings, Inter. Assoc. Hydraulic Res., Sept. 1967, Fort Collins, Colorado.
- Daniel, J.F. 1971. Channel movement of meandering Indiana streams. U.S. Geol. Survey Prof. Paper 732A: 18 p.
- Davis, T.R. and A.J. Sutherland. 1980. Resistance to flow past deformable boundaries. Earth Surface Processes 5: 175-179.
- de Vriend, H.J. 1977. A mathematical model of steady flow in a curved shallow channel. J. Hydraulics Res. 15: 37-54.
- de Vriend, H.J. 1980. Velocity distribution in curved rectangular channels. J. Fluid Mechanics 107: 423 - 439.
- Despard, R.A. and J.A. Miller. 1971. Separation in laminar boundary layer at channel bends. Transactions, Amer. Geophys. Union 35: 114-120.
- Dietrich, W.E., J.D. Smith and T. Dunne. 1979. Flow and sediment transport in a sand bedded meander. J. Geology 87: 305-315.
- Dietrich, W.E. and J.D. Smith. 1983. Influence of the point bar on flow through curved channels. Water Res. Research 19: 1173 - 1192.
- Dickinson, W.T. 1967. Accuracy of discharge determination. Hydrology Papers: 20: 2 - 6
- Dury, G.H. 1965. Principles of underfit streams. U.S. Geological Survey, Prof. Paper 452-H.
- Einstein H.A. and J.A. Harder. 1954. Velocity distribution and the boundary layer at channel bends. Transactions, Amer. Geophysical Union 35: 114-120.
- Einstein, H.A. and H. Li. 1958. Secondary currents in straight channels. Amer. Geophysical Union 39:
- Einstein, H.A. and H.W. Shen. 1964. A study of meandering in straight alluvial channels. Amer. Geophys. Res. 69: 5239 - 5246
- \_\_\_\_\_ 1972. On secondary currents and sediment motion. River Mechanics 1, H. W. Shen (ed.); Fort Collins, Colorado.
- Engelund, F. 1970. Instability of erodible beds. J. Fluid Mechanics 42: 225-244.
- Engelund, F. and O. Skovgaard. 1973. On the origin of meandering and braiding in alluvial streams. J. Fluid Mechanics 57: 289-302.

- Engelund, F. 1974. Flow and bed topography in channel bends. J. Hydraulics Div., Amer. Soc. Civil Engineers 100: 1631.
- Fenneman, N.M. 1906. Floodplains produced without floods. Geol. Soc. Amer. Bull. 38: 89-91.
- Ferguson, R.I. 1973. Regular meander path models. Water Res. Research 9: 1079 - 1086.
- Fisk, H.N. 1944. Geological investigations of alluvial valley of lower Mississippi River. Mississippi River Commission, Vicks., Miss.
- Fisk, H.N. 1952. Mississippi river valley geology relation to regime. Transactions, Amer. Soc. Civil Engineers. 117: 667 - 689.
- Fox, J.A. and D.J. Ball. 1968. The analysis of secondary flow in bends of open channels. Institution of Civil Engineers 39: 467-475.
- Francis, J.R.D. and A.F. Asfari. 1971. Velocity distribution in a wide curved open-channel flows. J. Hydraulic Res. 9: 73-90.
- Friedkin, J.F. 1945. A laboratory study of the meandering in alluvial rivers. U.S. Waterways Experiment Station, Vicksburg.
- Godfrey, R.G. 1958. Evaluation of current meters. U.S. Geological Survey. Research seminar.
- Gotz, W. 1975. Shear distribution in bends in rectangular channel. J. Hydraulic Div., Amer. Soc. Civil Engineers HY 12: 1771-1773.
- \_\_\_\_\_. 1980. Secondary flow and shear stress at river bends. Discussion. J. Hydraulics Div. 105: 1710-1713.
- \_\_\_\_\_. 1980. Calculation of strongly strongly curved open-channel flow. J. Hydraulics Div. 105: 1913-1714
- Hall, M.G. 1972. Vortex breakdown. Annual Review of Fluid Mechanics 4: 195 - 218.
- Hawthorne, W.R. 1951. Secondary circulation in fluid flow. Proceedings, Royal Soc. London 374-386.
- Hayashi, T. 1971. On the cause of meandering of rivers. Proceedings, Inter. Assoc. Hydraulic Res, Bangkok, 667-678.
- Hey, R.D. 1975. Flow separation in meander bends. Nature 253: 338-339.

- Hey, R.D. 1976. The geometry of river meanders. Nature 262: 482-484.
- Hey, R.D. 1978. Determinate hydraulic geometry. Amer. Soc. Civil Enginrs., J. Hydraulic Div. 104: 869 - 885.
- \_\_\_\_\_ and C.R. Thorne. 1975. Secondary flow in river channels. Area 7: 191-195.
- Hickin, E.J. 1969. A newly identified process of point bar formation in natural streams. Amer. J. Science 267: 999 - 1010.
- Hickin E.J. 1974. The development of meanders in natural river channels. Amer. J. Sci. 274: 414-442.
- \_\_\_\_\_ 1977. Hydraulic factors controlling channel migration. Research in Fluvial Geomorphology, Geo Abstracts, Norwich. R. Daidson-Arnott and W. Nickling (ed.): 59-66.
- \_\_\_\_\_ 1978. Mean flow structure in meanders of the Squamish River, British Columbia. Can. J. Earth Sci. 15 : 1833-1849.
- \_\_\_\_\_ 1979. Concave bank benches on the Squamish River. Can. J. Earth Sci. 16: 200-203.
- \_\_\_\_\_ and G.C. Nanson. 1975. The character of meander migration on the Beaton river, N.E. British Columbia. Geol. Amer. Bull. 86: 487-494.
- Hoffman, A. 1929. Loss in 90 degrees pipe bends of constant circular cross section. Hydraulic Inst. Munich Tech. University. Translated by Amer. Soc. Meach. Engineers, 1935.
- Hooke, Le B. 1975. Distribution of sediment transport and shear stress in a meander bend. J. Geology 83: 543-565.
- Hooke, LeB. 1980. Shear stress distribution in stable channel bends: Discussion. Amer. Soc. Civil. Enginrs., J. Hydraulic Div. 1271 - 1272.
- Hooke, LeB and W.L. Rohrer. 1979. Geometry of alluvial fans: effect of discharge and sediment size. Earth Surface Processes 4: 147 - 166.
- Hoyt, J.C. 1910. The use and care of current meter as practised by U.S. Geological Survey. Proc. Amer. Soc. Civil Engineers 66: 70 - 105
- Humphrey, J.A.C. and J.H. Witelaw. 1977. Measurements in curved ducts. Turbulence in Internal Flows, S.N.B. Murthy (ed.). Hemisphere.

- Humphrey, J.A.C, J.H. Whitelaw and G. Yee. 1981. Turbulent flow in a square duct with strong curvature. *J. Fluid Mechanics* 103: 443-463.
- Ikeda, S, G. Parker and K. Sawai. 1982. Bend theory of river meanders, part 1: Linear development. *J. Fluid Mechanics* 112: 363 - 377.
- Ippen, A.T. and R.T. Knapp. 1936. A study of high velocity in curved channels of rectangular cross section. *Transactions, Amer. Geophys. Union* 17: 516 - 521.
- Ippen A.P and P.A. Drinker. 1962. Boundary shear stress in a curved trapezoidal channel. *J. Hydraulics Div., Amer. Soc. Civil Engineers* 88: 143-180.
- Ito, H. Friction factors for turbulent flow in curved pipes. *Transactions, Amer. Soc. Mechanical Engineers* 81: 123-134.
- Jackson II, R.G. 1975 (a). Velocity-bedform-texture patterns of meander bends in the Lower Wabash River. *Geol. Soc. Amer. Bull.* 86: 1511-1522.
- Jackson II, R.G. 1975 (b). Depositional model of point bars in the Lower Wabash River. *J. Sed. Petrology* 46: 579-594.
- Jackson II, R.G. 1976. Sedimentological and fluid-dynamic implications of the turbulent bursting phenomenon in geophysical flows. *J. Fluid Mechanics* 77: 531-560.
- Kalinske, A.A. 1947. The role of turbulence in river hydraulics. *University of Iowa, Stud. Engineer. Bull.* 27: Iowa.
- Keller. E.A. 1972. Development of alluvial channels - a five stage model. *Geol. Soc. Amer. Bull.* 83: 1531-1536.
- Kennedy, J.F. 1963. The mechanics of dunes and antidunes in erodable bed-channels. *J. Hydraulics Div., Amer. Soc. Civil Engineers* 16: 521-544.
- Kikkawa, H., H. Ikeda and A. Katagawa. 1976. Flow and bed topography in curved open channels. *J. Hydraulics Div., Amer. Soc. Civil Engineers* 102: 1327-1342.
- Kirkby, M.J. 1977. Maximum sediment efficiency as a criterion for alluvial channels. *River Channel Changes*, K.J. Gregory (ed.), John Wiley and Sons.
- Knighton, A.D. 1973. Riverbank erosion in relation to streamflow conditions, R. Bollin-dean, Chesire. *East Midl. Geogr.* 5: 416-426.
- Kondrat'yev, N.Y. 1968. Hydromorphological principles of

- computations of free meandering. Soviet Hydrology, 309-339.
- Langbein, W.B. and L.B. Leopold. 1966. River meanders - Theory of minimum variance. U.S. Geol. Survey Prof. Paper 422-H.
- Leeder, M.R. 1980. On the stability of lower stage plane beds and the absence of current ripples in coarse sands. J. Geol. Soc. London 137: 423-429.
- Leeder, M.R. and P.H. Bridges. 1975. Flow separation in meander bends. Nature 253: 338 - 339.
- Leighly, J. 1936. Meandering arroyos of the dry southwest. Geog. Rev. 26: 270-282.
- Leopold, L.B. and M.G. Wolman. 1957. River channel patterns - braiding, meandering and straight. U.S. Geol. Survey Prof. Paper 282B.
- Leopold L.B et al. 1960. Flow resistance in sinuous irregular channels. U.S Geol. Survey, Prof Paper 282-D 134 p.
- \_\_\_\_\_. Wolman, M.G. and J.P. Miller. 1964. Fluvial Processes in Geomorphology. Freeman, San Francisco.
- Leschziner M.A. and W. Rodi. 1979. Calculation of strongly curved open channel flow. J. Hydraulics Div., Amer Soc. Civil Engineers 105: 1297-1313.
- Leliavsky, S. 1955. An Introduction to Fluvial Hydraulics. London, Constable.
- Lewin, J. 1976. Initiation of bedforms and meanders in coarse grained sediment. Geol. Bull. Amer. Bull. 87: 281-285.
- Lewin, J., D. Hughes and P.H. Bridges. 1977. Incidence of river erosion. Inst. Brit. Geogrs. 9: 177-180.
- Lewin, J. 1978. Meander development and floodplain sedimentation a case study from Mid Wales. J. Geology 13: 25-36.
- Lugh, H.L and H.J. Haussing. 1974. Laminar flow past an abruptly accelerated elliptic cylinder at 45 degrees incidence. J. Fluid Mechanics 65: 711 - 734.
- Maddock, T. 1970. Indeterminate hydraulics of alluvial channels. J. Hydraulics Div., Amer. Soc. Civil Engineers 96: 2309 - 2323.
- Marris, A.W. 1963. The generation of secondary vorticity in an incompressible fluid. J. Applied Mechanics 525-531.
- Mathes, G. 1947. Macroturbulence in a natural stream flow.

- Transactions, Amer. Geophysical Union 28: Washington.
- Melton, F.A. 1936. An empirical classification of floodplain streams. J. Geology 84: 593-609.
- Middleton, G.V. 1976. Hydraulic interpretation of sand size distributions. J. Geology 84: 405-414.
- Milne, M.S. 1971. On the formation of dunes and meanders. Iner. Assoc. Hydraulic Res., Proceedings 3: 1-8.
- Mockmore, C.A. 1937. Flow characteristics in elbow draft-tubes. Transactions, Amer. Soc. Civil Engineers : 402-415.
- Mockmore, C.A. 1943. Flow around bends in stable channels. Transactions, Amer. Soc. Civil Engineers 109: 335-360.
- Mosonyi, E and W.Gotz. 1973. Secondary currents in subsequent model bends. Internl. Asson. Hydraulic Res., Proceedings 1 :A-18, Bangkok, Thailand.
- Mullin, T and C.A. Greated. 1980. Oscillatory flow in curved pipes: The developing flow. J. Fluid Mechanics 98: 383-395.
- Muramoto, Y. 1967. Secondary flow in curved open channel. Proceedings of International Assoc. Hydraulic Research, Colorado.
- Nakagawa, T. 1980. Boundary effects on stream meandering and river morphology. Sedimentology 30: 117-127.
- Nakagawa, H. and T. Tsujimoto. 1980. Sand bed instability due to bedload motion. J. Hydraulic Div., Amer. Soc. Civil Engineers 106: 2029-2051.
- Nanson, G.C and E.J.Hickin. 1983. Channel migration and incision on the Beatton river. Amer. Soc. Civil Enginrs., J. Hydraulic Div. 109: 327 - 337.
- Nanson. C.G. 1977. Channel migration, floodplain formation, and forest succession in meandering-river floodplain, N.E. Bitish Columbia, Canada. Unpublished Ph.D. Thesis, Simon Fraser University.
- Noble, C.A. and R.C. Palmquist. 1968. Meander growth in artificially straightened streams. Iowa Acd. Sci. Proc. 75: 234-242.
- Nouh, M.A. and R.D. Townsend. 1979. Shear stress distribution in stable channel bends. J. Hydraulic Div., Amer. Soc. Civil Engineers 105: 1233=1245.
- Onishi, Y. et al. 1976. Effects of meandering in alluvial

- streams. J. Hydraulics Div., Amer. Soc Civil Engineers 102: 899-917.
- Parker, G. 1976. On the cause and characteristic scales of meandering and braiding in rivers. J. Fluid Mechanics 76: 457-480.
- Parker, G., K.Sawai and S. Ikeda. 1982. Bend theory of river meanders, part 2: Nonlinear deformation of finite amplitude bends. J. Fluid Mechanics 115: 303 - 314.
- Parsons, D.A. 1960. Effects of flood flow on channel boundaries. Proceedings, Amer. Soc. Civil Engineers 86: 21-34.
- Prandtl, L. Essentials of Fluid Mechanics. Blackie, London. 1949.
- Perkins, H.J. Formation of streamwise vorticity in turbulent flow. J. Fluid Mechanics 44: 721-740.
- Pratap, V.S. and D.B. Spalding. 1975. Numerical computations of flow in curved ducts. Aero. Quarterly 26: 219.
- Prus-Chacinski, T.M. 1956. Patterns of motion in open-channel bends. Inst. Water Engineers 10: 420-426.
- Quraishy, M.A. 1944. The origin of cuves in rivers. Current Sci. (india) 13: 36-39.
- Ratzlaff, J.R. 1981. Development and cut-off of big bend meander, Brazos R. Texas J. Sci. 33: 121-129.
- Ramamurthy, A.S and C.P. Ng. 1973. Effects of blockage on steady force coefficients. J. Engrn. Mech. Div., Amer. Soc. Civil Engineers 99: 755-772.
- Raudkivi, A.J. 1966. Bedforms in alluvial streams. J. Fluid Mechanics 26: 507-514.
- Richards, K.S. 1976. The morphology of riffle-pool sequences. Earth Surface Processes 1: 71-88.
- Richards, K.S. 1978. Channel geometry in riffle-pool sequences. Geografiska Annaler 60: 23-27.
- Roshko, A. 1961. Experiments of the flow past a circular cylinder at very high Reynolds number. J. Fluid Mechanics 10: 345-356.
- Rozovskii, I.L. 1961. Flow of water in bends of open channels. Acad. Sci., Ukranian S.S.R., Kiev.
- Rowe, M. 1970. Measurements and computations of flow in pipe bends. J. Fluid Mechanics 43: 771.



- Schumm, S.A. and H.R.Khan. 1972. Experimental study of channel patterns. Geol. Soc. Amer. Bull. 83: 1755-1770.
- Schumm, S.A. 1977. The Fluvial System. Wiley and sons, N.Y.
- Siebert, W and W. Gotz. 1976. A study of the deformation of secondary flow in models of rectangular meandering channels. Proceedings, Inter. Assoc Hydraulic Res.: 141-149.
- Shen, H.W. and S. Komura. 1968. Meandering tendencies in straight alluvial channels. J. Hydraulics Div., Amer. Soc. Civil Engineers 94: 997-1016.
- Shukry, A.H. 1949. Flow around bends in an open flume. Transactions, Amer. Soc. Civil Engineers 115: 751-779.
- \_\_\_\_\_. 1963. Boundary shear stress in curved trapezoidal channel. Discussion. J. Hydraulics Div., Amer. Soc. Civil Engineers 89: 333-345.
- Siebert W. and W. Gotz. 1975. A study of the deformation of secondary flow in models of rectangular meandering channels. Proceedings, Inter. Assoc. Hydraulic Res. 141-149.
- Simons, D.B., E.V. Richardson, and C.F. Nordin. 1966. Resistance to flow in alluvial channels. U.S. Geol. Survey Prof. Paper 422J.
- Smith, T.R. 1974. A derivation of the hydraulic geometry of steady-state channels from conservation principals and sediment transport laws. J. Geology 82: 98 - 104.
- Smith, F.T. 1976. Fluid flow in a curved pipe. Proceedings, Royal Society of London, A 351: 71-87.
- Soliman, M.M. and E.R. Tinney. 1968. Flow around 180 degrees bend in open rectangular channels. J. Hydraulic Div., Amer. Soc. Civil Engineers 97: 893-908.
- Squire, H.B and K.G. Winter. 1951. The secondary flow in a cascade of aerofoils in a nonuniform stream. J. Aero. Sci. 18: 271.
- Stuart, J.T. 1971. Nonlinear stability theory. Ann. Rev. Fluid Meach. 1: 347-370.
- Suga, K. 1967. The stable bed profiles of curved open channels beds. Interl. Assoc. Hydraulic Res. , Colorado. 487-496.
- Sundborg, A. 1956. The river Klaralven - a study of fluvial processes. Geografiska Annaler 38: 127-316.
- Taylor, G.I. 1929. Proceedings, Royal Soc. London 86: 124-243.

- Talbot, V.S. and K.O. Gong. 1983. Pulsatile entrance flow in a curved pipe. *J. Fluid Mechanics* 127: 1-25.
- Thompson, J. 1876. On the origin and winding of rivers in alluvial plains. *Proceedings, Royal Society of London* 25:
- Thorne, C.R. and R.D. Hey. 1979. Direct measurements of secondary currents at a river inflection point. *Nature* 280: 226 - 228
- van Dyke, M. 1970. Entry flow in a channel. *J. Fluid Mechanics* 44: 813 - 823.
- Varshey, D.V and R.J. Garde. 1975. Shear distribution in bends in rectangular channels. *J. Hydraulics Div., Amer. Soc. Civil Engineers* 101: 1053-1066.
- Wang, C.Y. 1980. Flow in narrow curved channels. *J. Fluid Mechanics* 47: 7-10.
- Wang, K.C. 1980. Three-dimensional boundary layer near the plane of symmetry of a spheroid at incidence. *J. Fluid Mechanics* 43: 187-209.
- Wilson, I.G. 1973. Equilibrium cross sections of meandering and braided rivers. *Nature* 241: 393-394.
- Wolman, M.G. and L.M. Brush. 1961. Factors controlling the size and shape of stream channels in coarse noncohesive sands. *U.S. Geol. Survey Prof. Paper* 282G.
- Woodyer, K.D. Concave-bank benches on the Barwin River, N.S.W., Australia. *Australian Geogr.* 13: 36-40.
- Yalin, M.S. 1971. On the formation of dunes and meanders. *Proceedings, Inter. Assoc. Hydraulic Res.* 3: 1 8.
- Yao, L.S. and S.A. Berger. 1975. Entry flow in a curved pipe. *J. Fluid Mechanics* 67: 177-196.
- Yang, C.T. 1971. On river meanders. *J. Hydrology* 13: 231-253.
- Yarnal, D.L and F.A. Nagler. 1934. Flow of water around bends in pipes. *Amer. Soc. Civil Engineers: HY3*, 1018-1032.
- Yarnkh, N.A. 1978. Channel and bank deformations in an acute meander. *Soviet Hydrology* 17: 278 - 281
- Yen, B.C. 1965. Bed Configuration and Characteristics of Subcritical flow in a meandering River. PhD Dissertation, 149p. University of Iowa, Iowa.
- Yen, B.C. 1967. Some aspects of flow in meandering channels.

Proceedings, Inter. Assoc. Hydraulic Res. 1: 465-471.

—— 1972. Spiral motion of developed flow in wide curved open channels. Sedimentation, H.W. Shen (ed.), Fort Collins, Colorado.

Yen, C.L. Bed configuration and characteristics of subcritical flow in meandering channel. Unpublished Ph.D dissertation, University of Iowa, Iowa.

Yen, C.L. and B.C. Yen. 1972. Water surface configuration in channel bends. J. Hydraulic Div., Amer. Soc. Civil Engineers 97: 303-321.

Zimmerman, C. 1978. Roughness effects on flow direction near curved stream beds. J. Hydraulic Res. 15: 73-85.